

**RECENT ADVANCES IN MARINE SCIENCE
AND TECHNOLOGY, 96**

**NARENDRA K. SAXENA
EDITOR**

**PACON INTERNATIONAL
P.O. BOX 11568
HONOLULU, HAWAII 96828 U.S.A.**

UNIVERSITY OF HAWAII AT MANOA
SEA GRANT COLLEGE PROGRAM
2525 CORREA ROAD, HIG 238
HONOLULU, HAWAII 96822



UNIHI-SEAGRANT-BB-95-03

RECENT ADVANCES IN MARINE SCIENCE
AND TECHNOLOGY, 96

Edited by

Narendra Saxena
Professor of Civil Engineering
University of Hawaii
Honolulu, Hawaii, U.S.A.

PACON INTERNATIONAL
1997

June 1997

Published by
PACON International
P.O. Box 11568
Honolulu, Hawaii 96828
U.S.A.

ISBN 0-9634343-2-2 (this volume)
ISBN 0-9634343 (series)

Printed in the United States of America

TABLE OF CONTENTS

PREFACE.....	ix
I. OCEAN SCIENCE AND TECHNOLOGY PAPERS	
THE USE OF MULTI-LEVEL IMAGERY IN MARINE ENVIRONMENTAL MAPPING Joseph H. J. Leach.....	1
A NEW METHOD FOR ESTIMATING VELOCITY FIELDS FROM SATELLITE IMAGES Zhihua Mao, Delu Pan, Yuqiu Pan, and Weigen Huang.....	11
ACOUSTIC DETECTION AND CLASSIFICATION OF BURIED UXO USING SYNTHETIC APERTURE SONAR Mark Neudorfer, Tony Luk, Dennis Garrod, Norman Lehtomaki and Mark Rognstad.....	19
EFFECTS OF SOUND SPEED PROFILE UNCERTAINTY ON ACCURACY OF DEPTH MEASUREMENTS Xueyi Geng and Adam Zielinski.....	33
MIRROR IMAGE ZONALITY ON MAGMATISM AND ORE DEPOSITS AROUND THE JAPAN SEA Valentina Baskina.....	45
TSUNAMI RISK ASSESSMENT FOR SHIKOKU ISLAND AND THE KII PENINSULA Hitoshi Murakami, Naoaki Yamamoto, Sadahiko Itoh, Yasunori Kozuki, and Hiroaki Sato.....	55
A LINEAR PROBLEM ON SUBSURFACE VARIATIONS AT A TSUNAMIGENIC EARTHQUAKE Shigehisa Nakamura.....	65
NUMERICAL MODELING OF COSMOGENIC TSUNAMIS Victor Petrenko and Andrei Marchuk.....	77
DIVING TO MARIANA TRENCH BY “KAIKO” Shinichi Takagawa, Taro Aoki and Ikuo Kawana.....	89
UNDERWATER TELEROBOTICS AND VIRTUAL REALITY: A NEW TECHNOLOGY PARTNERSHIP Steve Murray and Doug Murphy.....	97

A MODEL BASED SELF-DIAGNOSIS SYSTEM FOR AUTONOMOUS UNDERWATER VEHICLES USING NEURAL NETWORKS Motoyuki Takai and Tamaki Ura.....	107
VISUAL TRACKING FOR UNMANNED UNDERSEA VEHICLES B.A.A.P. Balasuriya and Tamaki Ura.....	119
TIME-INVARIANT BATHYMETRY: A NEW CONCEPT TO DEFINE AND SURVEY IT USING GPS Muneendra Kumar.....	131
PREDICTION OF THE LARGEST SURFACE WAVE HEIGHT IN WATER OF CONSTANT DEPTH Stanislaw Massel.....	141
WIND-WAVE-SURGE INTERACTION IN STORM SURGE PREDICTION Takao Yamashita and Gary Watson.....	153
STORM SURGES IN THE PACIFIC FORUM REGION J. L. Luick, R. F. Henry, and T. S. Murty.....	167
MODELING METHODOLOGIES FOR THE PREDICTION OF HURRICANE STORM SURGE Cheryl A. Blain.....	177
SHIP-BASED FREE ELECTRON LASER (FEL) LIDAR FOR OCEANIC AND ATMOSPHERIC RESEARCH S. K. Sharma, C. E. Helsley, R. J. Burke, D. M. Tratt, R. L. Collins, and C. K. N. Patel.....	191
SEDIMENTARY $\delta^{13}\text{C}$ AS A PROXY FOR THE SOURCE OF THE BULK SEDIMENT Deling Cai.....	205
NEW ANALYTICAL TECHNIQUE FOR THE SHIPBOARD DETERMINATION OF COBALT CONCENTRATION IN SEA-WATER AND HYDROTHERMAL SOLUTIONS Irina Y. Kolotyrkina, Alexander Malahoff, and Lilly K. Shpigun.....	217
LASER INDUCED RAMAN AND FLUORESCENCE SPECTRA OF CROWN-OF-THORNS STARFISH EGGS Shiv K. Sharma and Tenshi Ayukai.....	227
THE ANOMALY IN TROPICAL PACIFIC AND ITS EFFECT ON EL NINO Jilin Sun, Qinyu Liu and Baozhen Zhu.....	239

CORAL REEF ISLANDS - IMPLICATIONS OF MORE MODEST GLOBAL CHANGE PREDICTIONS	
David Hopley.....	249
LIGHT SCATTERED BY PARTICULATE MATTER IN SEA WATER: COMPUTER MODELING AND EXPERIENCE FROM SEA TRIALS	
T. Hall, T. Clark and G. Ludbrook.....	259
EFFECT OF DISPERSANTS ON ZOOPLANKTON MORTALITY IN KOREA	
Woong-Seo Kim, Man Chang, Soo Hyung Lee and Jong Soo Lee.....	269
MINIATURIZED GAS CHROMATOGRAPHY INSTRUMENTATION FOR DMS IN THE MARINE ATMOSPHERE	
Paul M. Holland, Robert V. Mustacich, James F. Everson and John W. H. Dacey.....	277
CORAL REEF NATURE RESERVE MANAGEMENT IN HAINAN PROVINCE	
Lu Wang.....	287
SEA LEVEL CONTROLLED SEDIMENTATION ON A CARBONATE RAMP - SOUTHERN GREAT BARRIER REEF, AUSTRALIA	
Alexa Troedson and Peter J. Davies.....	297
SUBMERGED SHELF-EDGE REEFS, CORAL REEFS, GREAT BARRIER REEF AUSTRALIA	
D. Hopley, T. L. Graham, and C. E. Rasmussen.....	305
MODELING OF HYDROTHERMAL PROCESSES ON THE OCEAN BOTTOM	
Nickolay Korchagin.....	317
 II. MARINE RESOURCE MANAGEMENT AND DEVELOPMENT	
A POLICY ROLE FOR PACON IN SUSTAINABLE MARINE RESOURCE DEVELOPMENT	
Linda M. B. Paul.....	329
THE WORLD COBALT MARKET AND ITS ABILITY TO SUPPORT MANGANESE CRUST MINING	
John C. Wiltshire.....	337
FORMULATION OF SPECIALTY GLASSES AND GLAZES EMPLOYING MARINE MINERAL TAILINGS	
G. F. Terry Lay and John C. Wiltshire.....	347

TRANSVERSE ZONES AND TRANSFORM FAULTS AS TARGETS IN SEARCHING FOR SUBMARINE MINERALIZATION Valentina A. Baskina.....	363
FUNCTION OF BACTERIAL (<i>HYPHOMONAS spp.</i>) CAPSULAR EXPOLYMERS IN BIOFOULING Ronald Weiner, Stephen Langille, Gill Geesey and Ernesto Quintero.....	373
INTERNAL WAVE INTERACTIONS WITH STEEP SLOPES AND THE RESULTANT INFLUENCE ON OCEAN OUTFALL PERFORMANCE Patrick K. Sullivan and Dayananda Vithanage.....	387
PROTECTING THE COASTAL RESOURCES OF PENANG STRAITS OF MALAYSIA: A MODELING PERSPECTIVE Hock-Lye Koh, Hooi-Ling Lee and Zubir Din.....	397
BASIC STUDY ON THE RENEWAL IN THE COASTAL ZONE OF METROPOLITAN AREAS Takamasa Miyazaki and Akira Minemura.....	411
REFLECTIONS ON THE DEVELOPMENT OF TROPICAL MARINE STUDIES FOR SOUTH PACIFIC SCHOOLS Stephen M. Ritchie and David Hopley.....	421
POST 1995 CHALLENGES TO MARITIME EDUCATION AND TRAINING ESTABLISHMENTS Rod Haigh.....	429
BASIC RESEARCH ON BARRIER-FREE COASTAL RECREATIONAL FACILITIES IN JAPAN Tsuyoshi Kobayashi, Takeo Kondo and Eiichi Matsuura.....	443
PARTICIPATION OF SEAWEEDS IN WATER PURIFICATION AND MARINE BIOTA PROTECTION O. N. Selivanova.....	451
THE SEISMIC SEQUENCE, GEOTECTONICS AND PETROLEUM GEOLOGY IN NANSHA REGION Shaoren Jiang and Xiaozhang Zhou.....	465
WILD DOLPHIN BASED TOURISM: MINIMIZING THE RISKS AND MAXIMIZING THE BENEFITS Mark B. Orams.....	477

INFRASTRUCTURE DEVELOPMENT IN CORAL REEF ENVIRONMENTS:
THE NEED FOR ENGINEERING GUIDELINES
Stanislaw Massel and I. R. Kapitzke.....491

COMPETITION AMONG NORTH AMERICAN CONTAINERPORTS:
CURRENT CHARACTERISTICS INVOLVED
Henry S. Marcus and William A. Cowart.....501

INDEX OF AUTHORS.....509

PREFACE

Recent Advances in Marine Science and Technology, 96 is the third refereed publication of a series based upon papers presented at the seventh Pacific Congress on Marine Science and Technology (PACON 96) held in Honolulu, Hawaii, 17-20 June 1996. A unique process was adopted to bring about this refereed publication: session chairs selected papers based on presentations at PACON 96 and recommended them for possible inclusion in this publication. Each manuscript was reviewed by the session chairman and an external reviewer. Some revised manuscripts were reviewed a second time by the initial reviewer to see that the modifications were duly made. Out of 181 PACON 96 presentations, 113 papers were recommended by session chairmen, 56 manuscripts were submitted, and finally 46 papers were accepted for this publication.

Since papers dealt in areas of ocean sciences, technology, management and policy, we have tried to group related papers to facilitate the reader's use of this publication. I hope that readers will find this volume of 46 papers useful. An index giving the alphabetized list of authors is presented at the end of this volume.

I wish to thank Paula Kuriyama and Richelle Tashima of PACON International, without whose untiring efforts this publication would not have been possible. Acknowledgment is also extended to Sunyeen Pai of the Pacific Mapping Program for assisting in editing this publication. This work was made possible due to the generous support of our sponsors: Alexander & Baldwin; CEROS, National Defense Center for Research in Ocean Sciences; Department of Business, Economic Development and Tourism (DBEDT), State of Hawaii; Hawaii Natural Energy Institute; Office of Sustainable Development and Intergovernmental Affairs, NOAA, U.S. Dept. of Commerce; PACON International; The Medical Foundation for the Study of the Environment and the Human Body Charitable Trust; U.S. Geological Survey (USGS); University of California, Sea Grant College Program; University of Hawaii at Manoa, College of Engineering; and University of Hawaii at Manoa, Sea Grant College Program.

Honolulu
June 25, 1997

Narendra K. Saxena

THE USE OF MULTI-LEVEL IMAGERY IN MARINE ENVIRONMENTAL MAPPING

Joseph H. J. Leach

University of Melbourne
Parkville, Victoria, AUSTRALIA

ABSTRACT

The proposed declaration of marine reserves and sanctuary areas has created a need for accurate mapping of the shallow marine environment. The large areas involved and the difficulty of access mean that remote sensing techniques are essential tools in this work. Satellites can penetrate to 20m depth and map large areas quickly and cheaply. There is a need for ground truth in interpreting satellite imagery. To meet this requirement the Geomatics Department at the University of Melbourne developed a semi-submersible vessel designed to provide high resolution imagery of the marine environment. This imagery provides an accurate idea of the complexity within the broad terrain types mapped by satellite. One difficulty in using the semi-submersible imagery to ground truth the satellite mapping is that the scales of the two imagery types are so different that the comparison can sometimes be difficult. Multi-spectral aircraft imagery is one way of overcoming this problem - providing comparable imagery of an intermediate scale which can act as a bridge between the broad area coverage of the satellite mapping and the high detail of the submersible imagery. Together, these three levels of imagery can accurately map the shallow marine environment. They also provide the means to map the shallow sea floor rapidly and cheaply so that management decisions, such as the siting of sanctuary zones, can be made on the basis of hard data.

INTRODUCTION

The importance of preserving marine resources is now being recognised by many countries. One manifestation of this awareness is the declaration of marine reserves to protect areas of particular scenic, environmental or historic importance. The state of Victoria, Australia, is currently undergoing a reevaluation of its marine reserves. In 1991 the government directed that the Land Conservation Council establish a system of marine parks and sanctuary zones (LCC 1995) in order to preserve biological diversity and conserve both recreational and commercial fish stocks. The proposed declaration of marine reserves and sanctuary areas has created a need for accurate mapping of the shallow marine environment. Not only do the sites of these reserves need to be chosen on the basis of reliable information, a criticism of the Victorian proposals is that they are based on inadequate data (Porter and Wescott 1995), but also once established, the sites must be monitored if their management is to have any meaning. The large areas involved and the difficulty of access mean that remote sensing techniques are essential tools in this

work. Since it is the sea floor habitat which is the target of these protected areas, in situ monitoring of these parks would be difficult, dangerous, and expensive. Even using remote sensing technology, mapping the sea floor environment is difficult. This study shows how data from different platforms and at different scales can be combined to provide effective environmental monitoring.

STUDY AREA

Port Phillip Bay is a large (1920 Sq Kms) tidal embayment on the southern coast of Australia (See figure 1). Melbourne, Australia's second largest city, is located on its north eastern shore and over four million people live by the bay or in its near environs. The bay is a nearly fully enclosed saucer shaped depression with a large tidal delta at its southern end. It is separated from Bass Strait by a very narrow entrance which channels tidal flow to very high velocities. Very few bays would have similar morphologies (Black et al. 1993).



Figure 1. Locality map showing: A - Location of the study area, B - City of Melbourne, C - Port Phillip Heads, D - Lonsdale Bight, E - Nepean Bay, and F - Mud Island and the tidal delta

The study area for this project was the region around the restricted entrance at the southern end of the bay, known as Port Phillip Heads. This region contains Marine, National, and State Parks and represents an important site for environmental monitoring. The entrance to the bay is dominated by a deep submarine gorge which has been described as a tidal colk (Bowler 1966) although it may also form part of the submerged valley of the ancestral Yarra River (Holdgate et al. 1981). The gorge is narrow (approximately 250m wide) with steep walls containing numerous overhangs (Malloy 1995). The gorge is bounded by two shallow, sub-tidal shelves which form the floor of

the Lonsdale Bight and Nepean Bay. Both of these areas contain intertidal rocky shelves which have a national heritage listing (LCC 1995) and form part of both the Harold Holt Marine Park and the Point Nepean National Park. Monitoring the environment of this region is important to the management of the environmental resources of the whole Port Phillip area.

SATELLITE IMAGERY

Under good water conditions, satellites can penetrate to 20m in depth (Jupp 1988) and map large areas quickly and cheaply. The depth zone to 20m is the region where human activity is at its greatest. It is in this region that correct conservation efforts are most critical and accurate information is most urgently needed. The water penetration is greatest in the blue region of the visible spectrum for clear ocean water but, because of the blue absorption by phytoplankton chlorophyll, moves towards the green in coastal waters (Neumann and Pierson 1966). This wavelength dependent light absorption means that satellites always have two independent variables which contribute to their result; the reflectance of the bottom terrain and the absorption of the water column which is related to depth. These can be separated by water column models if you can make some assumptions about the nature of the water mass (Lyon and Hutchinson, 1995; Beirwirth et al., 1993). In the study area this is difficult as water conditions can change dramatically over distances of less than one kilometre. The classification approach used in this study avoids this problem but might classify the same bottom type occurring at different depths as different classes. In the study area this proved not to be a problem as there was a clear relationship between depth and bottom type.

However, even if the ambiguities between the bottom type and the water column can be resolved, the relatively poor resolution of the satellite systems means that many small, ecologically distinct regions on the sea floor will be aggregated into the response of one pixel. This means that satellites can only provide broad terrain type classification.

The satellite data used in this study came from the LANDSAT TM instrument with 30m square pixels. The bands used in the study were TM bands one and two which image in the blue and green portions of the visible spectrum respectively. These bands have the best penetration of the water column and contain the highest signal level from the sea floor (Neumann and Pierson, 1966). The Near Infra-red band (TM band 4) was used to remove surface interference from the other two bands. Since surface effects such as sun glint and waves will effect Band 4 to the same degree as the other bands and since the Near Infra-red has a zero return over water bodies apart from these effects, it can be used as a mask. The Band 4 was subtracted from the other two bands and the resultant data were classified using an unsupervised classification routine. The results are shown in Figure 2.

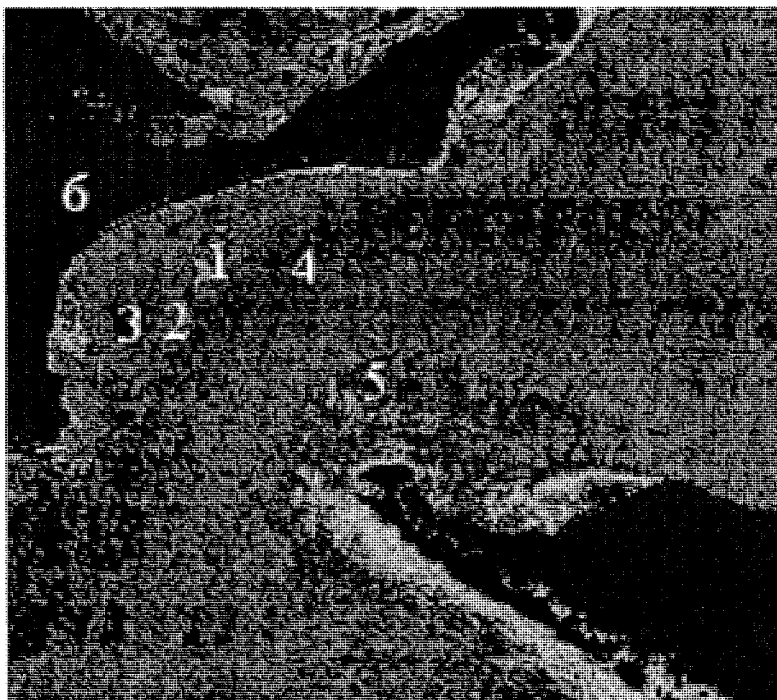


Figure 2. Classified Image of the Port Phillip Heads Region. Features shown are: 1 - Rocky reef with fringing kelp beds, 2 - Mixed seaweed and sand, 3 - Sandy Channels, 4 - Deep gorge, 5 - Turbid water, and 6 - Land.

In the Lonsdale Bight, Landsat TM has been able to distinguish sandy channels and banks, rocky reefs and kelp cover. These terrain types, however, are not simple or undifferentiated and the marine environment can display complex and significant variation on the meter scale. Also, while some interpretations can be made on the basis of the spectral return and a knowledge of the likely terrain types in the area, these must be treated with caution. There can be, for example, confusion between shallow rocky reef and shallow sand banks. Some reef areas have a dense and diverse kelp coverage which can be confused with areas of kelp forest, or even deep water. There is a need for ground truth in interpreting satellite imagery. Indeed, the scale of satellite imagery means that other data are always required for accurate environmental analysis.

"GROUND TRUTHING" PROBLEMS

The conventional means of ground truthing satellite imagery in this environment is quadrate mapping and in situ sampling by divers. This is difficult, expensive, and potentially dangerous. Also, the difficulties of precise location and data recording in the marine environment mean that this method is subjective and open to large statistical variations (Skewes and Long 1994). This means that there is no objective record of the variation at any given site and that individual sites can not be revisited as part of an ongoing monitoring program.

Photographs are often the only permanent record of sample sites. However, the hand held photographs taken by divers during sampling excursions are normally high detail obliques which are useful for illustration and sample documentation but which lack precise positioning and standard geometry and which are, as a consequence, difficult to place in their spatial context. They can not provide the complete area coverage needed for mapping and monitoring operations. Even when there has been an attempt to create an area coverage using hand held diver photography (Staniforth and Vickery, 1984), the lack of precision in image location, spacing and geometry creates difficulty in handling the resultant data.

Imaging sonar is the traditional method of acquiring image information underwater. It can operate to the greatest depths of the ocean basins and quickly provide a continuous cover over a large area. However, since its medium is sound rather than light, it mainly gives information on detailed bottom topography. It does not provide information on the nature and health of biological materials. In most cases the return echo is not purely from the surface but is an aggregate of both surface reflection and near surface volume scattering. Even systems which use the shape of the return signal to classify the bottom type have a poor response to biological material.

SEMI-SUBMERSIBLE IMAGERY

To overcome the difficulty of providing objective and precisely located ground truth data, the Geomatics Department at the University of Melbourne developed a semi-submersible vessel, named the Korrong - an Australian aboriginal word for boat, designed to provide high resolution imagery of the marine environment (Leach 1995).

The Platform design

The central Korrong platform is a semi-submersible vehicle specifically designed for submarine imaging. It is a 5.2m long aluminium monohull with a beam of 2.46m and a depth of 0.95m. The vessel can be considered as consisting of a fore and aft bay, separated by the console. The aft bay contains the navigation and control positions while the forward bay contains the observation pod and its lifting frame and moon pool. The deck layout of the vessel is given in Figure 3. The vessel is equipped with a Differential

Global Positioning System receiver (DGPS) so that the precise image position is available and specific sites can be revisited and rephotographed to provide an objective record for long term environmental monitoring. It also has a single frequency depth sounder to provide depth information and a mission control computer to coordinate all of the data inputs.

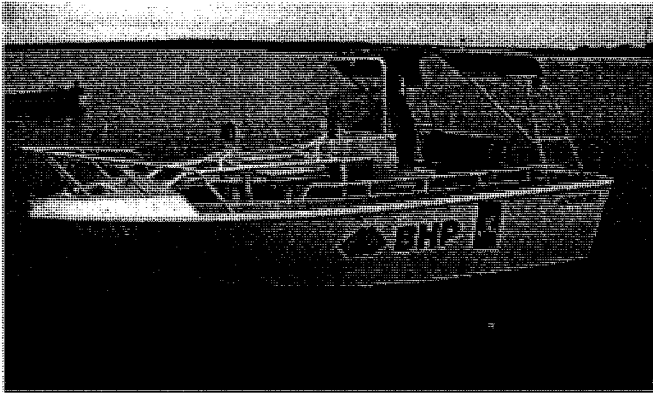


Figure 3. The *Korrong* shallow water imaging vessel.

The Observation Pod

The most important component of the Korrong system is the retractable observation pod which is lowered into position through a moon pool. The pod is elliptical in shape and



Figure 4. The observation pod in its raised position.

0.62 meters wide. When fully extended, the floor of the pod is one meter below the surface. The observation pod is designed to carry an observer and is equipped with three perspecks view ports to provide forward, port and starboard viewing. There are four camera ports in the floor of the pod, each of which has a generic camera mount associated with it. The system is designed to be flexible enough to take any reasonable imaging system with only minimal modifications. It is designed to be an imaging laboratory with direct access to the submarine environment so that a variety of imaging instrument prototypes can be evaluated. The pod is light tight from the surface and totally, sealed apart from a weather tight access hatch and the vents for the fan forced ventilation. Lead ballasting is used to take up the excess buoyancy when the pod is lowered and the pod is locked to the hull at three points to ensure that it remains at the correct operating depth.

In clear water, these camera ports in this pod can provide millimeter scale imagery at depths of up to 10 meters. The high resolution comes at the cost of area coverage, however, and it would be impractical to use this system for mapping large areas.

Results

In the Lonsdale Bight this system has been able to supply imagery detailed enough for algal species identification. Indeed, it can map the zonation in encrusting algae on rocky outcrops (see Figure 5). This imagery clearly shows the zonation of algal types around



Figure 5. *Korrong* image from Draper's Reef at the northern edge of Lonsdale Bight. The image shows: 1 - Rocky substrate, 2 - Encrusting coralline algae, 3 - Kelp fronds, and 4 - green seaweed. Depth 3m.

the rocky reefs and small bedform features in the sandy channels. This imagery provides an accurate idea of the complexity within the broad terrain types mapped by satellite and has been able to confirm the broad characterisation of the bottom reflectance classification.

AIRBORNE DATA

One difficulty in using the semi-submersible imagery to ground truth the satellite mapping is that the scales of the two imagery types are so different that the comparison can sometimes be difficult. The "mixel" problem is even more severe in the marine environment than it is on land. Multi-spectral aircraft imagery is one way of overcoming this problem - providing comparable imagery of an intermediate scale which can act as a bridge between the broad area coverage of the satellite mapping and the high detail of the submersible imagery. These data have been used very successfully in seafloor mapping exercises (eg. Ong et al., 1995). They do, however, require ground checking to the same degree as the satellite data.

The imagery used in this study was digitised multispectral air photography. This has a reduced water penetration relative to digital systems due to underexposure over the water if any land is included in the image. If there is no land in the image, the features can be difficult to locate accurately. The data were particularly important in areas close to the shore where the shallow depth and heavy swell would make it dangerous to operate the Korrong, see Figure 6. It is possible that the next generation of high resolution satellites, that are currently waiting to be launched, may make the airborne layer redundant.

CONCLUSION

Satellite imagery can rapidly map the shallow sea floor terrain over broad areas. It can map the major bottom types but it is an imprecise instrument and can not provide detailed information. The mapped divisions need to be checked to ensure that the ambiguities inherent in this style of mapping have not confused the result. Seaborne imagery can provide this checking. The imagery from the semi-submersible Korrong is very high in detail but with a very low area coverage. Airborne data can provide a bridge between the high resolution of the boat imagery and the broad coverage of the satellites. It is important as a primary checking tool in areas where the boat can not go. Together, these three levels of imagery can accurately map the shallow marine environment. They also provide the means to map the shallow sea floor rapidly and cheaply so that management decisions, such as the siting of sanctuary zones, can be made on the basis of hard data.

REFERENCES

- Beirwirth, P.N., Lee, T.J., and Burne, R.V., 1993. Shallow sea-floor reflectance and water depth derived by unmixing multispectral imagery. *Photogrammetric Engineering and Remote Sensing*, Vol **59**, No.3, pp 331-338.
- Black, K., Hatton, D. and Rosenberg, M. 1993. "Locally and externally-driven dynamics of a large semi-enclosed bay in Southern Australia." *Journal of Coastal Research* Vol. **9** (2) pp 509-538.
- Bowler, J. 1966. "Port Phillip Survey 1957-1963, The geology and geomorphology." *Memoirs of the National Museum of Victoria* No. 27, pp 1 9-68.
- Holdgate, G.R., Thompson, B.R. and Guerin, B. 1981. "Late Pleistocene Channels in Port Phillip." *Proceedings of the Royal Society of Victoria* Vol. **92**(1) pp 1 19-13 0.
- Land Conservation Council, 1995, *Marine and Coastal Special Investigation: Proposed Recommendations*,. Land Conservation Council, Melbourne.
- Leach, J.H.J., 1995. "High Resolution Multi-spectral Bottom Imaging Using A Semi-submersible Vessel." *Proceedings of the Third Thematic Conference: Remote Sensing for Marine and Coastal Environments*, ERIM, Michigan, Vol. **2**, pp 791-799.
- Lyon, J.G., and Hutchinson, W.S., 1995. Application of a radiometric model for evaluation of water depths and verification of results with airborne scanner data. *Photogrammetric Engineering and Remote Sensing*, Vol **61**, No.2, pp 161-166.
- Malloy, M. 1995. "Southern colours." *Sportdiving Magazine* No.53, pp 76-79.
- Neumann, G., and Pierson, W.J., 1966. *Principles of Physical Oceanography*. Prentice-Hall, New Jersey.
- Ong, C., Burt, J., Hick, P., and Wylie, A., 1995. "Marine Habitat Mapping Using Data from the Geoscan Airborne Multi-spectral Scanner". *Proceedings of the Third Thematic Conference: Remote Sensing for Marine and Coastal Environments*, ERIM, Michigan, Vol. **2**, pp 728-739.
- Porter, C.M. and Wescott, G.C. 1995. A Revolution in Marine Protected Areas in Victoria? *Proceedings of AMSA '95*. Australian Marine Sciences Association, Sydney.
- Skewes, D., and Long, B.G. (1994) *Sampling Marine Resources*. *GIS User*, No. 8 pp 31,32.
- Staniforth and Vickery (1984) *The Excavation of the William Salthouse Wreck Site*. Australian Institute of Maritime Archaeology Special Publication No. 3.

A NEW METHOD FOR ESTIMATING VELOCITY FIELDS FROM SATELLITE IMAGES

Zhihua Mao, Delu Pan, Yuqiu Pan and Weigen Huang
Second Institute of Oceanography, State Oceanic Administration
Hangzhou, China

ABSTRACT

The maximum correlation coefficient (MCC) method and correlation relaxation (CR) method have been widely used to estimate sea surface velocity fields from sequential satellite sea surface temperature (SST) images. The performance of the MCC and CR methods is dependent on the parameter values of pattern size and search range. The setting of parameters should correspond with the scale of the physical process in the same area. A new method called standard vector guidance (SVG), based on the MCC and CR methods, has been developed to improve the performance of the two methods.

The SVG method can provide a means to estimate sea surface velocity fields if satellite images and *in-situ* current measurements are simultaneously available. It combines both data and takes advantage of the large scale of satellite images to overcome the lack of *in-situ* current measurements and also take advantage of the accuracy of *in-situ* current measurements to reduce the flexibility of velocity fields from remote sensing data.

INTRODUCTION

Many methods have been developed to estimate sea surface velocities directly from high resolution satellite images. Lin *et al.*(1992) analyzed SST structure and derived the sea surface current systems from SST images in Taiwan Strait and its adjacent areas. Emery *et al.*(1986) applied the MCC method for estimating sea surface velocities from SST images. Wu *et al.*(1992 and 1995) applied the MCC method and CR technique on two time-lapsed images to estimate the current velocities. Wahl and Simpson (1991) decomposed the velocity vector into the normal and tangential components and used the MCC method to estimate the velocity vector.

The performance of the MCC and CR methods is dependent on the parameter values. A wrong choice of pattern size may cause an erroneous displacement vector in direction while a bad setting of search range may get an erroneous displacement vector in magnitude. Therefore, the settings of pattern size and search range should correspond with the scale of the physical process. For an image of a large area, however, different parts of the image should have different values of parameters. The optimal value setting of parameters, a function of the image coordinates, should be automatically changed according to the current velocity in the same position. A new method called standard vector guidance (SVG) has been developed to improve the situation of the MCC and CR methods.

METHODS

The MCC method to derive current velocities from SST images employs the pattern matching technique which depends on the cross correlation coefficient matrix given by

$$\rho(i, j) = \frac{\sum_k \sum_l ([s(k+i, l+j) - n_s(i, j)][p(k, l) - n_p])}{D} \quad (1)$$

where, $n_s(i, j) = E[S_{ij}(k, l)]$

$$n_p = E[p(k, l)]$$

$$D = \sqrt{\sum_k \sum_l [s(k+i, l+j) - n_s(i, j)]^2 \times \sum_k \sum_l [p(k, l) - n_p]^2}$$

and $S(k+i, l+j)$ is a subregion in the search window of the second image, $p(k, l)$ is a pattern in the first image. The vector with the maximum correlation coefficient in the correlation matrix is chosen as the displacement vector. The threshold of maximum correlation coefficients should be very carefully selected (Wahl and Simpson, 1990).

The consistency strength of two labels, where labels refer to all candidate vectors which have bigger correlation coefficient than a threshold, is given by (Wu and Pairman, 1995).

$$C = \exp(-d_1/d_0) \cdot \cos \theta \cdot \left(1 - \frac{|l_1| - |l_2|}{\max(|l_1|, |l_2|)} \right) \quad (2)$$

Therefore, the consistency strength is a function of three factors which are the distance d_1 of the two labels, the angle θ between the two labels and the magnitude of labels $|l_1|, |l_2|$. The signal of C decided by θ is that $C > 0$ when $-90^\circ < \theta < 90^\circ$ and $C < 0$ when two labels are opposite. A large value of C indicates good consistency between two labels.

The CR method uses the maximum probability to decide the displacement vector instead of maximum correlation coefficient. The probability is updated iteratively by (Rosenfeld and Kak, 1982)

$$P_{ij}^{n+1} = P_{ij}^n \cdot (1 + S_{ij}^n) / \sum_r (P_{ir}^n \cdot (1 + S_{ir}^n)) \quad (3)$$

where S_{ij}^n is a support for label l_{ij} obtained from all labels of neighboring feature points. A positive value of S_{ij}^n can increase its probability in the next iteration, while a negative one decreases its probability. The probability of the label changes according to the support condition

from other labels. S_{ij}^n is updated iteratively as follows

$$S_{ij}^n = \sum_h \sum_k C(i, j; h, k) \cdot P_{hk}^n \quad (4)$$

where, $C(i, j; h, k)$ is the consistency strength for label l_{ij} got from label l_{hk} . The label l_{hk} adds a positive support to the label l_{ij} when $C(i, j; h, k) > 0$, while it decreases the total support of l_{ij} when $C(i, j; h, k) < 0$.

The initial probability deduced from correlation coefficient matrix is given by

$$P_{ij}^0 = \rho_{ij} / \sum_r \rho_{ir} \quad (5)$$

It can be seen from (4) that a label with large values of C and P can add a big support to S_{ij}^n . If the value of P is enlarged by 10 times, the support will be also enlarged by 10 times and become the main part in S_{ij}^n . The label will become a prominent label to decide the value of S_{ij}^n and increase the probability of those labels with large C much faster than that of others and enhance their chances to become the maximum probability.

A standard vector given by a large correlation coefficient weight, for example 10, can play this role. Its correlation coefficient weight is more than 10 times larger than other labels. It can modify the probabilities of other labels much larger than other labels do. After a number of iterations, the probability of a label having a good consistency with the standard vector will become maximum in the labels of a point and be selected as the displacement vector. Therefore, the SVG method allows the standard vector to choose the displacement vectors from similar labels.

The standard vectors can be derived from *in-situ* current data. They are given by large correlation coefficient weight and be put into the initial label field. They can increase the probability of other labels which are similar to them. They can guide other vectors to be more consistent.

RESULTS

Two SST images dated on Dec. 5 and 6, 1989 have been used in this study. Because of no *in-situ* current measurements during that period of time in this area, two groups of standard vectors shown in Fig. 2 which were derived from Fig. 1 (Guan, 1986) have been used.

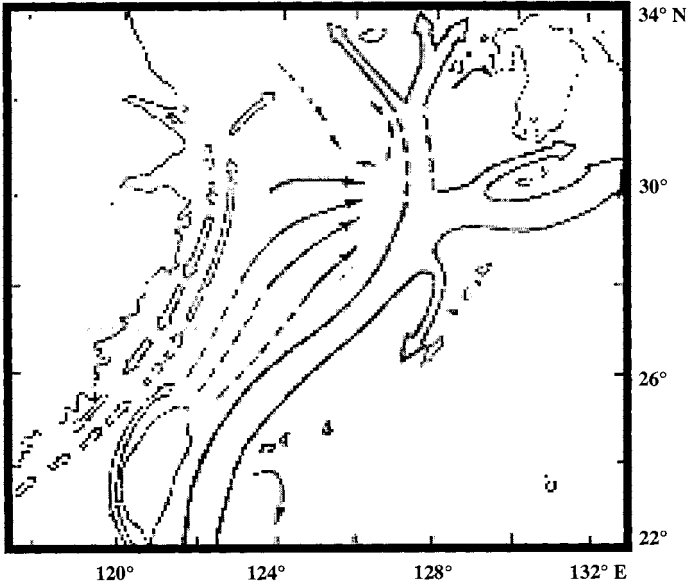


Fig. 1 The current systems in the East China Sea in winter (from Guan, 1986)

Fig. 3 and Fig. 4 illustrate the results obtained by the MCC and SVG methods respectively. Compared to the results of these two methods, it is obvious that the standard vectors can guide other vectors in direction and make the velocity field be much more consistent. The standard vectors can also modify the neighboring vectors in magnitude shown in table 1. It can be seen that the standard vectors smaller than average velocity can decrease the average velocity. For example, the standard vectors with 10 cm/s decreases the average velocity from 16.0 cm/s to 14.9 cm/s. On the other hand, the standard vectors larger than the average velocity can increase the average velocity. Therefore, the standard vectors can guide other vectors both in direction and in magnitude and make them be more consistent.

Table 1 The relationship between the standard vectors and the average velocity, showing how the standard vectors modify other vectors in magnitude.

velocity of standard vectors(cm/s)	average velocity(cm/s)	velocity difference(cm/s)
no standard vectors	16.0	0
10	14.9	-1.1
20	16.2	0.2
30	17.0	1.0
40	17.2	1.2
50	17.5	1.5

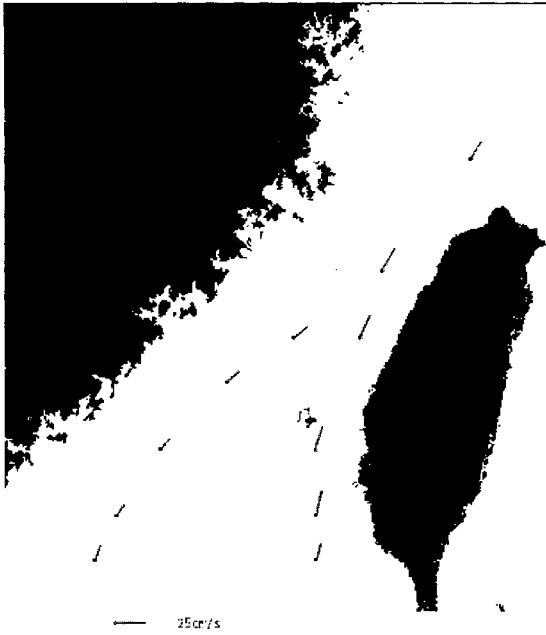


Fig. 2 Two groups of the standard vectors derived from Fig. 1.

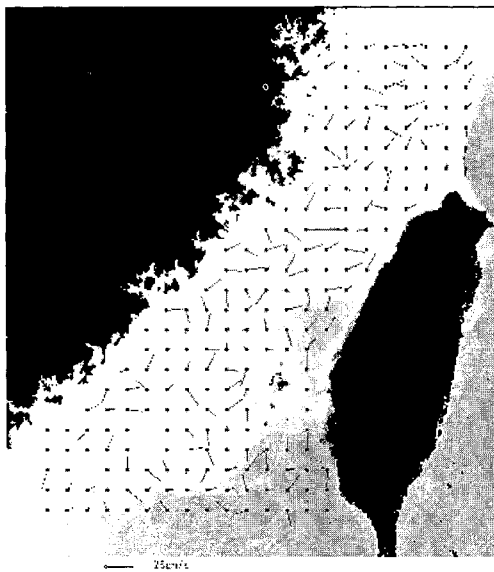


Fig. 3 The velocity field obtained by the MCC method

The velocity field in Fig. 4 reveals two current systems in Taiwan Strait in winter. In the east part of Taiwan Strait, a branch of Kuroshio stream enters Taiwan Strait and flows northward along the west coast of Taiwan island. The other one from the South China Sea flows northeastward in the west and middle parts of Taiwan Strait. The SVG method can make the disorderly vectors obtained by the MCC method be more consistent and the current systems be more obvious.

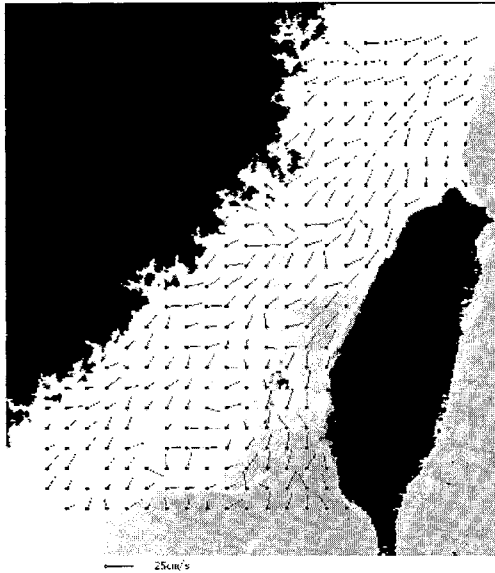


Fig. 4 The velocity field obtained by the SVG method using the standard vectors in Fig. 2

CONCLUSIONS

The standard vectors derived from *in-situ* current measurements can guide other vectors obtained from satellite SST images both in direction and in magnitude. The SVG method can combine these two kinds of data and take the advantages of the large scale of satellite images and of the accuracy of the *in-situ* current measurements. It can make the displacement vectors be in good order and the current system structure be obvious.

ACKNOWLEDGMENT

This study has been supported by a German-Chinese cooperative research project. The authors would like to express their gratitude to Prof. Guenter Warnecke and Dr. Lutz Bannehr of the Institute of Meteorology, Freie University Berlin, Germany and Frau. E. Hongsernant of DLR-IB, Germany and Dr. Q. X. Wu of DSIR Physical Sciences, New Zealand for their various assistance.

This research is supported by the National Natural Science Foundation of China NO:49376275 & NO:49493400 and BMFT of Germany.

REFERENCES

- Emery, W. J. *et al.* 1986. An objective method for computing advective surface velocities from sequential infrared satellite image. *J. Geophysical Research*. **91(C11)**:1286512878.
- Guan, B. 1986. A sketch of the current structure and eddy characteristics in the East China Sea. *Studia Marina Sinica*. **27**:1-21.
- Lin, M. *et al.* 1992. Preliminary analysis of surface temperature field and surface current system in Taiwan Strait in early winter of 1989. *J. Oceanography in Taiwan Strait*. **11(3)**:262-267.
- Rosenfeld, A. and A. C. Kak. 1982. Digital picture processing. Vol. 2. New York: Academic Press.
- Wahl, D. D., J. J. Simpson. 1990. Physical processes affecting the objective determination of near-surface velocity from satellite data. *J. Geophysical Research*. **95(C8)**: 1351113528
- Wahl, D. D. and J. J. Simpson. 1991. Satellite derived estimates of the normal and tangential components of near-surface flow. *Int. J. Remote Sensing*. **12(12)**: 25292571.
- Wu, Q.X. *et al.* 1992. Computing advective velocities from satellite images of sea surface temperature. *IEEE Trans. on Geoscience and Remote Sensing*. **30(1)**:166-176.
- Wu, Q.X. and D. Pairman 1995. A relaxation labeling technique for computing sea surface velocities from sea surface temperature. *IEEE Trans. on Geoscience and Remote Sensing*. **33(1)**:216-220.

ACOUSTIC DETECTION AND CLASSIFICATION OF BURIED UXO USING SYNTHETIC APERTURE SONAR

Mark Neudorfer¹, Tony Luk¹, Dennis Garrod¹, Norman Lehtomaki¹, and Mark Rogstad²

¹Alliant Techsystems Inc., Mukilteo, Washington, USA

²University of Hawaii, Honolulu, Hawaii, USA

ABSTRACT

There is a need for better detection and more accurate classification of objects buried below the ocean floor. This need is shared by environmental monitoring and cleanup tasks, and geological surveying. Unexploded ordnance (UXO) hunting is a specific concern of the U.S. Department of Defense and the State of Hawaii as part of the cleanup of the waters around the island of Kaho'olawe. When buried objects are to be retrieved, the high false alarm rate associated with current UXO hunting technology leads to increased costs due to unnecessary excavation.

This paper presents the results of testing a bottom-penetrating side-looking sonar. The sonar uses synthetic aperture techniques to achieve 10 cm resolution. Differential phase techniques were used to measure the depth of buried targets. Tests were conducted in the Halekeluni sand channel off Waikiki Beach, Hawaii, USA. Sonar images show UXO like objects buried to 0.6 meters in the sand.

INTRODUCTION

Conventional methods for subbottom object hunting use vertical probing of the ocean floor with acoustic profiling equipment. In shallow water this approach suffers from the effect of successive acoustic specular reflections between the ocean bottom and sonar platform. In addition, the profiling equipment used is typically small, portable, and low cost, resulting in small acoustic apertures with broad beams. This results in poor horizontal resolution making it difficult to identify the size and number of buried objects.

This paper describes an experiment demonstrating that differential phase data processed by a modified Synthetic Aperture Sonar (SAS) algorithm can produce images of objects buried in the subbottom. UXO-like objects were planted at known locations by divers in a test site off Waikiki. The HIGP Acoustic Wide Angle Imaging Instrument (HAWAII MR1) sonar platform was modified to collect the sonar data. Data gathered with multiple passes over the target site were post processed to produce the results presented. The test results demonstrated the use of:

1. Low frequency (12.5kHz) to detect and image objects buried in the sand,
2. SAS processing to improve the image resolution and contrast, and
3. Differential phase processing to measure depth of buried objects.

This test program was limited by the telemetry bandwidth available in the HAWAII MR1 sonar. The telemetry constraint dictated the characteristics of the physical hydrophone arrays, the processing bandwidth, and the swath width available for recording. Ultimately the effect of the

constraints was to limit the maximum resolution of SAS and the detection of weak objects, but did not affect the demonstration of a resolution improvement and detection of buried objects.

TECHNICAL APPROACH

Side Looking Sonar (SLS)

A classic side-looking sonar (SLS) makes images of the bottom, creating one line of pixels for each ping of the sonar. The energy in the sonar pulse is constrained to a beam looking to the side of the towfish. The sonar transmission is a short pulse that travels away from the towfish and reflects off objects in its path. Each line in the image is a time history of the echoes from this pulse. Multiple objects within the width of the sonar beam cannot be resolved. To improve the resolution, the sonar beam must be made narrower by making the sonar array longer. This reaches a practical limit that is usually restricted by towfish size.

Subbottom Sonar

When making sonar images of what lies below the seafloor, the rapid attenuation of sound in the sea bottom must be considered. Typical attenuation constants in a sand bottom are around 1 dB per wavelength. Getting sound to penetrate the sea floor is therefore done by using low frequencies, typically below 10 kHz.

Synthetic Aperture Sonar (SAS)

In order to penetrate the sea floor, low frequency (12.5 kHz) pulses were used for this experiment. However, low frequencies have the disadvantage that they result in large beam widths and low resolution. A longer array is needed to get more resolution. A synthetic aperture sonar artificially forms this longer array by coherently adding the signals from successive pings to form a longer synthetic aperture. Synthesizing this long array requires measuring the positions of the towfish with an accuracy much better than a wavelength. This is accomplished using inertial instruments in the towfish and by close examination of the sonar signals using the ATK proprietary Aperture Position Correction (APC) algorithms.

Features of SAS Sonars (Cutrona 1975)

- The best achievable resolution is 1/2 of the hydrophone element size. This is because a small element affords a wider field of view, which in turn allows a longer synthetic array length.
- The SAS beam width is one half the beam width of a physical array of the same length. In a physical array each physical element measures a phase shift due to the receive path. With a synthetic aperture, each synthetic aperture experiences a phase shift due to the round trip path, yielding twice the phase shift of a physical array and therefore one half the beam width.
- The resolution is fixed and doesn't vary with range. This is an improvement over an SLS system in which the resolution decreases with distance from the sonar due to beam spreading.
- To avoid grating lobes in the image, the towfish should not be towed more than one half of a hydrophone array length between pings. Hence, increasing the tow speed requires either a longer array (which means more hardware) or a faster ping rate (which restricts the maximum range of the system). The practical impact is that increasing the area coverage rate (tow

speed times maximum range) requires a longer array length. For a given resolution, the first rule implies the number of elements must be increased.

Differential Phase Bathymetry

Differential phase, or interferometric, techniques are commonly used to measure the depth of the sea floor with a SLS system (Blackinton, 1983). Two distinguishable sonar pulses are either generated at vertically separated projectors or received at vertically separated receivers. The two signals take different transmit times to hit bottom features such as rocks and return to the keel array. This time difference can be measured accurately using differential phase methods, and then used to calculate the direction from the sonar to the feature. Combining this direction with the transit time gives the depth of the feature as well as its horizontal position.

Data Acquisition System

The system used for the experiment was modified from an existing Backscatter/Swath bathymetry SLS, the HAWAII MR1. The HAWAII MR1 is an ocean floor mapping sonar designed and built at the Hawaii Institute of Geophysics and Planetology (HIGP), of the University of Hawaii. Towed behind a ship at a depth of 100 meters, it is capable of measuring both acoustic back scatter reflectivity and bathymetry over a swath up to 25 km wide, in all ocean depths. The tow vehicle itself is slightly positively buoyant, and houses the transducer arrays and subsurface electronics, packaged in two pressure housings. The vehicle is connected to a depressor weight by an umbilical; the depressor in turn is towed behind the survey ship with a steel armored coaxial towing cable.

The tow vehicle carries two arrays, each consisting of two rows of transducer elements spaced one-half wavelength apart. To reduce crosstalk, the port array operates at 11 kHz and the starboard at 12 kHz. Both rows are driven by 10 kW amplifiers, transmitting tone bursts 0.5-10 ms long. The output from the transducer arrays is passed through programmable gain amplifiers and then digitized by dual channel 18 bit A/D converters (Rognstad, 1992).

The modifications fall into three categories:

1. Tow vehicle modifications to accommodate new projectors and hydrophones
2. Modification of data acquisition electronics to interface to new projectors and hydrophones and motion sensors
3. Modification of data acquisition software

Two projectors (15 cm long) with 0.8 m center-to-center separation, tilted at 50 degrees were mounted on the aft end of the HAWAII MR1 as shown in Figure 1. A new hydrophone consisting of a single row of four 20 cm long elements was mounted on the starboard side of the MR1 tilted at 45 degrees. Both projectors and hydrophone were tuned for use at 12.5 kHz.

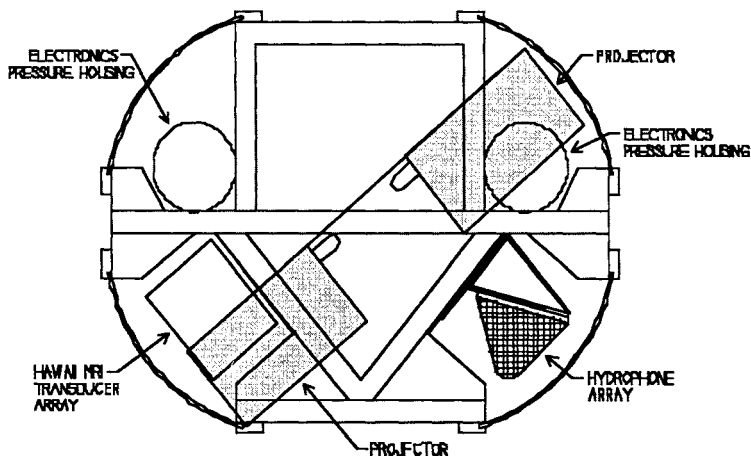


Figure 1. Aft View of HAWAII MR1 Showing Projector and Hydrophone Locations

Target Field

A 160' by 24' target field was set up near Waikiki in the Halekulani sand channel. Six types of targets installed in the target field:

1. Passive corner reflectors providing an approach line to the target field 90 feet long
2. 12 inch (30cm) diameter basketballs
3. Air cylinders 8 inches in diameter and 5 feet and filled with sand
4. One 8 inch diameter metal sphere
5. One 8 inch diameter plastic sphere
6. Four small cylinders, each filled with either air, gravel, sand, or foam

The basketballs were placed on the sea bed along the outer borders of the field. The 8 inch spheres and small air cylinders were placed at the far end of the target field on the sea floor. The remaining basketballs and large cylinders were placed with their upper surfaces flush with the sea floor, 1 foot below the sea floor, and 2 feet down. The targets were installed per plan by divers using a grid placed on the sea floor to aid in installation.

RESULTS

Acoustic Data Conditioning

The acoustic data were "conditioned" to remove any DC offsets and to normalize amplitudes across receiver elements. This conditioning process involves separately computing the DC offsets

(means) and standard deviations for each I and Q channel of each element. This is done over a relatively large region of the bottom where there is no obvious target echo. The means are then removed from the whole data set. The resulting data set is then divided by the standard deviations to give uniform element-to-element gains and used to generate SLS and SAS images.

Generation of SLS Images

The SLS images were generated by two methods. The first method simply maps the magnitude return from a single element into the range direction at the along track location corresponding to the current ping. This method is generally used to generate a real-time, quick look display. This method is not sensitive to the towfish motion due to the large element receive beamwidth. However, the along track resolution and signal to backscatter ratio degrade due to the large beamwidth.

The second method for generating SLS images involves forming shaded broadside beams using all four of the receive elements. This method results in a narrower beam which should give better along track resolution and signal to back scatter ratio. However, since the beam is broadside only to the array (not stabilized), the result would depend on the towfish motion and the scattering pattern of the target itself. If a target has a very narrow scattering pattern and the towfish has a significant yaw, then the receive broadside beam might not see the target at all even when the towfish passes over it.

Generation of SAS Images

The SAS images in this paper were generated in two steps. The first step is the aperture position correction (APC) to establish a set of towfish positions along the tow track. APC computes the x/y/z-axis corrections of the towfish positions relative to its nominal positions over the synthetic aperture so that echoes from detected point targets will add constructively across the aperture. APC corrections were made using the acoustic markers, the cylinder targets, and other “targets of opportunity”. The nominal towfish track was based on GPS position and velocity data.

The second step in generating an SAS image uses the corrected towfish positions as the SAS array element positions. An SAS beam is then steered to each volume element to be imaged by first forming steered physical beams for each ping and then summing them. An image pixel size small enough to assure over sampling the theoretical SAS beam (point spread function) in the resulting image was selected.

SLS and SAS Comparison

Figure 2 shows processed data from one pass over the target field. In the figure, traditional Side Look Sonar images are compared with a Synthetic Aperture Sonar image of the target field. Table 1 summarizes the method used to generate the images and compares the attributes of each image.

The SLS/SAS images in Figure 2 represent 2-D images at a depth corresponding to the bottom. The three images clearly show the four lead-in acoustic markers (zone A), all four buried

cylinders placed along the track (zones B, C, D and E), and three of the four proud, along track cylinders in zone F.

Table 1: Processed Image Comparison

	1-Element SLS	4-Element SLS	10 Ping SAS
Method	Sonar return of a single element from the receiver array	Form shaded broadside beams using the four receive elements	Synthetic aperture of ten pings limited by the speed and direction of the tow
Advantages	Least sensitive to towfish motion because of the large beamwidth	Improved along track resolution and signal to back scatter ratio (contrast)	Motion compensated, high resolution and high contrast images
Disadvantages	Along track resolution and signal to back scatter ratio poor because of large beamwidth of single element	Sensitive to towfish motion because of the narrower beamwidth and unstabilized beams	Target scattering response can effectively limit the number of pings in the aperture

The first two buried along track cylinders (zones C and D) appear blurred and weaker with the 4 element beam SLS image because the beam is not corrected for towfish motion. The cross track cylinders (normal to the tow track) are not seen because their orientations do not allow much specular reflection, and their back scatter strengths can be as much as 30 dB or more lower than the along track cylinders depending on incidence angle. However, at very low altitude (<5m), they can be detected (see Figure 9). Most of the basketballs are not detected because of strong back scatter from the sandy bottom. They have target strength of -22 dB compared to +1.6 dB for the along track cylinders. The targets labeled basketballs are detected in all images; but only the SAS image shows at least three targets in a line. The longer SAS aperture (2X) in a system developed for UXO hunting would increase the contrast of these basketballs so that an accurate classification of these objects could be made. Table 2 summarizes the SLS and SAS performance on the along track cylinders (ATC1 to ATC4), the cross track cylinders (CTC1 to CTC4) and the basketballs.

The SAS not only improved the images of the planned targets, but also other targets of opportunity. For example, the targets labeled as buried coral are more focused than in the SLS images. The depth of these object are estimated in the range of 2-4 feet.

Figure 3 depicts a cross-section plot through the second acoustic marker. Clearly shown is the contrast and resolution enhancement of the SAS image. The improvements shown are consistent with the theoretical values corresponding to the synthetic aperture length of ten pings used for the SAS image.

Table 2. SLS and SAS Performance Summary

Target	Alignment	Depth	4-Element SLS	10-Ping SAS
ATC1	Along track	Proud	Detected, contrast and resolution loss	Improved contrast and resolution
ATC2	Along track	1 foot	Detected, contrast and resolution loss	Improved contrast and resolution,
ATC3	Along track	2 feet	Detectable, significant contrast/resolution loss	Much improved contrast and resolution
ATC4	Along track	3 feet	Not detected	Not detected
CTC1 and CTC2	Cross track	Proud and 1 foot	Detectable, significant contrast and resolution loss	Much improved contrast and resolution
CTC3 and CTC4	Cross track	2 feet and 3 feet	Lack of good low altitude data to assess performance	Lack of good low altitude data to assess performance
Basket-balls	Spherical	Proud, buried	Not detected	Marginal detection

Discussion of SAS Processing Results

The important points to discuss about the SAS process are:

1. The SAS improvements in both resolution and signal to back scatter ratio are consistent with the theoretical values.
2. Three-dimensional SAS beamforming showed relative depth differences among the along track cylinders.
3. The cylindrical shape of the along track cylinders limits the length of the synthetic aperture.
4. The cross track cylinders can be detected only at very low towfish altitude.

SAS Resolution and SNR Improvements

The synthetic aperture used was ten pings long. With a tow speed of about 3 knots and a ping rate of ten per second, the synthetic aperture is about 1.5 meters long. Compared to the physical aperture length of 0.8 meter, the SAS aperture should give improvement in both along track resolution and signal to back scatter ratio. Figure 4 compares the theoretical beam patterns between the physical array and the 10-element synthetic array. The synthetic array has beams that are 3.5 times narrower and an array gain of about 6 dB (2 times in magnitude).

To assess the resolution and array gain improvements of the SAS, Figure 5 shows the SLS and SAS images and along track profiles for the second acoustic marker.

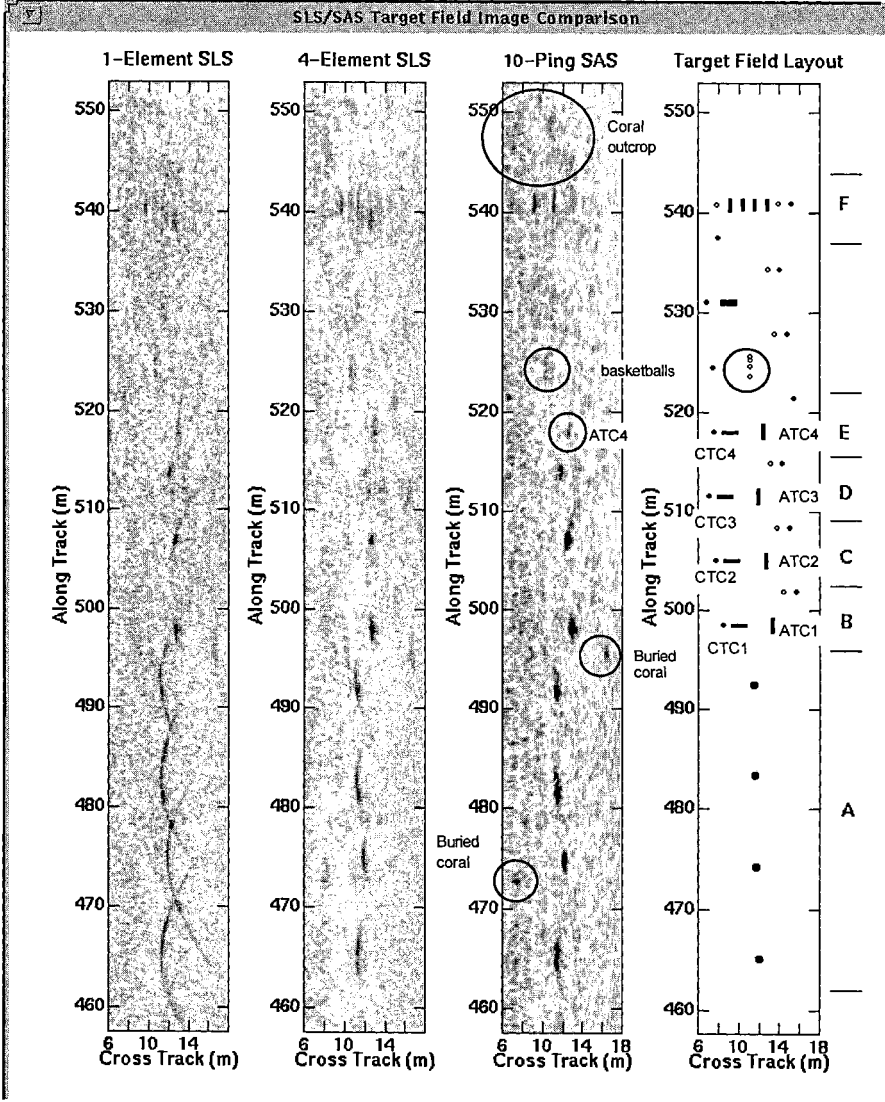


Figure 2. SLS/SAS Target Field Image Comparison

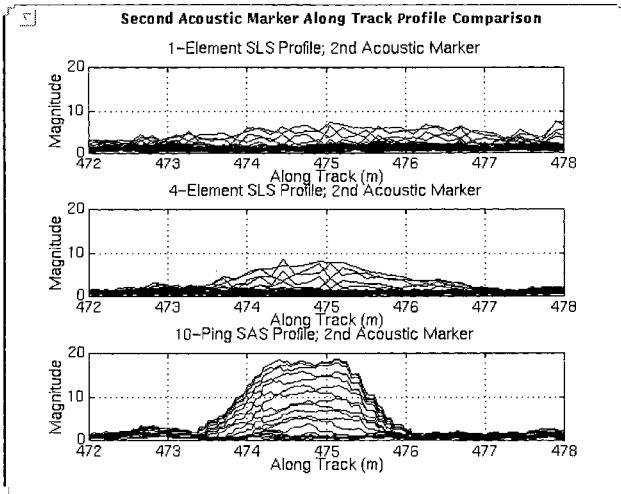


Figure 3. SLS and SAS Along Track Profile Comparison

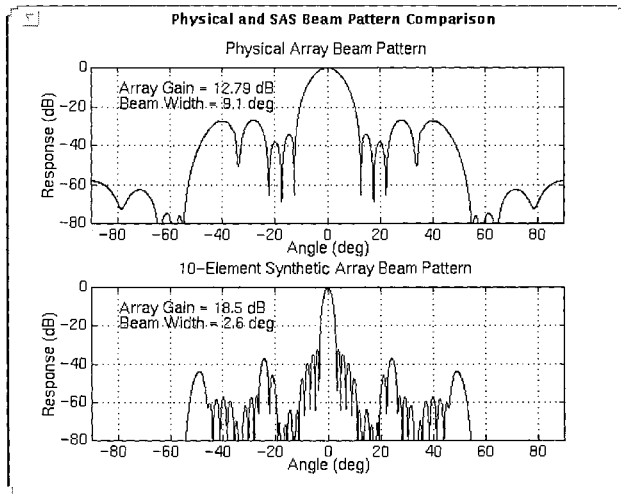


Figure 4. Physical and SAS Beam Pattern Comparison

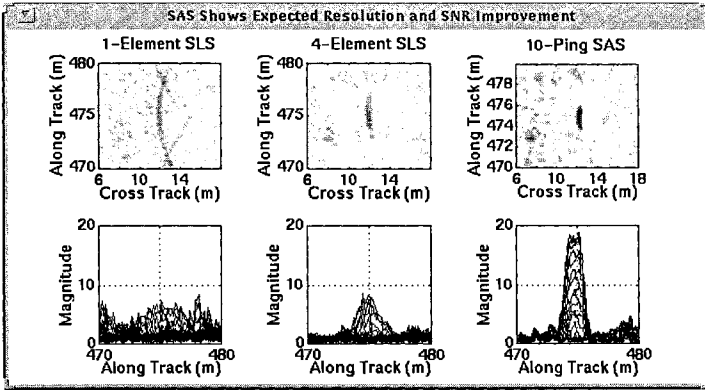


Figure 5. SAS Shows Expected Resolution and SNR Improvement

Although the markers are not small, if they are stationary, they should look like small point reflectors to the sonar. From visual inspection of the sonar data over different runs through the target field, the second marker appears to be the most stable. The improvements in the SAS image in Figure 5 are clearly seen. The measured array gain showed an improvement of about a factor of two which agrees with the theoretical value of 6 dB. In the SAS process, the theoretical width (-3 dB points) of a point target at a slant range of 17 meters is about 0.8 meter. The SAS profile plot shows the width to be about 1.2 meters. This can be expected since the marker is not a real point reflector.

Three-Dimension SAS Beamforming

With the two projectors, we have a small aperture (0.4m effectively) that will provide some directivity in the vertical plane. The SAS beamwidth in the vertical plane is about 4 degrees wide. At a slant range of around 17 meters, this translates to about 1.2 meters wide. Note that the grating lobes in the vertical plane are suppressed only by the vertical directivities of the transmit and receive elements which are rather broad. So there are significant grating lobes not too far from the vertical main lobe. It is difficult for human eyes to see the differences in depth from a 3-D intensity image when the differences are less than the resolution of the beamformer. Therefore, the differences need to be quantified differently.

Figure 6 shows the relative target magnitude as a function of depth from bottom for the four acoustic markers and the three detected along track cylinders. The curves show the markers and the first cylinder to be near the bottom, the second cylinder to be below the bottom, and the third cylinder to be significantly below the bottom. The results are consistent with the installed locations. The bottom was assumed to be flat in Figure 6.

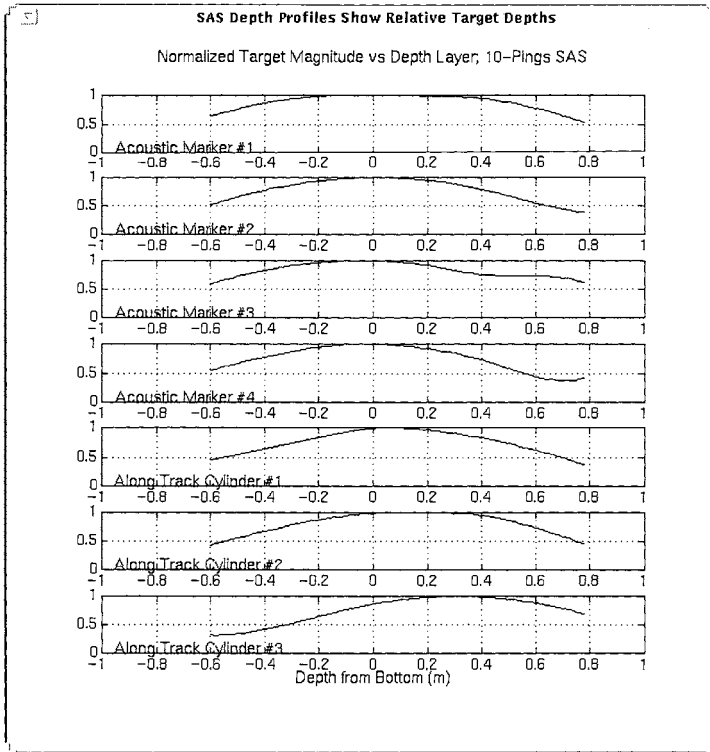


Figure 6. SAS Image Depth Profiles Show Relative Target Depths

SAS Aperture Length Consideration

Ideally, the longer the synthetic aperture is, the narrower the SAS beams will be. A narrower beam means higher resolution and array gain. However, the aperture length is limited by the following conditions:

1. The along track coverage of the physical array; that is, how far from array broadside the physical beam can be steered while suppressing the physical array grating lobes to an acceptable level.
2. The target scattering pattern (how many pings the target was seen in).

Condition 1 is driven by system design. The maximum steering angle of a physical beam defines the maximum synthetic aperture at a given range. However, this assumes a target can be seen at every point along the aperture. This is true if the target has an omnidirectional scattering pattern (i.e., aspect independent) or at least very broad. For a cylindrical shape object being viewed

along its length, this is no longer the case. If the synthetic aperture is so long such that the elements near each end do not see the target at all, then the SAS beam pattern on the target is distorted. Therefore, one would expect the performance to degrade.

Figure 7 compares the 10-ping SAS result with a 20-ping SAS on the second acoustic marker.

The top two plots show the images, and the bottom two plots show the corresponding along track profiles of the marker. For the marker, increasing the aperture to 20 pings improved the SAS performance since the marker looks omnidirectional. The profile plots shows improved resolution and array gain. The sharper profile using 20 pings suggests that the additional pings nullified some of the possible motion of the marker.

Figure 8 depicts the 10 and 20 pings SAS comparison on the second along track cylinder. In this case, the performance degraded with 20 pings. The image width is wider and the magnitude dropped. This is because some of the extra elements in the aperture do not see the cylinder at all.

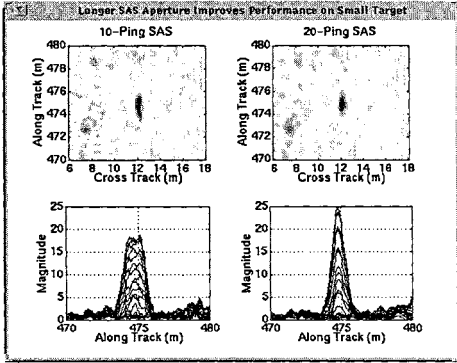


Figure 7. SAS Improves on Small Target Using 20 Pings

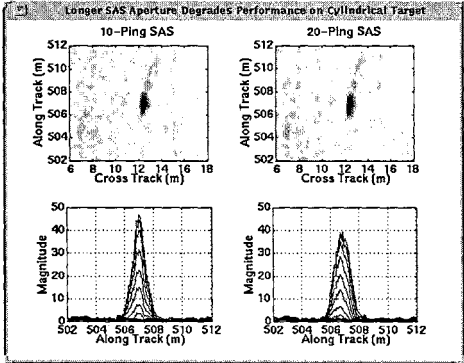


Figure 8. SAS Degrades on Cylindrical Target Using 20 Pings

Cross Track Cylinder Detection

Because of the orientation of the cross track cylinders relative to the sonar, detection relied mainly on back scatter instead of specular reflection utilized for the along track cylinders. The cross track cylinders are not detected against the bottom back scatter except for very low altitude runs. Figure 9 shows the SLS and SAS results for the first along track and cross track cylinders for an altitude run of about 5 meters.

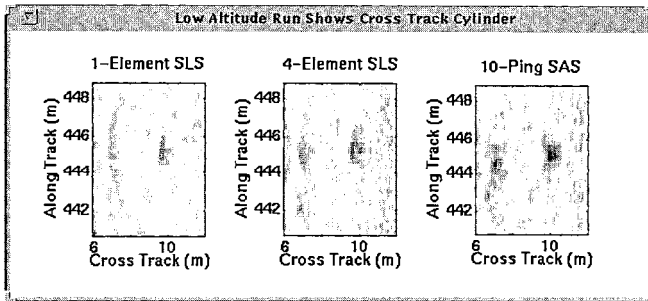


Figure 9. Low Altitude Run Shows Cross Track Cylinder

Differential Phase Processing

Differential phase processing provided accurate depth estimates of the strong targets; but did not provide good estimates of the bottom depth profile.

To determine depth of targets, traditional bathymetric sonar uses vertically separated receive arrays to obtain differential phase information. For this project, our existing towfish did not allow for a multi-row receive array. So two vertically separated projectors were installed to generate differential phase information by alternating the transmission (ping-pong). This approach is sound as long as the two successive pings have basically the same view, i.e., bottom and target characteristics do not change much. However, some decorrelation between the pings is expected. For this project, the target depths were estimated using the differential phase method, but the bottom depth could not be accurately estimated in the same way with the short data stream caused by the telemetry limitation. The lack of a long data stream prevented the filtering algorithm in the bathymetric process from sufficiently smoothing the bottom depth estimates. Instead, the towfish height off the bottom is estimated from the first bottom return, and the bottom is assumed flat in the cross track (range) direction. Figure 10 shows the estimated locations for the four acoustic markers (AM1 to AM4) and the three detected along track cylinders (ATC1 to ATC3). The estimated target depths agree very well with the planned depths.

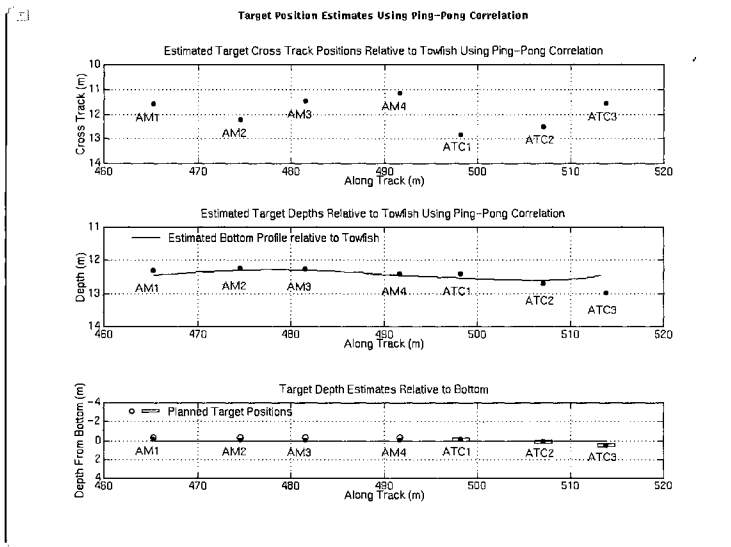


Figure 10. Target Position Estimates Using Differential Phase Techniques for Depth

REFERENCES

Blackinton, J. G., D. M. Hussong, and J. Kosalos, 1983. First results from a combination side-scan sonar and seafloor mapping system (SeaMARC II), *Offshore Technology Conference*, OTC 4478:307-11.

Cutrona, L.J., 1975, Comparison of Sonar System Performance Achievable using Synthetic Aperture Techniques with the Performance Achievable by more conventional Means, *J. Acoust. Soc. Am.*, **58**, p. 336.

Rognstad, Mark, (1992). HAWAII MR1: A New Underwater Mapping Tool. International Conference on Signal Processing and Technology, November 1992, p. 900.

EFFECTS OF SOUND SPEED PROFILE UNCERTAINTY ON ACCURACY OF DEPTH MEASUREMENTS

Xueyi Geng and Adam Zielinski
University of Victoria
British Columbia, Canada

ABSTRACT

Acoustic multi-beam and sidescan bathymetric systems are used to measure ocean depth. The maximum measurement error as specified by the International Hydrographic Organization is 1% for depth greater than 30 m and 0.3 m for depth less than 30 m (Anon, 1987). However, the lack of accurate sound speed profile data may be a source of significant errors. In this paper, a ray tracing method is used to investigate the effects of sound speed profile uncertainty on the accuracy of depth measurements. The sound velocity is usually available in form of a set of discrete data points. For ray tracing, these data points have to be suitably fitted by a continuous curve. It is found that curve fitting using linear interpolation and the associated ray tracing algorithm are most suitable for depth estimation. Thus, this ray tracing algorithm has been adopted for analysis. Analytical and simulation results are presented.

INTRODUCTION

Efficient management and use of the sea floor, especially within the Exclusive Economic Zone (EEZ) requires charts that accurately depict its form and composition. Therefore, precise measurements of the ocean depth is required. A traditional technique of surveying sea bottom relies on a ship-mounted echo sounder. Echo sounder measures the depth directly beneath the ship and area coverage is achieved by running a series of closely spaced parallel sounding lines. In recent years, acoustic multibeam and sidescan bathymetric systems have been used for ocean depth measurements. This kind of system is equivalent to a large number of echo sounders pointing perpendicularly to the direction of the travel with different inclination angles. A transmitted sound pulse propagates along a ray path through the water and impinges on the sea floor. It is then reflected back to the receiver along the same path. If the two-way travel time τ is measured, the coordinates of depth and horizontal range (z, x) can be estimated using a triangulation method as given by Eq. (1)

$$z - z_0 = \frac{c_0 \tau}{2} \cos \theta \quad \text{and} \quad x - x_0 = \frac{c_0 \tau}{2} \sin \theta \quad (1)$$

where (z_0, x_0) is the location of transducer array, θ is the inclination angle of the acoustic beam, and c_0 is the sound speed which is assumed to be constant versus depth. However, the actual sound speed is not constant and the actual ray path is not a straight line. The above method, therefore, will introduce errors in the measurement results. It can be shown that the errors depend on the inclination angle and, in some cases, can be much larger than 1% for depth larger than 30 m (Geng, 1996).

ACOUSTIC RAY TRACING FOR DEPTH MEASUREMENT

According to Snell's law (Urlick, 1975), the ray's grazing angle α and sound speed c must satisfy Eq. (2) along each ray path, that is

$$\frac{\cos \alpha}{c} = \mu \text{ (constant for each path)} \quad (2)$$

We assume that the sound speed profile is a function of depth z only, that is, $c = c(z)$. It can be shown that for a ray path starting at point (z_0, x_0) and ending at point (z_B, x_B) , the propagation time T and the horizontal range x_B are given by

$$T = \int_{z_0}^{z_B} \frac{1}{c(z)\sqrt{1-\mu^2 c^2(z)}} dz \quad (3)$$

$$x_B - x_0 = \int_{z_0}^{z_B} \frac{\mu c(z)}{\sqrt{1-\mu^2 c^2(z)}} dz \quad (4)$$

If the pulse propagation time T is known or measured, the depth z_B can be calculated from Eq. (3) and the horizontal range x_B can be calculated from Eq. (4). However, the close form solution to Eq. (3) and Eq. (4) exist only for special forms of function $c(z)$ (Weinberg, 1971; 1972). Numerical approximation methods can, however, be used to solve Eq. (3) and Eq. (4) for an arbitrary function $c(z)$ (Zielinski, 1996; Moler, 1970).

In practice, the sound speed is available in form of discrete data points $\{c_k, z_k\}$. Eq. (3) and Eq. (4) can be evaluated using numerical integration methods. Some numerical methods, like trapezoidal and midpoint approximations, use linear approximation of the integrand in each integration interval. An alternative approach is to fit the sound speed data with an interpolating function, and, either to integrate Eq. (3) and Eq. (4) in close form if possible, or to generate additional data points to be used in conjunction with standard numerical integration methods (Moler, 1970; Weinberg, 1971).

Because of the discrete nature of the available sound speed data, we divide the ocean into a number of layers corresponding to measured points. In the absence of information between each pair of the measured sound speed data points, it is reasonable to assume that the sound speed varies linearly with depth in each layer. As the layer becomes thinner, the accuracy of this linear interpolation increases. For linear sound speed profile within a layer, the associated ray path is a circular arc (Urlick, 1975). Applying the linear interpolation to sound speed profile, a piecewise constant sound speed gradient (CSSG) ray tracing algorithms is obtained, which allows the depth z_B and horizontal range x_B on the sea floor to be evaluated in close form (Geng, 1996). For this ray tracing algorithm, the accuracy of depth estimate depends only on the accuracy of linear interpolation. The results in this paper show that the depth estimate errors caused by linear interpolation are much less than 1% in most cases. Therefore, this piecewise CSSG ray tracing algorithm is a convenient and accurate method which can be used to improve the accuracy of depth measurements.

PERFORMANCE ANALYSIS OF PIECEWISE CSSG RAY TRACING ALGORITHM

We assume that N discrete sound speed data points $\{c_k, z_k\}$, $k = 0, 1, 2, \dots, N-1$, are known exactly, where depth z_{N-1} is in the vicinity of the sea floor z_B . Thus, the ocean is divided into N layers from depth z_0 to z_B . For the first $N-1$ layers, the pulse propagation time T_k in the k -th layer can be evaluated using Eq. (3). The propagation time in the last layer N is then calculated as

$$T_B = \frac{\tau}{2} - \sum_{k=1}^{N-1} T_k \quad (5)$$

where τ is known or measured two-way travel time. Substituting Eq. (5) to Eq. (3), the depth of the sea floor can be evaluated in close form (Geng, 1996) as

$$z_B = z_{N-1} + R_B \left[\cos \alpha_{N-1} + \frac{2g_B R_B (1 + \sin \alpha_{N-1}) c_{N-1} e^{\tau g_B}}{[g_B R_B (1 + \sin \alpha_{N-1})]^2 + [c_{N-1} e^{\tau g_B}]^2} \right] \quad (6)$$

where R_B is the radius of the ray path in the last layer near sea bottom, g_B is the sound speed gradient in the last layer and α_{N-1} is the grazing angle at depth z_{N-1} .

Normally, near sea bottom, especially in the deep ocean, the variation of sound speed gradient is small. We will assume, therefore, that the gradient g_B in the last layer is equal to g_{N-1} in the $(N-1)$ -th layer. Thus, all the values of R_B , g_B , α_{N-1} , c_{N-1} and z_{N-1} in Eq. (6) can be obtained exactly from the measured data points, and the error of z_B is caused only by the error of T_B estimate.

Accuracy of Depth Measurement

Generally, the actual sound speed values within a layer may not be exactly equal to those obtained by linear interpolation. Thus, the actual ray paths may be different from a circular arc path. However, according to Snell's law, both ray paths will have the same grazing angles at the boundaries of each layer. We denote the actual travel time of a sound pulse in the K th layer as T_k , and the estimated travel time along the circular arc path as \tilde{T}_k . The error of travel time estimate is $\Delta T_k = \tilde{T}_k - T_k$. Using Eq. (5), the error of the estimated travel time \tilde{T}_B in the last year is

$$\Delta T_B = \tilde{T}_B - T_B = -\sum_{K=1}^{N-1} \Delta T_k \quad (7)$$

where T_B is the actual travel time in the last layer. We define the relative error of total travel time estimate as

$$\varepsilon_T = \frac{\sum_{k=1}^{N-1} \Delta T_k}{\sum_{k=1}^{N-1} T_k} \quad (8)$$

Substitute Eq. (5) and Eq. (8) into Eq. (7), we have

$$\Delta T_B = -\varepsilon_T (\tau/2 - T_B) \quad (9)$$

In order to investigate the relationship between the error of depth measurement and the error of propagation time estimate, we assume that the actual depth of ocean bottom is at $z_B = z_{N-1}$ and that the estimated depth of ocean bottom is \tilde{z}_B . Then, the actual propagation time of a sound pulse in the last layer from depth z_{N-1} to z_B is $T_B = 0$. We define the relative error of the depth estimate as

$$\varepsilon_z = (\tilde{z}_B - z_B) / z_B \quad (10)$$

Substitute Eq. (6) and Eq. (9) to Eq. (10), we obtain, for $g_B \neq 0$

$$\varepsilon_z = -\frac{1}{z_B g_B \mu} \left[\frac{\mu c_{N-1}}{\mu^2 \left(1 + \sqrt{1 - \mu^2 c_{N-1}^2}\right)^2 + \left(c_{N-1} e^{-g_B \varepsilon_T (\tau/2)}\right)^2} - \frac{2 \left(1 + \sqrt{1 - \mu^2 c_{N-1}^2}\right) c_{N-1} e^{-g_B \varepsilon_T (\tau/2)}}{\mu^2 \left(1 + \sqrt{1 - \mu^2 c_{N-1}^2}\right)^2 + \left(c_{N-1} e^{-g_B \varepsilon_T (\tau/2)}\right)^2} \right] \quad (11)$$

Considering that the second speed gradient near sea bottom, g_B is in an order or a few hundredths of 1/second, and assuming the relative error of travel time $\varepsilon_T < 0.01$, numerical result shows that Eq. (11) can be simplified to

$$\varepsilon_z \approx -\varepsilon_T \quad (12)$$

Analysis of Sensitivity of Linear Interpolation

The accuracy of curve fitting using linear interpolation depends on the actual sound speed values between each pair of discrete sound speed data points. In linear interpolation, a straight line segment is used to approximate the sound speed profile in each layer. Typically, in most regions in the ocean, the gradient of sound speed is not larger than a few hundredths of 1/second. On rare occasions, in the sub-surface layer the gradient may reach a few tens hundredths 1/second. Therefore, the actual sound speed values will be in the vicinity of those given by the linear interpolation within a layer. Nevertheless, this approximation can lead to errors in the estimate of sound pulse propagation time in each year and therefore to errors in depth measurements.

Let us assume that in the layer between two measured sound speed data points $P_{k-1}(z_{k-1}, c_{k-1})$ and $P_k(z_k, c_k)$, there is one sub-layer $\delta z = z_b - z_a$ as shown in figure 1. In this sub-layer, the actual sound speed values deviate from the linear interpolation and are given by two line segments $P_a P_m$ and $P_m P_b$. Thus, the actual value of sound speed from depth z_{k-1} to z_k are assumed to be represented by the four straight segments $P_{k-1} P_a$, $P_a P_m$, $P_m P_b$ and $P_b P_k$. The maximum deviation of the sound speed value from linear interpolation is denoted by $\delta c = c_m - c_{m0}$.

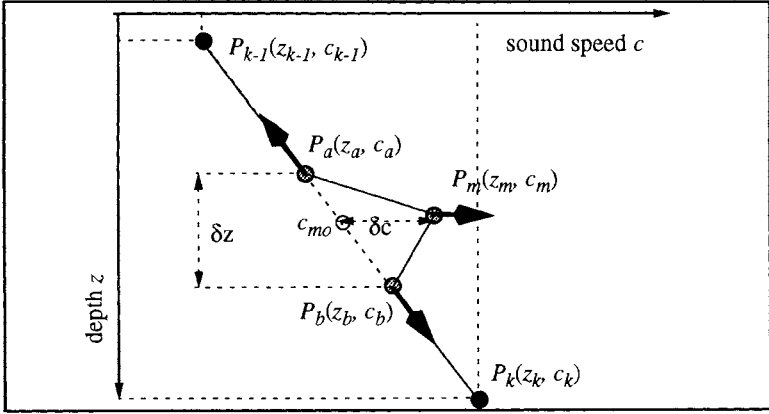


Figure 1. A diagram to illustrate the abnormality of sound speed profile

We will refer to such a deviation from linear interpolation as an abnormality. We define two parameters γ and ρ to describe the “size” of the abnormality region as

$$\gamma = \frac{z_b - z_a}{z_k - z_{k-1}} \times 100\% \quad (13)$$

$$\rho = \frac{c_m - c_{mo}}{c_k - c_{k-1}} \times 100\% \quad (14)$$

where $\Delta c = c_k - c_{k-1} \neq 0$ is the sound speed difference between two contiguous data points. γ describes the thickness of the sub-layer, and ρ describes the maximum error of sound speed in the sublayer. We define a relative error of propagation time in the k -th layer as $\varepsilon_T(k) = \Delta T_k / T_k$ which depends on γ , ρ and Δc in the layer, and also on the grazing angle α_{k-1} of a ray entering the layer from depth z_{k-1} . By extensive numerical calculations (Geng, 1996), we have found that $\varepsilon_T(k)$ in fact depends almost only on the product γ , ρ and Δc . We, therefore, define a new parameter

$$U = \rho \times \gamma \times \Delta c \quad (15)$$

Figure 2 shows the relative error $\varepsilon_T(k)$ as a function of α_{k-1} and U as a parameter. From Figure 2, we can determine a range of U and α_{k-1} for which the relative error of propagation time estimate associated with the abnormality is less than a certain value. For most reasonable values of U , the relative error $\varepsilon_T(k)$ is much less than 1% and can be neglected. Therefore, linear

interpolation of sound speed profile is relatively insensitive to this kind of abnormality in sound speed profile.

The parameter U can also be used to determine the minimum number of data points, for a given depth, which are needed to achieve a satisfactory accuracy of depth measurement,. Suppose we have some knowledge about the abnormality of sound speed profile. For instance, we know the range of the “size” of the abnormality. We select the required value of U to assure a required accuracy of travel time estimate. Then, for a given range of γ and ρ , we can determine the required Δc from Eq. (15). For example, we assume that the parameters γ and ρ of the abnormality may be as large as 100% in the sub-surface layer, while $\gamma=50\%$ and $\rho=10\%$ in the deep water. Suppose we want the relative error of travel time estimate to be less than 0.05%. Figure 2 gives the corresponding required value of parameter $U = 0.2$. Therefore, the sound speed data should be obtained in such a way that the difference between two contiguous points is less than 0.2m/s in the subsurface layer, while can be as large as 4m/s in the deep water.

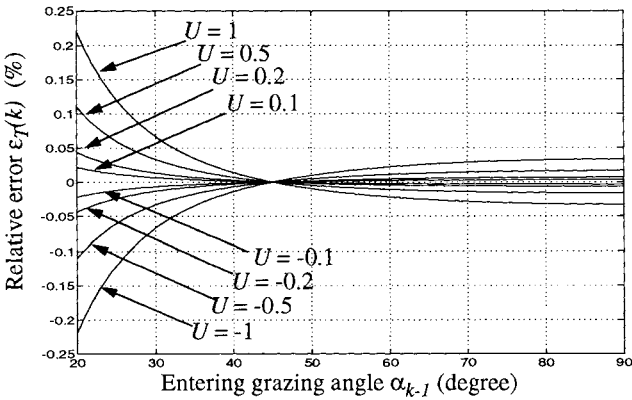


Figure 2 Relative errors of propagation time estimate associated with linear extrapolation

We will show that the relative error shown in Figure 2 represented the upper boundary of the relative error of the total travel time estimate. For simplicity, we assume that all the relative error of travel time estimate have the same value in each layer of the first $(N-1)$ layers. However, they may have different signs, which depend on the abnormality in each layer. Therefore, the relative error of the total travel time estimate is

$$|\epsilon_T| = \left| \frac{\Delta T_1 + \Delta T_2 + \dots + \Delta T_{N-1}}{T_1 + T_2 + \dots + T_{N-1}} \right| \leq \left| \frac{\Delta T_k}{T_k} \right| \quad (16)$$

Since $\varepsilon_z \approx -\varepsilon_T$ as given by Eq. (12), the relative error shown in Figure 2 is the approximate upper boundary of the relative error of depth estimate caused by the abnormality in sound speed profile.

Based on the above observation, we will assume that the sound speed data measured in such a way that the errors of depth estimate associated with linear interpolation are sufficiently small and can be neglected. Therefore, we will use this piecewise CSSG ray tracing algorithm to estimate the effects of sound speed profile uncertainty on the accuracy of acoustic bathymetry.

EFFECTS OF SOUND SPEED PROFILE UNCERTAINTY ON THE ACCURACY OF ACOUSTIC BATHYMETRY

The accuracy requirement of sound speed measurement depends on applications. Several types of devices are available for direct and indirect measurements. In this section, we will analyze the effects of the accuracy of sound speed data on the depth measurement.

Error Associated with Direct Measurement of Sound Speed

The relative error of sound speed is expressed as $\varepsilon_c(k) = \Delta c_k / c_k$, where Δc_k is the absolute error of c_k . We assume that the initial grazing angle α_0 is known exactly. The relative error of propagation time estimate in the k -th layer, $k > 1$, is

$$\varepsilon_T(k) = \frac{\Delta T_k}{T_k} = \frac{c_{k-1} \partial T_k}{T_k \partial c_{k-1}} \left[\frac{\Delta c_{k-1}}{c_{k-1}} \right] + \frac{c_k \partial T_k}{T_k \partial c_k} \left[\frac{\Delta c_k}{c_k} \right] + \frac{c_0 \partial T_k}{T_k \partial c_0} \left[\frac{\Delta c_0}{c_0} \right] \quad (17)$$

Typically, the errors of sound speed measurements have random character. In different layers, the error of propagation time estimate may have different signs. As indicated by Eq. (16), the relative error given by Eq. (17) is the upper boundary of the relative error of the total propagation time estimate.

We assume that the errors of sound speed in all points are independent of each other and the standard deviation δ_{ε_c} of the relative error is the same for every point. Therefore, the upper boundary of the standard deviation of the relative error of the total propagation time estimate can be obtained as

$$\sigma_{\varepsilon_T, \max} = \left\{ \left| \frac{c_{k-1} \partial T_k}{T_k \partial c_{k-1}} \right| + \left| \frac{c_k \partial T_k}{T_k \partial c_k} \right| + \left| \frac{c_0 \partial T_k}{T_k \partial c_0} \right| \right\} \sigma_{\varepsilon_c} \quad (18)$$

Two curves of the ratio of $\sigma_{\varepsilon_T, \max} / \sigma_{\varepsilon_c}$ are shown in Figure 3 as a function of grazing angle α_{k-1} . The upper one represents a case where there are errors in all data points including c_0 (the sound speed at the depth of transducer array). The lower curve represents a case with exact value of c_0 , but with errors in all other data points. We see profound reduction in the total error if c_0 is measured accurately. Thus it is advantageous to measure the sound speed c_0 precisely.

According to Eq. (12) $\varepsilon_z \approx -\varepsilon_T$, therefore, $\sigma_{\varepsilon_z} \approx \sigma_{\varepsilon_T}$. Then, using Figure 3 we can find that the standard deviation of relative error of depth estimate is less than $10\sigma_{\varepsilon_c}$ for most of the grazing angles. Therefore, if the required relative error of depth measurement is to be less than 1%, the relative error of sound speed should be less than 0.1%. Similar results can be obtained for horizontal range measurements (Geng, 1996).

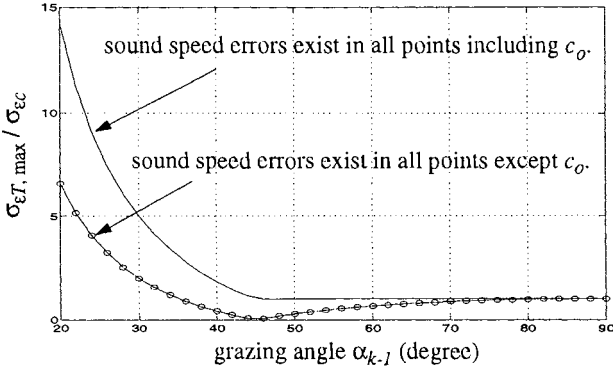


Figure 3 The ratio of $\sigma_{\varepsilon_T, \max} / \sigma_{\varepsilon_c}$

Simulation of the Effects of Sound Speed Errors

We use Munk's sound speed profile (Porter, 1987) as an example of actual sound speed profile, and add some random variables to the sampled data to assess the effects of the errors of sound speed on the accuracy of depth measurements by simulation. The sound speed data are sampled from Eq. (19)

$$\overline{c(z)} = 1500 \left\{ 1 + 0.00737 \left[\frac{(z-1300)}{650} - 1 + e^{\frac{-(z-1300)}{650}} \right] \right\} \quad (19)$$

at a depth interval of $\Delta z = 50$ m. The depth of the ocean bottoms is assumed to be $z_N = 5000$ m. The measurement errors are assumed to be Gaussian variables with zero mean and standard deviation of $\sigma_c(k) = 0.1\% \times \overline{c_k}$ at each point, where $\overline{c_k}$ is the mean sound speed value at the k-th point. It follows that the standard deviation of the relative error is $\sigma_{\varepsilon_c} = 0.1\%$. Shown in Figure 4 are the standard deviations of the relative depth error σ_{ε_z} as a function of sound speed error and initial grazing angle at α_0 , which are the statistical results of 500 simulations for each value of α_0 .

Similar to Figure 3, the lower curve is for the case of the initial sound speed c_0 known exactly. From the simulation results, we can see that the maximum value of standard deviation of the relative error of depth estimate is only 5 times that of the relative error of sound speed in this case. It also confirms that the sound speed c_0 has profound effect on the accuracy of depth estimate.

Error Associated with Indirect Measurement of Sound Speed

In many cases, indirect methods are used for sound speed measurements in the ocean. This is accomplished by measuring salinity (S) and temperature (T) at a given depth (D). From these data, sound speed can be calculated using an STD equation. The resulting errors in sea bottom measurement are related to accuracies of salinity and temperature measurement and accuracies of STD equations.

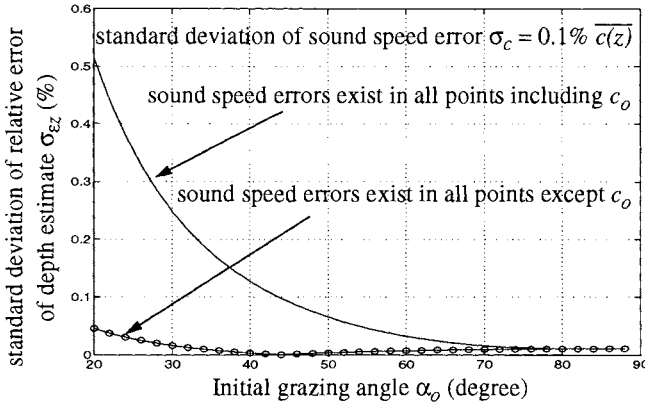


Figure 4 Simulation results of the effects of sound speed errors on accuracy of depth measurements

It is reported (Del Grosso, 1974) that Del Grosso's STD equation can provide sound speed values with a standard deviation of the errors as 0.05m/s in a range of pressure values from 0 to 1000kg/cm^2 , which corresponds to depth from 0 to nearly 10km . If the sound speed values in the ocean are in the range of 1400m/s to 1600m/s , the standard deviation of relative errors associated with Del Grosso's STD equation are in the range of 0.0036% to 0.0031% . Thus, according to the analysis and simulation results, the depth estimate errors caused by the STD equation are much less than the requirement of 1% and can be neglected. Therefore, Del Grosso's STD equation can provide enough accuracy for sound speed calculation for the application of depth measurements.

However, Del Grosso's STD equation is the most complicated one compared with other STD equations, like Medwin's STD equation (Medwin, 1975). Numerical results (Geng, 1996) show that in shallow water less than 1000m depth, this simpler STD equation provides a good approximation with relative sound speed error less than 0.02% compared with Del Grosso's equation. However, in the deep water, the relative sound speed error can reach 0.5% .

Numerical results show that, for large ranges of salinity and temperature values, the dependences of the relative sound speed error on the salinity and temperature measurement accuracies are in the ranges of

$$0.065\% \leq \left| \frac{dc/c}{dS} \right| \leq 0.095\% \text{ and } 0.1\% \leq \left| \frac{dc/c}{dT} \right| \leq 0.3\% \quad (20)$$

Most of the sensing devices can provide salinity and temperature data with error less than ± 0.02 ppt and $\pm 0.02^\circ\text{C}$ in routine use. The resulting errors of sound speed estimate are much less than 0.1%, and, therefore, the errors of depth estimate are much less than 1%.

Error Associated with micro-structure of temperature

Experimental results and theoretical analysis have shown that there exists micro-structure in the temperature distribution (Urick, 1975; Flatte, 1979). The temperature profile randomly fluctuates around the mean value. This will induce random component in the sound speed profile. Normally, the value of fluctuation is small compared with the mean value. An experiment shows that the temperature micro-structure has standard deviation $\sigma_T = 0.05^\circ\text{C}$ at depth 50m. For the average water temperature of 20°C and the salinity 33ppt, the relative errors of sound speed have standard deviation less than 0.01% as calculated using Medwin's STD equation. Therefore, the depth errors caused by the temperature micro-structure are also much less than 1%.

CONCLUSIONS

Depth calculations based on assumption of constant sound speed value can lead to significant errors in multibeam and sidescan bathymetric systems.

The linear interpolation for sound speed profile and the associated piecewise constant sound speed gradient ray tracing algorithm are found to be useful methods for improving the accuracy of depth measurements. The analysis and simulation results show that the maximum value of the standard deviation of relative depth error is less than 10 times the standard deviation of relative error of sound speed. Therefore, 0.1% relative error of sound speed measurement is sufficient to achieve the relative error of depth estimate less than 1%.

In most situations, the relative errors of depth estimate associated with indirect methods of sound speed measurement, such as STD equations, salinity and temperature measurement errors, as well as temperature micro-structure are much less than 1%. Therefore, these effects can be neglected.

REFERENCES

- Anon. 1987. IHO standards for hydrographic surveys. International Hydrographic Organization Special Publication. No. 44. Monaco.
- Del Grosso, V. 1974. New equation for the speed of sound in natural waters. *J. Acoust. Soc. Am.* **56**:1084-1091.
- Flatte, S. 1979. Sound Transmission Through a Fluctuating Ocean. Cambridge University Press.

- Geng, X. 1996. High Precision Acoustic Bathymetry. Masters thesis, Dept. of Electrical and Computer Engineering (in progress).
- Medwin, H. 1975. Speed of Sound in Water: A simple equation for realistic parameters. *J. Acoust. Soc. Am.* **58**:1318-1319.
- Moler, C. and L. Solomon. 1970. Use of splines and numerical integration in geometrical acoustics. *J. Acoust. Soc. Am.* **48**:739-744.
- Porter, M. and P. Bucker. 1987. Gaussian beam tracing for computing ocean acoustic fields. *J. Acoust. Soc. Am.* **82**:1349-1359.
- Urick, R. 1975. Principles of underwater sound for engineers. New York:McGraw-Hill.
- Weinberg, H. 1971. A continuous-gradient curve-fitting technique for acoustic ray analysis. *J. Acoust. Soc. Am.* **50**:975-984.
- Weinberg, N. and T. Dunderdale. 1972. Shallow water ray tracing with nonlinear velocity profiles. *J. Acoust. Soc. Am.* **52**:1000-1010.
- Zielinski, A. and X. Geng. 1996. Traveling wavefront ray tracing and its application. *J. Marine Geodesy.* **19**(2):165-179.

MIRROR-IMAGE ZONALITY OF MAGMATISM AND ORE DEPOSITS AROUND THE JAPAN SEA

Valentina A. Baskina

Institute of Geology of Ore Deposits, Petrography, Mineralogy and Geochemistry, (IGEM RAS)
Moscow, Russia

ABSTRACT

The late Cretaceous - Paleogene volcanic belts of East Sikhote-Alin and Southwest Japan are mostly regarded as model cases of subduction related volcanic belts. It is widely accepted that after Mesozoic accretion both the Sikhote-Alin and the Southwest Japan formed jointed parts of the Eurasian continental margin. In the period 100-50 m.a. ago, due to active subduction a marginal volcanic belt appeared over the subduction zone dipping west-north-west under eastern Japan, which covered most part of the eastern Sikhote-Alin and the Southwest Japan. Later the two areas parted in the course of the opening of the Japan Sea, probably in the Miocene. In the present paper the author analysed whether the magmatic and metallogenic zonality of the province fits into the above conception. As a matter of fact, no gradual unidirected lateral magmatic zonality occurs from the inferred front of the subduction related belt to its rare areas - i.e. from Sanyo belt in Southwest Japan westward to perivolcanic parts of the Sikhote-Alin belt. It makes a strong objection to the idea that the Late Cretaceous - Paleogene magmatism in the region was governed predominantly by subduction. In fact, symmetrical mirror-image zonality is characteristic of Late Cretaceous - Paleogene magmatic area around the Sea of Japan. The pattern of magmatic, geochemical and metallogenetic symmetry fits better into a conclusion that endogenic processes in the active margin segment between 132⁰-138⁰E were related to a persistent zone of extension which served later as the system of axes during opening of the Japan Sea.

INTRODUCTION

Lateral magmatic and metallogenic zonality typical of west Asian continental margins is generally regarded as one of the marks of the subduction related origin of the Late Cretaceous - Paleogene marginal volcanic belts, of which both the Sikhote-Alin (in the Far East Maritime region of Russia) and the Inner Zone of Southwest Japan are frequently described as model cases. (Zonenshain and Kuz'min, 1992; Cluzel, 1992; Filatova, 1990; Ueda and Miyashiro, 1974; and others). At the same time, strong evidence proves that prior to the development of the Late Cretaceous - Paleogene volcanic belts in the province, the south-western Japan as well as the Sikhote-Alin made a marginal part of the Eurasian continental plate. Thus originally a single marginal belt developed, which later split in two due to the opening of the Japan Sea (Takanashi, 1983; Taira and Ogawa, 1991; Ishihara, 1978a; b; Matsumoto, 1981). If this concept is true, a gradual unidirected transition of magmatic and metallogenic features should be observed from a front of the inferred volcanic arc inland, i.e. from the south border of the Inner Zone to western edges of the East Sikhote-Alin volcanic belt.

The present paper aims to compare zonality in the two mentioned areas. In fact, not unidirectional but mirror-image zonality about the Japan Sea is characteristic of the volcanic belts between 132°-138°E. In particular, older granites in both the Sikhote-Alin and the Southwest Japan dated as 95-75 m.a., are of ilmenite type, accompanied by tin and tungsten mineralization and distributed at the outer rim of the magmatic area. Younger granites, 65-55 m.a., of magnetite type, with lead-zinc-molybdenum mineralization emplaced closer to the sea shore and the youngest, 56-40 m.a., granophyres and subalkaline granites are exposed in shore cliffs on both sides of the sea. Rhyolites in both areas are synchronous and predominate in volume over other varieties. They show, like granites, gradual enrichment in potassium, rubidium, lithium, fluorine, and increase of La/Yb and Sr isotope ratios from the sea shore inland (i.e. in Japan oceanward). In both belts none of andesites fit in successions typical of a subduction volcanic front. The symmetry in zonality makes objections to the idea that the Late Cretaceous - Paleogene magmatism in this segment of the continental margin was governed to a great extent by a contemporaneous subduction of an ocean plate under Japan.

GEOLOGY OF LATE CRETACEOUS - PALEOGENE MAGMATIC ASSEMBLAGES

Late Cretaceous - Paleogene magmatic products in both the Sikhote-Alin volcanic belt and the Inner Zone of Southwest Japan in general are similar in age, succession, total volume, relative volumes of varieties, in predominance of acid to intermediate volcanics and comagmatic J - type plutonic masses; as well as by types of granite related mineral deposits and by zonal arrangement of magmatic and ore belts about the Japan Sea. At the same time a striking difference exists between two areas, as unlike Japan intermittent basalt and alkali basalt activity during the whole period is characteristic of the Sikhote-Alin. Basalt derived igneous suites of gabbro, monzonites, granosyenites and granites as well as multiphase swarms of basic dykes, though negligible in volume are considered to be a source or at least a very important factor in the localisation of economic sulphide - cassiterite and sheelite mineralization as well as tracers of persistent rift-like dislocations. In the present paper we have left aside basaltic activity in the Sikhote-Alin and directed attention to the main groups of intermediate to acid rocks, common to both areas .

Volcanics

In the Late Cretaceous - Paleogene volcanic succession andesites and basaltic andesites do not exceed 5 -10 % of the total volume. The earliest are dated as Aptian-Albian (Imaoka et al., 1993; Baskina, 1982; Volcanic Belts., 1984). They are mostly subaerial, underlain by thin beds of acid tuffs and lavas, comprise high potassium varieties of latite affinity along with tholeiitic volcanics. Early andesites, never observed close to the inferred Cretaceous volcanic arc front, are distributed in both the Sikhote-Alin and the Southwest Japan in axial parts of the north-east trending volcanic belts. The same position is characteristic of later, calc-alkaline Cenomanian - Turonian andesites and of Early Paleogene varieties in the Inner Zone of Japan. (Ichikawa et al., 1968). Paleogene andesites in the Sikhote-Alin are more abundant, and localised mostly within transverse longitudinal and latitudinal dislocations. Attempts to find unilateral petro-geochemical zonality in andesites of the South Sikhote-Alin was not a success (Baskina, 1982, 1988). Compositional features of andesite and basaltic-andesite suites like potassium content, tholeiitic or

calc-alkaline affinities and others, which are generally regarded as "key" to paleogeodynamics, vary from segment to segment, from one local volcano-tectonic structure to another. Enrichment in potassium and related incoherent microcomponents depends not on the distance from the Japan Sea shore, but on position in some thoroughgoing zones, thus proved to be spatially inherited. No seaward increase in relative volume of andesites and basaltic-andesites in the general volcanic succession takes place; on the contrary, their occurrence is even less in the subsided, submarine part of the Sikhote-Alin volcanic belt. Spatial distribution, mode of occurrence, and petrochemical variations of the Late Cretaceous - Paleogene andesites give no evidence to reconstruct an arc tectonic system or the position of the inferred deep seismic zone. Narrow north-east trending chains of polychronous andesites along axial parts of wide areas of acid volcanics both in the Sikhote-Alin and the Inner Zone of Japan probably trace persistent structures to control the main andesite activity since the Albian to Paleogene. The bulk of the volcanic pile in both areas is comprised of similar subaerial acid volcanics, up to 2.5 - 3 km. thick, predominantly welded tuffs, and tuff-lavas ignimbrites, related to domes and calderas. The thickness of the volcanic strata increases seaward in the Sikhote-Alin, as well as the prominence of the youngest, early Paleogene volcanics increases towards the Japan Sea in both areas. Unlike Japan, the Paleogene volcanics in the Sikhote-Alin penetrate far west along transverse dislocations due to intermittent activation of the latter, a phenomena never observed in Japan.

The general zonality of acid volcanics in the whole province is symmetric: from the shores of the Japan Sea inland younger volcanics (65 - 40 m.a.) give way to older ones (95 - 70 m.a.) as well as predominantly quartz porphyric, magnetite-bearing ignimbrites and tuff-lavas change to magnetite-free and sometimes garnet-bearing lavas. In the same direction contents of K, Rb, Be, F, Li, Sn, LREE, and initial Sr isotope ratios in rocks increase.

Granites

The Late Cretaceous - Paleogene granites in the province also display a mirror-image zonality around the Japan Sea with respect to their age, petrography, petrochemistry, isotope characteristics, and related metallogeny. Probably a difference in magma source is the ultimate reason for the above mentioned diversities. Evidences of zonality are the most detailed in the Southwest Japan due to thorough studies in petrology and isotope geochemistry (Arakawa, 1990; Shibata and Ishihara, 1979; Ishihara and Terashima, 1977; Ishihara, 1978a; Takanashi et al., 1980; Czamanske et al., 1981; Kagami et al., 1992; Takagi, 1993; and many others). Data for the Russian area are from Ivanov et al. (1980); Baskina (1982, 1988); Rub and Rub (1994).

The belts of the Late Cretaceous - Paleogene granites in both areas are as wide as 150 - 200 km. In the Inner Zone of Japan granites were divided into two groups due to systematic difference in radiometric age and petrography. They formed, respectively, the Sanin and the Sanyo belts, the former nearer to the Japan Sea (Murakami, 1974). This division is supported by many essential properties of granites, like belonging to magnetite or ilmenite type, carbon content, Sr isotope initial ratios; S, O, Nd isotope characteristics; age and type of granite related ore mineralization. (Ishihara, 1978a, b; Ishihara and Terashima, 1977; Shibata and Ishihara, 1979a; and others). The Sanyo granites, mostly Late Cretaceous (95 -70 m.a.), make granodiorite-granite to adamellite-granite suites. Rocks are medium to coarse-grained, crystallised in deeper, now more eroded

chambers. The granites, generally accompanied by W, Sn, Cu mineralization, are of the ilmenite-series, and nevertheless belong to I-type (Takanashi et al., 1980). The latter was also proved by Czamanske et al. (1980) by comparative study of rock-forming minerals and correlation of major and minor chemical constituents. According to cited authors, high aluminium, two-mica granites, to say nothing of "model" S-granites, are rare in the Sanyo belt. To the North a gradual transition is observed, sometimes within a single vast igneous body, to granites in the Sanin belt. They are Paleogene (65 - 55 m. a.), also of I-type, granodiorite-monzogranite suites of the magnetite-series. Bodies are generally smaller in size, less eroded, composed of fine to medium grained rocks. On the shore side of the Sanin belt small masses of younger granophyres and sometimes subalkaline granites are spread. The Sanin belt is an area of Mo, Pb, Zn granite related mineralization.

Similar but reversed zonality of granites takes place in the Sikhote-Alin region. Granites of distant west areas along the Central Suture are counterparts to the Sanyo belt, being Late Cretaceous (95 to 74 m.a), ilmenite-series of granodiorite-granite and adamellite-granite composition with predominantly hornblende-biotite mineral assemblages. These granites are mostly comagmatic to contemporary volcanics. High aluminium, two-mica, garnet bearing granites are more frequent than in the Sanyo belt. As it was mentioned above, activation of some transverse dislocations resulted in a notable amount of Paleogene granite stocks within Cretaceous granites, so the latter are mostly multiphase. Among Paleogene stocks some belong to A-type Li-F rich granites, and some acquired S-type affinities in the course of complete evolution of I-type magma chambers. The transition between ilmenite-series and magnetite-series areas in the Sikhote-Alin is concealed by a north-east trending zone of persistent rift-like dislocations which controls numerous central bodies and polychron dyke swarms of basaltic to alkali basaltic differentiated suites. Their emplacement spans time interval from the Jurassic- Early Cretaceous to the Late Paleogene and thus influenced properties of contemporaneous granites distributed in the transition zone.

Granites in the area close to the shore of the Japan Sea resemble even in minor details the granites of the Sanin belt in Japan. They are Paleogene (65-55 m.a), pyroxene-hornblende-biotite bearing, I-type granodiorite-granite suites of magnetite-series, accompanied with small amounts of earlier diorites or gabbro. Magmas crystallised in shallow to subvolcanic environments and at erosion level are displayed as small but generally multiphase bodies. Granite emplacement was completed by intrusion of granophyres and rare stocks of alkaline granites in the Paleocene - Eocene.

Many data were recently obtained on the systematic variations of the geochemical properties due to spatial position of the granites. After Kagami et al. (1992), granites in the Sanin belt contain less potassium and more magnesium and titanium than that of the Sanyo belt. A gradual transition takes place in geochemical features of granites and contemporaneous volcanics from the Median Tectonic Line to the North. It is best expressed as a change of Sr, Nd, O isotope ratios, in spite of the fact that the Cretaceous and Paleogene granites display close resemblance in petrography, mineralogy and petrochemistry. In the Sanin belt Sr isotope initial ratios in volcanics, granites, and related gabbro vary from 0.7050 to 0.7060, whereas in the major part of the Sanyo belt from 0.7060 to 0.7070. Variations of Nd ratios are, respectively, 0 to +5 and +1 to - 3. Isotope data on the Sikhote-Alin granites and volcanics are poorer than those for Japan. Nevertheless, those data reveal similar though reversed geochemical zonality. Closer to shore of the Japan Sea initial Sr

isotope ratios in acid to intermediate volcanics and granites vary from 0.7053 to 0.7061, whereas in the ilmenite-series and in Li-F rich granites inland, closer to the Central Suture, variations are much wider: 0.706 - 0.718.

On the base of isotope geochemistry of granites in the Inner Japan a conclusion is widely accepted that variations of major granite characteristics should be attributed to different magma sources: probably upper mantle under North Zone, i.e. the Sanin belt, and combination of upper mantle and low crust in Transition Zone - i.e. in the Sanyo belt. (Kagami et al., 1992; Arakawa, 1990; Shibata and Ishihara, 1979b).

METALLOGENIC ZONALITY

The Sikhote-Alin and the Inner Zone of Southwest Japan are well known metallogenic provinces rich in diversity of economic mineral accumulations, including large and exceptional ones. Among Late Cretaceous - Paleogene, in Japan there are granite related vein, skarn, and greizen deposits of Mo, W, Sn, Pb, Zn, Cu, Ag, Au, As, numbered in the hundreds. Radiometric ages of ores and vein minerals proved to be the same as the age of host granites. As well, ratios of sulphur isotopes both in granites and granite related ores are nearly similar, so a conclusion is widely accepted on close, direct connection between these ores and host granites (Ishihara, 1978, [1,2]; Ishihara and Sasaki, 1991; Kamitani and Kanazawa, 1993; Ishihara et al., 1975). In the Sikhote-Alin ore and mineral deposits of the same age, though less numerous, are also mostly granite related vein, skarn and to less extent greizen ones of Sn, W, Mo, Pb, Zn, Ag, B, Au. A radiometric time break of 2-5 m. a. between ore deposition and solidifying of host granites is frequently noted. Geological, mineralogical and geochemical evidences prove consanguinity of ores and intermediate to acid melts for the most of the mentioned deposits.

In Japan, in the Sanyo belt, older deposits of W, Cu, Sn are connected with ilmenite-type granites, while younger Pb, Zn, Mo, Au deposits occur in the Sanin belt in association with younger, magnetite-type granites. Only small masses of shallow to subvolcanic ilmenite-type granites, according to Shimazaki (1980), occur in the Sanin belt to host large Paleogene skarn polymetallic mineralization in the Kamioka and Nakatatsu deposits. In the Sikhote-Alin metallogenic zonalities is manifested by a continentward transit from Cu, Mo, Pb, Zn, Au deposits to predominantly Sn, W, Be. As in the Southwest Japan, the latter are generally of Late Cretaceous age, whereas deposits closer to the sea shore are mostly Paleogene (Figure 1). Thus, age and distribution of granite related ore deposits in the both areas display exactly the same mirror-image zonalities around the Japan Sea as magmatic rocks do. As well, in the both areas the largest mineral accumulations, despite their absolute size, age and mineral type, concentrate along some latitudinal, transverse, deep-rooted, persistent dislocations. Position of deposits within these structures also stress the general mirror zonalities: in the Sikhote-Alin, from the sea shore inland, the deposits are, for example, Dal'negorskoe (Pb, Zn, Ag B); then Kavalerovo and Tigrinoe (Sn, W); and Vostok 2 (W). (Baskina, 1982, 1988, 1996). In Japan, from the Japan Sea inland, there are, in particular, Daito (Mo), Kamioka (Pb, Zn, Au), Ikuno, Akenobe (Sn, W).

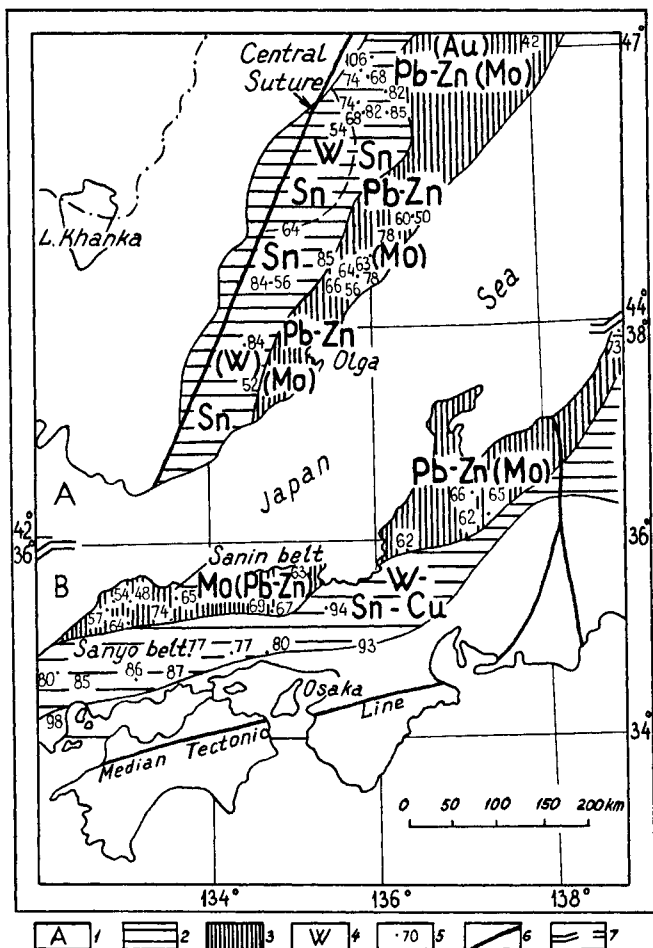


Figure 1. Zonal distribution of granites and related mineralization around the Japan Sea. Legend: 1- A. The Far East Maritime Region, Russia, B. The Southwest Japan; 2 - the belts of Late Cretaceous, ilmenite-type granites; 3 - the belts of Paleogene, magnetite-type granites; 4 - principal ore metals; 5 - the ages of ore deposits (in B. after Ishihara et al. 1988); 6 - tectonic lines; 7 - break.

CONCLUSIONS

Distribution and regular change of properties of magmatic rocks and related ores across marginal volcanic belts are widely used for paleogeodynamic reconstruction, even in provinces of predominating acid magmatism, like the West Pacific continental marginal belts.

Volcanic belts of the East Sikhote-Alin and the Inner zone of SW Japan are usually regarded as developed due to subduction of the oceanic plate dipping west-north-west under eastern Japan, when both Japan and the Sikhote-Alin composed a single part of the Eurasian continental plate. The conception is seriously constrained by the type of magmatic and metallogenic zonality in the region: it is revealed to be a symmetric, mirror-image one, instead of unilateral west-east transition, required by a subduction model. Younger, mantle-derived, magnetite-series magmatites and related ores emplaced in both areas around the Japan Sea, i.e. in the axial part of a once single whole of the volcanic area. The fact can be attributed neither to a unidirected convergent movement, nor to a combination of compression in front and extension at removed parts of the inferred over-subducted area.

According to petrologic and isotope studies, most properties of acid and intermediate rocks in the area, generally used as definite marks in paleogeodynamic reconstructions, depend on thickness of the crust. The history of pre-volcanic basement adds more to zonality than distance from a front of inferred contemporaneous deep seismic zone. Most "key" properties of magmatic assemblages and ores proved to be inherited. Under these circumstances, geological and petrochemical zonality of acid to intermediate volcanics, related granites and ore deposits gives no reliable ways for direct paleogeodynamic reconstruction.

Acknowledgements

A study was possible due to partial aid of the Russian Foundation for Basic Researches (Project 95-05-14525).

REFERENCES

- Arakawa, Y. 1990. Strontium isotopic composition of Mesozoic granitic rock in the Hida belt, Central Japan: diversities of magma sources and of processes of magma evolution in continental margin area. *Lithos*, **24**:261-273.
- Baskina, V. 1982. Magmatism of ore-concentrating structures in the Far-East Maritime Region. Moscow: Nauka (in Russian).
- Baskina, V. 1988. Granite magmatism and mineralization, associated with deep-reaching lineaments , Sikhote-Alin Range in the Far East Maritime region, USSR. In: Proc. Of 7 Quadr. IAGOD Symp. , Stuttgart.
- Baskina, V. 1996 . Transverse zones and transform faults as targets in searching for submarine mineralization. In: Recent Advances in marine science and technology' 96, Honolulu (this volume).
- Cluzel, D. 1992. Late Palaeozoic to Early Mesozoic geodynamic evolution of the Circum-Pacific orogenic belt in S. Korea and SW Japan. *Earth Planet. Sci. Lett.* **108**:289 -305.
- Czamanske, G., S. Ishihara, and S. Atkin. 1981. Chemistry of rock forming minerals in the Cretaceous- Paleogene batholith in South-western Japan and implication for magma genesis. *Journ. Geophys. Res.* **86**:10431-10469.
- Filatova, N. 1990. Mesozoic history of Korean - Japanese region. *Geotectonica*. **5**: 112 -124 (in Russian).
- Ichikawa, K., N. Murakami, A. Hase, and K. Wadatsumi. 1968. Late Mesozoic igneous activity in the Inner zone of Southwest Japan. *Pacific Geology*. **1**:96-116.
- Imaoka, T., T. Nakajima, and T. Ytaya. 1993. K-Ar ages of hornblendes in andesite and dacite from the Cretaceous Kwanmon group, SW Japan. *Jour. Miner. Petr. Econ. Geol.* **88**:265-271.
- Ishihara, S. 1978(a). Tin-tungsten-molybdenum metallogenic provinces in East Asia and some problems involved in their plate tectonic interpretation. In: Metallization associated with acid magmatism. **3**:29-36, Prague.
- Ishihara, S. 1978 (b). Metallogenesis in the Japanese island arc system. *Journ. Geol Soc. London*. **135**:389-406.
- Ishihara, S., T. Igarashi, and C. Nishiwaki. 1975. A re-examination of regional distribution of the Late Cenozoic ore deposits: East Japan arc. *Geol.Soc.Am. Bull.* **86**:293-297.
- Ishihara, S., and S. Terashima. 1977. Chemical variations in the Cretaceous Granitoids across South-western Japan. *Journ. Geol. Soc. Japan.* **83**:1-18.

- Ishihara, S., K. Shibata and S. Uciumi. 1988. K-Ar ages of ore deposits related to Cretaceous - Paleogene granitoids. *Bull. Geol. Surv. Japan*. **39**:81-94.
- Ishihara S., and A. Sasaki. 1991. Ore deposits related to granitic magmatism in Japan: a magmatic viewpoint. *Episodes*. **3-4**:286-296.
- Ivanov, V., I. Bur'anova, B. Zalishchak, G. Stepanov, and A. Strizhkova. 1980. Granites and monzonites in ore districts, Maritime Region. Moscow: Nauka (in Russian).
- Kagami, H., S. Isumi, Y. Tainosho and M. Owada. 1992. Spatial variations of Sr and Nd isotope ratios of Cretaceous-Paleogene granitoid rocks, SW Japan arc. *Contr. Miner. Petr.* **112**:165-177.
- Kamitani, M., and Y. Kanazawa. 1993. Potential of Au-Ag bearing ore deposits in Japan. *Bull Geol. Surv. Japan*. **44**:105-126.
- Matsumoto, T. 1981. Timing of geological events in the Circum Pacific Region. *Canad. Journ. Earth Sci.* **14**:346-358.
- Murakami, N. 1974. Some problems concerning Late Mesozoic to Early Tertiary igneous activity on the Inner side of Southwest Japan. *Pacific Geology*. **8**:139-151.
- Rub, M., and A. Rub. 1994. Rare-metal granites and associated mineralization of the Tigrinoc deposit, Central Sikhote-Alin. *Int. Geol. Rev.***36**:484 -502.
- Shibata, K., and S. Ishihara (a). 1979. Rb-Sr whole rock and K-Ar mineral ages of granite rocks in Japan. *Geochem. Journ.* **13**:113-119.
- Shibata, K. and S. Ishihara (b). 1979. Initial ^{87}Sr to ^{86}Sr ratios in plutonic rocks from Japan. *Contr. Miner. Petr.* **7**:381-390.
- Shimazaki, H. 1980. Characteristics of skarn deposits and related acid magmatism in Japan. *Ec. Geol.* **5**:173-183.
- Taira, A., and Y. Ogawa. 1991. Cretaceous to Holocene forearc evolution in Japan and its implications to crustal dynamics. *Episodes*. **14**:205-208.
- Takagi, T. 1993. Redox paths of magnetite-series and ilmenite-series granitoid magmas- examples from the Central to Eastern Chugoku districts, SW Japan. *Journ. Min. Petrol. Econ. Geol.* **88**:165-178.
- Takanashi, M. 1983. Space-Time distribution of Late Mesozoic to Early Cenozoic magmatism in Eastern Asia and its tectonic implications. In: Accretional and Collisional Eugeosynclinal Folded Systems in the Circum-Pacific Region. Tokyo.

Takanashi, M., S. Aramaki, and A. Ishihara. 1980. Magnetite-series / ilmenite-series vs. Y-type / S-type granitoids. *Min. Geol.* **8**:13-28.

Tanaka, K., and T. Nozawa. 1977. Geology and mineral resources of Japan. *Geol. Surv. Jap.* **1**:1-430 .

Ueda, S., and A. Miyashiro. 1974. Plate tectonics and the Japanese Islands - a synthesis. *Geol. Soc. Am. Bul.* **85**:1159-1170.

Volcanic Belts of Eastern Asia. 1984. Moscow: Nauka (In Russian) .

Zonenshine, L. and M. Kuz'min. 1992. Paleogeodynamics. Moscow: Nauka.

TSUNAMI RISK ASSESSMENT FOR SHIKOKU ISLAND AND THE KII PENINSULA

Hitoshi Murakami¹, Naoaki Yamamoto², Sadahiko Itoh³, Yasunori Kozuki¹
and Hiroaki Sato¹

¹University of Tokushima
Tokushima, Japan

²Shikoku Research Institute Inc.
Kagawa, Japan

³Kyoto University
Kyoto, Japan

ABSTRACT

The purpose of this study is estimating future tsunami risks along the coast of Shikoku island and the Kii peninsula, known as "Nankai-do" in Japan. Elliptically shaped tsunami sources were artificially moved to eight locations along the Nankai Trough, and the tsunami characteristics obtained by a refractive calculation method were analyzed. As a result, the tsunami risks was estimated in terms of arrival time, wave ray concentration, incident wave height and tsunami energy coming into the subjective area. The locations of the most dangerous tsunami sources are of great concern for local residents.

INTRODUCTION

Huge earthquakes have occurred at intervals of 100~150 years along the Nankai Trough. The coastal area of Nankai-do has frequently been damaged by large tsunamis. According to seismologists, the next large earthquake may occur in this area sometime around the year 2030 at the earliest.

Takahashi (1951) and Hatori (1977) estimated tsunami risks along the Japanese coast on the basis of the total energies of tsunami recorded in the past. However, there is no guarantee that tsunamis in the future will hit the same areas. For this reason, their data is not sufficient for predicting future tsunami risks. To solve this problem, Kawata et al (1994) described the characteristics of tsunami arrival times and heights of tsunami along the coast of Nankai-do by moving the fault model of the 1854 Ansei Nankai Earthquake (M8.4). The method they employed is useful in estimating tsunami inundation height in coastal areas and tsunami flow pattern in specified bays. However, the grid size and time interval used in this method must be narrowed if high accuracy is to be sought for. It is also necessary to use much data and complicated calculations for estimating tsunami risks in extensive areas. Thus, their calculation method is rather inconvenient in estimating tsunami risks along the entire coastal areas of Nankai-do.

In the present study, tsunami sources are derived from the data of past tsunami. Eight tsunami sources are artificially set on the north side along the Nankai Trough. A tsunami source is assumed to be elliptically shaped, and wave rays are start on an elliptic orbit in a refractive calculation. Using arrival time, wave ray concentration, incident wave height and energy for coastal area, the potential tsunami risks along the coast of Nankai-do are estimated. This method of calculation is far more simple and convenient for determining the spatial distribution of incident waves coming into the bay than a fault model method.

NUMERICAL CALCULATIONS

Equations and subjective area

The fundamental equations are given as follows:

$$\frac{D\alpha}{Dt} = \sin \alpha \cdot \frac{\partial c}{\partial x} - \cos \alpha \cdot \frac{\partial c}{\partial y} \quad (1)$$

$$\frac{H}{H_o} = k_r = \frac{1}{\sqrt{\beta}} \quad (2)$$

$$\frac{D^2\beta}{Dt^2} + p \cdot \frac{D\beta}{Dt} + q \cdot \beta = 0 \quad (3)$$

$$p = - \left(\frac{\partial c}{\partial x} \cos \alpha + \frac{\partial c}{\partial y} \sin \alpha \right) \quad (4)$$

$$q = c \left(\frac{\partial^2 c}{\partial x^2} \sin^2 \alpha - \frac{c \cdot \partial^2 c}{\partial x \cdot \partial y} 2 \sin \alpha \cdot \cos \alpha + \frac{\partial^2 c}{\partial y^2} \cos^2 \alpha \right) \quad (5)$$

where, α is the wave ray angle between the x axis and the direction of a wave ray at location (x, y) and time t , c is wave velocity, H is wave height, H_o is initial wave height (=1.0m), and β is the wave ray separation factor.

Fig. 1 shows a subjective area, of size 525.00 (km) X 243.75 (km). In the numerical calculation, the grid size is 1.25 km, and the time interval is 1 second. The wave rays start from each point at an interval of 1 km on the elliptic orbit. By carrying out refractive calculations, both the wave ray angle and the wave height were obtained per unit width of a wave ray (Griswold, 1963; Skovgaard, Johnson and Bertelsen, 1975).

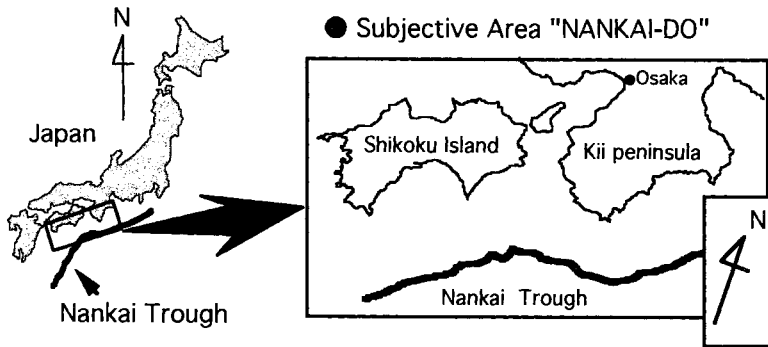


Figure 1. Subjective area

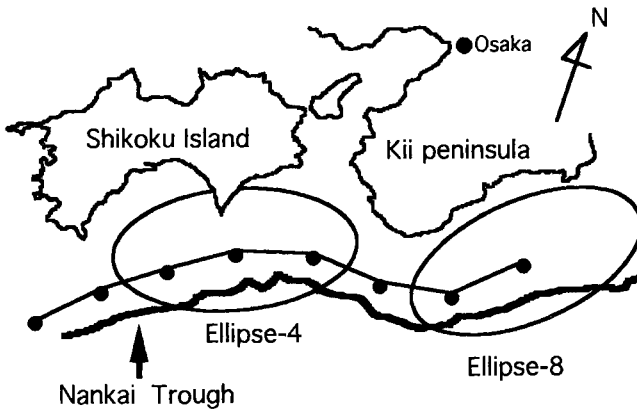


Figure 2. Tsunami sources and a baseline the tsunami source movement

Baseline for movement of the artificial tsunami sources

It is impossible to predict where and when the next huge earthquake will occur and how big such a quake will be. Therefore, the tsunami source was artificially moved to eight kinds of locations as shown in Fig. 2, which shows two examples of the locations of tsunami sources (Ellipse-4 and 8) and a baseline for the source movement. In the calculation, the following conditions are assumed:

- (1)The tsunami source is elliptical in shape with the minor axis 70 km and the major axis 126 km, and their sizes are equal to that of the 1946 Showa Nankai Tsunami. The direction of the major axis is parallel to the Nankai Trough.
- (2)The baseline is located on the north side along the Nankai Trough.

TSUNAMI RISK ASSESSMENT

In the consideration of tsunami risk, the coastal area along Nankai-do was divided into 14 regions of equal length of 43 km as shown in Fig. 3. The tsunamis in the Bungo channel and the Kii channel are not discussed as these tsunamis were not as big as those for the subject area.

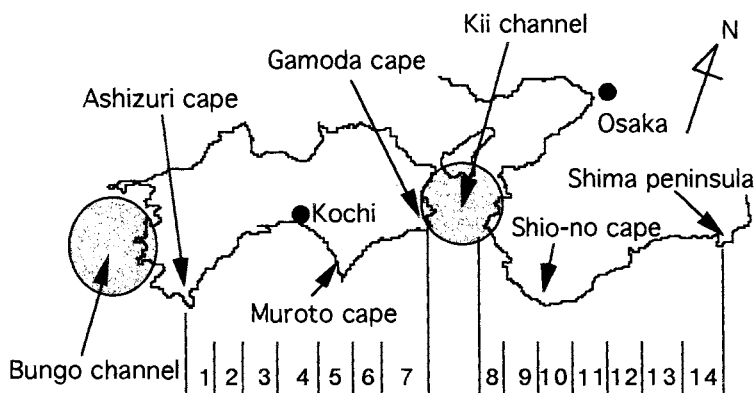


Figure 3. Definition of the 14-divided regions and main place names

Arrival time

Fig. 4 shows an example of the wave crest lines every 5 minutes from the tsunami source of Ellipse-4. In this case, the tsunami arrival time is about 5 minutes at the Shio-no cape, and about 20 minutes at Kochi.

Fig. 5 shows the spatial distribution of the arrival times T_a for each coastal region. The fluctuations of the arrival time T_a at each region are due to the different locations of the eight tsunami sources as shown in Fig. 2. The fastest tsunami reaches within about 5 minutes at the regions of 5, 6, 9, and 10, and within 20 minutes at the latest in all regions. The latest tsunami reaches within about 40 minutes at the region-2, and within 30-40 minutes at the other regions wherever the earthquake occurs along the Nankai Trough.

Wave ray concentration

Fig. 6 shows an example of the wave rays from the tsunami source of Ellipse-4. The high risk region can be seen from the behavior of tsunami propagation, especially that of both wave convergence and wave divergence.

Fig. 7 shows the degree of wave ray concentration C_w for each region. C_w is defined as the total number of wave rays coming into each region from the eight tsunami sources. The values of C_w are comparatively large at region-1, 2, 5, 7, 9, 10, and 14 as shown by the deep black area. These regions are located near peninsulas and capes.

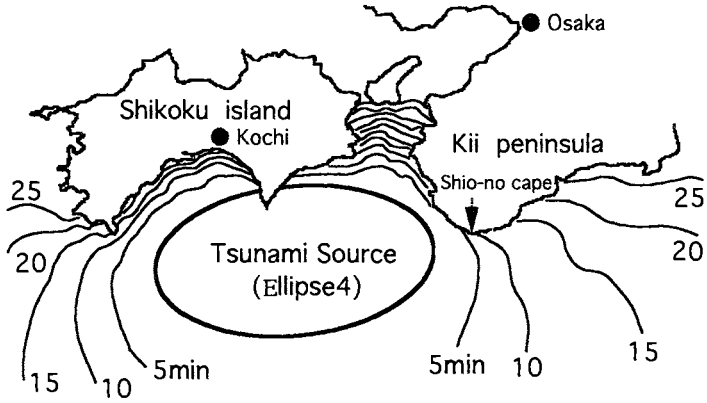


Figure 4. Wave crest lines every 5 minutes

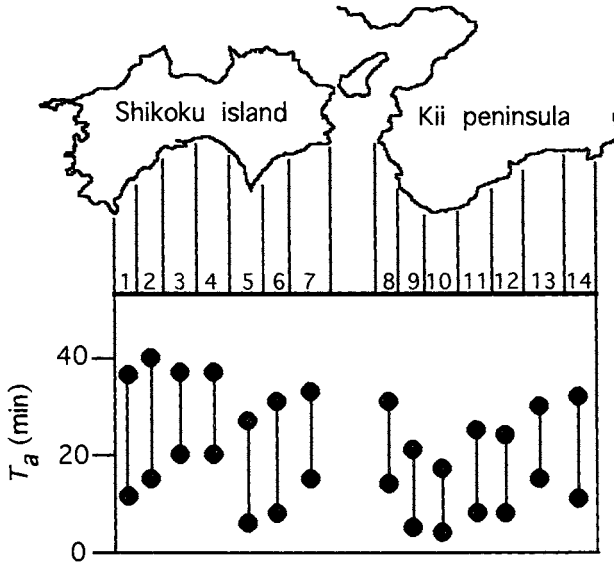


Figure 5. Spatial distribution of Arrival time T_a

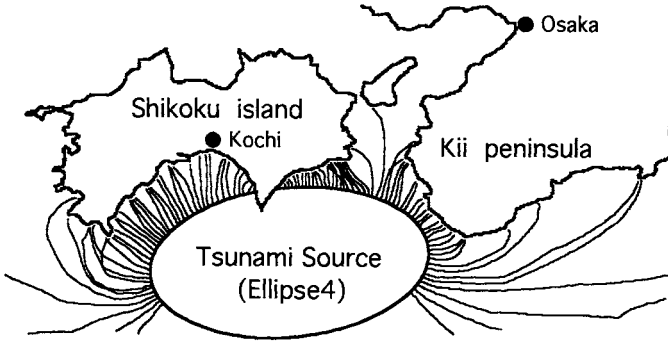


Figure 6. Wave Rays

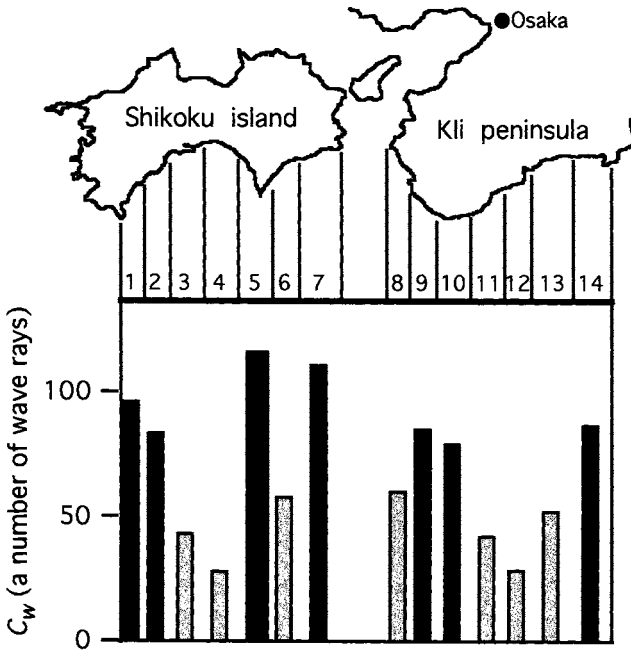


Figure 7. Wave ray concentrations

Tsunami Height

Fig. 8 shows the spatial distribution of the non-dimensional relative wave height H_r , together with wave ray concentration C_w as shown in Fig. 7. H_r is defined as the ratio of the average wave height H_a coming into each region to the initial wave height ($=1.0$ m everywhere) at the tsunami source. For instance, H_r will be equal to 3.0, when the average wave height H_a at an arbitrary region is 3m. To compare of incident wave height coming into each coastal area, H_r is used as a kind of factor of tsunami risk assessment. The spatial variation of H_r is not so big as that of C_w . The average values of H_r range between 2.3~2.9. The tsunami risk increases if the initial wave height becomes large such as in the 1707 and 1854 Earthquakes, because the magnitude of the 1946 Earthquake (M8.0) was not so great as those of the 1854 Earthquake (M8.4) and the 1707 Earthquake (M8.4).

Furthermore, this figure shows that the correlation between C_w and H_r is not always high.

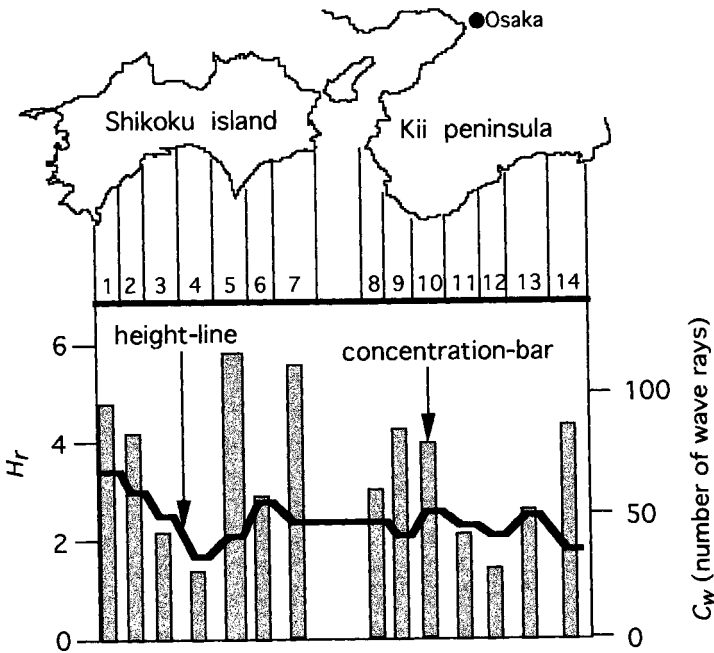


Figure 8. Relative wave height and wave ray concentration

Tsunami energy

Tsunami energy e_t is proportional to the product of the number of wave rays C_w and the second power of the average wave height H_a at each region. We redefined the tsunami energy E_t as follows:

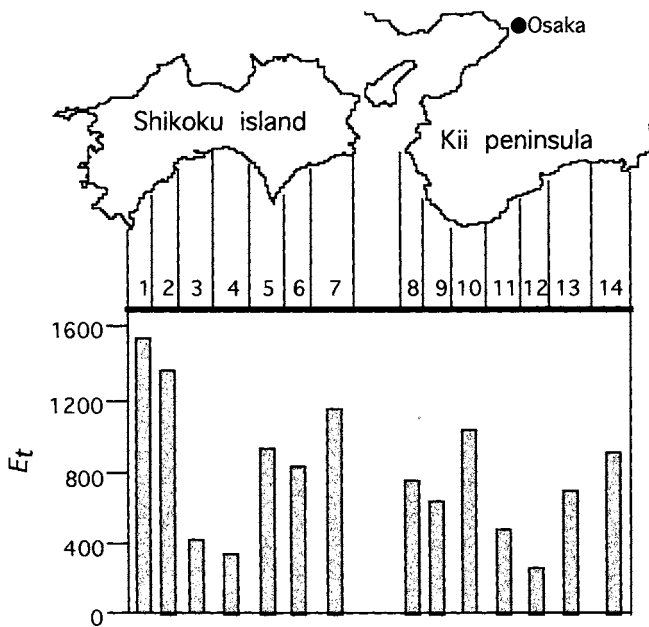


Figure 9. Tsunami energy

$$E_t = c_w \times Ha^2 \quad (6)$$

Fig. 9 shows the tsunami energy E_t for each region. The variation tendency of E_t is similar to that of C_w in Fig. 7. High risk regions for future tsunamis can be estimated from the total energy stored by eight tsunamis. It is shown that the total tsunami energy is largest for region-1 and 2. Region-5~7, 10 and 14 would also represent areas readily damaged by tsunamis.

Locations of the most dangerous tsunami source

The residents of each region along the coast of Nankai-do would surely wish to know location of the most dangerous tsunami source. We present this information based on the results of numerical calculations as follows: Fig. 10 is the result from the tsunami arrival time T_a . It can be seen that region-2~4 are most dangerous when the tsunami source is in Ellipse-3. In the same manner, the relationships between the two can be understood. Both Figs. 11 and 12 are the results from the wave ray concentration C_w and relative wave height H_r , respectively. The residents at region-6~9 must beware of a tsunami that occurs in Ellipse-4 or 5, and region-10, 12~14 in the case Ellipse-8.

As the location of the most dangerous tsunami source for each region is different from the results of T_a , C_w and H_r , it is necessary to consider two or more preventive systems against future tsunamis.

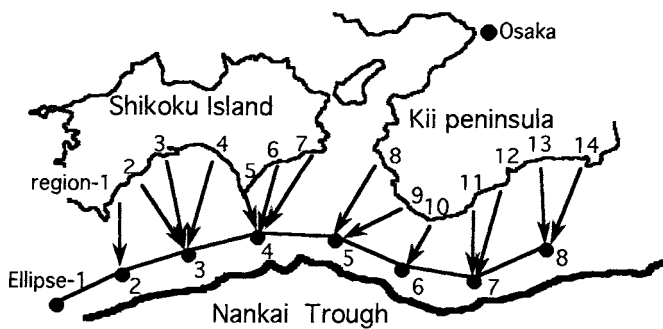


Figure 10. Locations of the most dangerous tsunami sources from viewpoint of arrival time

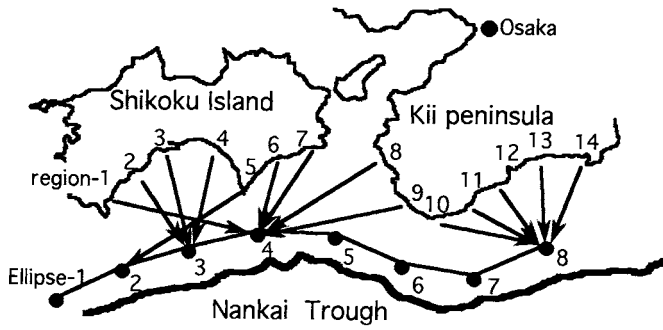


Figure 11. Locations of the most dangerous tsunami sources from viewpoint of wave ray concentration

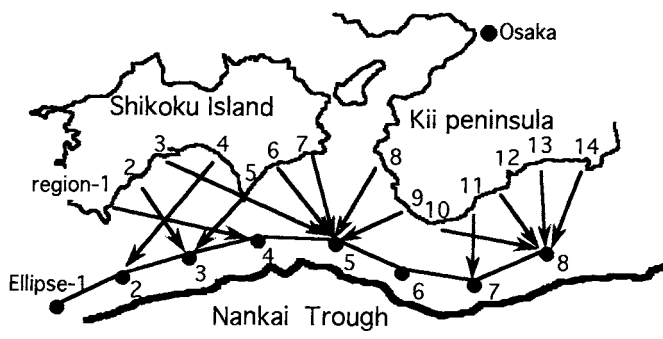


Figure 12. Locations of the most dangerous tsunami sources from viewpoint of relative wave height

CONCLUSION

In order to estimate potential tsunami risk along the coast of Nankai-do, an elliptical shaped tsunami source was artificially moved to eight locations, and the tsunami characteristics using the refractive calculation were analyzed. The following conclusions were drawn.

- (1) The fastest arrival times of tsunami are within approximately 5 minutes near the coast of Muroto cape and the Shio-no cape, and are within 20 minutes at most along every coast of Nankai-do.
- (2) The initial wave height (=unit height) at the tsunami source will become 1.9~3.5 higher at the coast of Nankai-do. Thus, the tsunami risk increases in the case of large initial wave height at the tsunami source such as has been caused by large earthquakes in the past.
- (3) The locations of the most dangerous tsunami sources where the residents want to know were clearly shown from the calculation of the arrival time, wave ray concentration and incident wave height.

ACKNOWLEDGMENTS

This study was partially supported by Grant-in-Aids for Scientific Research from the Ministry of Education, Science and Culture of Japan under Grant No. 07680490.

REFERENCES

- Griswold, G. M. 1963. Numerical calculation of wave refraction. *Jour. Geophysical Res.* **68(6)**: .
- Hatori, T. 1977. Distribution of Tsunami Energy along the Coast of Japan and Tsunami Travel Times. *Bull. Earthq. Res. Inst.* **26**:1-7. (in Japanese).
- Kawata, Y., N. Koike and T. Shimada. 1994. Proceeding of Coastal Engineering. *JSCE.* **41**:1181-1185. (in Japanese).
- Skovgaard, O., I. G. Johnson and J. A. Bertelsen. 1975. Computation of wave heights due to refraction and friction. Proc. ASCE. WW1.
- Takahashi, R. 1951. An estimate of future tsunami damage along the Pacific Coast of Japan. *Bull. Earthq. Res. Inst.* **29**:71-95.

A LINEAR PROBLEM ON SUBSURFACE VARIATIONS AT A TSUNAMIGENIC EARTHQUAKE

Shigehisa Nakamura
Kyoto University at Katada
Shirahama, Wakayama, Japan

ABSTRACT

A linear problem is studied in order to realize what processes were seen at a tsunamigenic earthquake. For example, in the case of the 1995 Hyogo South Earthquake, the epicenter of the earthquake was beneath the Akashi Strait located just next to Kobe and the areas of Hyogo South District. Hence, there must be tsunamis and subsurface variations in the sea. An eigenvalue problem of linealized hydrodynamics could give several specific normal modes of oscillations in Osaka Bay. In this work, an application of a finite segment method for mathematical contour integral is introduced to support the observed result before and after the earthquake. With the linear analysis, it could be understood what process was seen under the sea surface. Subsurface variations in relation to tsunamigenic earthquakes should be considered now for our complete understanding of the process induced by the earthquake. This could be helpful in considering an advanced tsunami warning and public protection system.

INTRODUCTION

A linear problem is studied in order to get a hydrodynamic understanding about what processes were seen at a tsunamigenic earthquake. A convenient way is to refer to past events. In this work, the case of the 1995 Hyogo South Earthquake is taken as a special reference for the author's study. The epicenter of the earthquake was in the area of the Akashi Strait located just next to Kobe and the surrounding urban areas of the coastal zones. When the epicenter is undersea, there must be tsunamis generated and induced subsurface variations in the sea. When the sea surface layer is stratified densimetrically or thermally, some expected subsurface variations can be seen as some horizontal motions of the sea waters around the epicenter.

For convenience, the author here considers that a linear problem is reversible when a hydrodynamic problem can be approximately expressed well in a form of Mathematics. With this, linealized problems are considered for a dynamic understanding of the water motions induced by a tsunamigenic earthquake. An eigenvalue problem of linealized hydrodynamics has given specific normal modes of oscillations in Osaka Bay (Nakamura, 1996). A finite segment method for a contour integral is considered in order to get a dynamic understanding of the interested problem. This method gives a solution to see whether resonant modes could be seen at the earthquake undersea. Referring to these reversed linear problems, we could see what is a reasonable understanding in relation to an advanced tsunami warning and public protection system.

ZONES OF TSUNAMIGENIC EARTHQUAKES

Hazardous earthquakes have occurred in the seismic active zones in the world. The circum-Pacific seismic zone is one of these zones. The Japanese Islands in the northwestern Pacific are located just in this zone. This fact can be seen by consulting the existing tsunami catalogs (for example, Iida et al., 1967; Soloviev and Gao, 1974; 1976; Watanabe, 1985).

As is well known at present, tsunamigenic earthquakes have been recorded not only in the circum-Pacific zone but also in the northeastern Indian Ocean including Sunda Trench and in the Mediterranean Sea.

The term "tsunami" is known as "tidal wave" in Europe. The earliest tsunami event must be documented in ancient Greece. In the medieval age, Spain and Portugal recorded the tsunamigenic earthquakes in the Atlantic Ocean. The Netherlands kept documents and reports of tsunami they had seen in the seas on the southeastern Asia during their activity in the 1600s. Several cases of the tsunamigenic earthquakes in the medieval age are not listed, except those that the scientists had noted even in the recent versions of the tsunami catalogs (Nakamura, 1996).

SEISMIC MAIN SHOCK AT THE 1995 HYOGO SOUTH EARTHQUAKE

A strong shock was felt in the early morning on 17th January 1995. This was the main shock of the seismic event named the "1995 Hyogo South Earthquake". As far as referring to the seismic processes at the previous earthquakes, there must have seen several foreshocks even though no one had paid attention and no threat of seismic hazards were felt in advance. The Japan Meteorological Agency (JMA) officially reported that the epicenter of the main shock was located at 34.601N and 135.033E (the location of the mark X in Figure 1), and this shock was at the depth of 17.73 km. The seismic magnitude of this main shock is 7.2 in the JMA's scaling. The maximum of the JMA seismicity scale 7 at this event is extraordinary and local so that it was hard to realize that this seismic event was severely hazardous in the urban areas in and around Kobe (cf. the location at K in the Figure 1). The aftershocks had been frequent for several days just after the main shock, with the frequency decreasing exponentially about a month after the main shock. As for the detailed seismic features of the main shock, some advanced studies have been analyzed by the seismological scientists though the author here concentrates on only a brief note to the terms interested in the sea water motions induced by the main shock.

At the main shock, the seismic fault was formed through the epicenter to the northeast and southwest directions. As seen in Figure 1, the epicenter (the mark X in Figure 1) is located under the sea in the Akashi strait: one fifth of the fault line formed at the main shock is to be under the sea and the rest on the land areas. Hence, the fault formation under the sea surely contributes to the generation of tsunamis and to the inducement of local oscillations of sea water around the epicenter.

As for seismicity, the main shocks were felt beyond the area shown in Figure 1. Examples are in Kyoto (more than 50 km away from the epicenter) and in Shirahama (about 100 km south of the epicenter just next to the mark T in the land area). Hence, the sea water in the interested area as shown in Figure 1 was surely excited at the seismic main shock, forcing some local oscillations in the coastal water zone. Unfortunately, the tide stations at Kobe and Osaka (cf. the mark D in Figure 1) malfunctioned just after marking the time of the seismic main shock. The tide station Sumoto (about 30 km south of the epicenter) some faint sea level variations had been seen. The induced variations after the main shock included a so-called local normal mode with a cycle of about 50 min (or about one hour) with its amplitude of about 20 cm, lasting for more than several hours and seen even in the afternoon.

TECTONIC FEATURE AND SEA WATER MOTIONS

As already noticed, the interested area as shown in Figure 1 is in the northwestern part of the circum-Pacific seismic zone (Nakamura, 1994a; b). Especially, the Kuril Islands, the Japanese Islands and the Ryukyu Islands are arc islands in the zone. The Pacific Plate (PAC) is subducting under the Eurasian Plate (EUR) off the southeast part of the main island of Japan, and under the Philippines Sea Plate (PHP) off the south part of the Japanese Islands and the Ryukyu Islands. The subduction is caused by interactions of the Pacific Plate and the other Plates noted just above. The trenches are seen as the boundaries of the Plates, for example, off the arc islands along the Japanese Islands. This subduction of the Pacific Plate suggests that the Eurasian Plate is deformed not to be flat but to be distorted to form some undulated crustal surfaces on the land and sea areas. Several parts of these undulations are the parts of the Japanese Islands as seen in the topographic or bathymetric pattern around the Japanese Islands including the area of Figure 1.

Nakamura (1994a; b) has noticed the long-term geodetic variations of the ground surface along a survey line on the coast of the south end of Japan. The variations in the interested area as shown in Figure 1 can be a convenient factor to detect what timely trend can be seen before and after the hazardous tsunamigenic earthquakes under the sea off the south Japan.

OFFSHORE TOWER

An offshore tower was constructed in 1993 off the south coast of the Japanese Islands facing the northwestern Pacific (at T in Figure 1). The tower is about 2 km off the coast and is settled at the top of a conical reef of a stratified sand rock. The water depth at the foot of the reef surrounding the tower is 32m, and the tidal range is about 1.8m in the area covering the author's interested sea area. Usually there are significant semidiurnal and diurnal tides. The location of the tower is just outside of a local wide-open bay and is next to the boundary of the coastal zone and the continental shelf. This allows the tower to be effective in detecting any hazardous variations in the ocean before the variations may be seen on the coast. At the tower, meteorological and oceanographical factors have been observed continuously to obtain real time data since the settling of the tower. The factors of observation at the tower are winds, air and water temperatures and dew-point temperature, sea surface waves, tides. The water temperatures at the

depth of 2.5m, 5m and 10m under the sea surface are monitored successively at every half minute.

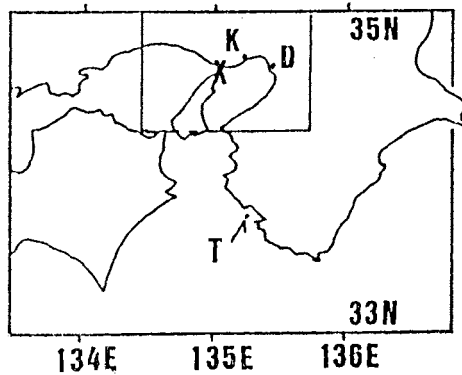


Figure 1. Coast lines around the epicenter of the 1995 Hyogo South Earthquake

OCEANIC AND ATMOSPHERIC CONDITIONS

The Kuroshio flow as a western boundary current is affecting to form a weak stratification of the surface layer in the area around the tower (cf. the mark T in Figure 1), and the coastal waters dynamically affect the sea surface layer around the tower. The Kuroshio water is flowing just South off the tower to affect the location of the Kuroshio front which is taken generally just next to the Kuroshio main flow as the oceanic western boundary flow. The Kuroshio water is a more haline water and a water of higher temperature than the coastal waters. The variations of the Kuroshio flow affect the temperature at the tower and the thermal pattern around the sea surface layer around the tower. The variations can be specified by salinity variations at the tower. Thermal variations at the tower can be one of the more convenient factors for the purpose of detecting the Kuroshio variations. Nevertheless, these do mean that the Kuroshio front crosses the location of the tower. The specific feature is an intrusion of the separated Kuroshio water into the coastal zone from the offshore zone to start the water temperature rise from the sea surface to the subsurface in the sea surface layer around the tower. Hence, it is hard to consider the thermal variations of the 1995 Hyogo South Earthquake as a case of the variation induced by the Kuroshio variations. For that day, no reference data is available to the author to certify what is noted above.

The violent effects of the meteorological variations disturb the skin water layer on the sea surface layer around the tower. Referring to the observed results at the tower which have been gathered for more than 20 years, a weakly stratified sea surface layer was usually seen. On the day of 17th January 1995, the weather was fine and calm. Hence, a possible abnormal motion of sea water as shown in Figure 1, can be aware in monitoring the observed data at the tower as the tectonic effect to the coastal waters covering the weakly stratified sea surface layer.

On the other hand, a branch of the Kuroshio warm water occasionally hits the tower when some variations appear in the Kuroshio flow variations. The Kuroshio warm water and the coastal waters interact with each other, and it is natural that the coastal waters are affected by the river discharges of the cold or low water temperature. River discharges spread on the coastal sea surface even though the river waters are colder than the coastal surface layer affected by the offshore oceanic water or the Kuroshio water in the interested zone. Then, the river discharges are also effective in affecting the thermal variations in the sea surface layer which can be monitored as the thermal variations of the sea waters just around the tower and in the interested zone. Adding to the above, horizontal motions of sea water can be found by observing the thermal front even when any vertical motion of the sea water is not significant enough to distinguish some specific variations in the sea water.

After the observed data, the semidiurnal and diurnal tides are significant though these effects are simply detected by the sea level variations at the tide stations on the coast and the current velocities induced by the tides. Considering a macroscopic scale of the sea water motion, no eddies and turbulent flow can be taken to be negligible so that a primitive linear problem may be possible at consideration of tidal currents in the interested sea area even though the sea surface layer is faintly stratified by the effects of the Kuroshio water and of the river discharges.

In the coastal zone as shown in Figure 1, the faint stratifications are maintained with little thermal variations in the range of 0.2°C in the sea surface layer for several years at the tower, even though the thermal variations are recorded every minute at the tower. It is hard to consider the water motions in the interested area as the baroclinic ones because the sea area is small enough not to consider the baroclinic currents except for the barotropic currents. Therefore, no variations can be seen as any internal waves or internal tides. At the passage of the typhoons and of the storms, the internal waves may be induced, and the thermal records at the tower suggest the vertical mixing is significant in the sea surface layer of 10m thick so that the internal waves must be faint even if those effects are included in the thermal records at the tower. At the seismic event on the 1995 January 17th, the specific thermal variations observed at Sumoto were quite similar to those at the tower. This fact suggests that the sea surface layer in the interested area must be affected directly by the tectonic effect to induce the local oscillations of the sea waters in the area of embayment. A small leak of waters at oscillations out of the area of embayment may cause to record the thermal variations at the tower accompanied to the oscillative motions of the sea water just after the seismic event for several hours.

SUBSURFACE THERMAL VARIATIONS

A strong shock was felt early in the morning (at 5:46 a.m. JST) on 17th January 1995. This was the main shock of the 1995 Hyogo South Earthquake. The location of the epicenter (the X in Figure 1) was in the sea area of the Akashi Strait just near the north end of the Awaji Island and the southwest of the urban area of Kobe(the K in Figure 1).

At the offshore tower introduced above, the main shock was felt even at a distance of about 100 km south. The tower recorded subsurface thermal variations as shown in Figure 2 (Nakamura,

1995; 1996). At 5:30 a.m. JST, the sea water temperature near the tower at a depth of 10m, started to decrease until 5:50 a.m. JST. After that, the thermal variations were found in the records at the depths of 2.5m and 5m.

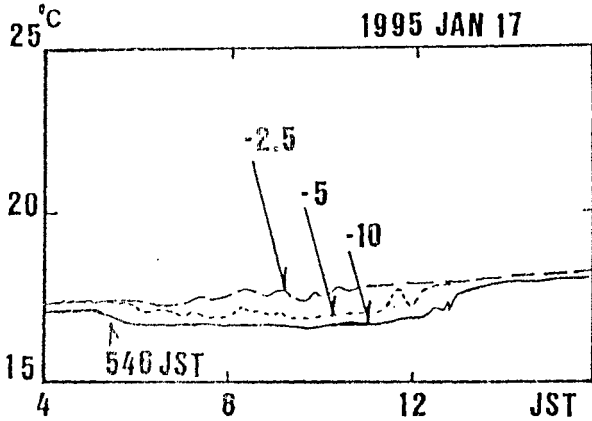


Figure 2. Subsurface thermal variations at the Offshore Tower

- 1) Full line for 10m under the sea surface
- 2) Dot line for 5m under the sea surface
- 3) Chain line for 2.5m under the sea surface

As for the thermal variations found before the main shock, there may be an effective tectonic variation which could be a trigger for the earthquake. Nevertheless, the author would consider the subsurface thermal variations only as an induced horizontal water motion in the surface layer of the sea. The temperature difference between the two depths of 2.5m and 5m was about 0.10°C. The temperature difference between the depths of 5m and 10m was about 0.5°C. Around the tower, the densimetric stability can be evaluated on the basis of the observed thermal stratification, though the density of the sea water is controlled by the main three factors, i.e., temperature, salinity and depth (pressure). The stability was maintained for more than 12 hours by the interaction of the coastal and offshore waters.

At the depth of 5m, the temperature was 17.2°C at 5:30 a.m. JST, though it had been 17.3°C earlier. By 5:56 a.m. JST, the temperature was 17.1°C JST, and was 17.0°C by 6:02 a.m. JST. At a depth of 2.5m, the thermal variations were not that significant and the temperature lowered to 17.2°C, although it had been 17.3°C earlier. These thermal patterns suggest that the subsurface thermal variations could be understood considering a tectonic process and the water motions in the wide area covering the western part of the Japanese Islands. It should be confirmed whether the crustal activity was contributive to making a change to the sea flood profile around the tower in order to realize why the thermal variations were observed at the tower at the time of the shock. When this process is clarified, a hypothetical understanding (for example, Nakamura, 1995a) could be well accepted as one of the dynamic factors for studying the interested problems. With the above fact, the author considers that it is preferred to note a

linear hydrodynamic problem which could give a solution. This problem is reversible so that the solution of the problem may be used to understand what was observed at the tower.

REVERSAL PROBLEM

In order to realize the motions of the sea surface layer induced by the seismic impact around the epicenter of the 1995 Hyogo South Earthquake, the author has considered a linearized reversal solution of the eigenvalue problem (Nakamura and Loomis, 1980; 1980a).

It can be well understood that a linear problem is reversible. Generally, then, a linear reversal problem can be easily solved if an ordinal problem is solved well for some expected normal modes and a forcing factor under some given boundary condition. The linear solution is utilized for the reversal problem at mathematical and hydrodynamical understanding of the solution under the given condition. The sea water motions during the 1995 Hyogo South Earthquake can fit for one case of the considering reversal problem. When the motions of waters around Kobe and in Osaka Bay are approximated as a kind of shallow water long waves in the gravity field, it can be expressed by a simple linear equation (for example, Stoker, 1957). Assuming the velocity potential to substituting, the equation can be rewritten. Solving the equation for the given frequency as an eigenvalue problem, an envelope function is obtained (Nakamura, 1980a). This is noted by Nakamura (1996) in relation to what the observed thermal variations of the sea surface layer at the tower. This is consistent to the reversal solution of the eigenvalue problem (Nakamura and Loomis, 1980a). Fortunately, the lowest modes obtained by Nakamura and Loomis(1980a) as the solutions in the numerical model of Osaka Bay support the expected reversal solution of free oscillation in this case.

CONTOUR ANALYSIS BY FINITE SEGMENT METHOD

Induced oscillation in Osaka at an incident wave is obtained by Nakamura (1979) after applying the work by Lee and Raichlen (1971).

First, assume water as a fluid to be irrotational and incompressible dynamically. Then, consider the problem of a solution for a Laplace equation under a certain condition. In this work, an application of contour integral while introducing a finite segment method is considered for realizing the water motion in Osaka Bay at the 1995 Hyogo South Earthquake. As for the case of Osaka Bay, the coastal configuration around the bay model is shown in Figure 3. An incident wave into the bay model across the section LN is assumed to be a sinusoidal cyclic- wave of small amplitude, and no water flow is considered across the segments corresponding to the coast. Then, the velocity potential can be obtained (Nakamura, 1976; 1996).

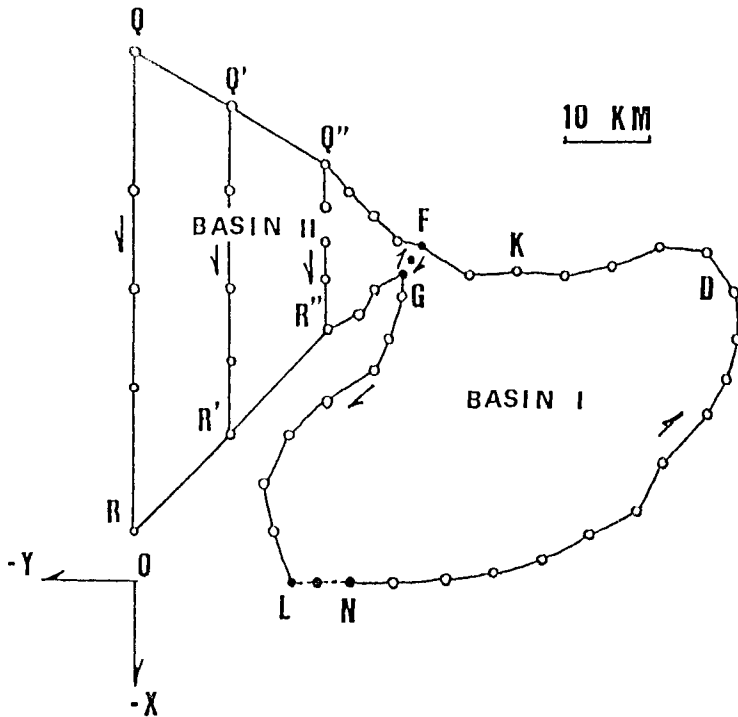


Figure 3. Osaka Bay model
 $i=1, 2, 3$ for the contours $GFQ''R''$, $GFQ'R'$, $GFQR$

Two water basins (basin I and basin II) are considered as shown in Figure 3. The segments between K and L are the south openings of the Osaka Bay model, and the segments between F and G are the northwest openings of Osaka Bay in the numerical model. Using Weber's solution, the function at any point of (x,y) in the basin corresponding to Osaka Bay can be obtained (Nakamura, 1996). The contour integral is performed along the boundary encircling the basin I as LNDKFGL as shown in Figure 3 (K for Kobe and FG for the model tsunami source). It is hard to practice the contour integral for an arbitrary shaped contour. Then, the integral equation is rewritten in the form of a matrix equation in order to get an approximated solution. The solution in the ocean can be expressed by a sum of the incident, reflected waves and the scattered wave. As far as considering the problem in the two basins, the function (f) in the ocean is not so important generally. Nevertheless the value of f on the formal- segments between LN as the opening of the bay facing the ocean should coincide to the value of f in basin I. Especially, for a case of an incident wave normal to the line LN, the evaluation of f on the line LN is written as a convolution of f and the first kind Hankel function of the zeroth order (Lee and Raichlen, 1971; Nakamura, 1979; 1996).

The obtained response function at D in the model (the point for Osaka) is shown in Figure 4 in which the parameter i is introduced to notice the effect of response depending on the water area in Basin II.

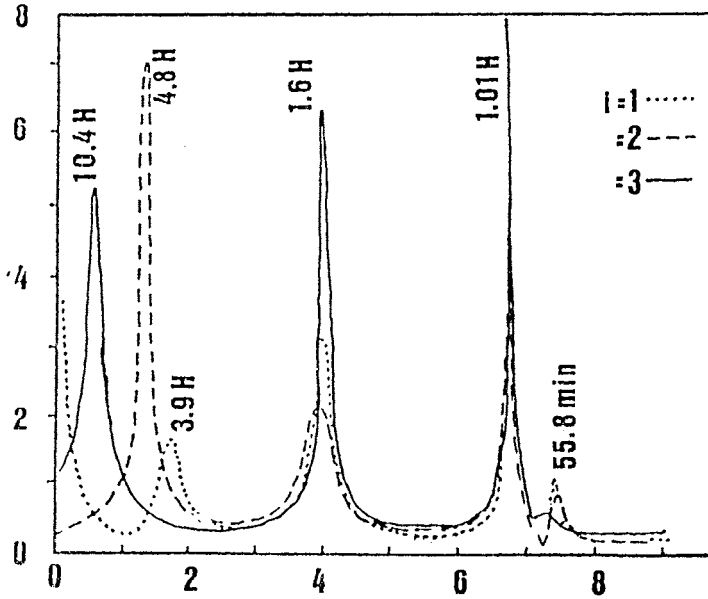


Figure 4. Response function at D (corresponding to Osaka) $i=1, 2, 3$ as in Figure 3.

The first eight resonant modes are shown in Figure 5. In the case of the 1995 Hyogo South Earthquake, several tide records had been obtained. These records suggest that the numerical model of the contour integral is enough to realize what variations of the sea level were seen by the impact the shock of the earthquake. As far as referring to the available observed data, the patterns in Figure 3 are consistent to the tsunami records in Osaka Bay.

CONCLUSION

A reversed linear problem is considered in order to realize what variations were seen in Osaka Bay at the 1995 Hyogo South Earthquake. A response function at a point (Osaka) in the model bay is obtained by using a contour integral by applying a finite segment method for the linealized shallow water wave equation. The patterns of numerical response in the Osaka Bay model suggest what variations of the sea surface layer in the bay were seen at the shock of the earthquake. Adding to the above, the solution in this work could be helpful at considering an advanced tsunami warning and public protection system.

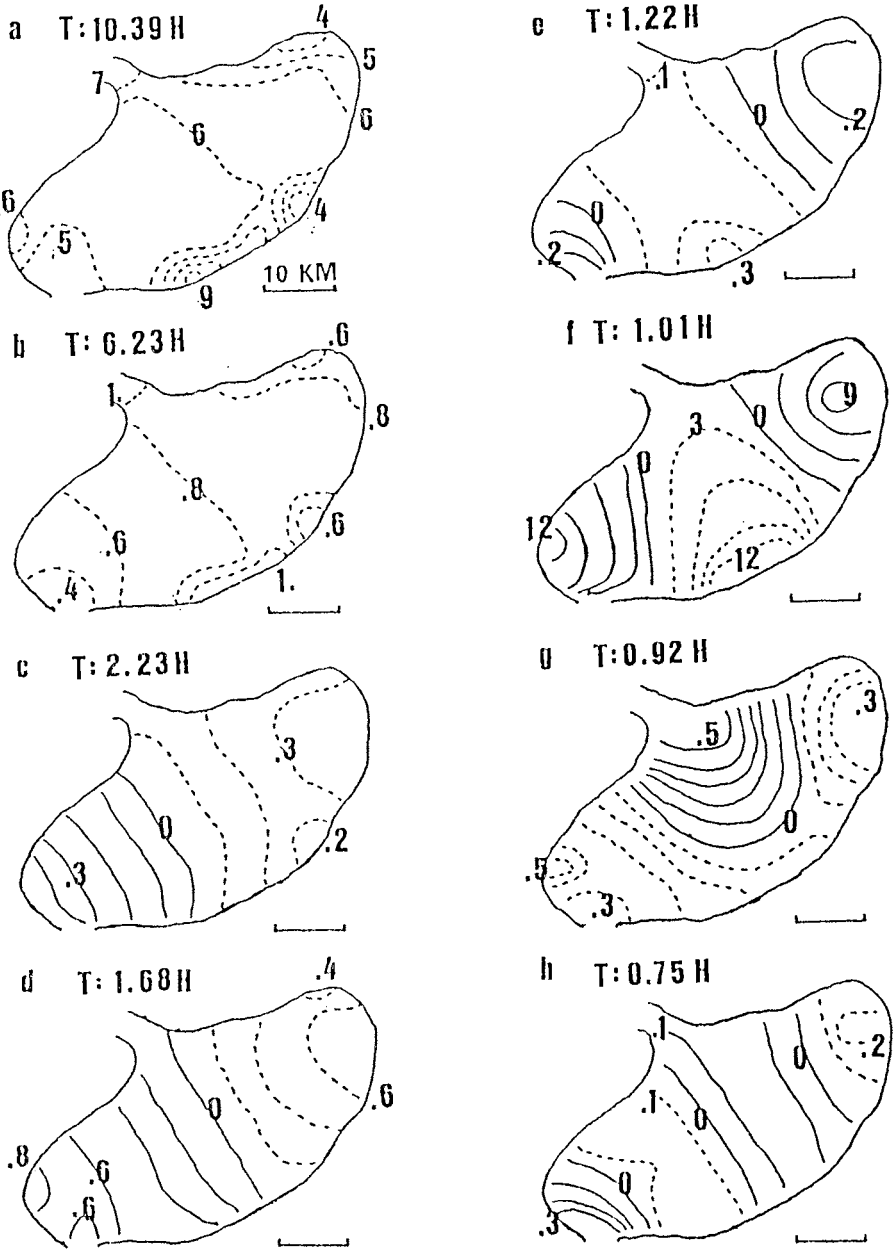


Figure 5. Patterns of response in Osaka Bay (T for period of oscillation)

REFERENCES

- Iida, K., D. Cox and G. Pararas-Carayannis. 1967. Preliminary Catalog of Tsunamis in the Pacific. HIG-67-10. Data Rep. No. 5.
- Lee, J. J. and F. Raichlen. 1971. Wave Induced Oscillations in Harbors with Connected Basins. CIT. Rep. No. KH-R-26.
- Nakamura, S. 1979. Oscillations of Osaka Bay in a numerical model. In: Proc. 26th Conf. Coastal Eng. in Japan. pp. 139-142.
- Nakamura, S. 1994a. Annual mean sea level variations in the Northwestern Pacific zone. *Marine Geodesy*. **17**:213--218.
- Nakamura, S. 1994b. Annual mean sea level and Tsunamigenic earthquake in the Northwestern Pacific. In: Proc. INSMAP'94 (International Symposium on Marine Positioning). pp. 577-584.
- Nakamura, S. 1995. Extent of sea water motions at the 1995 Hyogo South Earthquake. EOS (Trans. AGU). Supplement (1995 Spring Meeting). pp. 82-83.
- Nakamura, S. 1995a. Oceanic subsurface thermal variations during the 1995 Hyogo South Earthquake. *Sci. Tsunami Hazards. Int. J. Tsunami Soc.* **13**:53-56.
- Nakamura, S. 1996. An extent of sea surface layer affected by an earthquake. *Marine Geodesy*. **19**:281-289.
- Nakamura, S. and H. G. Loomis. 1980. Normal modes of oscillation in relation to storm surge and tsunami in Osaka Bay, Japan (1). *La Her.* **18**:69-75.
- Nakamura, S., and H. G. Loomis. 1980a. Normal modes of oscillation in relation to storm surge and tsunami in Osaka Bay, Japan (2). *La Mer.* **18**:76-81.
- Soloviev, S. L., and C. N. Gao. 1974. Katalog tsunami na zapadnom poberezie Tixogo okeana. Akad. Nauk(USSR). Leningrad:lzdat. Nank.
- Soloviev, S. L. and C. N. Gao. 1976. Katalog tsunami no bostochnom poberezie Tixogo Okeana. Akad. Nauk (USSR). Leningrad:lzdat. Nauk.
- Watanabe, H. 1985. Catalog of Hazardous Tsunamis around Japan. Tokyo:Univ. Tokyo Press.

NUMERICAL MODELING OF COSMOGENIC TSUNAMIS

Victor Petrenko and Andrei Marchuk
Computing Center, Siberian Division, Russian Academy of Sciences
Novosibirsk, Russia

ABSTRACT

Traditionally tsunami waves are considered as a result of strong submarine earthquakes, huge landslides or volcanic eruptions. However, there is one possible cause of tsunamis - the impact of cosmic bodies into ocean. It is known that the Earth is continuously attacked by meteorites and other cosmic bodies. A lot of traces of ancient meteorite impacts are discovered on the Earth surface. Some craters are found in shelf zones. It is evident that sometimes big cosmic bodies are impacting into ocean. Every such an event can produce water waves of tsunami type. Their amplitude and length depend on size, velocity and composition type of that cosmic body. Some results of the numerical simulation of cratering and ejecta dynamics, the generation and propagation of water waves caused by the impact of cosmic bodies into the ocean are presented. Estimations of the height of a deep water wave and earthquake magnitude caused by the impact as a function of impactor radius, velocity and composition type are given.

INTRODUCTION

The analysis of the available data on impact structures on the Earth surface shows that on the average, once in 50-100 years cosmic body of Tunguska size (50-100 m in diameter) falls down on the Earth. Events like Revelstoke bolide (1965) with the diameter 10-20 m can occur annually. The estimated frequency of meteorite impacts into oceans for scaled asteroids is 1 in 10^4 years for 0.5-1 km sized objects, 1 in 10^5 years for 5 km in diameter cosmic bodies and 1 in 50 million years for an asteroid with the diameter of 20 km. The probability of a kilometer-sized object colliding with the Earth within the next 100 years is 10^{-4} (Chapman and Morrison, 1994). If there are no erosive forces, some 2000 craters having sizes 10 km (or >10 km) should be recorded during the period of 200 million years (the age of present system of oceans). Figure 1 shows the location of some reliable significant impact structures discovered on the Earth surface. It is taken that about 70 percent of all meteorites are falling down into oceans. But only one crater was detected on the ocean bottom (Montagnais structure). It is located in the shelf zone of Nova Scotia. The age is about 50 million years and the size is about 30 km in diameter. Debris from a late Pliocene asteroid impact are thrown around on the 600 km area of ocean floor in the Southeast Pacific. The asteroid diameter was at least 0.5 km and did not produce a crater on the ocean floor because of significant (about 5 km) depth (Kyte, 1988). The analysis of the structure material makes it possible to estimate the age of craters and the frequency of cosmic body impacts of different size (energy). Most land impact structures have been identified by a combination of criteria, including the observation of circular topographic and geological formations and finding out high pressure polymorphs and other shock debris. There are insufficient data for a similar

search on the ocean floor. The cumulative frequency distribution of the kinetic energy of such celestial bodies is given by Shoemaker (1983) and shown in figure 2.

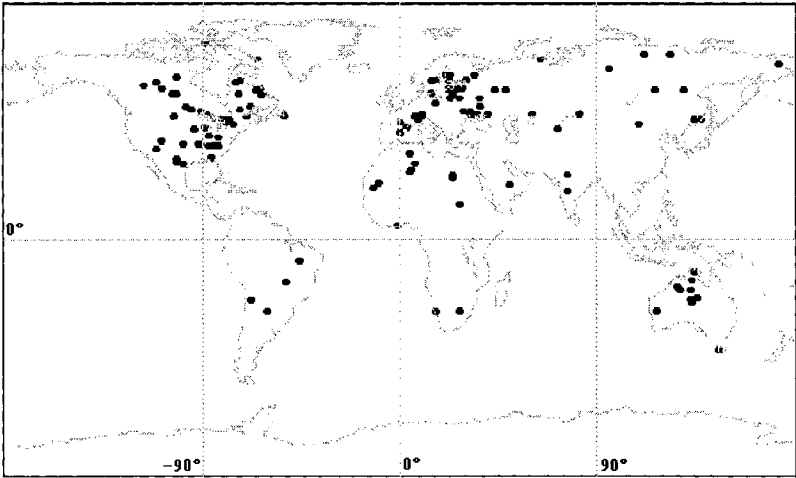


Figure 1. Reliable impact structures of the Earth surface.

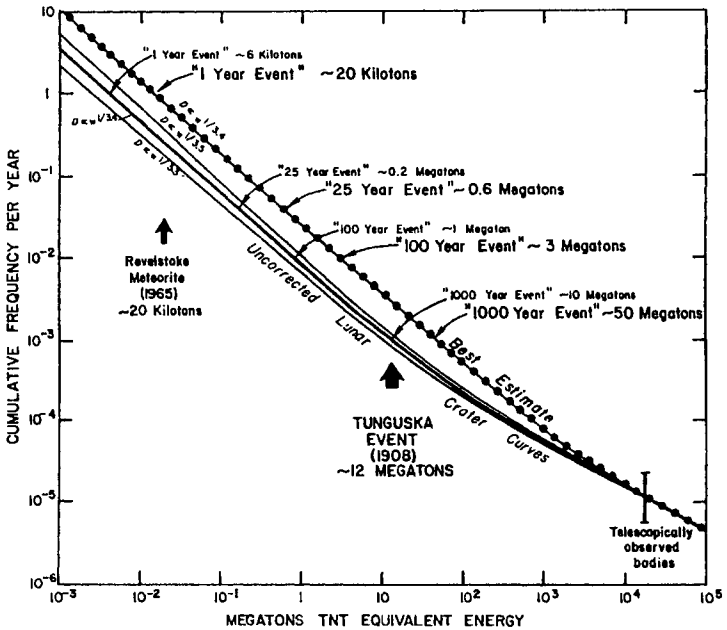


Figure 2. Cumulative frequency distribution of kinetic energy of falling celestial bodies

It is evident that the most part of cosmic bodies fell down into oceans and seas. But it is much more difficult to discover impact structures on the sea bottom than on the land. So, during the Earth's history there were a lot of regional events (tsunamis generated by the celestial body impact into the ocean) and some significant impacts which caused global catastrophes. During last decades some evidence of possible historical asteroid impacts into ocean has appeared (Kyte et al., 1988, Bourgeois et al., 1988). Paleo-tsunami deposits are discovered in different places. The most possible cause of 50-100 meter high tsunamis at the Cretaceous-Tertiary boundary is a bolide-ocean impact (Bourgeois et al., 1988). Some effects of tsunamis generated by cosmic body impacts were reviewed by Gault and Sonett (1982). Initial wave heights for bolide-water impacts depend on bolide radius, velocity, density, water depth and other factors such as atmospheric pressure (Gault and Sonett, 1982).

The impact of large cosmic bodies into the ocean leads to the forming of very high surface waves. The numerical simulation which was made by O'Keefe and Ahrens (1982) and by Roddy et al. (1987) gives the detailed picture of hydrodynamic processes caused by a vertical impact of the large asteroid.

For large asteroid (radius more than 1 km) impacts tsunami waves can be as high as the water depth at the impact site, i.e. up to 4-5 km for a deep ocean impact. Only a bolide-water impact can produce a far-field wave height from 10 m up to 100 m (Gault and Sonett, 1982).

ESTIMATIONS OF WATER WAVE HEIGHT

Rough estimations of the wave height in the deep ocean as the function of cosmic body parameters have been defined by following assumptions: 1) The impact into the deep ocean produces surface waves that do not dampen significantly when they run in deep water. 2) The estimation of the initial water cavity size is based on similarity scaling parameters for asteroid impacts with specified size, velocity, density and on some results of experiments with underwater nuclear explosions (Glasston and Dolan, 1977). 3) The height of a deep water wave is inverse to the distance from the impact point.

Such estimations of the height (in meters) of a deep water wave 1000 km from the impact point in the ocean are shown in Table 1. Wave heights are given in meters for three values of the impactor velocity (20 km/sec, 30 km/sec, 50 km/sec) and for three composition types ($\rho=8 \text{ g/cm}^3$, $\rho=3 \text{ g/cm}^3$, $\rho=0.5 \text{ g/cm}^3$), where ρ is the density of the impactor.

The wave period (which is determined by fill-in time of the water cavity) can be estimated very approximately from the phase velocity in the linear wave theory. It increases with the impact yield and is over than 2 min for asteroids with $D>300 \text{ m}$.

The deep water wave velocity is several hundred km/h. As the wave goes from the deep ocean to the shoal, its speed decreases and amplitude increases, the wave front becomes very steep until it breaks.

The average growth coefficient for the tsunami wave height when it moves from deep water to the land is about 40 times.

NUMERICAL MODELING OF COSMIC BODY IMPACT INTO OCEAN

Modeling cratering and ejecta dynamics, the generation and propagation of water waves arising as a result of the high-velocity cosmic body impact into ocean has been divided into four stages: 1) Impact crater formation in the water and ocean floor and ejection of the water, steam and rock from it. 2) Water cavity collapse and generation of central wave system. 3) Wave propagation in neighboring to water cavity zone. 4) Wave propagation in far areas.

On the first stage equations of compressible inviscid flow were used. On the second stage Navier-Stokes equations for incompressible flow or shallow water equations were used. The third and fourth stages of numerical modeling were based on shallow water equations.

Modeling cratering and ejecta has been performed using LPIC method (Petrenko, 1970), which has been developed for the calculation of the dynamics of compressible multi-substance fluids with large deformations in two dimensions for planar or axisymmetric geometry. LPIC typical features consist in the following: 1) the solid media is represented by finite-size particles; 2) the size of particles (lengths and widths) changes in time depending on local flow values; 3) the particles carry their current coordinates of the center and dimensions, mass, density, momentum, internal energy and substance sign; 4) particles can be divided into a few separate independent particles or united with other particles consisting of the same substance; 5) the system of compressible flow equations in the form of conservation laws is integrated for each particle by the explicit scheme of first/second order accuracy in space and first order accuracy in time; 6) rectangular Eulerian grid is constructed rather arbitrarily at each time step; 7) the interpolation forth and back between particles and grid, calculating, where necessary, derivatives by the finite difference on the grid and moving particles to simulate the advection are used; 8) special algorithms to define the contact boundary orientation and to follow the particle form are used.

LPIC time-step algorithm starts using particle values obtained at the previous time step and involves following stages. 1) Eulerian rectangular grid is constructed according to the flow dynamics. 2) The velocity and pressure (or in more general case - stress tensor components) are interpolated from particles to vertices of Eulerian grid. 3) Boundary conditions on the Eulerian grid are determined. 4) Velocity and pressure co-ordinate derivatives in the vertices of Eulerian grid are calculated. 5) The co-ordinate derivatives obtained in stage 4 are interpolated back from the vertices of Eulerian grid to the particles. 6) The new values of density, velocities, internal energy, coordinates and parameters of the particles are calculated by the difference analogies for density, momentum and energy equations and also by particle motion and form equations. 7) Dividing and uniting particles are produced. 8) The particle pressure is calculated by the equation of state which is a function of density and specific internal energy. The artificial viscosity is estimated.

Applying such an algorithm results in the following consequences: 1) It allows us to solve numerically many problems related to the behavior of solids (load history, phase transition, etc.), liquids (phase transition, formation of cavities and bubbles, etc.), and gases under high pressures/temperatures. 2) There is no problem with the pressure computation in mixed Eulerian cells. 3) There are no significant fluctuations of the numerical solution. 4) It is easy to model flows when density and pressure are varying in the range of several orders. 5) It is possible to perform calculations using only one particle per Eulerian cell that significantly reduces necessary computer resources and time. LPIC is robust and applicable to complex flows.

We carried out the numerical simulation of the high-velocity impact of cosmic bodies of different types, shapes, internal structures of layers and composition, including iron, stone, ice. Some results are presented here.

The numerical simulation of hydrodynamic processes caused by a vertical impact of the large asteroid (modeled as 20 km diameter iron sphere) with the velocity 20 km/sec into the ocean-bottom media was carried out. The ocean depth was 5 km. The rock under the ocean bottom was considered as two-layered. The thickness of the upper layer was 20 km. Every layer had different equations of state. The initial statement of the problem (Fig. 3.1) and results of numerical modeling are presented in figure 3.

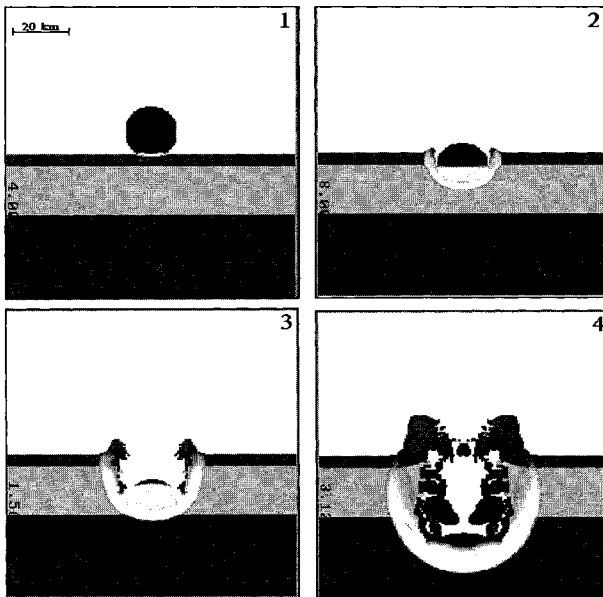


Figure 3. The big cosmic body impact into ocean-bottom media.

The field generated by the impact consists of an initial intensive pulse of the compression, associated with the excavation of oceanic crater followed by the system of waves resulting from the oscillation of the central peak. These waves then propagate outward losing energy to radial divergence.

The numerical simulation of the impact of the 200 m diameter stony asteroid with velocity 20 km/sec into 5 km deep ocean has showed that the first wave propagation velocity is equal to 120 m/sec while the propagation velocity of the second and third waves produced by the oscillation of the central peak is about 80 m/sec.

NUMERICAL SIMULATION OF THE WATER CAVITY COLLAPSE

The collapse of the cavity is quite different for the incompressible model of Navier-Stokes and shallow water model calculations. The cavity in Navier-Stokes calculations more slowly collapses from the bottom than that of shallow water calculations does from the side. The waves calculated by Navier-Stokes model have more complicated wave patterns. They quickly decay into the deep water, the fluid particle motion greatly decreasing, with depth increasing below the water surface.

Results of numerical simulation of the water cavity collapse and generation of the central system of waves for the shallow water model are shown in figure 4. The initial surface displacement was taken according to results of numerical modeling of the impact process. The semi-spherical cavity and the water elevation around it were used as the initial state of water surface. We assumed that water was first immobile. The initial position of water surface is shown in figure 4.1. In figures 4.2-4.4 the following stages of water wave generation process are shown. At the top of each figure 3D-view of water surface is given and at the bottom the profiles of generated waves is shown. The impact point is located at the left boundary of each figure and generated waves are propagating from the left to the right. Scale is given in figure 4.1. Two parallel horizontal dotted lines show plus 100 meter and minus 100 meter levels. In this series of computations the following parameters were used: ocean depth - 4 km, initial surface displacement in the center of cavity was -3.5 kilometers from the mean water level, maximum height of the initial water elevation was 1.5 km up from the mean water level. The diameter of the initial displacement was about 40 kilometers.

Here we have presented numerical simulation results on the initial stage of wave propagation process forming at the cavity collapse. The wave height will be inverse to the distance from the center of the water cavity. During the propagation the front of the second wave becomes very steep and wave breaking can occur. Wave forms obtained in this numerical computation are typical for this class of water gravity waves. The typical features of these waves are: relatively short period of waves, very steep front of the second wave (often the second wave transforms into bore) as a result of nonlinearity and significant wave amplitude.

The numerical simulation of a 10 km in diameter comet (modeled as a sphere of water) impact into 4 km deep ocean at the velocity 20 km/sec was carried out. The equation of state for a comet was the same as for oceanic water. At large distance the wave propagation was simulated using

the shallow water model. A N - type wave was formed (see, wave profiles at three time moments: 5 min, 8.5 min, 21 min, in fig. 5).

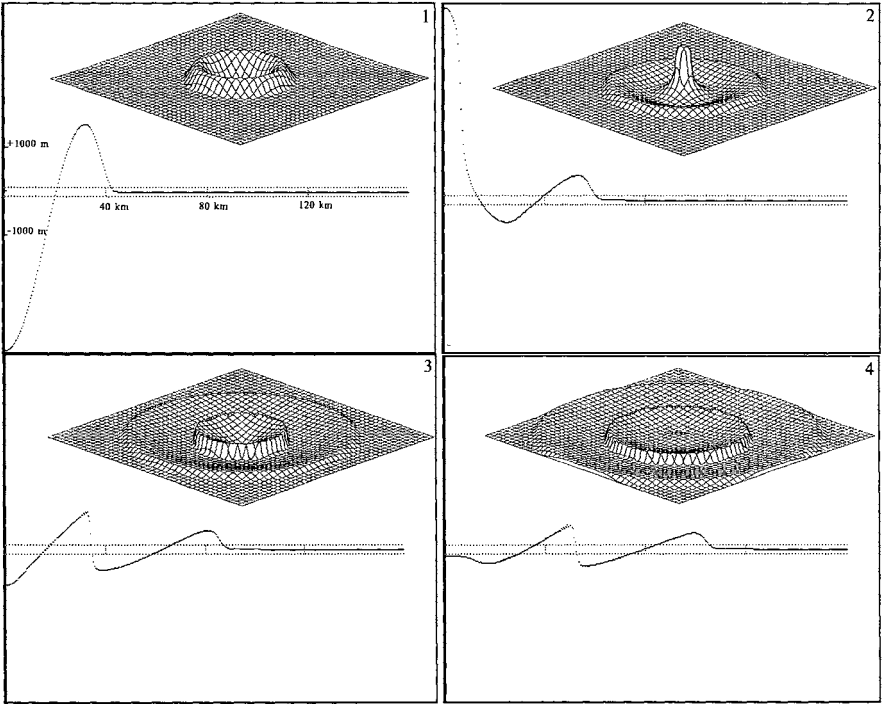


Figure 4. Numerical modeling of tsunami waves forming by initial water cavity.

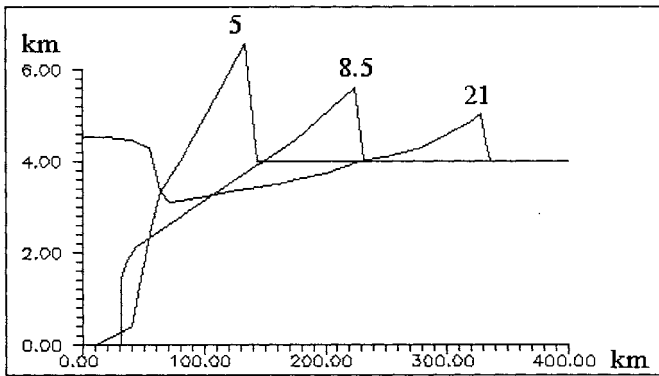


Fig. 5 Wave profiles for a 10 km in diameter comet impact.

NUMERICAL SIMULATION OF AN ASTEROID IMPACT INTO LAKE

Numerical modeling results of the stony asteroid impact into the lake is shown in figure 6. The asteroid was regarded as the sphere with diameter 100 m having velocity 20 km/sec. The diameter of the lake was 3 km and the depth was 500 m.

This problem solution illustrates the usage of translocation algorithm, which is applied in those cases when it is necessary to get more detailed picture of the initial impact stage. Calculated area dimensions change in the flow evolution. We start the problem solution with the highest spatial resolution and include the direct contact of colliding bodies. Then according to the shock wave propagation, steam and rock ejecta area the spatial resolution decreases saving the initial number of computational Eulerian cells and including a greater area of colliding objects.

Table 1. * Wave height in deep ocean 1000 km away from impact site of iron, stony asteroids and comets

Impact velocity 20 km/sec			
Density (g/cm^3)			
	8.0	3.0	0.5
Radius (m)	Wave height		
100.0	8.4	5.0	1.9
150.0	16.2	9.6	3.6
200.0	25.9	15.2	5.8
250.0	37.1	21.9	8.3
500.0	114.1	67.2	25.5

Impact velocity 30 km/sec			
Density (g/cm^3)			
	8.0	3.0	0.5
Radius (m)	Wave height		
100.0	13.0	7.7	2.9
150.0	25.1	14.8	5.6
200.0	40.1	23.6	9.0
250.0	57.5	33.9	12.9
500.0	176.8	104.1	39.6

Impact velocity 50 km/sec			
Density (g/cm^3)			
	8.0	3.0	0.5
Radius (m)	Wave height		
100.0	22.6	13.3	5.1
150.0	43.7	25.7	9.8
200.0	69.6	41.0	15.6
250.0	99.9	58.8	22.3
500.0	307.0	180.8	68.7

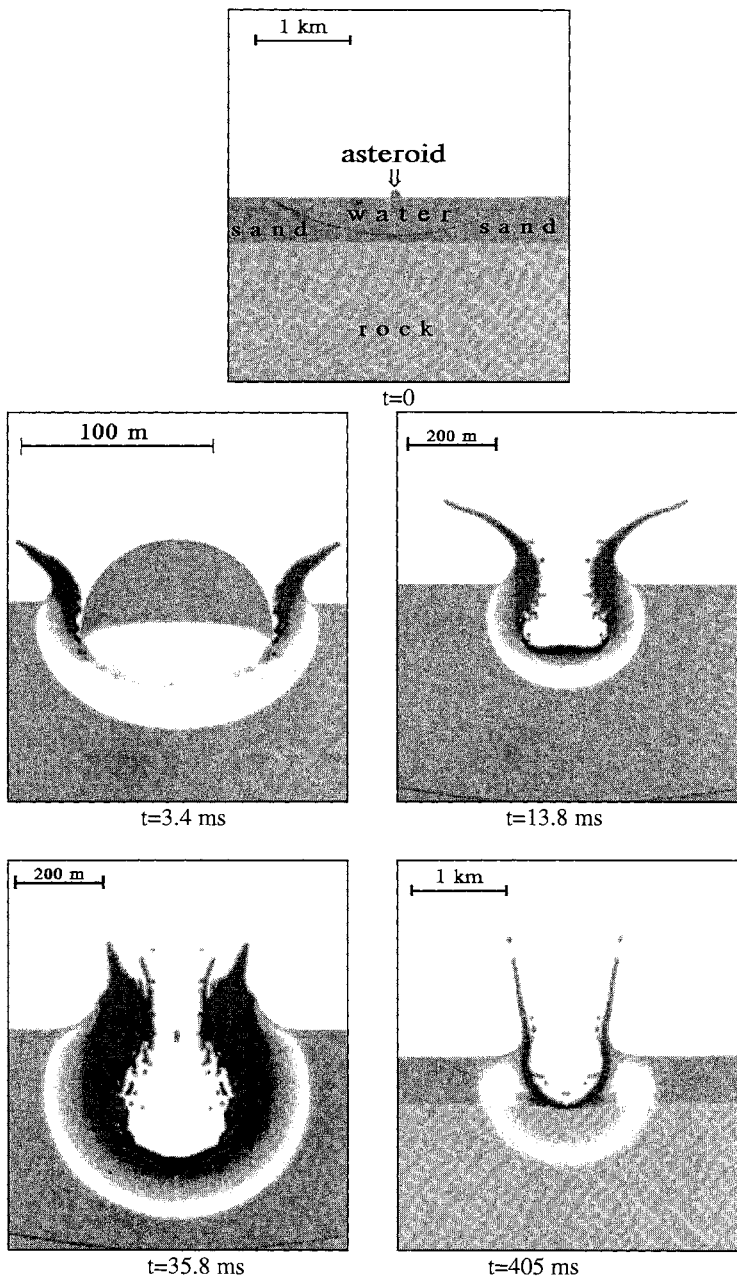


Figure 6. The asteroid impact into lake.

ESTIMATION OF SEISMIC EFFECT

If a celestial body produces a crater on the ocean floor, it must produce an earthquake. It is possible to estimate Richter scale magnitudes M of those earthquakes using the dependence of magnitudes M on buried nuclear explosive yield. Table 2 shows earthquake magnitudes as a function of impactor radius, velocity and composition type. The big impactor ($D \geq 10$ km) must produce an earthquake with the magnitude of $M \geq 11$.

Table 2. Event magnitude of the iron, stony asteroids and comet impact

Impact velocity 20 km/sec			
	Density (g/cm^3)		
	8.0	3.0	0.5
Radius (m)	Magnitude		
100.0	8.2	7.9	7.4
150.0	8.6	8.3	7.7
200.0	8.8	8.5	8.0
250.0	9.0	8.7	8.2
500.0	9.7	9.4	8.8

Impact velocity 30 km/sec			
	Density (g/cm^3)		
	8.0	3.0	0.5
Radius (m)	Magnitude		
100.0	8.4	8.1	7.6
150.0	8.8	8.5	8.0
200.0	9.1	8.8	8.2
250.0	9.3	9.0	8.4
500.0	9.9	9.6	9.1

Impact velocity 50 km/sec			
	Density (g/cm^3)		
	8.0	3.0	0.5
Radius (m)	Magnitude		
100.0	8.8	8.5	7.9
150.0	9.1	8.8	8.3
200.0	9.4	9.1	8.5
250.0	9.6	9.3	8.7
500.0	10.2	9.9	9.4

One of the goals of the study is to develop criteria of the cosmogenic tsunamis identification on the basis of the mathematical simulation.

As numerical computations have revealed, the characteristic features of cosmogenic tsunamis may be the following: a uniform wave radiation in all directions from the impact site, N-type wave profile at great distances from the impact site, a great run-up height with relatively short wave length. The short wave length means that forward momentum is strongly dispersed shoreward, decreasing the depth of a shoreward water invasion, thus diminishing the intensity of a consequent geological record. In the case of a big cosmic body impact huge water mass falling against the shore and coastal mountain ridge can produce rock displacement and landslides, which may result in specific relief changes and traces of paleotsunamis.

ACKNOWLEDGEMENT

The work was supported by Russian Foundation for Basic Research (grant 94-01-00293).

REFERENCES

- Bourgeois, J., T. A. Hansen, P. L. Wiberg, and E. G. Kauffman. 1988. A tsunami deposit in the Cretaceous-Tertiary boundary in Texas. *Science* **241**:167-169.
- Chapman, C. R. and D. Morrison. 1994. Impacts on the Earth by asteroids and comets; assessing the hazard. *Nature* **367**:33-40.
- Gault, D. E. and C. P. Sonett. 1982. Laboratory simulation of pelagic asteroidal impact: Atmospheric injection, benthic topography and the surface wave radiation field. *Geological Society of America, Special Paper* **190**:69-92.
- Glasston, S. and P. J. Dolan. 1977. The effects of nuclear weapons. Washington, DC: US Government Printing Office.
- Kyte, F. T., L. Zhou and J. T. Wasson. 1988. New evidence on the size and possible effects of a late Pliocene oceanic asteroid impact. *Science* **241**:63-65.
- O'Keefe, J. D. and Ahrens, T. J. 1982. The interaction of the Cretaceous/Tertiary extinction bolide with the atmosphere, ocean and solid Earth. *Geological Society of America, Special Paper* **190**:103-120.
- Petrenko, V. E. 1970. The Lagrangian Particle-in-Cell method for the calculation of the dynamics of compressible multi-substance fluids with large deformations. *Computer Center, Novosibirsk, Report* - 58a.
- Roddy, D. J., S. H. Schuster, M. Rosenblatt, L.S. Grant, P. J. Hassig, and K. N. Kreyenhagen. 1987. Computer simulation of large asteroid impacts into oceanic and continental sites - preliminary results on atmospheric cratering and ejecta dynamics. *Int.J.Impact Engng.* **5**:525-541.

Shoemaker, E. 1983. Asteroid and comet bombardment of the Earth. *Ann. Rev. Earth Planet. Sci.* **11**:461-494.

DIVING TO MARIANA TRENCH BY "KAIKO"

Shinichi Takagawa, Taro Aoki, Ikuo Kawana
Japan Marine Science and Technology Center
Yokosuka, Japan

ABSTRACT

Japan Marine Science and Technology Center (JAMSTEC) has completed the development of a full ocean depth research ROV "KAIKO" on March 1995 by the successful trial diving to Mariana Trench. It touched down the bottom and measured the water depth as 10,911.4 m with corrections by temperature and salinity distributions.

In FY1995, JAMSTEC started the training diving starting from the 1,000m water depth and ended with the dives to Mariana Trench. The training dives were successfully finished. Besides the training, JAMSTEC is now constructing a new vessel "KAIREI" ("Ridge" in English) dedicating its mission solely to the operation of the "KAIKO". This ship is scheduled to be completed at the end of March 1997.

During the sea trial and training diving of the "KAIKO", JAMSTEC experienced rotation of the primary cable. A survey of the cause of this rotation gave a new hypothesis on the rotation mechanism of the cable. An on-land experiment supported this hypothesis. JAMSTEC is now planning to establish a new methodology of fabricating the rotation-free cable under this hypothesis.

SEA TRIAL AND TRAINING DIVING

The First Sea Trial Diving to Mariana Trench --- A Failure (Kyo, 1995)

The present "KAIKO" system (see Fig. 1) consists of the free swimming "Vehicle", the "Launcher", which is an underwater stable platform, and the support vessel "YOKOSUKA". The subsystems are connected with cables as shown in Fig. 2.

The development and construction of the hardware of the "KAIKO" was completed in April, 1993. After that, a series of sea trials were carried out. The first diving to the Mariana Trench was carried out on March 1, 1994. But while cruising just above the sea floor of the Mariana Trench at the altitude of only 2m (the corrected water depth of the "Vehicle" was 10,909 m) the signal from the "Vehicle" suddenly blacked out.

JAMSTEC abandoned further trials and recovered the system onto the support vessel "YOKOSUKA". It was very strange that when the "KAIKO" was recovered, the signal transmission was in good condition.

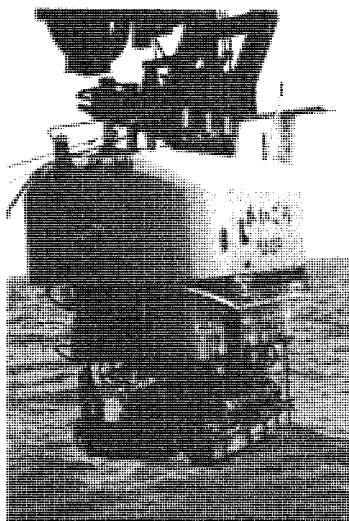


Fig. 1 The ROV "KAIKO"

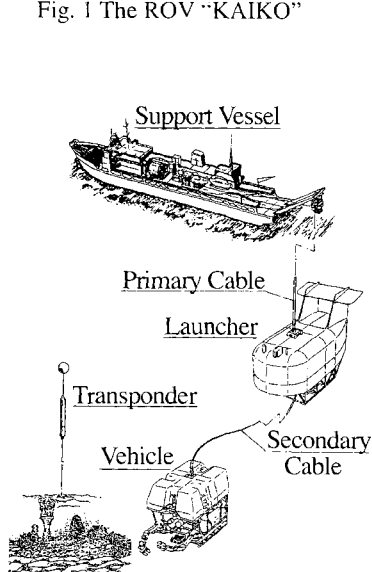


Fig. 2 General Concept of the "KAIKO"

The investigations of the cause of this black-out took a very long time, and finally it was found that the optical fiber in the secondary cable connecting between the "Launcher" and the "Vehicle" had buckled. The mechanism of this buckling was also clarified. The primary cable connecting the support vessel and the "Launcher" is a pressure compensated type cable, and the sea water enters into the gaps between the strength members made of Kevlar FRP (see Fig. 3). Whereas, the strength members of the secondary cable were covered with buoyant rubber, and the sea water cannot enter into the gaps through the rubber (see Fig. 4). The pressure compensation of the strength member is very important in order to keep the flexibility of the cable by allowing the mutual movement of the strength member. Thus, the secondary cable was designed to allow the sea water to enter into the gaps from both ends of the cable by capillarity to make it pressure compensated one.

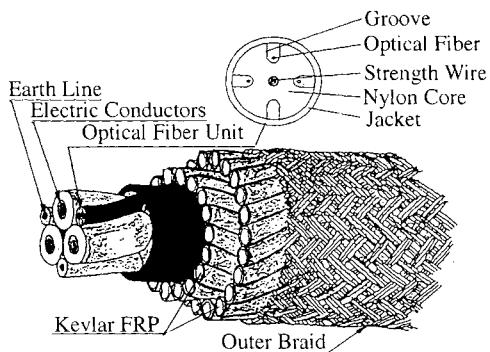


Fig. 3 Structure of the Primary Cable

After the blackout trouble, we found that the attenuation in the optical fiber became a little larger at a point by a few dB stepwise. We cut and opened the rubber around the position, and found that the Kevlar strength member was broken as if it was cut away by knife as shown in Fig. 5. Also, it was found that the sea water didn't enter into this position.

It became clear that the secondary cable was not pressure compensated at this point, and the flexibility was lost due to the very large water pressure. The flexibility-lost cable was bent at the sheave and at the reel, then the strength member was torn.

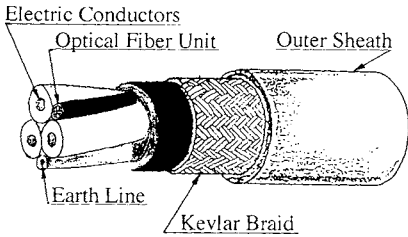


Fig. 4 Structure of the Secondary Cable
*Gelly Rubbed in while Manufacturing
 instead of Sea Water Introduction*

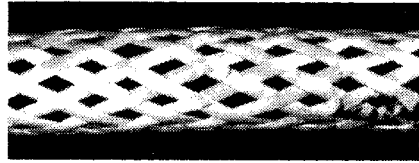


Fig. 5 Break out of the Kevlar Strength Member

The optical fiber in the cable received axial compression force because of the excess length, and it buckled elastically. When the water pressure became small by retrieving the "KAIKO", the flexibility of the cable recovered, and the elastically buckled optical fiber turned to the normal situation.

The break-out of the strength member lead to the loss of torsional rigidity, and the cable was easily twisted. By the twisting motion of the cable,

These are the series phenomena of the trouble which we have found out. Then, we proceeded to the modification method to keep the pressure compensation in any condition. What we did was to paste resin on the Kevlar. This resin acts as pressure compensation agent and also as lubricant agent, and it keeps the flexibility of the cable at any water depth.

The Second Sea Trial Diving to Mariana Trench --- Success (Kyo, 1995)

Using the new secondary cable, and of course after modifications of other subsystems, we conducted the second trial diving to Mariana Trench on 24th March, 1995. The operation was very smooth and the "Vehicle" touched the bottom of the Mariana Trench three hours after the launching from the support vessel. The temperature-salinity corrected depth of the bottom was measured as 10,911.4m. The targeted touch down position was 11° 22.400'N, 142° 35.550'E, whereas the touched down position was 11° 22.394'N, 142° 35.541'E. The difference is only about 20m. The "Vehicle" put down a memorial plate showing "KAIKO 1995.3.24" on the sea floor of the Mariana Trench.

While cruising around the touch down position keeping the altitude of 50cm, a white swarm of a few centimeters long was observed swimming with twisting its body. It was recorded in a video tape. A can was also found which was put on the sea floor at the first diving one year ago. This means that the diving position was the same as that of the last diving, showing the accuracy of the navigation system. When the "Vehicle" returned to the memorial plate, several shrimps were observed gathering to a bait which was put at the same

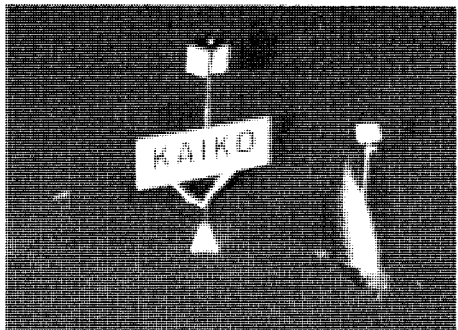


Fig. 6 Memorial Plate, a bait (Mackarel) and shrimps

position with the plate. They were also recorded in the video. Figure 6 shows the plate, the bait, and the shrimps. After observing these creatures, the "Vehicle" left the bottom and mated with the "Launcher", then the both were recovered onto the support vessel.

By this successful diving to the Mariana Trench, the development of the full ocean depth research ROV "KAIKO" was finished.

Training Diving

The training diving leg started on June 1995, starting from 1,000m water depth and finally ending at the diving to the Mariana Trench again. The sea trial was carried out by the manufacturers' operators, but the training diving was carried out by JAMSTEC's crew three times on February through March 1996. The diving point was about ten miles west of the sea trial point as shown in Fig. 7. These dives were also successful, and sampling of mud was carried out. The analyzing of the mud is now underway by microbiologists of JAMSTEC.

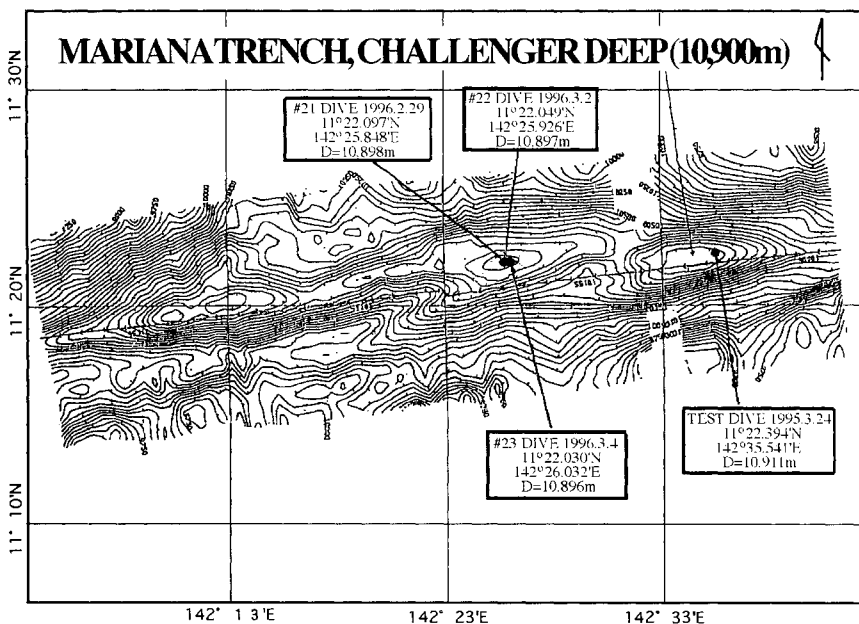


Fig. 7 Touch Down Points of the "KAIKO"

New Support Vessel "KAIREI"

The support vessel "YOKOSUKA" has been so designed and built as to be a support vessel both for the 6,500m manned submersible "SHINKAI 6500" and for the "KAIKO". However, the diving schedule of the two by one support vessel is very much crowded. So, Japanese

Government decided to construct a new support vessel dedicated for the "KAIKO". The construction started in 1995 and is scheduled to be completed on March 1997. The new vessel is named as "KAIREI", which means "Ridge" in English. The hull of the vessel is the same as the "YOKOSUKA", and both are sister ship. Fig. 8 shows the artist drawing of the new vessel "KAIREI". The "KAIREI"- "KAIKO" system will be used for the deep sea survey deeper than 6,500m water depth.

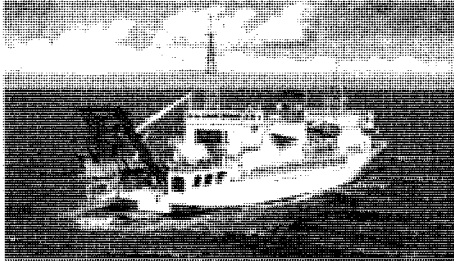


Fig. 8 New Support Vessel "KAIREI"

CABLE ROTATION PROBLEM

JAMSTEC has three tethered deep sea survey systems. The first is the research ROV "Dolphine 3K" capable to dive down to 3,300m deep. The second is the "Deep Tow" capable to dive down to 6,000m deep, and the third is the "KAIKO". All of the cables of these three systems show rotation problems while winding the cable off and up. The materials of the strength members of the cable are different, but the structure is the same, that means, double layered structure with the inner layer twisted in Z way (clockwise), and the outer layer in S way (counter clockwise).

"Dolphine 3K" has changed its cable three times and the No. 4 cable is the newest one. "Deep Tow" changed once and the No. 2 is the newest one. "KAIKO" has only one cable. These seven cables have the same structure of the strength member.

Except the No.4 cable of "Dolphine 3K", the other six cables showed the same rotation. That means, the cable rotated clockwise while winding off and rotated counter clock-wise while winding up. Clockwise rotation means loosing the S way twisted outer layer. The rotation rate is different in cable to cable, but around one turn in 50m to 100m length. However, the No.4 cable of "Dolphine 3K" rotates reverse.

The mechanism of the cable rotation was quite unknown. Furthermore, the reverse motion of the No.4 cable of "Dolphine 3K" made us very much confused.

During the maintenance work at the early stage of the training dive, we experienced twice the expansion of the outer layer strength member of the primary cable like a birdcage. This trouble was mended, but this phenomena indicated to us that the outer layer and the inner layer could slip longitudinally each other.

The torque balance of this type of cable is satisfied when the total tension is shared with the outer and inner strength members at the designed ratio. However, if both layers slip, the tension sharing ratio changes, and the torque balance changes, then the cable rotates.

We supposed that, when a cable passes through a sheave, the outer layer must delay a little as shown in Fig. 9. This delay causes the outer layer to have a larger ratio of tension than designed, which creates a loosening of the twist of the outer layer. This direction of rotation coincides with all cables except the No.4 cable of the "Dolphine 3K".

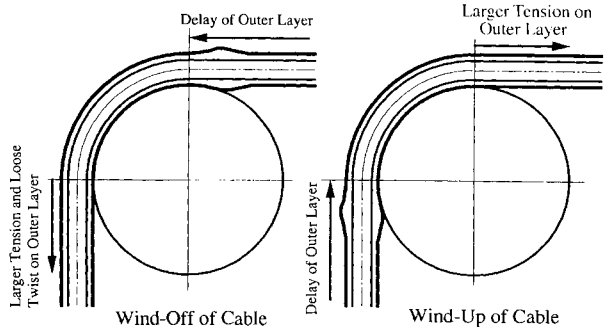


Fig. 9 Delay Run of the Outer Layer at Sheave

The further survey on the cable characteristics showed that the No.4 cable had a peculiarity that silicon oil was adhered on the surface of Kevlar FRP strength member. The cable winch is a friction drum type winch, and when the force is exerted on the cable, the force is transferred to the outer layer of the cable by friction, and then is transferred to the inner layer by friction also. If the friction between the two layers is very small, the force is not transferred so much, then the outer layer runs a little faster as shown in Fig. 10. This situation gives the reverse rotation on the cable just as the No.4 cable of the "Dolphine 3K". Thus, the rotation problem can be explained by the longitudinal slip of the outer and inner layers of the strength members.

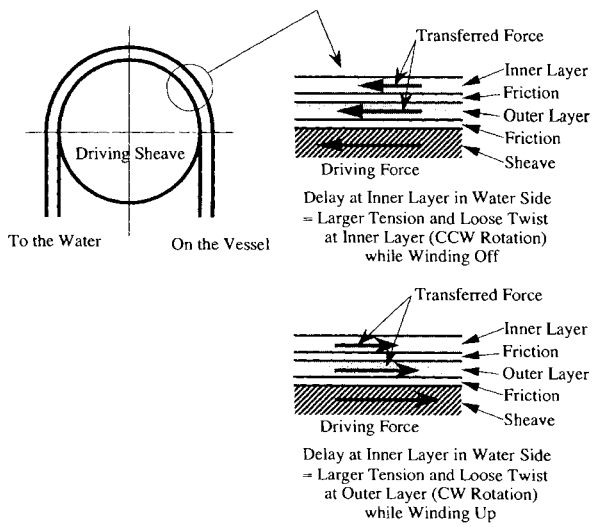


Fig. 10 Effect of Friction on the Delay Run

This is only a hypothesis, and requires verification by experiment. So, we carried out a simple on-land experiment as shown in Fig. 11 using a short primary cable of the "KAIKO". If the hypothesis is correct, both of Fig. 10 Effect of Friction on the Delay Run the angle indication bars on the swivel, seen from the driving sheave side, must turn clockwise when the swivel

moves to the free sheave and must turn counter clockwise when the swivel moves to the driving sheave. The test results showed the same motion as was expected as shown in Fig. 12.

Then, we moved to how to stop this rotation. The cause of the rotation must be longitudinal slip between both layers. The simple way to arrest the slip is to fix both layers, however, this must make the cable non-flexible. So, we introduced a method to fix both layers at a longitudinally straight line with a narrow width as shown in Fig. 13. By this method, each helical member is fixed at one point by every turn, and it is free to move at the other part. This gives free motions to each strength member, yet the longitudinal slip is not allowed.

The test method was the same as shown in Fig. 11, and the cable sample was so set as to make the fixed line face up the outer side of the bending curvature of the sheave. The reason is that there is no mutual motion between the two layers at the outer and inner side of the bending curvature of the sheave, and the outer side is stable position whereas the inner side is unstable position.

The test results were as we expected, and the angle indicator would not move as shown in Fig. 14.

We wanted to confirm the reverse motion as experienced by No.4 cable of the "Dolphine 3K" using the test equipment shown in the lower part of Fig. 11, which gave the tension difference around the sheave, but we had already consumed cable samples and we couldn't do it.

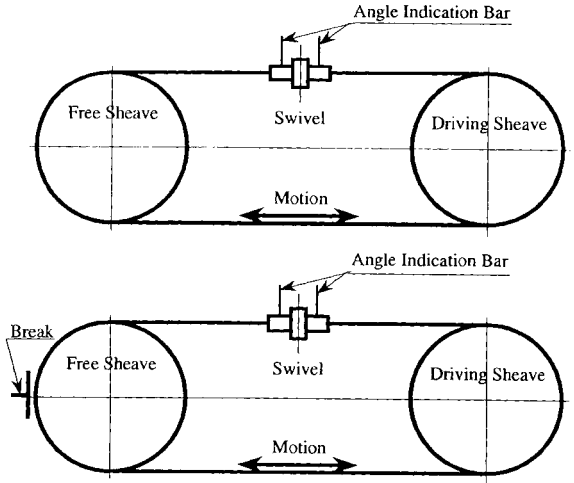


Fig. 11 Test Equipment for Cable Rotation

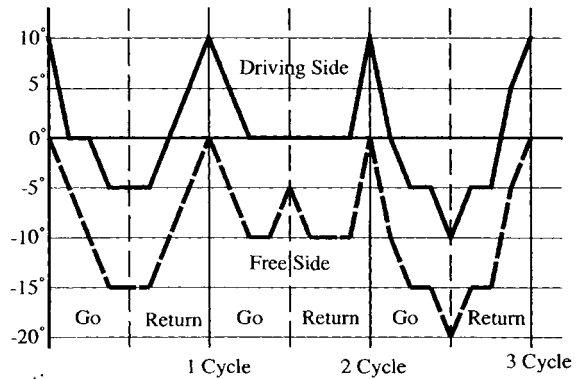


Fig. 12 Rotation of Normal Cable

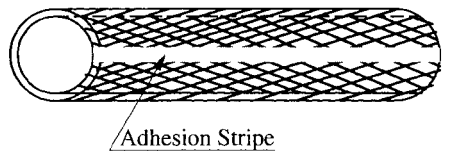


Fig. 13 Fixation Method by Adhesive Agent in One Line

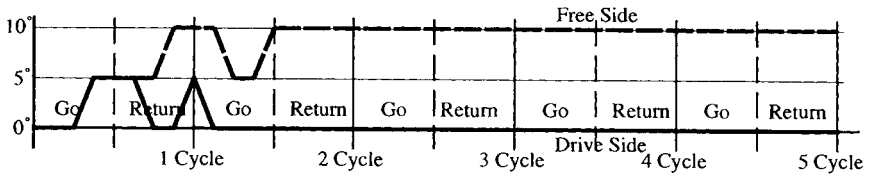


Fig. 14 Test Results of Rotation Free Cable

The hypothesis seems very good to explain the cable rotation problem, however, the method to adhere both layers is not good for actual application to the cable. The first reason is that the adhesive material is easily peeled off. The second reason is much more serious. As is mentioned above, the outer side of the bending curvature of the sheave is stable for the fixed line, and the fixation of both layers at one narrow line makes the cable loose omni-directionality.

We are planning alternative methods. One is to use braided plate with racks. These racks allow the strength member to move in a helical direction, but arrest the longitudinal slip, keeping the flexibility and omni-directionality.

REFERENCES

Kyo, M. 1995. The Sea Trial of "KAIKO", the Full Ocean Depth Research ROV. In: Oceans '95 Conference Proceedings. October.

UNDERWATER TELEROBOTICS AND VIRTUAL REALITY: A NEW TECHNOLOGY PARTNERSHIP

Steve Murray and Doug Murphy
Naval Command, Control and Ocean Surveillance Center
San Diego, CA, U.S.A.

ABSTRACT

Despite major advances in autonomous vehicle technologies, human-controlled ROVs (remotely-operated vehicles) continue to fill an important role in underwater work. To perform effectively, however, the human operator requires meaningful cues for spatial orientation, good workspace visibility, and tight feedback about manipulator behavior. These needs can be hard to support in actual undersea operations. Telerobot designers for space missions have addressed these challenges by presenting a graphic, virtual reality model of the workspace to the operator, who then performs tasks on this representation of the actual work site. Real-time graphic modeling can (1) maintain a continuous, clear depiction of the workspace that is largely independent of communications bandwidth, (2) allow arbitrary shading and perspective of the workspace, (3) provide integrated navigation and orienting cues, and (4) support a rich, multi-sensory feedback environment.

The use of virtual reality technologies for operator interface design is being investigated at NCCOSC for undersea ROV applications. A general-purpose virtual reality testbed is described which involves a dedicated virtual reality system for underwater applications, together with a manipulator system and supporting software. The objectives of the testbed are to examine fundamental human performance and engineering issues connected with operating on a virtual workspace for real telerobotic tasks, and to benchmark emerging telerobotic technologies in a standardized test environment.

INTRODUCTION

The U.S. Navy performs a wide range of undersea missions including deep water search and recovery, mine detection and removal, ship servicing, sensor placement, and support for scientific research. For many missions, the choice of telerobotic systems over human divers is driven by operational requirements (e.g., water depth, environmental hazards, etc.) and by concern for human safety. Unfortunately, an ROV is almost never as effective as a human diver performing the same work. While human perception, decision-making, and manipulation are essential for most underwater tasks, constrained sensory feedback from the work site (via cable or acoustic links) limits the performance that can be currently achieved with telerobotic systems and provides a relatively poor substitute for direct human presence (e.g., Pepper, 1986).

There are many impediments to good operator feedback. TV cameras and other imaging sensors, for example, are usually mounted at fixed points on the remote vehicle, with restricted

fields-of-view or adjustment ranges. Operator perspective on the environment is therefore tied to whatever "tunnel view" can be achieved through the sensors by vehicle positioning and self-contained lighting. Support references for navigating to the work site, orienting to the workspace (i.e., vehicle station-keeping), and manipulator operation are gathered through other devices and displays which the operator must mentally integrate into a single picture of the immediate environment. A representative operator station for performing these tasks is shown in Figure 1.

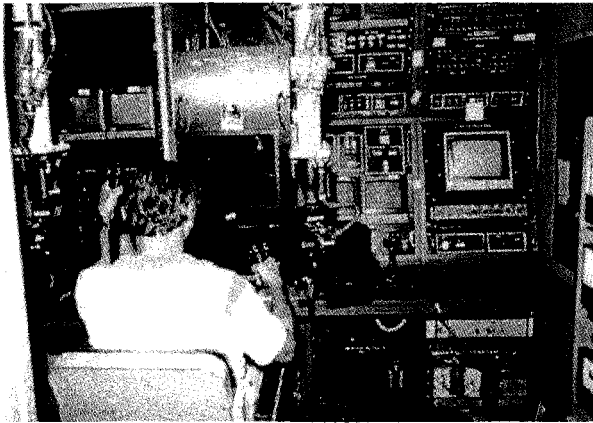


Figure 1. Conventional telerobotic control station

In addition, many tasks take place close to the ocean bottom, where sediment is stirred up by water currents or work activities. This further limits visibility of the workspace and reduces effectiveness by forcing divers or ROV operators to stop work until the sediment clears, i.e., a "move and wait" strategy.

Limited operator feedback and poor interface design constrain task productivity and extend task completion times. These effects, in turn, generate higher costs for surface support resources.

Mediated Telerobotics: the Virtual Reality Interface

Space telerobotic systems, being developed for satellite servicing missions, must support precise manipulation. This requires timely and accurate operator feedback about the remote work site, communicated with a limited-bandwidth, time-delayed channel (e.g., Sheridan, 1992). Designers of such systems have utilized graphical, predictive operator interfaces as a method for achieving the necessary feedback support with considerable success (e.g., Schenker, et al, 1991; Kim, 1993). The operator of such a telerobot acts on an artificial depiction of the work environment, while the computing subsystems process raw sensor information to ensure that the depiction is physically matched to the real environment. The operator can test and preview the effects of manipulator action in this surrogate environment before these actions are physically executed. Because most of the data processing occurs locally, i.e., at the operator station, the amount of command information that is actually sent to the telerobot site is minimized. This reduces the required bandwidth for communication with the remote vehicle.

Telerobotic interfaces are distinguished from the larger domain of virtual reality systems in that operator actions are ultimately realized in the physical world. Virtual reality is nevertheless an integral part of any telerobotic system, in that the operator is physically removed from the work

setting and all actions are based on its representation (i.e., via the operator's displays). Virtual reality techniques have been successfully used to support real-time operator performance in a great many physical environments including aircraft piloting (e.g., Furness, 1986), data visualization (e.g., Fisher et. al., 1987), and manipulation of scaled physical objects (e.g., Brooks, 1988), as well as telerobotics (e.g., Tachi et. al., 1994).

Virtual reality techniques can fuse real sensor data into an integrated depiction of the remote environment, and can enhance that depiction to support operator needs. Examples of such techniques include:

1. the ability to arbitrarily establish lighting and shadowing to support the best scene visibility. "Virtual lights" can be created and placed without regard for the constraints of physical equipment (Figure 2);

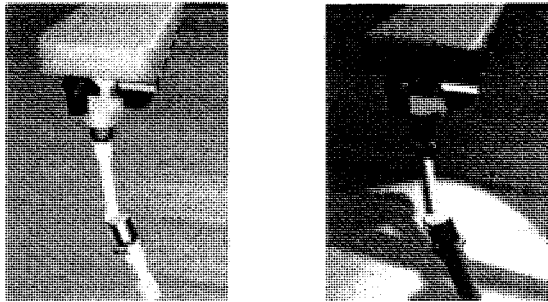


Figure 2. Virtual reality scene with and without arbitrary lighting and shading

2. the ability to establish arbitrary viewpoints of the work area (i.e., different viewing angles or distances, or multiple perspectives). Because all characteristics of the display are computer-generated, the operator controls "virtual sensors" that are independent of constraints at the work site, such as physical obstructions or visual interference by the manipulator itself (Figure 3). This can provide information about unseen features of the work space or unseen consequences of manipulation;

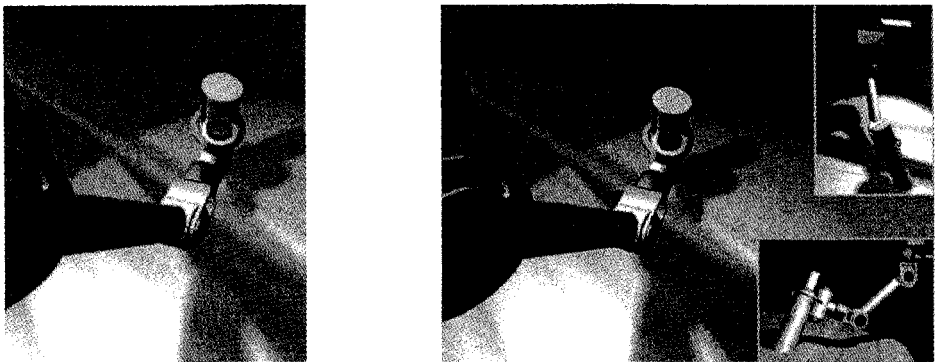


Figure 3. Multiple views of manipulator and work space combined in a single virtual reality interface

3. the ability to generate seamless, 360-degree views of the environment surrounding the work site, out to essentially arbitrary ranges. Such "virtual visibility" offers a large-scale context that can aid underwater navigation and search tasks, and can furnish a better sense of vehicle orientation in three-dimensions.
4. the capability to provide multi-sensory operator feedback, e.g., via integrated visual, auditory, and haptic displays. Human manipulation skills are almost entirely multi-sensory in nature and multi-sensory display has historically been a central thrust of virtual reality technology development (Burdea and Coiffet, 1994).

THE NCCOSC PROGRAM IN TELEROBOTICS AND VIRTUAL REALITY

The significant potential of virtual reality applications in telerobotic design is accompanied by an equally significant set of development issues requiring research and engineering attention. NCCOSC is addressing some of these issues by combining its experience with telerobot development (e.g., Shimamoto, 1993) and virtual reality systems (e.g., Murray, 1995) in a new research effort. The program focuses on benchmarking operator performance as a function of changes in virtual reality model characteristics. A unique, virtual reality-based testbed facility is being developed to support these investigations.

Research testbed facility

The NCCOSC test bed facility consists of a virtual environment interface and control system, a Western Space and Marine, Inc. MK-37 remote manipulator (typical of many systems used for underwater work) and a hardware/software architecture designed to support both in-house and collaborative research efforts.

The hub of the research facility consists of the Virtual Environment for Undersea Telepresence (VEUTel), a system developed by Innovation Associates, Inc. (Schebor, 1994) under a Small Business Innovation Research (SBIR) project. VEUTel (Figure 4) is a virtual reality interface system designed expressly for control of a remote underwater telerobot. VEUTel features:

1. an advanced three-dimensional, stereoscopic display of the remote telerobotic work space. The display can be implemented on a conventional flat-panel (CRT) display or on a head-slaved helmet-mounted display (HMD);
2. dynamic creation and updating of the virtual reality model using an integrated, vision-based tracking system at the remote vehicle to measure and correct deviations between the simulated and real environments;
3. an advanced human-machine interface employing an intuitive, virtual reality interface with multi-modal user interaction. The interface supports complete sensor and manipulator control through a conventional telerobot master system, through a computer-linked glove, and through voice command. All controls and system status data are integrated into the virtual

environment itself, so the operator can access any required information in a single, immersive display;

4. a flexible, object-oriented software architecture to generate remote scene environments and objects, and to accommodate alternate hardware configurations (e.g., alternative manipulators, arms, or control dynamics). Such flexibility will support the integration of tactile sensors into later phases of the research program without major changes to other VEUTel components.

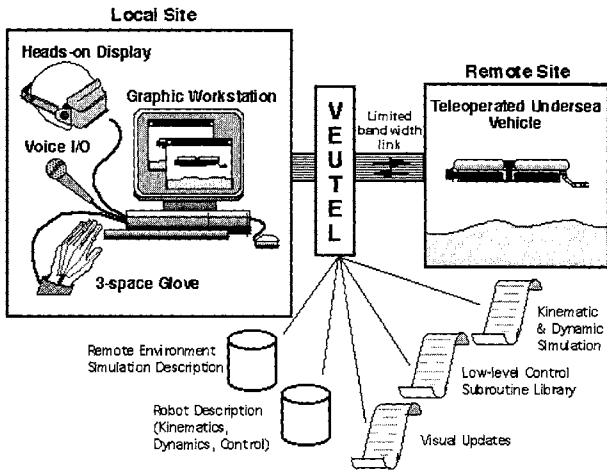


Figure 4. VEUTel system components and architecture

Research program

The NCCOSC research program seeks to develop data bases of operator performance as functions of interface characteristics. This is achieved in phases, by first measuring performance of basic operator actions, and then moving to more complex, operationally-relevant tasks. Visual interface features are examined first, followed by other forms of operator feedback, particularly haptic displays.

Operator performance benchmarks are generated through a standardized battery of perceptual-motor tasks. The test battery involves a series of very elemental actions (e.g., move, rotate, grasp, turn, etc.), which are individually measured and modeled for time and accuracy. Performance prediction for a complex task can then be done analytically, by breaking the complex task down into its constituent elemental actions and adding together the appropriate model data. The technique has an extensive history in human work performance measurement and its use as a human-machine performance tool has been advocated elsewhere (e.g., Pepper and Kaomea, 1988). Advantages of this approach are: (1) the test battery can be applied across different telerobot and display configurations for system comparisons, (2) the use of elemental

actions can help to identify specific engineering deficiencies in the human-machine system (e.g., backlash in the manipulator arm for linear movements of different lengths), and (3) predictions of "real world" performance can be made for novel tasks that may never have been performed before.

NCCOSC is located adjacent to several U.S. Navy communities that use ROVs and manned submersibles for underwater work. Volunteer operators from these communities will be used to generate the performance data bases for the perceptual-motor task series. Tests are conducted using direct vision as the baseline, i.e., where the operator can directly view the work space. The test battery is repeated using a set of virtual reality depictions with differing characteristics (e.g., with and without control of scene perspective, with and without control of light and shade, etc.). Because the physical work space and the virtual reality depiction are both implemented in the laboratory, model accuracy and performance measurement can be precisely controlled.

The second phase of the NCCOSC program involves testing with a set of operational tasks, defined by the Navy operators, under the same series of display conditions. Empirical performance with these more complex tasks will be compared to predicted performance from the modeling technique described earlier. If the results are in sufficient agreement, then two objectives will be achieved: (1) the use of standardized tasks as a benchmarking method will be validated. If such validation is obtained, then the methods can be applied across other telerobotic applications and systems, providing a reliable general-purpose tool for performance characterization and prediction, and (2) the relative contribution of different visual display features (e.g., perspective control, lighting control, etc.) to performance support can be evaluated by measuring the sensitivity of task performance to the presence or absence of these features. Such data can be used to model different telerobotic systems and tasks.

Research collaboration

NCCOSC expects to introduce haptic feedback and other multi-sensory displays into its research program through collaboration with other laboratories, where studies of haptic performance are already in place (e.g., Cutkosky et. al., 1992). Most human activities are multi-sensory in nature, and additional feedback modes can supplement the visual sense in important ways. Haptic feedback is a logical first choice for multi-sensory investigations in that the sense of touch and feel may provide the primary means for updating the underwater world model used for the virtual reality interface, especially if the location, orientation, or condition of the work space is not precisely known or if imaging sensors (e.g., video cameras, ultrasound, laser, etc.) cannot provide sufficient information. It has been demonstrated, for example, that a visual model of an unknown object can be built up solely by registering the physical locations of contact events from a telerobot end effector (e.g., Driels et al, 1992; Fyler, 1981).

The VEUTel architecture of the NCCOSC research testbed can be easily reconfigured to add haptic feedback, although the motor performance test battery used for visual displays will require extensions to include such task-relevant characteristics as slip detection and grip force. The fundamental testing concept is similar, however, for both visual and haptic feedback modes.

Further approaches to operator support

Generating an immersive, virtual reality scene for telerobotic operations is not difficult. Ensuring that the scene correctly represents the physical world, however, and that operations on that world are updated in a timely fashion is a formidable challenge. Moving a remote manipulator in the absence of accurate feedback can be both inefficient and dangerous. It falls to investigations such as those described here to determine exactly how accurate the virtual reality scene needs to be, and how rapidly it must be updated. Once such (probably task-dependent) data are developed, however, many interesting support tools can be added to the operator's display to assist performance.

Using an alternate application of virtual reality, the displayed scene might rely on raw imaging with graphical overlays to provide enhancements for recognizing task-critical elements of the work space. This approach has been taken in space applications studies for satellite repair missions (e.g., Bejczy et. al., 1990; Kim, 1993). It provides the operator with immediate recognition of a problem when the raw (although possibly degraded or time-late) scene image and its graphical overlay do not match. To the extent that the raw image must be updated, communication bandwidth requirements increase. With the use of high bandwidth fiber-optic data links in most current ROV systems, however, this is not a severe penalty. The performance gain comes from the design of the graphical overlays, which can contain special highlighting information to guide operator procedures, provide interactive decision support to the operator, or offer hazard warnings.

In addition to providing a clear view of the underwater work scene, a virtual reality interface can add elements to the image as necessary, to guide a desired operator behavior. "Virtual landmarks" or navigation grids, for example, with horizon lines or highlighted depictions of bottom terrain (from existing data bases or real-time mapping of the sea floor) could help the operator to navigate and orient to the work site. On a smaller scale, visual or haptic markers could be inserted into the environment as guides for a specific manipulator path, to help the operator locate particular regions of an object, or as barriers, to help the operator avoid certain sensitive or dangerous regions of the work site (e.g., Rosenberg, 1992; Sayers and Paul, 1994). The underlying theme of these virtual reality applications is that the relation between the real and artificial worlds need not be a one-to-one mapping; information can also be modified or enhanced to obtain a desired operator performance.

Summary

NCCOSC is beginning a new program in ROV operator interface development that focuses on immersive, virtual reality methods for system control. The program is distinguished from similar efforts in its use of a reconfigurable test bed (VEUTel) and a standardized benchmarking method for performance measurement. The objectives of the NCCOSC effort are to develop and demonstrate the utility of a virtual reality interface, to develop time and accuracy performance data for a core set of elemental actions as functions of virtual reality display features (e.g., perspective, scale, light and shadow, multiple views, etc.), and to define a model of human information processing that relates these display features to skilled task performance.

REFERENCES

- Bejczy, A., W. Kim, and S. Venema. 1990. The phantom robot: Predictive displays for teleoperation with time delay. In: Proceedings of the 1990 International Conference on Robotics and Automation. Cincinnati, OH. May.
- Brooks, F. 1988. Grasping reality through illusion: interactive graphics serving science. In: Proceedings of SIGCHI-88. May.
- Burdea, G. and P. Coiffet. 1994. Virtual Reality Technology. New York: John Wiley & Sons, Inc.
- Cutkosky, M., R. Howe, R. Johansson, G. Westling, and B. Edin. 1992. Tactile sensing and control in humans and robotic/teleoperated systems. Final report (Contract N0001490J4014). Stanford University Department of Mechanical Engineering.
- Driels, M., H. Spain, and W. Aviles. 1992. The effect of sensory feedback on the identification of objects using a teleoperator. In: Automation in Construction 1. Amsterdam: Elsevier.
- Fisher, S., M. McGreevy, J. Humphries, and W. Robinett. 1987. Virtual interface environment for telepresence applications. In: Proceedings of ANS International Topical Meeting on Remote systems and Robotics in Hostile Environments. J. Berger (Ed.).
- Furness, T. 1986. The super cockpit and its human factors challenges. In: Proceedings of the Annual Meeting of the Human Factors Society. vol. 1.
- Fyler, D. 1981. Computer graphic representation of remote environments using position tactile sensors. SM Thesis, Massachusetts Institute of Technology, August.
- Kim, W. 1993. Graphical operator interface for space telerobotics. In: Proceedings of IEEE International Conference on Robotics and Automation. Atlanta, GA.
- Murray, S. 1995. The NCCOSC Virtual Presence Program. HCI International, Yokohama, Japan. July.
- Pepper, R. 1986. Human factors in remote vehicle control. In: Proceedings of the Annual Meeting of the Human Factors Society. Santa Monica: HFS.
- Pepper, R. and P. Kaomea. 1988. Teleoperation: Telepresence and performance assessment. Presented at the International Ergonomics Society Annual Meeting, Bristol, UK.
- Rosenberg, L. 1992. The use of virtual fixtures as perceptual overlays to enhance operator performance in remote environments. Technical Report, Center for Design Research, Stanford University. September.

Sayers, C. and R. Paul. 1994. An operator interface for teleprogramming employing synthetic fixtures. *Presence*, 3(4).

Schebor, F. 1994. VEUTel: A virtual environment for undersea telepresence. Technical Operating Report, Innovation Associates (Navy Contract: N66001-94-C-7010).

Schenker, P. S., A. T. Bejczy, W. S. Kim and S. Lee. 1991. Advanced man-machine interfaces and control architecture for dexterous teleoperations. In: *Proceedings of IEEE Oceans '91*. Honolulu, HI.

Sheridan, T. B. 1992. *Telerobotics, automation, and human supervisory control*. Cambridge, MA: MIT Press.

Shimamoto, M. 1993. Teleoperator/telepresence system (TOPS) concept verification model (CVM) development. In: *Recent Advances in Marine Science and Technology 92*. N. Saxena (Ed.). pp. 97 - 104. Honolulu: PACON International.

Tachi, S. and K. Yasuda. 1994. Evaluation experiments of a teleexistence manipulation system. *Presence*. 3(1).

A MODEL BASED SELF-DIAGNOSIS SYSTEM FOR AUTONOMOUS UNDERWATER VEHICLES USING NEURAL NETWORKS

Motoyuki Takai and Tamaki Ura

University of Tokyo
Tokyo, JAPAN

ABSTRACT

In the underwater environment it is not easy to predict all situations and phenomena such as current force, sudden change of temperature and so on. Installation of a proper scheme to cope with unexpected troubles is, therefore, essential when Autonomous Underwater Vehicles (AUVs) carry out their mission out of human's reach. In order to supervise whether the vehicle operates itself in an appropriate way, this paper proposes a model based approach to self-diagnosis for AUVs. This system includes self-diagnosis which is carried out based on a dynamics model of an AUV and an active mechanism to get desirable information for diagnosis. The dynamics model is constructed by an artificial neural network taking advantage of its flexible learning capability. When a sensor is found to be defective, dead reckoning using its corresponding output of the dynamics model can be introduced in order to cope with the defect.

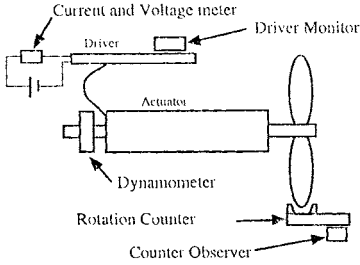
The performance of the proposed system was examined by implementing it to "The Twin-Burger", an actual test-bed AUV. It is shown that the system detects failures of onboard sensors and actuators without introducing extra sensors for the detection, and then selects a proper action scheme to reduce the damage to the AUV.

INTRODUCTION

In order to carry out the mission successfully under the unpredictable condition of high pressure and darkness of the sea, it is essential for Autonomous Underwater Vehicles (AUVs) to be implemented with high performance autonomies. The autonomies include an ability to supervise hardware conditions of the vehicle. Healey (1992) discussed a use of Kalman filters to identify the vehicle's dynamics and an artificial neural network for pattern classification, and Orrick et al. (1994) reported a method to detect failures by sensor fusion.

There are two ways of monitoring the condition of the vehicle: (1) A direct monitoring method which supervises the hardware condition using special sensors; and (2) An indirect monitoring method which checks the relation between causes and phenomena appeared to the vehicle. Figure 1-(1) shows an example of the method (1) referring to monitoring a propeller thruster. It is usual to attach a counter to measure the rotation. But it is impossible to tell either the propeller or the rotation counter is defective when the output of the counter is not as expected. In case that the counter is found to be defective, the vehicle may continue its mission disregarding its defect.

(1) Direct Monitoring



(2) Indirect Monitoring

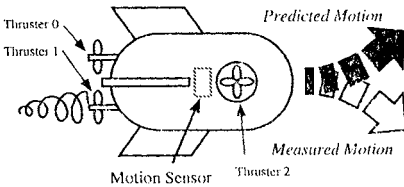


Figure 1. Two ways of self-diagnosis

Thus, we have to attach many supervising sensors in order to identify the defect as illustrated in Figure 1-(1). This method is straightforward and it leads the vehicle's hardware to be complex and heavy.

An alternative method is shown in Figure 1-(2) as the indirect monitoring. The AUV with three thrusters and a motion sensor is evaluated as not in normal condition when the motion sensor measures that the vehicle goes right even though only the right thruster is running. It is presumed that the right thruster or the motion sensor may be defective else unexpected force is applied on the vehicle. This indirect monitoring can be realized by comparing the predicted normal motion of the vehicle with the measured motion: i.e., comparing the outputs of a dynamics model of the vehicle with the actual sensor outputs.

In this paper, we propose a model based diagnosis system which contains a dynamics model constructed by an artificial neural network to predict sensor outputs induced by the motion of the vehicle. In order to diagnose in detail, the proposed system contains a mechanism to actively obtain necessary information for diagnosis. In case that a certain fault is detected, the system can select an action to cope with the trouble. The performance of the proposed self-diagnosis system is examined through tank tests using a test-bed AUV called "The Twin-Burger" (Fujii et al., 1993; Ura et al., 1993).

STRUCTURE OF SELF-DIAGNOSIS SYSTEM

Assumptions

In order to simplify the problem, four assumptions are introduced.

- (1) The vehicle is in steady environment: i.e., changes of the characteristics of the vehicle's motion depend on its hardware condition only.
- (2) In any instance, only one of onboard sensors and actuators may be defective.
- (3) For a particular sensor or an actuator, the condition is either normal or totally defective.
- (4) The defective condition lasts till the end of the self-diagnosis.

Subsystems of Self-Diagnosis

The Proposed self-diagnosis system consists of two subsystems.

(1) Model Matching Part (MMP)

The MMP includes a dynamics model which represents the characteristics of the vehicle's motion. The MMP produces index values which are the result of comparing the sensor outputs with the corresponding model outputs (cf. Figure 2).

(2) Diagnosis Part (DP)

In the DP, the index values from the MMP are used to identify the defective component of the vehicle and the next action scheme is decided to cope with the defect. When the information to identify the defective component is insufficient, the DP selects an appropriate predefined motion sequence of the vehicle for the purpose of collecting necessary information (cf. Figure 3).

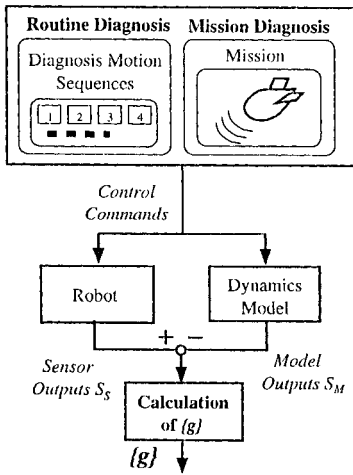


Figure 2. Structure of the Model Matching Part (MMP)

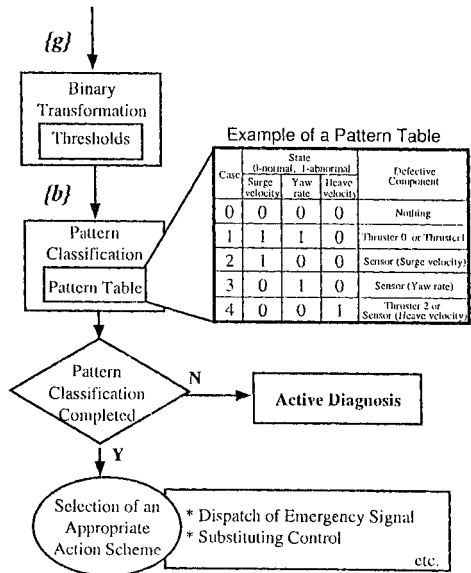


Figure 3. Structure of the Diagnosis Part (DP)

Routine Diagnosis and Mission Diagnosis

As shown in Figure 4, the proposed system introduces two procedures of diagnosis which are named “Routine Diagnosis” and “Mission Diagnosis” in accordance with the situation when the diagnosis is carried out.

Routine Diagnosis

The Routine Diagnosis (Takai et al., 1995) is designed to be carried out exclusively. For example, the vehicle executes the Routine Diagnosis before starting a mission in order to check the hardware.

In the Routine Diagnosis, the vehicle operates based on one of predefined motion sequences called “Diagnosis Motion Sequences (DMSs)”. The DMS is a fixed time history of control commands to the actuators. In order to design suitable DMSs for self-diagnosis, it is essential to take into account that the characteristics of the vehicle’s dynamics have to be measured by the onboard sensors. By carrying out one of the DMSs, the MMP compares the induced sensor outputs with the model outputs and calculates index values as their differences. Then, the DP determines whether the vehicle is in normal condition or not by referring to a predefined table called “Pattern Table”.

In some cases, execution of only one DMS may be insufficient to identify the defective component. Then, the Routine Diagnosis selects and carries out another DMS to narrow down the doubtful components.

Mission Diagnosis

The Mission Diagnosis is introduced to supervise hardware condition of an AUV all through a mission. The MMP continually compares the dynamics model outputs with the sensor outputs during the mission, and the DP verifies whether a fault exists or not. When a fault is detected, the system selects an appropriate action in order to cope with the fault: e.g., interruption of the mission or carrying out the Routine Diagnosis to identify the fault.

Structure of Model Matching Part (MMP)

Dynamics model

In underwater environment, the characteristics of AUV’s dynamics is usually nonlinear. Therefore, its mathematical model should be able to represent the nonlinearity. Furthermore the computational load for calculating the model outputs has to be minimized because the payload of the AUV is in general strictly limited.

Considering these situations, an artificial neural network is suitable for representing nonlinear dynamics of the system taking advantage of its flexible learning capability (Fujii et al., 1990 and 1994). It should be emphasized that the constructed network can be adapted quickly for changes

of vehicle's dynamics due to modifications of the vehicle's hardware: e.g., attaching new sensors.

Structure of dynamics model

The structure of the dynamics model based on an artificial neural network is shown in Figure 5 considering the following five points.

- (1) Inputs of the neural network are control commands to actuators and sensor outputs which correspond to the state variables of the vehicle.
- (2) In order to train quickly and refine the network, the outputs of the output layer are changes of sensor outputs in a specific time interval Δt (Ura et al., 1992).
- (3) In order that the neural network generates outputs without being affected by the failure of a sensor, input state variables to the input layer are given through RC_1 after integrating the outputs of the output layer (Ishii et al., 1994). Therefore, the initial values of inputs have to be fed based on the actual outputs of the sensors.
- (4) The neural network should have multiple inputs and multiple outputs to cover full degrees of dynamics' freedom, because there exist nontrivial interactions among dynamics modes: e.g., surge, sway, heave and yaw.
- (5) The neural network has recurrent connections RC_2 that hold the past sequences of vehicle's state variables.

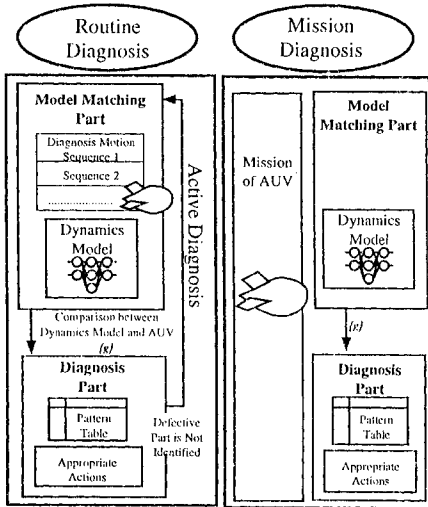


Figure 4. The Routine Diagnosis and the Mission Diagnosis

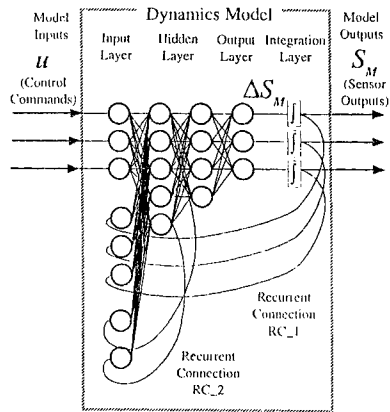


Figure 5. Dynamics model constructed by an artificial neural network

The neural network is trained well by dividing the process into some stages based on the proposal by Ishii (1995) and Takai et al. (1995) using Error Back Propagation method.

Model Matching Process

When the dynamics of the vehicle has been changed, the magnitude of the change can be expressed by introducing the index vector $\{g\}$ whose elements g_i are defined in equation (1):

$$g_i(k) = \frac{100}{KRi} \sum_{j=k-K}^k |SS_i(j) - SM_i(j)| \tag{1}$$

where i denotes the physical quantity to be measured by a sensor, and k the time step. S_{Si} and S_{Mi} are sensor and model outputs which correspond to index i , respectively. R_i is a constant to normalize the difference, and K is a sample time to be averaged. The g_i is expressed as a percentage being multiplied by one hundred.

Structure of Diagnosis Part (DP)

The DP identifies the defective component and selects an appropriate action to cope with the defect using the index vector $\{g\}$ passed from the MMP (cf. Figure 3).

In order to realize the function of the DP, g_i is transformed to a binary number b_i : i.e., if g_i is more than the threshold value in index i , b_i is 1, otherwise 0. The values of thresholds which can detect failures of components of the vehicle should be determined in advance by examining a time history of g_i when the component is defective. Then $\{b\}$ is a vector whose elements are either 0 or 1.

The DP classifies the vector $\{b\}$ on the basis of a table which is named "Pattern Table". The Pattern Table describes the correspondence between a vector $\{b\}$ and a fault. For example, in case of the vehicle shown in Figure 1 with three thrusters and motion sensors for surging, yawing and heaving velocities, the Pattern Table can be determined as shown in Figure 3. When the vector $\{b\}$ is $\{1,0,0\}$ of Case 2, it is concluded that the velocity sensor for surging is defective.

In the Routine Diagnosis, the DP classifies the vector $\{b\}$ after a selected DMS has been completed. There exist, however, some cases that the system can not identify the defective component: e.g., in Figure 3, when the vector $\{b\}$ is $\{1,1,0\}$ the system can only conclude that the Thruster 0 or 1 may be defective. For those cases, the DP selects an appropriate DMS to acquire necessary information for identification: this selection and the following execution of model matching and diagnosis is named "Active Diagnosis".

In the Mission Diagnosis, the DP continually classifies $\{b\}$ when the MMP calculates the $\{g\}$ all through the mission. When even one element of $\{b\}$ becomes 1, the system stops the mission and selects an appropriate action: e.g., dispatching emergency signals, discharging emergency ballast, ascending to the surface and returning to the operator using substituting control to be described in

the next paragraph. When the defective component is not identified, the Routine Diagnosis can be followed.

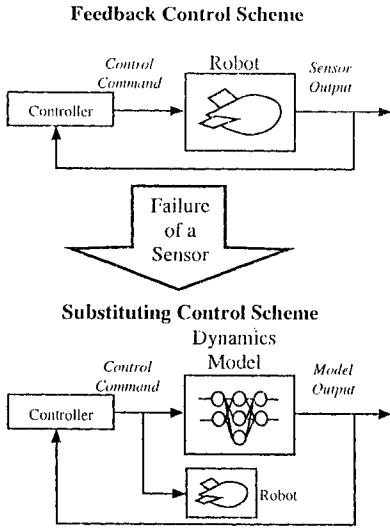


Figure 6. Substituting Control

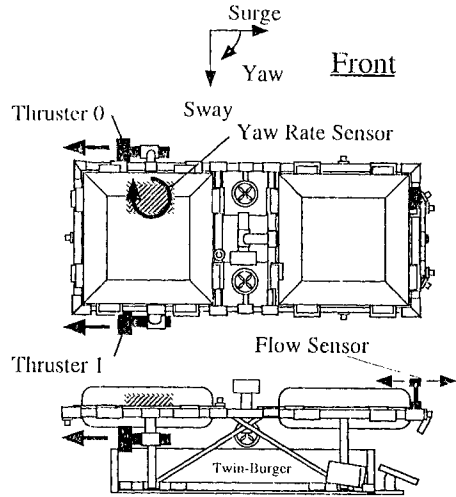


Figure 7. Top and side view of the Twin-Burger

Substituting Control

When a sensor failure is identified, the sensor outputs S_{Si} can not be used in feedback control loop. But the outputs of the dynamics model S_{Mi} is available instead of S_{Si} for control as shown in Figure 6 though it includes a little error. Consequently, the vehicle can proceed the mission using S_{Mi} in such an occasion. This control scheme is a kind of dead reckoning, which is named “Substituting Control”.

IMPLEMENTATION OF SELF-DIAGNOSIS SYSTEM

The proposed system is implemented to an actual AUV named “The Twin-Burger” as shown in Figure 7. The target components of the vehicle to be self-diagnosed are those involved in surging and yawing motions: i.e., “Flow Sensor” which measures the longitudinal relative flow velocity, “Yaw Rate Sensor” and actuators “Thruster 0” and “Thruster 1”.

Construction of Model Matching Part

Diagnosis Motion Sequences (DMSs)

Three kinds of Zigzag test are prepared for DMSs as illustrated in Figure 8. “ZA” where both Thruster 0 and 1 are concurrently actuated, is designed to be carried out at the first step in the Routine Diagnosis. “ZB” and “ZC” are the sequences where only one thruster (the Thruster 0 or 1) is actuated.

Construction of dynamics model

An artificial neural network shown in Figure 9 is constructed to represent the dynamics of the Twin-Burger. The inputs to the input layer are control commands to each thruster and sensor outputs, and the outputs of the output layer are the differences of sensor outputs in a specific time interval Δt . Teaching data are sampled by operating the vehicle in normal condition according to the ZA, ZB and ZC and also a mission scenario consisting of clockwise and counterclockwise square-path following of 5 by 2.5 meters.

The neural network is trained until its model output errors were reduced to about 0.0175 [m/s] for Flow Sensor and 0.0168 [rad/s] for Yaw Rate Sensor. Figure 10 shows the time history of teaching data and trained model outputs of a path following mission. Although some disagreement in Flow Sensor exists from forty seconds to sixty seconds when the vehicle is turning, it can be said that the trained neural network represents the dynamics of the vehicle in good precision for the proposed self-diagnosis.

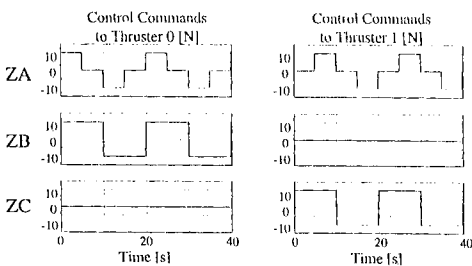


Figure 8. Diagnosis motion sequences (DMSs)

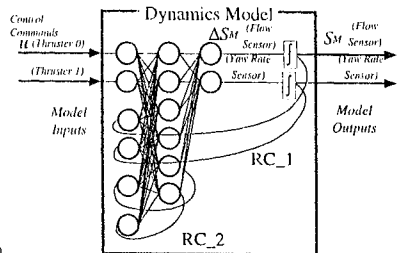


Figure 9. Dynamics model constructed for the Twin-Burger

Construction of Diagnosis Part

Threshold values

In order to determine the threshold values of g in Eq. 1 for binary transformation in the DP, the Twin-Burger was operated in defective conditions by decreasing the power of each thruster. The threshold values were determined as shown in Table 1. In this table, R in Eq. 1 were determined by the experiments: i.e., $R_{(Flow\ Sensor)}$ is 0.6 [m/s] and $R_{(Yaw\ Rate\ Sensor)}$ is 0.8 [rad/s]. The threshold values for the Mission Diagnosis are larger than those for the Routine Diagnosis considering the variety of the mission.

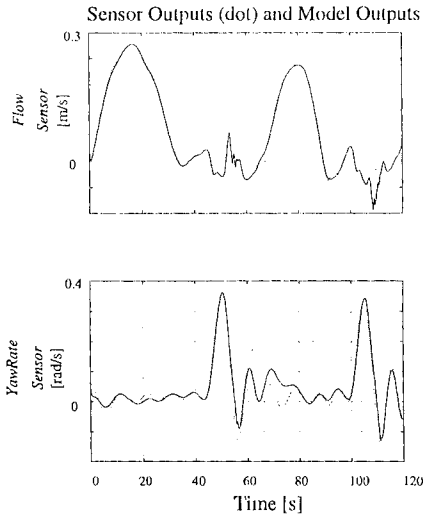


Figure 10. Sensor outputs and trained model outputs

Table 2. The Pattern Table defined for the Twin-Burger

Case	State		Defective Component
	0-Normal	1-Abnormal	
	Flow Sensor	Yaw Rate Sensor	
0	0	0	Nothing
1	1	1	Thruster 0 or Thruster 1
2	1	0	Flow Sensor
3	0	1	Yaw Rate Sensor

Table 1. Threshold values for binary transformation in the DP

		g Value Thresholds [%]	
		Flow Sensor	YawRate Sensor
Routine Diagnosis	ZA	8	7
	ZB	8	7
	ZC	8	7
Mission Diagnosis		15	10

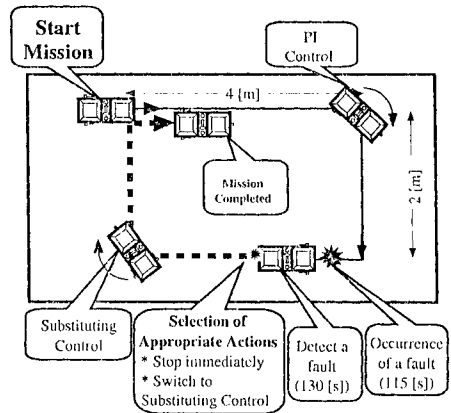


Figure 11. Experiment of the Mission Diagnosis

Pattern Table and Active Diagnosis

The Pattern Table of the Twin-Burger is determined as Table 2 by examining the configuration and performance of the onboard sensors and thrusters. When $\{b\}$ is calculated as $\{1,0\}$ after the ZA is carried out, it is concluded that the Flow Sensor is defective from Table 2. But when $\{b\}$ is calculated as $\{1,1\}$ the system only concludes that the Thruster 0 or 1 may be defective. In order to identify the defective component, the Active Diagnosis should be carried out. In this case, the vehicle carries out the ZB or the ZC. When the calculated $\{b\}$ after the ZB is not $\{0,0\}$, it is concluded that the Thruster 0 is defective because only the Thruster 0 is actuated in the ZB. The redundancy of the diagnosis can be raised by carrying out the ZC in the same way.

EXPERIMENT

In this section, we present an experiment of the Mission Diagnosis using the Twin-Burger which demonstrates that the proposed self-diagnosis system detects a sensor failure occurred during a mission. The vehicle follows the square-path of 4 by 2 meters keeping 0.7 meters of depth as shown in Figure 11. The Flow Sensor is covered at 115 seconds when the vehicle almost finishes turning and is going to move forward, so that the output of the sensor is zero after this time as shown in Figure 12.

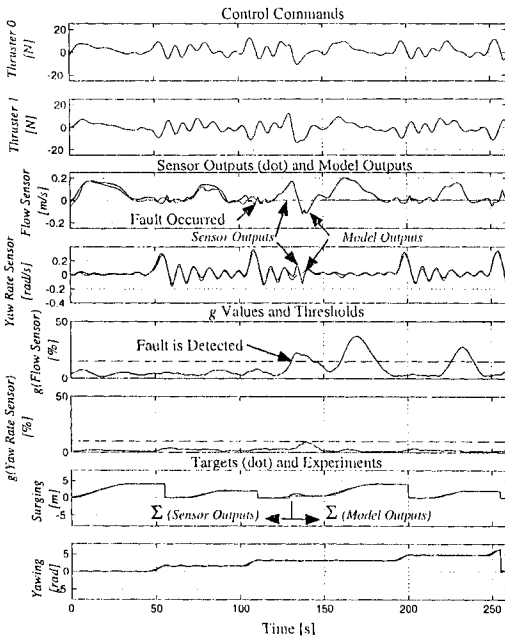


Figure 12. Experimental Results of the Mission Diagnosis

At about 130 seconds, $b_{(Flow\ Sensor)}$ is calculated as 1 because the value of $g_{(Flow\ Sensor)}$ becomes larger than the threshold value 15 in Table 2. Then the DP concludes that the vehicle is not in normal condition. It takes about fifteen seconds to detect the fault after its occurrence because forward velocity of the vehicle is very small when the fault occurs. It is identified that the Flow Sensor is defective because calculated $\{b\} = \{1,0\}$ corresponds to the Case 2 in the Table 2. After the fault detection, the vehicle proceeds the mission scenario based on the Substituting Control. Finally, the vehicle gets to the predetermined destination even though the Flow Sensor is in malfunction.

Consequently, the result of the experiment shows that the proposed self-diagnosis system can identify the fault

and succeeds in completing the given mission scenario based on the Substituting Control.

CONCLUSION

The work described in this paper demonstrates a fault detection for AUVs based on a dynamics model constructed by an artificial neural network. The proposed model based self-diagnosis system has three significant features: i.e., (1) It contains a neural network to represent nonlinear dynamics of the AUV; (2) It has a mechanism to obtain necessary information by "Active Diagnosis"; and (3) In case that a certain failure is detected, the system selects an appropriate action to cope with the defect including "Substituting Control". These functions are achieved by the Routine Diagnosis and the Mission Diagnosis whose structures consist of two subsystems: the Model Matching Part (MMP) and the Diagnosis Part (DP).

The performance of the proposed self-diagnosis system is examined through tank tests using an actual test-bed AUV. It is shown that the system can detect failures of the onboard sensors and actuators without introducing extra sensors, and select proper action in order to reduce the damage to the AUV. It can be concluded that inclusion of the proposed self-diagnosis system in the AUVs' software increases their reliability and ability of emergency management.

REFERENCES

- Fujii, T. and Ura, T. 1990. Development of motion control system for AUV using neural nets. In: Proceedings of IEEE Symposium on Autonomous Underwater Vehicle Technology, AUV Ô90. Washington, DC. 81-86.
- Fujii, T., Ura, T., Kuroda, Y., Chiba, H., Nose, Y. and Aramaki, K. 1993. Development of a versatile test-bed "Twin-Burger" toward realization of intelligent behaviors of autonomous underwater vehicles. In: Proceedings of IEEE OCEANS Ô93. Victoria. 186-191.
- Fujii, T. and Ura, T. 1994. Self-generation of neural-net controller by training in natural environment. In: COMPUTATIONAL INTELLIGENCE: Imitating Life ed. Zurada, J.M., Marks II, R. J., Robinson, C.J. IEEE PRESS. 340-351.
- Healey, A.J. 1992. A neural network approach to failure diagnostics for underwater vehicles. In: Proceedings of IEEE Symposium on Autonomous Underwater Vehicle Technology, AUV Ô92. 131-134.
- Ishii, K., Fujii, T. and Ura, T. 1994. A quick adaptation method in a neural network based control system for AUVs. In: Proceedings of IEEE Symposium on Autonomous Underwater Vehicle Technology, AUV Ô94. 269-274.
- Ishii, K., Fujii, T. and Ura, T. 1995. An on-line adaptation method in a neural network based control system for AUVs. In: IEEE Journal of Oceanic Engineering. **20**: No.3. July.

Orrick, A., McDermott, M., Barnett, D.M., Nelson, E.L. and Williams, G.N. 1994. Failure detection in an autonomous underwater vehicle. In: Proceedings of IEEE Symposium on Autonomous Underwater Vehicle Technology, AUV '94. 377-382.

Takai, M., Fujii, T., Ura, T. 1995. A model based diagnosis system for autonomous underwater vehicles using artificial neural networks. In: Proceedings of Ninth International Symposium on Unmanned Untethered Submersible Technology, UUST '95. 243-252. September.

Ura, T. and Suto, T. 1992. Generation of controller of an underwater robot for constant depth cruising by self-training. In: J. Soc. Naval Arch. Japan. **171**: 581-586 in Japanese.

Ura, T. and Kuroda, Y. 1993. Mission execution experiment with a newly developed AUV The Twin-Burger. In: Proceedings of Eighth International Symposium on Unmanned Untethered Submersible Technology, UUST '93. UN. 92-105.

VISUAL TRACKING FOR UNMANNED UNDERSEA VEHICLES

B. A. A. P. Balasuriya and Tamaki Ura
Institute of Industrial Science, University of Tokyo
Tokyo, Japan

ABSTRACT

This paper addresses the use of a vision sensor in the Underwater Vehicle (UV) feedback control loop. The nature of underwater images captured by CCD cameras is discussed. A pre-filter to reduce unwanted features unique to underwater environments, and two active vision algorithms are proposed for autonomous underwater object following. The two algorithms focus on typical underwater applications such as underwater cable tracking and underwater object following. Experimental results demonstrate that these algorithms can be implemented in real time with the use of small hardware systems.

INTRODUCTION

Current data acquisition methods for underwater vehicles, such as ROV's (Remotely Operated Vehicles) and AUV's (Autonomous Underwater Vehicles), are very costly and severely limited. Direct, long-duration exploration of the ocean by human is also limited and involves high risk even at depths of a few hundred meters (Blidberg, 1991).

AUV's must meet the needs of ocean exploration/exploitation while overcoming some of the limitations of humans and ROVs. Accordingly, AUV's must be intelligent enough to take decisions in unforeseen, highly complex underwater environments. In order to achieve completely autonomous underwater systems, it is necessary to integrate many types of sensors. At present acoustic sensors are widely used in underwater applications, although they encounter problems such as acoustic shading and multipath effect when close range sensing is considered. ROV operators find long duration tasks such as object search, cable tracking and object following very exhausting. An autonomous system that can assist ROV operators will make the operations more reliable and efficient. Considering the above mentioned reasons, this paper introduces the uses of visual sensors for target recognition and guidance of underwater vehicles (UV's) (Balasuriya and Ura, 1996).

Vision is a sensing modality rich with information in the short range, and provides very high resolution compared with acoustic sensing. There are, however, certain features which are unique to the underwater environment, yet undesirable for computer vision algorithms.

This paper discusses a filtering technique to minimize the effects due to the undesirable features of the underwater environment and proposes some techniques to use visual data for the guidance of UV'S. The performance of the proposed system is demonstrated through direct application to typical underwater missions, such as underwater cable tracking and object

following, based on the image captured by a commercially available Charge-Coupled Device (CCD) camera.

UNDERWATER VISUAL SENSING

Visual sensing plays a major role in autonomous systems on land, as it is unobtrusive, accurate, and has a high bandwidth. For underwater applications, there are, however, limitations due to both the environment and the technology currently available. Due to the little, or even the complete absence of ambient light, visibility is poor so that active light sources have to be used to illuminate the working environment, resulting in non-uniform lighting. In case of AUV's, it is almost impossible to place large hardware systems in their small pressure hulls.

Underwater Optical Properties

An underwater image is illuminated by several ambient light sources as shown in Fig. 1.

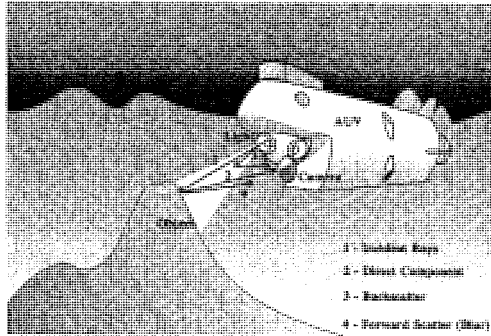


Figure 1. Underwater optical properties

The final image formed in the camera plane is the linear superposition of the three reflected quantities shown in Fig. 1;

$$I_t(x, y) = I_d(x, y) + I_{bk}(x, y) + I_b(x, y) \tag{1}$$

where,

I_t = the total intensity, I_d = the direct component: the light reflected from the target, I_{bk} = the backscatter component: light scattered by water and suspended particles with no illumination from the object, and I_b = the blur component (forward scatter): the light reflected from the target can also be scattered on its way to the camera.

Each quantities are given respectively by the following equation (Jaffe, 1990);

$$\begin{aligned}
 I_d(x, y) &= \frac{I_r}{R'^2}(x, y, z)Ke^{-cR} \\
 I_b(x, y) &= \frac{I_d}{e^{-cR}}(e^{-GR} - e^{cR}) * F^{-1}(e^{-BRf}) \\
 I_{bk}(x, y) &= \sum_{n=1}^{z/\Delta z} I_{bp}(x, y, z)
 \end{aligned}
 \tag{2}$$

where ,

I_r - reflectance intensity from the target, I_{bp} - the intensity at the backscatter plane, K - a function depending on the camera used, c - total attenuation coefficient, R - distance from the light source to the target, R' - distance from the target to the camera, G -empirical constant related to the power in the scattered component, B - empirical constant related to the angular attenuation, f - angular frequency in radians, F^{-1} - inverse Fourier transform, $*$ - convolution, Z - distance from the light source to the camera and ΔZ - increment in the z-direction.

Considering the frequency response of the above optical properties as shown in Fig. 2, it is clear that underwater images have spatial attenuation of high frequencies (blur) and predominance of low frequencies (backscatter). A filter should be designed to filter out some of the low frequency components and to boost some high frequency components which were attenuated.

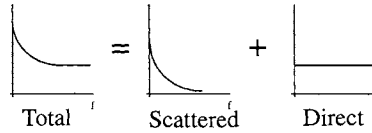


Figure 2. Frequency response of the underwater optical properties

Underwater Image Properties

Unique features of underwater images can be summarized into three categories;

Non-uniform lighting

Due to the light absorbed by water, far range objects will appear to be darker than close range objects, and highly directional active lighting make regions in the image to appear either darker or brighter. This will result in a non-uniform lighting condition in the underwater image which is undesirable for most of the available computer vision algorithms.

Suspended particles in water

Backscattering is mostly due to randomly moving particles suspended in water. As a result, the image consists of many bright spots. In case of marine snow the image could be improved with the use of filtering techniques. But in case of high turbidity, quality of the image will be difficult to improve.

Limited range

Due to absorption of light, the range of visibility underwater is limited.

To make underwater computer vision processing possible, filtering technique should be introduced to reduce the above mentioned effects to some extent.

FILTERING OF UNDERWATER IMAGES

The scattering of light underwater introduces low frequency components to the image. Marine snow introduces not only backscattering but also high frequency components due to the fast moving particles. Therefore, it can be concluded that band pass filters will be the best to reduce those effects observed in underwater images.

In this paper, we propose to use the Laplacian of Gaussian (LoG) filter as the band limiting filter for underwater images (Huertas and Medioni, 1986). The Laplacian portion will act as a high pass filter and the Gaussian as a low pass filter (Marks et al., 1993). The main advantage of this filter is that it can be implemented in real-time applications. The LoG mask in two dimensions is given in Eq. 3.

$$\nabla^2 G(x,y) = \left[K \left(2 - \frac{x^2 + y^2}{\sigma^2} \right) e^{\left[-\frac{x^2 + y^2}{2\sigma^2} \right]} \right] \tag{3}$$

The characteristic curve of the LoG mask is shown in Fig. 3(a).

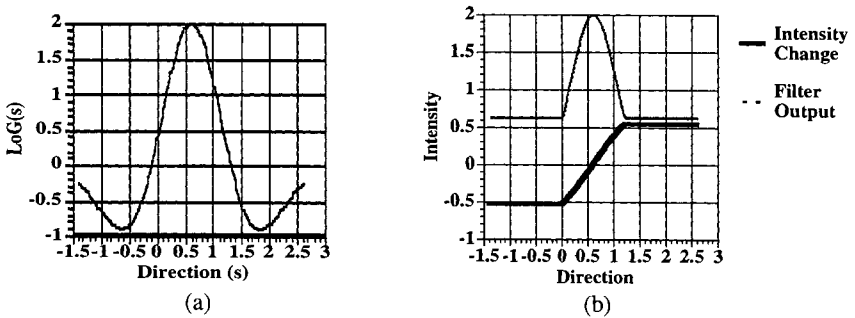


Figure 3 The LoG characteristic

The filter response to intensity variation in the image, in a particular direction is shown in Fig. 3(b). Note how the filter evaluates a zero at the local maxima. The zero crossings are locally more stable in the presence of noise than most other properties, thus making them more attractive for underwater images. Therefore, a signum function to extract the zero crossings from the LoG filtered image is proposed.

UNDERWATER OBJECT FOLLOWING

Although the use of vision for dynamically servoing an autonomous system is a well studied area, the applications are either for land navigation or for a structured environment, such as a production cell. UV navigation is more challenging due to the fact that it involves 6 degrees of freedom. The motion parameters of the object of interest which is to be followed can be derived with the pin-hole camera model shown in Fig. 4. A point P projects into a point p in the image plane with image coordinates (x,y) given by;

$$x = X_s / Z_s \text{ and } y = Y_s / Z_s \quad (4)$$

The perspective projection and the focal length is assumed to be unity. If the vehicle moves in a static environment with a translational velocity T and with an angular velocity R with respect to the vehicle frame, then the velocity of point P can be derived as;

$$\frac{dP}{dt} = -T - R \times P \quad (5)$$

By taking the time derivatives of the expressions for x and y and using (4) and (5), we obtain Eq. (6) which is used as the motion estimator in the proposed tracking algorithm (Papanikolopoulos and Khosla, 1993).

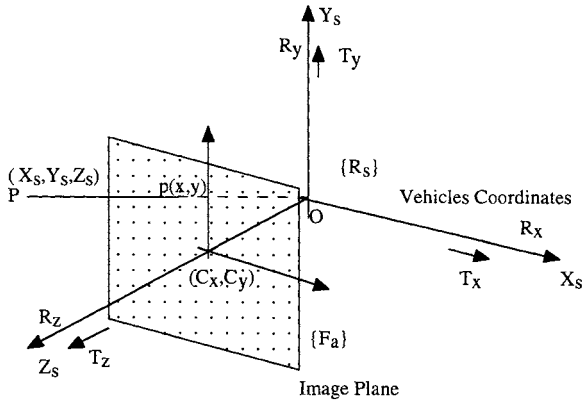


Figure 4 Image and vehicle coordinate systems. Where T_x - Sway, T_y - Heave, T_z - Surge, R_x - Pitch, R_y - Yaw, R_z - Roll.

Two real-time vision based tracking algorithms are proposed for underwater vehicles: (1) Feature based object following; (2) Template based object following. The general schematic diagram of the object following system is shown in Fig. 5.

$$\dot{x} = \left[x \frac{T_z}{Z_s} - \frac{T_x}{Z_s} \right] + \left[xyR_x - (1+x^2)R_y + yR_z \right]$$

$$\dot{y} = \left[y \frac{T_z}{Z_s} - \frac{T_y}{Z_s} \right] + \left[(1+y^2)R_x - xyR_y - xR_z \right]$$
(6)

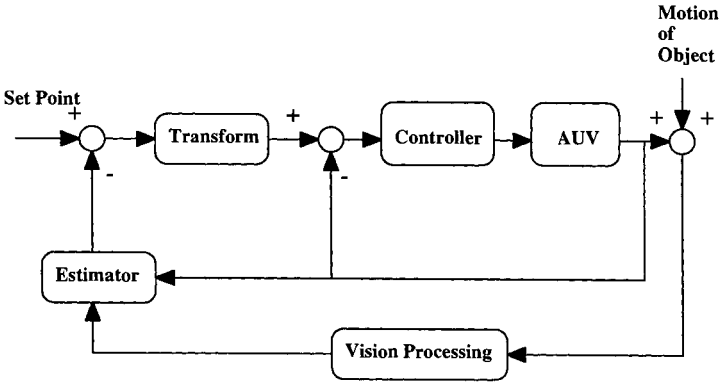


Figure 5. The general schematic diagram of the vision based tracking system

The set point is the target position desired in the image plane and the control commands are derived by comparing it with the current position of the target found by the vision processing algorithm. The estimator given in Eq.(6) will compensate the delay caused by the vision processing algorithm. The transform block in Fig. 6 will transform the error found in the 2D image plane to the 3D plane by using the pin-hole camera model.

Feature Based Object Following

This algorithm is capable of tracking objects with well defined geometric features which will not change with change in pose. A typical example is underwater cable tracking. Navigation commands are derived using the position of the cable in the image. The position of the cable is found by extracting the linear features in the image.

As shown in Fig. 6, the equation of the line found by the vision processor will be compared with the equation of the line at the desired location.

Line feature extraction

Hough transformation technique is used to extract the line features from the image. In this technique a line, given in Eq. (7), in the image plane (x,y) is transformed into the parametric plane. Here the parameters of the line are shown in Fig. 7(a). A straight line in the image plane

will correspond to a point in the parametric plane. During the transformation the number of pixels falling into each parametric coordinate will be counted as shown in Fig. 7(b). The highest

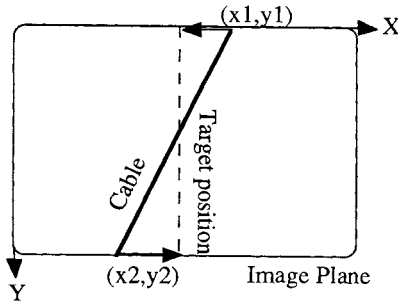


Figure 6 Cable tracking example

vote of pixels in the parametric plane will correspond to the longest line in the image plane. With the estimator given in Eq. (6), the whereabouts of the line can be predicted and Hough transformation will be necessary only in that region to get the details of the line. Thus the extraction will be much faster, enabling real-time operations and false detection of targets will be avoided. As underwater environments will have only a very few well defined geometric shapes, Hough transformation technique is found to be suitable for underwater cable detection.

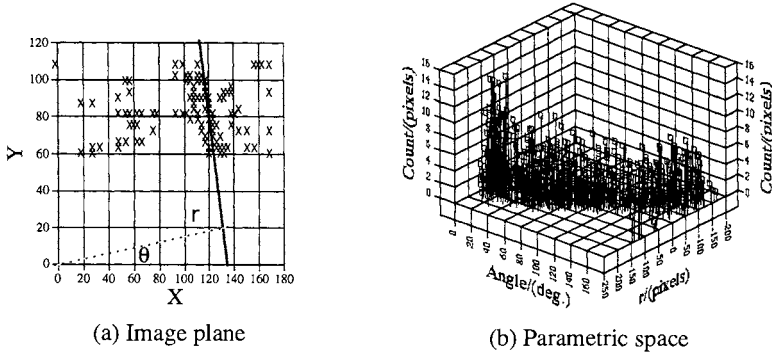


Figure 7 Hough transformation

$$r = x \cos(\theta) + y \sin(\theta) \tag{7}$$

Template Based Object Following

This technique is used in situations when a particular feature of the target cannot be defined. Fish following is a typical example of this nature. In this technique, a template will be derived using the image of the object to be tracked as shown in Fig. 8. This template will be correlated with the neighborhood in the next frame with the correlation function $R(u,v)$ given in Eq. (8). The best correlation will correspond to the new location of the object. In order to cater for the changing shape and size of the interested object, the template is updated according to the variance and the mean at the best correlation.

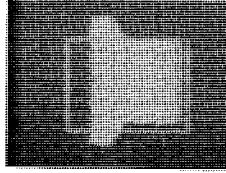


Figure 8. The template for tracking

$$R(u,v) = \sum_{j=1}^J \sum_{k=1}^K [I(j,k) \text{ XOR } I(j-u,k-v)] \quad (8)$$

where, u,v are the displacement of the target and $I(j,k)$ is the intensity of the pixel at (j,k) . With the Signum of LoG (SoLoG) filter a binary image is obtained. Therefore correlation can be easily calculated with the binary exclusive OR (XOR) operation.

EXPERIMENTAL RESULTS

Performance of the SoLoG Filter

The performance of the SoLoG filter was tested on real images captured at a depth of 1000m with a CCD camera mounted on the Dolphin 3K ROV. From the Figs. 9(a) and 10(a) it can be seen how the underwater images are corrupted with the features mentioned earlier.

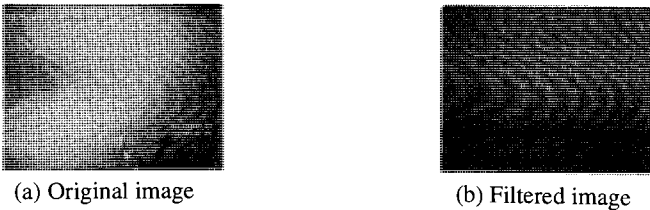


Figure 9. LoG filter example 1

In Fig. 9(a), there is an eel (left center), but due to the predominance of backscatter the details of the fish can hardly be seen. As it can be seen, the highly directional light source of the ROV had made the light condition non-uniform as well. Figure 9(b) shows how the filter had reduced the

noises making the details of the target visible. Similar effects are shown in Fig. 10(b). Note the marine snow effect in Fig. 10(a). Figure 10(c) shows the binary image as a result of the signum operation on the LoG filtered image. These results show the strength of the LoG filter in minimizing the special features discussed earlier.

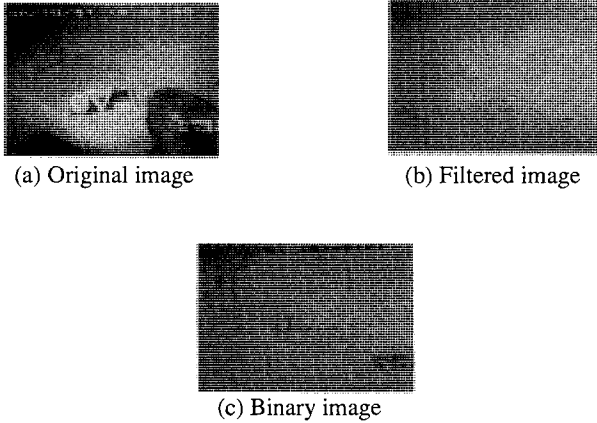


Figure 10. LoG filter example 2

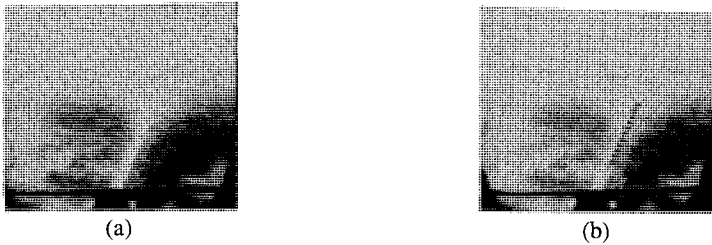


Figure 11. Feature extraction example 1

Feature Based Object Following

The experiments were carried out by placing a yellow cable on the lake bottom of lake Biwako and on the bottom of the experimental pool at the University of Tokyo. The algorithm discussed above was implemented in the hardware of the test-bed vehicle "The Twin-Burger". It is a INMOS B429 transputer based hardware system which can be placed easily in the pressure hull of an underwater vehicle. The processing time of the algorithm on this hardware is 3 decisions/sec.

Figure 11 shows how Hough transformation technique was successful in determining the position of the cable from the image of lake Biwako. The black dotted line in Fig. 11(b) represent the detected line. The performance of the algorithm was tested in a situation when there are many linear features in the environment as shown in Fig. 12. With the use of the estimator given in Eq. (6), the algorithm performed very well in following the cable. The white dotted line in Fig. 12(b) shows the position of the line detected by the algorithm. The proposed algorithm was successful in tracking a cable at the Lake Biwako during experiments on October 3-5, 1996. The algorithm was capable of handling the noises caused by many underwater objects.

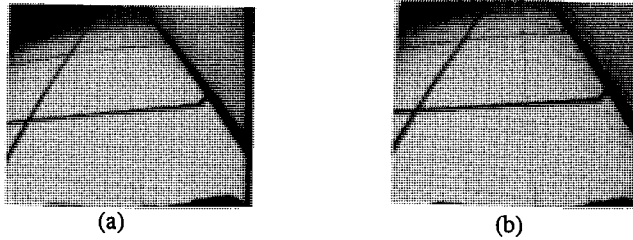


Figure 12. Feature extraction example 2

Template Based Object Following

The object in the template shown in Fig. 8 was moved in a known trajectory. Fig. 13 shows the movement of the object in a circular trajectory. From the trajectory of the coordinates of the template centroid as shown in Fig. 14, it can be concluded that the template followed the object successfully. The algorithm was implemented in the Max Video image processing board and the speed of the following of the target was at 4 frames/sec. This experiment shows how an object could be followed even if its features are undefinable. In general, selecting special features from underwater objects is a difficult task. Therefore template based following scheme will be suitable for such situations.

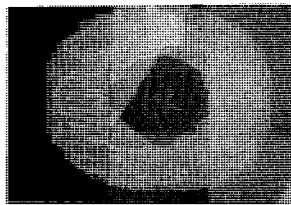


Figure 13. Template based object following

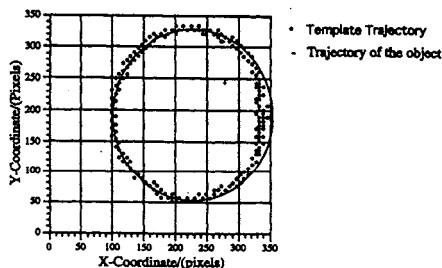


Figure 14. Trajectory of the centroid of the template

CONCLUSIONS

In this paper, the use of visual sensors for real-time decision making for underwater vehicles is addressed. The undesirable features which are unique to underwater images are described and a filter to reduce these effects is proposed. The potential of the proposed approaches have been demonstrated by experimental results from applications such as underwater cable tracking and underwater object following. The algorithms were developed in such a way that they can be implemented in small hardware systems which could be placed in pressure hulls of the underwater vehicles.

It can be concluded from the results that with proper filtering techniques, visual sensing is possible for underwater applications. Visual sensing provides enormous amounts of information on the environment making the fully autonomous system a reality.

ACKNOWLEDGMENTS

The authors would like to thank JAMSTEC (Japan Marine Science and Technology Center) and the Biwako Research Institute for providing underwater images.

REFERENCES

- Balasuriya, B. A. A. P. and T. Ura. 1996. Vision Based Tracking for Unmanned Underwater Vehicles. In:Proc. of SICE '96. July.
- Blidberg, R. 1991. Autonomous underwater vehicles, Current activities and research opportunities. *Int. Rob. Aut. Sys.*, 7(2-3):139-150.
- Huertas, A. and G. Medioni. 1986. Detection of Intensity Changes with Subpixel Accuracy Using Laplacian-Gaussian Masks. *IEEE Trans. on PAMI*. 8(5):651-664.

Jaffe, J. S. 1990. Computer Modeling and the Design of Optimal Underwater Imaging Systems. *IEEE J. of Oceanic Eng.*, **15**(2):101-111.

Marks, R. L., M. J. Lee and S. M. Rock. 1993. Automatic Object Tracking for an Unmanned Underwater Vehicle using Real-Time Filtering and Correlation. In:Proc. of IEEE Sys., Man and Cybernetics. October.

Papanikolopoulos, N. P. and P. K. Khosla. 1993. Adaptive Robotic Visual Tracking: Theory and Experiments. *IEEE Trans. on Automatic Control*. **38**(3):429-444.

TIME-INVARIANT BATHYMETRY A NEW CONCEPT TO DEFINE AND SURVEY IT USING GPS

Muneendra Kumar
Defense Mapping Agency
Fairfax, VA, U.S.A.

ABSTRACT

Currently, there are hundreds of vertical datums, both for land and ocean areas, in use all over the world. As we live on land, the land datums always got the priority attention. Thus, to update them either new datums, viz., the North American Datum (NAD) 1983, European Datum (ED) 1979, and EUREF 1989 have already been established or efforts to establish new datums, viz., SIRGAS for South America and KGS 1995 1994 for Korea have been started.

Another important point is that no rigorous horizontal datum has ever been defined over ocean areas; the practice has been to always extrapolate the land datums to map the charts over oceans. For nautical chart vertical datums, the situation is still more complicated by the lack of agreement on the definition(s) by different countries which in turn jeopardizes the safety of international navigation.

Further, the tidal surfaces used in the vertical datums to define elevations and bathymetry are time-variant and do not have a common zero. This generates apparent slopes between and along the coasts and prevents creation of consistent data sets for global usage.

This paper deals with the chart vertical datum problem and presents a new concept for defining/surveying a time-invariant bathymetry using a high accuracy geoid as the new zero reference surface. Details have also been included on how to realize this zero surface and use the same in real-time navigation. It would also be necessary to avoid use of different regional or global geoids to maintain consistency in the zero reference.

INTRODUCTION

In the complex mapping, charting, and geodetic world, there are hundreds of vertical datums in use. Some datums are properly defined, while in some cases there is hardly any validity in the definition. For many others, information is not available that can be used to determine an accurate height in the local system.

In the above environment, the definitions of the nautical chart datums and the depiction of all other related information useful for safe navigation to avoid underwater and/or overhead hazards vary from one chart to another, coast to coast, between charting agencies, and also between countries. Furthermore, in the hydrographic usage, statements like, "Owing to the many varied tidal characteristics, a precise scientific definition for chart datum, which could be used universally, has not been agreed upon" (IHO, 1993), can still be found. This situation arises due to our age old practice of measuring various time-dependent mean ocean surfaces, such as Mean High Tide (MHT), Mean High Water (MHW), Mean Lower Low Water (MLLW), Mean Sea Level (MSL), Mean Higher High Water (MHHW), Mean Low Water (MLW), Low Water (LW), High Water (HW), etc., and then using such tidal surfaces in relating them to land and nautical chart datums in depicting heights or ocean depths.

The above approach can and has varied from one country to another country and is dependent on the adopted definitions and tide models, surveying techniques, and duration (for computing “means” and instrumentation. As the sea level changes can be excessive and are also time-dependent, the knowledge of accurate tide modeling, which is always complex, becomes critical. Thus, in this complex and difficult to measure time-dependent scenario, it is quite obvious why internationally it would be difficult to agree to a common datum for nautical charts and ocean depths.

However, we now have the capability to compute a geoid of very high accuracy over ocean areas and thus define an accurate nautical chart vertical datum without using time-dependent tidal surfaces. Also, the availability of the Global Positioning System (GPS) makes it easy to establish this vertical datum for charts by surveying time-invariant depths in the field and then depicting them on charts. Then, reversing the survey mode, these charted depths can be measured in real-time during navigation to check depth clearances to avoid ship grounding.

This paper presents a new concept to define a nautical chart vertical datum completely independent of time, to establish the same through GPS surveys, and also to realize the seafloor depths during navigation. The approach thus eliminates the necessity for the time-dependent sea level and other tidal data as the primary source of information for navigation.

CURRENT TIDAL LEVELS

Figure 1 shows an illustrative depiction to define various tidal levels and charted data as this information is currently in use by some countries (NOAA, 1990), if not by all. For example, use of the Lowest Astronomical Tide (LAT) as the vertical datum in charts is increasing. There are some interesting conflicts and deviations between various definitions in Figure 1. Mariners using

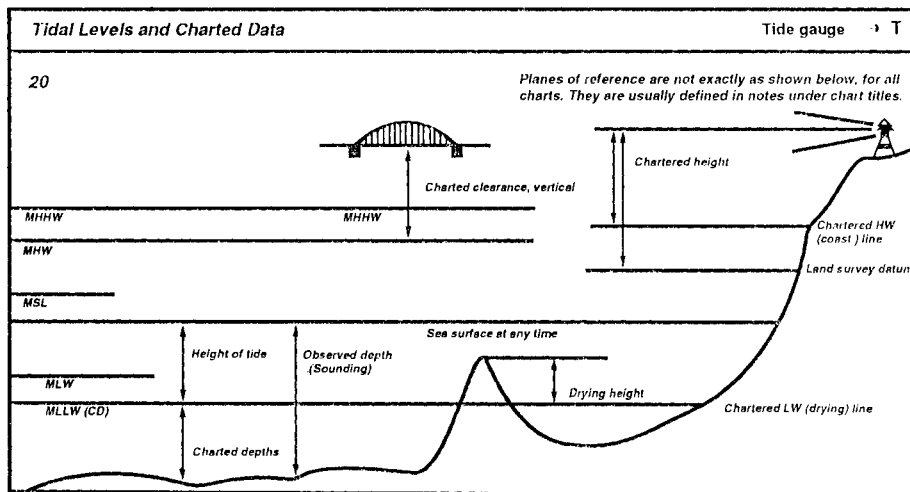


Figure 1. Tide Levels and Charted Data (NOAA, 1990)

the data based on these definitions would have a hard time understanding and correctly interpreting them, especially when hard pressed for time and faced with little margin of error. A few typical examples of such cases are:

- (1) Use of MLLW as chart datum (CD) to depict charted depths versus use of charted LW (drying) line to depict drying heights.
- (2) Use of Charted HW (coastal) line as land survey datum to depict charted heights. Here, MSL is shown separately, even though all the land vertical datums worldwide are defined with respect to it.
- (3) Both MHW and MHHW are shown differently from the charted HW (coastal) line.
- (4) While charted depths are defined with respect to MLLW, the charted vertical clearances are defined with respect to MHW, and not to MHHW. This definition may leave MHHW practically with no application, at least in Figure 1.
- (5) In Figure 1, the "height of tide," is defined with respect to MLLW (CD), while Tide and Current Glossary (NOAA, 1989) does not define this important item. Further, this glossary includes Half-Tide Level, also called Mean Tide Level, to define a tidal datum which is midway between MHW and MLW; but the same is not included in Figure 1.

Table 1¹

Tide Tables Referred to Datum of Soundings

Tidal Levels referred to Datum of Soundings		<i>Tabular statement of semi-diurnal or diurnal tides</i> <i>Note:</i> <i>The order of the columns of levels will be the same as that used in national tables of tidal predictions.</i>																					
Place	Lat N		Long E	Heights in meters above datum																			
				M-HWS	M-HWN	MLWN	MLWS																
30																							
			M-HLW0	M-LHW	M-HLW	M-LLW																	
31			<i>Tidal Stream table</i>				Tidal streams referred to: <table border="1" style="width: 100%; border-collapse: collapse;"> <thead> <tr> <th style="width: 10%; text-align: center;">Hours</th> <th style="width: 10%; text-align: center;">Geographical Position</th> </tr> </thead> <tbody> <tr> <td style="text-align: center;">6</td> <td rowspan="6" style="text-align: center; vertical-align: middle;"> </td> </tr> <tr><td style="text-align: center;">5</td></tr> <tr><td style="text-align: center;">4</td></tr> <tr><td style="text-align: center;">3</td></tr> <tr><td style="text-align: center;">2</td></tr> <tr><td style="text-align: center;">1</td></tr> <tr> <td style="text-align: center;">High Water</td> <td rowspan="6" style="text-align: center; vertical-align: middle;"> Directions of streams (degrees) Rates at spring tides (knots) Rates at neap tides (knots) </td> </tr> <tr><td style="text-align: center;">4</td></tr> <tr><td style="text-align: center;">3</td></tr> <tr><td style="text-align: center;">2</td></tr> <tr><td style="text-align: center;">1</td></tr> <tr><td style="text-align: center;">6</td></tr> </tbody> </table>	Hours	Geographical Position	6		5	4	3	2	1	High Water	Directions of streams (degrees) Rates at spring tides (knots) Rates at neap tides (knots)	4	3	2	1	6
Hours	Geographical Position																						
6																							
5																							
4																							
3																							
2																							
1																							
High Water	Directions of streams (degrees) Rates at spring tides (knots) Rates at neap tides (knots)																						
4																							
3																							
2																							
1																							
6																							

1 NOAA, 1990.

Table I (NOAA, 1990) shows a typical example of a tide table where tidal levels are related to "Datum of Soundings". Here, a user will then have to Solve or interpret a newer set of terms like MHWS, MHWN, MLHW, and MHLW. To make the usage of available information more complex and thus more difficult to interpret correctly, the note in Table 1 indicates that the order of the included tidal levels, as referred to all the sounding datums, may differ in national tables. If this statement is taken to be correct, the involved definitions of these terms may also be different (IHO, 1993).

Another important aspect in all of the above complexity of terminology and definitions is that all this information may also be time-dependent.

DEFINING TIME-INVARIANT ZERO REFERENCE SURFACE

On land, the orthometric heights or elevations are defined theoretically with respect to the geoid. However, in the past, due to our limitations to compute and establish the geoid with the desired accuracy, the Mean Sea Level (MSL) was and still is used to approximate the geoid, though the MSL does not coincide with an equi-potential surface. Another complication in using MSL to define a vertical datum is that it deviates from coast to coast, both in east-west and north-south directions. There are cases when the MSL has been very poorly "measured" in defining zero surface for the vertical datums and related elevations. In ocean areas, the bathymetric data, as available currently, is related to a zero reference surface which may be even more poorly defined than MSL for the land areas.

In view of our present capability with the newer technology and availability of accurate observed data sets, the geoid over ocean areas can now be computed easily with absolute accuracy of about ± 25 -30 cm. All indications reflect that this accuracy may be even better in the near future.

It is thus proposed to utilize the geoid as the zero surface for the nautical chart datum and reference all bathymetric data to it. This referencing will then provide a time-independent and globally consistent definition and facilitate easy integration of different data sets which would originate from newly surveyed projects under this definition.

Another important point, which requires clarification under the proposed concept, is that the geoid (to be used) is defined by the following equation:

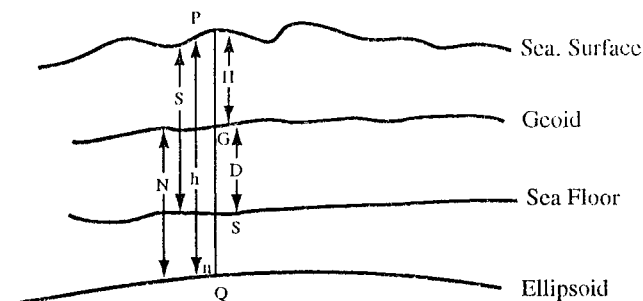
$$W(X, Y, Z) = W_0 \quad (1)$$

where the "W" is the earth's total gravity potential and "W₀" the geoid constant as specified by the International Association of Geodesy (Moritz, 1980). The computational task of such a high absolute accuracy geoidal solution using extensive data sets with coverage from all over the globe would be a very costly and time consuming effort. To eliminate conflicts between too many zero surfaces, the use of regional geoidal solutions will have to be avoided. In addition, to ensure consistent accuracy, worldwide proliferation of too many solutions must be checked. To achieve these two desirable goals, international institutions like the International Hydrographic organization, International Maritime Organization, International Commission on Geoid, and International Federation of Surveyors would play an important role in coordination and adoption of an accurate global geoidal solution by all.

SURVEYING CONSISTENT BATHYMETRY

Figure 2 illustrates a typical survey scenario using GPS. In open and deep ocean areas, where accuracy of measured depths will be less critical, the ellipsoidal height (h) of the ship can be

determined with GPS in navigation or single point positioning mode. As the survey scenario would approach the coast with shallower water depths, high accuracy requirements would also become more critical. In such cases, the ship's ellipsoidal height (h) would be established or surveyed with differential GPS technique where the survey can be designed to achieve desired higher accuracy in " h ".



PQ = Ellipsoidal height (h) of the survey ship surveyed with GPS

GQ = Geoidal height (N) computed with the Earth Gravity Model (EGM)

PS = Sounding (S) measured acoustically from the survey ship

GS = Depth of sea floor (D) from the geoid

Figure 2. Surveying the Time-Invariant Bathymetry

The surveyed ellipsoidal heights (h) of the ship can provide the h_p of the sea surface, which when combined with the computed geoidal height (N_p), would give the orthometric height (H_p) as:

$$H_p \approx h_p - N_p \tag{2}$$

Then, at the same epoch, the ship measures through sounding the distance S_p . Combining the S_p with sea surface orthometric height H_p (using equation 2), the depth D_p can be computed as:

$$D_p = S_p - H_p \tag{3}$$

While the surveyed h_p and S_p and computed H_p would be time variant with the moving sea surface, the geoidal height (N_p) and computed depth (D_p) would be time-independent. Further, as the heights h_p and N_p would be established in the globally consistent World Geodetic System (WGS) 1984 used by GPS, the computed depth D_p through ship's soundings would also be defined with respect to the WGS 84 geoid (DMA, 1991).

Once an area is surveyed with all the depths referenced to the WGS 84 geoid, the information can be utilized to contour the nautical charts. The data can also be stored as individual depths in a digital data base and will also be available for use with digital charts.

RECOVERING DEPTH AND HEIGHT CLEARANCES IN NAVIGATION

Depth Clearance

While navigating in an area with its nautical chart plotted and contoured for depths (Section 4-1), the height (H_p), using the GPS surveys and the computed geoidal height (N_p), depth (D_p) and the ship's hulk (HL) are configured in Figure 3.

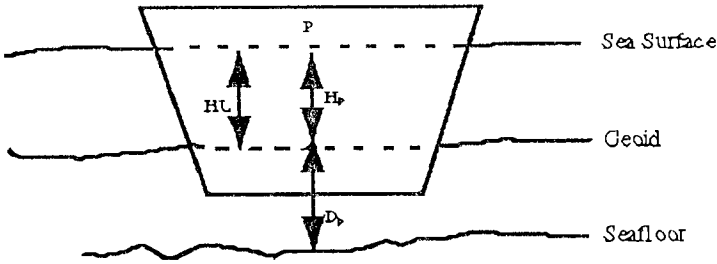


Figure 3. Surveying the Depth Clearance

A measure of depth clearance (or the safe distance between the ship's bottom and the seafloor) will then be given as :

$$HL < H_p + D_p \tag{4}$$

A new measurement of sounding (S_p) at the sailing time will then provide a check on the plotted depth D_p on the chart.

Height Clearance

While navigating in an area with its nautical chart plotted for height clearance, the height (H_p), using the GPS surveys and the computed geoidal height (N_p), the height (H_B) of a bridge and length of the ship's mast (HM) are configured in Figure 4.

A measure of height clearance (or the separation between the highest point of the ship's mast and the bridge bottom) will then be given as :

$$HM < H_B - H_p \tag{5}$$

It is important to point out that the distance from the sea surface to the GPS antenna would be a measured correction in all of the above relationships.

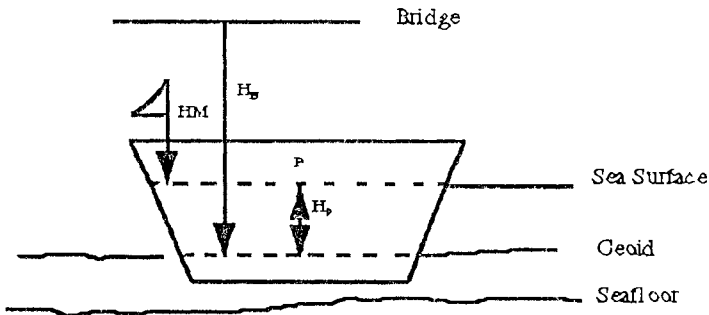


Figure 4. Surveying the Height Clearance

RELATING THE TIDAL SURFACES

At any tidal station, the absolute zero of the tidal staff can be established with the GPS absolute point positioning survey at a nearby station and then performing differential leveling to the staff (Figure 5). Its orthometric height H ($=h - N$) set to the geoidal zero will be consistent all over the globe.

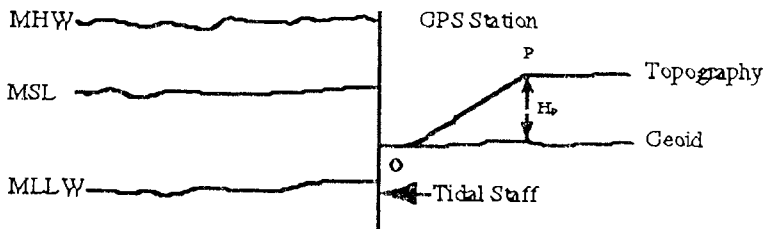


Figure 5. Surveying the Zero Height of the Tidal Staff

Then, all the tidal surfaces, e.g., MLLW, MLW, MSL, MHW, can be surveyed with respect to the zero of the tidal staff or to the geoid and used with consistent definition worldwide as auxiliary information with the time-invariant bathymetry.

Though the tidal surfaces will be tied to the same zero as the elevations and depths determined with the GPS surveys and a global geoid, it is emphasized that the tidal measurements and/or reductions would not be required when navigating with GPS fixings and using depths which are referenced to the geoid. In this mode, the ship navigator can use the high tide information as auxiliary data to compute the "safe" time when the high tide would improve ship's clearance to entering the shallower areas.

EVALUATING THE NEW CONCEPT

The proposed use of the geoid as the zero reference for a global vertical datum will enable us to integrate and analyze the depth and elevation data over the sea and land interface. It will also eliminate the numerous existing local tidal datums which are in use around the world.

However, the adoption of a new vertical datum would raise an immediate issue of what to do with the existing data sets based on the numerous tidal datums, each with its own definition and how to save this valuable information.

One solution for the integration of the existing data sets is datum transformations but this method would not improve the quality and accuracy of the data based on the numerous tidal and chart datums. However, it would definitely help in utilizing the existing information until the new and more accurate data sets are surveyed and integrated under consistent, time-invariant, and accurate definition.

It is also noted that the proposed method to determine the depths with respect to the geoid also involves the sounding data and the accuracy of final results would require accurate acoustic modeling. As the issue concerning the accuracy of the soundings is not a new one, the improvement in the acoustic modeling should be considered as an area for future research (section 5.).

ACCURACY ESTIMATION

In Figure 2, in offshore areas the ellipsoid height (h) can be surveyed using differential GPS with an accuracy of ± 1 meter in routine field surveys. Also, the achievable accuracy of the geoid over ocean areas should be within the desired range of about 25 cm in the near future, even though some doubts may still exist about the accuracy of the current geoidal model(s).

The above shifts the emphasis to the sounding measurements and their surveyed accuracy which would impact the final accuracy of the bathymetric data. Table 2, extracted from a National Oceanic and Atmospheric Administration publication (NOAA, 1978), is one such example which specifies the accuracy standards for measurement of soundings during field surveys. Another very important document, which specifies international standards and classification criteria for hydrographic surveys and soundings, is the IHO Special Publication No. 44 (IHO, 1987). The IHO's depth accuracy specifications have been tabulated in Table 3.

Table 2¹
Accuracy Standards for Soundings

Water Depth	Allowable Errors
0 - 20 meter	0.3 meter
20 - 100 meter	1 meter
> 100 meter	1% depth

¹ Extracted from NOAA, 1978.

Table 3

<u>Depth</u>	<u>Survey Error*</u>
0 to 30 meters	0.3 m
>30 meters	1% of depth

*Probability of at least 90%.

Though the above tables specify the desired survey accuracy requirements, standards, and classifications for soundings and related hydrographic surveys, the users would still be concerned about the accuracy actually achieved and/or obtained during any marine field survey over an area, especially when one would consider all the rapidly varying environmental conditions and use of different definitions. Thus, under the newly modified and more accurate survey scenarios with GPS techniques, the new concept of using a global geoid as zero reference would be very timely. Further, combining the use of modern instrumentation and techniques to measure soundings, a complete revision of achievable accuracy and specifications for the GPS and marine surveys and soundings, and setting of new international standards would also become desirable.

SUMMARY

The practical complexity and difficulties arising from the use of numerous vertical datums and various time-dependent tidal surfaces with inconsistent definitions are impeding the correct integration of valuable information. This also affects safe navigation over international waters.

The new concept of the geoid as the zero reference surface for the time-invariant bathymetry and elevations is practical and also realizable with sufficient accuracy using current technology and available data sets. The computation of a modern global geoid with an absolute accuracy of ± 25 cm is a costly project, but to accomplish the same at this time would be very timely. Problems arising from use of various relative and regional solutions and also of different global geoids with lower accuracy would have to be avoided. Use of local geodetic datums for differential GPS surveys would be another dangerous and critical problem. If the new survey data is not properly coordinated and collected under standardized specifications, the present complexity may crop up in a different form.

REFERENCES

- DMA. 1991. Department of Defense World Geodetic System 1984, its Definition and Relationship with Local Geodetic Datums, DMA TR 8360.2, Second Edition. Fairfax, VA: Defense Mapping Agency
- IHO. 1987. IHO Standards for Hydrographic Surveys Classification Criteria for Deep Sea Soundings and Procedures for Elimination of Doubtful Data. Special Publication No. 44. Monaco: International Hydrographic Organization.
- IHO. 1993. A Manual on Technical Aspects of the United Nations Convention on the Law of the sea - 1982. Special Publication 51. Monaco: International Hydrographic Organization.

Moritz, H., 1980. Fundamental Geodetic Constants. Report of the Special Study Group 5.39. Paris, France: International Association of Geodesy.

NOAA. 1978. Hydrographic Field Handbook. Silver Spring, MD: National Oceanic and Atmospheric Administration.

NOAA. 1989. Tide and Current Glossary. Silver Spring, MD: National Oceanic and Atmospheric Administration.

NOAA. 1990. Nautical Chart Symbols Abbreviations and Terms. USA Chart No. 1. Silver Spring, MD: National Oceanic and Atmospheric Administration.

PREDICTION OF THE LARGEST SURFACE WAVE HEIGHT IN WATER OF CONSTANT DEPTH

Stanislaw R. Massel
Australian Institute of Marine Science
Townsville, Australia

ABSTRACT

Extreme high waves and subsequent breaking play an important role in upper ocean dynamics, including surface currents and turbulent mixing. A reliable estimation of the maximum wave height at a particular location is a fundamental requirement in the protection of coastline against wave attack and in the design of offshore structures. There is experimental evidence that maximum wave height propagating over a constant water depth is much smaller than the limiting wave height ($0.78 h$), routinely used in practice. This paper discusses various theoretical approaches to clarify this discrepancy, observed for both regular and irregular waves propagating in water of constant depth. For the laboratory conditions, the higher harmonic generation mechanism reduces the maximum regular wave height to $\approx 0.60h$. Moreover, the computations based on the vertical acceleration threshold concept, applied for wind-induced waves, confirmed that the limiting wave steepness in deep water is lower than the steepness predicted by the Stokes limit. Also, for shallow water depth the limiting wave height is smaller than $0.55h$.

INTRODUCTION

The heights of waves are not increasing infinitely, being limited by breaking phenomenon or energy dissipation due to bottom friction. A reliable estimation of the maximum wave height at a particular location is a fundamental requirement in the design coastal or offshore structures, and management and protection of coastline. For structures located on the sea bottom of finite slope, the design criteria are based on the limiting wave height resulting from laboratory data. Shore Protection Manual (1984) provides a family of curves for slopes between 0.2 and 0.02. For slopes less than 0.02 the interpolation was assumed to be consistent with H_{\max} / h ratio of 0.78, predicted for solitary waves over a horizontal bottom.

Nelson in a series of papers (1985, 1987, 1994) showed that a significant discrepancy exists between the value 0.78 and that achieved in practice, when waves are propagating on water of constant depth. After reviewing of existing laboratory and field data for shallow water waves (Le Mehaute et al., 1968; Keating and Webber, 1977; Nelson, 1987; Hardy et al., 1990) he concluded that the upper limit value for the ratio H_{\max} / h is 0.55, which is less than 0.78.

Tucker et al. (1983) measured waves seaward and landward of a relatively flat off-shore bank off the east coast of England using two Waverider buoys. Minimum water depth over the bank was approximately 4.5 m at mid-tide level. The measured saturation level corresponding to a wave breaking showed that the ratio of maximum wave height to water depth is about 0.5.

Laboratory experiments on random waves, propagating over a horizontal bed, reported by Riedel and Byrne (1986), showed that the limiting $(H/h)_{\max}$ ratio of 0.55 applies equally well to random and monochromatic waves. A Pierson-Moskowitz spectral form was adopted and its shape modeled on measured wave spectra during cyclones off the north Australian coast with peak period in the range 8-12s ($0.0141 < h/gT^2 < 0.0318$). The corresponding highest values of H/h ranged from 0.44 to 0.54.

Sulaiman et al. (1994) reported the results of the similar experiments at Sanur Beach in Bali on maximum wave heights on the horizontal reef flat. For nondimensional water depth range of $1.7 \cdot 10^{-4} < (h/gT^2) < 0.17$, the ratio of maximum wave height to water depth is always smaller than 0.6, except for a very few cases when it was ≈ 0.65 .

In this paper, the theoretical explanations of the discrepancies between observations and routine prediction methods are proposed. The paper is limited to the horizontal bottom, and slopping, shoaling bottom case, when wave transformation occurs, is excluded from consideration. This paper is organized as follows. First, the limiting wave height is discussed for regular waves and influence of mechanical wave generation on the highest wave height is evaluated. Secondly, the upper limit of the wave height for irregular waves is determined applying the threshold acceleration criterion. In section five the conclusions are formulated.

LABORATORY REGULAR WAVES

Data sets, collected by Nelson (1994) and shown in Fig. 1, fall into two categories: sets where it is known which points were at or near the limit of stability and sets where no such distinction was made (shadow area in Fig. 1). Using these data sets, Nelson proposed an envelope curve for both transitional and shallow water waves in the form:

$$\left(\frac{H}{h}\right)_{\max} = \frac{F_c}{22 + 1.82F_c}, \quad (1)$$

in which F_c is the so called non-linearity parameter depending solely on the measurable wave parameters H , T , and h (Nelson, 1994):

$$F_c = \left(\frac{H}{h}\right)^{1/2} \left(T \sqrt{\frac{g}{h}}\right)^{5/2}, \quad (2)$$

in which H , T and h are wave height, wave period and water depth, respectively. From Eq (1) follows that the limiting value of $H/h = 0.55$ applies to shallow water waves for which $F_c \geq 500$. Equation (1) is transcendental for H/h because parameter F_c also depends on H/h . For practical calculations it is convenient to express H/h as a function of some independent variable, say h/gT^2 . Substitution of Eq. (2) into Eq. (1) gives:

$$\frac{H_{\max}}{h} = \left[\frac{\sqrt{1 + 0.01504h_*^{-2.5}} - 1}{0.1654h_*^{-1.25}} \right]^2, \quad (3)$$

in which $h_* = h / gT^2$. The non-dimensional maximum wave height (3) is shown in Fig. 2 versus h / gT^2 . Lower values of h / gT^2 correspond to shallow water while the higher values represent deep water.

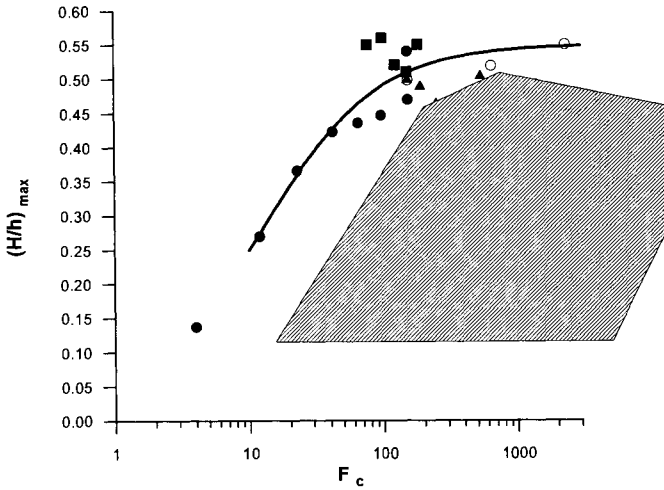


Figure 1: Maximum normalised wave height as a function of F_c . Solid line denotes the Nelson's envelope (Eq. 1). Points indicate various experimental data at or near the limit of stability. Shadow area represents other experimental data reported by Nelson (1994).

HIGHER APPROXIMATIONS OF STOKES' AND CNOIDAL THEORIES

One of the most comprehensive studies related with higher approximation of the Stokes' perturbation method was that by Cokelet (1977). He used the inverse plane method in which the velocity potential ϕ and the stream function ψ were adopted as the dependent variables rather than (x, z) of the common physical plane method (Massel, 1989). The resulting limiting breaking wave height asymptotically approaches to the solitary wave limit which approximately is equal to $0.8332h$ and is even higher than $0.78h$ suggested by SPM (1984).

The limiting ratio H/h is of special importance for shallow water, so for the estimation of the limiting wave height, the shallow wave theory is more appropriate to be used. The lowest theoretical approximation to the surface profile of progressive waves in shallow water is given by the cnoidal functions. In a series of papers Fenton (1979, 1990) developed higher approximations to the cnoidal wave theory up to the fifth order. The comparison of the

theoretical results based on the higher approximations of the cnoidal wave theory with experiments showed that the cnoidal theory predict much higher limiting waves than those observed in the experiments.

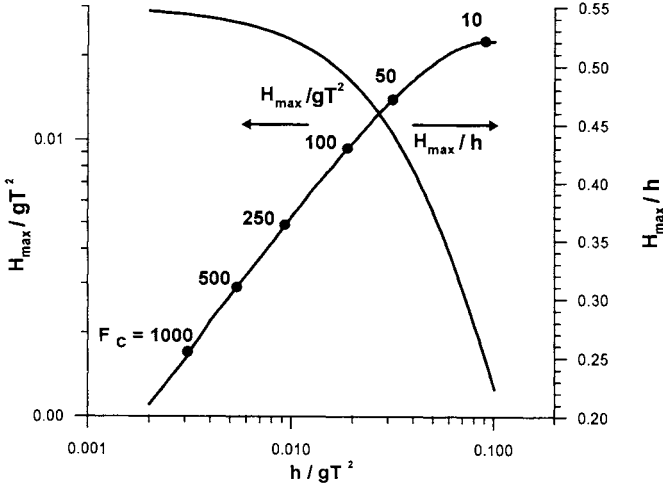


Figure 2: Maximum normalised wave height versus normalised water depth

INFLUENCE OF MECHANICAL WAVE GENERATION ON THE LIMITING WAVE HEIGHT

Most of the experimental data reported by Nelson are the results of experiments in wave flumes. The utilization of laboratory wave channels has become standard practice. However, laboratory studies of surface waves are complicated due to contamination contributed to the wave motion by wave-makers, as the simple harmonic motion produces a wave train not only with the wave-maker frequency but also with its higher harmonic. The sinusoidal motion of the generator does not match the water particle motion required by the wave that is naturally stable under the given conditions. When the higher harmonics generation mechanism (up to second order) is taken into account, the maximum wave height in a wave flume should satisfy the following kinematic breaking condition (Massel, 1996b):

$$\frac{gka}{\omega} \frac{\cosh k(\zeta_{\max} + h)}{\cosh kh} + \frac{3}{4} \omega ka^2 \frac{\cosh 2k(\zeta_{\max} + h)}{\sinh^4 kh} + \frac{gla^{(2)F}}{2\omega} \frac{\cosh l(\zeta_{\max} + h)}{\cosh lh} = C, \quad (4)$$

where ω is wave frequency, k is wave number of first harmonic, a is an amplitude of this harmonic, $a^{(2)F}$ and l are the amplitude and wave number of 'free' second harmonic, ζ_{\max} is ordinate of maximum crest and C is phase velocity. The maximum elevation ζ_{\max} is not known

a priori; therefore, to solve Eq. (4) a recurrent procedure is needed. Using the input data (water depth h and wave period T) from experiments, the kinematic breaking condition (4) was used to determine the possible maximum of the wave height over a horizontal bottom. The coincidence of the experimental and theoretical values of wave heights is good and the difference between experiments and theory is less than 20% (Fig. 3). Two points with the highest error are based on input data from Le Mehaute et al. (1968), when $F_c = 1403$ and 2314. Thus, they are clearly out of range of applicability of second order wave generation theory.

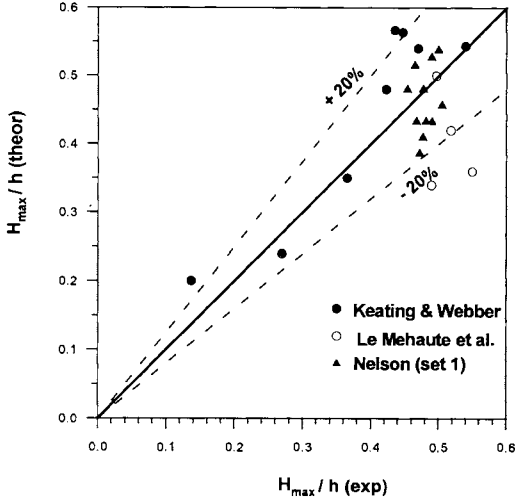


Figure 3: Comparison of theoretical and experimental maximum normalised wave height

BREAKING CRITERIA FOR IRREGULAR WAVES

For steep, limiting regular waves the crest attains sharp point with an angle of 120° and the particle acceleration at the crest is equal $\frac{1}{2}g$. To extend the above results to the case of irregular waves it is assumed that the downward acceleration at the crest of wave has to be greater than αg for breaking to occur, i.e.:

$$\left| \frac{d^2 \zeta}{dt^2} \right| > \alpha g, \quad (5)$$

in which α is a constant. Snyder et al. (1983) have found that α varies from 0.4 to 0.52 and $\alpha = 0.5$ gives good agreement between their experimental results and theory. The laboratory experiments of Ochi and Tsai (1983) provide the value $\alpha \approx 0.4$, used in this paper.

Srokosz (1986) showed that the vertical acceleration threshold (5) results in the following relationship for the probability that a crest of any height will break:

$$Prob_{br} = \exp\left(-\frac{\alpha^2 g^2}{2m_4}\right), \quad (6)$$

in which m_4 is a fourth spectral moment. The probability $Prob_{br}$ is independent of any assumption about the spectral width, assuming that moment m_4 exists. This remarkably simple result holds also for finite water depth under the assumption that probability density function is approximately true for finite water depth. $Prob_{br}$ represents the probability of occurrence of breaking at a crest at a given point on the sea surface. It can be shown that as $m_4 \rightarrow \infty$, $Prob_{br} \rightarrow 1$. The full evaluation of the breaking criteria for irregular waves is a subject of separate paper (Massel, 1996c).

For practical applications it will be more useful to present the limiting wave height (for example, significant wave height H_s) as a function of the spectral peak period T_p for a given level of probability of breaking (or fraction of breaking waves). Hence, we obtain:

$$H_s = 0.03029 \left[\frac{\alpha^2}{-\ln(Prob_{br})} \right]^{1/2} \cdot gT_p^2. \quad (7)$$

The above formula is based on the assumption that the wind waves can be represented by the JONSWAP spectrum and the Phillips' constant and peak frequency are given by the standard JONSWAP relationships (Hasselmann et al., 1973).

COMPARISON WITH EXPERIMENTS

The experimental data on probability of breaking are very limited, so the results of Holthuijsen and Herbers (1986) observation in the North Sea are used to compare the probability with experimental data. The observed significant wave height varied from 1.3m to 2.0m, with average peak period 5s, so, the significant wave steepness varied from 0.0053 to 0.00815 which is lower than limiting steepness predicted by Stokes, i.e. $H_{max} / gT_p^2 = 0.027$. The resulting theoretical probability of breaking varies from 2% to 13%, for α values changing from 0.40 to 0.52. Holthuijsen and Herbers (1986) reported that the fraction of breaking during their field experiment was 12%, what is consistent with the observations of Weissman et al. (1984). The low steepness associated with wave breaking in the field conditions may be explained by superimposing a sequence of a relatively short gravity wave riding on the back of a longer wave. According to Longuet-Higgins (1986) such superposition may induce a high downwards acceleration which causes the waves to break at lower values of steepness than do steady waves.

In fact the observations of Holthuijsen and Herbers (1986) do not correspond exactly to the deep water conditions as water depth at observation site was 17.5 m. Therefore, it is appropriate to

compare their results with limited depth model. Only the intermediate water depth, with the non-dimensional peak wave number $k_p h$ in the range (1.0, 3.0), will be discussed. To represent the spectral density for finite water depth the modified JONSWAP spectrum according Kitaigorodskii et al. (1975) is used. The limiting wave height, for selected probabilities of breaking, is presented in Fig. 4.

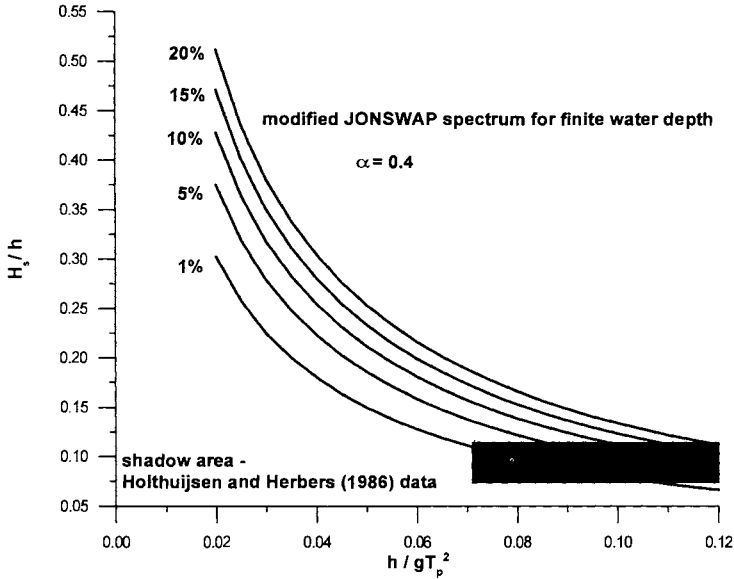


Figure 4: Non-dimensional significant wave height as a function of h/gT_p^2 for various levels of probability of breaking.

Shallow water limit 0.02 of the normalised water depth h/gT_p^2 corresponds to the nondimensional wave number $k_p h \approx 1$, while value 0.12 is associated with deep water. Holthuijsen and Herbers (1986) observed that at a water depth of 17.5 m a fraction of breaking waves was ~ 0.12 for significant wave height varying from 1.3 m to 2.0 m and for peak frequency of the energy spectrum close to 0.2 Hz. Therefore, H_s/h varied from 0.074 to 0.114, with $h/gT_p^2 > 0.071$. Using these values, the fraction of breaking varying from 1% to 20% depending on H_s and T_p values was obtained. The average fraction of breaking is about 10%, which agrees well with Holthuijsen and Herbers (1986) estimation of 12%. The onset of breaking is not related to one individual breaking wave but rather to some percentage of breaking waves which gives the justification for assumption that the observed waves start to break. Field and laboratory observations indicate that the non-breaking waves are at least 10 times more frequent than breaking waves. This crude estimation is used for transfer of the limiting significant wave height into limiting maximum wave height. From the Glukhovskiy's distribution for wave height in finite water depth (Massel, 1996a), the ratio of H_{max}/H_s is equal to 1.30, and

the ratio H_{max}/h for a given level of probability of breaking is obtained. In Fig. 5 this ratio for percentage of breaking of 10%, and the limiting maximum wave height given by Nelson's envelope curve 1, are presented. The ratio of the maximum wave height to water depth is smaller than 0.55 for $h/(gT_p^2) > 0.02$ and even smaller than the limiting value predicted by Nelson (1994).

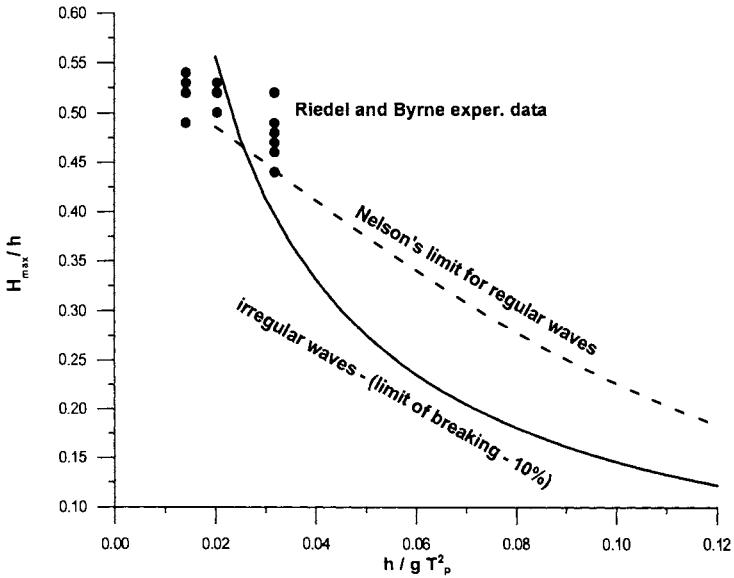


Figure 5: Non-dimensional maximum wave height as a function of h / gT_p^2 for 10% of probability of breaking

The Riedel and Byrne (1986) experimental data superimposed on the theoretical results are presented in Fig. 5. The limiting value of H_{max}/h is smaller than 0.55 and agree with theory. However, a dependence of the limiting wave height on $h / (gT_p^2)$ is weak.

CONCLUSIONS

The experiments in the wave flumes as well as in the field provided the evidence that the maximum possible wave height over a horizontal bottom was $0.55 h$ (h - wave depth). To justify the observed limiting values some theoretical explanations are proposed in this paper. The analysis showed that:

- The higher approximations of the Stoke's and cnoidal wave theories give the limiting wave heights close to $0.78 h$ which is commonly used in engineering practice, but is much higher than observed values.

- Nonlinear theory (second order approximation) of the mechanically generated waves and the kinematic breaking condition predict a maximum wave height less than $\approx 0.6h$, what is in agreement with observation within the $\pm 20\%$ error margin. Therefore, the inclusion of the mechanism of higher harmonics generation into kinematic breaking condition provides convincing explanation for the observed limiting wave height in the regular wave train propagating over constant water depth when F_c parameter is smaller than ≈ 1000 .
- The vertical downwards acceleration threshold concept yields simple computation of the probability of breaking for stochastic sea in deep and finite water depth.
- The computations confirmed the available field and laboratory observations that the limiting wave steepness in the deep water is lower than the limiting steepness predicted by Stokes: $H_{\max} / gT_p^2 = 0.027$. For commonly observed probability of breaking (3%-15%), the limiting significant wave steepness in the field is of order of 0.005.
- For the intermediate water depth ($1 < k_p h < 3$), the limiting wave height is smaller than $0.55h$ and that given by the Eq. (1), what is consistent with the field and wave tank observations.
- The comparison of the theoretical and the observational values can not be fully explored due to the lack of information on the fraction of breaking waves. The future studies should be focused on the more detailed experimental validation of the acceleration criterion.
- As waves usually break inside the wave groups, the relationship of the probability of breaking and wave grouping remains to be clarified.

REFERENCES

- Cokelet, E. D. 1977. Steep gravity waves in water of arbitrary uniform depth. *Phil. Trans. of Royal Soc.* **A286**: 183-230.
- Fenton, J. D. 1979. A high-order cnoidal wave theory. *Jour. Fluid Mech.* **94**:129-161.
- Fenton, J. D., 1990. Nonlinear wave theories. In Ed. B. Le Mehaute and D. M. Hanes. *Ocean Eng. Science.* **9**:3-25.
- Hardy, T. A., I. R. Young, R. C. Nelson, and M. R. Gourlay. 1990. Wave attenuation on an offshore coral reef. In: Proc. 22nd Coastal Eng. Conf. Vol. 1. 330-344.
- Hasselmann, K., T. P. Barnett, E. Bouws, H. Carlson, D. E. Cartwright, K. Enke, J. A. Ewing, H. Gienapp, D. E. Hasselmann, P. Kruseman, A. Meerburg, P. Mueller, D. J. Olbers, K. Richter, W. Sell and H. Walden. 1973. Measurements of wind-wave growth and swell decay during the Joint North Sea Wave Project (JONSWAP). *Deutsches Hydr. Zeit.* **A12**:1-95.

- Holthuijsen, L. H. and T. H. C. Herbers. 1986. Statistics of breaking waves observed as whitecaps in the open sea. *Journ. Physical Ocean.* **16**:290-297.
- Keating, T. and N. B. Webber. 1977. The generation of laboratory waves in a laboratory channel. A comparison between theory and experiment. In: Proc. Inst. Civil Eng. **63**:819-832.
- Kitaigorodskii, S. A., V. P. Krasitskii and M. M. Zaslavskii. 1975. On Phillips' theory of equilibrium range in the spectra of wind-generated gravity waves. *Jour. Phys. Oceanogr.* **5**:410-420.
- Le Mehaute, B., D. Divoky and A. Liu. 1968. Shallow water waves: a comparison of theories and experiments. In: Proc. Coastal Eng. Conf. **1**:86-107.
- Longuet-Higgins, M. S. 1986. Acceleration in steep gravity waves. *Jour. Phys. Ocean.* **15**:1570-1579.
- Massel, S. R. 1989. Hydrodynamics of coastal zones. Amsterdam: Elsevier.
- Massel, S. R. 1996a. Ocean Surface Waves: their Physics and Prediction. Singapore: World Scientific Publ.
- Massel, S. R. 1996b. On the largest wave height in water of constant depth. *Ocean Engng.* **23**:553-573.
- Massel, S. R. 1996c. The limiting wave height in wind induced wave train (submitted to *Ocean Engineering*).
- Nelson, R. C. 1985. Wave heights in depth limited conditions. Civil Eng. Trans., Inst. Eng. of Australia. **27**:210-215.
- Nelson, R. C. 1987. Design wave heights on very mild slopes. Civil Eng. Trans., Inst. Eng. of Australia. **29**:157-161.
- Nelson, R. C. 1994. Depth limited design wave heights in very flat regions. *Coastal Engng.* **23**:43-59.
- Ochi, M. K. and C. H. Tsai. 1983. Prediction of occurrence of breaking waves in deep water. *Jour. Phys. Ocean.* **13**:2008-2019.
- Riedel, H.P. and Byrne, A.P. 1986. Random breaking waves - horizontal seabed. In: Proc. 12th Coastal Eng. Conf. **1**:903-908.
- Shore Protection Manual (SPM). 1984. U.S. Army, Coastal Engineering Research Center. Washington. Vol. I.

Snyder, R. L., L. Smith and R. M. Kennedy. 1983. On the formation of whitecaps by a threshold mechanism. Part III: Field experiment and comparison with theory. *Jour. Phys. Oceanogr.* **13**:1505--1518.

Srokosz, M. A. 1986. On the probability of wave breaking in deep water. *Jour. Phys. Ocean.* **15**:382-385.

Sulaiman, D. M., S. Tsutsui, H. Yoshioka, T. Jamashita, S. Oshiro and Y. Tsuchiya. 1994. Prediction of the maximum wave on the coral flat. In: Proc. 24th Coastal Eng. Conf. Kobe. **1**:609-622.

Tucker, M. J., A. P. Car, and E. G. Pitt. 1983. The effect of an off-shore bank in attenuating waves. *Coastal Eng.* **7**:133-144.

Weissman, M. A., S. S Ataturk and K. B. Katsaros. 1984. Detection of breaking events in a wind-generated wave field. *Journ. Phys. Oceanogr.* **14**:1608-1619.

WIND-WAVE-SURGE INTERACTION IN STORM SURGE PREDICTION

Takao Yamashita and Gary Watson

Kyoto University
Uji, Kyoto, Japan

ABSTRACT

Storm surges and the associated high breaking waves present a severe and sometimes disastrous coastal hazard. During surges there are complex mutual interactions between wind, waves and currents. The wind generates waves, which influence the wind drag coefficient and hence the wind-driven currents and the surge height. In turn, the currents influence the wave field and the waves influence the wind field. In order more accurately to predict surges, waves and flooding, a thorough understanding of these air-sea interaction processes is important. This paper briefly considers some of them.

The phenomena by which wave conditions influence both the bottom friction and wind stress are briefly discussed. The relation between mean wind and wind stress, and the influence of waves on this relationship, is then investigated using data from a new observation tower about 2 km offshore in Tanabe Bay. This measures wave elevation, 20-m wind and 10-m depth current in about 30m of water. Wind stress and drag coefficient estimates are made using the inertial dissipation method. Data taken during a typhoon are found to show enhanced stress compared with values from empirical formulae in the literature.

The relevance of these ideas and results for improving the representation of wind drag forcing and bottom friction in storm surge models is discussed. As a first step, a wave model is used to predict the wave field in the Bay of Bengal during the April 1991 cyclone disaster.

INTRODUCTION

Many storm surge models have been developed over the years, but the forcing terms are empirical. Surge models commonly use equations similar to the following for mass and momentum conservation (non-linear shallow-water equations with some forcing terms):

$$\frac{\partial \zeta}{\partial t} + \frac{\partial(ud)}{\partial x} + \frac{\partial(vd)}{\partial y} = 0 \quad (1)$$

$$\frac{\partial u}{\partial t} + u \frac{\partial u}{\partial x} + v \frac{\partial u}{\partial y} = f v - g \frac{\partial \zeta}{\partial x} - \frac{1}{\rho} \frac{\partial p_a}{\partial x} + \frac{1}{\rho d} \tau_{sx} - \frac{1}{\rho d} \tau_{bx} + A \nabla^2 u \quad (2)$$

$$\frac{\partial v}{\partial t} + u \frac{\partial v}{\partial x} + v \frac{\partial v}{\partial y} = -f u - g \frac{\partial \zeta}{\partial y} - \frac{1}{\rho} \frac{\partial p_a}{\partial y} + \frac{1}{\rho d} \tau_{sy} - \frac{1}{\rho d} \tau_{by} + A \nabla^2 v \quad (3)$$

Where ζ is surface elevation, d is total water depth, and (u, v) is depth-averaged velocity. The acceleration terms on the right of the momentum equations (2) and (3) are due respectively to Coriolis force, surface slope, atmospheric pressure gradient, surface wind stress $\bar{\tau}_s = (\tau_{sx}, \tau_{sy})$, bottom friction stress $\bar{\tau}_b = (\tau_{bx}, \tau_{by})$, and eddy viscosity.

For storm surge modelling, the most important forcing terms are the atmospheric pressure, the surface wind stress and the bottom friction stress. The former is of course theoretically well-defined and depends only on a reasonably accurate knowledge of the relevant time-dependent pressure field. The stress terms however are not so simple and are normally represented using empirical approximations. These are based on what data are available, which are rather limited and scattered. There is much room for improving our physical understanding of these stresses and then the accuracy of the corresponding forcing terms.

One current area of research is the influence of waves, on both wind stress and bottom stress. Waves are a crucial and complex part of the process of momentum transfer between air and sea, involving the two-dimensional wave spectrum, wave growth and decay, nonlinear interactions, and wave breaking. A forcing term in which the surface stress is a simple function of wind speed is a useful first approximation, and produces acceptable results in many circumstances. However, it is certainly oversimplified and there may be important cases where it is inaccurate, especially in situations where the wind is rapidly changing (such as in tropical storms), near the coast where the water is shallow and the waves fetch-limited, or where the wave spectrum has more than one significant component. Such cases could potentially be more accurately represented by a theory which correctly accounts for momentum transfer between wind and waves, and between waves and the mean current. This paper introduces some work which is aimed in this direction, including recent measurements from the Kyoto University Storm Surge Observation Tower.

Another effect of waves which may be important in some circumstances is their influence on the bottom stress. In shallow water, wave orbital velocities can be quite large and the flow over the rough bottom produces turbulence. This increases the eddy viscosity experienced by the mean flow and thus the force acting between the mean flow and the bottom.

The effect of these processes on surge models may be estimated by using a wave model to predict wave conditions during surge generation, and then modifying the surface and bottom drag coefficients, depending on appropriate properties of the local wave spectrum as outlined below. An assessment of the size of such effects remains a subject for further investigation.

STORM SURGES - EFFECT OF WAVES

Dependence of Surface Wind Stress on Wave Conditions

The mean force acting on the surface of a body of water due to wind stress is usually approximated as

$$\bar{\tau}_s = \rho_a C_{D10} \bar{U}_{10} |\bar{U}_{10}| \quad (4)$$

where $\bar{\tau}_s$ is the wind stress at the surface (the horizontal force per unit area acting on the surface), ρ_a the air density, \bar{U}_{10} the mean wind at 10 m and C_{D10} the drag coefficient for wind at 10 m.

With a constant drag coefficient, this formula is found to be reasonable for air flow over solid rough surfaces. However, as wind speed increases over the sea, the waves get bigger and the surface gets rougher. Thus, for Eq. 4 to be useful, the drag coefficient must be allowed to vary with wind speed: $C_D(U)$.

For fully-developed seas in which the waves are approximately in equilibrium with the local wind, observations of wind stress as a function of wind speed have led to several empirical relations for $C_D(U)$. The data are scattered, but the relationships resulting from the various datasets are all quite similar. Four examples of such formulae are listed in Table 1. Note that these data mainly apply to wind speeds greater than about 5-10 ms^{-1} .

Table 1. Empirical Formulae for Wind Drag Coefficient as a Function of Wind Speed.

Yelland & Taylor (1996)	$C_{D10} = (0.60 + 0.070U_{10}) \times 10^{-3}$	$U > 6 \text{ ms}^{-1}$
Smith et al. (1992)	$C_{D10} = (0.66 + 0.072U_{10}) \times 10^{-3}$	(HEXOS data)
Anderson (1992)	$C_{D10} = (0.49 + 0.071U_{10}) \times 10^{-3}$	
Smith & Banke (1975)	$C_{D10} = (0.63 + 0.066U_{10}) \times 10^{-3}$	

However, these results only apply to well-developed seas in deep water. Higher values of C_D found both in growing waves, such as during the onset of a storm, and in shallow water. Both of these conditions are necessary for the development of a storm surge, so the effect is potentially important. However, what field data exist are hard to interpret because the effect is comparable in size with measurement errors, and therefore cannot be determined very accurately. It has not so far been possible to derive any empirical relationship between wind stress and wave conditions, based on the data. The following section of this paper discusses some new data which add to the existing database and may be useful for investigating the effect.

Janssen (1991) proposed a theory for this effect. This considers the extra momentum extracted from the wind by growing waves, and then passing into the mean flow. This enhancement of momentum transfer effectively increases the drag. An important

parameter here is the ratio of dominant wave phase speed to wind speed, known as the wave age c_p/U , which is a measure of whether or not the wind and waves should have reached equilibrium. Another approach is to use Charnock's formula, which tends to give lower values of the drag coefficient.

The effect is not usually incorporated in surge models, and it is uncertain how significant it may be. One aim of this work is to make such investigations, using an ocean wave model to predict the wave spectrum, and applying the appropriate theory or empirical relations to the results, thus estimating the change in local wind stress and the overall effect on the storm surge prediction.

Dependence of Bottom Stress on Wave Conditions

The mean retarding force acting on a body of water due to bottom friction is usually approximated as

$$\bar{\tau}_b = \rho_w C_{Db} \bar{u} |\bar{u}| \quad (5)$$

where $\bar{\tau}_b$ is the bottom stress, ρ the water density, \bar{u} the wave-averaged bottom current and C_{Db} a bottom drag coefficient. For many applications, it is found good enough to use a constant value for C_{Db} .

In shallow water, wave-induced flow near the bottom results in an increase in turbulence. Amongst other things, this increases the rate of vertical transfer of horizontal momentum, and hence the mean drag force between the water and the sea bed. This is represented theoretically as an increase in eddy viscosity (which parameterizes the effect of small-scale turbulence in increasing the shear stresses) and hence of the drag coefficient in Eq. 5.

Mastenbroek (1992) estimated the size of this effect for storm surges in the North Sea using the relationship between drag coefficient and significant wave height, $C_{Db}(H_s)$ shown in Figure 1. He found that in some shallow areas it could significantly affect the predicted surge, more so than the effect of a wave-dependent wind drag coefficient. However, the size of this effect is similar to that of geographical variations in C_{Db} due to variations in bed roughness. This makes practical implementation difficult because of the lack of sufficiently detailed data on bed roughness.

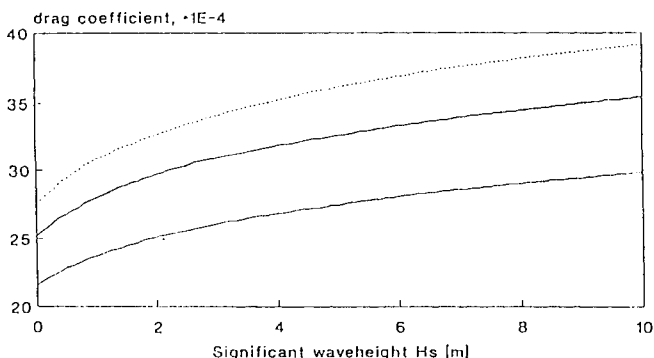


Figure 1. $C_{Db}(H_s)$ for 40-m depth water, 8-s waves and three different bed roughnesses. (Mastenbroek, 1992, Fig. 3.)

Wave Set-Up

For completeness, we also point out that another effect of waves on local water level at the coast is that of wave set-up. Depending on the beach topography and wave conditions, this can sometimes raise sea level within the surf zone by up to about 1 m. Although not the subject of this paper, it is an effect that should also be taken into account when considering the flood risk during storms and surges.

WIND AND WAVE DATA FROM THE OBSERVATION TOWER

The Kyoto University Disaster Prevention Research Institute's Tanabe-Nakajima Storm Surge Observation Tower (Figure 2) is located in 30 m of water, about 2 km from the coast near Tanabe, in southern Honshu Island, Japan (Wakayama Prefecture). The tower stands at the mouth of Tanabe Bay, on a plateau of about 10 m depth, around 100 m in diameter, in an area where the depth is predominantly 30 m. It is possible that this plateau will have some local influence on the waves, but this is difficult to determine. The site is in the approaches to the densely-populated area around Osaka Bay (No. 8 in Figure 3). Typhoons regularly cause surges in this area and defences against these form a significant element of coastal engineering works.

The main instruments of interest here are a 3-component ultrasonic anemometer at about 20 m height, and a downward-looking ultrasonic wave gauge. Data are recorded at 20 Hz during 20 minutes of each hour. There is also an electromagnetic current meter at a depth of 10 m.

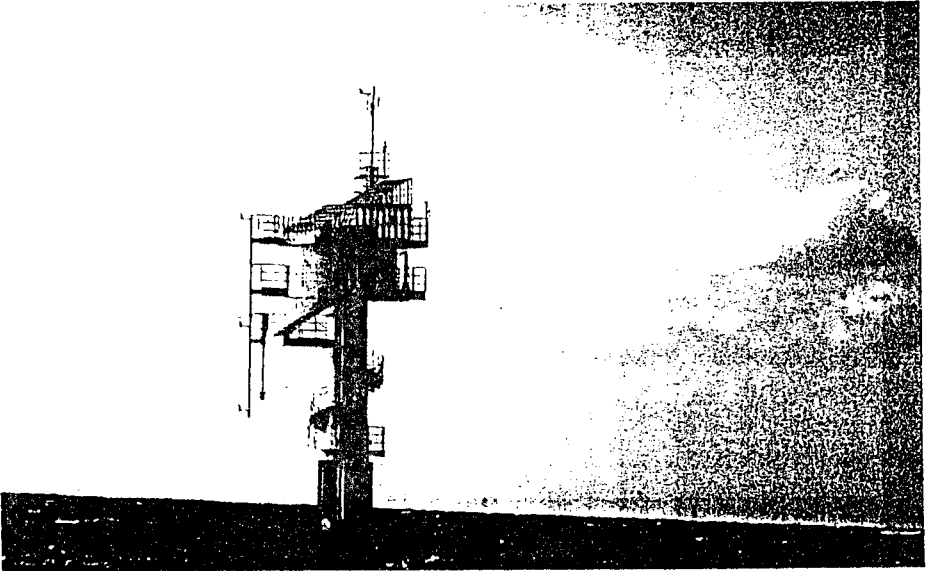


Figure 2: The Kyoto University DPRI Tanabe-Nakajima Storm Surge Observation Tower

Because the largest surges are generated by storms, data from a typhoon are considered first. On 29 Sept. 1994, Typhoon 9426 passed very close to the tower, with strong winds from the east rapidly changing to strong winds from the west. The central pressure was about 950 hPa when it passed the tower, where the minimum recorded was 965 hPa at about 19:00. Maximum recorded wind speed was 24 ms^{-1} from the west, about 2 hours later. Wave height peaked at around 5 m near 17:00. Wave period reduced from 13 s to 7 s as the typhoon passed, but direct measurements of wave direction are not available. These observations were reported in more detail by Yoshioka et al. (1995). The typhoon track is shown in Figure 3. Recorded wind speed and direction are shown in Figure 4 and wave height and period in Figure 5.

Following Yelland et al. (1994), wind stress was estimated from the anemometer data using the turbulent (or inertial) dissipation method. This is one of the two commonly-used methods, the other being the direct, or eddy-correlation method. The latter was also attempted but it was found that the 20-minute data samples were not long enough to give convergent results.

The turbulent dissipation method is based on the assumption of a cascade of energy from lower to higher frequencies, at a rate which is governed by the rate of dissipation of energy by turbulence at the high-frequency end of the spectrum. The turbulence is

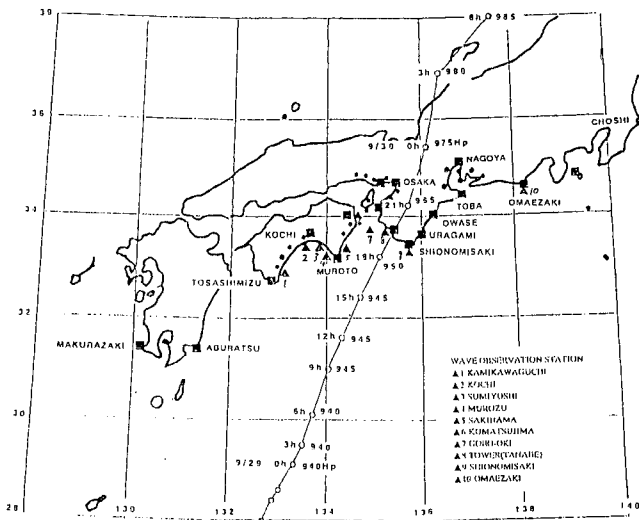


Figure 3: The track and central pressure of Typhoon 9426. (Yoshioka et al., 1995)

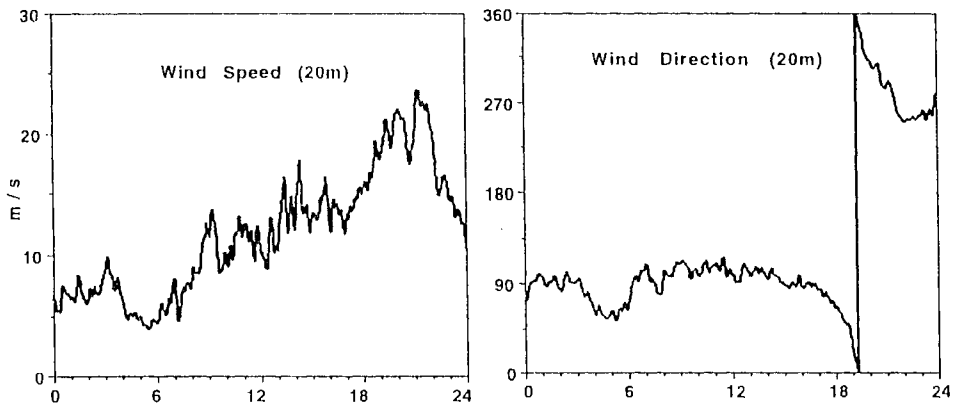


Figure 4: Wind speed and direction (Tower, T9426). (Yoshioka et al., 1995)

assumed to be "frozen", i.e. the time scales are slow compared with the time scale of advection past the observation point. These assumptions yield:

$$S(f) = Ke^{2/3} f^{-5/3} \left(\frac{U}{2\pi}\right)^{2/3} \quad (6)$$

where $S(f)$ is the power spectrum of the down-wind component, K is the 1-D Kolmogorov constant, taken as 0.55, and ε is the high-frequency turbulent dissipation rate. If the measured spectrum is found to obey the $f^{-5/3}$ law reasonably well, then an average value of $S(f)f^{5/3}$ over an appropriate frequency range (0.8-2.0 Hz was used here) may be used in (6) to estimate ε . The wind stress τ is then estimated from

$$\tau = \rho(k_v \varepsilon z)^{2/3} \tag{7}$$

where k_v is the von Karman constant (here taken as 0.4), and z is the measurement height (20 m). The drag coefficient is then obtained from (4) after correcting the observed mean wind to an estimated value at 10 m using the relation for a logarithmic boundary layer,

$$\frac{U(z)}{U(10)} = \frac{\ln(z/z_0)}{\ln(10/z_0)} \tag{8}$$

where z_0 is the roughness length $z_0 = z e^{-k_v / \sqrt{C_D}}$. It should be noted that (6) applies to neutral atmospheric stability. A correction is possible for non-neutral conditions, but was found to be small in this case.

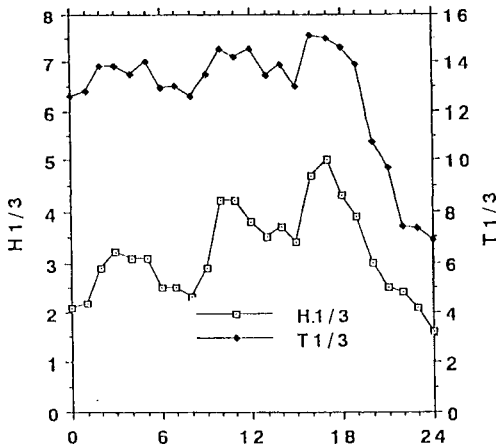


Figure 5: Wave height and period (Tower, T9426). (Yoshioka et al., 1995)

Figure 6 shows the power spectrum of the wind component in the direction of mean wind ('downwind component') multiplied by $f^{5/3}$ for each hour of the typhoon. Between 12:00 and 21:00, the spectrum in each case is almost constant over the frequency range used for the average (0.8-2.0 Hz, dotted lines). This permits Eq. 6 to be used with some confidence. For the data at 22:00 and 23:00 however there is a distinct slope, indicating that the $f^{5/3}$ power law does not apply, and that (6) should not be used. This is unfortunate, since results just after a rapid change of wind direction are of particular

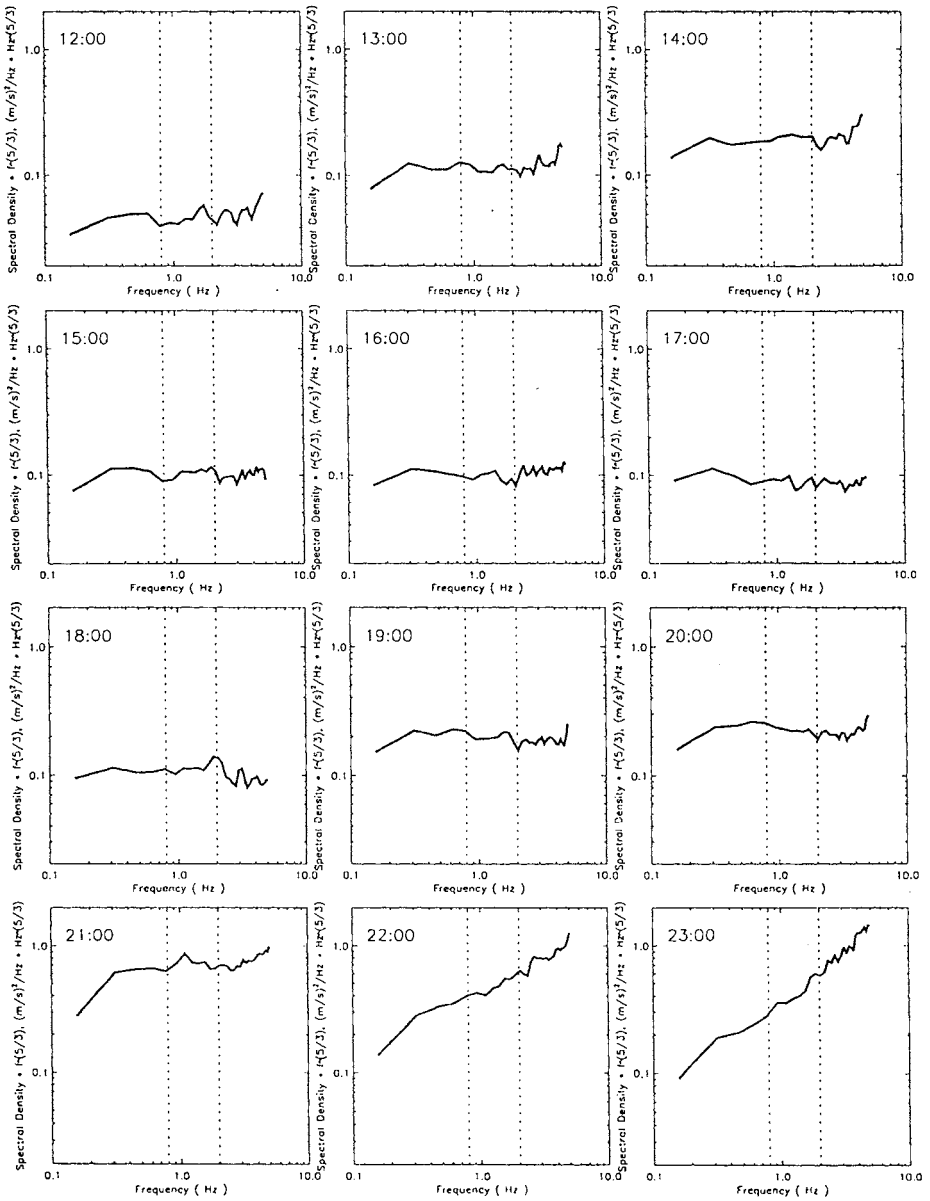


Figure 6: Wind Spectra ($S(f)f^{5/3}$), 12:00–23:00, 29 Sep 94 (T9426)

interest. The reason for the different spectral slope (these data have much more high-frequency content) are not clear but may be caused by interference of the anemometer structure with the flow. The problem requires further analysis. One must also be aware that flow distortion around the tower structure, although it should not much affect the turbulence and the stress estimate, will change the observed value of the mean wind, introducing an unknown error into the estimated drag coefficient. Plans are in hand to verify these values by comparison with estimates from anemometers in different positions on the tower, and from the eddy correlation method.

The final estimates of stress for this day, excluding the data from 22:00 and 23:00, are plotted against mean wind speed in Figure 7. The four empirical relations from Table 1 are plotted for comparison. Particularly at intermediate wind speeds (5-15 ms^{-1}), the data lie well above these curves. These data appear to be an example of departure from the standard formulae and are thus worthy of further investigation. There is no obvious trend with wind speed, and as with other such data, they are rather scattered. If anything, these data suggest that a constant drag coefficient may be appropriate in this instance. The mean value is 2.2×10^{-3} . However, this is only a small amount of data and it will be necessary to examine a larger amount, including normal wind conditions, in order to draw firm conclusions.

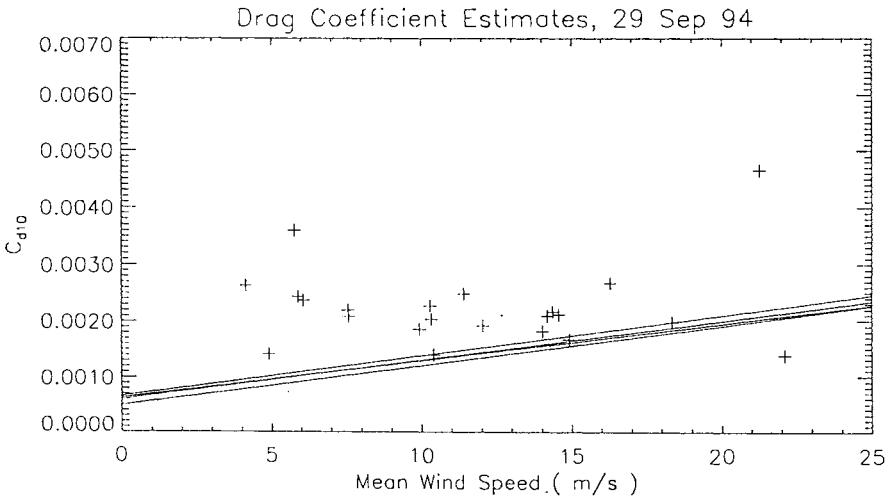


Figure 7: Drag coefficient estimates against wind speed during the typhoon.

INCORPORATION OF WAVE EFFECTS INTO SURGE MODELS

The next stage of this work, in addition to further analysis of the wind stress data, will be to incorporate wave effects into a surge model. The first step is to use an ocean wave model to predict the time-dependent wave field during the storm. This has been done for the cyclone which struck Bangladesh in April 1991, causing a severe disaster in which 150,000 people died. The model is that of Yamaguchi et al. (1979) and the main result is shown in Figure 8. It is a second-generation model, whereas third-generation models which include a more accurate calculation of nonlinear interactions, such as WAM, are now available. However, it is uncertain whether this would be any more applicable in the highly-nonlinear situation in the extensive shallow region near Bangladesh, and so the more convenient second-generation model was used. Qualitative differences are not expected.

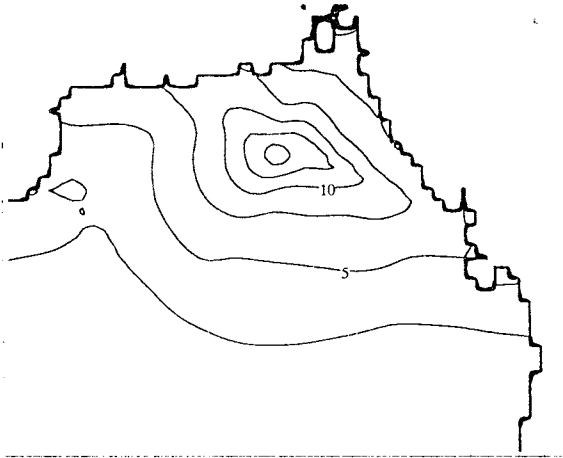


Figure 8: Wave height prediction for the Northern Bay of Bengal, 15:00, 29 April 1991.

The figure shows contours of significant wave height during the approach of the cyclone, with a maximum of about 15 m being predicted near the cyclone centre. The next step will be to take the results for wave height and use them to modify the surface and bottom drag coefficients in the surge model, as outlined above. In this way, the size of wave effects on the surge prediction will be assessed.

During the finalization of this paper, the authors became aware of the work of Zhang and Li (1996) who have implemented a coupled wave-surge model using Janssen's theory for

the effect of waves on wind stress, including radiation stress terms, but not considering the effect of waves on bottom stress.

DISCUSSION AND CONCLUSIONS

We have seen that wave effects on wind stress and bottom stress are likely to influence the size of a storm surge in some circumstances. These effects are not clearly understood and so are not included in surge models. There is room for improving our understanding of the physics of these processes. In the case of wind stress, this should come from comprehensive and accurate field measurements of wind stress in a range of wind and wave conditions.

Data taken during storms are particularly important for the storm surge problem. One such dataset, from a new tower, shows enhanced stress during a typhoon, in comparison with empirical formulae from the literature. Data from this tower add to those currently in existence and should be thoroughly analyzed as they become available. Eventually, a more accurate formulation of wave effects in surge models may be possible.

ACKNOWLEDGMENTS

Thanks are due to Dr. H. Yoshioka of DPRI for discussion and help with analysis of the tower data and for permission to use several figures; Prof. S. Nakamura of Kyoto University's Shirahama Oceanographic Observatory for permission to use the data; Ms. M. Yelland of Southampton Oceanography Centre for advice on the inertial dissipation method and Dr. S. Smith of Bedford Institute of Oceanography for advice on the eddy-correlation method.

REFERENCES

- Anderson, R.J. 1993. A study of wind stress and heat flux over the open ocean by the inertial dissipation method. *J. Phys. Oceanogr.* **23**: 2153-2161.
- Mastenbroek, C. 1992. The effect of waves on surges in the North Sea, Proc. 23rd Int. Conf. Coastal Eng., ASCE, 874-882.
- Janssen, P.A.E.M. 1991. Quasi-linear theory of wind wave generation applied to wave forecasting. *J. Phys. Oceanogr.* **21**: 1631-1642.
- Smith, S.D. and Banke, E.G. 1975. Variation of the sea surface drag coefficient with wind speed. *Quart. J. Roy. Meteorol. Soc.* **101**: 665--673.

Smith, S.D. et al.. 1992. Sea surface wind stress and drag coefficients: the HEXOS results. *Boundary-Layer Meteorology*. **60**: 109-142.

Yamaguchi, M. et al. 1979. Numerical prediction method for fetch-limited ocean waves. (in Japanese). Proc. 26th. Coastal Engineering Conf. (Japan), 96-100.

Yelland, M.J. et al. 1994. The use of the inertial dissipation technique for shipboard wind stress determination. *J. Atmos. Oceanic Technology*. **11**: 1093-1108.

Yelland, M.J. and Taylor, P.K. 1996. Wind stress measurements from the Open Ocean. *J. Phys. Oceanogr.* **26**: 541-558.

Zhang, M.Y. and Li, Y.S. 1996. The synchronous coupling of a third-generation wave model and a two-dimensional storm surge model. *Ocean Engineering*. **23**: 533-543.

Yoshioka, H. et al. 1995. The storm surge induced by Typhoon 9426. (in Japanese). *Ann. Disast. Prev. Res. Inst., Kyoto Univ.*, **38**, B-2: 581-598.

STORM SURGES IN THE PACIFIC FORUM REGION

J. L. Luick, R. F. Henry and T. S. Murty

National Tidal Facility
Adelaide, SA, AUSTRALIA

ABSTRACT

The South Pacific region consists of the following island nations: Cook Islands, Federated States of Micronesia, Fiji, Kingdom of Tonga, Marshall Islands, Niue, Papua New Guinea, Republic of Kiribati, Republic of Nauru, Solomon Islands, Tuvalu, Vanuatu, Western Samoa.

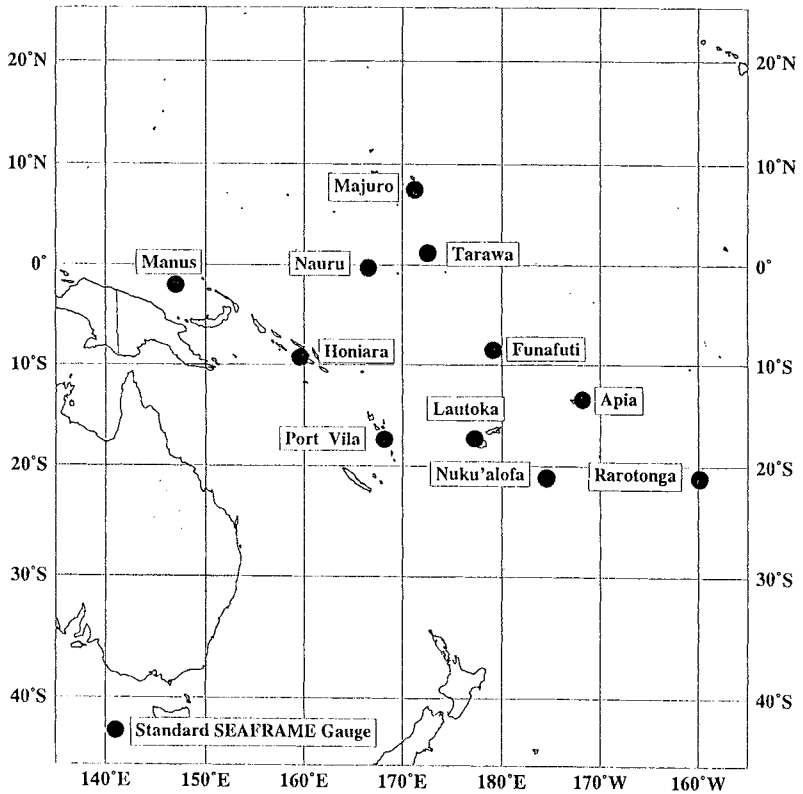
The nations mainly in the western part eg, Federated States of Micronesia (FSM) and Fiji, are subject at periodic intervals to tropical cyclones and the storm surges that are produced by them. Even though the lack of extensive continental shelves precludes the development of large amplitude surges such as those that occur in the Bay of Bengal and the Gulf of Mexico, nevertheless, moderate surges are generated. The inundation from such surges could cause problems in small islands with increased coastal erosion and salt water intrusion into coastal aquifers.

Because of the complex topography (several small islands interspersed over a large area), traditional finite-difference models are not very applicable. Instead more sophisticated irregular triangular grid models are being developed to include not only realistic bathymetry but also the state of the tide. The meteorological forcing terms for the models are the tangential surface wind stresses and the atmospheric sea level pressure fields which are space and time-dependent.

INTRODUCTION

A map of the South Pacific Forum region (Figure 1) gives the locations of the eleven SEAFRAME gauges in the region operated by the National Tidal Facility (NTF) of Australia. These gauges use acoustic signals and have a precision of about 1 mm as compared to an accuracy of about 1 cm for the more traditional gauges. These gauges were placed to monitor the relative sea level changes that may be caused by the Greenhouse warming.

However, these gauges record all forms of long gravity waves, such as tides, storm surges and tsunamis. Storm surges up to one metre have been noticed occasionally in the residuals of these tide gauge records.



NATIONAL TIDAL FACILITY

Figure 1: Locations of the SEAFRAME gauges in the Pacific operated by the National Tidal Facility

WHERE DO THE SURGES OCCUR?

Figure 2 shows the areas north and south of the equator where the tropical cyclones form. There is a clear break at the equator where there are none due to the absence of the coriolis force.

Tropical cyclones in the South Pacific tend to form in the "monsoonal trough" between 10° - 15° S in the western South Pacific. During El Nino years the monsoonal trough shifts to the east onto the Central Pacific. Very few cyclones intensify south of 20° S (due primarily to increasing westerlies in the upper troposphere).

In the southwest Pacific, tropical cyclones typically continue to intensify as they move southwards from their points of origin, decaying over cooler subtropical water. More than half, however, decay prior to reaching 30° S, while a third of tropical cyclones in the southwest Pacific eventually become extra-tropical depressions.

It is known (Murty 1984) that looking down the track of movement of a tropical cyclone, peak surges occur to the right of the track in the northern hemisphere and to the left in the southern hemisphere.

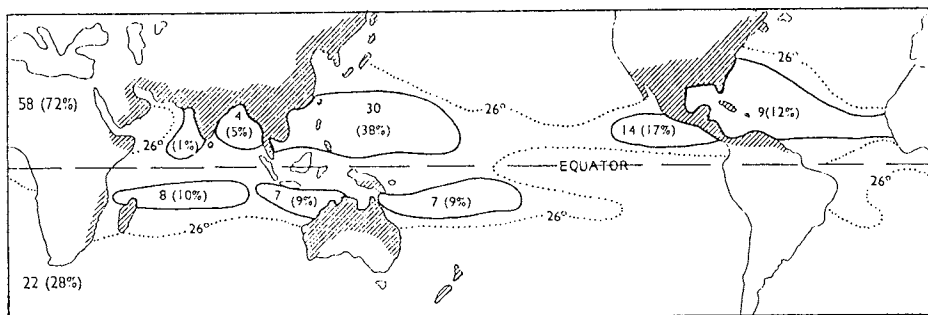


Figure 2: Areas of tropical cyclone occurrence (from Gray 1975).
Land areas affected by cyclones are shown hatched.

Figure 3 shows the track of Hurricane Bebe of 1972. Even though the track is over Viti Levu, there is no coast against which the tangential wind stress can push water to the left of the track and pile it up. On the other hand, depending upon the strength of the wind field a surge could occur on the island, Vanua Levu.

The tracks of five hurricanes near Viti Levu are shown in Figure 4. Again using the above rule of thumb, only the track for February 1965 should generate a peak surge on Viti Levu, depending upon the strength of the wind field.

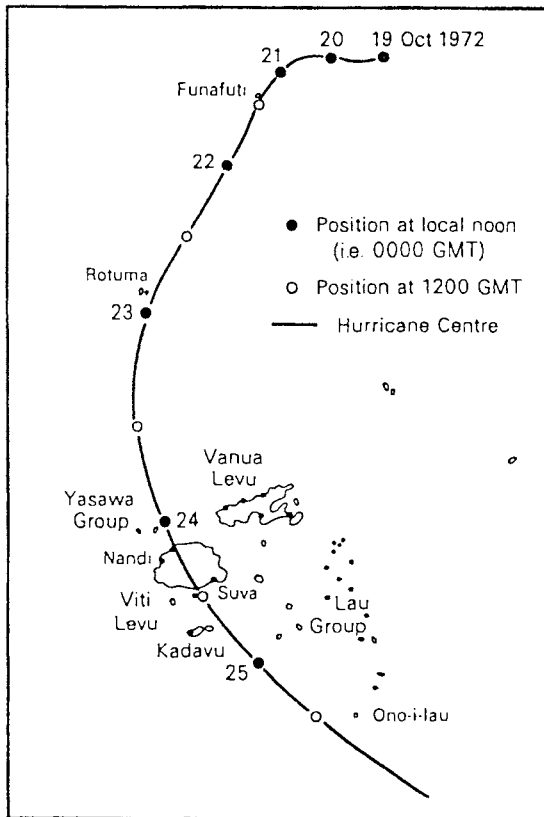


Figure 3: Track of Hurricane Bebe October 1972
(from New Zealand Meteorological Service)

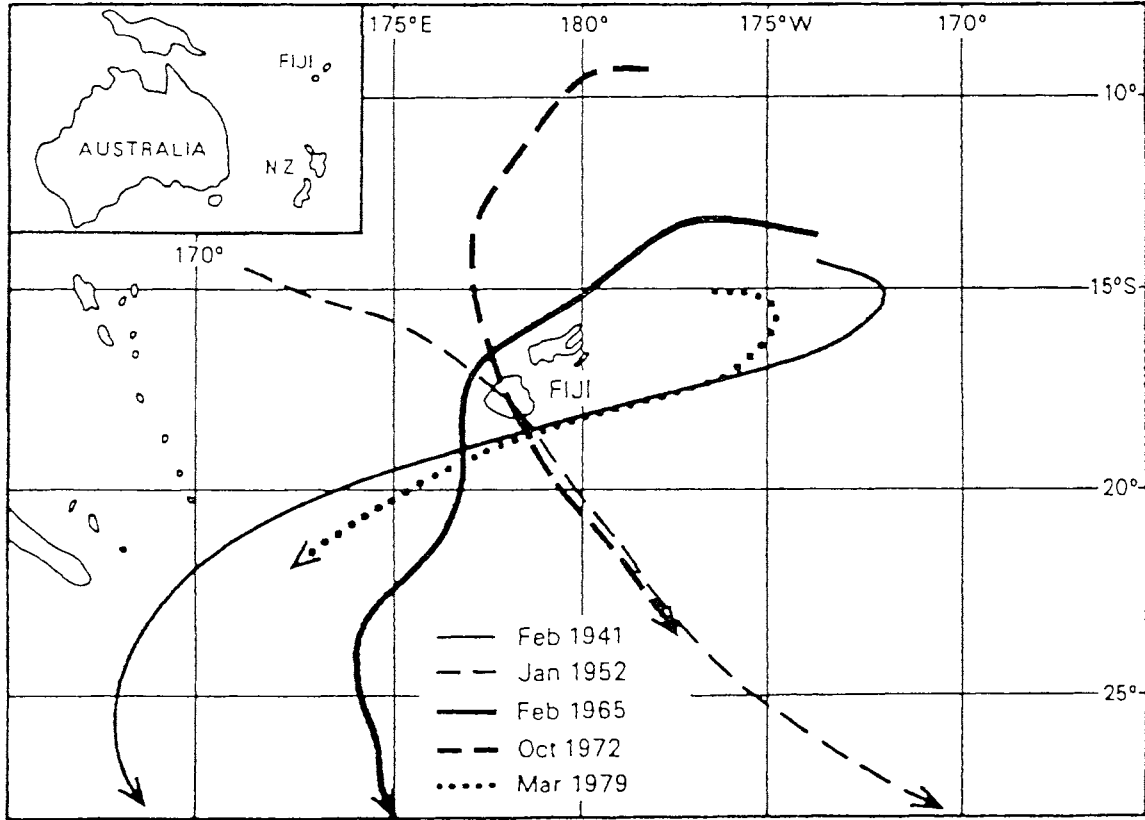


Figure 4: Tracks of severe hurricanes in the Fiji area between 1940 and 1979 (from Fiji Meteorological Service)

COMPUTATION OF STORM SURGE

During 15-16 January 1996, a minor storm surge occurred in Tonga and was recorded on the SEAFRAME as shown in Figure 5. The following information can be deduced from an examination of this figure.

Total residual or storm surge ~ 0.33 m.

Wind set-up (residual adjusted for the atmosphere pressure effect) ~ 0.18 m.

Inverse barometer effect = $0.33 - 0.18 = 0.15$ m. Pressure drop ~ 15 hPa (hectoPascals).

The wind set-up can be estimated roughly from the following simple calculation.

$$\frac{\partial \eta}{\partial x} = \frac{\rho_a C_D W^2}{\rho g D} \quad (1)$$

- η = amplitude of the surge (m)
- x = coordinate perpendicular to the shoreline
- ρ_a = density of air = 1.25 kg/m^3
- ρ = density of sea water = $1.026 \times 10^3 \text{ kg/m}^3$
- C_D = drag coefficient = 2.8×10^{-3} (dimensionless)
- g = gravity = 9.8 m/s^2
- D = average depth of the water = 10 m
- W = wind speed = 35 m/s

Using these values, we get

$$\frac{\partial \eta}{\partial x} = 0.42 \times 10^{-4} \quad (2)$$

Assuming a fetch of 5 km, one can write.

$$\eta = \frac{\partial \eta}{\partial x} x = 0.42 \times 10^{-4} \times 5 \times 10^3 \text{ m} = 0.21 \text{ m} \quad (3)$$

The amplitude of the wind set-up computed from the simple formula is 0.21 m which compares reasonably well with the observed wind set-up of 0.18 m. A numerical model will yield a better agreement.

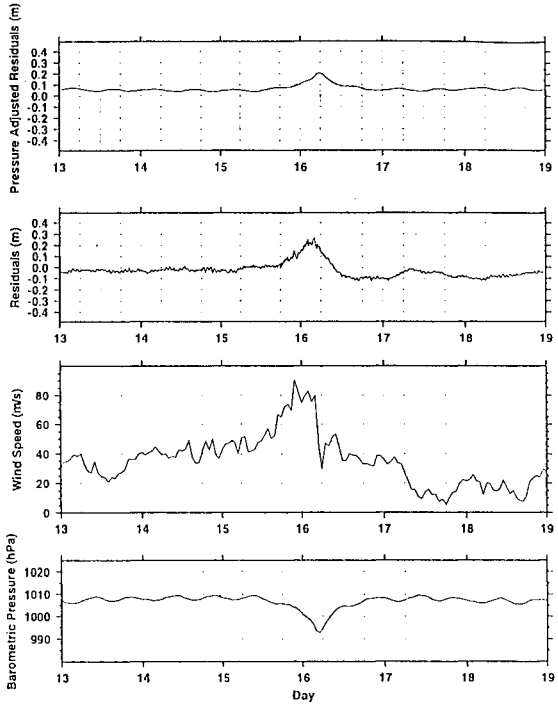


Figure 5: Wind gust, barometric pressure, adjusted residual and residual at Tonga SEAFRAME gauge for January 1996

Traditionally finite-difference numerical models have been used for storm surge computations. In recent years finite-element models with irregular triangular grids have increasingly been used. As can be seen from Figures 6 and 7, the irregular triangular grids can resolve the bathymetry much better than rectangular grids.

A finite element model supplied with tidal boundary conditions from Egbert et al. (1994) inverse analysis of Topex/Poseidon satellite altimeter observations is currently being tested to identify portions of the Fiji coasts which are particularly vulnerable to storm surges. Initial results show encouraging agreement with tide gauge observations at Lautoka and Suva.

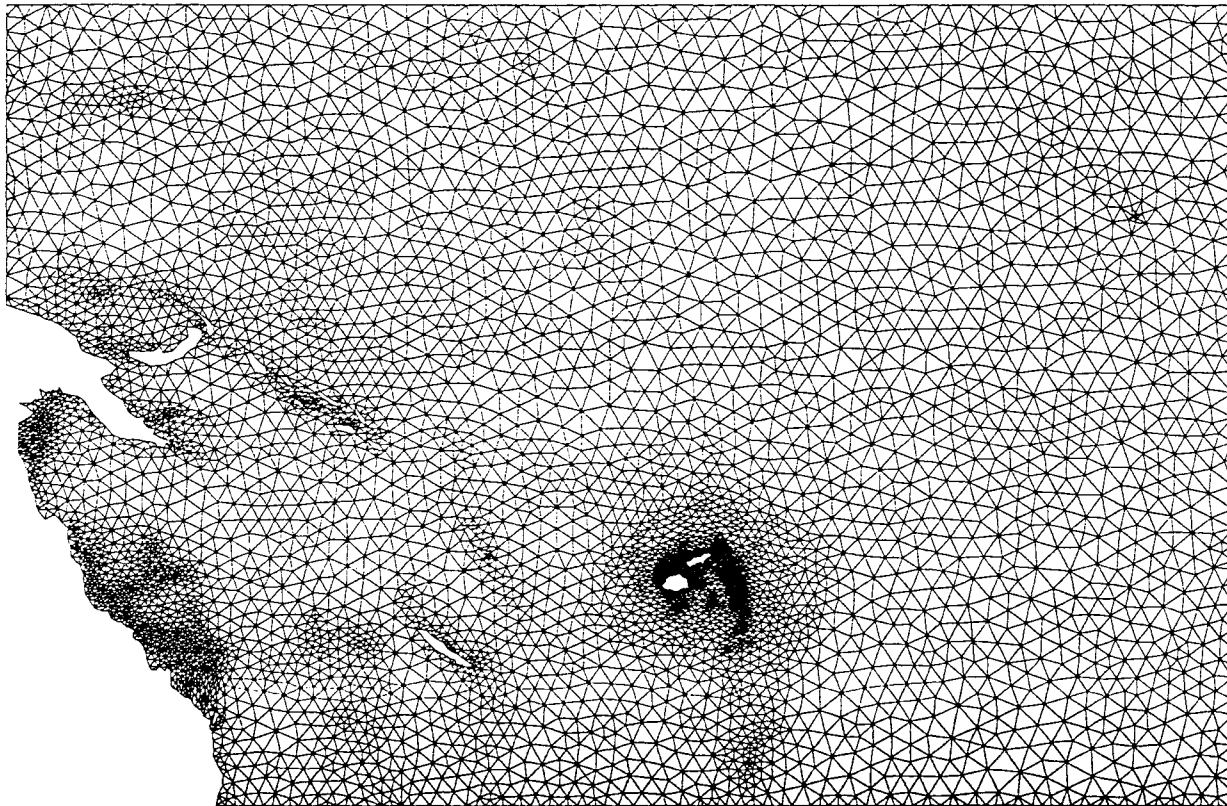


Figure 6: Irregular triangular Forum Area Region model grid

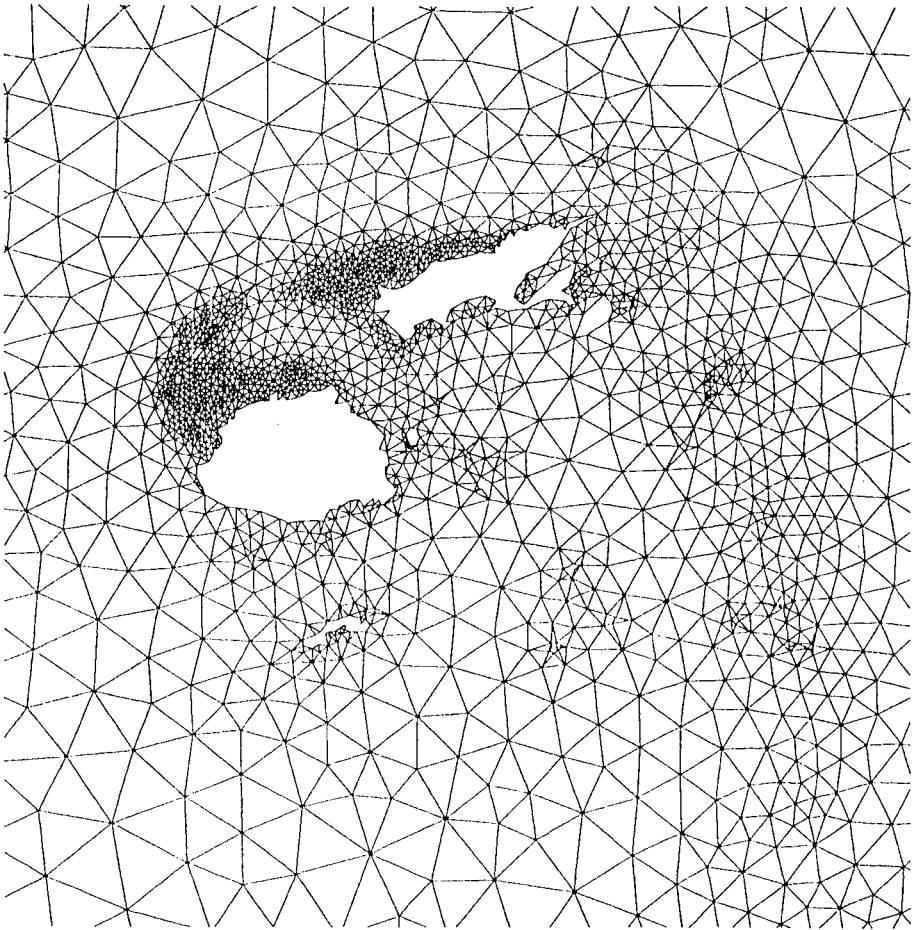


Figure 7. Close up view of irregular triangular grid for the Fiji area

REFERENCES

Egbert G. D., A. F. Bennett and M. G. G. Foreman. 1994. Topex/Poseidon tides estimated using a global inverse model. *J. Geophys. Res.* **99**, C12, 24821-24852.

Gray. 1975. Tropical Cyclone Genesis. Atmos. Sci. Paper 234, Colorado State University, Fort Collins, Colorado.

Murty, T. S. 1984. Storm Surges - Meteorological Ocean Tides. Ottawa: Department of Fisheries and Oceans.

Thompson, R. D. 1981. Weather. Bracknell, England, pp. 138-140.

MODELING METHODOLOGIES FOR THE PREDICTION OF HURRICANE STORM SURGE

Cheryl Ann Blain
Naval Research Laboratory
Stennis Space Center, MS USA

ABSTRACT

Both the size and discretization of the computational domain can significantly influence the model representation of storm surge generation in a coastal region. An appropriate modeling strategy for the prediction of hurricane storm surge includes the use of a very large domain which encompasses the coastal region of interest and extends out of resonant basins into deep ocean waters. A domain of this size allows proper generation and propagation of the storm surge throughout the domain and onto the continental shelf and minimizes the influence of the boundary condition specification. An additional strategy involves the use of a graded grid structure which yields low, uniform prediction errors throughout the domain and minimizes computational effort. High levels of grid resolution are necessary in near shore regions and at the coastline to accurately represent hurricane storm surge generation. In deep waters, resolution requirements on the order of the spatial scale of the hurricane are less restrictive. The recommended guidelines for model formulation with respect to the model domain size and grid discretization are summarized here and illustrated with applications to hurricanes Kate and Camille in the Gulf of Mexico. Further validation of the modeling methodology put forth is demonstrated in the prediction of tropical storm surge in the Yellow and East China Seas during the 1995 typhoon season.

INTRODUCTION

Numerical modeling is an increasingly important tool used for understanding the hydrodynamic behavior of the coastal ocean. Studies documenting numerical model performance with regard to grid spacing and domain size are often neglected yet are an extremely important component of any successful model application. This paper first summarizes the modeling strategy outlined by Blain et al. (1994, 1996) for selection of a model domain size and construction of a computational grid. This modeling strategy then is demonstrated through simulations of the storm surge generated by hurricanes Kate and Camille along the Gulf of Mexico coast. These applications using the recommended domain size and grid structure capture the significant features of the hurricane storm surge produced by these storms.

Storm surge generation from hurricane Kate, which made landfall on the Florida shelf in the Gulf of Mexico, is examined over three domain sizes which allows comparisons

between storm surge elevations computed over each domain. The sensitivity of boundary specification to domain size is evident. In a second example, storm surge computations over an idealized domain having regular and variably graded grid discretizations are compared using maximum prediction errors cast in the form of a Richardson based error estimate (Roache, 1994). The importance of near shore resolution and coastline refinement is illustrated. Low uniform errors in the prediction of storm surge along the Mississippi Gulf coast result when the gridding concepts are applied to the simulation of hurricane Camille. An independent test of the modeling strategy with respect to domain size and grid construction is undertaken in the simulation of storm surge generated by typhoon forcing in the Yellow and East China Seas during the 1995 season. An evaluation of model performance is presented to demonstrate the analyses that should accompany all storm surge model applications and confirm the validity of the storm surge modeling strategy put forth.

MODELING STRATEGY

Domain Size Selection

The work of Blain et al. (1994) suggests selection of a domain size which is large enough to allow proper generation and propagation of the storm surge throughout the domain onto the continental shelf and into coastal regions. Furthermore, the domain selected must

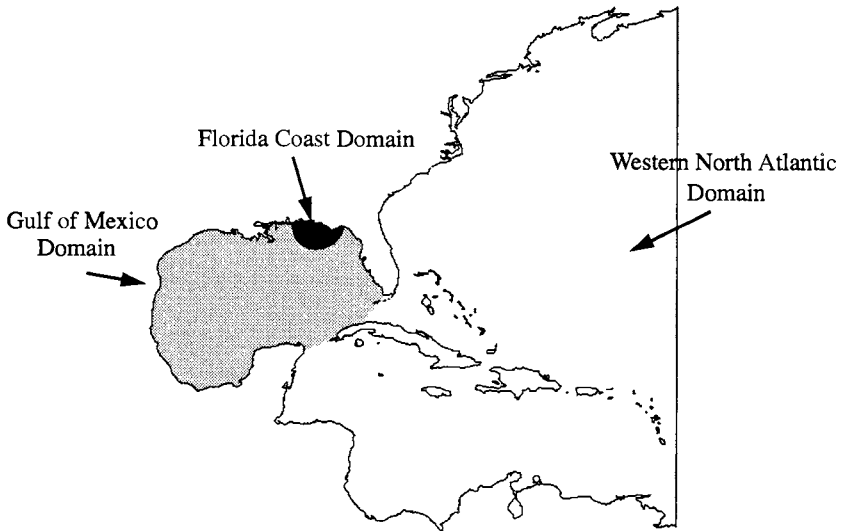


Figure 1. Three domain sizes evaluated in the prediction of storm surge on the U. S. Florida coast from hurricane Kate, 1985.

minimize the influence of the open boundary specification. Three domain sizes, shown in Figure 1, clearly demonstrate the relationship between domain size and open boundary elevation specification. The smallest domain considered, the Florida Coast domain, is a semi-circular basin which mainly lies on the continental shelf at depths less than 130 m and is similar to one used by the National Weather Service (Jelesnianski et al., 1992). The second domain, the Gulf of Mexico domain includes the entire Gulf of Mexico and is similar to domains used by other investigators for storm surge modeling studies in the Gulf of Mexico (e.g. Bunpapong et al., 1985). The final and largest domain is the Western North Atlantic (WNAT) domain which has been previously used by Blain et al. (1994) and Scheffner et al. (1994) to compute storm surge heights along the Gulf of Mexico and eastern U. S. coasts. The WNAT domain encompasses the Gulf of Mexico, contiguous basins, and extends out of resonant basins into the deep regions of the western North Atlantic ocean. A deep Atlantic ocean boundary lies along the W meridian, far from the coastal region of interest.

A series of simulations is conducted using a historical storm, hurricane Kate (1985), as the meteorological forcing. All domains have identical discretizations over corresponding regions and simulations were conducted using identical model parameters and wind and pressure forcing. Thus, any differences between the model responses are attributed solely to the domain size and/or the boundary elevation specification. Contours of the storm surge elevations generated by hurricane Kate forcing in the northeast Gulf of Mexico are shown in Figure 2a, 20 hours prior to landfall. Notice the substantial storm surge elevations occurring in the vicinity of the open ocean boundaries of the Florida Coast domain as water is pushed up on the shelf by hurricane winds. The storm surge hydrograph at Carrabelle along the Florida coast (dashed line in Figure 2b) clearly

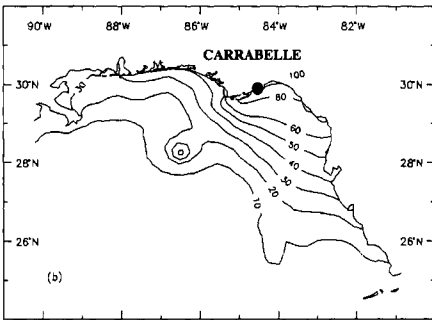


Figure 2a. Storm surge elevations (cm) in the northeast Gulf of Mexico from hurricane Kate 20 hours prior to landfall, November, 1985.

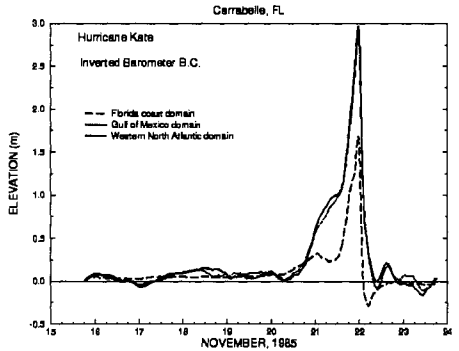


Figure 2b. Comparisons of storm surge elevations (m) for hurricane Kate at Carrabelle, FL computed over three domain sizes.

illustrates that a model domain such as the Florida Coast domain which is situated largely on the continental shelf and whose size is limited relative to the size of the storm significantly underestimates the primary storm surge response relative to the two larger domains. On the contrary, both the Gulf of Mexico and WNAT domains yield nearly identical predictions of the peak primary storm surge. The storm surge profile at Carrabelle is representative of conditions on the right-hand side of the hurricane, east of the hurricane landfall region and the region of significant storm surge generation.

The sensitivity of the boundary forcing is clearly evident in storm surge hydrographs at Carrabelle (Figures 3a and 3b) when comparing computed storm surge responses over a single domain which incorporates two different boundary elevation forcings. While the peak surges over the Gulf of Mexico domain closely correspond in Figure 3a, different oscillatory patterns before the peak storm surge are predicted. These oscillatory patterns are associated with resonant modes in the Gulf of Mexico basin and relate to the surge forerunner. While the predicted modes in the Gulf of Mexico domain appear to be very sensitive to the boundary forcing specified, modes in the WNAT domain solution exhibit no sensitivity to boundary condition specification as seen by identical storm surge profiles in Figure 3b.

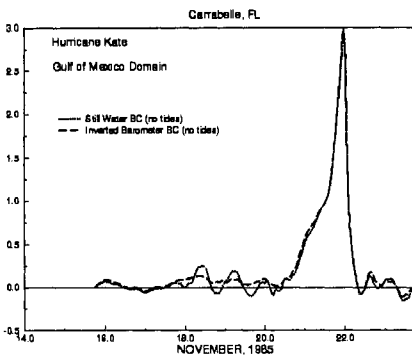


Figure 3a. Storm surge elevations (m) from hurricane Kate at Carrabelle, FL computed over the Gulf of Mexico domain using two different boundary forcings.

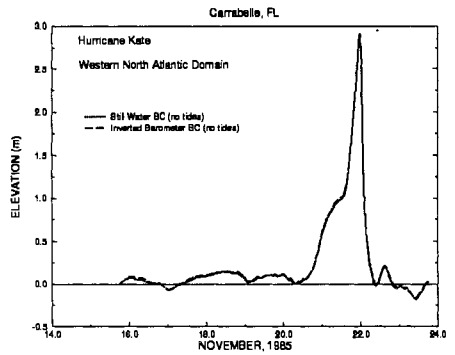


Figure 3b. Storm surge elevations (m) from hurricane Kate at Carrabelle, FL computed over the Western North Atlantic domain using two different boundary forcings.

Computations over the WNAT domain which includes the western North Atlantic ocean, the Gulf of Mexico, and the Caribbean Sea capture both the primary storm surge and the surge forerunner. The inclusion of contiguous basins allows the proper set up of basin resonant modes and facilitates the realistic propagation of storm surge throughout the domain onto the continental shelf where development of the storm surge is most critical. The main advantage of the WNAT domain is that the open boundaries lie within the deep Atlantic ocean and are far from the intricate processes occurring on the continental shelf and within the Gulf of Mexico basin in response to the storm. Such a large domain with remote, deep open ocean boundaries is recommended for storm surge model applications.

Grid Structure

A grid discretization which yields low, uniform prediction errors throughout the domain and minimizes computational effort is optimal. Blain et al. (1996) demonstrate that high levels of grid resolution are necessary at the coastline and in near shore regions to accurately capture primary hurricane storm surge generation. They state that resolution in open waters may be relatively coarse but should be at least on the order of the spatial scale of the hurricane and suggest implementation of a graded grid structure. Though not addressed here, refinement of the grid discretization also increases the resolution of the bottom topography. Luettich and Westerink (1995) demonstrate that bathymetric changes are important with regard to tidal phenomena and hence may also influence storm surge computations. The relative importance of the coastline detail versus bathymetric refinement remains an open question.

To evaluate the performance of the graded grid structure, a Richardson based error estimate is implemented as discussed by Roache (1994) and used by Blain et al. (1996). By comparing differences between solutions obtained over a graded and a fine, uniform grid, an estimate of the error associated with the graded grid is made. Error estimates are computed using extreme and normalized overprediction and underprediction errors. Extreme errors are determined with respect to the entire domain at a specific point in time. Normalization of these errors is achieved with respect to the absolute extreme surge over the entire period of simulation. Normalization allows comparison of the errors within a storm simulation. The depths at which extreme errors occur are also tracked.

A synthetic hurricane, which makes landfall along a path perpendicular to a straight coastline is applied as forcing over a rectangular domain. This domain is discretized using both a regular and graded grid structure. A uniform grid, G03, has regular nodal spacings of 12.5 km. In the graded grid, VG02, refinement at the 12.5 km level extends from the shoreline to 25 km offshore and 25 km spacing covers the remainder of the continental shelf with 50 km spacing elsewhere. Storm surge predictions computed over grids G03 and VG02 are compared in Figure 4 using the Richardson based error estimates just described.

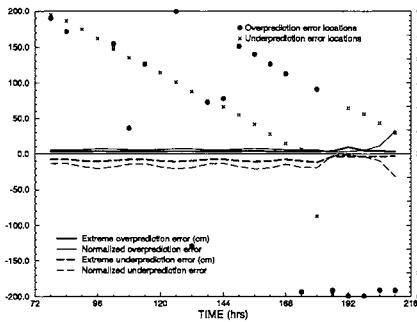


Figure 4. Error estimates (cm) for storm surge computed over the graded grid, VG02, as compared to the uniform grid, G03.

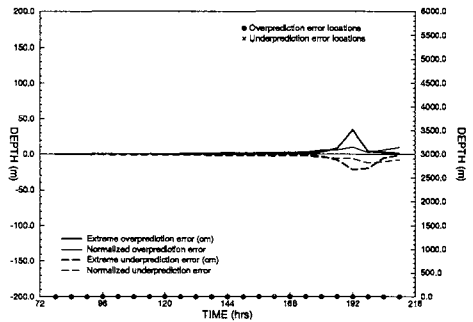


Figure 5. Error estimates (cm) for storm surge computed over identical, uniform grids having two different refinements of a sinusoidally varying coastline.

The largest errors over grid VG02 are due to an underprediction of the inverted barometer effect of the hurricane in deep waters. A slight increase in the overprediction error is seen at the time of peak surge and is concentrated on the continental shelf nearest the shoreline. In general, the maximum errors computed over grid VG02 are relatively uniform in time and space and utilize 1/12 the nodal density of grid G03. A graded mesh clearly provides an optimal grid structure for minimizing storm surge prediction errors and maximizing computational efficiency.

To demonstrate the importance of the shoreline representation itself, errors associated with storm surge elevations computed over two uniform grids of resolution 12.5 km each having different refinements of a sinusoidally varying coastline are compared in Figure 5. The large errors seen in Figure 5 clearly show that misrepresentation of the coastline detail by way of coarse resolution can lead to rather significant errors in the predicted storm surge elevations.

Illustration of Modeling Concepts

As a illustration of the modeling strategy just described, the storm surge generated by hurricane Camille which made landfall on the Mississippi Gulf coast in August, 1969 is simulated. The WNAT model domain is selected and its discrete representation is the graded structure of grid SG01. Grid SG01 has maximum nodal spacings of 98 km in the

deep Atlantic ocean and 45 km in the Gulf of Mexico. Near shore regions, shown in Figure 6, are highly discretized with grid resolution ranging from 0.5 km to 2.0 km with the finest spacing located at entrances to inlets where the set up of exchange processes with the coastal ocean are important. Error estimates for storm surge computations over grid SG01, shown in Figure 7, are derived through comparison to a doubly refined grid.

Hurricane Camille follows a path over the deep portions of the Gulf of Mexico and Atlantic Ocean where a ratio of nearly one is maintained between the resolution in grid SG01 and the spatial scale of the hurricane. Figure 7 indicates that normalized errors do not occur in the deep ocean but in fact are located adjacent to the coast. The level of resolution provided by grid SG01 over deeper waters is adequate to capture the inverted barometer effect of this hurricane.

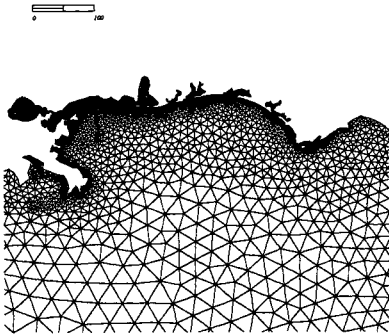


Figure 6. Graded discretization of grid SG01 in the northeast Gulf of Mexico.

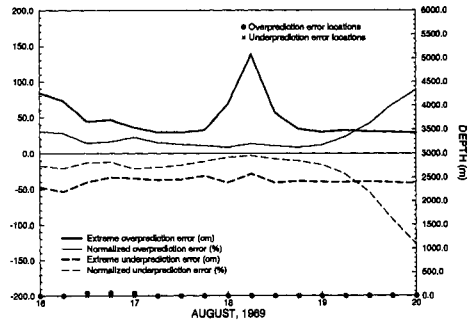


Figure 7. Error estimates for storm surge elevations computed over grid SG01 during hurricane Camille forcing.

Prior to peak surge development, Figure 7 indicates both over- and underprediction errors are important and occur adjacent to the shore. Normalized errors remain fairly uniform during the approach and movement of hurricane Camille through the Gulf of Mexico. Initially, large errors occur as Camille approaches and passes over Cuba, an area not highly resolved because of its remote distance from the coastal region. At the time of peak surge, August 18, 1969, extreme overprediction errors dominate as seen in Figure 7. From spatial distributions of error, high magnitudes of the extreme overprediction error are confined to very localized areas where resolution is insufficient and coastline detail is highly irregular. Normalized errors, however, are at low levels near 15% as hurricane Camille approaches the Gulf Coast and makes landfall. A rise in the normalized errors

following the peak surge is due to a combination of residual errors at the coastline following landfall of the hurricane and the presence of minimal surge elevations as the hurricane moves inland.

APPLICATION OF THE MODELING STRATEGY

Previously the recommendations for modeling storm surge generation are described using examples of applications undertaken during developmental stages of the modeling strategy. A true test of the approach put forth comes only when the methodology is applied in a new, untested region. The Yellow and East China Seas, which are often subject to tropical storms and typhoons during the summer and fall months, provide an appropriate location to test the storm surge modeling approach presented.

Hydrodynamic Model and Meteorological Forcing

Hydrodynamic computations for this application in the Yellow and East China Seas are performed using the finite element model, ADCIRC-2DDI (Luettich et al., 1992), which uses the vertically averaged equations of mass and momentum conservation, subject to the hydrostatic pressure approximation. The standard quadratic parameterization for bottom stress is implemented and baroclinic as well as lateral diffusion/dispersion terms are neglected. The resulting conservation statements cast in primitive, non-conservative form are expressed in a spherical coordinate system (Kolar et al., 1994). For computational purposes these equations are reformulated into a generalized wave continuity equation (GWCE) and are subsequently discretized using the finite element (FE) method, e.g. Lynch and Gray (1979); Kinnmark (1984).

The storms of record selected as forcing are tropical storm Janis and typhoon Ryan which entered the East China Sea generating surge in the Yellow Sea during portions of August and September, 1995, respectively. Wind stress fields associated with these storms are obtained from the Navy Operational Global Atmospheric Prediction System (NOGAPS) (Hogan et al., 1991). Shown in Figure 8 are the paths of these storms as they enter and exit the model domain. Storm surge hydrograph locations are also indicated in Figure 6.

Storm Surge Predictions in the Yellow and East China Seas

Several simulations are conducted using the historical storms, Janis and Ryan, as meteorological forcing. All simulations for each storm use identical model parameters and wind forcing. Note, however, that no atmospheric pressure is applied which can lead to negative surge elevations. Any differences between the model responses are attributed solely to the domain size or the grid discretization. The largest domain considered, shown in Figure 8, includes the Yellow and East China Seas and the Sea of Japan. The open boundary of this domain extends well into the deep waters of the Pacific ocean beyond the influence of the strong and highly variable Kuroshio Current. The smaller domain, shaded in Figure 8, excludes the Sea of Japan and places an open boundary at the

Tsushima Strait. In open waters this domain is severed near the base of the steep continental slope in the East China Sea where depths drop rapidly from 1000 m to nearly 7000 m. The discrete representations for both domains have a variable nodal density and are identical in overlapping regions using 8340 points for the smaller domain and 11773 points (grid YESSOJ) for the larger domain. The dynamic near shore regions off the west coast of Korea are the most resolved with nodal spacings near 2.5 km. In the deep waters of the Pacific ocean grid refinement is on the order of 100 km.

Comparisons of storm surge computations made over the two model domain sizes reinforce the necessity of using large domains to capture the full storm surge response in coastal areas. The two storm surge hydrographs in Figure 9 are representative of coastal locations near landfall on the right side of tropical storm Janis. Surge elevations computed over the smaller domain consistently underpredict the peak primary storm surge relative to surges predicted over the largest domain. This pattern is similar to that seen in the prediction of storm surge from hurricane Kate in the Gulf of Mexico. In this case, even though the smallest domain extends off the shelf into deeper waters, surge generation over the continental slope and onto the shelf is not adequately captured by this limited domain which crosses the continental slope.

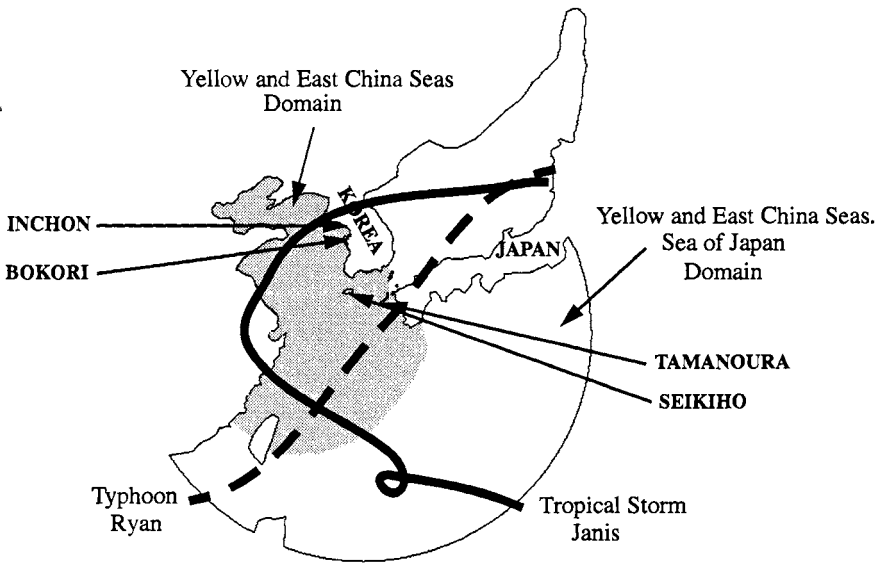


Figure 8. Two domain sizes for the Yellow and East China Seas region, together with the paths of tropical storm Janis (August, 1995) and typhoon Ryan (September, 1995) and four hydrograph station locations.

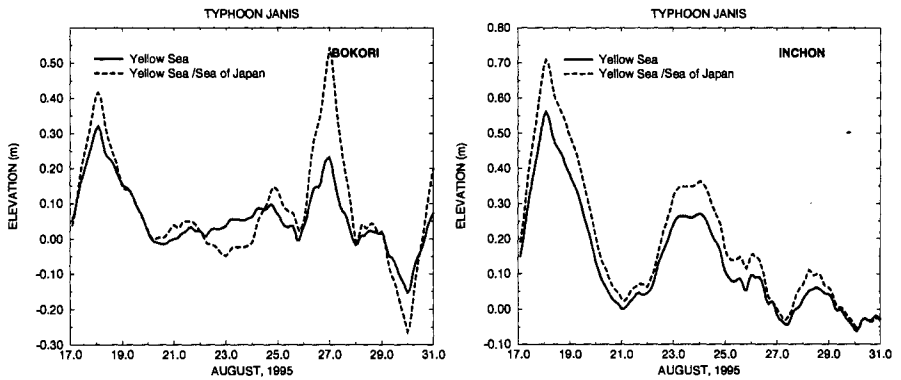


Figure 9. Comparisons of the storm surge hydrographs computed over two domain sizes at Bokori and Incheon on the west coast of Korea near the point of landfall for tropical storm Janis, August, 1995.

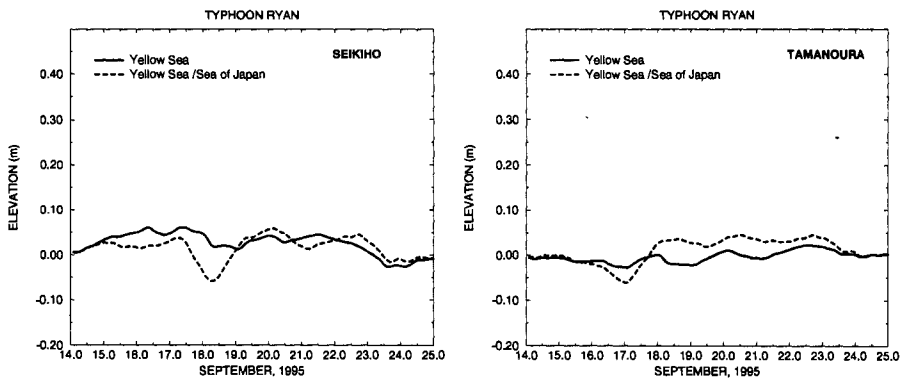


Figure 10. Comparisons of the storm surge hydrographs computed over two domain sizes at Seikho and Tamanoura near Kyushu, Japan near the landfall point for typhoon Ryan, September, 1995.

Computed storm surge elevations from typhoon Ryan are shown in Figure 10 at locations near Kyushu, Japan, the point of landfall of the storm. Magnitudes of the surge associated with typhoon Ryan are considerably smaller than those produced by tropical storm Janis a consequence of the storm's path over relatively deep water. However, largely different surge patterns for typhoon Ryan are evident between computations made over each domain size as seen in Figure 10. The path of typhoon Ryan winds back and forth over the continental slope and shelf break making surge prediction difficult for a limited area domain. Note although typhoon Ryan remains in the East China Sea, the surge generated

by this storm propagates up into the Yellow Sea. Proper representation of the storm surge generation in Yellow Sea coastal areas comes through implementation of a model domain which extends far into the deep Pacific ocean water.

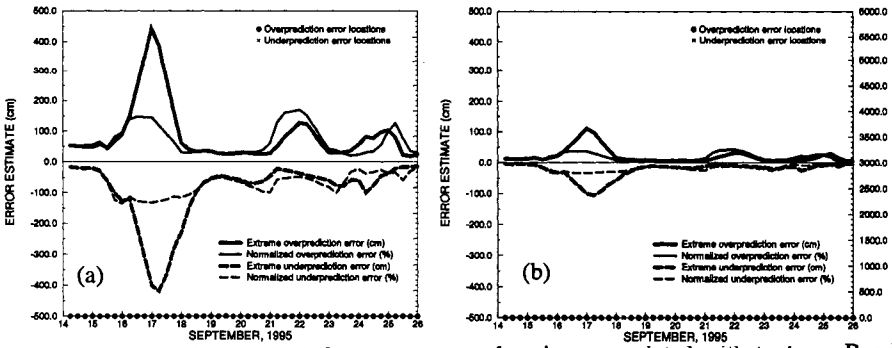


Figure 11. Error estimates (cm) for storm surge elevations associated with typhoon Ryan computed over (a) YESSOJ, a graded discretization of the large Yellow and East China Seas and Sea of Japan domain and (b) YESSOJ2, a doubly refined discretization of grid YESSOJ.

Comparisons between storm surge computations over the graded grid YESSOJ associated with the largest domain and a double refinement of that grid, YESSOJ2, result in error estimates for each of these grid discretizations with respect to storm surge prediction. Depths at the location of all extreme and normalized error estimates for both grids YESSOJ and YESSOJ2, shown in Figures 11a and 11b, are indicative of very shallow water near the coastline. Rather significant errors in the simulation of typhoon Ryan over grid YESSOJ (Figure 11a) are recorded and can be attributed to the relatively coarse 2.5 km grid refinement for near shore areas. Doubling the resolution in coastal areas, as done in grid YESSOJ2, noticeably reduces the levels of the extreme overprediction error coinciding with peak surges. Normalized errors throughout the simulation over grid YESSOJ2 are maintained at a rather uniform level. Most changes in the error magnitudes occur at times of peak surge indicating that over deep waters the coarse resolution of graded grid YESSOJ is adequate for simulation of primary storm surge. With the addition of a relatively few number of points, refinements of the grid discretization of grid YESSOJ in very shallow coastal areas should result in further error reduction.

CONCLUSIONS

Both the size and discretization of the computational domain influence storm surge generation in the coastal region. To minimize the effect of cross shelf boundary specification and properly represent the resonant characteristics of a domain, a very large domain which encompasses the coastal region of interest, adjacent basins, and extends out into the deep ocean is most appropriate for modeling storm surge generation. A variable grid structure which has extensive refinement in the near shore region leads to low uniform errors throughout the domain.

ture which has extensive refinement in the near shore region leads to low uniform errors throughout the domain.

A simple but effective test of model performance with respect to the grid discretization is demonstrated using a Richardson based error measure. The computation of Richardson based error measures provide an estimate of the errors associated with a graded grid and a grid having twice the resolution everywhere. Since discretization errors can never be completely eliminated, uniform errors over a mesh are desired with an acceptable magnitude of these errors representing a balance between computational effort and required accuracy.

The modeling strategy outlined for the prediction of hurricane storm surge which incorporates the use of a very large domain in conjunction with a variably graded grid structure having higher levels of coastal refinement is applied to the simulation of tropical storm Janis and typhoon Ryan in the Yellow and East China Seas. These applications reinforce the modeling methodology presented and demonstrate implementation of this approach in the context of capturing the essential components of storm surge generation.

Acknowledgments. This work was funded through the Office of Naval Research's Navy Ocean Modeling and Prediction Program (Program element 62435N). This paper, NRL contribution JA-7322-96-0029, is proved for public release; distribution is unlimited.

REFERENCES

- Blain, C.A., J.J. Westerink, and R.A. Luetlich. 1994. The influence of domain size on the response characteristics of a hurricane storm surge model, *J. of Geophys. Res.*, **99 (C9)**, 18467-18479.
- Blain, C.A., J.J. Westerink, and R.A. Luetlich. 1996. Grid convergence studies for the prediction of hurricane storm surge, *Int. J. of Numer. Meth. in Fluids*, accepted.
- Bunpamong, M., R.O. Reid and R.E. Whitaker. 1985. An Investigation of hurricane-induced forerunner surge in the Gulf of Mexico, Coastal Engineering Research Center, U.S. Army Engineers, Technical Report CERC-85-5.
- Hogan, T.F., T.E. Rosmond and R. Gelaro. 1991. The description of the Navy Operational Global Atmospheric Prediction System's Forecast Model, NOARL Technical Report 13, Naval Research Laboratory, Monterey, CA.
- Jelesnianski, C.P., J. Chen and W.A. Shaffer. 1992. SLOSH: Sea, Lake, and Overland Surges from Hurricanes, NOAA Technical Report NWS 48.
- Kinmark, I.P.E. 1984. The Shallow Water Wave Equations: Formulation, Analysis and Application, Ph.D. Dissertation, Department of Civil Engineering, Princeton University.

Kolar, R.L., W.G. Gray, J.J. Westerink, and R.A. Luettich. 1994. Shallow water modeling in spherical coordinates: Equation formulation, numerical implementation, and application, *J. Hydraul. Res.*, **32**, 3-24.

Luettich, R.A. and J.J. Westerink. 1995. Continental shelf scale convergence studies with a barotropic model, Quantitative Skill Assessment for Coastal Ocean Models, Coastal and Estuarine Studies Vol. 47, American Geophysical Union, 349-371.

Luettich, R.A., J.J. Westerink, and N.W. Scheffner. 1992. ADCIRC: An Advanced Three-Dimensional Circulation Model for Shelves, Coasts and Estuaries, Report 1: Theory and Methodology of ADCIRC-2DDI and ADCIRC-3DL, Dept. of the Army, Tech. Report DRP-92-6.

Lynch, D.R. and W.G. Gray. 1979. A Wave equation model for finite element tidal computations, *Comp. Fluids*, **7**, 207-228.

Roache, P.J. 1994. Perspective: A method for uniform reporting of grid refinement studies, *J. of Fluids Eng.*, **116**, 405-413.

Scheffner, N.W., D.J. Mark, C.A. Blain, J.J. Westerink, and R.A. Luettich. 1994. A Tropical Storm Data Base for the East and Gulf Coasts of the United States, Department of the Army, U.S. Army Corps of Engineers. Washington, D.C.

SHIP-BASED FREE ELECTRON LASER (FEL) LIDAR FOR OCEANIC AND ATMOSPHERIC RESEARCH

S. K. Sharma¹, C. E. Helsley¹, R. J. Burke², D. M. Tratt³, R. L. Collins⁴, and C. K. N. Patel⁵

¹University of Hawaii
Honolulu, Hawaii, U.S.A.

²Arcata Systems, McKinleyville, California, U.S.A.

³California Institute of Technology
Pasadena, California, U.S.A.

⁴University of Alaska-Fairbanks
Fairbanks, Alaska, U.S.A.

⁵University of California
Los Angeles, California, U.S.A.

ABSTRACT

Growth of the world's population and increased per capita use of energy and other resources have created an exponentially increasing burden on the global environment of anthropogenically generated byproducts. A complete and systematic understanding of the complex environmental impact of these results of human activities demands detailed and often simultaneous measurements of numerous compounds in various stages of their evolution. Optical techniques provide remote sensing mechanisms to carry out these measurements over large land and sea masses. To take advantage of these techniques, a consortium of Pacific Rim institutions is proposing a new FEL lidar (laser radar) platform for global environmental research. This platform is called PEARL, for Pan-Oceanic Environmental and Atmosphere Research Laboratory.

The free electron laser (FEL) at the heart of the PEARL platform will have the robust capabilities needed to carry out these measurements effectively. While conventional lidar systems have the potential for the necessary studies, their performance has heretofore been restricted by the low power and limited wavelength tunability of laser sources. In contrast, the FEL lidar will have continuous wavelength tunability from 250 nm to 20 μ m and the power to project beams over large ocean expanses and basin-sized land regions. Examination of examples of the wide range of measurements that will be possible with this powerful instrument shows that the FEL lidar aboard a ship promises to be a revolutionary tool for environmental research—having, for instance, the capability to make detailed and simultaneous observations of the vertical structure of the ocean and the atmosphere in real time.

INTRODUCTION

A FEL lidar aboard a ship promises to be a revolutionary tool for environmental research—providing a powerful remote-sensing system for the atmosphere, marine boundary layer, and upper ocean. Operating in various environments (Fig. 1), the mobile PEARL facility will be able to attack a wide range of scientific problems—problems as diverse as the origin of noctilucent (night luminous) clouds in the polar upper mesosphere (altitude 80 to 90 km), the concentration of water vapor in the stratosphere, the dispersal of Arctic haze, smog in urban areas, and the effect of volcanic emissions on the albedo and temperature of the earth. Along the track between

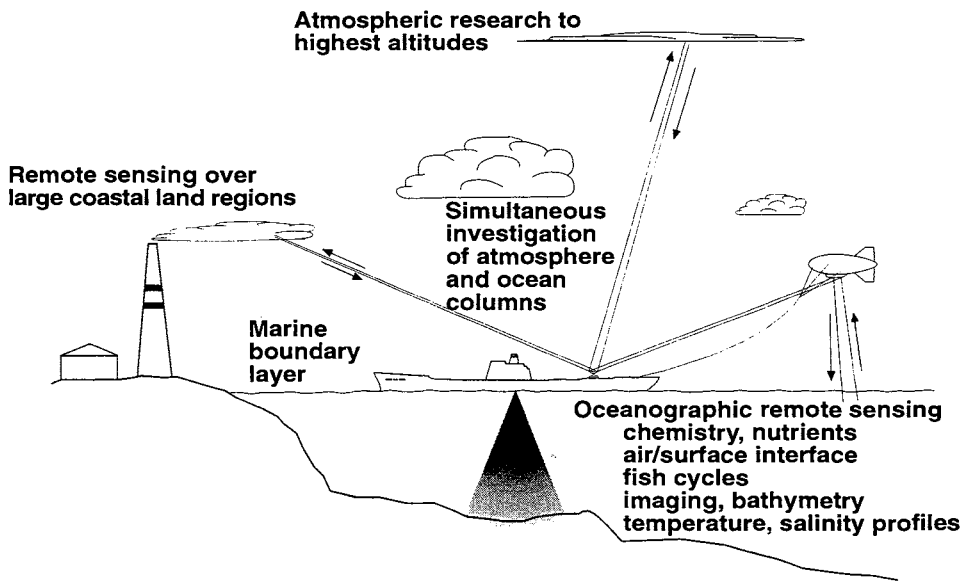


Fig. 1. Schematics of the PEARL platform indicating some of the research capabilities.

the sites for these studies, or as targeted studies in and of themselves, the facility could gather precise information about the physical, chemical and biological properties of the upper ocean, the bathymetry of coastal regions to a depth of 100 to 200 meters, the distribution of phytoplankton and other particulate matter in the upper ocean, the variation of the optical properties of the sea and the marine boundary layer in various environments, and the variation of water vapor in the atmosphere as a function of height and lateral position.

The remote sensing capabilities of the FEL aboard the PEARL are ideally suited for a variety of defense related applications, in peace time as well as in potential conflicts. The mobile PEARL platform will allow studying propagation of coherent light in a variety of coastal environments, and provide information on how the scattering and attenuation of light over a wide spectral range is affected under various meteorological conditions. Scattering and attenuation of natural and artificial light in the marine boundary layer (MBL) is of concern for both civilian and military operations. Atmospheric attenuation adversely affects laser target ranging, optical data communications, remote sensing and visibility, and the FEL is a powerful tool for understanding the factors affecting this attenuation: aerosol composition and concentration, Mie-Rayleigh scattering, water vapor content, and temperature inhomogeneity. Finally, there is now an increased emphasis on deployment of remote detection and characterization systems for identifying biological and chemical agents of warfare. PEARL's continuous (and rapid) wavelength tuning will address compounds with diverse—and complex—spectroscopic signatures, and the FEL's power will allow long stand-off distances by using optical relays with the ship-based system.

Since a ship moves slowly while the FEL puts out 10^{22} photons per second, the best use of resources suggests that large areas should be scanned wherever the ship goes. Moreover the FEL produces sufficient light-energy that the atmosphere, air-sea interface and the sea can all be scanned simultaneously in some cases, utilizing the ability to rapidly change wavelength. The direction of the laser beam is precisely controllable with current optical technology, making it practical to use a remote relay to redirect the beam launched from the ship—downward to wide expanses of the ocean surface and laterally over the ocean or inland. This will increase the ability to rapidly gather data from large regions of the environment, adding to the distant destinations in the atmosphere accessible in a direct line from the ship. To effect this relay, we plan to use a mirror and suitable receivers mounted on an aerostat or other UAV (Unmanned Aerial Vehicle), scanning large areas as needed with a down looking lidar.

The key components for the PEARL facility are the ship, the free electron laser, a large aperture telescope and optical beam train, an aerostat, and optical detecting devices characteristically found in lidar and spectroscopy laboratories. Most of these systems exist, have been tested and deployed to various degrees in other projects, and are currently in storage at various facilities.

TECHNOLOGY

The special capabilities of the PEARL facility are a result of the wavelength tunability and peak and average power of a free electron laser. Heretofore in atmospheric lidar experiments, the workhorse laser in the infra-red region is the carbon dioxide (CO₂) laser which can be used to generate nanosecond-length pulses in the infrared between 9 μm and 11 μm . Solid state and other gas lasers are also used but all are intrinsically restricted to narrow wavelength ranges, are often not continuously tunable over those ranges, and are limited in optical power. Tunable solid-state and dye lasers do provide tunability, but with low output power and hence a limited monitoring range. Figure 2 exhibits the PEARL FEL with these light sources as well as atmospheric attenuation in the infrared as a function of wavelengths. By operating FEL in the DIAL (Differential Absorption Lidar) modes in the 8 - 12 μm window in the atmosphere, minute amounts (ppb to ppm) of pollutant species can be detected (Manheimer, 1994).

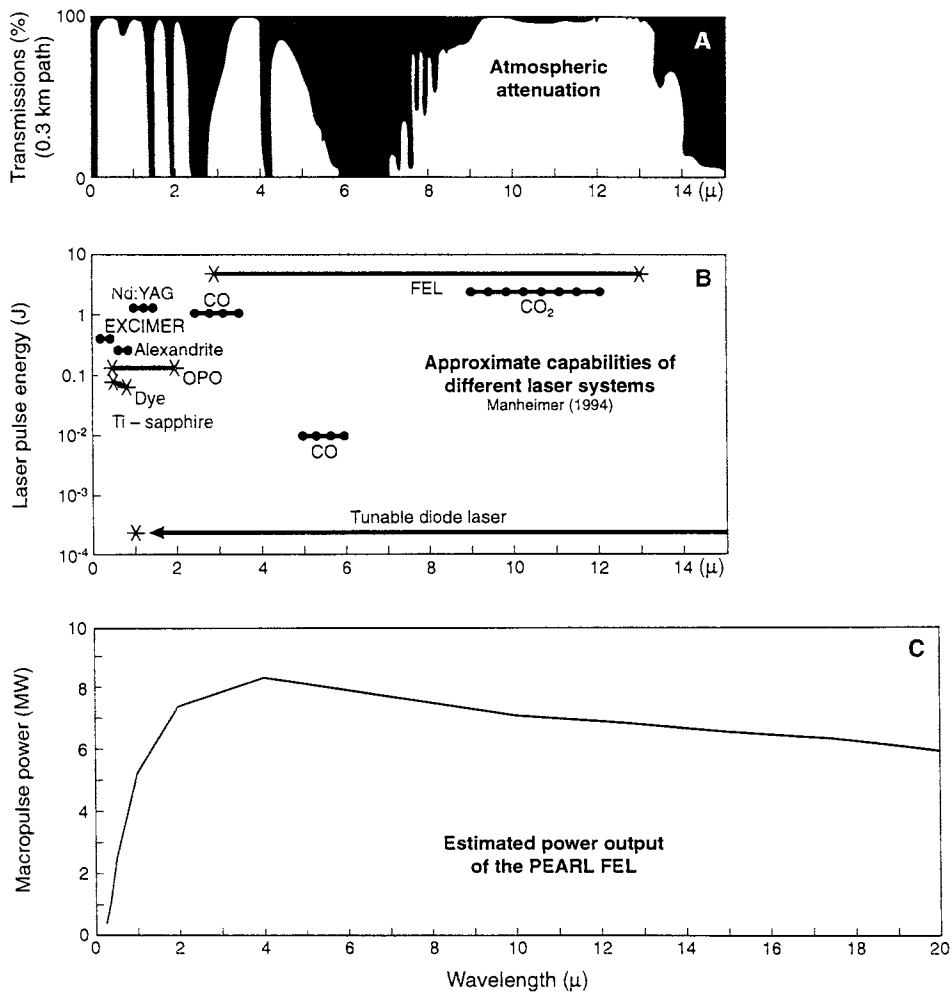


Fig. 2. (A) Atmospheric transmission, (B) comparison of output power spectrum of various laser systems (Lines with dots indicate line tunable lasers, and continuous lines indicate continuously tunable lasers). The output curve for IR FEL represents some generic infrared FEL, and (C) estimated tunable output of PEARL FEL.

The FEL's unique wavelength tunability has long been exploited for medical and materials research in land-based facilities, and the ability to scale this type of laser to high power made it the laser of choice for ground-based Strategic Defense Initiative (SDI) work. The inherent wavelength flexibility of the FEL, and its ability to produce substantial power, make it possible to realize an extremely powerful remote sensing system for atmospheric and marine research.

The PEARL FEL will use apparatus initially built by Rockwell International Corporation for development of advanced FEL technology in support of a SDI program. The design (Cover *et al.*, 1991) is a direct descendant of the highly successful Mark III FEL (Benson *et al.*, 1988; Benson, 1995), incorporating the results of the collaboration between Rockwell and the Mark III FEL group at Stanford University and Duke University. The basic FEL system is currently complete but in storage. Modification of the existing hardware to make it serviceable in a shipboard environment will provide the mobility that has heretofore prevented FELs from being instruments for field research.

CHARACTERISTICS OF THE PEARL FEL

FELs use gain media that are not subject to the same restrictions as conventional lasers. In a FEL, perturbation of a relativistic electron beam by a periodic magnetic field generates tunable laser light (for a review see Benson, 1995). The optical wavelength is determined by the electron energy and the period and strength of the magnetic field, and tunability is becoming a normal operating feature of many FELs. The FEL wavelength is given by

$$\lambda = \frac{\lambda_{\text{wiggler}}}{2\gamma_e^2} \times f(B_{\text{wiggler}}) \tag{1}$$

where λ_{wiggler} is the magnetic field wiggler periodicity, γ_e is the relativistic energy of the electrons, and $f(B_{\text{wiggler}})$ is a function that determines the dependence of the FEL wavelength on the magnetic field of the wiggler.

The pulse format of the laser beam mimics that of the electron beam produced by the accelerator. With the existing 3 GHz RF accelerator, the PEARL's output will be a train of "micro pulses" of a few picoseconds duration within a "macro pulse" whose duration and repetition rate match the switching of the RF power to the accelerator (Fig. 3).

Depending on the research objectives that they support, operational FELs have been designed to produce laser output in selected spectral ranges from the ultraviolet to the far infrared. For the PEARL, an existing accelerator will provide the range of electron beam energy needed to tune the FEL from the near ultraviolet to the far infrared. To allow rapid wavelength changes over substantial wavelength ranges, a short accelerator section will be inserted in the optical resonator, just upstream of the magnetic wiggler. The short accelerator will provide $\delta\gamma_e$ of energy to the electron beam. This auxiliary accelerator can be used to change wavelength from one macropulse to the next at 180 Hz. With the auxiliary accelerator excited at one-half the frequency of the main accelerator, the wavelength can be switched from one micropulse to the next—giving an ability to switch wavelengths at rates up to 1.5 GHz, as illustrated in Fig. 4. To cover the full spectral range, the optical resonator will have two sets of mirrors, and therefore gross spectral changes will be substantially slower.

With no conventional gain medium to overheat, a FEL can be designed for extremely high average power. Based on the existing system, the PEARL's FEL will provide continuous average power of 2 KW in the near infrared, somewhat more in the mid-IR, and somewhat less for operation in the visible and ultraviolet parts of the spectrum. Figure 5 shows an estimated output power spectrum of the FEL as a function of wavelength. Peak powers in the picosecond-long

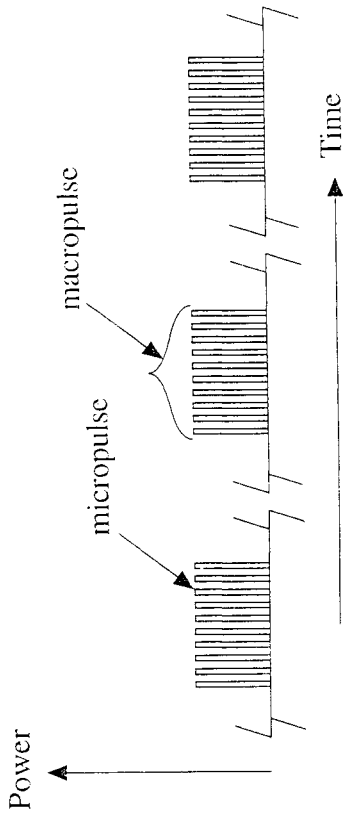


Fig. 3. Macro and micropulse structure of FEL output.

Wavelength Agile FEL: Two Wavelengths Beam In Every RF Bucket

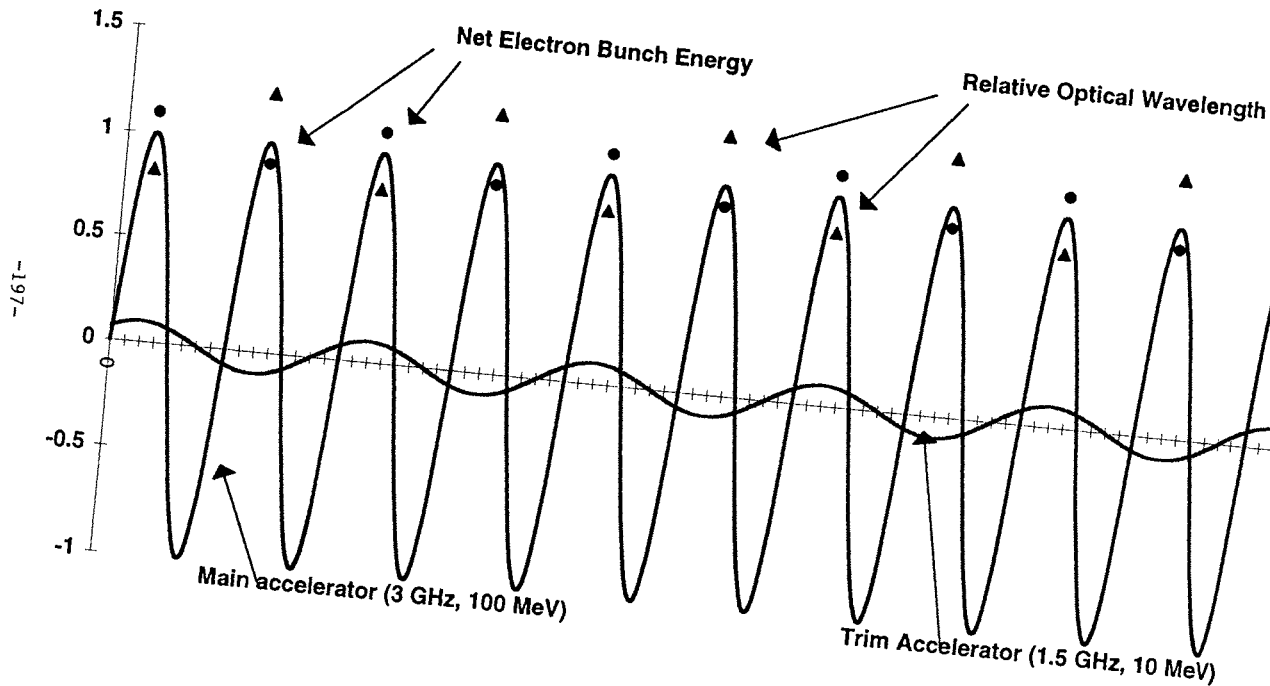


Fig. 4. Micropulse wavelength agility of PEARL FEL output.

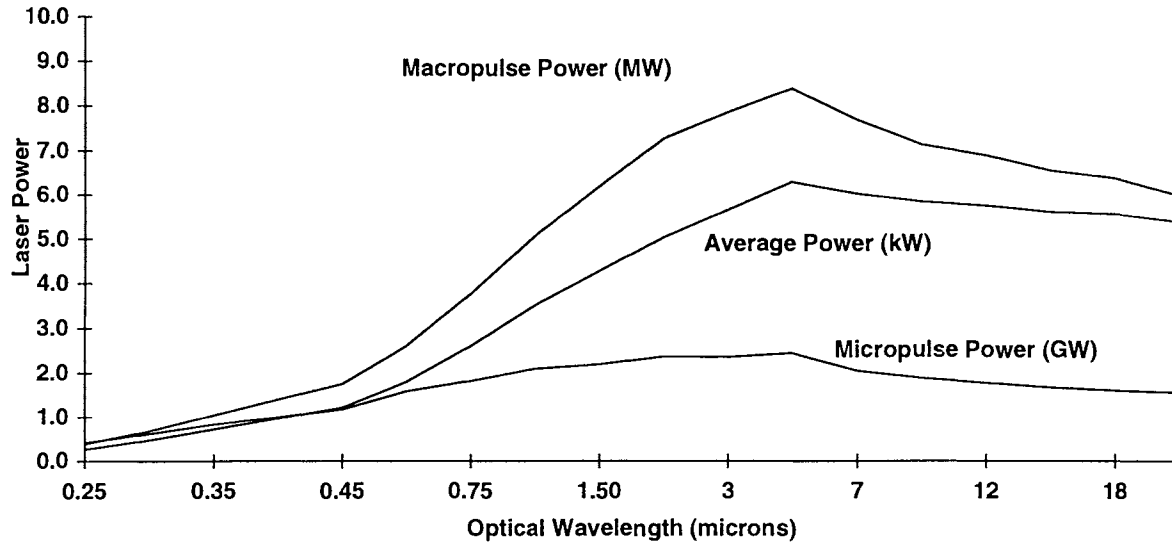


Fig. 5. Estimated power output spectrum of the PEARL FEL

micro pulses will reach gigawatts, and these will average to megawatts over the microsec-long macro pulses. The characteristics of the FEL in the PEARL are given in Table 1.

The FEL must be mobile to be most useful and to address the full program we have identified. The size of the device and the need for massive radiation shielding makes this difficult, if not impossible, for transport methods such as by conventional trucks. Our plan to mount the FEL in a large ship satisfies the space requirements and has the added advantage that water tanks can be used for shielding. Using one of several existing ships that we have identified will avoid a major element of the cost of completing the PEARL facility. To be compatible with the proposed ship environment, the FEL's "centerline" components will be mounted on a full-length optical table integrated within a large-diameter steel tube for structural strength. This assembly will be supported by a kinematic mount with dampening to isolate the system from the twisting, bending, and accelerations of the ship motion. The practicality of this installation plan is owing to the fact that the components thus mounted do not include the most massive parts of a FEL—the radiation shielding and the radio frequency power system that excites the accelerator.

Table 1. The PEARL FEL Parameters

• Wavelength tuning range	250nm to 20 μ m (to 50nm at greatly reduced power)
• Wavelength switching rate	up to 100%* at up to 1.5 GHz; full range of each resonator optical systems at ~1 Hz; between ranges of resonator optics sets to be determined.
• Spectral Purity	6 to 40 wavenumbers for raw pulses, <0.5 wavenumber with optical pulse conditioning.
• Micro pulse repetition rate	1 per macro pulse to 3 GHz during a macropulse
• Macro pulse repetition rate	1 to 180 pulses per sec (pps) (upgradable to 1000 pps)
• Macro pulse duration	600 fsec to 5 psec (electrons), 200 fsec to 60 psec (with optical pulse conditioning)
• Micro pulse peak optical power	to 1000 MW*
• Macro pulse duration	1 micro pulse duration to 5 μ sec
• Macro pulse optical power	up to 1MW*
• Average optical power	up to 4kW* (upgradable to >20 kW*)

*asterisked parameters are optical-wavelength dependent

Lidar Performance Simulations

The power of the PEARL FEL as a tool for atmospheric research is apparent from lidar performance simulations. The projections discussed here were generated using the USAF

BACKSCAT version 4.0 software package (Longtin *et al.*, 1994), assuming the zenith viewing configuration and a 150-cm transmitter diameter. The transmit pulse duration will be variable from a few psec (single micropulse) to 4 μ sec (full macropulse). For the following cases we have chosen to treat the full 4- μ sec. macropulse and also a 200-nsec sub-macropulse, which although containing less energy illustrates a FEL pulse format that would allow for range resolution more commensurate with typical atmospheric science requirements. The pulse energy at each of the selected transmit wavelengths derives from Fig. 5. An alternate means of achieving necessary range resolution would be to modulate the macropulse envelope using a pseudorandom coding scheme. (e.g., Takeuchi *et al.*, 1986).

Elastic (Rayleigh-Mie) Backscatter

Figure 6 shows the simulated dependence of the single pulse signal-to-noise ratio (SNR) on altitude above median sea-level (MSL) for selected lidar wavelengths from the UV to the mid-IR, as indicated. The US Standard Atmosphere is assumed.

Unity SNR denotes the point at which signal return from the atmosphere is indistinguishable from system noise, and therefore defines the limit of observation for a single pulse measurement. Increased measurement range can be achieved by averaging multiple pulses, but this is at the expense of temporal resolution. The very favorable single-pulse range limits indicated by Fig. 6 should permit much more rapid scanning and greater temporal resolution than is typically obtained using conventional lidar instruments.

Eye-safety Considerations

Operation of the PEARL will involve precautions for eye-safety, and reductions of some capabilities near populated areas is anticipated. Although PEARL's crew and visitors will use protective devices such as filtering goggles and be trained in laser safety, and eye-safety requirements will be less stringent for operation in remote areas, the laser design and the facility's operating procedures will demonstrate a high degree of care for aircraft, humans, and wildlife which may be in the vicinity.

A primary design feature will be means to rapidly cease laser beam transmission, which is easily built into the control system for the pulsed device. In addition to devices such as surveillance radar, control inputs—including laser interdiction—will be made by assigned human observers. In addition, an eyesafe pilot beam will be sent out a short time (e.g., 1 μ sec) before each intense pulse. Only if no return is received from the pilot pulse will the main pulse be permitted.

Figure 7 depicts the maximum permitted ocular exposure (MPE) across the PEARL output wavelength spectrum. This calculation is based on a single pulse direct exposure using American National Standards Institute guidelines ANSI Z136.1-1992 for a dark-adapted eye (Spiers, 1996). The dependence of MPE on pulse length can be seen to be minor above about 2.4 microns and effectively zero at shorter wavelengths.

Also shown in this figure is the expected PEARL output energy density for the laser parameters in the performance simulations above. For wavelengths above 1.3 μ m, it can be seen that PEARL is eyesafe in the single pulse exposure regime. For operation at shorter wavelengths, special circumstances will have to obtain for atmospheric operation in populated areas. In such instances, special precautions and regulatory waivers would be required as is the case with conventional lidar systems operating in the UV-visible part of the spectrum.

Care must be exercised in applying the single pulse results to the case of multiple pulse exposure—the maximum PRF of PEARL being 180 Hz. Different considerations apply to various spectral ranges. In some cases, for example, the applicable exposure dose is additive over a 24-

hour period regardless of PRF. In others, the MPE for one day depends on the expected dose on succeeding days. And for others, the MPE for a single pulse must be adjusted by a corrective factor to protect against cumulative damage from sub-threshold pulses, and thermal or photochemically-induced injury.

DISCUSSION

In this work we have focused on technological aspects of PEARL's FEL and its use as a lidar transmitter both for up-looking and down-looking lidar receivers. The atmospheric lidar technology with conventional solid-state lasers has made significant advances in recent years (for review see Measures, 1984; Grant, 1995, McGee *et al.* 1995). The lack of suitable tunable and high power lasers in the mid-infrared has so far restricted our ability to detect trace (ppb) amounts of chemical species in the atmosphere (e.g., Measures, 1984; Manheimer, 1994). For a given compound, the PEARL lidar, when operated in differential absorption light-scattering (DIAL) mode would have at least ten to fifty times the range and much finer spatial resolution than the existing lidar systems. An existing DIAL system has yielded a 2km x 2km x 10m map of SO₂ in 45 min (Buschner *et al.*, 1992). The FEL based DIAL system could scan the volume in a few seconds, limited only by the slewing of the beam optics. The FEL lidar would allow not only characterization of atmospheric aerosols, but also detection of precursors of illegal drugs, such as amphetamines, cocaine, etc., and of chemical warfare agents. Most of the biological warfare agents can be detected using UV excited fluorescence by operating PEARL FEL in the UV region. A down looking UV-fluorescence PEARL lidar could also provide valuable information about the dissolved organic carbon (DOC) in near surface waters (see for example, Vodacek *et al.*, 1995; Coble *et al.*, 1993).

The tunability and the high power (1 KW) of the PEARL FEL in the blue-green region of spectrum would allow the beam to penetrate up to 200 meters of open-ocean water. The PEARL FEL would allow 2 pico-second micropulses at 500 MHz with different optical wavelengths on successive micro-pulses in the blue-green region of the spectrum. The pico-second micro-pulses would allow centimeter depth resolution with appropriate gated receivers. At 488 nm, 3 μ sec macropulses at 180 Hz with average power of \geq 1KW would allow examination of the sea-floor with variable depth resolution by modulating the macropulse envelope using a pseudo-random coding scheme (e.g., Takeuchi *et al.*, 1986).

CONCLUSIONS

A FEL lidar aboard a ship has potential for greatly increasing the capabilities of remotely monitoring oceanic and atmospheric environments on a regional scale around the globe. PEARL's high power and tunable FEL lidar would allow rapid multi-wavelength long range measurements of atmospheric aerosols, vertical distribution of phytoplankton and DOC in the ocean at unprecedented scales. Such measurements would greatly enhance our understanding of sources and sinks of natural and anthropogenic aerosols, and might have extensive applications in the studies of ocean and atmospheric circulation and exchange. The DIAL measurements with the FEL system in the mid-infrared region would be most valuable in long range surveillance programs for civilian and military agencies.

ACKNOWLEDGEMENTS

Portions of this work were carried out by the Jet Propulsion Laboratory, California Institute of Technology, under contract with the National Aeronautics and Space Administration. This is SOEST contribution no. 4187 and HIGP contribution no.928.

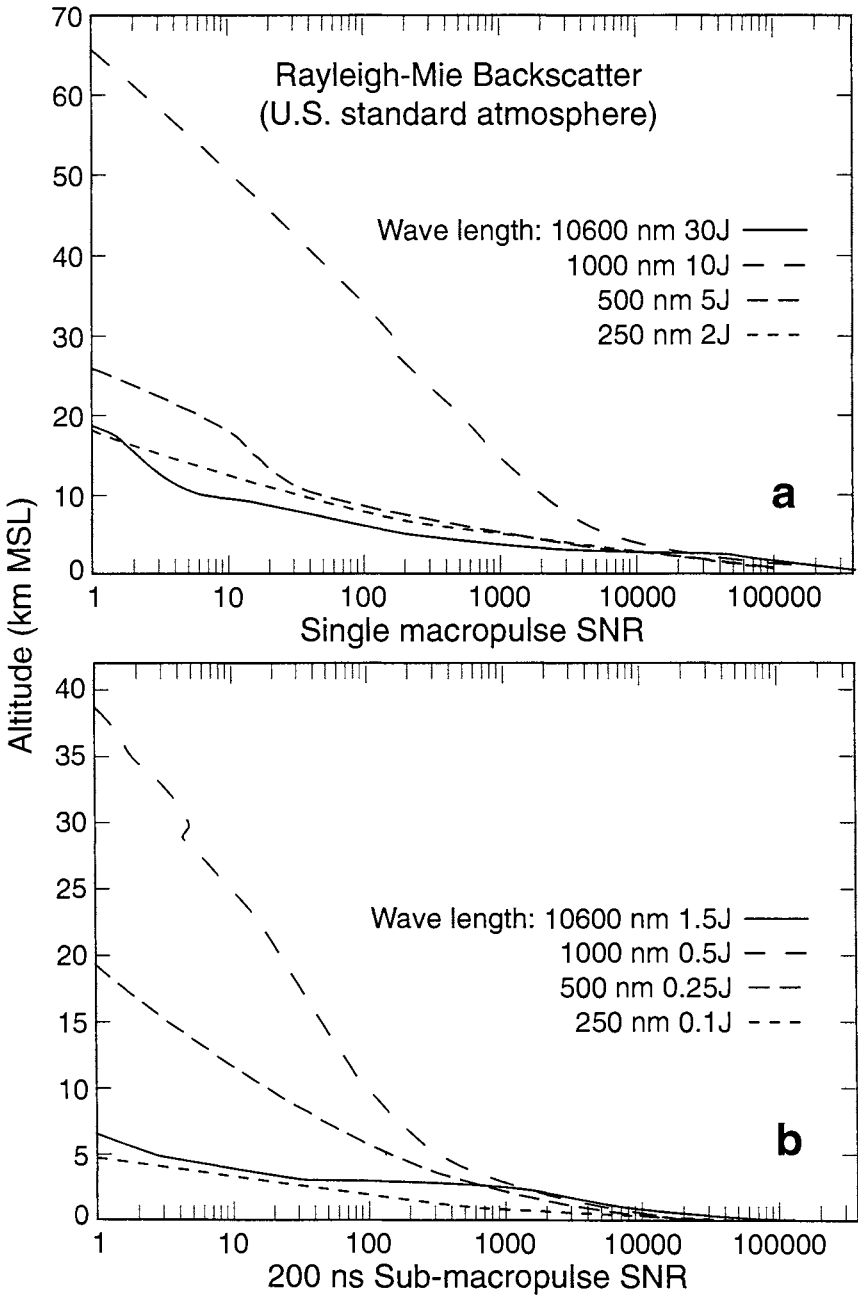


Fig. 6. Dependence of lidar SNR on retrieval altitude above median sea-level (MSL), and wavelength for (a) in full 4 micro-sec FEL macropulse; and (b) a 200 nano-sec submacropulse.

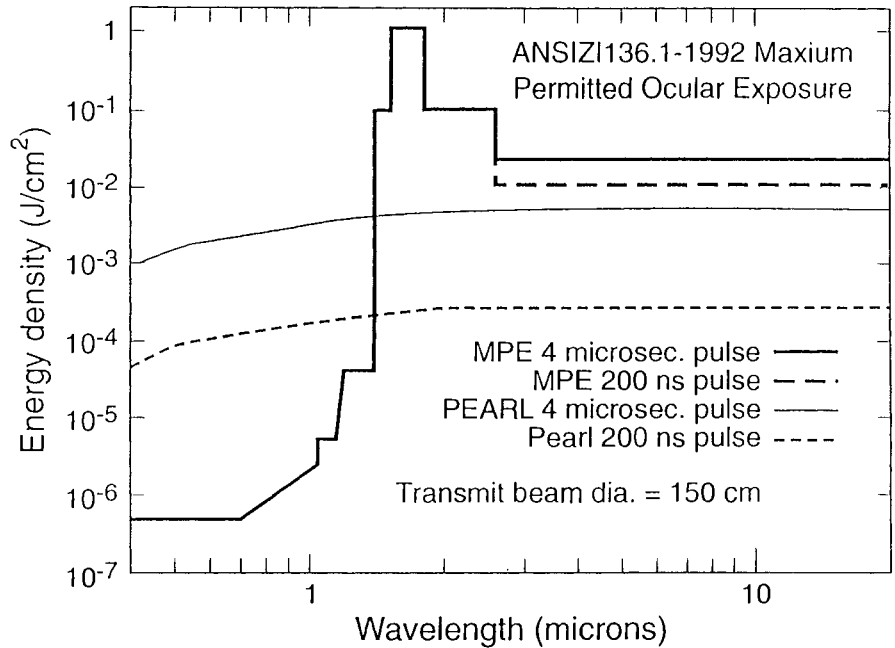


Fig. 7. Dependence of Maximum Permitted-Ocular Exposure (MPE) on wavelength and pulse duration. The output energy of the PEARL FEL are also shown for the full 4 micro-sec macropulse, and a 200 nano-sec sub-macropulse.

REFERENCES

- Benson, S. V. 1995. Tunable Free Electron Laser, in F. Duarte (ed.), *Tunable Laser Handbook*, New York: Academic Press, pp. 443-470.
- Benson, S., J. Schultz, B. Hooper, R. Crane, and J. Madey. 1988. Status Report on the Stanford Mark III infrared free electron laser, *Nucl. Instrum. Methods*, **A272**, 22-28.
- Buschner, R., M. Kolm, U.-A. Gorys, and C. Weitkamp. 1992. ARGOS -A vanborne system for remote air pollution measurement, in R. J. Becherer and C. Werner (eds.), *Lidar for Remote Sensing*, Proc. SPIE, **1714**, 39-45 .
- Coble, P. G., C. A. Schultz, and K. Mopper. 1993. Fluorescence contouring analysis of DOC intercalibration experiments samples: a comparison of techniques. *Marine Chem.* **41**, 173-178.
- Cover, R. A., G. T. Bennett, R. J. Burke, M. S. Curtin, M. C. Lampel, and G. Rakowsky. 1991. Simulations of the Rocketdyne Free-Electron Laser, *IEEE Quantum Electronics*, **27**, 2598-2604.
- Grant, W. B. 1995. Lidar for Atmospheric and Hydrographic studies in F. Duarte(ed.), *Tunable Laser Handbook*, New York: Academic Press, pp. 213-305.
- Longtin, D. R., M. G. Cheifetz, J. R. Jones, and J. R. Hummel. 1994. BACKSCAT Lidar Simulation Version 4.0: Technical Documentation and Users Guide, USAF Phillips Laboratory Report PL-TR-94-2170, pp. 137.
- Manheimer, W. M. 1994. Gyrotrons and Free Electron Lasers as Atmospheric Sensors. *Phys. Plasmas* **1**, 1721-1929.
- Measures, R. M.. 1984. *Laser remote Sensing*, New York: Wiley Intersci. Publications. pp. 510.
- McGee, T. J., M. R. Gross, U. N. Singh, J. J. Butler and P. E. Kimreilakani. 1995. Improved Stratospheric Ozone Lidar. *Optical Engineering* **34**, 1421-1430.
- Spiers, G. D., (University of Alabama at Huntsville), private communication, 1996.
- Takeuchi, N., H. Baba, K. Sakurai, and T. Ueno. 1986. Diode laser random-modulation cw lidar. *Appl. Optics*, **2**, 63-67.
- Vodacek, A. F., E. Hoge, R. N. Swift, J. K. Yungel, E. T. Peltzer, and M. V. Blough. 1995. The use of in situ and airborne fluorescence measurements to determine UV absorption coefficients and DOC concentrations in surface waters. *Limnol Oceanogr.* **40**, 411-415.

SEDIMENTARY $\delta^{13}\text{C}$ AS A PROXY FOR THE SOURCE OF THE BULK SEDIMENT

Deling Cai
First Institute of Oceanography, SOA
Qingdao, China

ABSTRACT

Sedimentary organic carbon isotope ratios have been used extensively to calculate the relative contributions of marine and terrestrial organic matter to coastal sediments. A question that has not yet been addressed is whether the source, as determined from the isotopic composition of the organic matter, can be used to trace other components of the sediment. To investigate this problem, the organic carbon content, the isotopic composition of organic carbon, grain-size parameters, and light mineral constituents of sediments from the Okinawa Trough have been analyzed. Correlation between these parameters have been used to show that the same processes that affect the source of organic matter to this hemi-abyssal basin also affect the source of other components of the bulk sediment.

INTRODUCTION

The carbon isotope composition of modern marine sedimentary organic matter ($\delta^{13}\text{C}_{\text{SOM}}$) has been investigated worldwide since the fifties. Deines (1976) compiled values for more than 1600 samples that had been published in the literature before 1976, showing variations in $\delta^{13}\text{C}$ values ranging from -10‰ to -30‰ . Only a few samples were lighter than -30‰ , and more than 90% of the samples had values between -20‰ and -27‰ . The $\delta^{13}\text{C}$ values of these sediments were in the main close to that of living plants and animals collected in the overlying water column from the corresponding area.

Stable carbon isotopes have been used extensively in estuaries to study the source and fate of organic carbon. The largest estuaries in the world such as the Amazon (Cai et al., 1988), the Mississippi (Shultz and Carder, 1976), the Yangtze (Tan et al., 1991), the Yellow (Cai, 1994), the St. Lawrence (Tan and Strain, 1979, 1983), the Congo (Mariotti et al., 1991) and the Orinoco (Tan and Edmond, 1993) have been investigated, showing that the carbon isotopic composition in particulate organic matter ($\delta^{13}\text{C}_{\text{POM}}$) can provide a valuable tracer for the transport of riverine material into the coastal waters (Sharp, 1991).

In the early 1960's, based on the meager amount of stable carbon isotope data available for marine and terrestrial plants, Sackett and Thompson (1963) demonstrated that the difference between the characteristic isotopic compositions of these two plants from these two environments could be used to determine the relative amounts of terrestrial and marine plant organic debris in near shore clastic sediments. Sediments in several rivers flowing into Mississippi Sound and Mobil Bay were found to have $\delta^{13}\text{C}_{\text{SOM}}$ values of about -27‰ , reflecting

terrestrial plant composition. $\delta^{13}\text{C}_{\text{SOM}}$ values increased across the Mississippi estuary and Sound and out into the open Gulf of Mexico reaching a maximum value of about -19‰ , which reflected the isotopic composition of plankton in the overlying water column. Subsequent studies by Hunt (1970) for sediments in Chesapeake Bay, Delaware Bay, Pamlico and Albemarle Sound at Cape Hatteras and in various estuaries along the southeastern Atlantic coast of the US showed a similar range of values. The $\delta^{13}\text{C}_{\text{SOM}}$ values are often used to establish the marine versus terrestrial contribution in marine sediments (Degens, 1969; Peter et al., 1978; Fontugne and Calvert, 1992).

In this paper, the sedimentary organic carbon isotope ratios have been used as a tracer to study quantitatively the material sources of the sediments to the Okinawa Trough, a hemi-abyssal basin.

BACKGROUND KNOWLEDGE OF MATERIAL SOURCES IN THE SHELF OF THE EAST CHINA SEA AND OKINAWA TROUGH

The sediments from the shelf of the East China Sea and Okinawa Trough come from three main sources: (1) the terrestrial material carried by the Yangtze River and the other rivers around the East China Sea, (2) the suspended or resuspended material, mostly from the Yellow River, carried by the alongshore currents of the Yellow Sea, (3) *in situ* produced marine plankton and the pelagic organisms carried by the Kuroshio or Taiwan warm currents. The first two are terrestrial in origin and the last is marine (Jin, 1989).

The main rivers emptying into the East China Sea are the Yangtze, the Qiantang, the Oujiang, the Minjiang, the Jiulongjiang and the Dushuixi in Taiwan. The total annual mean sediment load for these rivers is 485×10^6 t, to which the Yangtze contributes 468×10^6 t, making up 96.4 % of the total. The deposited material from the disused Yellow River Estuary makes a large contribution to the suspended or resuspended material of the Yellow Sea. This has a considerable effect on the East China Sea. Therefore it is clear that the terrestrial material affecting this area originates in the Yangtze and the Yellow Rivers, especially the former, and amounts of material from islands are minimal, influencing only small adjacent areas.

COLLECTION AND ANALYSES OF SAMPLES

Particulate matter from the Yangtze River was collected at the last hydrographic station (Datong station) to monitor seasonal variations. The sampling took place at Datong station in the lower reaches during a period from January to December of 1993. The station is 624 km from the river mouth and it is still a tidal channel during the dry season. Sampling was undertaken midstream on the 22nd of each month.

Surface and demersal water samples (2 dm^3) were collected using a Niskin water sampler. Water samples were filtered under vacuum through precombusted $1 \mu\text{m}$ glass fiber filters of 60 mm

diameter produced by Shanghai Hongguang paper mill. The filters were stored frozen at -20°C for subsequent laboratory analyses.

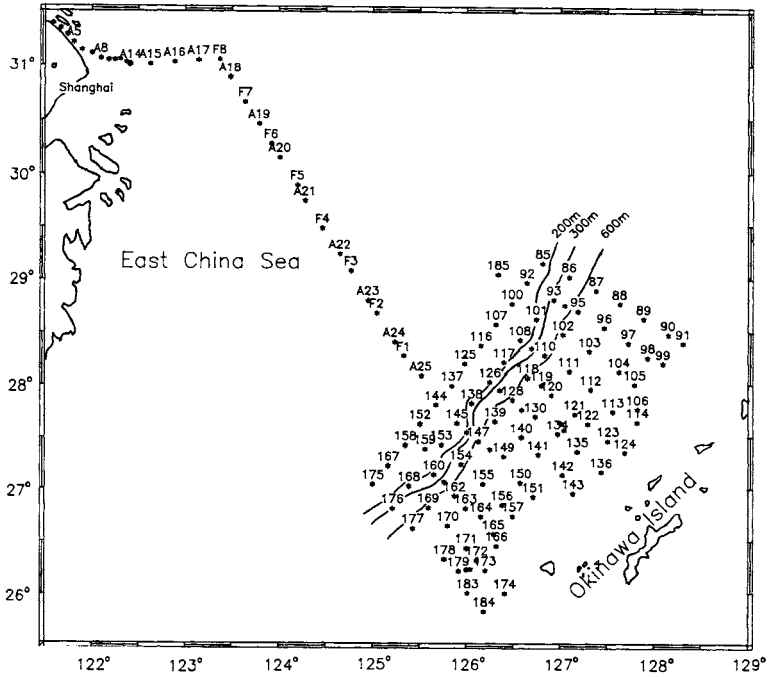


Fig. 1 Locations of surface sediment samples in the middle part of the Okinawa Trough

Surface sediment samples from the middle part of the Okinawa Trough were collected on RV Xiangyanghong 16 from June 12 to July 22, 1993. The locations of the 126 stations sampled are summarized in Fig. 1.

The concentrations of particulate organic carbon, sedimentary organic carbon and their isotopic compositions were determined by a high-temperature combustion method. This procedure is similar to that described by the literature (Tan and Strain, 1979; 1983; Cai et al., 1988; Cai, 1994). The $\delta^{13}\text{C}$ values of samples were measured on a Finigan MAT DELTA E mass spectrometer, reported as a reference with PDB international standard. Replicate sample analysis showed that the precision of the isotopic analysis of samples was $\pm 0.2\text{‰}$.

RESULTS

Seasonal Variations of the Particulate Organic Carbon Concentration and its Isotopic Composition in the Freshwater of the Yangtze

Based on the statistical data from daily measurements at Datong hydrographic station in 1993, the annual flow through the Yangtze is 976.7 km^3 and the annual sediment load $368.3 \times 10^6 \text{ t}$.

The seasonal variations in the POC concentration and its isotopic composition in the lower freshwater regions of the Yangtze are shown in Fig. 2. It can be seen from figure 2 that the POC maximum, 0.44 mmol/dm^3 , appeared in September. However this did not correspond to the sediment load maximum which occurred in August. The POC minimum (0.098 mmol/dm^3) is seen in February, and is in line with the value for suspended matter. The particulate organic carbon concentrations in the freshwater of the Yangtze are much lower than that of the Yellow River (0.68 to 6.16 mmol/dm^3).

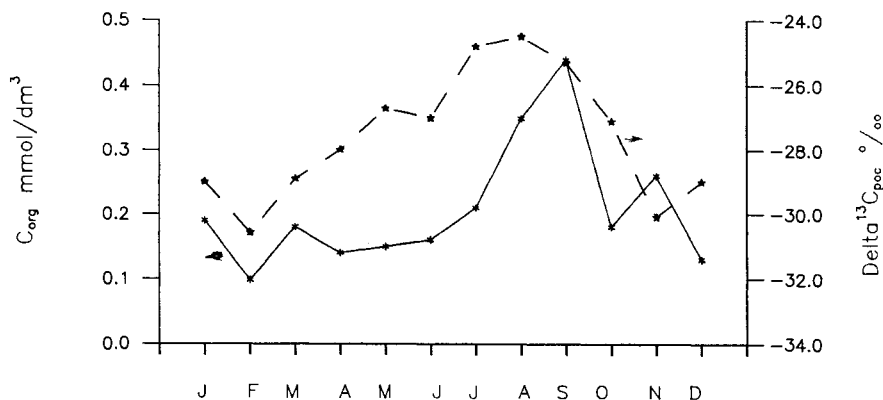


Fig. 2 Seasonal variations of the POC concentration and $\delta^{13}\text{C}_{\text{POC}}$ values in freshwater of the lower reaches of the Yangtze river

It can also be seen that the isotopic composition of the POC for the Yangtze River shows seasonal variation. The $\delta^{13}\text{C}_{\text{POC}}$ values in the flood season were heavier, maximum -24.5 ‰ in August, whereas those in the dry season become lighter and decrease to a minimum of -30.6 ‰ in February. The variation over a whole year was approximately 6 ‰ . This pattern of seasonal variation is very similar to that of the Yellow River. The $\delta^{13}\text{C}_{\text{POC}}$ of the Yellow River ranged from -25.1 to -29.2 ‰ . The annually weighted average value of $\delta^{13}\text{C}_{\text{POC}}$ in the freshwater of the Yangtze was -26.2 ‰ . This is a typical carbon isotope composition for terrestrial organic matter and close to that of the Yellow River (-26.5 ‰) (Cai, 1994).

Particulate organic carbon concentrations in the freshwater of the Yangtze have positive correlation with monthly means of runoff and suspended matter. The correlative coefficients

were 0.72 and 0.81, respectively. Similarly, $\delta^{13}\text{C}_{\text{POC}}$ had good positive correlation with these two parameters and the coefficients of 0.92 and 0.88, respectively. This feature is also similar to that of the Yellow River (Cai, 1994).

Since the sediment load from the Yangtze River is the predominant source of total sediment load entering the sea in this area, it can be considered that the annual weighted mean of the Yangtze (-26.2‰) is the endmember value of carbon isotopes of the terrestrial organic matter ($\delta^{13}\text{C}_t$) in the area.

Measurements of the Endmember Value of Carbon Isotopes of Marine Plankton in the Study Area

To determine the marine endmember in the sampling area, we collected two samples of marine plankton from water depths of 0 to 150 m at station Nos. 103 and 106 with a planktonic net (mesh number 38). Their isotopic values were -20.2‰ and -19.5‰ , respectively. The mean (-19.9‰) was used as the marine endmember for the area ($\delta^{13}\text{C}_m$).

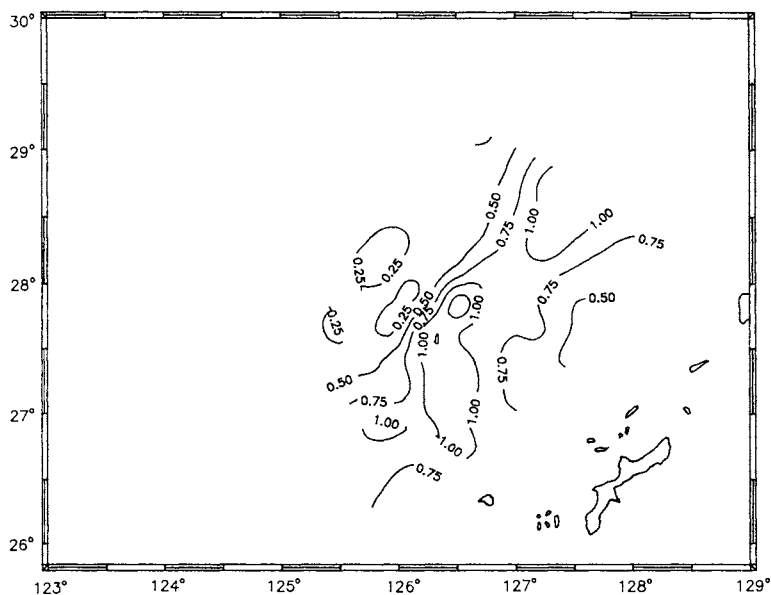


Fig. 3 The isopleth of sedimentary organic carbon percentage

The Concentration of Sedimentary Organic Carbon and its Isotopic Composition in the Middle Section of the Okinawa Trough

The concentration of sedimentary organic carbon and $\delta^{13}\text{C}_{\text{SOM}}$ from the shelf to the middle part of the Okinawa Trough are shown in Figs. 3 and 4. The concentrations of sedimentary organic carbon on the shelf of the East China Sea are usually below 0.3 %. It can be seen that the

isopleth of 0.5 % for sedimentary organic carbon concentration on the west side of the trough is basically in line with the isobath of 300 m water depth in the area, and the isopleth of 0.75 % corresponds mostly to the isobath of 600 m. There are few areas of high organic carbon content (more than 1%) in the north and south of the basin bottom in the middle of the Okinawa Trough, and the contents had a decreasing trend eastwards over the trough bottom. There is another isopleth of 0.75 % in the slope on the east side of the trough and an area of lower values (less than 0.5 %) more eastwards.

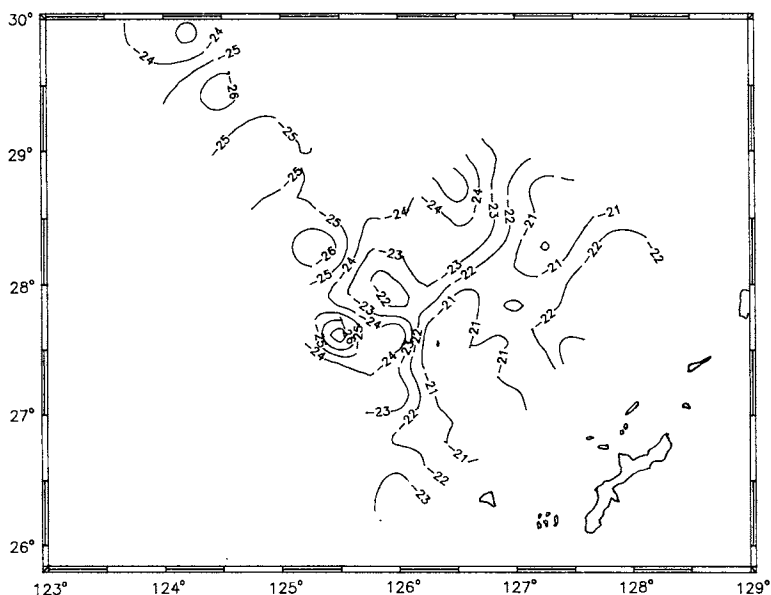


Fig. 4 The distribution of sedimentary $\delta^{13}\text{C}_{\text{org}}$ values (‰)

It is suggested from the distribution of $\delta^{13}\text{C}_{\text{SOM}}$ that the isopleth of -24‰ follows the trend of the isobath at 200 m. The isopleth of 0.75 % for organic carbon contents is in line with an isopleth $\delta^{13}\text{C}_{\text{SOM}}$ of -23‰ in the southern region, but follows the isopleth of -22‰ in the northern region. Two areas having heavier values (more than -21‰) correspond to that of the higher (more than 1%) carbon contents. On the eastern slope of the trough the isopleth of -22‰ , for isotopic values, matches that of the isopleth of 0.75 % for carbon contents.

DISCUSSION

From the literature published in China and abroad some sediments in the Okinawa Trough have been identified as terrestrial in origin. Jiang et al. (1984) considered monoterpenes as terrestrial markers as they originate from the remains of higher plants. Three kinds of monoterpenes were detected in sediments from the Okinawa Trough. These were thought to

originate from the shelf around the trough. Sediments collected south of Cheju Island, at the northern end of the Okinawa Trough, have been shown to be clay rich and contain calcite (Milliman, 1985). The presence of calcite suggested that this material originally derived from the Yellow River. However, these studies had a common limitation, i.e. they could only be used to make a qualitative judgment of the existence of terrestrial matter, with no way of estimating it quantitatively. The application of stable isotope tracer technology opens up a new way to overcome this difficulty.

As stated before, even though the sediments in this area may have many origins, the sediment composition has only two sources, namely: terrestrial and marine. The material from the Yangtze and the Yellow rivers predominate the terrestrial source with material from the other smaller rivers and islands making only very minor contributions. The annual weighted mean of $\delta^{13}\text{C}_{\text{POM}}$ in particulate matter from the Yellow River is very close to that from the Yangtze, and the Yangtze value of -26.2‰ was taken as an appropriate endmember value of the terrestrial material. The endmember of marine material in the area was determined to be -19.9‰ . In the light of a simple mass balance the following equation can be established:

$$F_t \delta^{13}\text{C}_t + (1 - F_t) \delta^{13}\text{C}_m = \delta^{13}\text{C}_{\text{SOC}} \quad (1)$$

where, $\delta^{13}\text{C}_t$ = endmember isotopic value for terrestrial organic matter, $\delta^{13}\text{C}_m$ = endmember isotopic value for marine plankton, $\delta^{13}\text{C}_{\text{SOC}}$ = the isotopic value of total organic carbon in a sediment sample, and F_t = the percentage of terrestrial material in the sediment (%). The following formula can be derived:

$$F_t = \frac{\delta^{13}\text{C}_m - \delta^{13}\text{C}_{\text{SOC}}}{\delta^{13}\text{C}_m - \delta^{13}\text{C}_t} \quad (2)$$

Therefore the percentage of terrestrial material in a sediment can quantitatively be derived from the $\delta^{13}\text{C}_{\text{SOC}}$ if the isotopic composition of the two source terms are known. The isopleth of percentages of terrestrial material in sediments from the Okinawa Trough is shown in Fig. 5. It can be seen that the isopleth of 60 % is basically in line with the isobath of 200 m in water depth. Water column temperature and salinity data collected on the same cruise show an intrusion of more saline, warmer water at 28°N and a landward deviation from the isobath of 200 m in at 28°N was also observed in the percentage of terrestrial material. The isopleth of 40 % is in line with the isobath of 600 m in water depth. There are two areas of lower percentages in the middle of the basin bottom, being below 20 %, illustrating that the sedimentary organic matter was predominantly of marine origin. On the east slope of the trough the percentage of terrestrial material increased slightly, reflecting local island-origin material (see Fig. 1).

We calculated directly the relative marine and terrestrial contributions for sedimentary organic matter based on the sedimentary carbon isotopic compositions. However, the significance of the estimation need not be limited to organic matter itself and should lie in the fact that it can be used to trace the sources of other material components in these sediments. Therefore, we examined

the correlation of sedimentary organic carbon concentration and its isotopic composition with grain size, light mineral components etc. (Table 1).

Table 1. Summary of correlation factors

	$\delta^{13}\text{C}_{\text{org}}$	C_{org}	grain-size parameters			light mineral component	
			sand content	silt content	clay content	terrestrial clastic	biological clastic
$\delta^{13}\text{C}_{\text{org}}$	—	0.65	-0.65	0.57	0.62	-0.57	0.58
C_{org}	0.65	—	-0.81	0.68	0.79	-0.66	0.69
F_1	-1.00	-0.65	0.65	-0.57	-0.62	0.57	-0.58

It can be seen clearly that the sedimentary organic carbon concentration and the $\delta^{13}\text{C}_{\text{SOM}}$ both have a good correlation with grain-size parameters in the sediments, showing a negative correlation with sand contents, but a positive correlation with silt and clay contents.

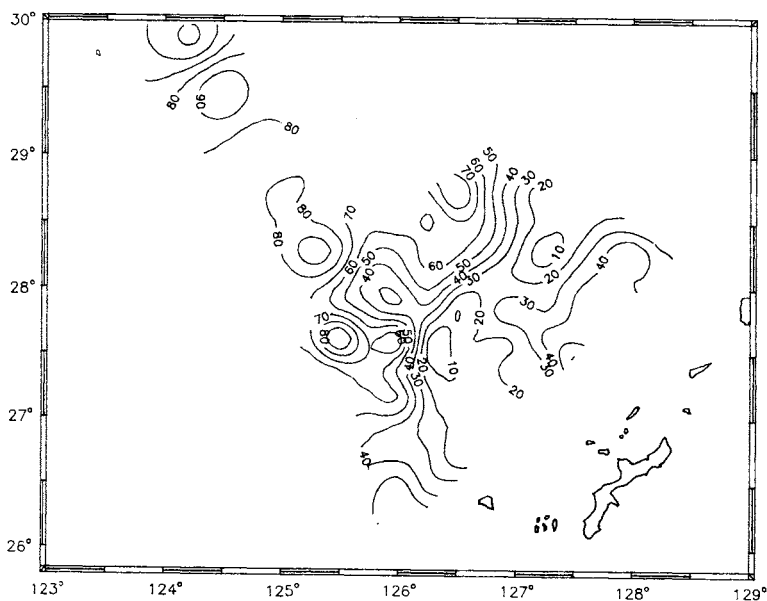


Fig . 5 The isopleth of terrestrial material percentage

The distribution of sand in and around the trough shows that there is an area of more than 70 % of sand contents in sediments at the margin of the continental shelf in the East China Sea. This area corresponds to the one where the organic carbon concentration in the sediments was, in general, less than 0.5 % and $\delta^{13}\text{C}_{\text{org}}$ values lower than -22‰ . The area of low (less than 20 %) sand contents is located further east and south.

sand content is distributed basically at the bottom of the trough. In this region, the organic carbon concentration was usually more than 0.5 % and $\delta^{13}\text{C}_{\text{org}}$ values more than -24‰ . Thus the sand-grade component in sediments has a lower organic carbon content and ^{13}C depleted isotopic composition.

In contrast with sand, the silt- and clay-grade contents have positive correlation with sedimentary organic carbon concentrations and its isotopic composition, illustrating that these fine-grade sediments had high organic carbon contents and ^{13}C -rich isotopic composition. When silt content was lower than 25 % or clay content lower than 20 %, the organic carbon content was mostly below 0.5 %, and $\delta^{13}\text{C}_{\text{org}}$ ranged from -28 to -22‰ ; while silt content was higher than 30% or clay content higher than 40 %, organic carbon content was usually larger than 0.5 % and $\delta^{13}\text{C}_{\text{org}}$ had a range of -24 to -20‰ . The area of highest clay content (more than 50 %) is found both in the north and south of the trough bottom. This is in line with the areas of high organic carbon content (above 1 %) and the high $\delta^{13}\text{C}_{\text{SOM}}$ (more than -21‰).

A similar relationship between sedimentary organic carbon and its isotopic composition with light mineral component (density $<$ 2.85) in sediments has been shown (Table 1). The light mineral components of the sediment in the grain-size range of 0.063 to 0.25 mm were determined quantitatively. The light mineral in the study area consists of four kinds: continental-origin debris, bioclastic, volcanic and authigenic. Both the continental-origin debris and the bioclastic minerals hold a dominant position, usually over 90 % at most of the stations. The terrestrial debris had a negative correlation with organic carbon and its isotopic ratios, showing organic-rich sediments usually had a lower content of terrestrial debris. The bioclastic content had a contrary trend and a positive correlation with organic carbon and its isotopic composition. This is easy to understand as the percentage of material originating from marine sources increases, then so will the percentage of organic carbon, while the isotopic composition will increase to heavier values than that of terrestrial matter. Therefore, the information originated from organic carbon content and its isotopic composition in the sediment reflects also relative content of terrestrial debris and bioclastic mineral as the majority of mineral constituents. Only two stations (Nos. 86 and 93) at the northern end of the sampling site had an authigenic mineral content of above 5 %. There were eight stations (Nos. 87, 91, 96, 98, 99, 104, 106 and 123), where volcanic mineral content was higher than 10 %. The highest content appeared at station 99, up to 35.6 %.

Thus it is shown that there are good homologous relationships of sedimentary organic carbon and its isotopic ratios with grain-size parameters and light mineral components of sediments in the middle part of the Okinawa Trough. These homologous relationships are not occasional, and show for example that sedimentary organic matter has a close relation with the grain-size grade of sediments, and that these relationships hold true for a wide range of grain-size from sand to clay. Therefore, the information on material sources represented by sedimentary organic carbon and its isotopic composition need not be used only for organic matter itself, but can also be used to derive information about the source of the bulk sediments.

In conclusion, organic carbon isotope ratios as a proxy of material sources of sediments from the middle part of the Okinawa Trough have been further substantiated with evidence from

sedimentary grain-size and light mineral constituents, showing the quantitative estimation for contents of terrestrial material on the basis of this tracer is suitable for the majority of sediments from the middle part of the Okinawa Trough. Gravel which has grain-size of larger than 2 mm has not been considered and the method is not suitable for volcanic and inorganic authigenic minerals because these constituents had, in general, very low contents in sediments of the Okinawa Trough.

The higher percentage of terrestrial material in the sediments at the continental shelf slope of the East China Sea does not mean the lower production of marine plankton in this region but active reconstruction of sediments caused by strong hydrodynamic conditions. As a consequence, most of the clay-grade sediments were transported to the bottom of the trough and the grain size of the residual became coarser. Our conclusion coincides with the qualitative judgment that there is more terrestrial material around the west slope of the trough on the basis of mineral constituents and spore-pollen analysis in sediments (Yuan et al., 1978).

CONCLUSION

With a linear equation for the mixing of marine and terrestrial material, the percentage of terrestrial matter in sediments could quantitatively be calculated from $\delta^{13}\text{C}_{\text{org}}$ values in surface sediments from the middle part of the Okinawa Trough. The percentage of terrestrial material correlated negatively with sedimentary organic carbon concentration, silt- and clay-grade content and bioclastic content in the light mineral components, but positively with sand-grade content and continental debris content. It has been shown that the material sources of sediments can be determined by sedimentary organic carbon isotopic ratios, representing not only the source for organic matter itself, but also for other bulk constituents of the sediment.

ACKNOWLEDGMENTS

This project was supported by a grant (85-904-03-02) from the National Science and Technology commission of China and by a grant (49473191) from the National Natural Science Foundation of China. My colleagues at the institute, in particular, Han Yibing, Gao Sulan, Prof. Wu Shiyang, and Bai Liming are acknowledged for doing part of the analysis. To Dr. Hilary Kennedy of the University of Wales-Bangor, UK, I extend my gratitude for critically reading the manuscript.

REFERENCES

- Cai, D. L., F. C. Tan, and J. M. Edmond. 1988. Sources and transport of particulate organic carbon in the Amazon River and Estuary. *Estua., Coast. Shelf Sci.* **26**(1):1-14.
- Cai, D. L. 1994. Geochemical studies on organic carbon isotope of the Huanghe River (Yellow River) Estuary. *Science in China, Series B.* **37**(8):1001-1015.

Degens, E. T. 1969. Biogeochemistry of stable carbon isotopes. In: Organic Geochemistry. Berlin, Heidelberg. New York: Springer Verlag. pp. 304-329.

Deines, P. 1976. The isotopic composition of reduced organic carbon, In: Handbook of Environmental isotope Geochemistry. vol. 1. Amsterdam: Elsevier. pp. 329-406.

Fontugne, M. R. and S. E. Calvert. 1992. Late Pleistocene variability of the carbon isotopic composition of organic matter in the eastern Mediterranean: Monitor of changes in carbon sources and atmospheric concentrations. *Palaeoceanography*. **7**:1-20.

Hunt. J. M. 1970. The significance of carbon isotope variations in marine sediments. In: Advances in Organic Geochemistry. pp. 27-35.

Jiang, S., J. Fu and Z. Luan. 1984. Monoterpenes as terrigenous markers in Okinawa Trough sediment. *Geochimica*. **2**:161-165 (in Chinese).

Jin, X. (ed.) 1989. Marine Geology of the East China Sea. Beijing: Ocean Press.(in Chinese)

Mariotti, A., F. Giresse and Kingamouzeo. 1991. Carbon isotope composition and geochemistry of particulate organic-matter in the Congo River (central-Africa) application to the study of Quaternary sediments off the mouth of the river. *Chemical Geology*. **86(4)**:345-357.

Milliman, J. D. 1985. Modern Huanghe-derived muds on the outer shelf of the East China Sea: Identification and potential transport mechanisms. *Continental Shelf Research*. **4(1/2)**:175-188.

Peters, K. E., R. E. Sweeney and I. R. Kaplan. 1978. Correlation of carbon and nitrogen stable isotope ratios in sedimentary organic matter. *Limnol. Oceanogr.* **23**:598-604.

Sackett, W. M. and R. R. Thompson. 1963. Isotopic organic carbon composition of recent continental derived clastic sediments of Eastern Gulf Coast, Gulf of Mexico. *Bull. Am. Assoc. Pet. Geol.* **47**:525-528.

Sharp, J. H. 1991. Review of carbon, nitrogen and phosphorous biogeochemistry. In: U. S. National Report to International Union of Geodesy and Geophysics 1987-1990. pp. 648-657.

Shultz, D. J. and J. A. Carder, 1976. Organic carbon $^{13}\text{C}/^{12}\text{C}$ variations in estuarine sediments. *Geochim. et Cosmochim. Acta*. **40**:381-385.

Tan, F. C., D. L. Cai and J. M. Edmond, 1991. Carbon isotope geochemistry of the Changjiang Estuary. *Estua. Coast. Shelf Sci.* **32(4)**:395-403.

Tan, F. C. and J. M. Edmond, 1993. Carbon isotope geochemistry of the Orinoco Basin. *Estua. Coast. Shelf Sci.* **36(6)**:541-547.

Tan, F. C. and P. M. Strain. 1979. Carbon isotope ratios of particulate oceanic matter in the Gulf of St. Lawrence. *J. Fish. Res. Board Can.* **36**:678-682.

Tan, F. C. and P. M. Strain. 1983. Source, Sinks, and distribution of organic carbon in the St. Lawrence Estuary, Canada. *Geochim, et Cosmochim. Acta.* **47**:125-132.

Yuan, Y., G. Chen, W. Yang, et al. 1987. Characteristics of sediments from the Okinawa Trough. *Acta Oceanologica Sinica.* **9**(3):353-359 (in Chinese).

NEW ANALYTICAL TECHNIQUE FOR THE SHIPBOARD DETERMINATION OF COBALT CONCENTRATION IN SEA-WATER AND HYDROTHERMAL SOLUTIONS

Irina Ya. Kolotyrkina¹, Alexander Malahoff², Lilly K. Shpigun¹,

¹Russian Academy of Sciences
Moscow, RUSSIA

²University of Hawaii
Honolulu, HI USA

ABSTRACT

A new flow-injection technique for the determination of cobalt in sea-water and hydro-thermal sea-water solutions has been developed and tested in the field. It is based on the catalytic effect of cobalt(II) on the oxidation of N,N'-diethyl-p-phenylendiamine by hydrogen peroxide in the presence of Tiron as an activator. The catalytic activity of cobalt (II) was found to be significantly enhanced by the presence of sea-water matrix components, especially by calcium ions, improving the sensitivity of cobalt determination in sea-water. The comparatively weak basic medium (pH 8.7-9.0) of the reaction and its relative freedom from co-existing ions allowed the direct analysis of sea-water to be effectively conducted without any preliminary steps. A sampling rate was 50 h⁻¹. The limit of detection for cobalt was 1 ng l⁻¹ and the relative standard deviation at the level of 10-1000 ng l⁻¹ was (1-8) % (n=5). The technique was confirmed to be accurate on the basis of analysis of the standard sea-water solutions CASS-2 and NASS-2. Artificial hydro-thermal solution samples as well as samples taken from a hydrothermal plume were analyzed by the proposed technique and the results were in good agreement with data obtained by ICP-MS.

INTRODUCTION

It is known that the oceanic concentration of cobalt is very low and in deep ocean water is less than 1 ng l⁻¹ (Bruland, 1983). From the geochemical point of view this metal is interesting because anomalous concentrations of cobalt up to 300 ng/l have been detected in deep sea-water around hydrothermal vent fields (Sakai *et al.*, 1987). One good approach for measurement of trace metals is to use very sensitive catalytic reactions. The application of this types of reactions has been especially developed recently with the developing of flow-injection analysis (FIA) (Kawashima *et al.*, 1992). This methodology greatly simplifies all kinetic measurements. Advantages of FIA catalytic procedure over the kinetic batch measurements at fixed time are obvious. Beside rapid and reproducible mixing of reagents at regular time intervals which this methology provides it also gives an opportunityt a unigue possibility of carrying out relative kinetic measurements by controlling a signal produced by a metal-catalysed reaction and a signal related to uncatalysed reaction at the same time.

Significant progress has been made recently in applying flow injection (FI) catalytic methods for trace metal determination in sea-water. This approach has proved to be very adaptable for marine chemical research aboard a ship (Sakamoto-Arnold *et al*, 1987, Kolotyrkina *et al*, 1991; Resing *et al*, 1992; Kolotyrkina *et al*, 1995). Several such systems have been developed for detection of cobalt in sea-water samples (Kawashima *et al*, 1985; Sakamoto-Arnold *et al*, 1987, Isshiki *et al*, 1987; Yamane *et al*, 1988). Most of them were based on the spectrophotometric monitoring the well-known catalytic reactions of the oxidation of o-dihydroxybenzene derivatives, like tiron, and protocatechuic acid in a basic medium. Unfortunately, the strong alkaline media of all cobalt catalyzed indicator reactions (pH > 10), a lack of selectivity and often an insufficient sensitivity prevented the direct determination of cobalt in sea-water and a preliminary separation /preconcentration step was required.

In order to provide direct tracing of dissolved cobalt in sea-water it was necessary to find a sensitive catalytic reaction which can be carried out in the range of pH close to that of sea-water. Our work was devoted to the investigation of the catalytic activity of cobalt in the oxidation of two organic reagents mixture: N,N'-Diethyl-p-phenylendiamine and Tiron. Hydrogen peroxide was an oxidant in this reaction. The purpose of this research was to develop an FI technique for direct analysis of cobalt in sea-water.

Apparatus

A FIAstar 5010 Flow Injection Analyzer (Tecator) equipped with FIAstar 5023 spectrophotometer with 18 μ l flow-through cell (light path, 10 mm) and a Model 5032 controller or IBM computer was used. All tubing was made from poly(tetrafluoroethylene) (0.7 mm i.d.). The Chemifold II (Tecator) was used in order to provide the necessary FI manifold configuration.

RESULTS AND DISCUSSIONS

The catalytic reaction

Though the catalytic activity of cobalt in the reaction mixture of N,N'-Diethyl-p-Phenylendiamine (DePD), Tiron (Tr) and hydrogen peroxide (Fig.2) mainly appears at the pH level of more than 11 for pure metal solutions, it was found that it is strongly dependent on the matrix composition and on the pH level in the reaction zone.

Absorption spectra for the reaction mixture with pH 9 in the presence of cobalt and without are shown in Fig.2. The spectra were obtained by scanning during the first 30s of the reaction. It was noticed that the presence of sea-water matrix compounds in the reaction mixture solution significantly enhanced the catalytic effect of cobalt. By comparing the obtained spectra with the absorption spectra obtained with the presence of only one organic reagent the primary oxidation of DePD in the triple reaction mixture at pH 9 was identified. It was suggested that Tr play role of activator in the reaction significantly increasing the rate of the catalytic reaction.

It was noticed that cobalt analytical signal is dependent on the time of reaction. Kinetic curves for the reaction in the presence of cobalt and without it showed that the strongest catalytic effect could be observed during the first 15-30 s of the reaction. After that time the uncatalysed reaction proceeded very quickly and at a reaction time of more than 100 s the difference between the two reactions was insignificant. The described kinetic dependences once again demonstrate the advantages of the FIA technique over batch techniques, as it is obvious that analytical measurements of cobalt concentrations by the catalytic indicator reaction described in this paper would be impossible, without the FI technique.

Flow-Injection Configuration

The established fact that the cobalt-catalyzed oxidation of DePD significantly accelerated by the sea-water matrix at pH of 9 allowed us to develop a FI technique which we could be used for the determination of cobalt in sea-water.

As a result of a detailed study of chemical and hydrodynamic variable influences on the analytical signal for cobalt (II) the configuration of the FI manifold was proposed (Fig.4). The volume of 200 μ l of sea-water sample was injected into the carrier stream of sea-water matrix, then subsequently mixed with streams of the reagents: R₁ = (DePD + Tr), R₂ = (NaOH or buffer solution + H₂O₂). After mixing of all the reagents in the reaction coil the developing coloration of the reaction was monitored by the spectrophotometer.

Investigation of the catalytic reaction in the presence of sea-water matrix

As noted before, the catalytic activity of cobalt (II) was increased with the addition of sea-water matrix components in the reaction zone. In order to clarify this observation, the effect of the individual macrocomponents of sea-water was investigated. It can be seen that the analytical signal of cobalt grows proportionally with the increasing concentration of sodium chloride in the reaction zone. The variation of ionic strength from 0.4 to 0.6 made the peak height vary by about ± 15 %. The most significant effect on the catalytic activity of cobalt in this reaction was with addition of calcium to the reaction zone. Even an addition of small concentrations of calcium increased the cobalt peak by several magnitudes. A fifteen fold increase in the peak height of 0.5 $\mu\text{g l}^{-1}$ cobalt concentration was achieved by the addition of $1 \times 10^{-2} \text{ mol l}^{-1}$ of CaCl₂ solutions to the matrix solution. The effect of magnesium was smaller but still could not be completely attributed to the ionic strength effect. At the same time only a negligible salt effect on the studied oxidation reaction in the absence of cobalt was observed.

Considering the conservative nature of the macrocomponents in the open ocean, and the plateau on the calcium dependence, which is situated within the range of the average concentration of calcium in sea-water, it can be stated that there is no risk of interferences from the sea-water matrix on the results of analysis of real sea-water samples.

In order to make it possible to analyse real sea-water samples especially those collected from hydrothermal plumes, which can be significantly enriched in metals, the effect of various metal

ions on the determination of cobalt (II) was examined. As can be seen from the Table 1, aluminium (Al), lead (Pb) and zinc (Zn) at 20,000 fold concentration do not interfere with cobalt determination. At the same time manganese, nickel and iron shows interference estimated as 5% of relative error at 30, 100 and 1000 ratio to cobalt concentration respectively.

Table1. Tolerance of diverse ions on the determination of 100 ng l⁻¹ of cobalt.

Diverse ion	[Me] / [Co] ratio	Recovery (%)
Mn (II)	1 : 30	104
	1 : 50	108
	1 : 150	118
Ni (II)	1 : 100	105
	1 : 200	109
	1 : 400	116
	1 : 500	120
	1 : 2000	130
Fe (III)	1 : 1000	103
	1 : 2000	106
	1 : 5000	123
Cr (VI)	1 : 2000	102
	1 : 5000	108
	1 : 10,000	119
Cu (II)	1 : 2000	105
	1 : 5000	114
	1 : 10,000	125
Al (III)	1 : 20,000	104
Pb (II)	1 : 20,000	100
Zn (II)	1 : 20,000	98

Analytical Characteristics and Applications

The typical calibration graph of cobalt obtained for cobalt standards prepared with sea-water matrix, under the chosen optimal conditions, was linear over the range 0-1000 ng l⁻¹ of cobalt(II) concentration. The regression equation was $\Delta A = 6.026 + 3.370 C$ with correlation coefficient of 0.999389. The detection limit was 1 ng l⁻¹ and the sampling rate was 50 samples per hour. The data for the recovery experiments, are shown in Table 2. The accuracy of the method was tested by analyzing Coastal Atlantic Standard Sea-water -2 (CASS-2) and North Atlantic Sea-water-2 (NASS-2) reference materials. The results obtained by this method were in good agreement with the certified cobalt concentrations (Table 3).

The applicability of this method was also demonstrated by analyzing artificial hydrothermal solutions obtained from the geochemical experiments with basalt-water system. The

concentration values obtained by our method were in a good agreement with the values obtained by ICP-MS method using sample splits (Table 3).

Analysis of the hydrothermal vent water taken from a newly formed pit crater on Loihi submarine volcano (Hawaii) with vents located at the bottom and rim of pit crater produced elevated cobalt values. These samples were taken at the end of intense episode of earthquake activity on Loihi during 7 August 1996. The results show highly elevated cobalt values of up to $\sim 2.2 \mu\text{g/l}$ dissolved and $\sim 15.5 \mu\text{g/l}$ total at the water depth of 1200 m. In these samples the elevated cobalt concentrations were accompanied by elevated iron values of up to 20 mg/l and manganese up to 0.4 mg/l, so it is important to note that the cobalt values determined in these studies should be regarded as tentative. The linear range of the method was extended up to $5 \mu\text{g/l}$ by the addition to the described FI system (Fig.4) of one more line for the dilution the injected sample.

The obtained cobalt values are fifty times greater than those determined by Sakai et al. (1987) for Loihi vent waters before the 1996 tectonic event. The high cobalt, manganese and iron values coincide with the tectonic crisis and the probable release of high temperature hydrothermal endmembers. As a comparison samples taken in the vicinity of the Loihi vent area in 1995 showed low cobalt values of less than 4 ng/l and only a couple of samples had values of about 10 ng/l.

Table 2. Recovery of cobalt added to sea-water matrix solutions ($p=0.95$; $n=5$).

Co (II) added ng l^{-1}	Co (II) found ng l^{-1}	S_r (%)	Recovery (%)
4	4.8 ± 0.5	10.6	113
10	10.1 ± 1.1	8.5	101
30	31.3 ± 1.7	4.4	104
100	103.0 ± 2.0	1.6	103

Table 3. Results of the determination of cobalt in sea-water samples ($p=0.95$)

Sample	n	Cobalt (II) concentration / ng l^{-1}			
		FI method	S_r / %	ICP-MS	Certified value
NASS-2	4	3.1 ± 0.5	10.4	-	4 ± 1
CASS-2	14	27.1 ± 0.4	2.8	-	25 ± 6
Sea-water (Pacific Ocean)	4	10.5 ± 1.6	9.4	-	-
Artificial hydrothermal solutions	5	35 ± 3	5.8	33 ± 1	-
	5	175 ± 5	2.5	165 ± 5	-

CONCLUSION

A new FI procedure for the spectrophotometric determination of cobalt in sea-water based on the catalytic effect of Co(II) on the oxidation of DePD by hydrogen peroxide has been developed and successfully applied to the direct shipboard determination of cobalt concentration in hydrothermal solutions sampled from Loihi submarine volcano (Hawaii). This new method provides results that have satisfactory reproducibility, accuracy and recovery.

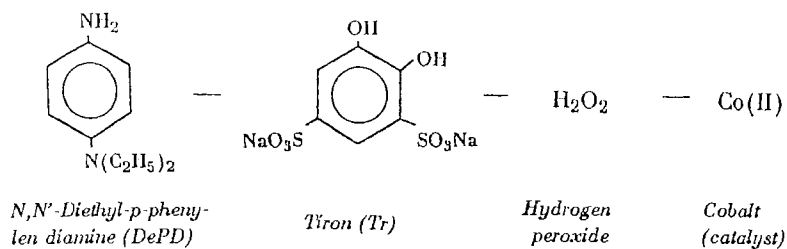


Figure 1. The reagents involved in catalytic reaction used.

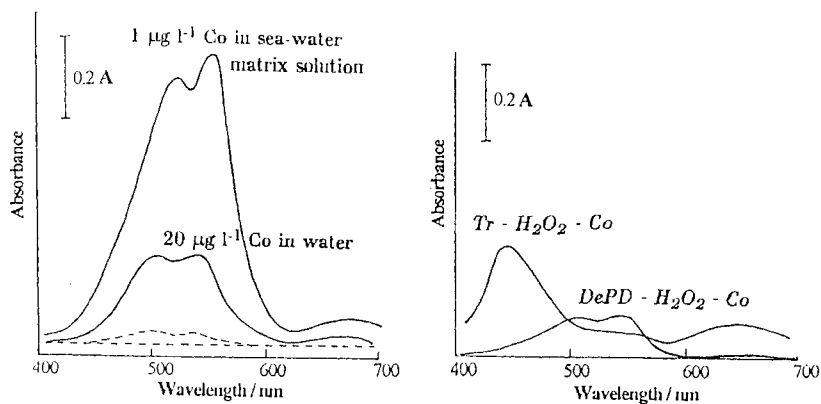


Figure 2. Absorption spectra of solutions (pH9) containing (a) - DePD-Tr-H₂O₂ : ---- without cobalt; ---- with cobalt; (b) - Individual reagent-H₂O₂ with 20 µg l⁻¹ of cobalt in sea-water matrix solution.

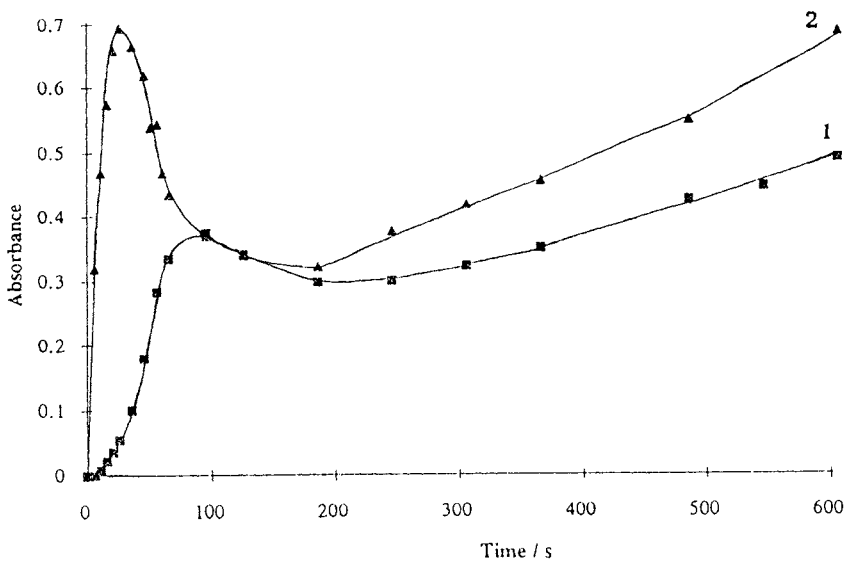


Figure 3. Kinetic curves for the reaction of oxidation of DePD by hydrogen peroxide in the presence of Tr: 1, uncatyzed reaction; 2, cobalt-catalyzed reaction obtained with injection of $1 \mu\text{g l}^{-1}$ of cobalt.

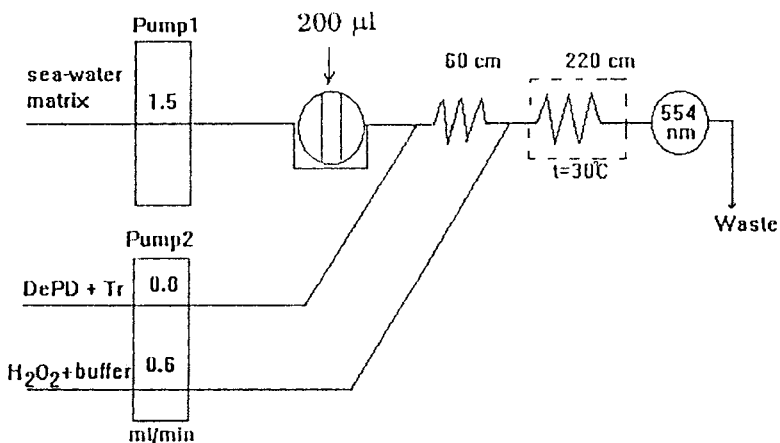


Figure 4. Schematic diagram of FI manifold used for the catalytic determination of cobalt(II).

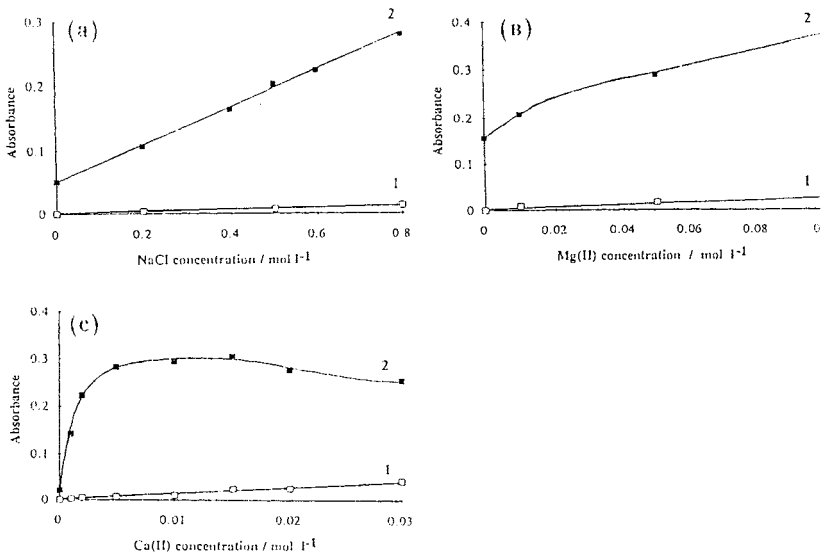


Figure 5. Effect of macrocomponents in sea-water on the FI signal.

(a) NaCl: 1, without cobalt; 2, with $4 \mu\text{g l}^{-1}$ of cobalt.

(b) Mg(II): 1, without cobalt; 2, with $4 \mu\text{g l}^{-1}$ of cobalt.

(c) Ca(II): 1, without cobalt; 2, with $0.5 \mu\text{g l}^{-1}$ of cobalt.

REFERENCES

- Bruland, K.W. 1983. In: *Chemical Oceanography*, eds.Riley, J.P., Chester, R., Academic: London, 11.
- Isshiki, K., and Nakayama, E. 1987. *Talanta*. **34**:277.
- Kawashima, T., Minami, T., Ata, M., Kamada, M., and Nakano, S. 1985. *Flow Inject. Anal.* **2**:40.
- Kawashima, T., Nakano, S. 1992. *Anal. Chim. Acta.* 261:167-182.
- Kolotyrkina, I. Ya., Shpigun, L.K., Zolotov, Yu.A., and Tsysin, G.I. 1991. *Analyst*. **116**:707.
- Kolotyrkina, I. Ya., Shpigun, L.K., Zolotov, Yu.A., and Malahoff, A. 1995. *Analyst*. **120**:201.
- Sakai, H., Tsubota, H., Nakai, T., etc. 1987. *Geochem. Journ.* **21**:1134.
- Sakamoto-Arnold, C.M., Johnson, S. 1987. *Anal. Chem.* **59**:1789.
- Resing, J.A., and Mottl, M.J. 1992. *Anal. Chem.* **64**:2682.
- Yamane, T., and Watanabe, K. 1988. *Anal. Chem. Acta.* **207**:331.

LASER-INDUCED RAMAN AND FLUORESCENCE SPECTRA OF CROWN-OF-THORNS STARFISH EGGS

Shiv K. Sharma¹ and Tenshi Ayukai²

¹University of Hawaii
Honolulu, Hawaii, U.S.A.

²Australian Institute of Marine Science
Townsville M. C., Queensland, AUSTRALIA

ABSTRACT

Outbreaks of crown-of-thorns starfish (COTS, *Acanthaster planci*) can cause devastating damages on coral reefs and are serious concern to scientists and managers. Synchronous mass spawning has long been considered as one of the triggering mechanisms of COTS outbreaks. However, observations of COTS spawning in the field are rare and the timing and scale of their spawning events are essentially unknown. In this study, the potential of a LIDAR is examined to solve this problem. Laser-induced Raman and fluorescence spectra of COTS eggs are measured using 488.0 and 514.5 nm laser lines from an Ar⁺ laser.

COTS were collected on the fringing reefs around Lizard Island, Australia. Gonad samples were dissected from female COTS, rinsed gently in 0.4 μm glass fiber filtered seawater and placed on filter papers to remove excess seawater. These samples were kept frozen in liquid nitrogen, except during the transport between laboratories (in dry ice). The mature eggs exhibit red color where as one sample of immature eggs was pale white. Under the exposure to blue laser light (488 nm), the mature eggs from four female COTS consistently emitted strong and broad fluorescence peak in the range 527-556 nm, with distinguishable Raman peaks at 1010, 1160 and 1530 cm^{-1} . The sharp peaks at 1160 and 1530 cm^{-1} are, respectively, attributed to characteristic ν_1 (-C=C-) and ν_2 (-C-C-) stretching modes in the resonance Raman spectrum of carotenoid pigment in the eggs. The immature pale white eggs did not show resonance Raman bands of carotenoid pigment indicating that either the pigment was lacking or was below the detection limit in this sample.

These Raman and fluorescence features of mature COTS eggs were observed while the eggs were submerged in seawater. The signals did not deteriorate over a period of several days. These results clearly indicate potential of optical remote sensing technique for observation of COTS spawning in the field. Further work is, however, necessary to exploit the application of a blue-green lidar for remote *in situ* surveying of the COTS - eggs distribution in the field as well as for evaluating coupling of COTS spawning with phytoplankton blooms.

INTRODUCTION

Over the past 3 - 4 decades, outbreaks of crown-of-thorns starfish (COTS) have caused devastating damages on a number of coral reefs in the Indo-Pacific region and been dealt with as a major scientific and management problem (Birkeland and Lucas 1990 for review). The causality of COTS outbreaks has been vigorously investigated, yet still remains uncertain.

COTS has very high fecundity, with mature females being able to produce over 100 million eggs over three or four successive breeding seasons (Conand, 1985; Lucas, 1986; Kettle and Lucas, 1987). This investment towards reproduction can, however, be wasted without strategies to increase the chance of fertilization. Synchronous spawning is one of such strategies. Some workers suggested pheromones as proximate cues for COTS spawning (Beach et al., 1975). Based on the studies of temperate marine invertebrates (e.g., Minchin, 1987; Starr et al., 1990, 1993), others speculated the involvement of environmental parameters, such as temperature and phytoplankton concentration, in COTS spawning (Brodie, 1992; Babcock et al., 1992). COTS spawning has been sighted and described by some workers (Birkeland and Lucas, 1990 for review; Babcock and Mundy, 1992). None of these studies, however, have sufficient information for identifying proximate spawning cues (divers are not ready to do anything, but observe). Our inability to monitor/locate spawning COTS populations systematically is one big stumbling block for resolving this important problem.

A number of hydrodynamic models have been developed and tested for understanding the dispersal of COTS larvae in Great Barrier Reef waters (e.g., Dight et al., 1990a,b; Black and Moran, 1991). After the success in simulating the migration of COTS outbreak populations, some models were used for identifying source reefs, which initially supplied a large mass of larvae to downstream reefs. This attempt is, however, problematic. In addition to the use of a number of assumptions, the models generate a spawning event and track COTS eggs and larvae using randomly selected tide and wind histories. Model outputs can vastly lack the reality if COTS spawning is not a random event or occurs in environmental response to the onset of certain conditions. Clearly, the temporal and spatial scales of COTS spawning events is needed not only to evaluate these models but also to fully understand the COTS outbreaks. In this work, we have examined the laser-induced Raman and fluorescence characteristics of COTS egg, with the intent to use these characteristics as optical signature for field monitoring of the eggs using lidar technique (e.g., Sharma et al., 1994; Gauldie et al., 1996).

EXPERIMENTAL METHODS

COTS were collected on the fringing reefs around Lizard Island, Australia, during December 1994 and again during summer of 1995. Gonard samples were dissected from female COTS, rinsed gently with (0.4 μm glass fiber) filtered seawater and placed on filter paper to remove excess seawater. The egg samples collected from four COTS female were red in color with the exception of one sample that was pale white. No other female COTS collected during summer of 1994 and 1995 was found to contain pale white eggs. The pale white eggs sample is referred to

as immature COTS eggs as far as the pigmentation is concerned. All of these samples were kept frozen in liquid nitrogen, except during transportation between laboratories in dry ice.

Both blue (488.0 nm) and green (514.5 nm) lines of Ar⁺ ion laser (spectra-physics 2020) were used to excite the samples in nearly 180° scattering geometry. With laser power of 10 or 20 mW at the sample, the laser beam was focused to a spot of 20 micro-meter diameter. At higher laser power a defocused beam was used to avoid damage to the COTS eggs sample. Scattered light was collected with a convex lens (focal length, 4.8 cm; aperture diameter, 4.3 cm) Spectra were recorded with a Spex 1403 double monochromator equipped with a thermo-electrically cooled photomultiplier tube and a photon counting detection system. The spectra of eggs were measured both in air, and with the eggs submerged in seawater.

RESULTS AND DISCUSSION

Figure 1 shows the spectra of COTS eggs, excited with 488 and 514.5 nm lines of Ar⁺ laser in air. The mature and immature COTS eggs give distinct spectra. In the spectrum of immature eggs sample (COTS-94-2), the O-H stretching bands of water are clearly observed, and there is weak fluorescence at ~573 nm with 514.5 nm excitation (Fig. 1b). The mature red COTS eggs on the other hand produce strong and broad fluorescence at ~546 nm with distinct and sharp peaks at 1160 and 1530 cm⁻¹ and weak peaks at lower and higher wavenumbers (Fig. 1). Figure 2 exhibits spectra of three samples of COTS eggs collected during the summer of 1995. All these samples show broad fluorescence with distinct peaks shifted from the excitation line by 1010, 1160, 1530 cm⁻¹ and weak peaks at higher wavenumbers. These COTS eggs show the same distinct peaks when excited with 514.5 nm (green) laser line indicating that these peaks originate from the Raman scattering in the eggs. In Fig. 1, the fluorescence band maximum observed at ~546 nm, appear at ~556 nm for COTS-95-5 and for COTS-95 -6, and at ~546 nm for COTS-95-4 sample. Figure 3 shows the effect of high laser power on the spectra of COTS eggs. The Raman bands positions are not affected. However, the fluorescence maxima appear at lower wavelengths ~527 nm for COTS-95-4 and ~538 nm for COTS-95-5. These observations indicate desirability of using low laser power for exciting fluorescence of COTS eggs.

Figure 4 shows the Raman spectral peaks of COTS eggs, collected from three distinct females, in the 900-1600 cm⁻¹ region. The sharp peaks at 1010, 1160 and 1530 cm⁻¹ are typical of a trans conjugated double bond system with bond alteration (Rimai et al. 1973). These modes have been attributed to originate in the spectra of beta-carotene from resonance Raman modes of C=C stretch (1520 cm⁻¹, ν_1) C-C stretching mode with strong mixing of C-H bending (1160 cm⁻¹, ν_2) and the CH₃ in plan rocking (1010 cm⁻¹, ν_3) (e.g., Clark et al., 1980; Merlin, 1985; Merlin and Dele-Dubois, 1986; Urmos and Sharma, 1991; Sharma, et al., 1995). The 1100-1400 cm⁻¹ spectral range is called the “fingerprint region” of carotenoid. The weak bands observed in the wider spectral merge (1600-5000 cm⁻¹) are the combination and overtone bands. The presence of 1010, 1160 and 1530 cm⁻¹ resonance Raman bands in the spectra of COTS eggs indicate that these eggs have carotenoid pigments and thus give unique resonance Raman signatures, that can be used for remote sensing. The presence of ν_1 band of COTS eggs at higher wavenumber (1530 cm⁻¹) indicates that the number of carbon atoms in the carotenoid chain is

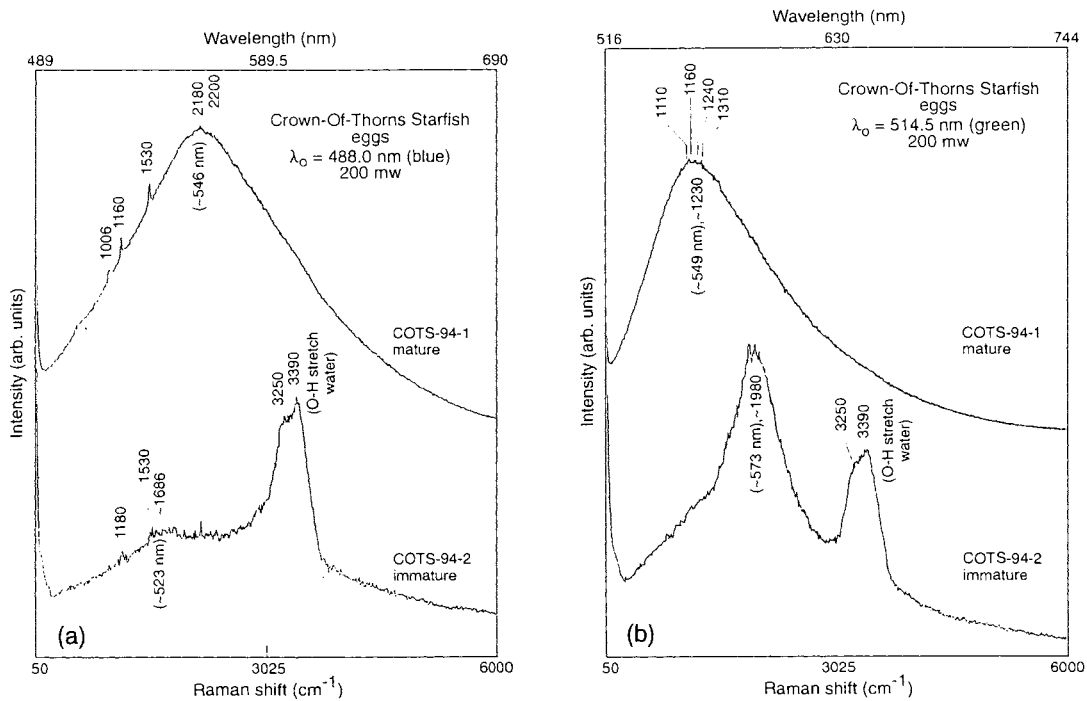


Figure 1. Raman and fluorescence spectra of crown-of-thorns starfish (COTS) eggs, collected during December 1994, excited with (a) 488.0 nm (blue) and (b) with 514.5 nm (green) laser light.

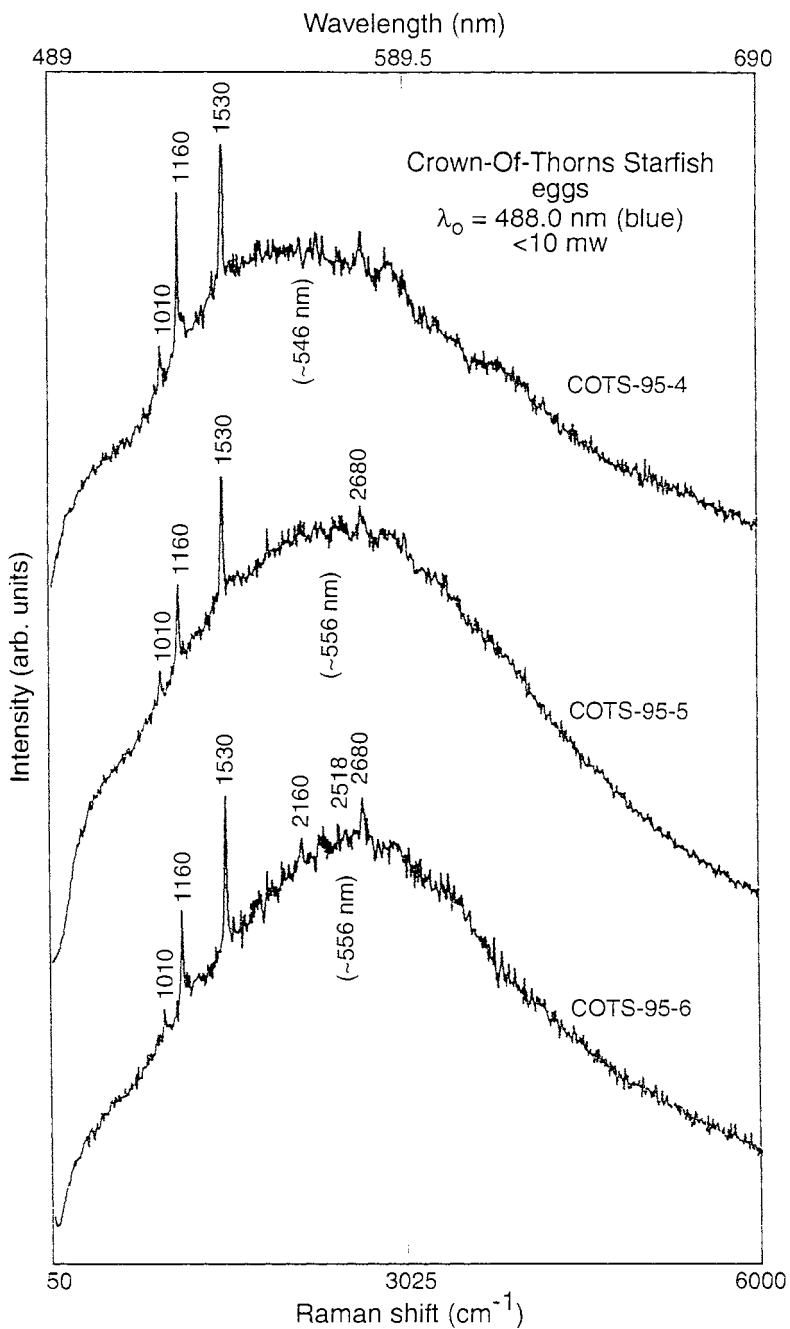


Figure 2. Raman and fluorescence spectra of COTS eggs, collected during summer of 1995, excited with $< 10 \text{ mW}$ of blue (488.0 nm) laser beam.

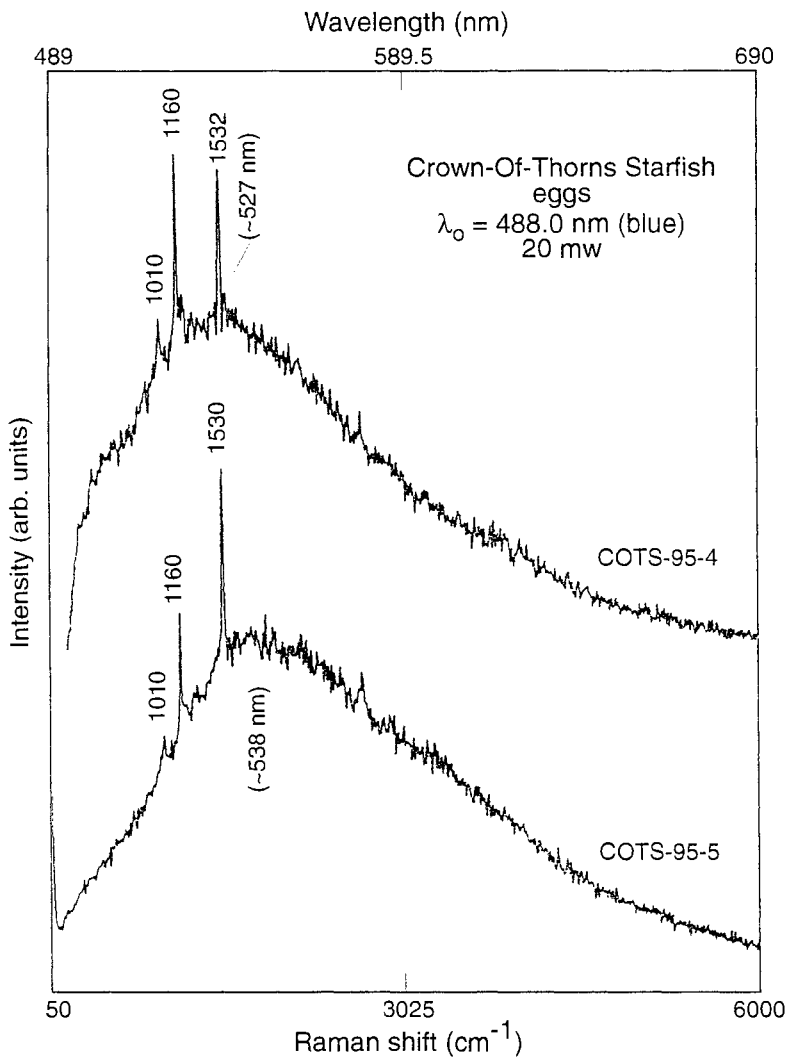


Figure 3. Raman and fluorescence spectra of COTS eggs, collected during summer of 1995, excited with 20 mW of blue (488.0 nm) laser beam.

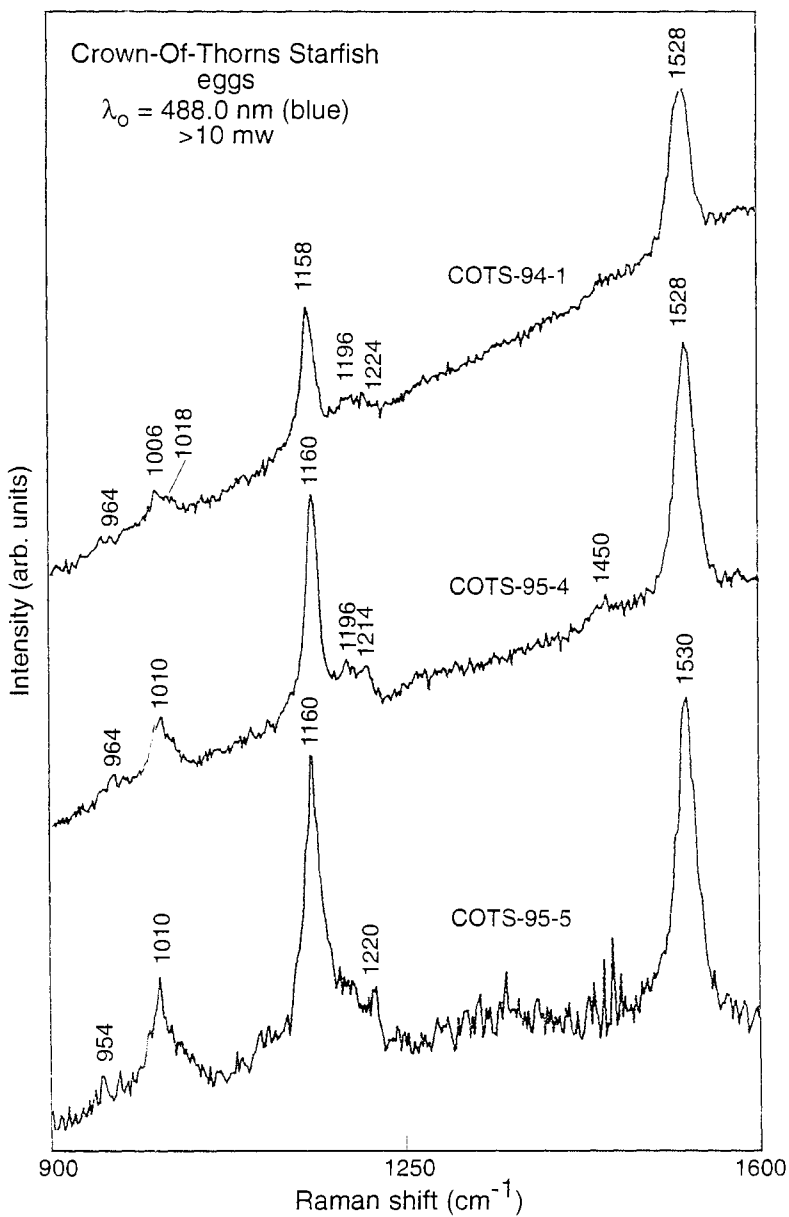


Figure 4. Resonance Raman spectra of COTS eggs in the 900-1600 cm^{-1} region.

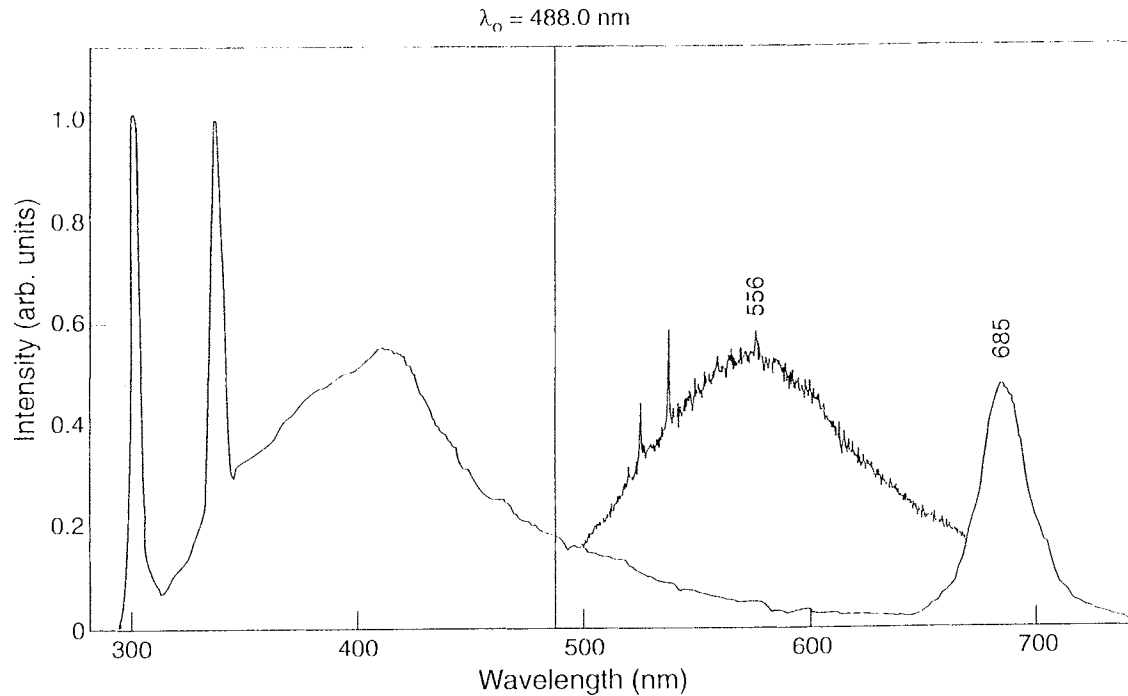


Figure 5. COTS eggs fluorescence spectra has been overlaid (shaded area) on the fluorescence and Raman spectra of natural water excited with an uv-laser. The peaks at 420 and 685 nm are, respectively due to dissolved organic carbon and chlorophyll-a.

more than that in beta-carotene (e.g, Merlin, 1985). It is interesting to note here that the eggs of Chinook salmon, and Mahimahi fish also contain carotenoid pigments and give rise to characteristic fluorescence when excited with the blue-green laser lines (Sharma, et al., 1995).

Fluorescence excitation and emission spectral studies of a number of carotenoids in carbon disulfide have shown that beta-carotene give rise to a broad fluorescence with maxima at 570 nm with natural radiative lifetime of 1-10 nanosec (e.g., Gillbro and Gogdell, 1989). The observed broad fluorescence bands with band maxima at the range 527-556 nm in COTS eggs can be attributed to originate from the carotenoid pigments present in the COTS eggs. As is evident from Fig. 5 the fluorescence band associated with COTS eggs do not overlap with the fluorescence normally observed in ocean water, and therefore, is easy to detect along with the fluorescence from chlorophyll-a associated with phytoplankton. Simultaneous monitoring of fluorescence of COTS eggs and phytoplankton in the field could provide valuable information for evaluating coupling of COTS spawning with phytoplankton blooms.

The fast (1-10 nanosec) emission lifetime of carotenoid pigments and the fact that the fluorescence can be excited at ≤ 535 nm are suitable characteristics of COTS eggs for airborne remote sensing with a lidar using 532 nm frequency doubled Nd:YAG laser excitation such as in NASA's oceanic lidar (e.g., Hoge and Swift, 1981; Measures, 1984) and LADS (Sinclair, 1995). These systems would, however, require sensitive detectors and suitable optics for operation at fluorescence (~ 546 nm) and resonance Raman wave lengths.

CONCLUSIONS

We have detected for the first time the presence of carotenoid pigment signatures in laser-induced Raman and fluorescence spectra of COTS eggs. These results clearly indicate potential of lidar techniques for observing COTS spawning in the field. Additional work is, however, needed to characterize spectroscopic properties of COTS larvae. Future collaboration between spectroscopists, biologists and physicists could lead to development of powerful remote sensing method for monitoring COTS temporal and spatial spawning events and for evaluating coupling of COTS spawning with phytoplankton blooms.

ACKNOWLEDGMENTS

The idea of investigating spectroscopic properties of COTS eggs was originated during discussions with Dr. David Cartwright, at PACON '94 Meeting in Townsville, Australia. We would like to thank Dr. Cartwright for his interest and for making this collaboration possible. One of us (TA) would like to thank Miss Carina Cartwright for her assistance and Great Barrier Reef Marine Park Authority for funding. This is School of Ocean and Earth Science and Technology (SOEST) contribution no. 4188, and HIGP contribution no. 929.

REFERENCES

- Babcock, R. C. and C. N. Mundy. 1992. Reproductive biology, spawning and field fertilization rates of *Acanthaster planci*. *Aust. J. Mar. Freshwater Res.* 43: 525-534.
- Babcock, R. C., C. N. Mundy, J. K. Keesing and J. Oliver. 1992. Predictable and unpredictable spawning events: *in situ* behavioural data from free-spawning coral reef invertebrates. *Invertebrate Reproduction and Development* 22: 213-228.
- Beach, D. H., N. J. Hanscomb and R. F. G. Ormond. 1975. Spawning pheromone in crown-of-thorns starfish. *Nature* 254: 135-136.
- Birkeland, C. and J. S. Lucas. 1990. *Acanthaster planci*: major management problem of coral reefs. CRC Press, Boca Raton, 257.
- Black, K. P. and Moran P. J. 1991. Influence of hydrodynamics on the passive dispersal and initial recruitment of larvae of *Acanthaster planci* (Echinodermata: Asteroidea) on the Great Barrier Reef. *Mar. Ecol. Prog. Ser.* 69: 55-65.
- Brodie, J.E. 1992. Enhancement of larval and juvenile survival and recruitment in *Acanthaster planci* from the effects of terrestrial runoff: a review. *Aust. J. Mar. Freshwater Res.*, 43: 539-554.
- Clark, R. J. H., N. R. D'Urso and P. F. Zagalsky. 1980. Excitation profiles, absorption and resonance Raman spectra of carotenoid protein octorubin, and a resonance Raman study of some other astaxanthin proteins. *J. Am. Chem. Soc.* 102, 6693-6698.
- Conand, C. 1985. Distribution, reproductive cycle and morphometric relationships of *Acanthaster planci* (Echinodermata: Asteroidea) in New Caledonia, western tropical Pacific. Proc. 5th Intl. Echin. Conf., Balkema, Rotterdam, 499-506.
- Dight, I. J., L. Bode and M. K. James. 1990a. Modelling the larval dispersal of *Acanthaster planci*: I. Large scale hydrodynamics, Cairns Section, Great Barrier Reef Marine Park. *Coral Reefs* 9: 115-123.
- Dight, I. J., L. Bode and M.K. James. 1990b. Modelling the larval dispersal of *Acanthaster planci*: II. Patterns of reef connectivity. *Coral Reefs* 9: 125-134.
- Gauldie, R. W., S. K. Sharma and C. E. Helsley. 1996. LIDAR applications to fisheries monitoring problem. *Canad. J. Fish. Aquat. Sci.* 53, 1459-1468.
- Gillbro, T. and R. J. Cogdell. 1989. Carotenoid fluorescence. *Chem. Phys. Lett.* 158, 312-316.

Hoge, F. E. and R. N. Swift. 1981. Airborne simultaneous spectroscopic detection of laser-induced water column back scatter and fluorescence from chlorophyll-a and other naturally occurring pigments. *Appl. Optics* **20**, 3191-3205.

Kettle, B. T. and J. S. Lucas. 1987. Biometric relationships between organ indices, fecundity, oxygen consumption and body size in *Acanthaster planci* (L.), *Bull. Mar. Sci.*, **41**: 541-551.

Lucas, J.S. 1986. The crown-of-thorns starfish. *Oceanus*, **29**: 55-64.

Measures, R. M. 1984. Laser remote sensing. Wiley-Intersci. Publications, New York, pp. 510.

Merlin, J. C. 1985. Resonance Raman spectroscopy of carotenoids and carotenoid containing system. *Pure and Appl. Chem.* **67**, 785-792.

Merlin, J. C. and M. L. Dele-Dubois. 1986. Resonance Raman characterization of polyacetylenic pigments in the calcareous skeleton. *Comp. Biochem. Physiol.* **84B**: 97-103.

Minchin, D. 1987. Seawater temperature and spawning behaviour in the seastar *Marhasterias glacialis*. *Mar. Biol.*, **95**: 139-143.

Rimai, L., M. E. Heyde and D. Gill. 1973. Vibrational spectra of some carotenoids and related linear polyenes. A Raman spectral study. *J. Am. Chem. Soc.* **95**, 4493-4501.

Sharma, S. K., R. W. Gauldie, C. E. Helsley and C. Schoen. 1995. Laser-induced Raman spectra and fluorescence in fish eggs. In O. Bellwood, H. Choat and N. Saxena (eds.). Recent advances in Marine Science and Technology '94, PACON Int. and James Cook Univ. of North Queensland, Australia. pp.323-331.

Sinclair, M. J. 1985. Laser airborne depth sounder. In O. Bellwood, H. Choat and N. Saxena (eds.). Recent advances in Marine Science and Technology '94, PACON Int. and James Cook Univ. of North Queensland, Australia. pp.345-349.

Starr, M., Himmelman, J.H., Therriault, J.C. 1990. Direct coupling of marine invertebrate spawning with phytoplankton blooms. *Science*, **247**: 1071-1074.

Starr, M., Himmelman, J.H., Therriault, J.C. 1993. Environmental control of green sea urchin, *Strongylocentrotus droebachiensis*, spawning in the St. Lawrence estuary. *Can. J. Fish. Aquat. Sci.*, **50**: 894-901.

Urmos, J., S. K. Sharma and F. T. Mackenzie. 1991. Characterization of some biogenic carbonates with Raman spectroscopy. *Amer. Min.* **76**, 641-646.

THE ANOMALY IN TROPICAL PACIFIC AND ITS EFFECT ON EL NINO

Sun Jilin¹, Liu Qinyu¹, and Zhu Baozhen²

¹Ocean University of Qingdao
Qingdao, China

²Institute of Atmospheric Physics
Beijing, China

ABSTRACT

The oceanic stationary anomalies in the Tropical Pacific were found both in observational results and in numerical tropical ocean model studies. They appeared as a prelude of the development of the El Nino events. Model studies showed that the formation of the stationary waves in the tropical ocean have some thing to do with the Doppler effect made by the westward moving equatorial current on the second baroclinic Kelvin mode. The stationary phenomenon is also involved with the phase speed of the second baroclinic Kelvin wave: the reduction of upper layer depth and nonlinearity also favors the standing of such waves. When the stationary wave formed, the upper layer temperature was much influenced. Experiment also showed that the stationary waves could be generated by a westerly bursts at intraseasonal time scales on the Western Equatorial Pacific. Some possible mechanisms are presented to explain the relation between the oceanic stationary wave and the onset of the El Nino event.

INTRODUCTION

Much progresses have been made in the ENSO(El Nino/Southern Oscillation) dynamical studies. Theories and hypotheses were presented and used to explain the development and quasi-circle of the ENSO event(e.g.Hirst,1986; Battisti, 1988). Typical ENSO events summarized by Rasmuson and Carpenter (1982) were well simulated in some air-sea coupled models (e.g. Zebiak and Cane,1987). The feature of this kind of El Nino occurred in the coupled model such as the westward moving of positive SST anomaly and also the anomalous westerly responding to SST anomaly migration. Yet there are still some problems which need to be solved. For example, since the 1982 - 1983, El Nino event it always appears that a positive SST anomaly moves eastward from west of the Pacific basin to the east and, up to now, no satisfactory explanations have been given . Philander et al(1985) better simulated the 1982-1983 El Nino event with an ocean GCM forced by observed wind field, and their simulations gave the impression that the El Nino was a forced event but no exact physical processes were given. Fig.1 is an observed results from "Climate Diagnostics Bulletin ". It can be seen from Fig. 1 that the El Nino event which happened recently also had the same features with a positive SST anomaly moving eastward. That is, the anomaly first occurred at the central Equatorial Pacific, then spread eastward(Fig. 1a) Corresponding to the central Pacific warming, a much wider westerly anomaly overlies the

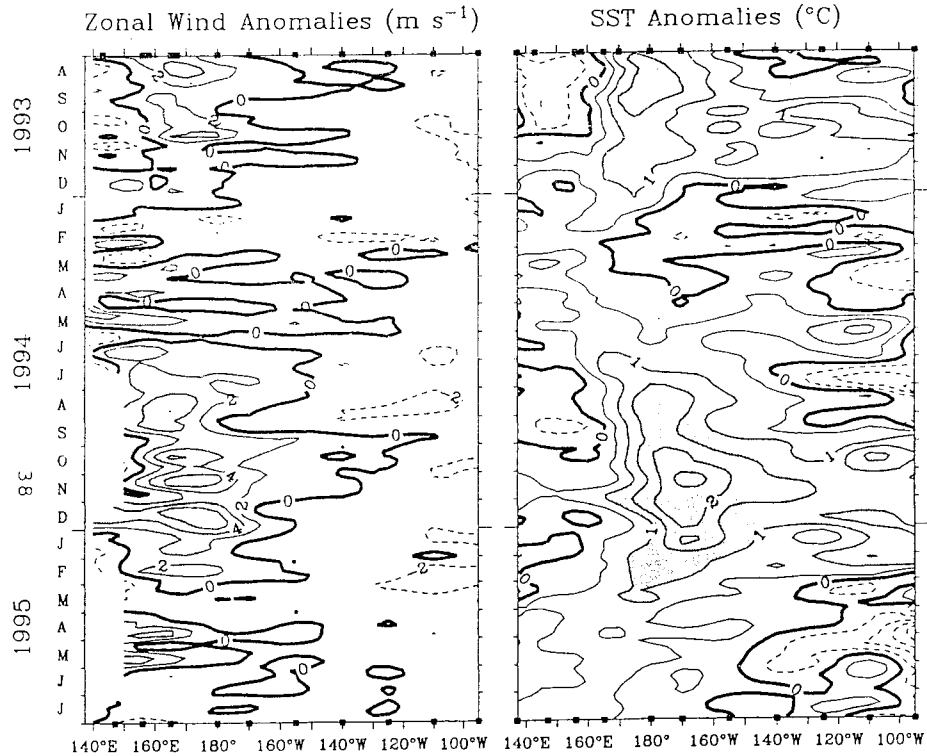


Fig.1 Time/longitude section of anomalies in surface zonal winds (in $m s^{-1}$), sea surface temperature (in $^{\circ}C$) for the past two years. Analysis is based on 5-day averages between $2^{\circ}N - 2^{\circ}S$ of moored data from the TAO Array (from Climate Diagnostics Bulletin)

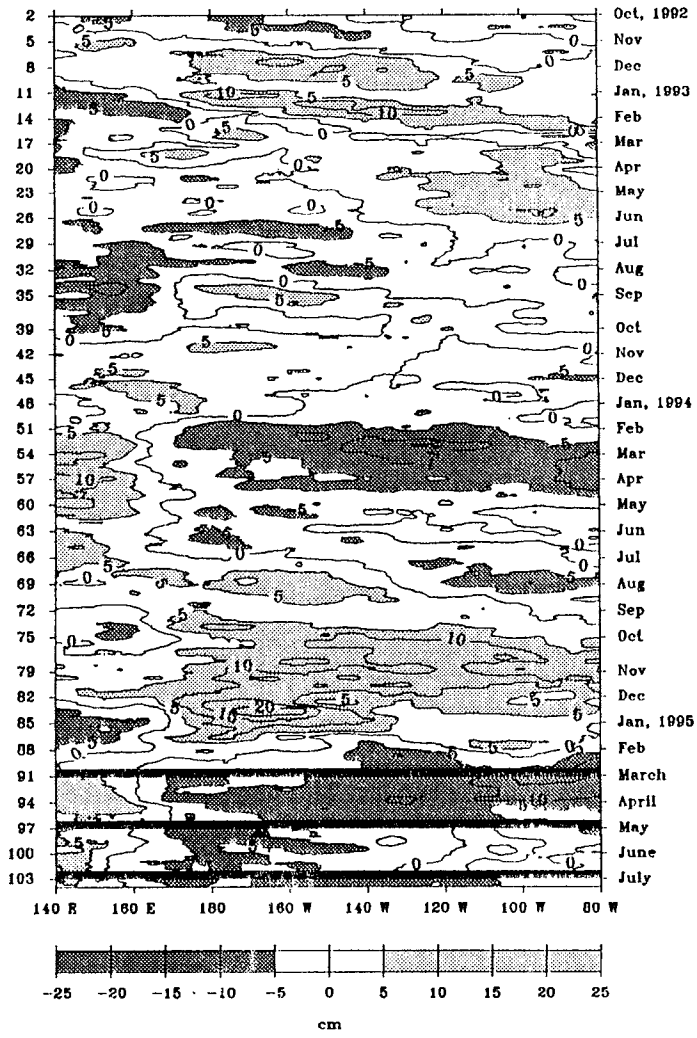


Fig.2 Time/longitude sections of 10-day averaged sea level (2°N - 2°S) observed by TOPEX/POSEIDON(TP) (from Climate Diagnostics Bulletin)

whole western Pacific(Fig. 1b). The time scale for the westerly anomaly was intraseasonal. Lau(1986) guessed that the intraseasonal time scale oscillations in the tropical atmosphere might be a trigger factor in the occurrence of an El Nino event. 10 years have passed since his presentation, yet the mechanisms of the connections between the atmospheric intraseasonal oscillation and the happening of the El Nino event are still not revealed. In this paper, by using a two and half layer tropical ocean model, we tested how the stationary waves formed and, with the assumption of stationary waves existence, we present mechanisms to illustrate how intraseasonal time scale atmospheric oscillations affect the development of the El Nino event. Problems are also discussed from the proposed air-sea interaction mechanisms.

STATIONARY ANOMALIES IN OBSERVATION AND WAVES IN THE OCEANIC MODEL EXPERIMENT

Fig. 2 gives the sea level anomaly along the equator from Oct. 1992 to July 1995(also from "Climate Diagnostics Bulletin").

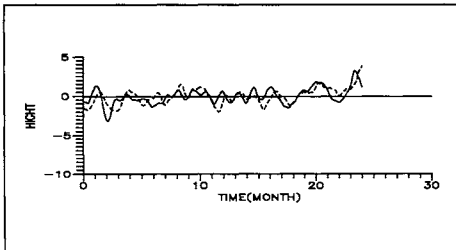


Fig. 3a Band-filtered sea level deviations at Tarawa (solid; 1°N, 173°E) and Christmas (dashed; 2°N, 157°W) from Jan., 1985 to Dec., 1986

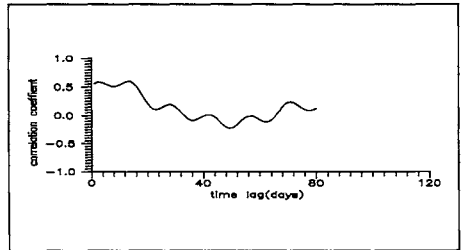


Fig. 3b Correlation coefficients between Tarawa (1°N, 173°E) and Christmas (2°N, 157°W)

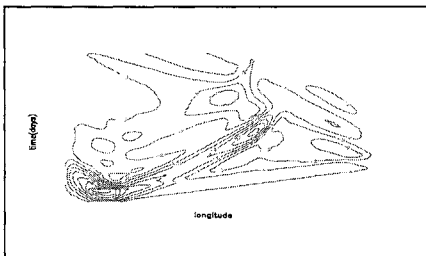


Fig.4a Time-longitude cross section of anomalous zonal current forced by an anomalous westerly (at zonal grid 10-19 and meridional grid 14-19) added on the initial ideal patch of wind field for 25 days (interval 6cm/s)

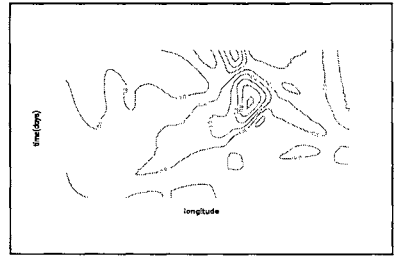


Fig.4b Time-longitude cross section of anomalous upper layer temperature forced by anomalous westerly (grid 10-19 and 14-19) added on the initial patch of wind field for 25 days (interval 0.2°C)

A pronounced feature in Fig.2 is the nearly stationary sea level anomaly in the central Equatorial Pacific just before the two El Nino events (the 1993 and 1994 El Nino event). Comparing Fig.2 with Fig. 1 , it can be easily found that, in the region of stationary positive sea level anomaly in 1994, a positive SST anomaly existed. Thus the stationary waves(if we regard it as a wave) have characteristics of a warm temperature anomaly. To illustrate the phenomenon in Fig 2 further, we analyse the data in Fig. 3. The time series in Fig. 3a gives band filtered (15 - 150 day band pass filter) sea level deviations and Fig. 3b gives their correlation results from Jan. 1985 to Dec.1986 at two islands in the central tropical Pacific. It can be seen from Fig.3a that during the next half year of 1986, sea level amplitude at the two islands became larger and oscillated nearly simultaneously. Since the distance between the two islands is over 3000 Km, we may regard the waves as standing if the sea level variations were caused by waves. In order to explain such phenomenon mentioned above, some numerical experiment are given in Fig.4 which gives the experimented result from a two and half layer oceanic model beginning from a nearly equilibrium state of the model ocean.

The model used in this paper was initially created by McCreary and Yu(1992) with some modifications. In producing the nearly equilibrium state, the model was first driven by a meridional uniform westward wind field (McCreary & Yu 1992) with maximum stress at N 61 (the grid in the experiment is 1*1 degree both in zonal and meridional directions) for 1080 days. Then the anomalous fields were calculated by a westerly anomaly wind patch being added to the region from grid 10 to 19 in a zonal direction and from grid 14 to 19 in a meridional direction across the equator for 25 days. The most pronounced feature in Fig. 4 is the stationary waves in the central and east part of the model basin. There are two signals propagating from the west to the east in the baroclinic basin. Since the model contains only two baroclinic modes, we call them the first baroclinic Kelvin mode and the second baroclinic mode corresponding to the faster traveling and slower traveling signals in the model, respectively. By examining the model experiment we found that the stationary waves in the model results also have the characteristics of a positive upper layer depth anomaly corresponding to the positive temperature anomaly. So the characteristics in Fig.2, Fig. 3 and Fig.4 are similar. Why do stationary waves exist prior to the happening of El Nino event? How were the stationary waves formed? What connected the stationary waves and the El Nino development? To answer these questions we need further experiment as explained in the late sections of this paper.

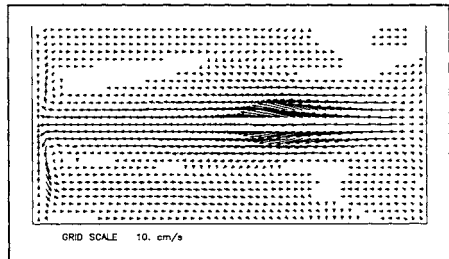


Fig.5a The upper layer current at model day 1080 forced by an ideal patch of wind

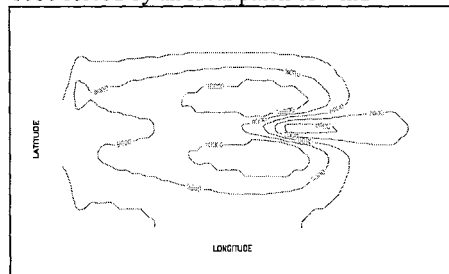
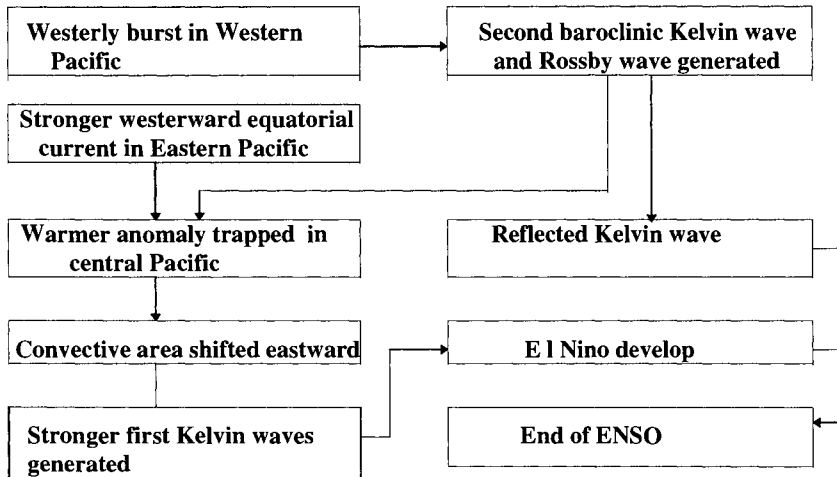


Fig.5b The upper layer depth at model day 1080 forced by an ideal patch of wind

THE REASON FOR THE SECOND BAROCLINIC KELVIN WAVE STANDING AND SOME MECHANISMS PRESENTED IN ILLUSTRATING THE AIR - SEA INTERACTION

Fig.5 gives the calculated upper layer currents and depth at model day 1080 integrated from a calm ocean. It can be seen that corresponding to the maximum westward wind stress, the strongest westward current is also located at the same longitude in the upper layer(Fig. 5a). Thus the Doppler effect may be the most important factor in affecting the standing of the second baroclinic Kelvin wave mode. Fig.6 shows an some other numerical experiment forced by the same westerly anomaly on a initially motionless model ocean. The phase speed of the eastward propagating mode is faster in the deep upper layer depth case than in the shallow upper layer case(Fig.6a, 6b). It took 30 to 40 days less to reach the eastern boundary in the deep case(100m) compared to the shallow case(50m). Nonlinearity also took effect on the propagation of the Kelvin wave. Waves in the linear model travel faster than in the nonlinear model(Fig.6c, 6d). Since the Kelvin wave phase speed has close relations with layer depth, when the second baroclinic wave propagated to the region with shallow depth, its phase speed must be reduced. The distribution of upper layer depth in the model equilibrium state(Fig.5b) has characters that minimum value at grid around 60 along the equator. Combining the features discussed above, the contributions to the second baroclinic Kelvin wave standing are the Doppler effect, the reduced upper layer depth and the nonlinear effects.

A schematic diagram to illustrate how the intraseasonal westerly bursts affect the El Nino event is presented:



First, with the westerly burst in the Western Tropical Pacific(stage 1), two kinds of Kelvin waves are generated. As they propagate eastward, the second baroclinic Kelvin wave becomes stationary with a moderately stronger westward current existing in the equatorial upper layer of the east part of the Pacific Ocean. The stationary waves in the central Pacific with positive SST

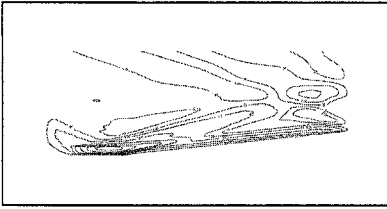


Fig. 6a Time-longitude cross section of upper layer zonal current at equator by 25 days westerly burst ($H_1=50\text{m}$, $H_2=150\text{m}$)

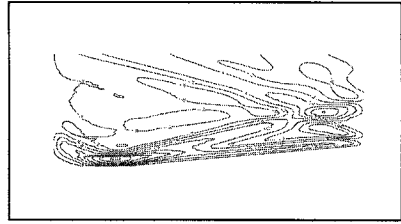


Fig. 6b As in Fig. 6a but $H_1=100\text{m}$, $H_2=200\text{m}$

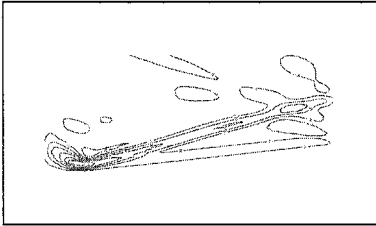


Fig. 6c As in Fig. 6a but $H_1=75\text{m}$, $H_2=175\text{m}$

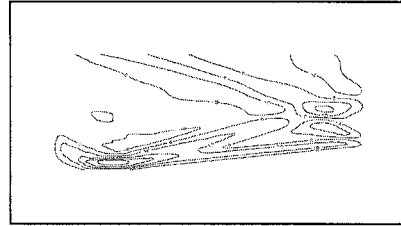


Fig. 6d As in Fig 6c but for the linear case

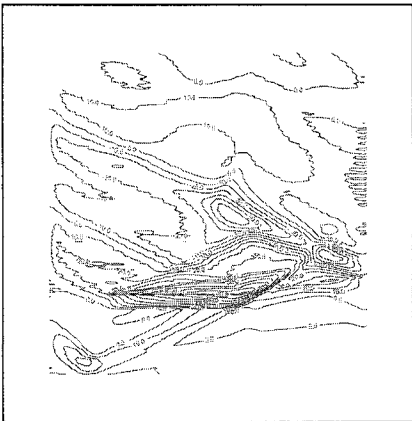


Fig. 7a Time-longitude cross section of anomalous zonal current response to two time anomalous westerly forced at model day 1080 and 1190 for 25 days respectively (interval 10 cm/s)

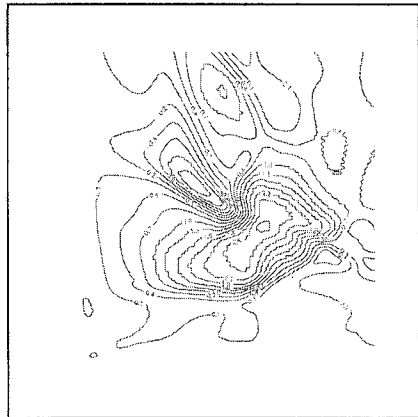


Fig. 7b Time-longitude cross section of anomalous upper layer temperature response to twice anomalous westerly wind added on the ideal patch of wind for 25 days respectively (interval 0.3°C)

anomaly will enhance the convective movement in the atmosphere and the westerly anomaly will prevail to the west of regions that stationary waves occupy(stage 2). If this happens, the westerly anomaly with wider area will generate stronger first Kelvin wave(Fig. 7), the anomalous westerly wind (from grid 10 to 16 and from 14 to 19) will be added to the ideal patch of wind field for 25 days from model day 1080 for the first time. Another anomalous westerly wind (from grid 22 to 45 and 14 to 19) will be added to the ideal patch of wind field for 25 days from model day 1190 for the second time, respectively), and the first baroclinic Kelvin wave will raise the temperature of the east part of the Equatorial Pacific upper layer, and produce an El Nino(stage 3).

From Fig. 7a, the amplitudes of the two kinds of Kelvin waves rely on the area of wind patch

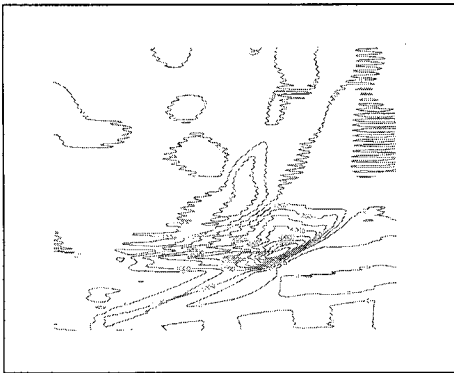


Fig. 7c Time-longitude cross section of anomalous upper layer depth response to twice anomalous westerly wind added on the ideal patch of wind for 25 days respectively (interval 10m)

which can be clearly seen. A wider area of westerly anomaly generates the first Kelvin wave more effectively than a less wide westerly anomaly. This may be the reason why intraseasonal oscillations in tropical atmosphere are more frequent and El Nino event happen irregularly. It can be seen from Fig.7b that for two of the anomalous westerly bursts, the migration of positive SST anomaly was from west to the east in the model ocean. Thus our work in this paper can provide a reasonable explanation for the kind of El Nino event with a positive SST anomaly spreading from west to the east in the tropical Pacific Ocean. Comparing Fig. 7c with the diagnostic result in Fig. 7d, the roles of the two baroclinic Kelvin waves in the formation of El Nino events may cautiously give support to the mechanism we present.

CONCLUSIONS AND DISCUSSION

Some tentative conclusions may be made primarily from the discussion in the previous parts of this paper:

1. since the westerly anomaly forced the model ocean with a time scale half the intraseasonal oscillations of atmosphere, Lau's ideas in the 1980s, that intraseasonal atmospheric oscillation might be one triggering factor of El Nino events is possibly true;
2. the location of stationary waves in the central Pacific before an El Nino happening may be the key factor for the development of El Nino events with a positive SST anomaly moved from west to the east.

Further problems in ENSO dynamical studies may need to be resolved if our staged mechanism of ENSO is true. First, how is the intermittent feature of air-sea interaction in the coupled air-sea models concludes? Second, the ENSO event and the intraseasonal atmospheric oscillation have different time scales. The mechanisms we presented in this paper are actually interactions between systems of tropical ocean and atmosphere with different time scale characteristics. How do the details of interaction between these systems operate? To answer these questions much more work needs to be done. To some extent our work presented here is preliminary and needs to be taken further.

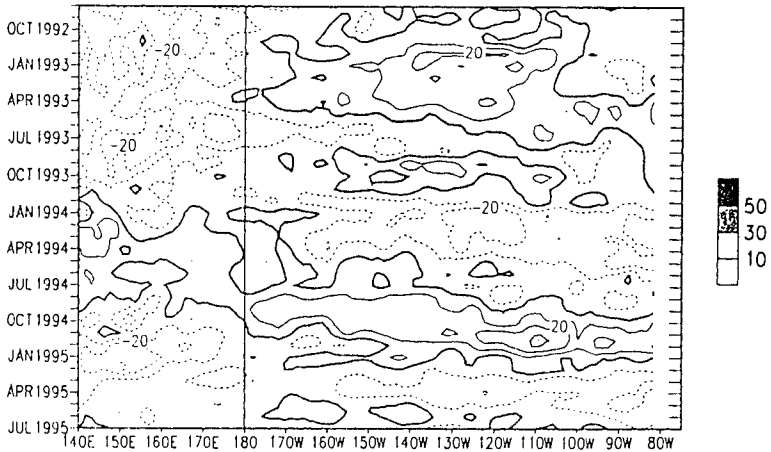


Figure 7d Time/longitude sections of anomalous depth of the 20° C isotherm for 5 N - 5S in the Pacific Ocean (U.S. National Meteorological Center).

ACKNOWLEDGMENTS

This project is supported by the National Natural Scientific Foundation of China (49376258).

REFERENCES

- Battisti, D. S. 1988. The dynamics and thermodynamics of a warming event in a coupled tropical atmosphere-ocean model. *J. Atmos. Sci.* **45**:2899-2919.
- Hirst, A. C. 1986. Unstable and damped equatorial modes in simple coupled ocean-atmosphere models. *J. Atmos. Sci.* **43**:606-630.
- Lau, K.M. and Chan, P.H. 1986, The 40 - 50 day oscillation and the El Nino Southern Oscillation. *Bull. Am.Meteorol. Soc.* **67**:533-534.

McCreary J.P. and Yu Z. 1992, Equatorial dynamics in a $2^{1/2}$ layer model. *Prog. Oceanogr.* **29**:61 - 132

National Meteorological Center of U.S. Climate Diagnostics Bulletin. 1995

Philander, S. G. H. 1990 El Nino, La Nina and the Southern Oscillation. Academic Press.

Rasmusson, E. M. and Carpenter, T. H. 1982. Variations in tropical sea surface temperature and surface wind field associated with the Southern Oscillation/El Nino. *Mon. Wea. Rev.* **110**:354-384.

Zebiak S. E. and Cane M. A. 1987. A model ENSO/Southern Oscillation. *Mon. Wea. Rev.* **115**:2262-2278.

CORAL REEF ISLANDS - IMPLICATIONS OF MORE MODEST GLOBAL CHANGE PREDICTIONS

David Hopley
James Cook University of North Queensland
Townsville, Australia

ABSTRACT

Over the last ten years global climate change has gained prominence with maximum impact identified in small low lying coral island states, such as the Maldives and Kiribati associated with sea-level rise. Early concerns may have been alarmist as researchers with no experience of coral reefs, simply moved shorelines upwards by anything up to 3.45 metres. Current methods now are to use either the Bruun model or fully consider the sediment budgets and processes operating on coral islands and reef-fronted beaches of high islands. Simultaneously, the estimates of change have become more moderate (a modal value of 0.5 m for sea level rise by the year 2100 is now accepted).

As the predicted ranges of change become more moderate, they have also become more precise. Coral reefs will respond both positively and negatively to the predicted changes. However, the more conservative prediction for a rise in sea-level may mean that some of the positive changes will be less certain as the ecological response of reefs to the slower rise will be different.

The positive responses of reefs and adjacent shorelines, assumes that coral reefs remain healthy. Unfortunately climate change is only one of many factors currently impacting on coral reefs. Strategies which address all environmental problems of the coast and near shore areas will ultimately go a long way to overcoming the pressures related specifically to global climate change.

INTRODUCTION

Previous work by this author and colleagues (Hopley and Kinsey, 1988; Kinsey and Hopley, 1991) has suggested that coral reefs may be one of the few coastal-marine ecosystems which benefit from the range of environmental changes predicted as part of the Greenhouse scenario over the next 100 years. It was hypothesised that rising sea-levels may initially inundate reef-flats dominated by sediments which have evolved over a long period of relatively stable sea-level of approximately 6,000 years. Indeed, at least some reef flats have achieved their present elevation and morphology as the result of a c.1m falling sea-level since the mid-Holocene (Hopley, 1987). As sea-level rises over these old, high reef flats which characterise Pacific reefs, it was predicted that renewed coral growth would take place and reef flats would become aesthetically more pleasing and more productive of calcium carbonate. This was the response until about 2100, beyond which reefs may start to lag behind the sea-level rise and slowly drown.

Contrary to many reports (see summary, Hopley, 1993) it is also predicted that the impact of sea-level rise on reef islands also may not be as drastic as originally considered. A rising sea-level would initially create deeper water over the reef flat and inundation over a longer portion of each tidal cycle. Thus sediment accumulated over 6,000 years on these reef flats would be moved more efficiently towards reef islands. Changes to wave form may occur to produce an increase in height of the beach berm, even greater than the rise in sea-level. (Gourlay and Hacker, 1991). In addition, as the water deepens, reef flats would change from sediment cover to living coral cover, to significantly increase the productivity of calcium carbonate, at least a proportion of which would be transported by waves towards reef islands.

Similar conclusions were reached for atoll motus for which similar processes would operate. The greater incidence of tropical storms as predicted within the Greenhouse scenario, may also benefit motus, increases in island size being associated with greater frequency of storms in the past, (Bayliss-Smith, 1988).

These predictions were based on the best available estimates of environmental, particularly sea-level, changes. Subsequently intense work has focused on improving these predictions and the latest to come from the Inter-governmental Panel on Climate Change (1996), though much more certain, are of much smaller magnitude than incorporated into these predictions for coral reef islands. This paper examines the implications of these more modest predictions for coral reefs over the next 100 years or so.

CHANGES TO PREDICTIONS OF GLOBAL CHANGE

The reef responses as described above (Hopley and Kinsey, 1988) were based on the best available predictions of global environmental change in the 1980's (Table 1). The best estimate of sea level rise was 1.8m by 2100. By 1990 this estimate of sea-level rise had been reduced to 31-110cm with a mid-point 0.66m (IPCC, 1990). The revised estimates of the Intergovernmental Panel on Climatic Change (1996) reduced the range to 25-80cm with a best estimate of only 50cm sea-level rise by 2100. Thus over an approximate ten year period the rate of sea-level rise predicted was reduced from approximately 15mm a year to less than 5mm a year during the next century. These new estimates require a revision of the responses of coral reefs, particularly as the new estimates of sea-level rise no longer exceed the threshold beyond which coral reefs are able to keep up with rising water level. Both geological records from coring data (eg. Davies and Hopley, 1983) and calcification rates best based on metabolic data (Kinsey, 1985) indicate that reefs can maintain upward growth rates of up to 8mm per year, and a calcification rate of $10\text{kg m}^{-2}\text{yr}^{-1}$.

With an average rate of sea-level rise of approximately 4.8mm a year now predicted, including an even slower rate during the early part of the century, coral reefs need to be re-examined to see if the ecological changes previously forecast are still feasible and in particular if the changes which were described as beneficial to reef islands will still take place. As atoll islands (motus) have been described as being one of the most susceptible coastal environments of all to sea-level rise (Falk and Brownlow, 1989), this paper models the response of atoll reef flats and adjacent islands

Table 1. Changes to estimates in global climate change by year 2100

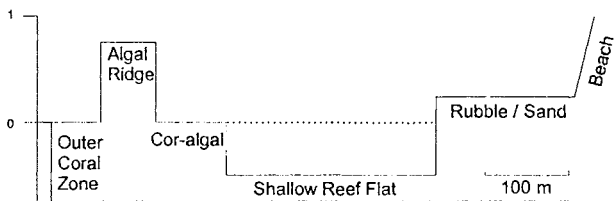
	1980s (Variety of Sources)	1995 (IPCC, 1996)
Global T° (c)	2.3 - 7.0	1.0 - 4.0
Sea-level (m)	1.80	0.50
Best estimate range	0.56 - 3.45	0.25 - 0.75
Cyclones / Typhoons	30% - 60% intensity	Debatable - no consensus
Ozone	Debatable - no agreement	1.1% to 10.6% Depletion

to both the higher and more recent lower estimates of sea-level rise. However, it is stressed that this is a notional model and uses only the IPCC estimate of *global* sea-level rise. Actual behaviour of local sea-level at any specific site will depend as much on local tectonic and isostatic factors which in some locations may dominate over the Greenhouse rise. (For review of these factors in relation to the Pacific see Hopley, 1987)

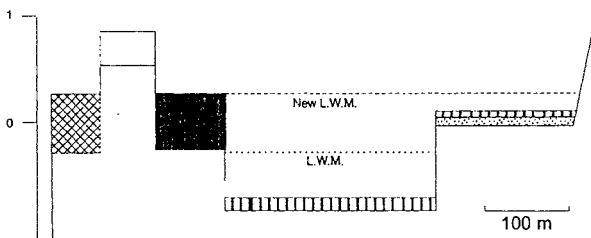
THE NOTIONAL ATOLL REEF FLAT (Figure 1)

The starting point for this exercise is the typical reef flat of Pacific atolls, which has formed in response to a sea-level which achieved its modern position as much as 6,000 years ago (Hopley, 1987). Such a reef flat has grown to its maximum possible elevation which in some examples may have been further heightened by a c.1m fall in relative sea-level in the intervening period. Production of calcium carbonate over such a reef flat is far from the optimum $10\text{kg m}^{-2}\text{yr}^{-1}$ and much of what there is, is converted into sediment and moved laterally across the reef. Maximum productivity is limited to the outer slope of the reef from which periodically during high energy events produced by tropical cyclones and hurricanes, there is a major transport of material to the reef flat. Reef boulders remain close to the reef edge but even relatively large material can be swept leewards to form significant shingle banks which contribute to motu development (Maragos *et al.*, 1973). At other times normal wave action is limited due to tidal exposure and is insufficient to significantly move either the sediment originating from the reef front or the smaller amounts produced by organisms of the reef flat.

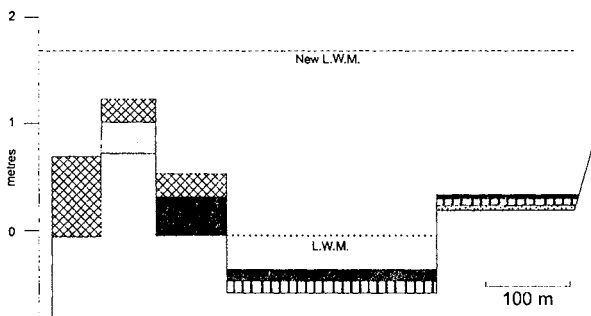
Characteristic zonations are found on most Pacific and Indian Ocean atoll windward margins. For modelling purposes the detailed descriptions of Emery *et al* (1954) of Bikini and nearby atolls have been used to obtain both typical zonation and heights and widths of these zones. Table 2 summarises the data of a synthesised transect to which have been added the rates of present calcium carbonate productivity based on Kinsey (1985). This morphology and zonation is used as the starting point for predictions over the next 100 years.



1. Notional Atoll Reef Flat



2. Change in Response to Sea Level Rise of 0.5 m



3. Change in Response to Sea Level Rise of 1.8 m



Figure 1. Response of notional atoll reef flat to rises of sea level of 0.5m and 1.8m in next 100 years

Table 2. CaCO₃ Productivity changes in an atoll reef flat

Zone	Nominal Width (m)	Nominal Height (m) in relation to L.W.M.	Present Productivity Kg m ⁻² yr ⁻¹	Equivalent Upward Growth rate mm yr ⁻¹	Present Production Kg Ca CO ₃ yr ⁻¹ m wide transect	Production 1.8m SL rise by 2100	Production 0.5m SL rise by 2100
Outer Coral	65	0	10	7	650	650	650
Algal ridge	80	+0.75	4	3	320	800	320
Coral-algal zone	100	0	5	3.5	500	1000	500 perhaps less
Shallow reef flat	300	-0.5	1.5	1	450	1500	450
Rubble / sanded reef flat	200	+0.25	0.5	0.3	100	1000	300
Total	770				2020	4950	2220

REEF RESPONSE TO A 1.8m SEA-LEVEL RISE BY 2100

Figures 1 and 2 show the modelled response to a sea-level rise of 1.8m by the year 2100, an average inundation rate of approximately 15mm per year. In each zone the response is as follows:

- Living coral zone**

This continues as a coral zone, growing upwards at maximum of 7mm per year but lagging behind the rise in sea-level. By 2100 this zone is approximately 1m below Low Water Mark (L.W.M.). (n.b. no further refinement of L.W.M. is attempted here as the relationship to the upper limit of reef growth varies with tidal range, but on the notional atoll reef flat it is approximately Low Water Spring tides).
- Algal ridge**

Because of its height the algal ridge remains above LWM until approximately the year 2070, at this point it becomes permanently inundated and it is predicted that change from an algal to a coral cover will take place. The change in upward growth rate will be from 3mm a year up to 2070, up to 7mm a year by the end of the century, at which time the algal ridge will be approximately 0.5m below LWM.

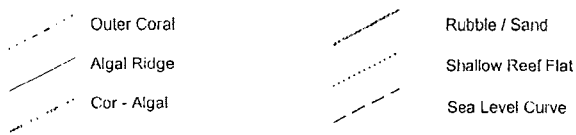
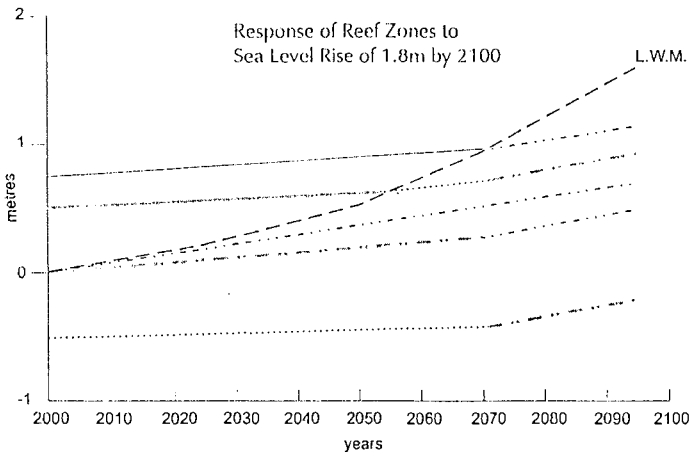
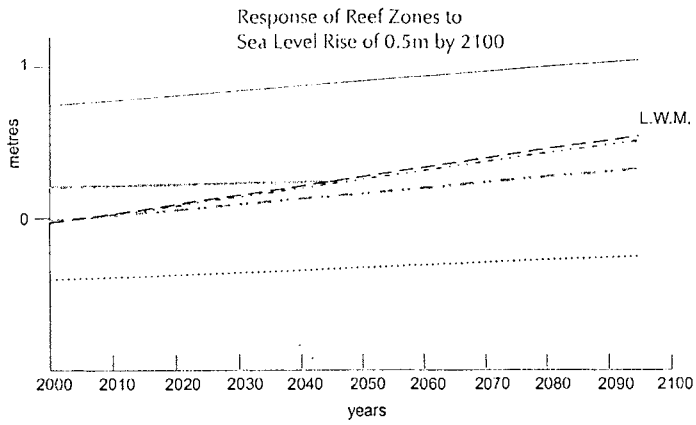


Figure 2. Upward growth rates of reef zones in response to a sea level rise of 0.5m and 1.8m in next 100 years

- **Coral-algal zone**

Coral algal zone will continue to grow upwards at approximately 3.5mm a year until 2070. It is then suggested that as the algal ridge which currently protects this zone is inundated permanently, this zone will change to a full coral cover with maximum $10\text{kg m}^{-2}\text{ yr}^{-1}$ productivity. By the end of the century it will be 1.2m below LWM.

- **Shallow reef flat**

The shallow reef flat will continue to grow upwards at only 1mm a year until 2070, by which time it is suggested there will be an upward change in productivity, perhaps equivalent to the present coral-algal zone. Initially only 0.5m below LWM, by the end of the century this zone could be as much as 1.8m below LWM. However, it is also likely that this is the zone which will receive much of the sediment transported across the reef.

- **The innermost rubble and sanded reef flat zone**

This zone has lowest productivity and the slowest vertical accretion rate. Although 0.25m above LWM rising sea-level will inundate the zone before 2030, transforming the ecology into a zone similar to the present shallow reef flat with a productivity of $1.5\text{kg m}^{-2}\text{ yr}^{-1}$ and an upward growth rate increasing to 1mm yr^{-1} . With inundation of the algal rim below LWM about 2070, it is suggested that this zone may further increase its productivity to that approaching the present coral-algal zone by the end of the century by which time the zone will be almost 1.5m below LWM.

REEF RESPONSE TO AN 0.5m SEA-LEVEL RISE BY 2100

Figures 1 and 2 also show the model response to a sea-level rise of 0.5m by the year 2100, an average inundation rate of approximately 4.8mm per year. In this instance only one zone changes its ecology during the century. The inner rubble and sand zone is inundated by approximately mid century, changing a low productivity of $0.5\text{kg m}^{-2}\text{ yr}^{-1}$ to rates similar to the shallow reef flat ($1.5\text{kg m}^{-2}\text{ yr}^{-1}$). All other zones remain the same in response to the rising sea-level, indeed, the outer living coral zone has the potential to grow more rapidly than the rising sea-level and will be constrained, particularly in the early part of the century by the rate of rise. All other zones have a rate of upward growth less than the overall rate of sea-level rise. By the end of the century their elevation will be slightly different to that of the starting point, though not significantly.

IMPLICATIONS FOR CORAL REEFS AND ISLANDS

The modelled response of the reef flats to sea-level rise clearly supports the earlier contention of a positive response with renewed coral growth if the rise exceeds the rate at which the reef can grow upwards. The original reef flat zonation is slowly replaced by a near monotone of living coral veneer. For a 1m wide transect across the entire reef flat (Table 2), present productivity is estimated at $2020\text{kg CaCO}_3\text{ m}^{-2}\text{ yr}^{-1}$. By 2100 when the reef flat is entirely inundated it is estimated that this has more than doubled to approximately $4950\text{kg CaCO}_3\text{ m}^{-2}\text{ yr}^{-1}$. In addition the flat will become inundated throughout the tidal cycle, thus allowing wave action to move

loose sediment much more effectively than at the present time. At high tide larger waves will be able to move across the reef front and onto the reef flat, thus giving the conditions for the construction of a higher berm as suggested above. Although not built into the models (Figures 1 and 2) lateral movement of a proportion of the new carbonate sediments produced is presumed as:

- i) much of the new growth in the reef flat is in the form of easily broken branching corals; and
- ii) wave efficiency in transportation increases.

However, as a 7mm yr^{-1} upward growth rate is considered minimal for such assemblages (eg. see Davies and Hopley, 1983), even 25% loss of material from the outer reef flat will possibly not alter the predicted elevation, though infilling of the shallow reef flat may be more significant.

A very different result is produced by a sea-level rise of only 0.5m by 2100. The zonation remains almost exactly the same as present and with deeper water over the coral-algal zone, the productivity here may actually decrease, thus, cancelling out the small increase which will result from inundation of the inner, rubble, sanded reef flat. There is little change to the total productivity of the reef flat and the extra inundation by the end of century is only 15cm greater than present. This is regarded as insignificant in terms of efficiency of sediment movement.

Nonetheless, without significant amounts of new sediment entering the beach storage system, such a rise can result in significant shoreline retreat whatever recession model is used (see for example Pilkey and Davis, 1987). Because of the contrasting nature of reefal sediments compared to those of generally high latitude mainland beaches, for which models have been developed, it is superfluous to try and attempt to estimate the actual amount of erosion which could take place. Internal cementation within motus and cays may also retard the erosion rate. Nonetheless, enigmatically a smaller rise in sea-level is likely to see a greater impact on coral reef islands.

There are other chain reactions to the lower predicted sea-level rise, for example, lack of increase in island size will not see a proportionate increase in the freshwater lens if the Ghyben-Herzberg model is applied or the layered aquifer model is applied, will more of the low permeability aquifer become available for the retention of freshwater (see Hopley, 1993, for discussion).

It was further argued that a higher sea-level would help in increasing lagoon circulation, increasing biological productivity of the lagoon. Examination of the model response to a 0.5m rise in sea-level clearly shows that this is now unlikely. During the 1980s it was also suggested that there could be increased cyclone activity, both in terms of frequency of occurrence and severity. However, this too is now less certain. Whilst this may retard erosion rates in some circumstances, the island building activities associated with such storms, will also not increase.

Reduction in the estimate for temperature rise may be of some relief to coral reefs, although many believe that widespread bleaching of coral reefs, due to the expulsion of the symbiotic zooxanthellae (see Wilkinson and Buddemeier, 1994) from many areas, is due to the small

amount of global warming which has already taken place. A new factor not anticipated in the 1980s has now to be considered. Depletion of ozone in the upper atmosphere, though of greater proportional significance to high latitudes, is still taking place in the tropics and may lead to an increase in UV radiation which is particularly harmful to corals and other reef flat organisms (eg. Jokiel, 1980).

CONCLUSION

The more moderate predictions of sea-level rise during the next century, are probably good news for most of the world's coastal environments but not for many coral reefs. Because the potential for reefs to grow upwards is no longer exceeded by the predicted rate of sea-level rise, changes to the ecology of reef flats previously forecast are not likely to take place. Concomitantly, increased production of calcium carbonate on reef flats and increased efficiency of wave transport produced by deepening waters will also not take place and produce the build-up of coral island beaches as previously predicted, and at least some erosion is inevitable.

As the predicted ranges of change have become more moderate they have also become more certain and, indeed, both temperature and sea-level rise are generally accepted as already taking place. The uncertainty which in many areas retarded political response in the 1980s can now be replaced by planning processes which incorporate the more modest predictions.

Whilst the predicted reef response does little more than maintain the status quo and the future of coral reef islands again becomes dubious, the serious implications for coral reef islands would be both accelerated and aggravated were reef flats to respond even less than is suggested in this paper. The responses modelled here presume that coral reefs remain healthy. Unfortunately, climate change is only one of many factors currently impacting on coral reefs. Population growth, coastal development and resource exploitation are all impacting adversely on the coastal zone. Strategies which address all environmental problems of the coast and near-shore areas of coral reefs and islands, are still required to retard the pressures related specifically to global climate change.

ACKNOWLEDGMENT

This paper has benefited from discussions with several colleagues and especially Dr DW Kinsey whose help is gratefully acknowledged.

REFERENCES

Bayliss-Smith, T.P. (1988) The role of hurricanes in the development of reef islands, Ontong Java Atoll, Solomon Islands. *Geographical Journal*, **154**: 377-391

Davies, P.J. and Hopley, D. (1983) Growth facies and growth rates of Holocene reefs in the Great Barrier Reef. *B.M.R.J. Australian Geol. Geophys.*, **8**:237-251.

Emery, K.O., Tracey, J.I. and Ladd, H-S. (1954) Geology of Bikini and nearby atolls. *US Geological Survey Prof. Papers*, **260(A)**:1-265.

Falk, J. and Brownlow, A. (1989) *The Greenhouse Challenge: What's to be done?* Penguin Books, Ringwood, Victoria, 341 pp.

Gourlay, M.R. and Hacker, J.L.F. (1991) Raine Island coastal processes and sedimentology. Rept. CH40/91, Dept. Civil Engin., Univ. of Queensland, 68pp.

Hopley, D. (1987) Holocene sea-level changes in Australia and the Southern Pacific. In Derooy R.J.N. (ed.) *Sea Surface Studies*, Crown Helm, London, pp. 375-408.

Hopley, D. (1993) Coral reef islands in a period of global sea-level rise. In Saxena, N. (ed.) *Recent Advances in Marine Science and Technology 1992*, PACON International, Honolulu, pp. 453-462.

Hopley, D. and Kinsey, D.W. (1988) The effects of rapid short term sea-level rise on the Great Barrier Reef. In Pearman, G.I. (ed.) *Greenhouse: Planning for Climatic Change*, pp. 189-201.

Intergovernmental Panel on Climatic Change (IPCC), 1990. *The IPCC Science Assessment*, CUP, Cambridge.

Intergovernmental Panel on Climatic Change (IPCC), 1996. *Climate Change 1995. Impacts, Adaptations and Mitigation of Climate Change: Scientific-Technical Analyses*. CUP Cambridge.

Jokiel, P.L. (1980) Solar ultra-violet radiation and coral reef epifauna. *Science*, **207**:1069-1071.

Kinsey, D.W. (1985) Metabolism, calcification and carbon production: I Systems level studies. *Proceedings Fifth International Coral Reef Congress, Tahiti*, **4**:505-526.

Kinsey, D.W. and Hopley, D. (1991) The significance of coral reefs as global carbon sinks - response to Greenhouse. *Palaeogeog. Palaeoclimatol. Palaeoecol.* **89**:1-15.

Maragos, J.F., Baines, G.B.K. and Beveridge, P.J. (1973) Tropical cyclone creates a new land formation on Funafuti Atoll. *Science*, **181**:1161-1164.

Pilkey, O.H. and Davis, T.W. (1987) An analysis of coastal recession models: North Carolina coast. In Nummedal, D., Pilkey, O.H. and Skidaway, J.D. (eds.) *Sea-level fluctuation and coastal evolution*. Soc. Econ. Paleo. and Min. Spec. Publication, **41**:59-68.

Wilkinson, C.R. and Buddemeier, R.W. (1994) *Global Climatic Change and Coral Reefs: Implications for People and Reefs*. Report of the UNEP-IOC-IUCN Global Task Team, 124 pp.

LIGHT SCATTERED BY PARTICULATE MATTER IN SEA WATER: COMPUTER MODELLING AND EXPERIENCE FROM SEA TRIALS

T. Hall¹, T. Clark¹ and G. Ludbrook²

¹Defence and Evaluation Research Agency, Haslar,
Gosport, Hampshire, PO12 2AG, United Kingdom

²Defence and Evaluation Research Agency, Malvern,
Malvern, Worcs. U.K.

ABSTRACT

Light scattering by particles suspended in sea water reduces both underwater visibility and the available contrast in underwater imaging systems. However, light scattering measurements can also provide information on the nature of the particulate suspension. A theoretical means of predicting light propagation through turbid sea water is therefore of potential benefit both for underwater imaging system design and water characterisation purposes.

A PC-based computer model has been developed to calculate the inherent optical properties and the Modulation Transfer Function (MTF) of a turbid medium for mono-disperse and polydisperse spherical scattering suspensions. This was described at PACON 94. The model has since been extended to calculate the scattering from coated and uncoated aspherical particles having elliptical, cylindrical and irregular geometries. Calculations are presented which give the phase function for scattering from cylindrical particles as a function of orientation with respect to the incident beam. The calculations were designed to support both laboratory and trials measurements of particulate scattering in sea water. These results are presented.

INTRODUCTION

Suspended particles are a natural feature of the oceans. The particle distribution is affected by many of the natural processes that take place in its upper layers (photic zone, eg. BROWN 1995, JERLOV 1976). Knowledge of the size, composition and distribution of such particles is of interest to many workers. These include those studying the natural processes, those wishing to characterise bodies of water and those developing underwater imaging systems. This paper describes the use of an improved computer model of light scattering by suspended particles and our initial experience with a novel instrument designed to measure such suspensions at sea. The instrument has been described elsewhere (CLARK, 1996) It uses an array of detectors to measure forward scatter and incorporates a nephelometer which measures 90° scattering and a transmissometer. By combining this instrument with conventional sensors for CTD (Conductivity, Temperature and Depth) and optical backscatter, we are able to characterise changes in the scattering behaviour found in the sea in

some detail. The development of the instrument and the interpretation of its measurements have been helped by the use of the computer model.

COMPUTER MODELLING

The general problem of characterising a medium containing a set of particles from a set of scattering measurements (the phase function) cannot be solved. (BOHREN & HUFFMAN, 1983) However, for a given size, shape and distribution of particles we can predict the scattering properties of the system using a computer model. By comparing scattering measurements of realistic suspensions in the laboratory and during sea trials with predictions from such a computer model we can obtain a greater insight into the nature of the particles. For example, we can estimate total weight assuming a size range and composition.

The computer model we use is simply called the “Combined Model” (FAIRBANKS 1994, WOLFENDEN 1994). It combines IPHASE developed at DREV, Canada (EVANS, 1993) with a Monte Carlo simulation developed at The University of Florence (BRUSCAGLIONI, 1991). IPHASE includes calculation of the scattering from coated and uncoated aspherical particles having elliptical, cylindrical and irregular geometries. The Monte Carlo simulation was previously limited to spherical particles. An example of the results from the model studies is shown in Figure 1. This is our attempt to model a more realistic change in scattering intensity with orientation of asymmetric particles.

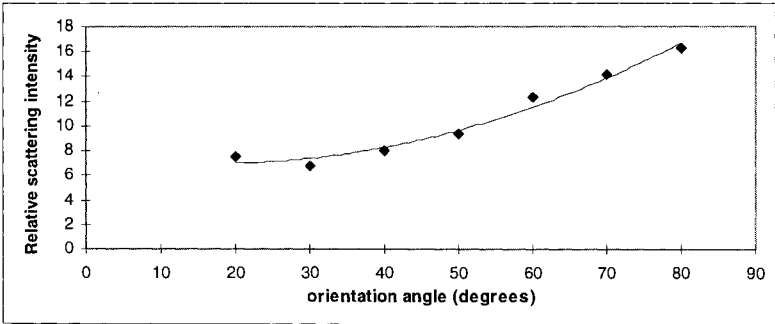


Figure 1. Example of Combined Model. Effect of the change in forward scattering as the axis of a cylindrical particle is rotated.

If there are a significant number of asymmetric particles in a body of water we predict a change in their orientation will result in a significant change in the forward scattered signal. The phase function may also change if the orientation of the particles is disturbed, for example by turbulence.

The Combined Model is subject to the usual constraints of computer modelling. Some combinations of parameters can become numerically unstable and fail to reach a solution,

especially for larger particles and complex shapes. These restrictions are detailed in the above references.

DESCRIPTION OF INSTRUMENT

The Light Scattering Device (CHELSEA INSTRUMENTS, 1996) was developed in co-operation with a commercial oceanographic instrument maker in the UK. It can be seen in Figure 2 about to be deployed. For brevity it is called LUCY.

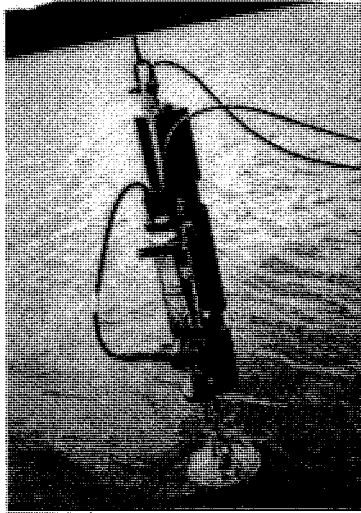


Figure 2 The Light Scattering Device, LUCY MkII (far side of support) and CTD (near side of support) and optical backscatter instrument (attached to cable in foreground) being deployed from a small fishing class vessel in coastal waters.

The instrument is pressure resistant to 100m and is light and portable enough to be used as a supplement to existing oceanographic survey instruments. It can be towed at speeds of a few knots without degradation of performance.

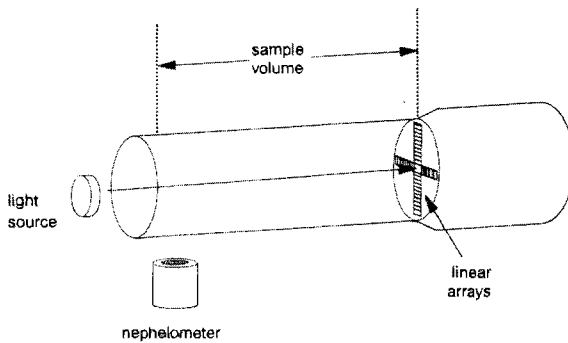


Figure 3. Schematic Diagram of LUCY's Construction.

The construction of LUCY is shown in Figure 3. In the MkII instrument, a custom made planar array of 4 by 12 elements detects forward scattered light from a cylindrical volume (250mm by 10 mm diameter). This gives the instrument a resolution of better than 1/2 a degree within a forward angle of +/- 5 degrees. At the centre of this array is an aperture which prevents interference from the non scattered beam and allows it to be monitored as in a conventional transmissometer. The light source is a red solid state laser, wavelength 670nm. It is modulated at about 30% of full output and detected using a phase sensitive detector to reduce the effects of ambient light. The output of all sensors (51 channels) is available once a second.

The design of LUCY benefited from the use of the computer model described above. We were able to confirm our assumptions about the size of the forward scattering angle. Figure 4 shows that the calculated forward scattered light is dominant for spheres greater than 5 microns in size. For asymmetric particles the calculated effect of orientation is shown in figure 5.

Iphase Sphere

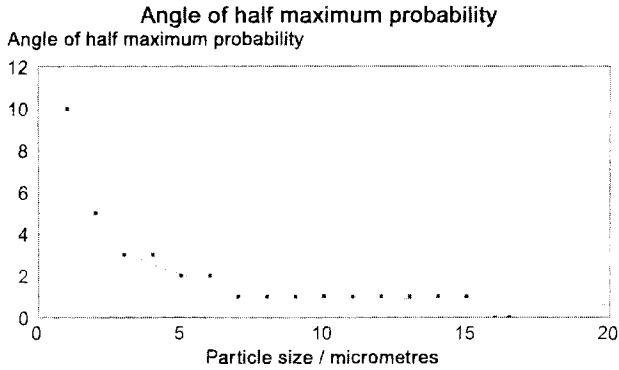


Figure 4. Model Calculation: The effect of particle size on probability of scattering angle

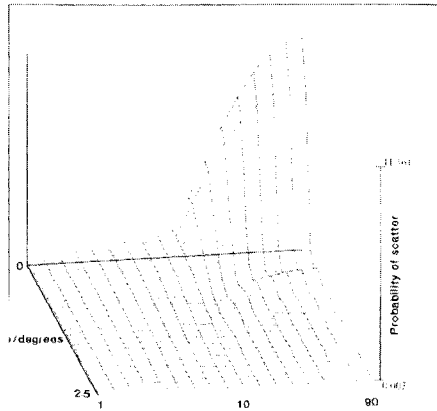


Figure 5. Computer Calculation: The effect of orientation of asymmetric particles on forward scattering angle

If such asymmetric particles play a significant role in oceanic scattering there will be a change in scattering cross section as the orientation changes.

The optics and sensors of the LUCY instrument were designed to allow use of multifrequency operation in a future version.

LABORATORY MEASUREMENTS

Making scattering standards to test the performance of an optical instrument is notoriously difficult. We have investigated the response of LUCY in the laboratory using easily available

particles such as sephadex (Aldrich Chemical Co.) and silica (Merk Ltd.) as well as polymeric size standards. The particles are assumed spherical within a range of diameters. The relative refractive index depends on the material. Figure 6 shows the output from the instrument as increasing quantities of particles were added to the sample volume.

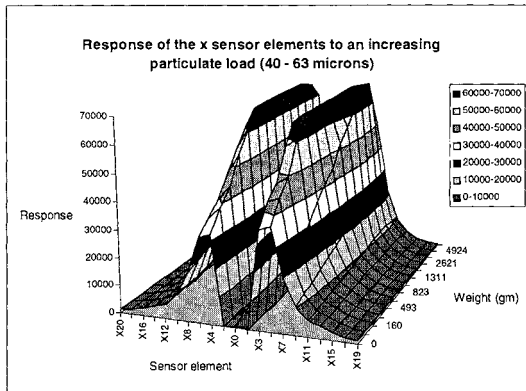


Figure 6. Laboratory Measurements: Effect of increasing particle loading on forward scattering signal.

The weight increments are not all equal. The horizontal sensors (labelled X) show a characteristic pattern in part due to varying gain of the detectors. The nephelometer has been plotted in the X0 position. Several features can be seen from this figure. Even with no particles added (pure deionised water) there is a characteristic response pattern. This is due to the difficulty of separating the direct beam from the forward scattered beam. The response is approximately linear initially for each of the forward scattering channels. The shape of the beam does not change with particle concentration until the digitising electronics saturates (at 16 bits). Results with silica particles of three size ranges are summarised in Figure 7.

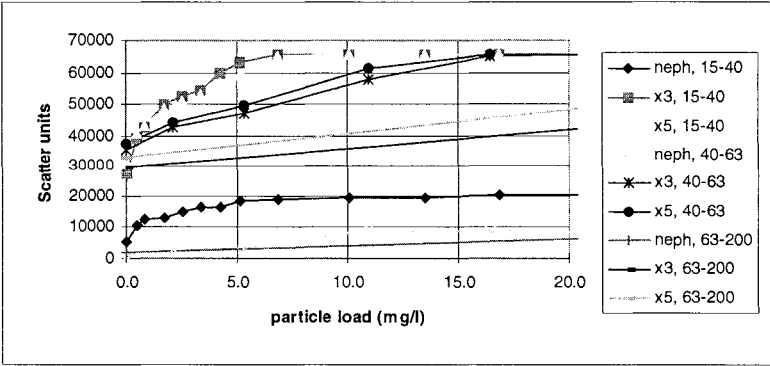


Figure 7. Laboratory Measurements: Effect of different size distributions (diameter μm) on forward scattering signal.

The top half of the graph shows three pairs of curves from the forward scattering sensors, the lower part that from the nephelometer (90 degree scattering). The main feature is a decrease in the slope of the curves as the average particle size increases. This is not surprising as scattering is dominated by particle number. Even with such a simple situation there is uncertainty in the size distribution of particles which makes comparison between model and experiment difficult. Note, these particle size distributions may not be typical of those found in the ocean.

EXPERIENCE WITH SEA TRIALS

LUCY underwent trials in the comparatively sheltered waters of a Scottish sea loch. The site was chosen partly because they have relatively clear waters, representative of deep oceans, and partly because this region has been well characterised by scientists at the local Dunstaffnage Marine Laboratory. Our initial experience over two seasons and several trials shows that LUCY is sensitive to changes in the marine environment. A typical example is shown in Fig. 8.

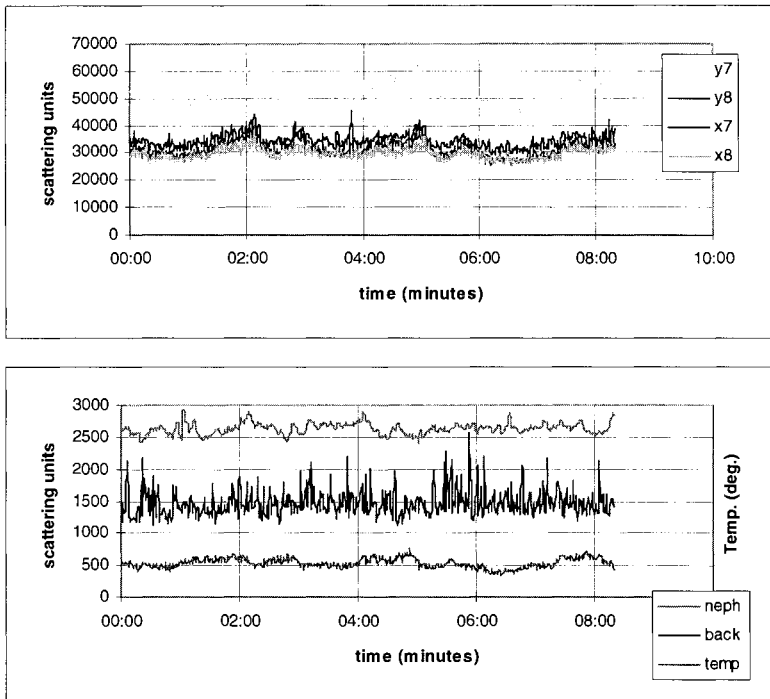


Figure 8. Trials Measurements: Response of LUCY to changes in the marine environment, depth 10m.

The top part of figure 8 shows the response of four symmetrically placed sensors over a period of 8 minutes. The bottom shows the response of some of the supporting instrumentation including the nephelometer. All the scattering signals are reasonably well correlated with changes in the environment as measured by the temperature sensor (and the salinity probe not shown). The forward scattering sensors are more sensitive than the nephelometer and the backscattering device. The fluctuations in the amplitude of the forward scattering signal have a Gaussian distribution. LUCY is capable of measuring changes in the symmetry of the beam pattern but during the above trial the changes found were attributed to misalignment of the detector optics. In particular we found changes in the scattering intensity from layers of water with depth and with local fronts (patches of less salty water ~30g/litre).

Although we want to measure particle scattering, other effects such as salinity or temperature fluctuations, can potentially cause changes in the forward beam pattern. However, the size of these fluctuations is likely to be larger than the active volume of the instrument and will therefore refract the beam as a whole. In future we hope to be able to detect any asymmetry in the forward scattering pattern and to compare this with the nephelometer and backscattered

signals. The instrument has only recently undergone the improvements that will allow us to make these measurements.

SUMMARY

Our Combined Model of light scattering by small particles of various shapes allows us to tackle a range of scenarios of interest in measuring scattering effects in the sea. We are now testing the model predictions both in the laboratory and on sea trials using a novel instrument especially designed to measure forward scatter. However, in a medium as variable as the sea there are many factors we are not able to measure or control. And therefore make precise predictions. We expect to use our model to aid interpretation of measurements made during sea trials.

We believe an instrument such as LUCY could prove a useful addition to the devices currently available for taking measurements of the marine environment.

REFERENCES

Aldrich Chemical Company, Gillingham, Dorset, SP8 4BC, U.K.

Bohren, C.F & Huffman, D.R. 1983, Absorption and Scattering of Light by Small Particles, New York, John Wiley & Sons

Brown, E, et al, 1995, Seawater: Its composition, Properties and Behaviour, 2nd edition, Oxford, Elsevier.

Bruscaglioni, P, et al, 1991, A numerical procedure for calculating the effect of a turbid medium on the MTF of an optical system, Physics Dept. University of Florence, Italy.

Chelsea Instruments Ltd, 1996, Light Scattering Device Handbook Mk2, ref. HB173, East Molesey, Surrey, KT8 0QX, U.K.

Clark, T, Hall, T J, Williams, T H, Walton J R. A new approach to the measurement of light scattering in the ocean.. Oceanology International 96, Conference Proceedings, Vol 2, 157.

Evans, B.T.N 1993, Integrated Program Host for Absorption, Scattering and Extinction Calculations, version 2.4, DREV, Quebec, Canada.

Fairbanks, M.C, 1994, Software Design Specifications for models of Light Scattering in a Turbid Medium, 6A003D002/1.0, Smith System Engineering, Guildford, UK.

van de Hulst, H.C 1981, Light scattering by small Particles, New York, Dover Pubs.

Jerlov N.G 1976, Marine Optics, 2nd Edition, Amsterdam, Elsevier

Merk Ltd. Poole, Dorset, BH15 1TD, U.K.

Wolfenden, T.D. 1994, Specification of changes performed by Smith to DREV IPHASE routine and to the Smith small angle scattering model, 6A003D004/1.0, Smith System Engineering, Guildford, UK.

EFFECT OF DISPERSANTS ON ZOOPLANKTON MORTALITY IN KOREA

Woong-Seo Kim, Man Chang, Soo Hyung Lee and Jong Soo Lee
Korea Ocean Research and Development Institute
Seoul, Korea

ABSTRACT

Oil spill accidents happened frequently in the coastal waters of Korea, and various oil dispersants were widely used to treat spilled oil. In this study, microcosm experiments were carried out to investigate short-term high-dose effects of three dispersants (Enersperse 1037, Gamasol LT-A and Hi-Clean) on the mortality of zooplankton in the southern coastal waters of Korea. Dispersants varied widely in toxicity effect on zooplankton depending on the kinds of dispersants and zooplankton taxa. Mortality of zooplankton in Enersperse 1037 was higher than that in Gamasol LT-A, and at the same exposure time and concentration mortality was slightly higher in Gamasol LT-A than in Hi-Clean. Mortality of copepods was significantly higher than that of polychaete larvae when they were exposed to the same concentration of dispersant. In general, mortality of zooplankton increased as concentration of dispersants, incubation time, and incubation temperature increased.

INTRODUCTION

As oil is visible and easily recognizable, it has been considered a marine contaminant more than any other pollutants. To treat spilled oil, various dispersants such as Gamasol LT-A and Hi-Clean have been widely used in Korea. However, using too much of a dispersant was suspected to cause red tides by increasing mortality of herbivorous zooplankton (Tang *et al.*, 1992). Zooplankton play an important role in the planktonic ecosystem to transfer organic materials from primary producers to higher trophic levels. Therefore, the high mortality of zooplankton may cause a serious problem to the entire ecosystem through food webs. Reduced zooplankton due to the toxic effect of dispersants may release grazing pressure on phytoplankton populations resulting in an increase of algal biomass, and making a food-limited environment for the higher trophic levels resulting in a decrease of marine living resources. Thus, information on the increased mortality of zooplankton due to various dispersants will be essential to evaluate damages of the ecosystem.

Oil spills due to accidents involving oil tankers and other ships have frequently happened in the coastal waters of Korea, and damaged marine ecosystem, fishery and aquaculture industries severely. A total of 3,534 accidents related to marine pollution occurred in Korea from 1978 to 1994, and 91.0% of them were oil spill accidents. The numbers of accidents have continuously increased (Fig. 1). Most of the accidents happened near the large ports such as Pusan (24.5%)

and Incheon (19.8%), and almost half of them (47.2%) occurred in the southern sea (Data from the Korea Maritime Police).

In 1995, there were three major oil spill accidents in the southern coastal waters of Korea. Dispersants were widely used to treat the spilled oil on the accident site, even though some scientists suggested negative impact of the dispersants on the ecosystem. Two months after the oil spill accident, we experienced the worst red tide of *Cochlodinium* sp. in September with the monetary loss of about 100 million US\$ in mariculture industry. It was hypothesized that the increased zooplankton mortality due to dispersants caused the algal bloom. However, the hypothesis has not been tested yet, and data of the dispersant effects on zooplankton mortality are very limited in Korea. In this study, microcosm experiments were carried out to investigate the effects of dispersants on the mortality of zooplankton in the southern coastal waters of Korea.

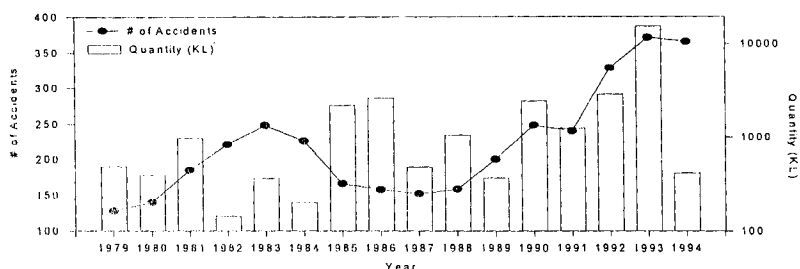


Figure 1. Increasing trend of oil spill accidents in Korea from 1979 to 1994. Dots show the number of oil spill accidents and bars show the amount of spilled oil in the unit of kiloliters. (Data from an unpublished document of the Korea Maritime Police Agency, 1995)

MATERIALS AND METHODS

Microcosm experiments were conducted to investigate short-term high-dose effects of three different kinds of dispersants (Enersperse 1037, Gamasol LT-A, and Hi-Clean) on the zooplankton mortality and to compare the relative toxic effects among dispersants in Masan Bay of the southern coast of Korea using 2-l Nalgene bottles from November 1995 to April 1996. Incubation bottles were filled with sea water with net-collected (250- μ m mesh) zooplankton. Zooplankton abundance in the experimental bottles were 3 to 4 times higher than natural abundance. Incubation bottles with and without (control) dispersants were incubated in the laboratory at the same temperature as *in situ* temperature. At the end of the 24-hr incubation period, zooplankton were examined whether they were alive or dead under a dissecting microscope. Live and dead zooplankton were enumerated using a zooplankton counting chamber. Mortality was calculated as the percentage of dead zooplankton to the total (live+dead) abundance. Target organisms were dominant zooplankton in the study area such as copepods and polychaete larvae. To investigate the relative toxicity of Gamasol LT-A and Hi-Clean, copepods, which were the most dominant zooplankton in March, were incubated at three different experimental bottles (n=3 in each treatment); control, Gamasol LT-A (1,000 ppm), and Hi-Clean

(1,000 ppm) for 24 hours. Analysis of variance (ANOVA) was performed to compare the relative toxicity of Gamasol LT-A and Hi-Clean on the mortality of zooplankton.

RESULTS AND DISCUSSION

Dispersants are mixtures of several surfactants dissolved and dispersed in polar and nonpolar solvents (Wells, 1984a). The chemical compositions of dispersants used in these experiments are as follows. Gamasol LT-A contains polyethyleneglycol mono-oleate, sorbitan mono-oleate, and orbitol mono-oleate in a denormalised and dearomatised middle distillate such as liquid paraffin, and two individual n-alkanes (C_{14} and C_{15}) as minor components. Hi-Clean comprises of polyethyleneglycol mono-oleate in a denormalised and dearomatised middle distillate such as liquid paraffin. The average carbon number of this distillate is slightly higher than that for Gamasol LT-A (analysed by M-Scan Ltd.). Concentrate Enersperse 1037 contains polyethyleneglycol mono-oleate, alkylbenzene sulfonate, and high molecular weight anionic detergents. Generally concentrated dispersants are more toxic than the water-immiscible or water-miscible products, and a less toxic product would be preferable to one more toxic.

When copepods were exposed to concentrate Enersperse 1037 at the concentration of 50 ppm, 82.1% of the copepods were dead after a 24-hr incubation period (Fig. 2). The 24-h LC_{50} was less than 50 ppm for copepods, and between 100 and 500 ppm for polychaete larvae. At 500 ppm, 100% of the copepods and 97% of the polychaete larvae were dead. Mortality of copepods was more than 4 times higher than that of polychaete larvae when they were exposed at 50 and 100 ppm. This result showed that copepods were more vulnerable to Enersperse 1037 than polychaete larvae. Polychaete larvae formed an important constituent especially in the heavily polluted coastal waters such as the study area (KORDI, 1994). This fact implicated that polychaete larvae represented a higher tolerance to various pollutants than copepods.

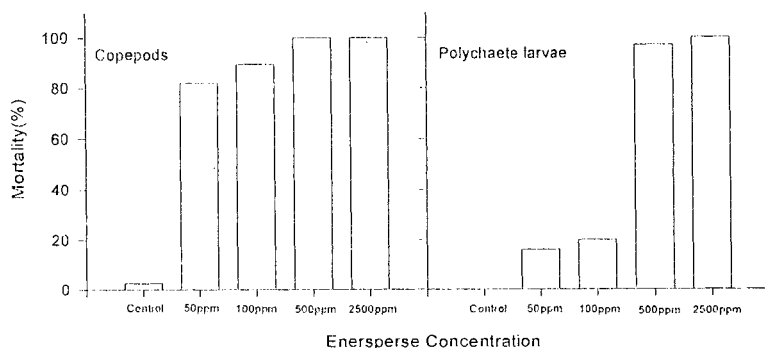


Figure 2. Mortality of copepods and polychaete larvae when they were exposed to Enersperse 1037 at the concentration of 0, 50, 100, 500, 2,500 ppm for 24 hours in November 1995.

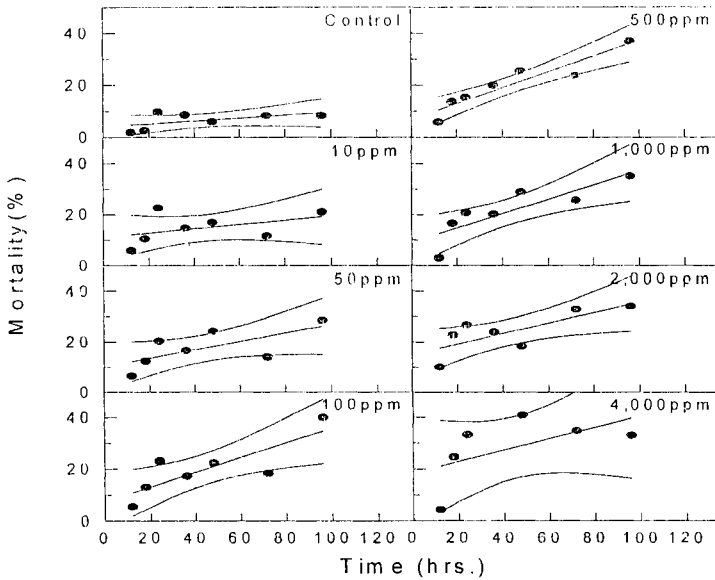


Figure 3. Mortality of copepods exposed to Gamasol LT-A at the various concentrations (0, 10, 50, 100, 500, 1000, 2000, 4000 ppm) for 12, 18, 24, 36, 48, 72, 96 hours. Linear lines are regression lines and curved lines show a 95% confidence level. Incubation temperature was 6° C.

Figure 3 shows the effect of concentration Gamasol LT-A and exposure time on copepod mortality. Mortality of copepods generally increased as the concentration of the dispersant and exposure time increased. Gamasol LT-A was less toxic in terms of copepod mortality, compared with concentrate Enersperse 1037. At the control microcosm without dispersant, copepod mortality was less than 10% during the 96-hour incubation period, however, at the concentration of 4,000 ppm, mortality reached up to 40.9% after 48-hour incubation. Copepods were exposed to the dispersant at the concentration up to 4,000 ppm for 96 hours in the experiment, however, LC₅₀ was not found during the incubation period. Considering low concentration of dispersants and short exposure time in the field (Butler, 1989), the effects of dispersant on zooplankton mortality would be less than we expect from the laboratory results.

The results of relative toxicity of two dispersants currently in use in Korea, Gamasol LT-A and Hi-Clean, on the mortality of copepods are in Figure 4. There was a highly significant ($p < 0.001$) addition of dispersants at the concentration of 1,000 ppm on the mortality of copepods. However, the effects of two different dispersants were not significantly ($p > 0.5$) different at the same concentration, even though mean mortality (37.2%) in Gamasol LT-A was slightly higher than that (36.9%) in Hi-Clean. In the repeated experiment in April, mortality was significantly higher ($p < 0.05$) in Gamasol LT-A than in Hi-Clean in most cases.

Comparison experiments were repeated with Gamasol LT-A and Hi-Clean at the concentrations of 1,000 and 4,000 ppm. Mortalities of copepods and polychaete larvae, which were dominant in April, in the control bottles were 8.3% and 0.9%, respectively. The result "higher mortality in higher concentration" of the April experiment was the same as that of the larvae in Gamasol of 1,000 ppm. Mortality of copepods was higher than that of polychaete larvae in most cases. Compared with Hi-Clean, Gamasol LT-A seemed to be more toxic to zooplankton. Mortality of copepods increased by 15.0% and 1.9% in Gamasol LT-A and Hi-Clean, respectively, when the water temperature was 15° C in April, compared with the result in March when the water temperature was 9° C at the same concentration of 1,000 ppm. Increased mortality was possibly due to the high incubation temperature which accelerated metabolism rates of the experimental animals or diminished DO.

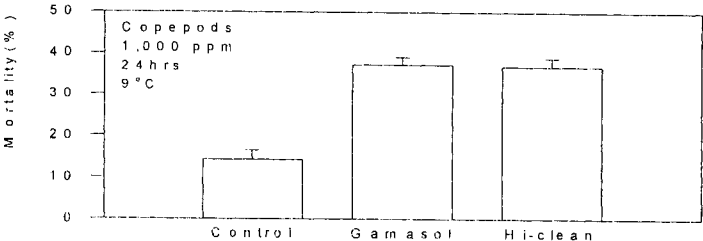


Figure 4. Comparison of the effect of two different dispersants, Gamasol LT-A and Hi-Clean, on the mortality of copepods during 24-h incubation period. Experiment was conducted in March and incubation temperature was 9° C previous experiment except for polychaete

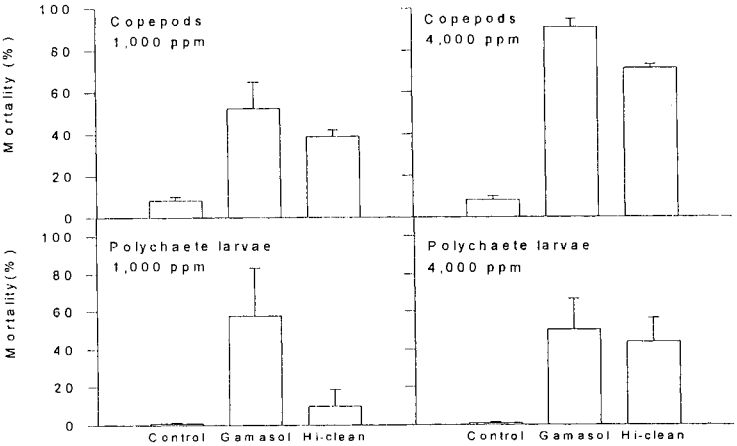


Figure 5. Mortality of copepods and polychaete larvae exposed to Gamasol LT-A and Hi-Clean. Experiment was conducted in April and incubation temperature was 15°C.

The 24-hour median lethal concentrations (24-h LC₅₀) for a copepod *Pseudocalanus minutus* varied depending on the type of dispersants (Wells, 1984b). The LC₅₀ of concentrated dispersants were in the order of 10 to 100, however, water miscible and immiscible dispersants were in the order of thousand ppm. The results of this study for the copepod assemblages are shown in the following table with previous data.

Table 1. Acute toxicity threshold expressed as ranges of one-day median lethal concentrations in mg/l for *Pseudocalanus minutus* (from P. G. Wells, 1984b)

Dispersants		LC ₅₀ of copepods
Concentrate	Corexit 9527	10.8 - 17.5
Concentrate	BP1100WD	460
Water immiscible	Corexit 8667	1,320 - 6,300
Water immiscible	BP1100X	5,500 - 6,700
Water miscible	Corexit 7664	2,450 - 10,000
*Concentrate	Enersperse 1037	< 50
	*Gammamol LT-A	1,000 - 4,000
	Hi-Clean	1,000 - 4,000

* result from this study for assemblages of various copepod

There are many factors influencing toxicity threshold of dispersants. The factors may be chemical compositions of dispersants, chemical stability and age of dispersants, concentration and exposure time, environmental factors such as temperature, salinity, DO, and biological characteristics of exposed organisms such as species, age, stage of development and physiological conditions (Overton et al., 1994). With a series of experiments, mortality of various zooplankton seemed to be dependent on the chemical composition and concentration of the dispersants, exposure time, incubation temperature, and zooplankton taxa. In conclusion, mortality of copepods was generally higher than that of polychaete larvae when they were exposed to dispersants, and mortalities of zooplankton were higher in Gammamol LT-A than in Hi-Clean.

Further *in situ* incubation experiments are now being performed in order to compare relative toxicity among various kinds of oil dispersants and a mixture of crude oil and dispersant. As the mortalities of zooplankton observed in the microcosm occurred at higher concentrations than those in the water column during treatment of spilled oil at sea (1 to 10 ppm), and for longer time than predicted exposures during oil dispersal at sea (1 to 3 hours; Butler, 1989), investigation on the short-term (less than 3 hours) impact on the mortality of various zooplankton at lower concentrations of dispersants will be needed.

REFERENCES

- Anonymous. 1994. Marine environmental assessment based on the benthic faunal community in Chinhae Bay, Korea. KORDI (Korea Ocean Research and Development Institute, Seoul, Korea. BSPE 00417-684-3. pp 73.
- KORDI (Korea Ocean Research and Development Institute), 1994. Marine environmental assessment based on the benthic faunal community in Chinhae Bay, Korea. BSPE 00417-684-3. 73pp.
- Butler, J. N. 1989. Using oil spill dispersants on the sea. In: Proceedings 1989 Oil Spill Conference (Prevention, Behavior, Control, Cleanup). American Petroleum Institute. pp. 343-345.
- Overton, E. B., W. D. Sharp and P. Roberts. 1994. Toxicity of petroleum. In: Basic Environmental Toxicology. Cockerham, L. G. and B. S. Shane (eds). CRC Press. pp. 133-156.
- Tang, S-M., X-L. Chen and D-F. Zhuang. 1992. The effects of BP- 1100X dispersant and dispersed Shengli crude oil on the ecosystem - Marine ecosystem enclosure experiment. *Acta Ecol. Sinica*. 12(4):361-367. (in Chinese with English abstract)
- Wells, P.G. 1984a. Marine ecotoxicological tests with zooplankton. In: Ecotoxicological Testing for the Marine Environment. Persoone, G., E. Jaspers and C. Claus (eds). State Univ. Ghent and Inst. Mar. Scient. Res., Bredene, Belgium. Vol. 1. pp. 215-256.
- Wells, P.G. 1984b. The toxicity of oil spill dispersants to marine organisms: A current perspective. In: Oil Spill Chemical Dispersants: Research, Experience, and Recommendations. STP 840. Tom E. Allen (ed), American Society for Testing and Materials, Philadelphia. pp. 177-202.

MINIATURIZED GAS CHROMATOGRAPHY INSTRUMENTATION FOR DMS IN THE MARINE ATMOSPHERE

¹Paul M. Holland, ¹Robert V. Mustacich, ¹James F. Everson and ²John W. H. Dacey

¹RVM Scientific, Inc.
Santa Barbara, California, U.S.A.

²Woods Hole Oceanographic Institution
Woods Hole, Massachusetts, U.S.A

ABSTRACT

New instrumentation approaches will be important in extending studies to the spatial and temporal scales required to understand the role of dimethylsulfide (DMS) and other species in the marine boundary layer. In response to this need, we are developing miniaturized, automated gas chromatography (GC) instrumentation for the measurement of DMS and other trace sulfur species in the marine atmosphere. Our modular design includes a sample inlet scrubber for oxidants, miniature preconcentrator based on molecular sieve adsorbents, miniaturized fast GC with pulsed flame photometric detector, and automated signal processing and control software, with planned telemetry of data in near real-time from research platforms such as remotely piloted aircraft. The use of a modular design approach provides flexibility for future incorporation of a variety of additional modules for sampling, preconcentration, and detection. This would allow instrument configurations for other analytes, measurements of DMS in seawater, and deployment for long term monitoring from other types of platforms such as buoys and moorings.

INTRODUCTION

A new generation of chemical instrumentation and sampling technology is needed for the collection and telemetry of data in near real-time, allowing studies on appropriate spatial and temporal scales from research platforms such as remotely piloted aircraft and autonomous underwater vehicles (Pellenbarg, et al., 1994; Dacey and Cooper, 1994). With near real-time data telemetry, data collection plans may be modified as needed to study transient or anomalous features. Related instrumentation will provide the capability for long-term unattended monitoring from buoys, moorings and innovative low cost platforms such as "ships of opportunity". Advantages of miniaturizing and automating chemical instrumentation include small size, reduced use of power and other consumables, improved robustness for "real world" environments and unattended operation, and the potential for low cost manufacturing. Substantial productivity gains and cost savings in data collection may also be realized with automated instrumentation. Such benefits are highlighted by the high operational costs of research vessels and aircraft, where onboard laboratory space and instrument payloads are often limited.

DMS in the oceans is produced by biological activity and it is the primary source of gaseous sulfur in the marine atmosphere (Andreae, 1990). Observed concentrations of DMS in the ocean

and marine atmosphere vary widely, exhibiting complex dynamics and distribution. A summary of sources and sinks for DMS in the oceans and atmosphere (after Charlson et al., 1987; Ledyard and Dacey, 1996) is illustrated in Figure 1. Here, the primary source of DMS is seen to be DMSP (dimethylsulfoniopropionate) which is produced in marine algae. Conversion to DMS can occur when particulate or intercellular DMSP in these phytoplankton is released into seawater and undergoes cleavage to acrylic acid and DMS. The major sinks for DMS in seawater are transport across the sea/air interface and photochemical or bacterial oxidation. Its residence time in seawater is estimated to be several days to a week. DMS in surface waters is highly variable in coastal environments ranging up to 40-fold in concentration on scales of kilometers (unpublished data), and in even in open ocean waters it can vary as much as five-fold in a few days.

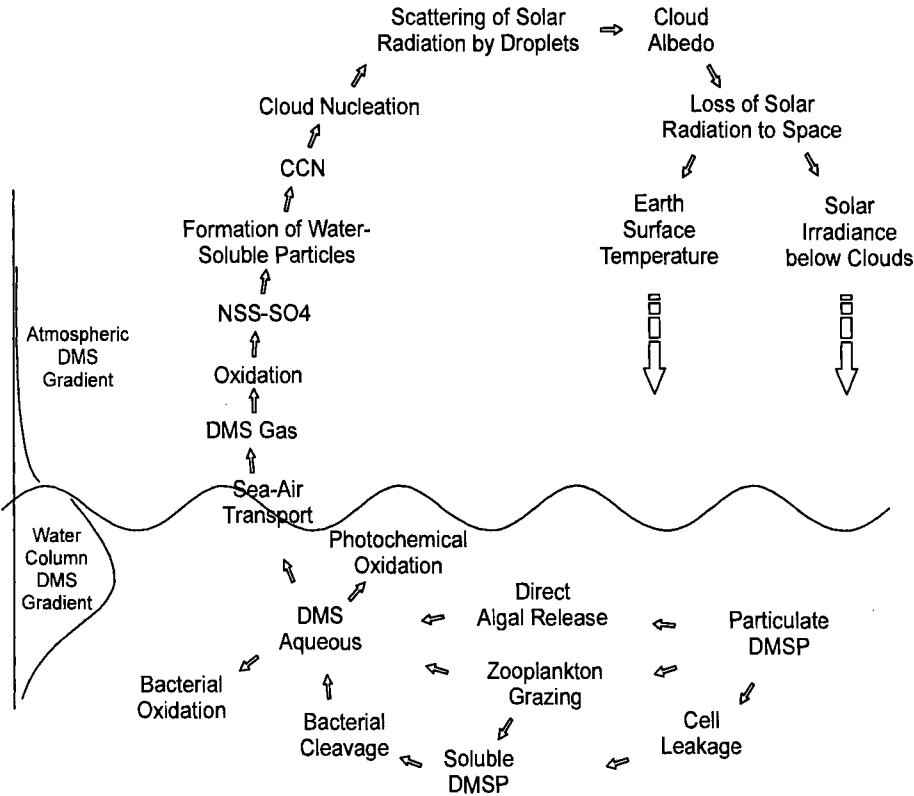


Figure 1. Sources and sinks for DMS in the marine environment.

The pool of DMS in the mixed layer of the water column is typically 1-30 times the size of that in the atmospheric boundary layer. The observed rapid turnover of this massive seawater reservoir of DMS suggests that even relatively minor changes in one of its source or sink terms could lead to a substantial changes in concentration and therefore to the DMS flux across the air/sea interface. We know little about the relative contributions of biological, chemical and physical processes in controlling DMS in seawater. While some moderately quantitative data for DMS in seawater exists for a limited set of conditions, it is not adequate for generating predictive models. The residence time for DMS in the atmosphere is even shorter than that in seawater.

Once in the atmosphere, DMS rapidly reacts with hydroxyl free radical and is oxidized to methane sulfonic acid and sulfur dioxide (Andreae, 1990). These species, in turn, are precursors to atmospheric sulfuric acid, leading to the formation of cloud condensation nuclei (Pandis, et al., 1994). Cloud formation results in the scattering of incoming solar radiation, affecting the Earth's albedo, the Earth's surface temperature, and ultimately the amount of sunlight reaching the sea surface to contribute to algae growth (Charlson et al., 1987). This overall process can thus be viewed as forming a "feedback loop" related to global climate, and investigating these relationships is becoming an active area of research.

Understanding the production and fate of DMS in the oceans and the atmosphere is an important component in global climate change modeling and prediction, and is of direct importance in understanding the formation of aerosol particles and clouds in the marine environment. It is the global aspect of the problem, which ranges from remote open ocean environments to biologically rich coastal upwelling areas, that make measurement needs so demanding. Some specific measurement needs for DMS include: spatial and temporal distributions of DMS in the marine atmosphere and surface waters over a full range of oceanic environments; profiles of DMS at low altitude to examine the effects of wind shear on transport across the sea/air interface; and higher altitude measurements of DMS and other sulfur species to help assess oxidation kinetics in the marine atmosphere and the impact on aerosol formation. Measurements of DMS may also provide a means of performing fundamental studies of gas transport across the sea/air interface, since DMS is already present in seawater with a strong partial pressure gradient between seawater and air (due to the atmospheric sink for DMS). This makes DMS a nearly optimal gas for such studies.

INSTRUMENTATION APPROACH

In order to meet measurement needs for DMS and other atmospheric sulfur species, it will be important to bring the analytical capability of laboratory instrumentation to the field. This means new approaches to instrumentation focused on robustness, compact size, automated operation, reduced power and consumables requirements, and fast analysis times, all *without* sacrificing low detection limits. Basic requirements for such instrumentation packages are that they be self-contained, have sufficient detection sensitivity, are capable of remote operation with automated signal processing, and that they provide excellent chemical selectivity against background.

We have selected a modular design approach for developing miniaturized gas chromatography instrumentation for DMS in the marine atmosphere. This approach provides design flexibility

for meeting a variety of future instrumentation needs, including measurements of DMS in seawater, long term unattended monitoring from buoys and moorings, and for measurements of other analytes in the marine environment.

Our modular design is built around a miniaturized fast gas chromatography module with automated signal processing. Gas chromatography (GC) is an especially powerful method of separating complex mixtures of compounds by passing them in a "carrier gas" through a column (narrow tube) coated with materials with affinity for the compounds to be separated. Different compounds in the mixture spend varying fractions of their time being "carried" through the column in the gas stream depending on these affinities, and thus emerge from the column into the detector at different times. Coupling GC to a "selective" detector, which responds only to compounds of a particular type such as sulfur containing species, allows even trace levels to be detected against complex chemical backgrounds. In fast GC, smaller and shorter columns are used to achieve separations on time scales of seconds, rather than the minutes typical for conventional laboratory GC. An overview of the functional elements of our modular design is shown in Figure 2.

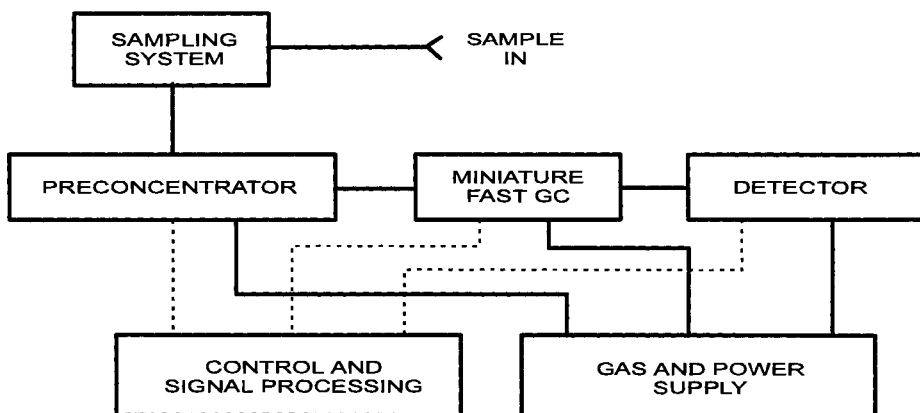


Figure 2. Overview of modular design of instrument.

Here, various "front end" sampling modules can be used for the particular species and sampling mode of interest, such as: direct air sampling, air sampling through an oxidant scrubber, or purging of seawater samples to remove dissolved gases for analysis. At the trace levels where many of the species of interest occur, preconcentration is required. For this, relatively large volumes of air (liters) can be passed through a trap preconcentrator, which strongly adsorbs the species of interest at ambient temperatures. On heating the trap, these preconcentrated compounds can be thermally desorbed (released) into much smaller volumes (milliliters), thus providing preconcentration factors of up to several orders of magnitude. Depending on the species of interest, various trap preconcentrators based on different sorbents and required

sampling volumes can be substituted. The choice of detector for the instrument depends on the species to be analyzed, detection sensitivity and selectivity needed, and requirements for ruggedness, size and consumables use. In the case of sulfur species, various flame photometric detector (FPD) designs can be used. Gases required for instrument operation may be supplied from small cylinders, air pumps or devices such as hydrogen generators, with power supplied from aircraft or shipboard systems, or by battery. The use of a modular design makes it possible to adapt the instrument for other measurements, generally by changing the sampling system, preconcentrator, GC column and detector.

Details of our instrument design for GC measurements of DMS in the marine atmosphere are shown in the schematic in Figure 3. Miniature valves and other components are used throughout. Air samples are introduced via a Teflon sampling line through an oxidant scrubber to the trap preconcentrator by the use of computer controlled miniature valves and small sampling pump (far left). The scrubber is needed to remove ozone and other oxidants before they can react with DMS in the preconcentrator (Andreae et al., 1985). While a variety of approaches can be used for scrubbing oxidants, our current design incorporates the cotton scrubber described by Hofmann et al., (1992), Andreae et al. (1993), and Persson and Leck (1994). This scrubber is easily changed in the field, and unlike solution-based scrubbers employing bubblers, can be used in any attitude.

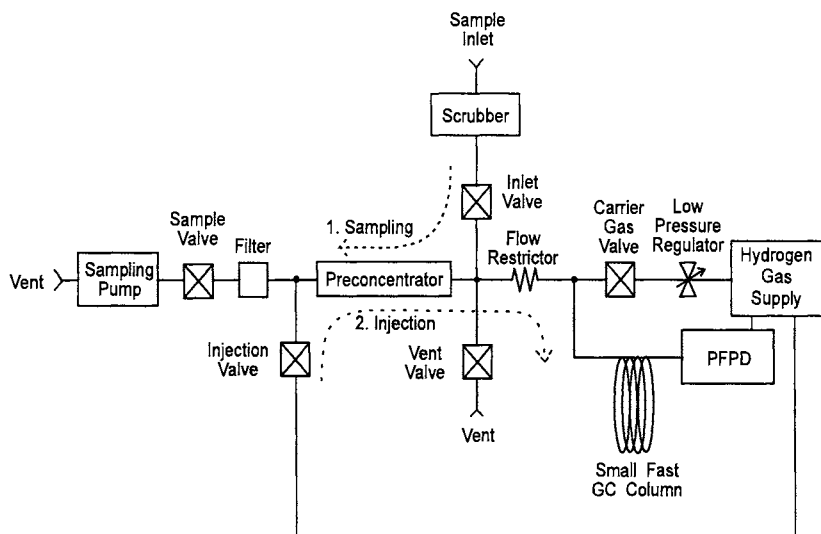


Figure 3. Miniature GC Instrument design for DMS.

An important part of our effort has been to develop approaches for ambient temperature preconcentration of DMS and other atmospheric sulfur species of interest, thus avoiding the need for the use of cryogenics. There has been substantial previous work demonstrating that gold

surfaces can provide a useful approach for preconcentrating DMS from the atmosphere (Andreae et al., 1985; Ayers et al., 1995), and recent work that aluminosilicate based molecular sieves can be effective for DMS (Davison, 1994; Benner, 1996). While we have utilized both of these methods for preconcentrating DMS from air, our current preconcentrator design is based on the use of carbon molecular sieve materials, such as Carboxen 1000 (Supelco, Bellefonte PA).

Carboxen is created by the pyrolysis of polymeric precursors and is hydrophobic, making it a good choice for tolerating the significant amounts of water vapor that will be encountered in atmospheric sampling. Surface areas are on the order of 750 m²/g, and our measurements indicate that the breakthrough volume for DMS at 1 ppm on Carboxen 1000 is more than 10⁶ mL/g at ambient temperature. This means that the trap preconcentrator need only contain a few milligrams of adsorbent, which has allowed us to go to 1/16" o.d. tubing for the trap body, thus minimizing dead volume and providing for more complete injections of preconcentrated analyte onto the GC column for analysis. Because the adsorbent bed is short, even at 1/16" trap diameter flow rates of 0.5-1 L/min are feasible. With such miniaturized traps, temperatures of 200 °C can be achieved in several seconds using low voltage and modest current. Results for other atmospheric sulfur species such as SO₂ also look promising with this miniature preconcentrator design, as seen in Figure 4.

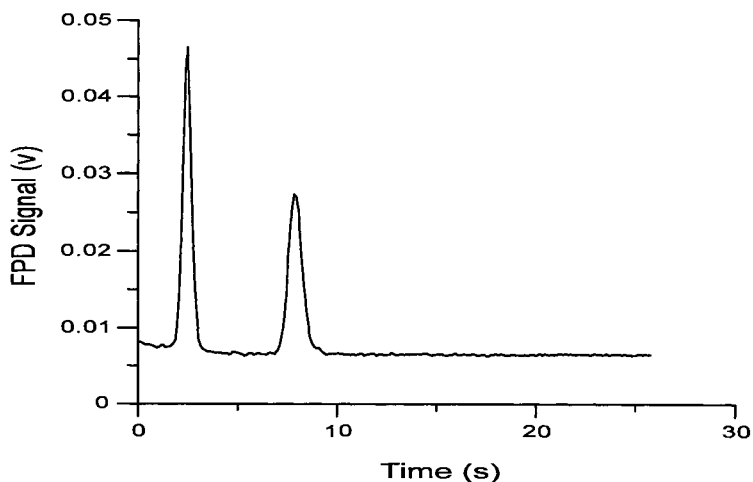


Figure 4. Chromatogram of SO₂ and DMS desorbed from Carboxen trap.

After heating the preconcentrator, the sample is desorbed and introduced into the gas chromatograph by "injection" through a flow restrictor (at the right of the preconcentrator in the schematic). Here, the gas sampling and carrier gas valves are closed, while the injection valve is opened to create a reverse flow from the preconcentrator across the flow restrictor. This injects thermally desorbed analytes onto the head of the GC column. The fast GC itself consists of a short length of capillary column and regulated flow of carrier gas to the column. In the present design, hydrogen carrier gas is supplied from a small hydrogen gas cylinder. After separation on the GC column, the analyte enters the detector.

Three flame photometric detector (FPD) configurations have been evaluated for the instrument. These include a miniature FPD developed using a miniaturized PMT coupled to a flame source by fiber optic cable, a larger conventional FPD design where the PMT directly stares at the flame through heat shielding glass, and a compact, new pulsed FPD (PFPD) design. The results of this evaluation strongly favored PFPD for measurements of DMS in the marine atmosphere.

PFPD is based on time-gated temporal and spectral emissions created in a self-terminated propagating flame (Cheskis, et al., 1993). For sulfur detection, this also provides nearly infinite selectivity against carbon, due to the delay in sulfur emission. The newly available commercial form of this detector (OI Analytical, College Station, TX) which we have incorporated into the DMS instrument is very compact and provides $< \text{pg/sec}$ detection sensitivity for sulfur, much lower than other FPD detectors. With the trap preconcentrator, this provides good detection sensitivity for DMS at typical atmospheric levels as shown in Figure 5. Pulsed operation of the PFPD has other potential advantages for field instrumentation. The flame pulses occur at about 3-4 Hz in the presence of a continuous "glowplug" ignition source by using a flow rate of combustible gas that cannot sustain a continuous flame. Besides providing start times for gating the spectral emissions, pulsing eliminates difficulties associated with lighting and maintaining a flame, and results in much lower consumption of both hydrogen and air compared to conventional FPD. These are both important advantages for remote operation.

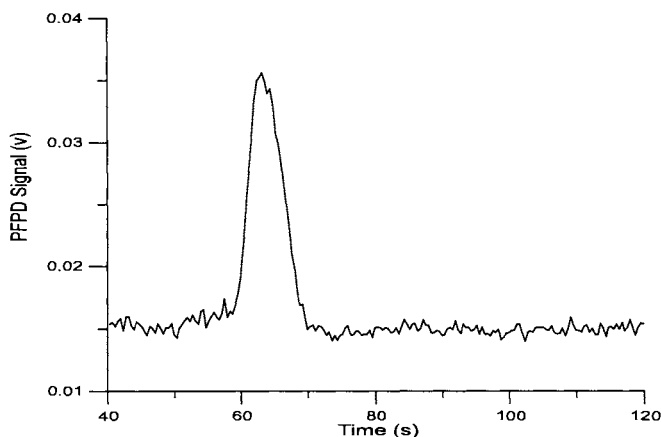


Figure 5. Chromatogram of 100 ppt DMS preconcentrated on Carboxen trap.

Our instrument for DMS measurements is designed as a self-contained instrumentation package for mounting in the payload bay of a remotely piloted aircraft, with the compact dimensions of 15x25x37cm as shown in Figure 6. The design incorporates a cotton inlet scrubber, miniature ambient temperature trap preconcentrators based on carbon molecular sieve adsorbents, a miniaturized fast capillary column GC coupled to a pulsed flame photometric detector (PFPD), with control software for automated data acquisition, chromatographic peak detection and integration. Support hardware includes a 24-bit data acquisition board, GC controller board, on-

board processing and data logging, with computer control of pump, valves, heater and temperature controls, and trap cooling fan. The instrument package is designed to communicate with the central aircraft computer for master control and data telemetry via a serial link. Power for instrument operation will be directly obtained from the 28 V DC supplied by aircraft using DC/DC converters packaged within the housing, with gas supply from lecture bottles providing sustained operation times of up to 35 hours.

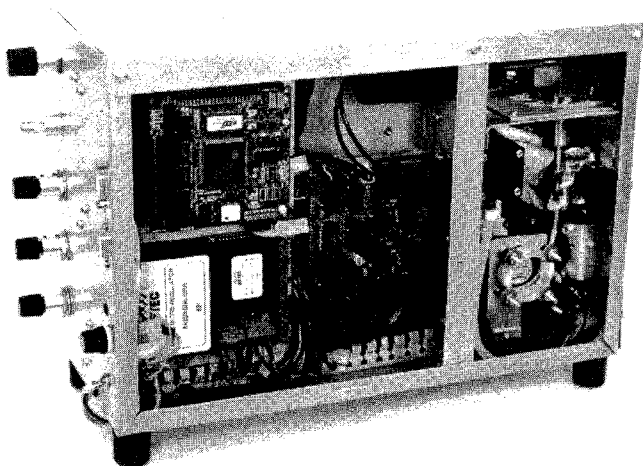


Figure 6. Miniaturized GC instrumentation package for DMS measurements.

The miniature GC instrumentation package described here, is designed to provide near real-time measurements of DMS and other sulfur species from remotely piloted aircraft, with telemetry of results. Such measurements will help lead to a better understanding of the relationship between biogenic production, distribution, transport of DMS from ocean to atmosphere, and its impact on aerosol formation in the marine environment.

The modularity of the present instrument design should allow it to be adapted for other applications. These include measurements for other analytes, and the use of alternative methods of sampling, such as automated purge and trap analysis of seawater samples. For long term unattended operation of instrumentation on moorings, buoys, or "ships of opportunity," a hydrogen generator could be incorporated to provide chromatographic carrier and detector fuel gas. In this case, only water and power would be required for the instrument, and storage and transportation of hazardous fuel gases such as hydrogen would be eliminated. Telemetry of data would also allow near real-time data acquisition and diagnostic monitoring of the instrument over long time periods.

The potential low cost and autonomous operation of such instrumentation may also allow it to be used in hazardous locations and under conditions where human operators or high value assets

cannot be risked regardless of the potential scientific payoffs. An example is low altitude measurements near the sea surface in severe weather to monitor enhanced transport of environmentally important species across the sea-air interface as a function of sea state.

The automated, miniature gas chromatograph for DMS measurements, is one example of the new generation of oceanographic instrumentation, sensors and sampling technology that is being developed by the ocean sciences community. Such new capability will provide the potential for measurements and monitoring of the marine environment on spatial and temporal scales previously beyond reach, and this is likely to lead to a more complete understanding of the relationship between the world's oceans and global climate.

ACKNOWLEDGEMENTS

Support of this work by the Office of Naval Research under contract N00014-95-C-0386 is gratefully acknowledged.

REFERENCES

- Andreae, M. O. 1990. Ocean-atmosphere interactions in the global biogeochemical sulfur cycle. *Marine Chemistry* **30**:1-29.
- Andreae, M. O., R. O. Ferek, F. Bermond, K. P. Byrd, R. T. Engstrom, S. Hardin, P. D. Houmère, F. LeMarrec, H. Raemdonck, and R. B. Chatfield. 1985. Dimethylsulfide in the marine atmosphere. *J. Geophys. Res.* **90**: 12891-12900.
- Andreae, T. W., M. O. Andreae, and H. G. Bingemer. 1993. Measurements of dimethyl sulfide and H₂S over the western north Atlantic and the tropical Atlantic. *J. Geophys. Res.* **98**: 23389-23396.
- Ayers, G. P., S. T. Bentley, J. P. Ivey and B. W. Forgan. 1995. Dimethylsulfide in marine air at Cape Grimm, 41°S. *J. Geophys. Res.* **100**: 21013-21021.
- Benner, R. L. 1996. Personal communication.
- Charlson, R. J., J. E. Lovelock, M. O. Andreae, and S. G. Warren. 1987. Oceanic phytoplankton, atmospheric sulphur, cloud albedo and climate. *Nature* **326**:655-661.
- Cheskis, S., E. Atar, and A. Amirav. 1993. Pulsed-flame photometer: a novel gas chromatography detector. *Anal. Chem.* **65**: 539-555.
- Dacey, J. W. H. and D. J. Cooper. 1994. Dynamics of dimethylsulfide in coastal waters and the marine atmosphere: a need for platform observations. *Mar. Tech. Soc. J.* **27**:72-77.
- Davison, B.M. and A. G. Allen. 1994. A method for sampling dimethylsulfide in polluted and remote marine atmospheres. *Atmos. Environ.* **28**:1721-1729.

Hofmann, U., R. Hofmann, and J. Kesselmeier. 1992. Cryogenic trapping of reduced sulfur compounds using a nafion drier and cotton wadding as an oxidant scavenger. *Atmos. Environ.* **26A**: 2445-2449.

Ledyard, K. M. and J. W. H. Dacey. 1996. Microbial cycling of DMSP and DMS in coastal and oligotrophic seawater. *Limnol. Oceanogr.* **41**:33-40.

Pandis, S. N., L. M. Russell, and J. H. Seinfeld. 1994. The relationship between DMS flux and CCN concentration in remote marine regions. *J. Geophys. Res.* **99**: 945-957.

Pellenberg, R. E., R. A. Morris, D. H. Johnson and S. J. Martin. 1994. MarChem 93: a workshop focused on concerns of the marine chemistry community. *Marine Chemistry* **48**:83-86.

Persson, C. And C. Leck. 1994. Determination of reduced sulfur compounds in the atmosphere using a cotton scrubber for oxidant removal and gas chromatography with flame photometric detection. *Anal. Chem.* **66**: 983-987.

CORAL REEF NATURE RESERVE MANAGEMENT IN HAINAN PROVINCE

Lu Wang

Hainan Marine Development Planning and Design Institute
Haikou, Hainan, P.R. CHINA

ABSTRACT

There are about 600 islands in Hainan province and most of them consist of coral reef. Till 1995 there are 7 nature reserves related to coral reef of which total area is 2.45 millions ha. In this paper we describe the present situation, successes and lessons in nature reserves management.

INTRODUCTION

Hainan Province is located in the most southern part of China and combined by Hainan Island and islands, shoals, sea territory in South China Sea. Its land area is about 34,000 km² and sea area is about 2 million km² which take 2/3 sea area of China. Hainan Coast line is about 1,800 km long. In Hainan coast there is about 300 km of fringe coral reef. In South China Sea, almost all islands consist of atoll coral reef. Because these coral reefs benefit fishery, coast and island protection, bio-environment and tourism, it is very important for us to protect and properly use this area. From 1980, 7 nature reserves have been set up in Hainan. Following the economic boom after 1988 set up province in Hainan, the nature reserve management is more complex and important.

SURVEY OF HAINAN CORAL REEF NATURE RESERVES

Till 1995 there are 7 nature reserves related to coral reef ecosystem protection in Hainan. Among them one belongs to national level, four to provincial, one to county and one to city. These reserves total area is about 2.45 million ha., of which 50,000 ha. is distributed around Hainan island. These nature reserves are distributed from 15 to 20 N latitude. Regional annual average water temperature is in 24-27.5° C and salinity is 31-34. Tidal range is 1-2m and wave height is about 1 m. Sea water transparent in this region is among 5-30m. Water quality is good and with reef and rock in the bottom. The 7 nature reserves are:

1. Sanya coral reef national nature reserve (national)

Set up in 1990. Area is 8,500 ha. and including Sanya near shore fringe reef and 6 coral reef islands. Mainly protect fringe coral reef and its ecosystem. Hard coral and soft coral is widely distributed along the coast and island. Now some zones are protected well and some are destroyed before protection.
2. Sanya Dadonghai coral reef nature reserve (city level)

Set up in 1989. Area is 13.45 ha. Mainly protect fringe coral reef and its ecosystem. Now damage still happened. Main coral is hard coral.
3. Lingao coral reef nature reserve (county level)

Set up in 1986. Total area is 32,400 ha.. Mainly protect Pinctada Maxina ecosystem including coral reef. Coral reef in this area is comparatively sparse. Only hard coral exists in this area.
4. Wenchang Baohu Kylin nature reserve (provincial level)

Set up in 1983. Area is 2,500 ha. Mainly protect Kylin ecosystem which is in coral reef zone. Now this zone coral reef suffered serious damage.
5. Wenchang Tongguzui Kylin nature reserve (provincial level)

Set up in 1983. Area is about 4,000 ha.. Mainly protect Kylin ecosystem which is in coral reef zone. Hard coral is the main coral in this area and coral reef suffered some damage.
6. Qionghai Kylin nature reserve (provincial level)

Set up in 1983. Area is about 2,500 ha. Mainly protect Kylin ecosystem and coral reef. Hard coral is dominant in this area and protected well.
7. West, south and middle sand islands nature reserve (provincial level)

Set up in 1980. Area is about 2.4 million ha. Located in west, south and middle islands and their surrounding area. Coral reef and some special species are the main protected resources. Hard coral and soft coral are widely distributed. Now suffer some damage.

Among the 7 nature reserve areas, reserve 1, 6, 7 ecosystem and scenery protected better than other reserve zone.

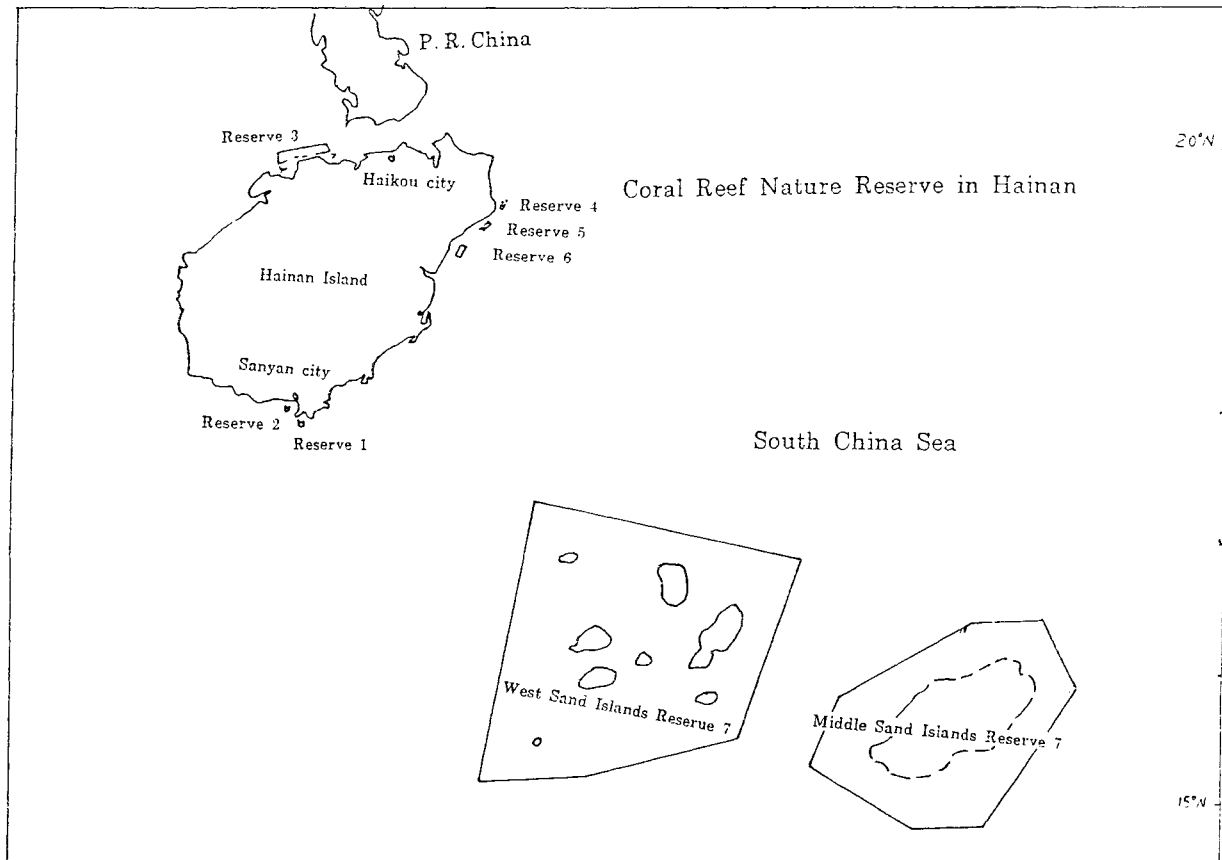


Table: Nature Reserve Related to Coral Reef

Reserve Zone Number	1	2	3	4	5	6	7
Location	Sanya Near shore	Dadong Bay	Lingao county	Wenchang county	Wenchang county	Qionghai city	West, middle, and south sand island
Area (ha)	8,500	13.45	32,400	2,500	4,000	2,500	2.4 million
Protect aim			<i>Pinctada maxina</i>	Kylin	Kylin	Kylin	Special species
Biosystem	Coral	Coral	Coral	Coral	Coral	Coral	Coral
Start time	1990	1989	1986	1983	1983	1983	1980
Admin Office	Hainan Marine Dept.	City Environment Protection	Fishery Administration Bureau	same as 3	same as 3	same as 3	same as 3
Status	Some degreee of damage	same as 1		Seriously damaged	Same as 4	Protected well	Some degree damage
Research	Coral species investigation Coral transplantation					Kylin transplantation	Biological investigation
Utilization	Biosystem tourism education	Education	Seed of <i>Pinctada Maxina</i>			Kylin culture	Fishery capture and scenery tourism
Planning Fulltime supervisor	yes 1996 yes <20	no no	no no	no no	no no	no yes <20	no yes <20

THE RULE AND ITS IMPLEMENT IN THE NATURE RESERVES

1. Main rules related to the nature reserve:

a. Nature reserve regulation of People's Republic of China. Passed by state council committee in Sept. 1994 and implement from Dec. 1st 1994. This regulation includes five chapters:

Chapter one:	General rule
Chapter two:	Construction of nature reserve
Chapter three:	Management of nature reserve
Chapter four:	Legal duty
Chapter five:	Supplementary articles

b. Marine nature reserve management measure. Approved by State Science and Technology committee in May 1995 and implemented on May 29th 1995.

c. Hainan province nature reserve management regulation.

d. Sanya city bulletin on coral reef nature reserve protection. In these rules, there are three main function zones in nature reserves. First is core zone. In this zone, except the special approved scientific research, all other activities are forbidden. Second is buffer zone. In this area we can do some approved activities such scientific research and education, viewing etc. Third is experiment zone. In this area we can do tourism,, aquaculture and research activities.

2. Rule Implement and management

- a. Master plan and EIA before development.
- b. Ship cruiser
- c. Fish boat check by Fishery Administration.
- d. Marine monitoring: by ship, airplane, station and buoy
- e. Public supervise network
- f. Market control: ban to sell coral in market
- g. Coral reef ecosystem science research

PLANNING AND RESEARCH IN THE NATURE RESERVE

1. Planning

Till now only a part of reserve zone I (Sanya coral reef nature reserve) has been made a planning. This plan is mainly on the preservation and sustainable development of coral reef ecosystem and we will discuss it later.

2. Research

- a. Reserve zone 1 (Sanya): on coral transplantation, coral reef ecosystem investigation, water quality monitoring, coral species investigation
- b. Reserve zone 2 (Dadonghai): coral reef ecosystem and coral scenery investigation
- c. Reserve zone 3: Pinctada Maxina culture research
- d. Reserve zone 4: Kylin culture research
- e. Reserve zone 5: Kylin culture research
- f. Reserve zone 6 (Qionghai): coral scenery research and Kylin culture research
- g. Reserve zone 7: have done synthetic research on resources and its environment

3. Research result

- a. Zone 1: There are distributed over 200 species soft and hard coral in Sanya near shore. This coast coral reef belongs to fringe reef. The beautiful crowded hard and soft coral zone is distributed separately in 2-6m and 79m depth. Also in these zones distributed hundred species of coral fishes. In 1993 we have made coral transplantation test in this zone. We transplant 18 species madreporaria and 1 hydrozoan. The coral alive rate reach 94% and grow well.
- b. Zone 6: This area distributed a long band dense fringe hard coral reef in 2-6m depth. We estimate the hard coral species are over 100.
- c. Zone 7: The hundreds islands and reefs are scattered in about 0.5 million km² sea areas. All the coral reef is atoll reef. There are about 500 coral species and several hundred angel fishes.

OUTLINE OF YALONG BAY PLANNING (IN RESERVE 1)

Yalong bay is in the east coast of Sanya city and also a part of Sanya state coral reef nature reserve. Its reserve area is about 9 km² where located in the 40 km² area Yalong bay. From 1995 to 1996, we have made a preservation and development plan for this zone. In this plan we have consider:

- a. Master plan of Yalong bay
- b. Regional social and economic development
- c. Marine nature condition
- d. Biologic distribution and biosystem environment
- e. Other countries related information as a reference

1. The principle of the plan

- a. Bioeconomic principle
- b. Integrate principle
- c. Sustainable principle
- d. Selecting principle
- e. Feasibility Principle compare to economic development

2. The rule this plan rely on:

- a. People's Republic of China Nature Reserve Regulation
- b. Marine Nature Reserve Management Rule of China
- c. Hainan Nature Reserve Management Regulation
- d. State council, State Oceanic Administration and Hainan marine

Department Document on Yalong Bay Nature Reserve

3. Zoning plan

In this plan we divide this area into Three zones:

- a. Core Zone: protect coral and its ecosystem. Ban to human activities except special approve. This zone takes about 5% of total reserve area.
- b. Buffer Zone: buffer area for core zone. In this area human activities are limited. Generally this area takes 5 -1 0% of total reserve area.
- c. Experiment zone: in this area we choose tourism, research and education as the main sustainable development activities. Also we make a function plan in this area.

4. Function plan

In experiment zone, according to different use, we put 5 subfunction zones as below:

- a. Management zone- for management use. Such as port, monitoring station.
- b. Tourism zone: for tourism use. Such as diving, subsea boat touring and snorkel.
- c. Scientific research and education zone: for research and public education.
- d. Reservation zone: to reserve some area for future use.
- e. Defense zone: area for military use.

The main functions in this area are preservation, tourism, scientific research and education. We also give the preservation plan and phase one program in the near five years. At last, we suggest to set up a marine park in this area and give out the implement way.

RESERVE ZONE UTILIZATION

The 7 nature reserve zones main utilization function is different as follow:

- a. Reserve 1: Main utilization function is tourism, preservation, science research and education. In the near future we will begin subsea viewing, diving, islands tour, coral transplantation, marine animal culture test, science research and education activities. It is about 1 million tourists in this area per year.
- b. Reserve 2: Main function is tourism, science research and education. Will begin snorkel viewing, coral transplantation test and middle school marine education. It is over ten thousand tourists in this area per year.
- c. Reserve 3: Main function is Pinctada Maxima protection and culture.
- d. Reserve 4-5: Main function is Kylin culture and coral reef reform.
- e. Reserve 6: Main function is Kylin culture, coral viewing, science research and education. It is about 3 to 5 thousand tons Kylin production from this area. Coral tourism will begin in the near future.
- f. Reserve 7: Main function is fishery and tourism. The fishery production in this area is over 300,000 tons per year.

SUCCESS, LESSON AND SUGGESTION

1. Success

For some reserve zone protect well, the success experiences are:

- a. Pay attention to reserve zone planning
Such as reserve I start regional planning and EIA before development.
Control random human activities.
- b. Enforce the executive force
Including team and equipment construction. For example, Yalong bay in reserve 1 with its 9 km² area has four motor ships and 7 persons to start local management. They do 24 hours cruiser watching this reserve.
- c. Introduce public activities to the main function of the reserve
Government of the reserve zone not only manage and supervise this area, but also introduce enterprise and local people do production activities to the main function of this reserve zone. For example, in reserve 6 the reserve station also set up a Kylin product processing plant. This promote local people to culture Kylin and protect the coral reef.
- d. Propagate and education
In TV and broadcast propagate the importance of marine reserves and environment protection to public, government official and student. Announce bulletin of reserve management. Also put marine knowledge education into the middle school course.

- e. Enforce environment monitoring and public supervise net work
- f. Integrate management: Such as management from production to market.

2. Lesson

- a. Manage office is not unified such as different reserve management under different department. Management unit is not perfect and this affect executive force. For example, some reserves have not full time officer to manage the area and can not take in time treatment to the damage activities in reserve area.
- b. Some reserve zones have not combined management with the main utilization function of the reserve. Have not create condition to introduce public product activities. For example, in reserve 3 and 4 have not introduce and manage well, local people main activities are to dig coral for ornament sell and construction material. This bring the ecosystem heavily damaged.
- c. Budget shortage, can not equip enough management team and equipment.

3. Suggestion

- a. Unified the management of the marine nature reserve. Set up perfect management unit and strengthen the executive force.
- b. Make regional preservation and development plan and EIA before utilization.
- c. Use the reserve to support reserve and solve the management funds shortage. Such as use the zone main utilization function to carry out proper activities and replenish management money shortage.
- d. Perfect the public supervise network
- e. Perfect integrate management from production to market
- f. Take international exchange and corporation. Learn advanced experience from other country.

REFERENCE

Allen, G. R. and R. Steene. 1994. Coral reef. In: Tropical Reef Research. Singapore.

Hainan Islands Resources Investigation Team. 1996. Hainan islands resources investigation report. Beijing: China Marine Press.

Hainan Marine.Department. 1992. Hainan marine function plan. Beijing: China Marine Press.

Wang, L. and W. Daoru, etc., 1996. Yalong bay nature reserve protection and development plan (interior report of HMDPDI).

Wang, L. and C. Gang, etc., 1995. Sanya subsea tourism scenery investigation and research report (interior report of HMDPDI).

Zou R. L., 1995. The research status and conservation strategy of coral reefs in China. In: Advances in biodiversity Research. Beijing: Chinese Science and Technology Press.

SEA-LEVEL CONTROLLED SEDIMENTATION ON A CARBONATE RAMP - SOUTHERN GREAT BARRIER REEF, AUSTRALIA.

Alexa Troedson and Peter J. Davies

University of Sydney
Sydney, N.S.W., AUSTRALIA

ABSTRACT

A post-last glacial change from siliciclastic to carbonate-dominated sedimentation on the upper slope of the Southern Great Barrier Reef is related to both a reduction in the clastic sediment source, and an increase in carbonate sediment accumulation. This change occurred 11ka ago during the middle of the post-glacial transgression. Regional sea-level curves suggest that sea-level was probably between -42 and -52m at that time. Seaward of 50-60m deep, the margin gradient changes from near-horizontal to $>2^\circ$ in this region. The observed facies change is believed to reflect a rapid switch-off of the seaward transport of siliciclastics, and switch-on of shelf carbonate production, in response to the change in margin morphology resulting from sea-level transgression across this change in gradient. We suggest that the response of upper slope facies to sea-level change is dependent on margin morphology, and that facies boundaries will therefore be diachronous between localities.

INTRODUCTION

The continental margin of the Great Barrier Reef region is commonly classified as a rimmed carbonate platform (Maxwell, 1968). However, the southernmost Great Barrier Reef is an exception and is defined instead, by us, as a distally-steepened carbonate ramp. In that region the continental shelf is greater than 70km wide, the shelf-break is poorly defined, and the reefs of the Capricorn-Bunker Group form isolated structures on the mid to outer shelf, rather than creating a significant outer shelf barrier (Fig. 1). The first expression of the shelf-break in the region occurs approximately 10km seaward of these reefs as the western edge of the Capricorn Channel, an outer shelf to upper slope embayment. While the surface sediments and seismic stratigraphy of the Channel have been documented previously (eg. Marshall, 1977), no sub-surface sampling had been carried out in the Channel prior to this study.

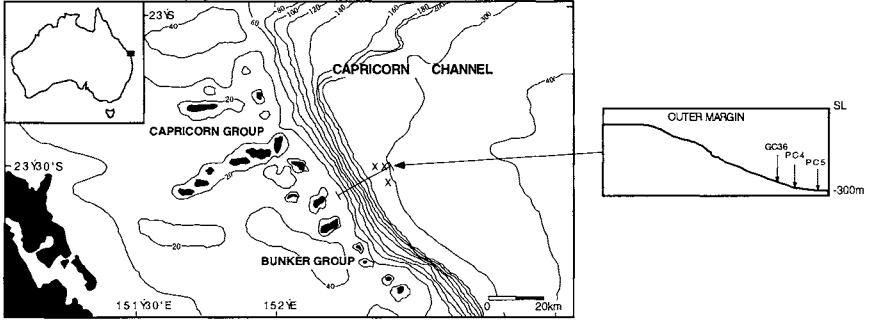


Figure 1. Bathymetric map of the Southern Great Barrier Reef region. Core sites are shown as crosses on the map, and arrows on the cross-section.

Data from three representative cores from the western Capricorn Channel floor is presented in this paper, to illustrate the relationship between sea-level and upper slope sedimentation on a carbonate ramp within the Great Barrier Reef province. The cores were collected in water depths of 251 to 281 metres in the localities listed in Table 1. Core 105GC36 is a gravity core, while JK/PC4 and JK/PC5 are piston cores. The data presented here includes carbonate content, magnetic susceptibility and grainsize variations, and 10 AMS radiocarbon dates. Oxygen-isotope data is also presented for one core. This paper focuses on the post-last glacial maximum sediment record (ie. post 20-18ka) as, for that period, radiocarbon dating is reasonably precise and regional sea-level curves provide some constraints on sea-level magnitude. Rapid global eustatic sea-level rise from ~-120m to present sea-level occurred within that time (Fairbanks, 1989).

Table 1. Core details

Core	Latitude	Longitude	Depth (m)	Length(m)
105GC36	23°30.0S	152°17.4E	251	3.0
JK/PC4	23°33.0S	152°20.2E	271	2.4
JK/PC5	23°30.0S	152°18.3E	281	2.5

RESULTS

The core locations are shown in Figure 1. GC36 was collected from the Capricorn Channel flank in 251m of water. Some sedimentological data from this core is presented in Figure 2. The sediments are a mixture of siliciclastic material and biogenic carbonate. In general, carbonate content varies between 30% and 70%, and sediment texture varies from sandy-mud to muddy-sand. The carbonate fraction includes a mixture of pelagic, autochthonous benthic, and shelf-derived benthic material. A major feature of this core is a gradational down-core transition from carbonate to siliciclastic-dominated sediments between 90cm and 120cm. This transition is evident in both the carbonate content variations (especially mud fraction carbonate), and the magnetic susceptibility signal, which is essentially an insoluble sediment proxy in this locality. Six radiocarbon dates provide good age control for this core. The dates indicate that the magnetic susceptibility peak at 200cm coincides approximately with the last glacial maximum (17-19ka BP), and that the facies transition from 90-120cm occurred between 9.6ka and 12.8ka.

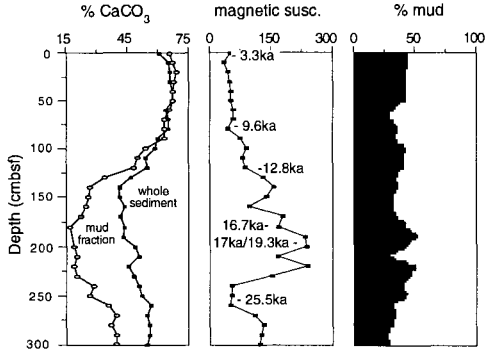


Figure 2. Carbonate content, magnetic susceptibility and mud content data from GC36.

PC4 was obtained from the base of the Channel flank in a water depth of 271m. This core contains two carbonate content/magnetic susceptibility facies cycles (Fig. 3). A corresponding cyclicity is also evident in the oxygen-isotope signal ($\delta^{18}\text{O}$) obtained from the planktonic foraminifer *G. ruber*. The relatively high $\delta^{18}\text{O}$ values in the low carbonate beds suggest that these were deposited during glacial periods. Radiocarbon dates confirm that the upper low carbonate bed was deposited during the last glacial period, and that deposition of the core-top high carbonate bed began ~11ka ago.

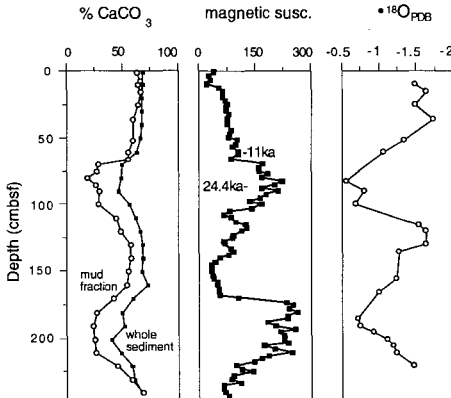


Figure 3. Carbonate content, magnetic susceptibility and oxygen-isotope data from PC4.

Lithofacies, chronostratigraphic data and magnetic susceptibility variations for GC36 and PC4 are illustrated in Figure 4, together with some additional data from a third core, PC5. A date of 10.7ka BP was obtained from the base of the core-top, carbonate-dominated facies in PC5. Therefore an age of ~11ka BP can consistently be inferred for the post-last glacial transition from siliciclastic to carbonate-dominated sedimentation in this locality.

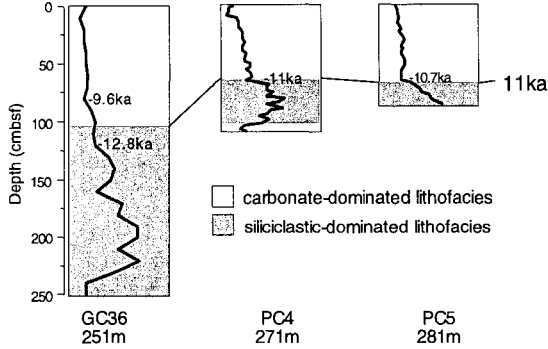


Figure 4. Lithofacies, chronostratigraphic data and magnetic susceptibility variations for each core. The consistent 11 ka age of the facies change is evident.

To determine the controls on sedimentation in the region, it is necessary to understand the nature of variations in sediment flux through time. GC36 contains a continuous relatively high resolution record, and has a well-constrained age model. Figure 5 illustrates variations in carbonate and insoluble mud accumulation rates calculated for this core ($\% \text{carbonate} / \text{insoluble mud} \times \text{sedimentation rate} \times \text{dry bulk density}$). The data is smoothed and plotted against age, and clearly indicates that the facies change at $\sim 11 \text{ ka BP}$ is related to both a decrease in insoluble mud accumulation rate, and an increase in carbonate mud accumulation rate.

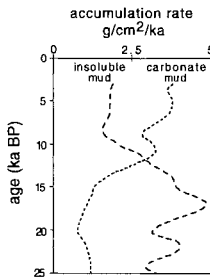


Figure 5. Variations in carbonate and insoluble mud accumulation rate in GC36.

DISCUSSION

The results indicate that a major post-glacial facies change occurred at 11 ka BP. This was a time of rapid eustatic sea-level rise, and corresponds to the middle period of the post-last glacial transgression (eg. Fairbanks, 1989). Thus the siliciclastic-dominated sediments can be associated with a period of sea-level lowstand and early transgression, while the carbonate-dominated sediments were deposited during the late transgression and subsequent sea-level highstand/stillstand (Fig. 6).

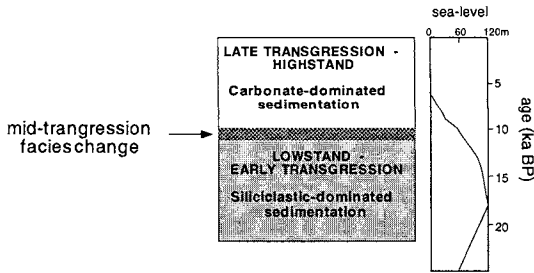


Figure 6. Relationship between last glacial to present stratigraphy and sea-level changes.

The essential differences between maximum highstand and lowstand depositional regimes are illustrated in Figure 7. During sea-level lowstand the shelf is exposed as an alluvial plain, siliciclastic mud can be delivered to the upper slope through fluvial channels, and there is no shallow water carbonate source (Fig. 7a). In contrast, during sea-level highstand shelf carbonate may be transported to the upper slope, contributing to relatively high carbonate accumulation rates (Fig. 7b).

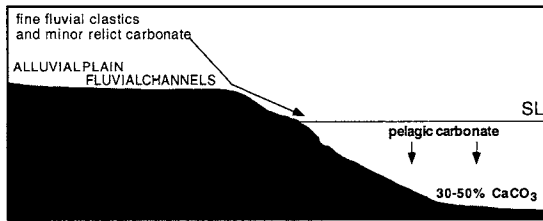


Figure 7a. Cross-section showing main outer margin sedimentary processes and products during maximum lowstand (SL at ~120m).

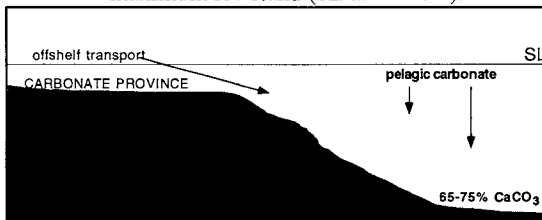


Figure 7b. Cross-section showing main outer margin sedimentary processes and products during maximum highstand.

Two regional sea-level curves have been consulted to determine sea-level position at 11ka BP. A Holocene sea-level envelope for the south-east Australian margin gives a possible upper limit of -36 to -48m (Thom & Roy, 1985), while a recently published curve based on data from the central Great Barrier Reef provides a lower estimate of -45 to -59m (Larcombe et al., 1995). For

the purposes of this discussion a sea-level range of 42-52m has been accepted based on the median points of these two estimates. The relationship of this range to outer margin bathymetry is illustrated in Figure 8.

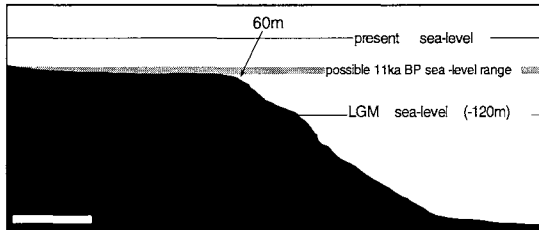


Figure 8. West-east diagrammatic cross-section of outer shelf to upper slope bathymetry showing present sea level, LGM sea level and possible sea level range at 11ka BP. The white bar represents 3 km.

This indicates that, by 11ka BP, the sea had transgressed the flank of the Capricorn Channel (which has a gradient of 2-3°), and was starting to flood the near-horizontal shelf. We propose that the upper slope facies change is a response to sea-level transgression across this change in shelf gradient. The change in shelf morphology, combined with a rapid landward shift of the coastal zone would have greatly reduced the amount of clastics delivered to the slope, and allowed expansion and colonisation of the shelf by carbonate producers. If, as we suggest, margin morphology exerts a critical control on upper slope facies patterns, the boundaries between such facies will be diachronous between localities so cannot be used for regional correlation.

CONCLUSIONS

The main findings of this study are as follows:

- (1) Sea-level variations regulate the flux of both terrigenous and carbonate sediment into the Capricorn Channel, and have resulted in cyclic variations from low carbonate to high carbonate facies. Highstand sedimentary processes include seaward transport of carbonate sediment from the shelf. During lowstand conditions there is an increase in detrital input to the Channel, and carbonate accumulation decreases due to sub-aerial exposure of the shelf carbonate source region.
- (2) A transition from siliciclastic to carbonate-dominated sedimentation occurred in the Channel at ~11ka BP. Thus the siliciclastic-dominated facies is associated with sea-level lowstand and early transgression, the carbonate-dominated facies is associated with late transgression and highstand, and the major facies change is associated with the mid-transgression. This situation differs from the sequence stratigraphic model which predicts the development of distinct lowstand, transgressive and highstand deposits.

(3) The 11ka sedimentary change can be related to a change in shelf morphology associated with sea-level transgression. This demonstrates the importance of local factors in controlling upper slope facies development. Furthermore, it suggests that the boundaries of rhythmically-bedded slope facies may be diachronous even within a single basin.

ACKNOWLEDGMENTS

The gravity core GC36 was collected on a research cruise jointly sponsored by the Japanese National Oil Company (JNOC) and the Australian Geological Survey Organisation (AGSO). The AMS radiocarbon dates quoted for this core were obtained by JNOC scientists. This paper is a contribution to IGCP Project no. 396 'Continental Shelves in the Quaternary'.

REFERENCES

- Fairbanks R. G., 1989. A 17,000 year glacio-eustatic sea level record: Influence of glacial melting rates on the Younger Dryas event and deep-ocean circulation. *Nature* 342: 637-642.
- Larcombe, P., Carter, R.M., Dye, J., Gagan, M.K. and Johnson, D.P., 1995. New evidence for episodic post-glacial sea level rise, central Great Barrier Reef, Australia. *Marine Geology* 127: 1-44.
- Marshall, J. F., 1977. Marine Geology of the Capricorn Channel Area. BMR Bull. 163, 81pp.
- Maxwell, W.G.H., 1968. Atlas of the Great Barrier Reef. Elsevier, 258pp.
- Thom, B.G., & Roy, P.S., 1985. Relative sea levels and coastal sedimentation in southeast Australia in the Holocene. *J. Sed. Pet.* 55: 257-264.

SUBMERGED SHELF-EDGE REEFS, CORAL REEFS, GREAT BARRIER REEF AUSTRALIA

D. Hopley, T.L. Graham*, C.E. Rasmussen
Sir George Fisher Centre, James Cook University of North Queensland
Townsville, Australia

* currently Australian Geological Survey Office, Canberra, Australia

ABSTRACT

Submerged shelf-edge reefs have been described from many areas of the world and their formation and probable demise has been attributed to changing water quality including temperature, the effects of hurricanes, and stepped sea-level rise.

On the Great Barrier Reef, shelf-edge submerged reefs are relatively common. Detailed examinations have been undertaken of a small area, off Moss Reef, on the North Central Great Barrier Reef. Two submerged parallel systems have been studied using seismic profiling, and sediment grab sampling. The deepest system on the shoulder of the continental shelf is in approximately 70m water and observations have indicated that it is almost entirely dead, though constructed by shallow water assemblages.

The shelf-edge reefs are complex features predating the post-glacial marine transgression during which they were recolonised for a short period. Sediment shed from upslope reefs, decline in water quality and rapid sea-level rise all appear to have played a part in reducing the structures to effectively fossil reefs capped by only a few slow growing fragile hermatypic corals.

INTRODUCTION

Submerged coral reefs located on the edge of continental shelves or close to the drop off zones off oceanic islands and banks, have been recognised from many different areas of the world. The uppermost level of these reefs is often tens of metres below present sea-level and in some instances more than 100m below. For this reason without direct evidence they are often presumed to be dead, although it would appear that this is not always so. Because of their location, little is known of the age or evolution of these submerged reefs.

On the Great Barrier Reef shelf-edged submerged reefs are probably more ubiquitous than previously thought. Detailed examinations have been undertaken of one of these reefs, near Moss Reef on the North Central Great Barrier Reef, and the results of these surveys are examined in the light of the previous literature.

LOCATION OF SUBMERGED SHELF-EDGE REEFS

The majority of reports of submerged shelf-edge reefs come from the Caribbean in general (Macintyre, 1972 and 1988) and more specifically Florida (Lighty, 1977; Lighty *et al.*, 1978 and 1979), Barbados (Macintyre, 1967; Ott, 1975; Macintyre *et al.*, 1991), Jamaica (Goreau and Goreau, 1973; Goreau and Land, 1974), Belize (James and Ginsburg, 1979, Burke, 1982), St Croix (Adey *et al.*, 1977; Hubbard *et al.*, 1986) and Grand Cayman (Rigby and Roberts, 1976; Blanchon, 1995).

However, the first description and partial mapping of a submerged reef system occurred on the Great Barrier Reef (Paradice, 1925; see also Hopley, 1982). Paradice and later Fairbridge (1950) noted that submerged linear reefs are common between Cairns and Townsville where narrow shoals parallel to the shelf-edge appear to be a drowned continuation of the more northerly ribbon reefs which form a continuous barrier north of Cairns. They noted that the depth of the shoal is generally between 35-50m and is very persistent. Further work (Harris and Davies, 1989; Hopley, 1995; and recent 1:250000 bathymetric maps, Division of National Mapping, Canberra) have indicated that the distribution of these reefs is even greater than formerly thought. What appear to be single linear submerged features, extend along the shelf-edge from Townsville southwards. Outside the Pompey Complex Reefs of the South Central Great Barrier Reef more complex parallel sets of submerged reefs are located at and just behind the shelf-edge. Further, submersible surveys outside the ribbon reefs (Ribbon No. 5) by this author and colleagues (CVG Phipps and PJ Davies) in 1984 discovered submerged -50m and -70m reefs on even this very steeply sloping continental shelf margin.

This paper concentrates on an area of shelf-edge reefs located outside Moss Reef (17° 57'S) 140km north of Townsville and just south of the area which Paradice originally mapped in the 1920s. These reefs are also within the area chosen by one of us (TLG) as part of a more extensive geological and geomorphological study which included extensive continuous seismic profiling and is written up as a PhD thesis (Graham, 1993).

WHY A PREFERENTIAL SHELF-EDGE LOCATION FOR REEFS?

There is little disagreement in the literature that at the margins of topographic highs or at the top of drop-offs, hydrological conditions are very suitable for the initiation and growth of coral reefs. However, many different reasons have been given for the formation of such topographically favoured locations on shelf margins. For example, Graham (1993), suggested that erosional or depositional terraces of earlier interstadial ages may have formed the favourable topographic features from which the Great Barrier Reef shelf-edge reefs rise. On Grand Cayman the seaward sloping nature of the shelf terraces and the landward sloping nature of emergent reef formed terraces has suggested to Blanchon and Jones (1995) that there is a genetic relationship between the sea-level cycle and terrace forming processes. During sea-level rise episodes bedrock terraces are cut by erosion and marine planation, whereas during falling sea-levels sedimentary terraces are formed by reef accretion.

Formation of such terraces will be aided by an appropriate regional slope which is neither too shallow nor too steep and such geometry is found frequently on the shoulder of the continental shelf or on the edge of oceanic islands and banks. Harris and Davies (1989) suggested that the Central Great Barrier Reef has such appropriate shelf geometry whereas the Northern Great Barrier Reef is generally too steep for the formation of significant terrace features and therefore lacks significant submerged reefs apart from the small features described, for example, on the outside of Ribbon No. 5.

Terrace formation will be reinforced topographically if the level of the terrace coincides with a stillstand in sea-level, particularly during the post-glacial transgression. Such a mechanism has been suggested, for example, by Carter and Johnson (1986) for the level of submerged reefs along the Great Barrier Reef. However, as Harris and Davies (1989) have noted, even within relatively small areas there may be a lack of correlation in the depth/height of submerged features which suggests that sea-level alone may not be responsible for their location. Indeed, they have suggested that some reefs at least may be associated with shelf-edge rotational fault scarps. Given the wide range of depths from which shelf-edge reefs are reported world wide, the variable shelf geometries on which they are found and the differences in the size and morphology of the reefs, it is likely that there are multiple reasons for location of submerged shelf-edge reefs.

REASONS FOR DROWNING AND/OR PRESUMED DEMISE OF SHELF-EDGE REEFS

The simplest explanation for the deaths of the submerged shelf-edge reefs has been drowning during the earlier part of the post-glacial transgression when the rapid rise in sea-level, greater than 15mm a year, was too fast for reef growth to keep up (i.e. Carter and Johnson, 1986). In some instances it appears that shallow-water hermatypic corals have been succeeded by deep water biota dominated by sponges and ahermatypic corals as described in Barbados by Macintyre *et al.* (1991). Obviously once this community change has taken place the reefs ability to grow upwards is even further handicapped.

Probably the most popular explanation for the demise of shelf-edge reefs has been a decline in water quality as sea-level has crept up over the continental margin and onto the continental shelf. The death of the shelf-edge reefs has variously been referred to as "being shot in the back by your own lagoon" (Neumann and Macintyre, 1985) or "killed off by inimical bank waters" (e.g. Schlager, 1981). Hallock and Schlager (1986) attribute the demise of these reefs almost entirely to eutrophication due to release of nutrients from a submerging shelf at a time when sea-level was still rising rapidly. At high latitudes these shelf waters in winter may also have been too cool for reef growth in comparison to the deep oceanic water outside the reefs. However, Marshall (1988) has suggested that changes to upwelling patterns at the shelf-edge after the shelf is flooded may also have produced decreases in temperature and increase in nutrients through the rise of deep oceanic water sufficient to kill off these shelf-edge reefs.

Other explanations may have a more local application. Goreau and Land (1974) and Blanchon (1995) have suggested that as sea-level rises and reefs grow upslope of the shelf-edge structures,

sediment from the higher reefs will rain down on the lower reef causing its demise (clastic control). For some higher shelf-edge reefs Blanchon (1995) suggests that the upper limit of growth is limited by the trimming action of low frequency hurricane waves. As with reasons for the location of shelf-edge reefs their demise, where it can be demonstrated, is probably due to a number of causes.

THE MOSS REEF INVESTIGATION

So far, two research cruises have been dedicated to the examination of submerged reefs to the seaward of Moss Reef on the Great Barrier Reef (Figures 1 and 2). A number of methodologies have been applied and results, although preliminary, help to explain the age and the evolution of these reefs.

Echo-sounding

A series of echo-sounding traverses were undertaken between Moss Reef and the shelf-edge normal to the shelf margin and finishing in water depths of more than 200m. Two of these transects are shown in Figure 1. The shelf margin is located approximately 6km seawards of the outer edge of Moss Reef. The first of the submerged reefs occurs approximately 3.5km seawards of Moss Reef and is separated from it by relatively flat sea floor, approximately 70m deep. This first reef, approximately 1km wide is a very persistent feature on this part of the shelf and rises to within a few metres of present sea-level although nowhere breaking the surface. In places it is as much as 55m below present sea-level (see Figure 2).

Two kilometres to seawards of this is the shelf-edge proper and here a smaller but also persistent reef occurs, rising from a depth of approximately 70m, to approximately 45m below the present sea surface. A smaller but deeper reef appearing only as a pinnacle on the echo-sounding traces is found to seawards. From its base at ca.80m depth the shelf slopes away with an average gradient of approximately 1 in 20, although there are also terrace like features, particularly at approximately 90m, 100m and 120m depth.

Remotely Operated Vehicle (ROV) Observations

The ROV investigations were particularly enlightening. They indicated that:

- the sea floor between Moss Reef and the inner submerged reef is a monotonous sediment covered relatively flat surface;
- the inner submerged reef has a luxurious cover of living coral, even at depth;
- the area between the first and second submerged reefs is relatively flat but containing areas of coral rubble;
- the outer submerged reefs are largely dead, i.e. with only a few living corals on the summits of the reefs; and
- the terraces on the upper reef slope are much less distinctive as visible features and are largely sediment covered.

MOSS REEF

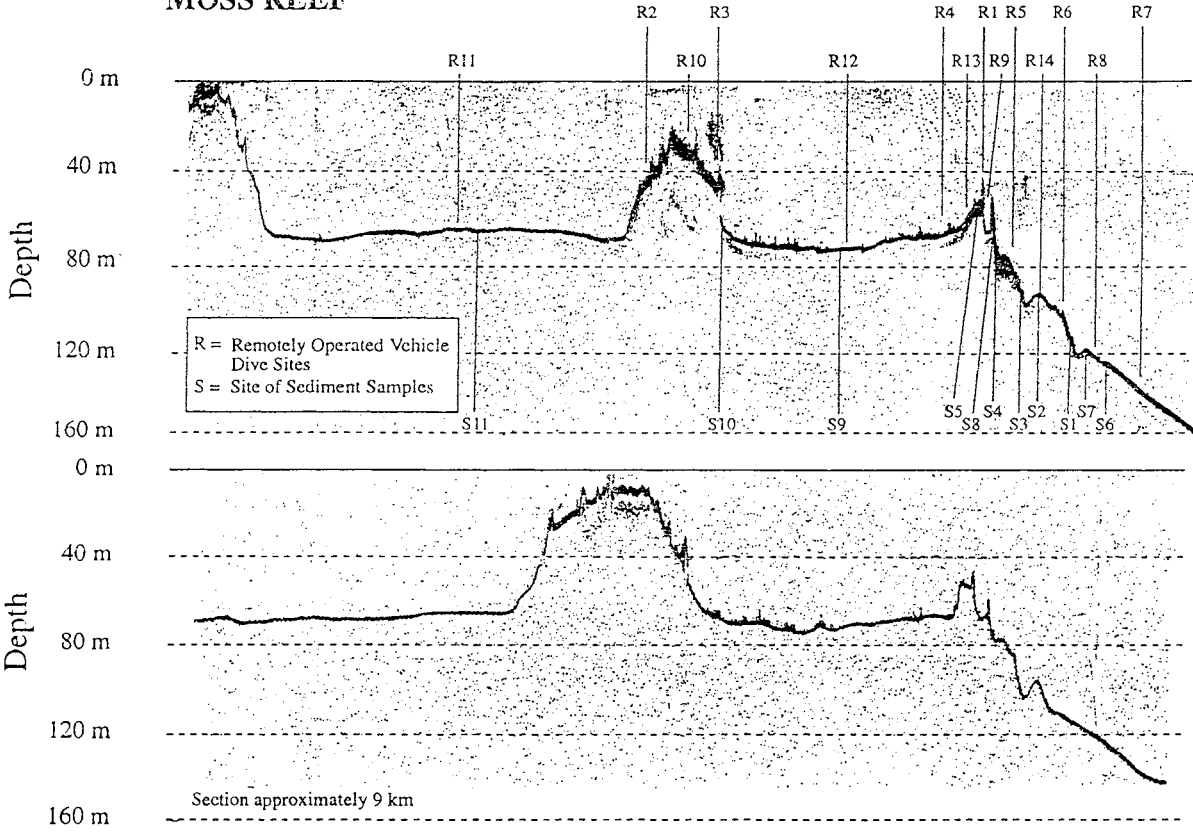


Figure 1. Moss Reef profiles and research sites. Horizontal scale is approximately 9km

Seismic Profiling (Figure 2)

Figure 2 is but one of a series of seismic profiles which provide information on the shelf-edge reefs, most are north of Moss Reef and the conclusions given below are taken from all data available (Graham, 1993):

- The modern shelf marginal and immediate pre-modern submerged shelf-edge reefs generally grow from more extensive older carbonate platforms actually buried under a shallow sediment cover.
- Reef initiation appears to have been favoured on the edge of steep dropoffs such as on the margin of older carbonate platforms or erosional features, but particularly on the continental break-of-slope.
- The upper continental slope and shelf-edge reefs display a complex history of both growth and erosional notching and planation, with erosional terraces becoming the preferred site of reoccupation in subsequent sea-level rise events. Shelf-edge reefs are clearly multi-cyclic. The most recent (Holocene) phase of growth is represented by a veneer of pinnacles, which is probably a characteristic mode of growth for these reefs as they are stranded by rapidly rising sea-level events.
- The clastic control of reefs of Goreau and Land (1973) is clearly shown in a number of instances on the shelf margin, reef pinnacles clearly being inundated by sediments from upslope.
- A hypothesis for the parallel lineation of submerged reefs observed inside the present shelf-edge group is that they have preferentially occupied the top of an erosional scarp formed during a previous sea-level stillstand.
- Interpretation of past sea-levels from the morphological and seismic data is extremely complex. Many features are a combination of erosion and depositional episodes with the evidence actually related to a particular sea-level often buried beneath the present surface.

Sediments and Grab Sampling

Size and compositional characteristics of the grab samples collected were as expected. Close to the submerged reefs sediments were coarser and of higher carbonate content, becoming finer and largely terrigenous away from the reefs.

Particular attention was given to the samples taken from depths greater than 80m which were largely non-carbonate. These samples were examined to see if any of the fauna they contained was shallow water, i.e. relict fauna. No species were found which would be unusual for the relevant depths and this appears to confirm the thickness of the recent sediment cover as indicated by the seismic surveys.

Of particular interest, however, was a grab sample taken from the top of the outer submerged reef at approximately 50m depth. This sample contained a number of platy living corals including *Oxypora lacera*, *Hydnophora* sp. and *Echinophyllia echinata*. These corals were taken from the upper most surface of the submerged reef, all are hermatypic normally found on protected reef slopes. The ROV observations indicated that such corals were not common on the outer submerged reef and were generally small where they did occur. Their location suggests that they

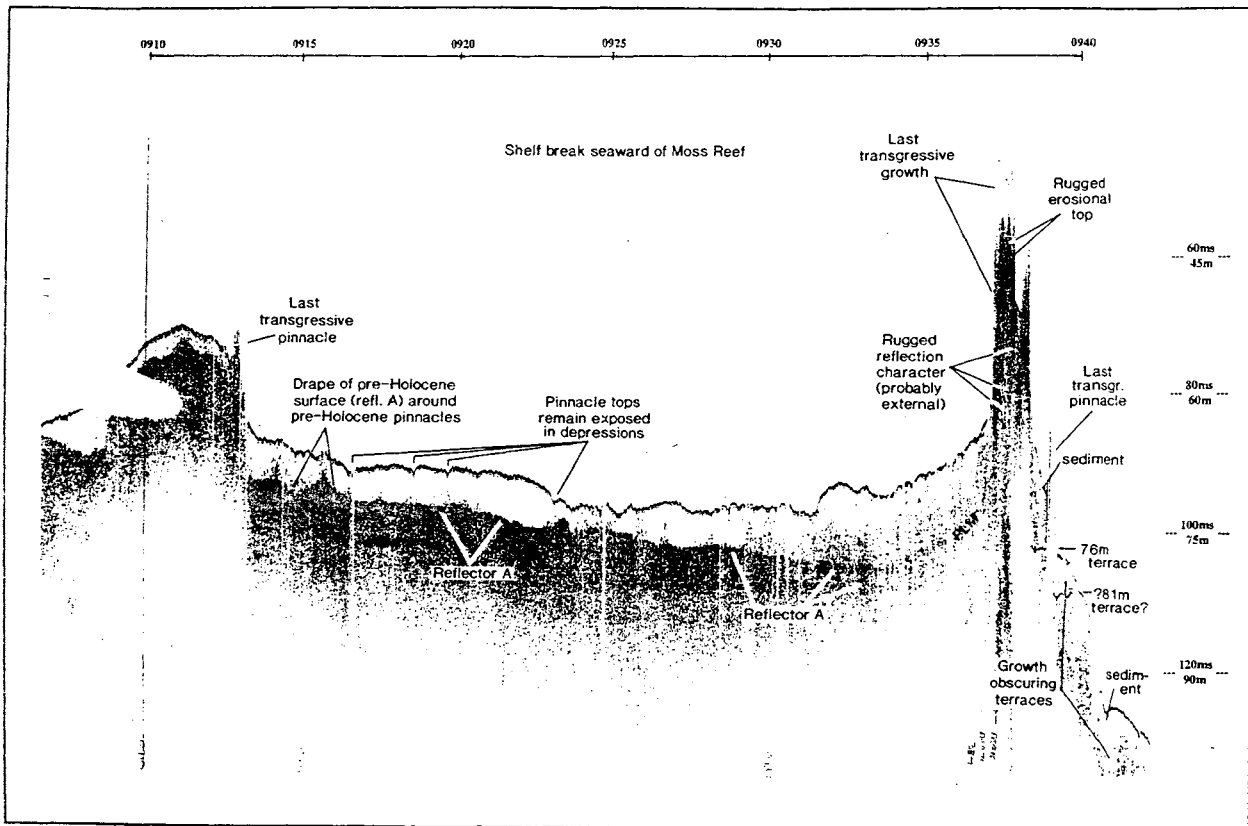


Figure 2. Interpretation of Seismic profile of Moss Reef. Horizontal distance is approximately 4km.

are below normal wave base, however, their small size and the dated rubble (see below) also suggest that very low frequency cyclonic waves may affect depths greater than 40m.

Radiocarbon Dating

Grab sampling failed to retrieve any material which appeared to be framework and which was suitable for radiocarbon dating from the top of the outer submerged reef. However, on the presumption that the rubble slopes on either side of the reef, represented material accumulated there whilst it was an 'active' reef system, three *Acropora* clasts were chosen for dating (Table 1).

Table 1. ¹⁴C Dates

IDENTIFICATION	DEPTH	MATERIAL	UNCORRECTED ¹⁴ C y.B.P.
ANU-10188	-64m	Rubble in front of outer submerged reef	Modern
ANU-10187	-50m	Rubble behind outer submerged reef	250±60
ANU-10189	-50m	Rubble in front of inner submerged reef	1130±60

Unfortunately the ages throw little light on the age of the outer submerged reef. They are however, interesting in that it would appear that the rubble slopes either side of the reef are still accumulating, though probably very slowly. Whilst disintegration of the reef through agencies such as bio-erosion may be taking place it is also possible that the upper most part of this reef is still just within the wave base of the largest cyclonic waves, particularly as the corals on the reef top are extremely fragile. The outer shelf is completely unprotected and significant wave heights for the Coral Sea of 10m or more have been calculated (e.g. Hopley, 1982). At least a small amount of trimming at the present time may be responsible for the maintenance of the depth of shelf-edge reefs along the Great Barrier Reef.

CONCLUSIONS

This has been a preliminary investigation of only a short section of what appears to be a very continuous set of outer shelf submerged reefs on the Great Barrier Reef. Already there is sufficient evidence to suggest that these reefs have a history as complex as that of the main Great Barrier Reef complex. They are not simple features formed only during the post-glacial marine transgression since about 18000 yrsBP. Their origin on what appear to be marine erosional terraces relates to earlier glacial or stadial low sea-levels and their reoccupation during the post-glacial transgression appears to have been for a short period only.

The reason for their demise is also problematic and probably complex. At least locally the clastic control mechanism appears to have resulted in the burying of some shelf-edge reefs but is probably that several mechanisms have been working as sea-level rose quickly through the

depths found at the shelf-edge. Almost certainly, water quality did decline for a number of reasons (see for example Hopley, 1995). Some deep water coral communities appear to have hung on, equivalent to the deep water communities observed in Barbados but they are slow growing and appear to be trimmed back by very occasional cyclonic wave action.

Irrespective of the accumulation of factors that led to the demise of these reefs during sea-level rise, their subsequent inability to continue to sea-level has probably been due simply to the positive forces of the 'reef accretionary ledger' (i.e. coral and algal carbonate growth, plus sediment retention), being outweighed by the negative forces of erosion (i.e. bioerosion, current removal and cyclone wave damage).

Further work is planned on these reefs, in particular, using a portable remotely operated drill (PJ Davies, pers. comm.). We believe that these features can provide important information particularly at a time when many reefs worldwide are under stress, a situation which global environmental change is likely to aggravate. Thus the reasons for the demise of shelf-edge reefs, at times of rising sea-level and poor water quality, may help in determining strategies for future reef management.

There is also direct evidence of sea-level change in the shelf-edge features, which although complex, may be deciphered by further seismic work and most importantly, drilling into the structures. This information will also add to data on the tectonic stability of the shelf margin. Finally, these reefs are important and major structures but have only recently appeared on the first bathymetric maps. They are not included in the inventory of reefs managed by the Great Barrier Reef Marine Park Authority even though they lie within the Marine Park. Already the video from the ROV has indicated that they may contain a flora and fauna very different from the modern reefs of the continental shelf. Questions raised at the present time can only be answered by further research.

ACKNOWLEDGEMENT

The research reported here has been helped greatly by assistance from the Masters and crew of the R.V. 'James Kirby'; the technical input of John Morrison; aid in seismic interpretation from John Marshall and Ron Boyd; in fauna recognition by Peter Arnold; and general assistance from Jeremy Taylor, Robert Fietz and Kay Johnston.

This paper is a contribution to I.G.C.P. Project no. 396 'Continental Shelves in the Quaternary'.

REFERENCES

Adey, W.H., Macintyre, I.G., Stuckenrath, R. And Dill, R.F. (1977) Relict barrier reef system off St Croix: its implications with respect to late Cenozoic coral reef development in the Western Atlantic. In: Proceedings of Third International Coral Reef Symposium, 2:15-21.

- Blanchon, P. (1995) Control on modern reef development around Grand Cayman. Unpublished PhD thesis, University of Alberta, 204pp.
- Blanchon, P. and Jones, B. (1995) Marine planation terraces in the shelf around Grand Cayman: a result of stepped Holocene sea-level rise. *Journal of Coastal Research*, **11**:1-33.
- Burke, R.B. (1982) Reconnaissance study of the geomorphology and benthic communities of the outer barrier reef platform, Belize. *Smithsonian Contributions to Marine Science*, **12**:509-526.
- Carter, R.M. and Johnson, D.P. (1986) Sea-level controls of the post-glacial development of the Great Barrier Reef, Queensland. *Marine Geology*, **71**:137-164.
- Fairbridge, R.W. (1950) Recent and Pleistocene coral reefs of Australia. *Journal of Geography*, **58**:330-401.
- Goreau, T.F. and Goreau, N.I. (1973) The ecology of Jamaican coral reefs II geomorphology, zonation and sedimentary phases. *Bulletin of Marine Science*, **23**:399-464.
- Goreau, T.F. and Land, L.S. (1974) Fore-reef morphology and depositional processes, North Jamaica. In: Laporte, L.F. (ed.), *Reefs in Time and Space*, Society of Economic Palaeontologists and Mineralogists. Special Publication, **18**:77-89.
- Graham, T.L. (1993) Geomorphological response of continental shelf and coastal environments to the Holocene transgression - Central Great Barrier Reef. Unpublished PhD thesis, James Cook University of North Queensland.
- Hallock, P. and Schlager, W. (1986) Nutrient excess and the demise of coral reefs and carbonate platforms. *Palaios*, **1**:389-398.
- Harris, P.T. and Davies, P.J. (1989) Submerged reefs and terraces in the shelf-edge of the Great Barrier Reef, Australia. Morphology, occurrence and implications for reef evolution. *Coral Reefs*, **8**:87-98.
- Hopley, D. (1982) *Geomorphology of the Great Barrier Reef: Quaternary development of coral reefs*. John Wiley, Interscience, New York, 453pp.
- Hopley, D. (1995) Continental shelf reef systems. In: Carter, R.W.G. and Woodroffe, C.D. (eds.), *Coastal Evolution: Late Quaternary Shoreline Morphodynamics*. C.U.P. pp. 303-340.
- Hubbard, D.K., Burke, R.B. and Gill, I.P. (1986) Styles of reef accretion along a steep shelf edge reef, St Croix, U.S. Virgin Islands. *Journal of Sedimentary Petrology*, **56**:848-861.
- Lighty, R.G. (1977) Relict shelf-edge Holocene coral reef: south-east coast of Florida. *Proceedings of the Third International Coral Reef Symposium*, **2**:215-221.

- Lighty, R.G., Macintyre, I.G. and Stuckenrath, R. (1978) Submerged early Holocene barrier reef south-east Florida shelf. *Nature*, **276**:59-60.
- Lighty, R.G., Macintyre, I.G. and Stuckenrath, R. (1979) Holocene reef growth on the edge of the Florida shelf. *Nature*, **278**:281-282.
- James, N.P. and Ginsburg, R.N. (1979) The seaward margins of Belize barrier and atoll reefs. *International Association Sedimentology, Special Publication 3*, 191pp.
- Macintyre, I.G. (1967) Submerged coral reefs, west coast of Barbados, West Indies. *Canadian Journal of Earth Science*, **4**:461-474.
- Macintyre, I.G. (1972) Submerged reefs of the eastern Caribbean. *American Association Petroleum Geologists Bulletin*, **56**:720-738.
- Macintyre, I.G. (1988) Modern coral reefs of the western Atlantic: new geological perspective. *American Association Petroleum Geologists Bulletin*, **72**:1360-1369.
- Macintyre, I.G., Rutzler, K., Norris, J.N., Smith, K.P. Cairns, S.D., Bucher, K.E. and Steneck, R.S. (1991) An early Holocene reef in the western Atlantic submersible investigations of a deep relict reef off the west coast of Barbados, West Indies. *Coral Reefs*, **10**:167-174.
- Marshall, J.F. (1988) Potential effects of oceanic deep waters on the 'initiation and demise of coral reefs. *Proceedings of the 6th International Coral Reef Symposium*, **3**:509-512.
- Neumann, A.C. and Macintyre, I.G. (1985) Reef response to sea-level rise: keep up, catch up or give up. *Proceedings of the 5th International Coral Reef Symposium*, **3**:105-110.
- Ott, B. (1975) Community patterns on a submerged barrier reef at Barbados, West Indies. *Internationale Revue der Gesamten Hydrobiologie*, **60**:719-736.
- Paradice, W.E.J. (1925) The pinnacle or mushroom-shaped coral growths in connection with the reefs of the outer barrier. *Reports of the Great Barrier Reef Committee*, **1**:52-59.
- Rigby, J.K. and Roberts, H.H. (1976) Grand Cayman Island: geology, sediments and marine communities. *Brigham Young University Geological Studies Special Publication*, **4**:17-26.
- Schlager, W. (1981) The paradox of drowned reefs and carbonate platforms. *Geological Society American Bulletin*, **92**:197-211.

MODELING OF HYDROTHERMAL PROCESSES ON THE OCEAN BOTTOM

Nikolay Korchagin

Academy of Science of Russia
Moscow, RUSSIA

ABSTRACT

A new approach to the problem of the closure of the system of integral equations (SIE) describing the dynamics of a buoyant turbulent jet (BTJ) in a stratified fluid is suggested. As a result an analytical expression of the Taylor's "entrainment constant" was obtained from the parameters of the jet form. The suggested approach to the closure of the SIE in its turn shows one of the ways to describe the mechanism of the entrainment of a resting fluid into a turbulent area of the same fluid. The solution of the SIE was made by the numerical Runge-Kutta method of the fourth order of accuracy. The validation of the numerical model of the BTJ was carried out using the observational data of the characteristics of high temperature fluid flows entering the bottom water from hydrothermal vents ("black smokers") in two regions of the ocean. A model construction of the BTJ is suggested, the use of which in the SIE allows us to obtain an analytical expression of the maximum height for the rising jet, H_m , depending on the boundary parameters of the flow at the exit from the vent and on the stratification of the surrounding waters. The value of H_m was compared with the calculation of the maximum height of the rising jet using the Turner's empirical formula suggested more than 30 years ago; this comparison showed a good agreement with H_m which was calculated using the two formulas.

INTRODUCTION

Researching of hydrothermal processes on the ocean bottom is a difficult problem. Therefore it is better to construct adequate physical models in the first approximation for the solution of this problem. However it's difficult to construct a single complete model of the hydrothermal phenomenon at all stages of its development, because it is a combination of problems of different nature: hydrophysical, geological, chemical and geophysical ones. So it is convenient to divide the theoretical description of a hydrothermal action in the rift zones of the ocean into three parts :

- 1) the bottom circulation in crustal fissure systems of the ocean crust, leading to the outflow of high temperature ore-forming liquids from the ocean bottom surface and to the formation of polymetal ore deposits in the form of huge hills with "black smokers" at their summits;

- 2) the carrying out of endogenetic material into ocean waters in the form of jet-like high temperature turbulent flows saturated with soluble elements and fine dispersions of ore component particles;
- 3) the formation of anomalous water (plumes) at the termination of the jets. These "plumes" play an important role in controlling of the processes of heat and mass transportation in the deep and bottom layers of the ocean.

MODEL OF THE FORMATION OF "BLACK SMOKERS"

In the first part the processes of convective circulation of bottom waters in the crustal fissure systems in ocean spreading rift zones in the area of magma chamber geothermal field influence are investigated (Korchagin, Sorokhtin, 1992). Using a model for fluid motion in a U-shaped tube the possible mechanisms for waters circulation in different thermal and dynamic conditions are analyzed. It is shown that cold seawater descends along fine cracks, heating in the field of the magma chamber and being enriched with ore minerals on the way, and rises along broader channels, pouring out into the bottom water as hydrothermal jets. When hydrothermal water rises along cracks of the ocean crust, its temperature decreases and therefore a partial discharge of ore minerals already occurs in cracks. Later such cracks are blocked and the emergence of hydrothermal water finally concentrates in the central cracks. Further, a model for the evolution of the functioning of the system of chaotically distributed cracks in the spreading regions and their associated processes of ore hills formation with "black smokers" at their tops are considered.

MODEL OF THE FORMATION OF PLUMES

In the third part the formation of anomalous water (plumes) in their hydrophysical and hydrochemical characteristics near hot vents on the ocean floor is regarded as the mixing of three different water volumes: from the hydrothermal vent itself, entrained during the ascent of a jet of near bottom water and water from the depth of horizontal spreading of the plume (Korchagin and Gordeev 1993). An integral physical model is proposed for computing the relative volume of each of the three parts of water in the plume. Testing of the model in the computation of a relative volume was made on the basis of measurements of temperature and salinity using a Neil Brown CTD probe near a "black smoker" in the rift valley of the Mid-Atlantic Ridge, 26°N (the TAG study area). From the practical point of view, the structure of the model allows us to compute the concentration of any chemical element or soluble component directly in a thermal spring. In particular, computations were made of the concentration of soluble manganese and silicon, which were in a good agreement with the direct measurements of the corresponding concentrations in "black smoker" vents. Besides, the model allows us to estimate the approximate time of the ore hills formation. It turned out that the formation time of the ore hills was about 10 thousand years in the TAG area, that confirms the current information on the time of hydrothermal activity.

MODEL OF VERTICAL JET

In the second part a new method of closing of the system of integral equations which describes the dynamics of a buoyant turbulent jet has been developed. The application of the similarity theory to axially symmetric jet flow leads to a simplification of the equations system, if these equations are integrated over the cross section of the jet :

$$\frac{d}{dz} (R_T^2 \cdot W) = -2\alpha \cdot (r \cdot u)_\infty, \quad (1)$$

$$\frac{d}{dz} (R_T^2 \cdot W^2) = \frac{2\alpha}{\gamma} \cdot R_T^2 \cdot G, \quad (2)$$

$$\frac{d}{dz} (R_T^2 \cdot W \cdot G) = -\frac{\alpha + \gamma}{\gamma} \cdot R_T^2 \cdot W \cdot N_e^2. \quad (3)$$

Here α, γ are the constants of the Gaussian curve formed in the jet's parameters in the form

$$w = W(z) \cdot \exp(-\alpha \cdot \eta^2), \quad g' = G(z) \cdot \exp(-\gamma \cdot \eta^2), \quad (1a)$$

where $W(z), G(z)$ are the velocity and the buoyancy along the jet axis; $\eta = r / R_T(z)$; $R_T(z)$ is the local radius of the jet where the parameters of the flow $w[z, R_T(z)]$ and $g'[z, R_T(z)]$ decrease "e" times with respect to $W(z)$ and $G(z)$; N_e is the mean value of the Brunt-Vaisala frequency; u is the radial component of the fluid speed in the jet. Thus, the system of three nonlinear equations (1-3) contains 4 unknown variables $W, G, R_T, (ru)_\infty$. The closure of the system (1-3) becomes one of the problems in the hydrodynamics of buoyant jets in a fluid.

The value u_∞ is interpreted as the velocity of entrainment fluid in the jet varying as it was shown by Batchelor (1954) proportionally to $u_\infty \sim z^{-\frac{1}{3}}$. Introducing a coefficient of proportionality E_0 and defining it as the "entrainment constant" in equation (1) it is presented in the form (Morton et al., 1956)

$$\frac{d}{dz} (W \cdot R_T^2) = -2\alpha \cdot E \cdot (W \cdot R_T), \quad E = E_0 / \sqrt{2} \quad (4)$$

The numerical value of the "entrainment constant" can be determined only from laboratory experiments. However, the dispersion of the value E_0 indicates that the "entrainment constant" is not universal. Nevertheless, since 1956 the hypothesis of Taylor was generally used for the closure of the equation system (2-4) where the values of E_0 were chosen by means of laboratory estimates.

A new approach to the problem of the closure of the SIE describing the dynamics of a buoyant turbulent jet in a stratified fluid is suggested. A sharp boundary observed

between the fluid structures of the flow and the surrounding medium at the stage of the jet rising has on the average a regular conical form (Figure 1)

$$f_i[z, R(z)] = R(z) / z - \text{const} = 0. \quad (5)$$

As the equations (1-3) were obtained from the averaged Navier-Stokes equations and the parameters of the jet were averaged over an ensemble of profiles $w_i(z, r)$ and $g'_i(z, r)$ the jet boundary can be naturally considered as a line averaged over an ensemble of the curves :

$$f[z, R(z)] = \overline{f_i[z, R(z)]}, i=1,2,\dots \quad (6)$$

In this case (6) will describe a smooth line not curved by individual eddies and forming an angle $\theta = 12.5^\circ$ with the jet axis at the exit from the source (Morton et al., 1956).

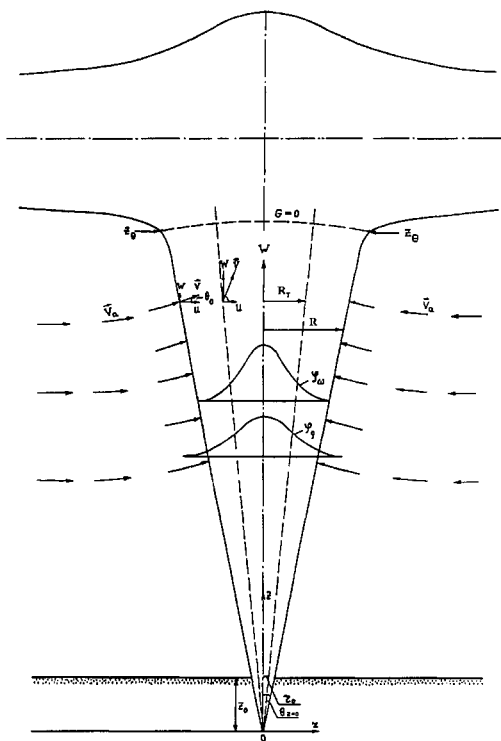


Figure 1. Schematic model of the hydrothermal jet.

According to the continuity equation the vertical and horizontal components of the fluid velocity in every point of the curve (6) at both sides of the boundary "jet-medium" are

correspondingly equal one another. At the same time the presence of a fixed in space sharp boundary of the jet dividing different structures of the fluid motion allows us to propose there is no mean motion along the line (6). It follows that the maximum values of the entrained fluid velocity $\bar{v}_\alpha(z, r)$ are reached at the boundary of the buoyant jet normal to the average position of the boundary line. We note that the analysis of the photographs of the turbulent jets in a fluid does not contradict the assumption of the normal position of $\bar{v}_\alpha(z, r)$ to the mean boundary of the jet.

Equations (1-3) were obtained by integration of the Navier-Stokes equations across the jet within the limits $0 \leq r \leq \infty$. However, the sharp boundary between the jet and the surrounding media allows us to restrict the limits of integration of the original equations in a transverse section of the jet by the radius $R(z)$, which is obtained from equation (6). Then the integration of the original equations within the limits $0 \leq r \leq R(z)$ leads to:

$$\frac{d}{dz} (R_T^2 \cdot W) = -\frac{2\alpha}{C_\alpha} \cdot \lim_{r \rightarrow R(z)} [r \cdot u(z, r)], \quad (7)$$

$$\frac{d}{dz} (R_T^2 \cdot W^2) = \frac{2\alpha}{\gamma} \cdot \frac{C_\gamma}{C_{2\alpha}} \cdot R_T^2 \cdot G, \quad (8)$$

$$\frac{d}{dz} (R_T^2 \cdot W \cdot G) = -\frac{\alpha + \gamma}{\alpha} \cdot \frac{C_\alpha}{C_{\alpha\gamma}} \cdot R_T^2 \cdot W \cdot N_e^2, \quad (9)$$

$C_\alpha = 1 - \exp(-\alpha \cdot \eta_R^2)$; $C_{2\alpha} = 1 - \exp(-2\alpha \cdot \eta_R^2)$; $C_\gamma = 1 - \exp(-\gamma \cdot \eta_R^2)$; $C_{\alpha\gamma} = 1 - \exp(-(\alpha + \gamma) \cdot \eta_R^2)$. According to the assumption of the normal position of the vector $\bar{v}_\alpha[z, R(z)]$ at the boundary "jet-medium" the equation (7) is transformed to the form

$$\frac{d}{dz} (R_T^2 \cdot W) = \frac{2\alpha}{C_\alpha} \cdot R \cdot W \cdot \text{ctg}\theta_z \cdot \exp(-\alpha \cdot \eta_R^2). \quad (10)$$

θ_z is the angle between the tangent to the boundary line $R(z)$ in the point z and the vertical. In this case $\text{ctg}\theta_z = \frac{dR(z)}{dz}$. Thus, the equations (8-10) form a closed system of nonlinear equations with respect to W, G, R . The solution of this system depends on the constants α, γ, η which numerical values are interdependent as shown by the laboratory experiments. As an example the empirical expressions for the functions $\varphi_w(\eta) = \exp(-\alpha \cdot \eta_R^2)$ and $\varphi_g(\eta) = \exp(-\gamma \cdot \eta_R^2)$ in the form (1a) were obtained in the experiment of Rouse et.al. (1952). They have shown that $\varphi_g(\eta)$ has a flatter form than $\varphi_w(\eta)$, that is to say $\gamma = \alpha$. At the same time the empirical expressions for $\varphi_w(\eta)$ and $\varphi_g(\eta)$ allow us to correlate the parameters α and γ between themselves: $\alpha = 1.344 \cdot \gamma$.

In a later work (Morton, 1959) the relation was defined as $\alpha / \gamma = 1.346$ and in the monograph of Fischer and others (1979) it was defined as $\alpha / \gamma = 1.440$. The latter relation is used in numerical calculations of the system (2-4) where the value of the constant $C_{\alpha,\gamma}$ is defined as unity and $\gamma = 0.690$.

It was shown in Landau & Lifschitz (1986) that the value of $\varphi_w(\eta)$ on the boundary of the flow in a nonbuoyant jet is within the limits 0.01-0.005. In this case the average value $\eta = R(z) / R_T(z)$ is 2.220. It follows from the empirical expressions for $\varphi_w(\eta)$ and $\varphi_g(\eta)$ obtained in the experiments of Rouse et al. (1952) that $R(z) / R_T(z) \approx 2.13$. Thus if we take into account the estimates of $\alpha \cdot \gamma$ and γ we obtain that the coefficients $C_{\alpha,\gamma}$ in the equations (8-10) are practically equal to 1. Comparing the equations (4) & (10) we obtain the expression for the Taylor's "entrainment constant"

$$E_0 = \frac{\sqrt{2} \cdot \eta_R \cdot \exp(-\eta_R^2)}{C_{\alpha} \cdot \text{tg}\theta_z} \cong \frac{\sqrt{2} \cdot \eta \cdot \exp(-\eta^2)}{R'(z)}; \quad (11)$$

It follows from it that the Taylor's "universal constant" is not a constant but it depends on the variation of the form of the buoyant turbulent jet, that is to say on the curvature of the flow boundary line. E_0 is constant only under the condition of the regular conical form of the flow when $R'(z) = \text{const} = \text{tg}\theta_0$. In this case, if we assume that $E_0 = \text{const} = 0.1$ the equations (8-10) are equivalent to the system (2)-(4). Thus, assuming $E_0 = 0.1$ and $\theta_z = \theta_0 = 12.5^\circ$ in (11), we obtain $\eta = R(z) / R_T(z) = 2.225$.

RESULTS

The solution of the system of nonlinear equations (8-10) is possible only by a numerical approach. The solution of the system of integral equations was made by the numerical Runge-Kutta method of the fourth order of accuracy. The validation of the numerical model of the buoyant turbulent jet was carried out using the observational data of the characteristics of high temperature fluid flows entering the bottom waters from hydrothermal vents (black smokers) in two regions of the ocean (see Figure 2).

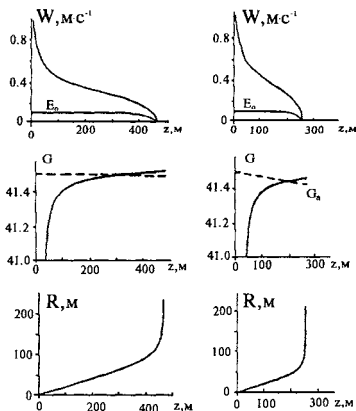


Figure 2. Examples of the calculations of hydrothermal jet parameters on the numerical model: TAG are the left graphics, EPR are the right ones.

The examples of calculations of the flow parameters W, G, R & E_0 using the numerical scheme Runge-Kutta are shown in Fig.2 for two regions of the ocean significantly different because of the density differences over the scale of the jet length. In the region of the intensive concentration of black smokers on the East Pacific Rise (EPR) the difference in the potential density is $A / \rho_0 = 2.8 \cdot 10^{-7} m^{-1}$ ($A = d\rho_a / dz$). But in the TAG study area $A / \rho_0 = 5.4 \cdot 10^{-8} m^{-1}$. The calculations were carried out at the known initial conditions for the hydrothermal vents: $R_0 = 0.1m$, $W_0 = 1.0m / s$, $G_0 / g = 0.3$. We emphasize that unlike the system (2-4) where the solutions depend on the parameters α and γ another parameter η is also included into the system (8-10) which estimate slightly varies (see above). A refinement of the numerical value of η can be done by an expert estimate of the jet maximum elevation H_m , which is an important characteristic of the jet obtained by the comparison of H_m obtained using the numerical scheme Runge-Kutta and the validated empirical Turner's formula (Turner, 1973):

$$H_m = 3.8 \cdot (G_0 \cdot W_0 \cdot \pi \cdot R_0^2)^{1/4} \cdot N_e^{-3/4}, \quad (12)$$

The calculation by the formula (12) showed that $H_m = 472m$ in the TAG region while in the region of the East Pacific Rise it was $H_m = 255m$. The similar estimates of H_m using the Runge-Kutta scheme were obtained at the common value of $\eta = 2.210$ under the same boundary conditions.

The graph of the dependence of H_m on the function $F_0 = (G_0 \cdot W_0 \cdot \pi \cdot R_0^2)^{1/4} \cdot N_e^{-3/4}$ is shown in Fig.3 in a logarithmic scale calculated both using the Runge-Kutta scheme and empirical formula (12). As it is seen in Fig.3 the values of H_m obtained using the Runge-Kutta scheme are close to the values calculated using the validated formula (12) for different sets of boundary data and stratification. Consequently the solutions of the

numerical model adequately describe the behavior of the buoyant turbulent jet in the stratified fluid.

The quasiconical form of the buoyant jet in its upper part is transformed in the deep ocean layers under the influence of the stratification of the surrounding waters into a turbulent area elongated form in the horizontal direction, "plume", in which the change of the mean characteristics of the flow occurs differently. In this area of the flow "...the formulation of the problem on the basis of entrainment becomes more than doubtful..." (Turner, 1973). The formation of an anomalous area in the upper part of the jet begins with a sharp deformation of the flow boundary approximately at a level z_G where $G(z_G) = 0$ (Morton et al, 1956). The fluid in the flow after reaching the level z_G continues its upward motion due to a "residual" momentum. Reaching the maximum elevation the fluid lowers down under the influence of the negative buoyancy and spreads in the horizontal mixing zones with the surrounding waters, thus forming a "plume". The position of the lower boundary of the anomalous area corresponds approximately to a level z_G and the upper boundary of the "plume" is formed at a level z_w , where $W = 0$. Unlike the experimental observations, the calculation of the parameters of the jet using the Runge-Kutta scheme or other numerical methods due to certain restrictions (stationarity condition, Gaussian form of the distribution of parameters) reveal only the upper boundary of the flow, where the calculation of the problem (8-10) terminates in the point z_w and $W(z_w) = 0$, while $G(z_w) < 0$. Thus the system (8-10) adequately describes only the first part of the phenomenon, that is to say the variation of the parameters W, G, R at the stage of the jet elevation from the nozzle of the vent z_0 until $z = z_w$. It is natural to assume that thereafter as the level z_w is reached, the fluid in the flow (as in the experiment) will lower down until the level z_G under the influence of the negative buoyancy, mixing on its way with the surrounding waters, thus forming a "plume".

One of the main parameters describing the behavior of the hydrothermal jet in the bottom waters is the jet elevation which can be estimated in the following way. The quasiconical form of the jet obtained in the numerical calculations and observed in the experiments allows us to describe the form of its boundary (in a projection on a plane) by a rather simple expression (Figure 3):

$$R(z) \equiv H \cdot \operatorname{tg} \theta_m \cdot \left[1 - \left(1 - \frac{z}{H} \right)^{1/p} \right], \quad (13)$$

where H is the elevation of the jet which is the sought parameter of the curve $R(z)$; $\theta_m > \theta_0 = 12.5^\circ$. The curve $R(z)$ is presented by three arbitrary parameters H, θ_m, p which requires additional conditions to find the optimal form of the model curve. We define the value θ_m by the requirement :

$R(z_G) = z_G \cdot \operatorname{tg} \theta_0$ in the point z_G . It follows that on $F_0 = (G_0 \cdot W_0 \cdot \pi \cdot R_0^2)^{1/4} \cdot N_0^{-3/4}$ under different boundary data. The right graph is the model form (13) of the jet radius.

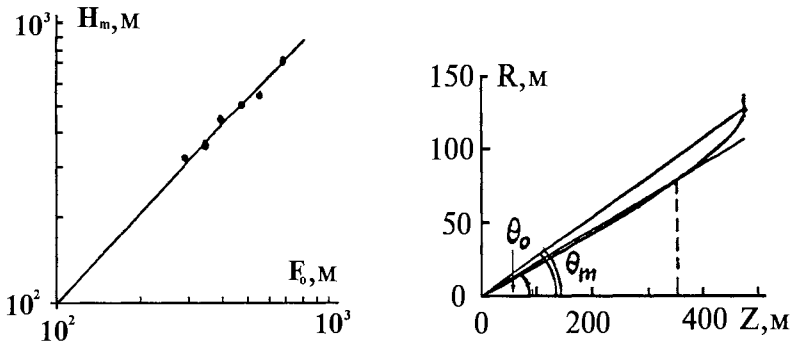


Fig.3. Graph of the dependence of the jet maximum elevation H_m

$$\operatorname{tg} \theta_m = \operatorname{tg} \theta_0 \cdot \frac{\varepsilon}{1 - (1 - \varepsilon)^{1/p}}, \quad (14)$$

$\varepsilon = z_G / H$ and $0 < \varepsilon < 1$. The numerical calculations of the parameters of the flow by the Runge-Kutta scheme under different boundary conditions on the section of the source indicate that the relation $\varepsilon = z_G / H$ is practically constant and $\varepsilon = 0.75$ for $E = \text{const}$ and $\varepsilon = 0.76$ for $E = \text{const}$. In the case $p \rightarrow 1$ it follows from (13-14) that $R(z) \cong z \cdot \operatorname{tg} \theta_0$ and for $z = H$ $R(H) \cong H \cdot \operatorname{tg} \theta_0$. At the same time for any $p > 1$ $R'(H) = \infty$ which means that a discontinuity of the jet boundary line is modeled in the point $z = H$.

Let us integrate the equation (10) in the system (8-10) to define the second parameter p of the curve $R(z)$ compatible with $R(z)$:

$$W = W_0 \cdot \left(\frac{R_0}{R} \right)^2 \cdot \exp(A \cdot J_R),$$

$$J_R = \int_{z_0}^z \frac{dz}{R \cdot R'} = -p \cdot \operatorname{ctg}^2 \theta_m \cdot \int_1^t \frac{t^q \cdot dt}{(1 - t^{1/p})} \quad (15)$$

where $A = 2 \cdot \alpha \cdot \eta_R^2 \cdot \exp(-\alpha \cdot \eta_R^2)$; $t = 1 - z / H$; $q = (p - 1) / p$. We have after opening the equation (9) taking into account (15)

$$2 \cdot W^2 \cdot [A - (R')^2] / \left(\frac{2\alpha}{\gamma} \cdot R' \cdot R \right) = G. \quad (16)$$

It follows, that at the level z_G , where $G = 0$,

$$R'(z_G) = \text{tg}\theta_0 = \sqrt{A} \quad (17)$$

Substituting the expression for the derivative of the jet radius $R'(z)$ from (13-14) into (17) we get:

$$\frac{(1-\varepsilon)^{(p-1)/p} - (1-\varepsilon)}{\varepsilon} = \frac{1}{p} \cdot \frac{\text{tg}\theta_0}{\sqrt{A}}, \quad (18)$$

Then we substitute the mentioned values of ε into (18) and get a transcendental equation from which it follows with an accuracy of about 5% that $p=1.25$, which defines finally an optimal form of the modeled curve (13)-(14).

We further integrate (11) taking into account (18) and get

$$G = (G_0 + C \cdot N_e^2 \cdot I_R) \cdot [\exp(A \cdot J_R)]^{-1}, \quad (19)$$

where $C = \frac{\alpha + \gamma}{\alpha} \cong 1.69$; $I_R = \int_{z_0}^z \exp(A \cdot J_R) \cdot dz = -H \cdot \int_1^t \exp(A \cdot J_R) \cdot dt = -H \cdot I_R$.

Then it follows from (19) that at the level $z = z_G$

$$H = \frac{G_0}{C \cdot N_e^2 \cdot I_R}. \quad (20)$$

Substituting the initial data at the exit from the source in (20) $R_0 = 0.1m$, $W_0 = 1m/s$, $G_0 / \sigma = 0.3$ and $N_a = -5.4 \cdot 10^{-7} c^{-1}$, we obtain $H_m = 475m$ which practically coincides with the estimate of H_m calculated using the empirical formula (12) suggested by Turner in 1973. A graph of the curve (13-14) is shown in Fig.3 calculated for the TAG study area. The behavior of the model curve $R(z)$ in Fig.3 is fairly well compatible with the graph $R(z)$ calculated using the Runge-Kutta scheme and the values H_m in both cases practically coincide with each other. We emphasize that the graphs of $W(z)$ and $G(z)$ calculated using the formulas (15) & (19) respectively, after the data of the model curve (13) are substituted into them, are very close and compatible with the corresponding curves $W(z)$ and $G(z)$ obtained using the numerical model of the Runge-Kutta scheme.

REFERENCES

- Batchelor G.K. 1954. Heat convection and buoyancy effects in fluids. Quart.Jour.Roy.Met.Soc. 80, 339-358.
- Fischer, H. B., J. R. List, J. Koh. 1979. Mixing in Inland and Coastal Waters. NY: Academic Press. pp. 315-389.

Korchagin N.N., Sorokhtin • O.G. 1992. Evolution model of hydrothermal springs in ocean spreading regions. *Oceanology*. 32, 1026-1032.

Korchagin N.N., Gordeev V.V. 1993. The integral model of anomalous waters formation near hydrothermal sources. *Oceanology* 33, 663-669.

Landau L.D., Lifschitz E.M. 1986. *Theoretical physics V.VI. Hydrodynamics*. MÆoscow: Nauka. 736 p.

Morton B.R. 1959. Forced plumes. *J.Fluid Mech.*5, 151-163.

Morton B.R., Taylor G., Turner J.S. 1956. Turbulent gravitational convection from maintained and instantaneous sources. *Proc.R.Soc. London. Ser.A234*, 1-23.

Rouse H., Yih C.S., Humphreys H.W. 1952. Gravitational convection from a boundary source. *Tellus*. 4, 201-210.

Turner J.S. 1973. *Buoyancy Effect in Fluids*. Cambridge. University Press.

A POLICY ROLE FOR PACON IN SUSTAINABLE MARINE RESOURCE DEVELOPMENT

Linda M.B. Paul

Ocean Law & Policy Institute, Pacific Forum CSIS
Honolulu, Hawaii, U.S.A.

ABSTRACT

Sustainable marine resource development requires increased communication, interaction, and cooperation between the scientific and technical community and the policy makers on matters involving marine resource assessment, conservation, and management. Such cooperation is urgently needed to facilitate important exchanges of information, encourage cooperative research efforts, prevent duplication, and promote sound objectives and policies. Several chronic coastal zone management problems require a cooperative approach, including 1) conflicts among coastal uses and users that negatively impact planning and management; 2) short term political and technology pressures that cause development to overtake planning processes; 3) weak and poorly defined linkages between natural systems and socio-economic systems; and 4) the failure to assign realistic values to non commercial resources and assess the impact of their loss on coastal communities. There are, however, both practical and political impediments that must be overcome before productive cooperation can take place.

The impetus for this paper comes from the recognition that the business of science is to collect and analyze data; data that is expensive to procure yet poorly utilized, particularly for policy making purposes. Among the "policy challenges" identified are 1) the need to translate technical and scientific issues for policy makers; 2) the need for multidisciplinary preparation and knowledge; and 3) the need to forge new linkages and investigate new ways of doing business between scientific organizations, agencies, and funding institutions that conserve, manage and develop marine resources. This integrated approach is discussed in the context of coastal zone development, land-based sources of pollution, and fish habitat loss.

INTRODUCTION

In 1992 the United Nations finalized the language of the oceans chapter (Chapter 17) of Agenda 21 in conjunction with the United Nations Conference on Environment and Development ("UNCED"). The UNCED participants sought to reconcile economic development with the need to maintain production of renewable resources and preserve the integrity of global ecosystems. The watch word became "sustainable development". Chapter 17 recognizes that the protection and sustainable development of the marine and coastal environment and its resources would require new management approaches that "are integrated in content, and are precautionary and anticipatory in ambit" (UNCED 1992). The first itemized objective in the oceans chapter, section 17.5, states that in order to accomplish sustainable development, it is necessary to "[p]rovide for an integrated

policy and decision-making process, including all involved sectors, to promote compatibility and a balance of uses" in the marine and coastal zones.

Such integration requires more than a high-level policy planning body that merely consults with the academic and management sectors, as suggested in Section 17.6. What is needed is an integration of the academic and resource management sectors into the planning and decision-making processes themselves. Although these sectors are often consulted at the initial fact-finding stages, they are generally not included in later stages when decisions, and compromises, are ultimately made. A classic example is the definition of optimum sustainable yield ("OSY") that was drafted into article 61 of the United Nations Convention on the Law of the Sea (United Nations 1982) and article 5 of the United Nations Agreement Relating to the Conservation and Management of Straddling Fish Stocks and Highly Migratory Fish Stocks (United Nations 1995). Both of those agreements specify that OSY is the maximum sustainable yield ("MSY") "as qualified by relevant environmental and economic factors." The use of the term "as qualified" instead of "reduced" means that states may adopt policies that will allow fishing at levels greater than MSY, a practice that will inevitably yield the collapse of the resource. To date this has happened in a large number of fisheries, most notably the North Atlantic cod fishery. The policy makers that drafted this language apparently failed to understand why fishery biologists cannot predict with any degree of certainty just exactly what MSY is from year to year and why a healthy margin of safety must be mandated to avoid exceeding it.

In the Fall of 1995 the Asia Pacific Economic Cooperation's Marine Resource Conservation Working Group convened a workshop on international coastal zone management policies and activities (APEC MRCWG, 1995). Representatives from organizations involved in multilateral initiatives in coastal zone planning concluded that the failure of technical people to translate technical issues for, and effectively communicate with, decision makers has contributed to a number of coastal zone management problems, including 1) conflicts among coastal uses and users that negatively impact planning and management; 2) short term political and technology pressures that cause development to overtake planning processes; 3) weak and poorly defined linkages between natural systems and socio-economic systems; and 4) the failure to assign realistic values to non commercial resources and to assess the impact of their loss on coastal economies.

COASTAL ZONE DEVELOPMENT

Management of marine and coastal zones is usually spread over multiple agencies and multiple levels of government. For example, in the United States the Department of Commerce has jurisdiction over fisheries, the Army Corps of Engineers has jurisdiction over navigable waters, the Department of Transportation has jurisdiction over maritime matters, the Environmental Protection Agency and the states share pollution monitoring responsibilities, the states share jurisdiction over coastal zone planning with the federal government, and the federal government, states, counties and cities share jurisdiction over ports and harbors. Planning, if there is any, is generally piece meal, short-term, and heavily influenced by special interests.

Integrated management in the marine and coastal zone requires that this traditional sector-specific management approach be changed to a multisectoral approach. The following recommendations have been made by members of the APEC Marine Resource Conservation Working Group and representatives from other institutions such as the Intergovernmental Oceanographic Commission (IOC), and the Western Pacific Fisheries Consultative Committee (WPFCC): 1) develop comprehensive, integrated, multisectoral long-term planning and management frameworks; 2) conduct comprehensive economic assessments of the impact of development on coastal resources and environment; 3) identify and evaluate competing coastal uses and users; 4) assess social and economic costs and benefits of these uses, including intangible benefits; 5) develop, strengthen and integrate coastal management institutions, including clarifying mandates, assigning responsibilities, and improving coordination between sectors; 6) encourage community participation in planning, implementation, and enforcement; 7) reduce vulnerability to short term development pressures by anticipating future coastal growth patterns and environmental change; 8) investigate new ways that scientific organizations, agencies, and funding institutions can work together, e.g. coordinate a multisectoral effort to solve single, high priority problems one at a time; and 9) expand, pool and integrate marine and coastal zone resource data bases.

LAND-BASED SOURCES OF POLLUTION

Some 22 billion tons of pollutants of all types are washed into the coastal zone every year and still more enter the ocean from atmospheric sources (Viders, 1993). Air and land-based pollutants travel long distances, and persistent materials contaminate a wide spectrum of marine organisms and are concentrated as they move through oceanic food chains. The main causes of marine pollution are well known, as are the technological solutions. The main problems are

poor management, poor communication between scientists and managers, weak institutional structures and manpower capabilities, a sectoral approach to environmental management, lack of cooperation between the public and private sectors, and the widespread notion in political circles that the seemingly drastic and costly changes and measures advocated by natural and technical sciences are economically, politically and socially impractical and unrealistic." (Dahl, 1993)

Section B of Chapter 17 lists a number of management measures that should be used to address these problems at national, subregional and regional levels. The measures need to be closely associated with integrated coastal zone management and be based on the precautionary and polluter pays principles. Management suggestions put forth by Agenda 21, the Montreal Guidelines (Montreal, 1985), the United Nations Environmental Program (see e.g. Report of the First Intergovernmental Meeting on the Northwest Pacific Action Plan (UNEP, 1994)), the UN Joint Group of Experts on the Scientific Aspects of Marine Pollution (GESAMP, 1991), and others (Dahl, 1993; Cote, 1993) include the following: 1) prepare scientifically sound and tested methods

for determining levels of contamination and biological effects; 2) inventory both pollution levels and potential sources and risks; 3) quantify ecosystem, habitat, and other relevant damage from land-based sources; 4) establish regional data and information exchange networks; 5) establish or improve monitoring and response programs; 6) assess social and economic costs; 7) promote risk and environmental assessment; 9) establish institutional structures that correspond to the geographic area where management is needed, e.g. watersheds; and 10) establish inter-agency control over development activity and permits.

FISH HABITAT LOSS

The global depletion of fish stocks and drastically declining catches are due in large measure to the unremitting destruction of fish habitat, particularly nursery habitat. Estuaries, coral reefs, mangroves, seagrass beds and shallow nearshore waters are the spawning and rearing grounds for approximately two-thirds of the commercial seafood production (Anon. 1992). There are numerous causes for habitat loss: pollution, construction, dredging, filling, mining, diversions, and destructive fishing techniques such as bottom trawls, dredges, explosives, chemicals and poisons. Coastal development projects are altering both coastlines and current patterns. Diversions of rivers and streams are drying out wetlands and destroying estuarine systems. Coral reefs, which support a third of all fish species, are being mined and quarried for sand and construction materials with consequences not only for diminishing marine productivity but also for coastal protection during storm surges.

In 1994 the head of the United States National Marine Fisheries Service stated

the loss of nearshore ocean and estuarine fishery habitat is probably the greatest long term threat to U.S. marine fisheries productivity. Habitat loss and degradation are among the major factors contributing to poor harvest, depletion, endangerment and extinction of living marine resources. Thus, managing stocks for long-term yield and promoting recovery of depleted stocks is no longer sufficient (Schmittner, 1994).

The North American Fisheries Policy drafted by the American Fisheries Society (Starnes, 1996) states that to support an ecosystem approach to management, researchers and administrators need to focus on developing an understanding of the multidimensional and interconnected nature of aquatic resource communities and their habitats. The needs of all ecosystem components, including all life stages of involved species, should be considered during planning, implementing, and monitoring of habitat management activities and coastal development projects. Habitat protection measures must include both a No Net Loss policy and a Net Gain policy. The preservation of natural marine areas, with no human use, to ensure maintenance of biodiversity is also required.

THE POLICY MAKING PROCESS

Integrated policy and decision making requires increased communication, interaction, and cooperation between the scientific and technical community and the policy makers at all levels. Such integration is urgently needed to facilitate important exchanges of information, encourage cooperative research efforts, prevent duplication, generate adequate funding and promote sound objectives and policies. There are, however, both practical and political impediments that must be overcome before this cooperative interaction can take place. The business of science is to collect and analyze data. That data is expensive to procure, yet is poorly utilized, particularly for policy making purposes. The reason for the poor utilization is a failure to communicate or even to recognize what needs to be communicated, how it must be explained, and how it can be utilized. Scientists, engineers, resource managers, and policy makers all too often believe they know more about each other's subject areas than they actually do, and they frequently make careless, oversimplified assumptions they would never make regarding matters within their own discipline.

Policy makers need to be sensitive to the need for a solid factual base to support policy initiatives. That base is what builds public and private support. They need to appreciate the time and cost requirements of data and information collection, analysis and other steps that must be taken before the creation of sensible and enforceable policies. Policy makers also need to communicate clearly about what they want and need from the scientific community and when they need it. They also need to understand the limits of science, why scientists cannot say for certain why or if things are or are not so, and why a precautionary safety factor must be built into policy mandates. Policy makers need to know and understand the implications of the facts and data that are being presented to them. They need to understand why or when, in the course of compromising and balancing competing interests, which they must and will do, they should not ignore those implications. And they need to be reminded of this all the way up to the time when decisions are ultimately made.

Scientists, engineers and resource managers need to understand the task of the policy maker. Policy makers are brokers, which means they must compromise and accommodate competing interests. They do not need the degree of certainty required by the scientific discipline to prove or disprove an hypothesis. They don't need to know all there is to know; they don't have the time. Generally they need just the basic facts that would be taught in an introductory course in the matter and a ball park estimate; that is, whether it is more likely than not that something may happen. In the policy making world there is no "right" or "wrong"; there are just differing points of view, all of which demand accommodation. That said, the accommodation choices will be disastrous if based on inaccurate assumptions, and scientists and resource managers have a responsibility to educate both the policy makers and society.

MULTIDISCIPLINARY PREPARATION

It is not enough to be an expert in one's own field. There is a need to understand the big picture that cannot be met merely by forming a committee and the mechanisms for communication and

understanding must be in place as well. It is useful to think of it as educational biodiversity; the need to understand the natural, social, economic and political ecosystems in which one must operate. It will affect what problems one chooses to address and the approach to take. It will also enable each group to speak each other's language and ask the pertinent questions.

Interdisciplinary studies should be required in all disciplines. Many of today's current disciplines would have been considered multidisciplinary 50 years ago. A biological oceanographer needs to understand chemistry, physics, geology, and mathematics, as well as the production and distribution of plankton, nekton and benthic communities. A fisheries manager needs to understand economics, sociology, anthropology, and psychology (as well as the population dynamics of fish stocks), since fishery managers manage people, not fish. Environmental lawyers need to understand biology, chemistry, economics, history, and politics in order to choose what issues to argue and what remedies to pursue.

Ethics should also be a required course in every discipline. Single purpose research, management or policy decisions, made by persons with limited areas of concern or experience, may have unanticipated, unintended consequences. Everyone needs to be sensitive to the fact that what they do and what choices they make may negatively impact other segments of society in ways they often don't fully appreciate.

HOW THE SCIENTIFIC COMMUNITY CAN MAKE A DIFFERENCE

1. It is important that scientists, engineers and technical people remember to speak and write in plain language when explaining technical and scientific concepts to policy makers. It is also important to explain the short and long term implications of what you are saying and to check to make sure you are being understood. Laws must be drafted into language that will convey the same meaning to everyone and do what they are intended to do. Joan Bondareff, counsel to the U.S. House of Representatives Committee on Merchant Marine and Fisheries in 1991, once remarked that "policymakers are not good listeners and the scientists are not good speakers to the policy issues" and recommended promoting a dialogue between the two.
2. To create an opportunity to educate and inform, offer to translate technical and scientific issues for policy makers. A particularly needy area is the lack of volunteer panels of experts available to review environmental impact statements and assessments for both governmental agencies and non governmental organizations. Policy makers need and rely on experts, yet all too frequently rely on people who merely pass themselves off as experts. It is also important to clarify for policy makers how you can be most effective as experts, i.e. the need for regulatory and monetary support for research, and assurances that you will not be exploited in the policy-making process.
3. If you feel strongly about the need for a particular law or regulation, draft the law or regulation yourself and find a legislator or agency head who will introduce it. Many laws and

regulations are initially drafted by or at the request of special interest groups. Better the experts do it than the non experts. It is not necessary to draft it in legalese; it will almost always be redrafted as it goes through the hearing process anyway. As a rule of thumb non-binding resolutions and laws and regulations that don't cost much have better chances of being enacted.

4. If a certain issue is not important it is generally better strategy to compromise. It is also a good idea to present needed changes in small increments if there is significant opposition. Sometimes it just takes time and education for someone to get used to an idea, and new policy implementation in the face of emotional or uninformed resistance is easier if it is done in small steps.

5. If long-term coastal zone planning is ever going to happen, it is important that the scientific community make the effort to do some lobbying. Compile and make available studies and draft reports that project where unplanned coastal zone development is headed and what it means in terms of degradation of coastal resources and the long-term costs to the public. Write legislative testimony and op-ed pieces; call, write, fax and e-mail policy makers; make appointments and meet with them and their staff; and don't forget that briefing the media can help educate voters.

6. The formation of public/private task forces will often help solve specific problems by helping groups with a stake in the outcome feel an ownership in the solution and an interest in enforcing it. Meetings facilitated by experts in communication, collaboration, and process-building can also assist participants to effectively communicate and coordinate their efforts toward mutually-understood common goals.

7. It is a good idea to include experts from other disciplines as members of your professional organizations. They can be very helpful in the development of practical methodologies that policy makers can use to incorporate scientific input into their decision-making processes at all levels.

8. Seminars, workshops, public forums, and field trips are particularly good ways to inform and educate the policy-making and user communities. Policy-making bodies should also be provided with reference sources that indicate where information can be found on particular subjects, what information is not available, but needs to be, and the means by which the missing information can be obtained, including needed legislation, cooperative agreements, and research and data base funding. Impress upon policy makers that good scientific and technical information can make tough decisions easier and will improve the substantive decision-making process. Suggest that scientific and technically trained people be included on the legislative staff.

REFERENCES

- Anon. 1992. Marine Fisheries and the Law of the Sea: A Decade of Change. FAO, Rome, 132-157.
- APEC MRCWG, 1995. Proceedings of Workshop on International Coastal Zone Management

Policies and Activities, 26-27 October 1995, Honolulu. APEC #95-MR-04.1.

Cote, R., 1993. Marine Environmental Management: Status and Prospects. Marine Pollution Bulletin. Vol. 25, No. 1-4, 18-22.

Dahl, A.L., 1993. Land-based pollution and integrated coastal management. Marine Policy. Vol. 11, 561-572, 566.

GESAMP, 1991. Global Strategies for Marine Environmental Protection. Rep. Stud. GESAMP (45), IMO, London.

Montreal, 1985. Montreal Guidelines for the Protection of the Marine Environment against Pollution from Land-based Sources, Environmental Law Guidelines and Principle No 7, UNEP, Nairobi, 1985.

Schmitt, R., 1994. NMFS responds to AFS editorial on habitat protection program. Fisheries Vol. 19, No. 5, 4.

Starnes, L., G. Compean-Jiminez, D. Dodge, G. Huntman, P. Janik, J. Lloyd, N. Prosser, W. Royce, and W. Taylor, 1996. North American Fisheries Policy. Fisheries. Vol 21, No. 3, 26-29.

UNCED, 1992. Introduction to Agenda 21 Oceans Chapter, as adopted at UNCED, June 14, 1992. A/CONF.151/4 (Part II).

UNEP, 1994. Report of the First Intergovernmental Meeting on the Northwest Pacific Action Plan, Seoul, 14 Sept. 1994. UNEP (OCA)/NOWPAP IG.1/5.

United Nations, 1982. U.N. Doc. A/CONF.62/122.

United Nations, 1995. Opened for signature December 4, 1995. 34 I.L.M. 1542 (1995).

Viders, H. 1993. Where Have All the Fish Gone? Sources. May/June, 41-48, 42.

THE WORLD COBALT MARKET AND ITS ABILITY TO SUPPORT MANGANESE CRUST MINING

John C. Wiltshire

University of Hawaii
Honolulu, Hawaii, U.S.A.

ABSTRACT

To be profitable a marine manganese crust mining operation would largely depend on cobalt sales. However, compared to other metals markets, the cobalt market is smaller, more volatile and inherently less predictable. The key factors shaping the cobalt market include its relative smallness, the wide variety of products which use cobalt, the relatively few numbers of large producers and consumers compared to other metals, the fact that most cobalt is mined as a byproduct of copper and nickel, and the highly politically unstable nature of some of the major cobalt producers. At the current growth rate of 4%, the annual cobalt demand will be 50,000 tons by the year 2015. At present, the world demand for cobalt and available supply are in equilibrium at today's high cobalt prices. This supply/demand balance on the world market is maintained by several factors. These are stockpile sales, metal substitution and new sources of cobalt coming on line. If 10,000 tons of new production comes on line by the year 2005, this could give a world primary supply of over 30,000 tons a year. If the current cobalt growth rate was maintained, demand in 2005 would be over 34,000 tons or a potential market shortfall of several thousand tons. Much more new production could cause a 30-40% price drop which would probably stimulate a 20-30% increase (shift) in market demand. A best long term guess on market size would be 30-35,000 tons after the year 2000. Such a market could support one 3,000 ton per year manganese crust operation coming on line in the year 2000. By contrast, the world cobalt market could not support several such marine mining operations without a major change in the present nature of supply and demand.

INTRODUCTION

Compared to other metals markets, the cobalt market is more volatile, inherently less predictable and, at present, highly lucrative for cobalt producers who have reaped windfall profits over the last ten years. There are a number of fundamental structural elements of the market which cause this and are unlikely to change for the next several decades. These include: the relative smallness of the world market, the wide variety of products which use cobalt, the relatively few number of large producers and consumers compared to other metals, the fact that most cobalt is mined as a byproduct of copper and nickel mining operations and the highly politically unstable nature of some of the major cobalt producers. Each of these factors will be looked at in turn to shed light on the future market.

The situation is further complicated by a significant growth in cobalt demand presently ongoing and projected to accelerate over the next several years. New uses for cobalt and high cobalt price are driving major terrestrial exploration efforts for cobalt. A significant number of new cobalt deposits have been found and are in the process of development. Most of these deposits are nickel deposits. Although the world nickel market is expanding, it is not expanding at the rate of the cobalt market. This limits the number of these deposits that can be brought on line at any given time. It is in this context of growing demand and growing supply that the question of a potential market share for a manganese crust mining venture is addressed.

This study follows on from earlier work by Loudat *et al* (1994, 1995) which examined the economics of manganese crust mining using several different techniques. Loudat *et al.* showed that provided engineering challenges could be overcome as projected, crust mining should be an economic venture. Further they showed that in calculating crust mining economics only a very few variables made much difference. The two most significant were the price of cobalt and the cobalt grade in crusts. While it may make sense to extract other metals at the same time as cobalt is removed, the decision as to whether mining manganese crusts is potentially viable rests on the contribution of cobalt to the venture. In turn, to achieve any economy of scale significant tonnages of cobalt must be mined and sold. Probably a successful crust mining venture would need to sell between two and five thousand tons of cobalt a year (U.S. Department of the Interior, 1990). This paper will address the question of whether the world cobalt market can support this much addition by a manganese crust mining operation without such a decrease in price as to render the venture uneconomic. To answer this question we will have to look at future cobalt supply and demand. This necessitates first looking at the current supply and demand patterns and then attempting to project trends. Such projections for market change are of necessity generalizations and subject to unpredictable occurrences particularly as they project farther into the future. In the past, the world cobalt market has been subject to severe unforeseen perturbations. If the past is the key to the future, we may anticipate more of the same.

PRESENT COBALT DEMAND

According to Union Miniere (Gellens, 1995), the Cobalt Development Institute (1996a) and the U. S. Bureau of Mines the size of the world cobalt market in 1994 was about 22,000 tons, in 1995 about 24,400 tons and should show a considerable increase in this number in 1996. All agree that the market is growing fairly rapidly. The apparent growth was 14% from '93 to '94 and 9% from '94 to '95 with some major sectors of the market experiencing over 20% growth. The cobalt market is, in actuality, a series of approximately 10 smaller, quite independent markets. These are shown on Table 1. None of these markets is declining, all are growing or at least maintaining their current level of use. The major cobalt sub markets are 1) super alloys, 2) carbides and cutting tools (pressed fired powders) 3) coloring (cobalt blue), 4) magnets, 5) industrial soaps and dryers, 6) audio and video tape and computer disk drives 7) catalysts 8) hard facings on engine and industrial parts, 9) medical applications (cobalt -60 for radiation treatment, prosthetics, vitamin and fertilizer additives), 10) batteries. Most of the major cobalt

applications are high tech and many of the applications have excellent prospects for dramatic growth early in the next century. In particular, these high growth areas include: computer applications, superconductors, super alloys, high capacity batteries, and catalysts for industrial environmentally mandated cleanup applications. Most of the cobalt applications in these areas have no other viable substitutes.

Tonnages projected in Table 1 are based on work by the Cobalt Development Institute (1996a), Garvey (1996), Abraham (1995) and Day (1996). These figures include both primary cobalt production, stock pile sales and recycling.

Table 1: The World Cobalt Market

Sub Markets	Projected 1996 Tonnage Used	Market %	Growth/year
1. Superalloys	7,100	26	8.4%
2. Carbides and Tools	4,100	15	moderate
3. Colors	3,500	13	level
4. Magnets	3,000	11	0.5%
5. Catalysts	2,800	10	moderate
6. Soaps, Driers Tire Adhesives	2,800	10	level
7. Recording Media Electrowinning Hard Disks	1,550	6	high
8. Hardfacings	1,500	6	level
9. Batteries	500	2	32%
10. Orthopedics	400	1	8.0%
Totals	27,250	100	7-10%

FUTURE COBALT DEMAND

At an average growth rate of 4%, the annual cobalt demand will be 50,000 tons by the year 2015. The Cobalt Development Institute (the main industry association) allows that a world wide demand of 40,000 tons is conceivable within a decade. The cobalt market is highly segmented. Many of the segments have very high anticipated future demands. Most notable among these is batteries. The current consumption rate for batteries is about 500 tons/year. This is anticipated to grow at a rate of 32% a year over the next half decade because of new battery technologies using cobalt. If electric cars become an

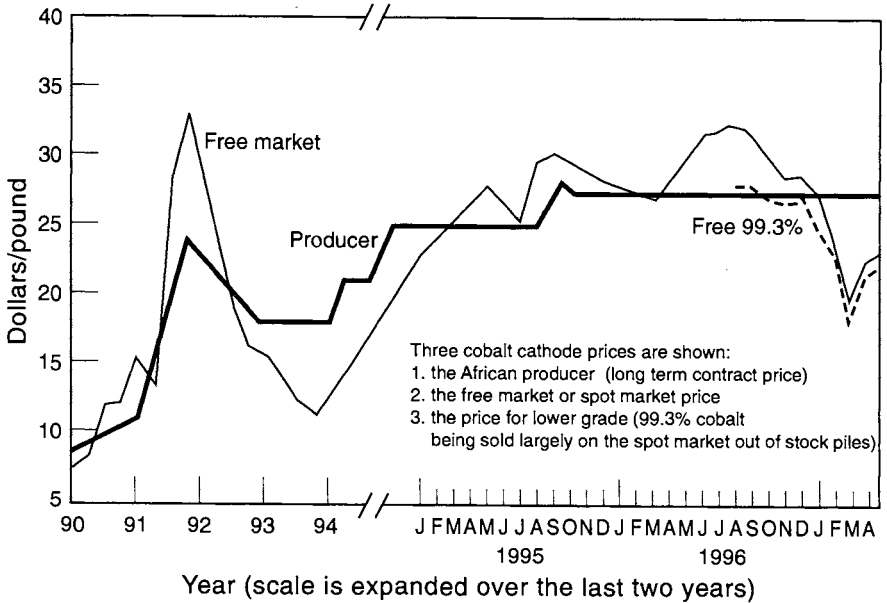
important mode of transportation early in the next century then the demand for cobalt will skyrocket as most major solutions to the electric car battery problem require cobalt. These include lithium cobalt dioxide batteries production of which for 1995 grew at a rate of 96% according to the Japanese Battery Industrial Association (Cobalt Development Institute, 1996b). The demand for cobalt in super alloys is rising at 8-9% a year. This is anticipated to continue through the rest of the century and early into the next century as the demand for specialty steels continues to rise. Similarly the demand for cobalt based orthopedics is increasing at a steady 8% a year. Again with an aging population in the west, this trend will certainly continue if not accelerate.

Overall long-term demand for cobalt appears to be increasing at in excess of 3-4% a year. If the period 1994-96 alone is considered, the growth is much higher. However, this is balanced by a period in the early 1990's of considerably reduced cobalt demand and production which corresponded to a world recession and rapid rise of cobalt prices. It is safe to say that in a time of relative world prosperity and increasing industrial production that the demand for cobalt will continue to rise particularly as new uses come into increasing demand.

PRESENT COBALT SUPPLY

A significant factor constraining cobalt market growth is near-term shortness of supply. Much of the world's cobalt supply is mined in Zaire and Zambia as a byproduct of copper mining. This area has been subject to intense political and economic instability in the last few years and many of the mines are in substandard condition. One of the major mines, the Kamoto mine, collapsed and most of its production has been lost. Furthermore, AIDS is rapidly becoming a serious problem with the mine workers and the possibilities of major new foreign investment are poor. The mines are largely low grade, open pit copper mines with low grade cobalt as a minor byproduct. The profitability of these mines is determined by the copper price. The copper market is suffering downward pressure as copper wire for communications (a major market share) is replaced by silicon fiber optics and cellular phones. This makes expansion or perhaps even continued operation of these mines problematic over the long-term. If the mines shut down or lose production because of the copper market then this source of cobalt is eliminated. A loss of all of these African Copper Belt mines would take 50% of the cobalt off the world market. This combination of new high tech applications and instability in the African supply has caused the cobalt price rise over the last several years (see Figure 1). At present, the world demand for cobalt and available supply are in equilibrium at today's \$27/lb cobalt producer price. This supply/ demand balance on the world market is maintained by several factors.

Figure 1 Cobalt Cathode Price 1990-1996



The first of these is stockpile sales. Up to 20% of the present world market is being supplied out of stockpiles. These are primarily from three sources, the U.S. Defense Logistics Agency (DLA) stockpile, the Russian stockpile and largely Japanese heavy industry stockpiles (Sumitomo and Mitsubishi). The U.S. Government has an extremely large cobalt stockpile (19,480 tons as of 1996). This was maintained in case the U.S. was ever cut off from cobalt supplies for a decade. Several years ago, after having spent \$4.5 million on a manganese crust EIS and associated research, the argument was made by the State of Hawaii to the DLA that vast high grade cobalt resources had been located on U.S. controlled seabeds which could be mined within several weeks by simply putting a conventional coal drag line on a dredging barge, albeit at very high cost. Given this premise, it made no sense to maintain a large cobalt stockpile. DLA agreed and they have been slowly selling the U.S. stockpile at considerable profit because of the high current cobalt price. For similar reasons, as well as to realize a significant profit, the other stockpiles are being sold. The industrial stockpiles are now virtually gone. The DLA stockpile will be sufficiently reduced in a few years at current rates of sale (generally about 1,500 tons a year) that these sales will stop.

The second factor maintaining the cobalt supply/demand balance is metal substitution. Both the spot market and long term cobalt prices are very high, relative to historical prices. The cobalt market is divided into long-term contract prices sold by the major African producers (known as the African Producer price- currently \$27/lb) and daily spot

prices on the London metals market largely controlled by speculators at the big London metals houses (currently running around \$23/lb). This high price causes many users to reduce the amount of cobalt in their products, switch to poorer but cheaper alloys, delay introduction of new high cobalt demand products etc. It seems reasonable to assume that more cobalt coming onto the market at a lower price would be quickly consumed. Recycling which is now about 10% of the market may be anticipated to increase.

The third factor maintaining the current supply/demand balance is new sources of cobalt coming on line. There are at least 20 mining projects world wide which are in varying stages of completion or are attempting to raise capital. The coming advent of this new supply has stabilized the market and reduced the fear of anticipated massive future short falls in supply. This has resulted in the development of new cobalt applications and has somewhat slowed the desire to shift to substitute metals (usually a nickel alloy) for traditional cobalt applications.

The pattern of current supply is changing. Both Zaire and Zambia are losing prominence as the world's largest suppliers. These traditional African sources are struggling to maintain production in the face of a transition to newer more efficient mines in the politically stable developed world. New sources in Canada, Australia and Cuba are projected to be the future large volume cobalt suppliers. This trend will likely dampen the very volatile price swings experienced by the cobalt market in recent years and make the metal more attractive for users because of anticipated price stability.

FUTURE COBALT SUPPLY

Unlike the cobalt supply in the recent past, the future projected supply of cobalt is very good. Among other factors, the high cobalt price has fostered an exploration boom on land which by means of new successful exploration techniques has resulted in the discovery of over 20 significant cobalt-bearing deposits. A number, but not all, of these will be developed. The first should begin to come on line in 1997. Over the next decade they could annually put 15,000 to 20,000 new tons of cobalt onto the market. Different authors place varying estimates on this range of potential new deposits which could come on line in the next decade. The range includes: Cobalt Development Institute, 19,000 tons; Seddon (1996), 15,000-19,600 tons; and Garvey (1996), 17,150 tons. Table two is derived from these sources. It gives a list of new cobalt sources over 500 tons which have at least some reasonable potential of being developed in the next decade in the thinking of three leading industry experts. If every one of the major and minor deposits presently located was fully developed, 50,000-80,000 new tons/year of cobalt supply would be put on the market early in the next century (Garvey, 1996 ; Gellens, 1995). This is far more than any conceivable demand could absorb. Any massive infusion of cobalt unto the small world market would have the effect of significantly decreasing cobalt prices.

Table 2 : Potential New Cobalt Sources Projected at Over 500 Tons per Year

Site	Country	Projected Tonnage	
From Nickel Production			
Yakabindie	Australia	600	
Murin Murin	Australia	3,000	
Bulong	Australia	1,270	
Voisey's Bay	Canada	2,500	
Moa/Punta Gorda	Cuba	2,200	
Kabanga	Tanzania	1,600	
From Copper Production			
Boleo	Mexico	2,000	
Ernest Henry	Australia	1,500	from tailings
Kilembe	Uganda	1,000	
Nkana	Zambia	500	copper slags
Konkola Deeps	Zambia	500	
Mt. Isa	Australia	600	from tailings
Total		17,270	

Given the potential of a large number of new terrestrial sources it would seem that a potentially higher cost ocean source would have little chance to compete. However, manganese crusts are one of the few deposit types that is actually a cobalt deposit and not a deposit of another metal taking cobalt out as a low grade byproduct. This is very important as most of the new cobalt sources are actually nickel prospects that must mine very large tonnages of nickel to be profitable. Further, the chances of bringing this many world-class nickel projects on line in one decade is inconceivable given the relatively slow growth and good world supply of nickel. The world nickel market could never support this much addition of nickel, even if the world mining community had this much spare capital to develop this many new projects. A historical perspective suggests that about half of these projects will ultimately come on line over the next ten to twenty years, most with lower than anticipated production, particularly for byproduct metals such as cobalt. Only the largest tonnage, lowest production cost nickel prospects will come on line, such as the International Nickel Company's Voisey's Bay prospect in Labrador. The other prospects will wait to supply nickel at a future time of higher prices. The potential contribution of the cobalt in these deposits will be limited by the world nickel market .

FUTURE SUPPLY/DEMAND SCENARIOS

Given our current understanding of the cobalt market let us look at two supply scenarios for the next decade. First, being conservative let us suggest that 10,000 tons of new production comes on line by the year 2005. At the same time we may expect to lose 3-4,000 tons of traditional production due to deposits being depleted and African political problems. We will also lose probably 2,000 tons a year of sales from stockpiles which will have been sold off. Recycling, which is growing trend, may add up to 2,000 tons to the market. This would give a world supply of about 30,000 tons a year a decade from now. If the conservative long term cobalt growth rate was maintained, demand in 2005

would be over 34,000 tons or a market shortfall of 4,000 tons when compared against this supply scenario. If a 4% growth were maintained demand in 2005 would be 39,000 tons. It would be difficult to imagine that the average 10% growth experienced over the last two years would continue for a decade. However, if it did, demand in 2005 would be 64,000 tons. This supply/demand scenario suggests a price in excess or equivalent to today's high level and plenty of room for new manganese crust ventures.

An alternate scenario is that almost all the proposed new production comes on line driven by the high cobalt price. Assuming a very high production of 40,000 tons a year of cobalt by 2005 we would anticipate a cobalt price drop. A 30-40% price drop could easily stimulate a 20-30% increase (shift) in market demand. This would give a projected supply/demand balance in the market at 40,000 tons/year production in the year 2005. Such demand shifts due to lower cobalt prices are complex and difficult to assess because of the small, sectored nature of the market and significant demand in new areas. The best published guesses and those given by several metals experts at recent conferences are that long term cobalt price will fall but that a fall below about \$16 / lb for a period of several years or more (the spot market can do anything on the short term) would be very unlikely. A standard price used by many for the most likely low end price for cobalt over the next decade is \$18/lb (a 33% price drop over the present producer price). This second scenario is much more cautious than the first in terms of the ocean miner. It basically says that there is enough elasticity in the demand to accommodate a very high future supply of material albeit at a significant price reduction.

For the manganese crust miner either of these scenarios bodes relatively well. In the first case new nickel production will not be able to come on line massively enough to catch the ballooning cobalt demand caused by new technological innovation. This will leave ample room for cobalt produced from crusts. In the second scenario, cobalt production could be very high but market demand will absorb it by taking it at a lower price. This is still acceptable to the crust miner provided ocean mining costs can be kept to a minimum. Studies by Loudat *et al.* (1994) suggest that a cobalt production cost below \$10/lb would be reasonable for a crust venture. Given this case then an operation mining manganese crusts in the 3,000 ton/year range should be viable.

CONCLUSIONS

In summary, the cobalt market is a complex market serving independent sectors from a limited supply base. The price is high at the moment, as supply is only just meeting high cost demand by selling off stockpiles. The long term price may drop as some new sources come on line. This new supply will be taken up by unmet lower cost demand. A best guess long term cobalt price would be \$18/lb with a market of 30-40,000 tons after the year 2000. Such a market could stand a 3,000 ton per year ocean minerals operation coming on line in the year 2000. The market could not support many such operations without an inconceivable change in the present nature of supply and demand.

For the manganese crust miner this means both caution and optimism are required. The crust miner has the advantage that crusts are a cobalt ore not a nickel ore trying to compete in the relatively slowly expanding nickel market. On the other hand the cobalt

market is highly volatile and subject both to oversupply and price collapse. Looking at the fundamentals of the cobalt market and projecting on the basis of global economic prosperity and continued industrial expansion, there should be no problem for one prosperous manganese crust venture to exist. If this venture became highly publicized for its success, it could encourage a second or third such venture. The world cobalt market probably could not support three large highly profitable crust mining ventures. Therefore the initial crust miner would want to structure a venture of considerable flexibility. This would entail making back the capital cost of the venture in the first several years of operation. Further it would entail limiting capital exposure or having other potential uses for major capital assets.

One possibility here would be to process the manganese crusts aboard a ship which could be converted easily to another purpose if the economics changed. A modular processing plant installed on a large dynamically positioned vessel that could be converted into an offshore floating, storage and production vessel in the oil industry would be a good possibility. The same vessel would be used to mine and process the manganese crusts. If built in a modular fashion to allow easy and rapid substitution of modules it might be possible to switch back and forth between crust mining and oil operations as the market for either commodity peaked or subsided. This could be an effective way of covering a potential downside of dealing with the high volatility of the cobalt market. It could also be an effective way to recover capital if too many other producers were attracted to the business.

Manganese crusts are the largest tonnage source of cobalt known on the planet. The higher grade crusts are some of the richest cobalt deposits ever discovered. Unlike traditional sources of cobalt where the metal is mined as a byproduct, the crusts are a cobalt ore. Significant work has been done over the last decade mapping and defining the crust fields. It appears that they are technically minable and that this can be done in an economically viable fashion. Understanding the very complex market into which this ocean derived cobalt would have to fit is the next key part to assessing the future viability of a crust mining operation. This analysis of the current situation suggests that the ballooning demand in the face of the rising supply in the world cobalt market projected for the next half decade would allow the entry of one manganese crust mining operation. However, the cobalt market is the most volatile of major metals markets. Past predictions in this market have been fraught with errors because of unforeseen circumstances. For the future ocean miner this will present a worthy challenge and a great opportunity.

ACKNOWLEDGMENTS

This work has been supported by the U.S. Department of the Interior's Mineral Institute Program administered by the U.S. Minerals Management service through the Marine Minerals Technology Center, Ocean Basins Division under grant number G1115128. This work is also supported by the State of Hawaii and is Hawaii Department of Business Economic Development and Tourism, Ocean Resources Branch Contribution Number 129.

REFERENCES

Abraham, T. A. 1995. Magnets and Magnetic Materials: A Technical Economic Analysis. *Journal of Metals*. v.41 n.1 pp.16-18.

Cobalt Development Institute.1996a. *Cobalt News*. Six Monthly Production Statistics. October 1996, p. 11. Cobalt Development Institute, Wickford, U.K.

Cobalt Development Institute.1996b. Cobalt in Batteries. *Cobalt News*. January, 1996, p. 12-14. Cobalt Development Institute, Wickford, U.K.

Day, Martyn. 1996. Future Sources of Cobalt. *Cobalt News*. March 1996, p. 11-16. Cobalt Development Institute, Wickford, U.K.

Gellens, Luc. 1995. Cobalt by the Year 2000: Supply Issues and Growth. In: The Proceedings of Cobalt '95. Gorham/Intertech Consulting, Gorham, Maine.

Garvey, R.M. 1996. Two Thousand-The Era of New Supply. In: The Proceedings of Cobalt Industry Restructuring. September, 1996, New York City, Gorham/Intertech Consulting, Gorham, Maine.

Loudat T., J. Wiltshire, K. Zaiger, J. Allen and W. Hirt, 1994, *An Economic Analysis of the Feasibility of Manganese Crust Mining and Processing*, State of Hawaii Department of Business, Economic Development and Tourism Technical Report. 105p.

Loudat, T.A., K. Zaiger and J.C. Wiltshire, 1995, Solution Mining of Johnston Island Manganese Crusts: An Economic Evaluation, *Proceedings of the Ocean's '95 Conference, Marine Technology Society*, San Diego, 10 pp.

Seddon, M. 1996. An Update on New Mining Projects. In: The Proceedings of Cobalt Industry Restructuring. September, 1996, New York City, Gorham/Intertech Consulting, Gorham, Maine.

U.S. Department of the Interior, Minerals Management Service (MMS). 1990. *Final Environmental Impact Statement: Proposed Marine Mineral Lease Sale in the Hawaiian Archipelago and Johnston Island EEZs*. U.S. Department of the Interior, Washington, D.C.

FORMULATION OF SPECIALTY GLASSES AND GLAZES EMPLOYING MARINE MINERAL TAILINGS

G. F. Terry Lay¹ and John Wiltshire²

¹Department of Mining and Metallurgical Engineering
Technical University of Nova Scotia, Halifax, Nova Scotia, Canada

²Hawaii Undersea Research Laboratory, University of Hawaii
1000 Pope Road, Honolulu, Hawaii, USA

ABSTRACT

Processed manganese tailings have been melted under controlled conditions in a laboratory kiln to form various glasses and glazes. Fluxes were added to influence the chemical resistance, working characteristics and oxygen release from the glass melts. Frits were added to aid melt homogenation and reduce costs by increasing firing times. Complete mixing of melt components was also necessary to achieve homogeneity and pore-free glass. Nucleating agents were added to enhance the devitrification process, thus producing a fine-grained material free of residual stresses. Several mixtures of nodules/BHP tailings and borax/lithium tetraborate have produced hard, crack-free, semi-transparent, relatively homogeneous glass, with minor inclusions and equivalence in sizing of nucleation centers.

Glaze slips were produced from mixtures of frits and tailings. Binders were added to control the rate of water removal. Several glazes developed may be employed as protective coatings for clay bricks, concrete blocks and tiles, and as a protective finish for decorative ceramics and pottery wares. A brown, opaque glaze for bricks and blocks developed from tailings, borax, frit and modifiers is currently under ASTM testing.

A single phase manganese borosilicate glass yielding high durability and low leach rate may be acceptable as a nuclear waste glass. Preliminary heat treatment trials on manganese borosilicate mixtures suggests that production of glass ceramics for use as tiles and industrial fixtures may be feasible. Manganese borosilicate glass may also be useful as; a water repellent agent, a thermal coating on bricks, an additive to polymer composites and for cement reinforcement.

INTRODUCTION

Due to major factors such as i) the legal clarification provided by the Law of the Sea Treaty now in full effect, ii) the rapid economic growth in East Asia and iii) the sharp rise in world cobalt prices, the Chinese Ocean Mining Company has announced plans that it will begin mining manganese nodules and crust resources early in the next century. One of the major concerns with this development is the creation of environmental pressures. Current studies suggest that

80% of the environmental effect will be associated with ore processing, particularly tailings disposal.

The focus of ongoing research at the Nova Scotia Technical College and the University of Hawaii has been the development of useful products for the construction industry from marine manganese tailings which have been hydrometallurgically processed. Two sources of tailings have been investigated. These are tailings derived from processed manganese nodules from the Eastern Pacific and the BHP Groote Eylandt deposit, which is an elevated crust deposit just off the northern coast of Australia. The nodules (Table 1) have been treated by a high temperature, high pressure sulphuric acid leach process, to separate the major constituents copper, nickel, cobalt and manganese, resulting in tailings comprised of approximately 30-40% manganese dioxide by weight, along with silica, oxides and aluminosilicates (Haynes et al. , 1985). The BHP tailings (Table 1) have been mined from an open pit operation with the ore being processed to extract manganese as the main economic mineral, resulting in tailings containing mainly residual manganese fines (30-40% manganese dioxide) and kaolinite. Although manganese is considered a relatively benign element, its ability as an oxidizer characterizes it as a potential environmental hazard when in close proximity to other potentially harmful oxides which it can concentrate. These concentrations of oxides may create toxic conditions for living organisms by contaminating sources of sustenance and water.

Table 1. Chemistry of Manganese Nodules and BHP Slimes (wt. %)

	SiO ₂	Al ₂ O ₃	MnO ₂	FeO	PbO	K ₂ O	CuO	CaO	MgO	BaO	TiO ₂	Na ₂ O
Nod	16.8	2.0	33.9	9.6	0.03	0.98	0.12	1.5	0.05	0.35	0.71	0.95
Slime	28.1	20.3	36.0	5.6	-----	0.34	-----	0.04	0.14	0.60	0.48	-----

DESCRIPTION OF GLASS MATERIALS

Fluxes

The chemistry of the raw materials in glass melts is important since the ratio of glass formers (eg. SiO₂, B₂O₃, P₂O₅, V₂O₅) to glass intermediates (eg. TiO₂, ZrO₂, Al₂O₃, ZnO₂) plus modifiers (eg. LiO₂, BaO, SrO₂, K₂O, Na₂O, MgO, MnO₂) will determine how high the temperature must reach for the raw materials to melt (liquidus temperature), how viscous will be the melt, and when nucleation of the melt will occur to change a glass to a ceramic. Glasses with greater than 30% borate are considered borosilicates, while those with greater than 30% aluminum are considered aluminosilicates (McMillan, 1979). Greater than 20% Mn in a melt has tended to produce slag, thus sufficient glass formers should be added to maintain Mn at < 20% of the total melt volume.

Fluxes are oxides which react in the glass batch at relatively low temperatures. Glasses with high percentages of fluxes tend to have low chemical resistance (eg. Group I alkaline oxides). Stabilizers (eg. CaO, MgO, BaO, Al₂O₃) are oxides which impart to the glass a high degree of chemical resistance. They control along with fluxes, the working characteristics of glasses (eg. CaO, MgO, BaO, Al₂O₃). Fluorine is useful as a fining agent to inhibit gas release, since it displaces oxygen. The common alkali earth metals (Na, K) are used as fluxes, while alkaline earth metals (eg. Ca, Mg) act as network modifiers in frits.

Frits

Frits are proven raw material melt combinations of glass formers and additives prepared by heating to a high temperature a mixture of sundry inorganic acidic and basic oxides, which will speed up the melting process and aid homogenation of the melt to achieve high quality glass and ceramics. A homogenous melt free from inclusions and bubbles can be achieved through heating for a sufficient period of time (Doyle, 1979). Silica is the main acid constituent in frits with boron as an additional actor. Acting as an additional fluxing agent, frits are essential components of industrial glazes maturing below 1150 C degrees. Frits permit faster firing times and thus production cost savings. Crushed glass has been employed as a frit, thus saving time during the firing cycle by requiring less time for evolution of gases from new materials (eg. CO₂ from carbonates, H₂O vapor from clays and O₂ from manganese) (Taylor and Bull, 1986). Wide differences in particle size, shape, density and surface character make homogeneous blending quite difficult, and poorly blended frits will adversely affect frit quality. Usually, the smaller the new raw material grain size, the faster will be frit forming reactions (Potts et al, 1944), although fine grained materials inhibit escape of gases (Doyle, 1979). It is desirable to restrict iron oxide from the frit batch (Handbook, 1990).

Glasses

Glasses are non-crystalline silicates containing various oxides (eg. SiO₂, CaO, Na₂O, K₂O, Al₂O₃ and MnO₂). A glass is formed when a molten composition is cooled so rapidly that the atoms do not have sufficient time to arrange themselves in a periodic structure (Richerson, 1992). There is no definite temperature at which the liquid transforms to a solid as with crystalline materials. For crystalline materials, there is a discontinuous decrease in volume at the melting temperature. For most uses, the glass product should be homogeneous and pore-free. Homogeneity is achieved by complete mixing of the raw ingredients. Porosity results from small gas bubbles that are produced in the melt. These bubbles must be absorbed into the melt or otherwise eliminated, which requires proper adjustment of the molten material (Callister, 1985). Several mixtures of nodules/BHP tailings and borax/lithium tetra borate have produced crack-free, hard, semi-transparent, brownish glass, with potential for commercial applications.

Most inorganic glasses can be transformed from a non-crystalline state to crystalline by proper high temperature heat treatment (devitrification). This process may produce weak, non-transparent glass due to the polycrystalline state, along with the introduction of stresses during

volume changes. Addition of a nucleating agent can produce a fine-grained material that is free of these residual stresses (Callister,1985). A nucleating agent is an additive which either causes volume crystallization of a melt (after suitable heat treatment) or increases low volume nucleation. Metallic particles have been employed as nucleating agents along with oxides such as TiO_2 , P_2O_5 and ZrO_2 , although their influence is specific to certain systems (Lewis, 1989).

Phase separation in glasses

Phase separation in glasses is caused by a reduction in the thermodynamic free energy of the system. Phase separated glass may have an interconnected microstructure from either spinoidal separation or a nucleation and growth process, or the phase separation may consist of droplets of one phase in a matrix of the other. The properties of glass ceramic materials depend primarily upon the physico-chemical properties of the main crystalline phase, which occupies a greater portion of the volume of the material. If this crystalline phase is known, then its physico-chemical properties can be found from tabulated data, leading to estimations of the main properties of the glass ceramic material. These properties are also influenced by the properties of the residual glass phase, depending upon the amount and morphology present in the total bulk material (Lewis, 1989). The physico-chemical properties of the residual glass phase depend primarily upon its chemical composition.

The analytical determination of the glass phase composition in a multi-component system is most difficult. Generally, the composition can be estimated from the chemical composition and amount of the precipitated crystalline phase, and from the chemical composition of the initial glass. The properties of glass and glass ceramic materials are dependent not only upon the phase composition, but also upon; the character of the interface formed between the crystalline and glassy phase, and on the crystal size and overall morphology of the crystalline and glass phases (Lewis, 1989).

Glazes

Bourry (1901) suggested that glazes were vitreous coatings with which we cover bodies either to decorate them or to make them impermeable, and we may “consider them glass in the widest sense of the word “. Glaze also describes a prepared mixture of minerals being either a powder or suspension in water, used as a spray or dip for ceramic ware. Glazes are designed to fit a particular specification and will vitrify as does ceramic glass. Glazes are usually ground powders with the majority of particles <75um or 200 mesh. Raw glazes based upon mineral fluxes such as quartz and clays, do not contain any preformed glassy phase (frit) and are often employed in a once-fire process where body and glaze mature together. A glaze slip (mixture) may contain a mix of several frits, ceramic materials, insoluble manufactured chemicals and possibly flocculants and dyes. A binder is included to control the rate of removal of water from

the slip (Taylor and Bull, 1986).

The thermal expansion coefficient (TEC) for glazes is an additive property depending upon the composition, as each component contributes to the total expansion by a characteristic factor (English and Turner, 1929). Stresses in glaze layers often result from differential thermal expansion, between glaze and substrate as they cool from setting to room temperatures (Taylor and Bull, 1986). An adequate margin of safety against stresses is provided if the percentage linear expansion of the body exceeds that of the glaze by an amount between 0.02% and 0.06% (Bruce and Wilkinson, 1966). In crystallized material, phases develop which have different thermal expansions from the parent glassy glaze, with the expansions differing dependent upon the composition of the individual phases (Taylor and Bull, 1986).

Glaze quality is directly related to the size and amount of free silica in the body, and by inference to how many large free silica grain crystals occur at the glaze-body interface, with best glaze appearance resulting from the lowest free silica content. High alkali content tends to increase thermal expansion, decrease durability and increase costs (Taylor and Bull, 1986), thus substitution for (Na and K) by Mn could offset these negative effects. Lead oxide, barium oxide and strontium oxide will increase quality of glazes, although Pb and Ba are toxic and Sr is expensive (Gray, 1979). Opaque glazes are used when it is desirable to hide an undesirable body colour, whereas a transparent glaze coating is applied to desirable substrates (Taylor and Bull, 1986). Manganese can exist in several valencies (MnO^{II} , $\text{Mn}_2\text{O}_3^{\text{III}}$, MnO_2^{IV}) (Haynes et al., 1985), yielding a number of derived colours which can be modified by changes in composition.

Glass Ceramics

Glass ceramics are polycrystalline solids containing a residual glass phase, prepared by melting glass and forming it into products that are subjected to controlled crystallization. Controlled crystallization involves separation of a glassy phase in the form of tiny crystals, where the number of crystals, their growth rate and final size are controlled by suitable heat treatment. Controlled crystallization is specific to glass ceramic production with standard procedures that include, preparation of the glass batch, glass melting and glass forming. The purity of the glass ceramic material to be produced determines the degree of purity of the raw materials employed. Impurities or additives must always be considered, since they can act as nucleation catalysts or centers, thus having considerable effect upon the final properties of the melt (Shackleford, 1985).

The main qualities required in a glass ceramic used in the construction industry are: resistance to corrosion, freedom from oxidation, high hardness, excellent abrasion resistance, chemical durability, low thermal expansion coefficient and high thermal shock resistance (Partridge, 1994).

CURRENT RESEARCH BACKGROUND

For this research project, glazes are being developed as protective coverings for clay bricks, concrete blocks and tiles, and as a protective finish for decorative ceramics (eg. household

fixtures) for the construction industry. Other glazes are being developed for applications in the pottery industry as a finishing cover for fired wares. These glazes will exhibit opacity and several shades of semi-transparent colouration. Several widely used industrial, low thermal expansion glazes contain proportions of major ingredients such as; SiO₂= 50-54%, Al₂O₃= 27-29%, TiO₂= 3-9%, PbO= 1-3%, B₂O₃= 2-4% and Li₂O= 0-6% (Taylor and Bull, 1986). MnO₂ has been substituted for varying percentages of Al₂O₃, TiO₂, PbO and SiO₂ in the development of comparable glazes for clay bricks and concrete/cement blocks and tiles.

Structural Clay Products

Thermal expansion values for clays differ according to; the position of strata in the source deposit, contraction from dry to fired dimensions and the level of soluble salts, which can change between different sites within the same deposit. Climatic variations also affect glazed structural clay products. A good bond between glaze and body is most important. Pre-fired brick is the preferred substrate for glazing because the absence of body reactions allows rapid firing schedules. Lead oxide has been the main component of low firing glaze, not only because of its fluxing powers, but also due to its ability to lower surface tension and improve mechanical properties. Low surface tension glazes will coat porous brick bodies and cover imperfections in the brick surface. To produce adequate adhesion and handling properties, many additives have been included in industrial glaze compositions (eg. organic hardeners which prevent flaking of the dried unfired glaze and induce strength) (Taylor and Bull, 1986).

High fire glazes are usually free from imperfections and have been used with engobes to avoid crawling (excess flow) on heavy clay products. Engobes are mixtures of clays, fluxes and fillers which coat the substance with a permanent opaque layer. Heavy construction clayware is subjected to weathering and the exposed glazed surfaces thus should be acid resistant (ASTM, 1994). When the fired colour of the ceramic body is dark (eg. manganese tile) and the colour of glaze is to be light, or where it is necessary to equalize differences in stress between body and glaze, an engobe is interposed as a compensating layer. This layer can be weatherproof and lies between glaze and clay. When pigmented, engobes can be used to hide the colour of an undesirable clay base (Taylor and Bull, 1986). Engobes can be applied by spraying, brushing, dipping, or rolling (Verba, 1958). Any tendency for the engobe to peel or be rejected by the brick due to the presence of high levels of soluble salts in the clay can be overcome by addition of up to 1% BaCO₃ to the body, which also eliminates scumming in the clay and engobe (Taylor and Bull, 1986).

Concrete and Cement Building Blocks

Concrete building blocks have been glazed at low temperatures. Cement glaze has been produced by coating the article with an alkali metal silicate, drying the coating and applying a

second coating of an alkaline earth metal salt, which converts the original layer to silica. For concrete and cement blocks, glossy or matt flame-sprayed high lead glaze coatings have proven feasible. A two-stage process of engobe, then glaze was optimal. Pinholing in the final coating was avoided by applying to the substrate a wash coat containing potassium silicate and Al_2O_3 as an engobe before spraying a thin coating of glaze. Optimal results were obtained by researchers who applied a thin flame spray coating of a frit (Taylor and Bull, 1986).

Tiles

The manner in which tiles are to be used (internal verses external) influences the properties which must be built into the body and glaze (eg. external tiles must be frost resistant, thus tile porosity must be at a minimum), whereas for internal uses, porous tiles are acceptable. External floor tiles are usually vitreous which negates frost damage and enhances strength. Vitreous tiles are normally more expensive than low-fired tiles. Tiles must be slip-resistant, scratch proof, and resistant to staining and the effects of chemical cleaning agents. These properties are usually introduced through the glaze coating. Fast-firing techniques are primarily used in producing ceramic tile. Glazes for porous wall tiles are at least partially fritted to enable compositions to mature quickly without vitrification of the body taking place. Leadless formulations can be employed for white or coloured opaque glazes, but usually a small amount of lead bisilicate is added to reduce the viscosity of the glaze. Opaque glazes usually employ zircon as the opacifying phase. It is added as a mill addition or frit component. High lead glazes may be used to achieve patterned effects (Taylor and Bull, 1986).

The industry standard for tiles is 55 to 75 (wt. %) of glaze particles being <0.01 mm. in diameter. The viscosity of the slip is affected by changes in particle sizing. Viscosity is adjusted until the condition of the glaze is appropriate for the size, design, and type of ware, and the chosen method of application. A glaze should normally have a thermal expansion coefficient lower than its substrate. Compression is induced in glazes during cooling when the contraction of the body slightly exceeds the contraction of the glaze. Peeling occurs when the contraction of the body exceeds that of the glaze by too much, and the body cannot resist the stress (Taylor and Bull, 1986).

EXPERIMENTAL PROCEDURES AND RESULTS

Slimes and Additives

In this study, various additives (eg. zinc oxide) were mixed with BHP tailings (slimes) to produce glazes which would possess the outward appearance, strength, durability and thermal expansion coefficient, TEC, required to qualify as marketable glazes. The main objective was to produce glazes which were not prone to imperfections such as; crazing, crawling, pinholing, peeling and blistering. Tests indicated that mixtures containing less than 29 (wt. %) borax flux did not produce satisfactory glass, thus when preparing melts, slimes content was held under 70% by weight. Mixtures containing from 10% to 20 % lithium tetraborate with 90% to 80%

slimes produced acceptable quality glass. Further testing indicated that when lithium plus boric oxide replaced lithium tetraborate, glass could not be formed from 900 to 1300 C degrees, which represents the cheaper and more common range for glass formation.

Considering the chemical composition of slimes, it was concluded that additives would be required to produce acceptable quality glazes. The simplest and possibly least costly approach was to add known frits to the slimes to substitute for missing network formers and modifiers such as SiO₂, B₂O₃, Na₂O, CaO and K₂O. The main frits employed were; Frit 3134, Gerstley borate and Custer feldspar.

Slimes and Frit

A mixture of slimes (50%) and Frit 3134 (50%) was heated to 1120 C degrees for approximately 4 hours and yielded an excellent quality, dark-brown glaze, exhibiting no crazing, crawling, peeling or bubbling. It was concluded that this mixture possessed a similar TEC to the number 10 Raku clay substrate. Testing to ASTM standards is required to determine the mechanical properties of this glaze and hence its potential value as a marketable glaze.

Slimes and Borate (50-50)

A mixture of slimes (50%) and Gerstley borate (50%) was fired at Cone 2 (1100 C degrees) for 4 hours to produce a light-brown, sandy glaze with slight crawling feature (irregularly shaped areas which are either glazed or unglazed), and rough surface texture. The same mixture fired at Cone 4 (1150 C degrees) for 4 hours produced a medium-brown glaze with low viscosity, no noticeable crawling and moderate pinholing (small holes due to gas release). Both firings resulted in glazes with rough surface textures, possibly too coarse for wall tiles, but acceptable for production of patio tiles.

Slimes and Borate (80-20)

A mixture of slimes (80%) and Gerstley borate (20%) heated to Cone 10 (1300 C degrees) for 1 hour, then heated at 1250 C degrees for 40 minutes, then at 1300 C degrees for 40 minutes, produced a medium luster grey glass with no major defects. Mechanical testing may prove that this glaze would be a useful coating for wall, floor or patio tiles. Mixtures of tailings/borax have produced relatively homogenous single phase glasses, with minor inclusions and equivalence in sizing of nucleation centers, which suggests the glasses could have commercial applications. Figure 1 shows an SEM photograph (x30,000) of a glass produced by heating a mixture of 50/50 borax/BHP tailings to approximately 1300 C degrees, followed by air cooling. The glass exhibits distinctive homogeneity and a one phase relationship between raw materials.

Slimes, Feldspar and Frit

A mixture of slimes (50%), Custer feldspar (25%) and Frit 3134 (25%) was fired at Cone 4 (1150 C degrees) to form a dark-brown glaze which exhibited no noticeable crazing, crawling, bubbling or peeling, and minor pinholing. A second firing at Cone 10 (1300 C degrees) produced a light-brown glaze with higher viscosity and minor pinholing yielding a rough surface. Correction of this defect could yield a glaze useful for coating interior or exterior tiles, dependent upon the results of mechanical properties testing. It was concluded that Frit 3134 could be very useful in glaze development, but the high alkali content could decrease durability in a glaze product. Custer feldspar was found to be very useful for providing additional silica to increase luster in glazes and Gerstley borate may prove useful as an ingredient in glaze and glass.

Slimes and Borax/Lithium Tetraborate

The main properties desired in a glaze are; adhesion to substrate, correspondence of thermal expansion between glaze and substrate, transparency or opacity, surface texture and resistance to chemical attack (Taylor and Bull, 1986). Two glazes (BHA and BHB) developed to cover a number 10 cone Raku clay substrate are compared to a known glaze (GL1)(Maki and Tashiro, 1966) as follows in Table 2:

Table 2. Tailings Glaze Melt Composition Compared to an Existing Commercial Glaze (wt. %)

	SiO ₂	Al ₂ O ₃	MnO ₂	Na ₂ O	Fe ₂ O ₃	B ₂ O ₃	LiO ₂	TiO ₂	K ₂ O	PbO	ZrO ₂	P ₂ O ₃
BHA	37.3	10.1	18.0	5.0	2.8	11.6	-----	0.24	0.17	-----	-----	0.04
BHB	48.5	18.9	18.0	1.5	2.8	-----	-----	0.24	5.37	-----	-----	0.04
GL1	50.4	29.2	-----	1.0	-----	2.8	5.9	2.6	1.0	2.8	1.7	2.6

BHA is a mix of 50% BHP tailings with frit #3134 (Ferro Corporation) and BHB is a mix of 50% tailings with 50% Custer feldspar (Pacer Corporation, S. Dakota). Another glaze has been developed consisting of tailings, borax and frit, with several modifiers. This brown, opaque glaze is currently being modified to yield a semi-transparent glaze through which chosen engobes may produce several colour variations for bricks and blocks. Glaze properties are being tested for acceptance by ASTM standards.

Comparison With Commercial Glass

The characteristics desirable in a manganese borosilicate glass based upon known borosilicate glasses would be; maximum alkaline durability, high strength, stiffness, wear resistance, chemical inertness, hardness and cheapness. This study has produced specimens which are of similar chemical composition to existing commercial glasses. Commercial Glass A seals to Kovar, Nilo and Fernico, and is used in small seals or in large seals of tubular design. Commercial glass B with a lower TEC, seals to tungsten, and commercial glass C with a high melting point and low alkali content is produced as continuous fiber for glass fiber reinforced

composite materials for weaving into glass textiles used in electrical insulation. The chemistry of commercial glasses A,B and C is compared to the chemistry of experimental glass M1 (70/30, slimes/borax) and M2 (50/50, slimes/borax) in Table 3.

Table 3. Comparison of the Chemistry of Existing Commercial Glasses to Experimental Glasses

	SiO ₂	Al ₂ O ₃	B ₂ O ₃	MgO	CaO	PbO	Na ₂ O	K ₂ O	Fe ₂ O ₃	MnO ₂
A	67.5	2.5	21.7	----	----	----	3.2	4.2	----	----
B	75.5	2.6	16.0	----	----	----	3.7	1.7	----	----
C	52.9	14.5	9.2	4.4	17.4	----	0.5	0.5	----	----
M1	19.7	14.2	11.0	0.10	0.03	----	6.1	0.24	3.92	25.2
M2	14.05	10.13	18.3	0.07	0.02	----	9.0	0.17	2.80	18.0

FUTURE RESEARCH

Nuclear Waste Glasses

Borosilicate glass is currently the nuclear waste form of choice for most countries. Its selection is based upon; an anticipated ease of processing (ie. glass frit and waste are mixed, melted at relatively low temperatures and poured into canisters), the technology is well demonstrated for real radioactive wastes, and the assumption is that glass as an aperiodic solid will easily accommodate wide variations in waste stream composition (up to 30 components). Also, the processing technology for waste materials is quite similar to demonstrated technology for borosilicate glass, the main difference being the final heat treatment (Ewing and Lutz, 1994). The glass forming, non-radioactive constituents determine the maximum waste loading obtainable. The chemical composition (frit and waste) determines the formation (melting) temperature and other properties (eg. viscosity and electrical conductivity of the melt). Critical characteristics of the waste form are phase transformations (upon cooling), mechanical integrity, chemical durability and effects of radiation upon any of the properties (especially chemical durability).

Polyphase assemblages are more common than single phase due to waste stream complexity. Even when a ceramic displays a dominant single phase, one expects to find other phases (glass and crystalline) segregated along grain boundaries. Research suggests that the redox state of the glass, existence and composition of crystals, and the presence of glass-in-glass phase separation can affect durability (Sproull et al, 1994). Thus, phase separation (glass-in-glass) should be avoided due to potential for decrease in durability, as radionuclides tend to concentrate in the less durable phase (Ewing and Lutze, 1994).

Referring to Figure 1, this single phase manganese borosilicate glass may provide a feasible basic mixture to which can be added radioactive waste that will produce a glass of acceptable durability and leach rate. Reaction of manganese borosilicate glasses with various radioactive waste mixtures and the leach rates of the resultant glasses within natural earth materials remains to be tested.

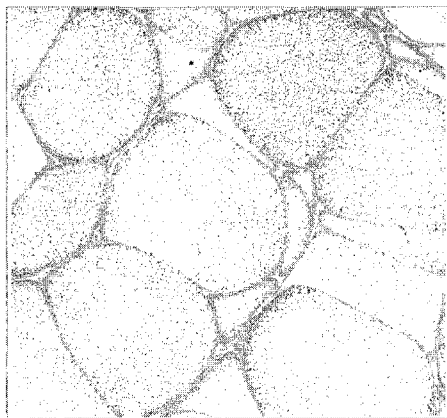


Figure 1. SEM Microphotograph of 50/50 Borax/Slimes Glass Product

At least 27 major nuclear waste glasses have been produced by many nations and all fall within a narrow range of compositions. Researchers suggest that for a single phase waste glass, the alkali oxide content should be greater than approximately 17%, plus aluminum oxide levels should be below 70 wt. %. In Figure 2 (Hench, 1985), numbered contours outline the areas of composition within which the calculated leach rate (90 C degrees and 28 day leach test) is not more than the contour value. The preferred range of leach rate is 0. 1 to 0. 2 g. m⁻². d⁻¹. Substitution of Mn for Na in this ternary association may be a plausible approach to increase durability, by decreasing the alkali content. Previous research also indicated that leachability decreased markedly with increasing waste product loading, possibility due to formation of a protective layer rich in various elements (eg. Fe, Ni, Mn, Ti and Zr).

Waste glasses may be subjected to corrosion processes when immersed in aqueous solutions or to weathering processes where they may undergo leaching and dissolution of some components leading to formation of numerous secondary phases. Previous research suggests that corrosion and weathering are due to processes such as; ion exchange of network formers, hydrolysis of the glass network, dissolution of glass components, and nucleation and precipitation of secondary

phases and products through surface alteration layers (Sproull et al, 1994).

Future waste glass composition development is dependent upon the technical feasibility of production (ie. formation temperature, process specific requirements, viscosity and electrical resistivity, and by the waste composition (Sproull et al, 1994). For a manganese based waste glass to be competitive, it would require a lower melting temperature and higher waste loading than existing forms (eg. sphene @ 1300 C and 15% loading). Industry has compiled a library of reference frits (Sproull et al, 1994), which have been used on a large scale, and which can be employed as standards for comparison and determination of the acceptability of new compositions.

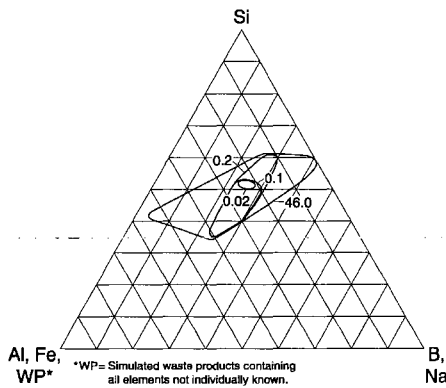


Figure 2. Areas of Composition and Leach Rates For a Single Phase Waste Glass

Fiberglass

Fibers for fiberglass are produced using several manufacturing processes, then sprayed with an organic binder (eg. phenol-formaldehyde resin), then passed through an oven to cure the binder. Ceramic fibers can be made into aggregates, blankets and fiberboards. Oxide and silicate fiber compositions are available in fiber bundles, woven cloth or blankets and hardboard (Richerson, 1992). Marketable products available from glass fibers include; loose wool for hand-packed thermal insulation, flexible rolls for thermal and acoustical insulation and rigid sheets, slabs and standard shapes, and thermal and acoustical insulation. Binders may contain various additives for functions such as fire retardation and water repellancy (Rawson, 1991). Due to the release of

O₂ from MnO₂, manganese based glass may not be suitable as a fire retardant unless the O₂ can be contained by a binder or other material added to the glass melt. Manganese borosilicate glass could perform adequately as a water repellent agent.

Fiberglass is normally employed as backup to brick insulation. It is conceivable that bricks glazed with a manganese borosilicate coating may provide equivalent thermal retention to bricks plus insulation. Alkali resistant fiberglass has been employed for reinforcing cement. Alkali-free glasses have displayed high electrical resistivity and good chemical durability in neutral and mildly acid environments. These characteristics and high strength make them suitable for use in polymer composites and cement reinforcement (Rawson, 1991). Manganese borosilicate glass, being alkali-free, may find similar usage. Silica glasses containing 15-20% ZrO₂ have proven resistant to cement paste alkaline environments (pH 11-12) in glass reinforced cement (Proctor, 1985), thus zircon could be considered an additive to a manganese based glass. Typical compositions of glass mineral, insulation and high temperature fiber products are presented in Table 4 (Mohr and Rowe, 1978).

Table 4. Compositions of Glass Mineral, Insulation and High Temperature Fiber Products

	SiO ₂	Al ₂ O ₃	Fe ₂ O ₃	CaO	MgO	Na ₂ O	K ₂ O	B ₂ O ₃	F ₂ O
Glass mineral	50	10	1	25	14	-----	-----	-----	-----
Insulation	63	6	trace	7	3	14	1	6	0.7
High-Temp	50	40	trace	6	4	-----	1	0.7	-----

Glass Ceramics

Tailings compositions have similar silica and alumina oxide values to existing products (Table 1). The challenge is to maintain suitable characteristics after partial substitution of MnO₂ for these oxides along with the calcium, magnesium and sodium oxides. Preliminary heat treatment schedules have been established indicating that production of glass ceramics for use as tiles and industrial fixtures may be feasible. Specific heat treatment schedules for specific mixtures are required to produce reliable ceramic products for ASTM testing.

CONCLUSIONS

This research has shown that manganese tailings can be employed to produce glass, glazes and eventually ceramic-glass which could have commercial applications. Additional research is required to determine whether the individual characteristics of these specimens will meet industry demands and whether new products can be produced economically. It is probable that various glass ceramics can be developed from tailings based glasses by employing effective heat

treatment schedules. Based upon findings, future research should result in producing additional acceptable quality glass, waste glass and glass ceramic products.

ACKNOWLEDGEMENT

This work was funded in part by the Broken Hill Proprietary Company (BHP), the State of Hawaii and National Atmospheric Administration project R/CM-1, which is sponsored by the University of Hawaii Sea Grant College Program, SOEST, under Institutional Grant No. NA 36RG0507 from NOAA Office of Sea Grant, Department of Commerce. The views expressed herein are those of the authors and not necessarily those of the funding sources. This is Ocean Resources Branch Contribution number 131 and UNIHI-SEAGRANT-CR-97-02.

REFERENCES

- ASTM 126. 1994. Specification for ceramic glazed structural clay, facing tile and solid masonry unit.
- Bourry, E. 1901. Treatise on the Ceramics Industries (translated by W. P. Rix), Scott Greenwood.
- Bruce, R. H. and W. T. Wilkinson. 1966. Trans. Brit. Ceramic Soc. , **65**, pp. 233-276.
- Callister Jr. , W. D. 1985. Material Science for Engineering, Wiley, pp. 302-309.
- Doyle, P. 1979. Glass Making Today, (Ed.), Portcullis Press, pp. 170-175.
- English, S. and W. E. S. Turner. 1929. J. Am. Cer. Soc. , **28**, pp. 52-62.
- Ewing, R. C. and W. Lutze. 1994. High Level Nuclear Waste Immobilization With Ceramics, Ceramics Intl. , 17, pp. 287-293,1991. J. F. Sproull, S. L. Marra and C. M. Jantzen, High Level radioactive waste glass production and product description, Mat. Res. Soc. Sym. Proc. , vol. **333**, Mat. Res. Soc. , pp. 15-25.
- Gray, T. J. 1979. Bull. Amer. Ceram. Soc. , **58**, pp. 768-770.
- Handbook of Glass Manufacture. 1990. vol. 1, Sect. 09, pp 517-579.
- Haynes, B. W. , Barron, D. C. ,Kramer, G. W. , Maeda, R. and M. J. Magyar. 1985.

- Laboratory processing and manganese nodules, U. S. Bur. Mines RI8938, pp. 1213.
- Hench, L. L. 1985. Leaching of nuclear waste glasses, In: Wright, A. F. and Dupuy, J (eds.) Glass. . . . Current Issues. NATO ASI series, Series E: Applied Sciences No. 92, Martinus Nijhoff Dordrecht, Boston, Lancaster, pp. 631-637.
- Lewis, M. H. 1989. (ed.), Glasses and Glass-Ceramics, Chapman and Hall, pp. 203-209, 1989.
- Maki, T. and T. J. Tashiro. 1966. J. Ceram. Assoc. , Japan, **74**, pp. 89.
- McMillan, P. W. 1979. Glass -Ceramics, Academic Press, pp. 285.
- Mohr, J. G. and W. P. Rowe. 1978. Fiberglass, Van Nostrand Reinhold Co. , N. Y. , pp. 338.
- Patridge, G. 1994. An overview of glass ceramics, Part 1. Development and principal bulk applications, Glass Technology, vol. **35**, No. 3, June, pp. 116-127.
- Potts, J. C. Brookover, G and O. G. Burch. 1944. J. Am. Cer. Soc. **12**, pp. 760.
- Proctor, B. A. 1985. Alkali resistant fiber for reinforcement of cement. In: A. F. Wright, and J. Dupuy (eds.), Glass Current Issues. NATO ASI series. Series E: Applied Sciences, No. 92, Martinus Nijhoff. Dordrecht, Boston, Lancaster, pp. 555-573.
- Rawson, H. 1991. Glasses and Their Applications, The Institute of Metals, Ch. 13, p. 130-135.
- Richerson, D. W. 1992. Modern Ceramic Engineering, 2nd ed. , Dekker, pp. 22-23.
- Shackelford, S. 1985. Introduction to Materials Science for Engineers, MacMillan, pp. 353-360.
- Sproull, J. F. , Marra, S. L. and C. M. Jantzen. 1994. High level radioactive waste glass production and product description, Mat. Res. Soc. Sym. Proc. , vol. **333**, Mat. Res. Soc. , pp. 15-25.
- Taylor, J. R. and A. C. Bull. 1986. Ceramics Glaze Technology, Pergamon Press, pp. 263.
- Verba, R. J. 1958. J. Bull. Amer. Ceram. Soc. **37**, pp. 364-365.

TRANSVERSE ZONES AND TRANSFORM FAULTS AS TARGETS IN SEARCHING FOR SUBMARINE MINERALIZATION

Valentina A. Baskina

Institute of Ore Deposit Geology, Petrography, Mineralogy and Geochemistry, (IGEM RAS)
Moscow, Russia

ABSTRACT

Deep-rooted dislocations transverse to continental - ocean margins are widely regarded as important in the control of submarine economic mineralization around the Pacific. Zones of this type were recently distinguished in SW Japan. In the ocean plate to the East of Japan, a set of transverse faults was traced at 80 to 500 km. depth as boundaries of segments of a deep seismic zone and the corresponding parts of the trench. On the island surface in SW Japan, continuation of the transform along the latitudinal zone of $34^{\circ}30'$ - $35^{\circ}N$ is marked by a chain of large economic deposits of various types and ages. Those are deposits of Mo, Sn, W, Pb, Zn, Au, Ag, Cu, U, Fe, Mn, of vein, greizen, skarn and stratabound type, in particular Daito, Ikuno, Otani, Kune, and others, their age spans the interval from Paleozoic to Neogene. Similar polychronic chains of the largest deposits trace islandward continuations of other transform faults, probably marking hidden throughgoing structures, adjusted to the same long-living set of dislocations. Transverse ore belts of SW Japan possess typical features of so-called "ore-concentrating" zones. The latter are agreed to serve persistently as passways of heat, juvenile magmas, gases and fluids and as a result - as areas of unusually high polygenetic ore concentrations in each metallogenetic epoch, as well as of oil and gas. Both oceanward and seaward continuations of these zones deserve to be the prime target in searching for submarine mineralization.

INTRODUCTION

In searching for new mineral sources in continental crust, special attention is now paid to exceptional ore accumulations (like large and giant deposits and their clusters), which are considered to be first-rate targets. As it was earlier noted, tectonic setting and endogenetic evolution of large deposits differs from that of smaller deposits of the same age and mineral composition. This is true for each mineral province, despite "absolute" size of most valuable deposits in it. (Billingsley and Locke, 1941; Favorskaya, 1971; Favorskaya et al. 1974; Kutina, 1980; Baskina, 1982; and others). Large deposits display as chains arranged along some persistent linear geofractures, mostly latitudinal and meridional, probably parts of a global deep-rooted regmatic shear system. The chains usually cut through boundaries of folded belts as well as the boundaries of the continent - transition zone, thus belonging to throughgoing or transverse dislocations. Generally each chain comprises deposits of various ages and types. Magmatic assemblages as well as geophysical data prove the deep-seated origin and multiple interchange of compression and extension in geologic history of these dislocations. Similarity in tectonic setting and endogenetic regimes of mineral superaccumulations (despite differences in their age, type and mineral composition) was shown. We regard the zones as persistent pathways of heat,

juvenile magmas and fluids which influenced evolution of crustal acid chambers resulted in accumulation of large deposits of W, Mo, Sn, Pb, Zn, Cu, Au, Ag, Mn and some nonmetallic ones.

As transverse ore-concentrating zones often control recent endogenetic activity, we suggest their submarine propagation to be among first targets in searching for submarine economic mineralization. Japan and surrounding areas are no exception. Ishihara et al. (1975) noted, that among Neogene- Quaternary deposits of sulfur, gold and base metals, the largest ones are confined to the land continuation of latitudinal transform faults. These data lead us to analyze the spatial position of large economic deposits in Japan, regardless to their age and metal composition. As a result, some new long - living latitudinal zones were proposed. This contribution describes a newly revealed transverse ore-concentrating zones in Japan, as a case, so far rarely proved, of direct transition between transform faults on ocean floor and long-living hidden transverse dislocations in continental folded belts.

DISTRIBUTION OF ORE DEPOSITS AND TRANSVERSE ORE-CONCENTRATING ZONES IN JAPAN

Economic ore deposits in Japan are counted by the hundreds. Mostly those are of small and medium size, but some tens belong to large and even to giant accumulations. According to recent standards (Laznicka, 1985), some clusters, like Daito, Hirase (Mo), Otani-Kaneuchi (W), Hokuroku (base metals, Au), Konomai (Au) belong to giant ones. The role of large deposits in Japanese economics can hardly be overestimated. For example, of more than 500 gold and silver minable accumulations, over 80 % of total gold comes from 10 % of veins (Kamitani and Kanazawa, 1993). Spatial distribution of large deposits in SW Japan proves both the crucial role of persistent transverse dislocations in their localization and direct transition of those dislocations to ocean plate transform faults.

Transform faults around Japan, which were studied, in particular, by Carr and coworkers (Carr et al, 1973), make a set of latitudinal faults traced by geophysical methods from 85 km to 500 km of depth. The faults serve as borders between segments of the deep seismic zone. Each segment, 100 - 300 km wide, differs from its neighbor by total depth, focal depth, dip trend, and seismic activity. Projections of transform faults to the ocean bottom divide the ocean trench into segments, which vary by width, depth, trend, and relief of slopes. Projections to the island surface control many geologic and morphostructural features. Among the latter there are bends in the trend of chains of recent volcanoes, the position of the largest calderas, the configuration of shore line and, as it is shown below, the control of the richest ore accumulations.

Having compared data on the metallogeny of southwest Japan we put special attention on the distribution of large and superlarge mineral accumulations and stressed the differences in spatial position of the latter versus small and medium deposits.

Distribution of Neogene gold-silver deposits and their clusters were recently described by Kamitani and Kanazawa (1993). All deposits - small, medium and large are confined to areas of

Neogene volcanics, with a single exclusion which proved to be a Cretaceous granite-related vein deposit. Data on the distribution of the youngest, Pliocene- Quaternary volcanogenic deposits of gold-silver, sulfur and base metals were presented by Ishihara et al. (1975). As cited authors noted, the largest subaerial deposits of those groups were localized along projections of transform faults. Spatial distribution of Late Paleozoic - Early Mesozoic volcanogenic deposits of massive sulfides and base metals were considered by T. Tatsumi (1970). It is easy to note from these data that the bulk of Bessi-type massive sulfide deposits are confined to NEE trending geosyncline belts, while the largest ones, like Hitachi, Kuno as well as a single Early Cretaceous large kuroko-type deposit Taro, occur at intersections of some dislocations with projections of transform faults.

The spatial position of granite related vein, skarn, and greizen deposits of rare, nonferrous and base metals (Sn, W, Mo, Pb, Zn, Sb, As, Au, Ag) is confined to SW - NE trending areas of Late Cretaceous - Paleocene volcanic-plutonic assemblages, the so called Sanin and Sanjo belts. (Murakami, 1974). These belts were distinguished by a systematic difference in radiometric age, petrology of volcanics and related granites and was later proved by differences in Sr, O, N, S isotope characteristics as well as in age and type of granite related ores. As it is evident from various data (Doi et al., 1975; Imai, 1978; Ishihara, 1971, 1978; Ishihara et al., 1975, 1988, 1991) on a background of SW - NE areas of evenly scattered small and medium deposits, the biggest ones make clusters within the same narrow throughgoing latitudinal belts - projections of transform faults. Thus, the occurrence of the largest granite related and telethermal deposits is in no doubt connected with transverse dislocations.

One of the most pronounced transverse zones to control large ore deposits in Japan is that of $34^{\circ}30'$ - $35^{\circ}N$. It controls the position of at least 8-9 large mineral accumulations, their age spanning the time interval from Late Paleozoic to Early Neogene. These are the clusters of granite related, volcanogenic and distant hydrothermal deposits of Sn, W, Mo, Pb, Zn, Ag, Au, Cu, Fe as well as manganese, and uranium (Doi et al. 1975) The largest pyrophyllite accumulations mentioned by K. Sato (1994) also belong to the same zone both in southwest Japan and in south Korea. The seaward continuation of the transverse ore belt, is a very important transform fault: it divides the Izu - Bonin and North Japan arcs, which trend respectively $N 30^{\circ}E$ and NS , and borders on two different parts of the oceanic trench - of 9 km of depth to the South and of 6 km of depth to the North (Carr et al., 1973). Its surface projection coincides with a boundary between contrasting gravity fields: positive to the North and negative to the South (A Bouger Gravity Anomaly Map. 1994).

Distribution of some large versus small and medium volcanogenic and granite-related ore deposits, and the general pattern of transverse ore belts in relation to transform faults in SW Japan are shown below (Figures 1 and 2).

Each transform fault on figures 1 and 2 is named after the mark of a neighboring segment of deep seismic zone, after Carr et al. (1973). The main polychronic latitudinal belts are coincided with B1 (about $34^{\circ}30'N$ - $35^{\circ}N$) and H1 faults. Neogene Au-Ag deposits are controlled mostly by meridional dislocations parallel to the North Japan trench.

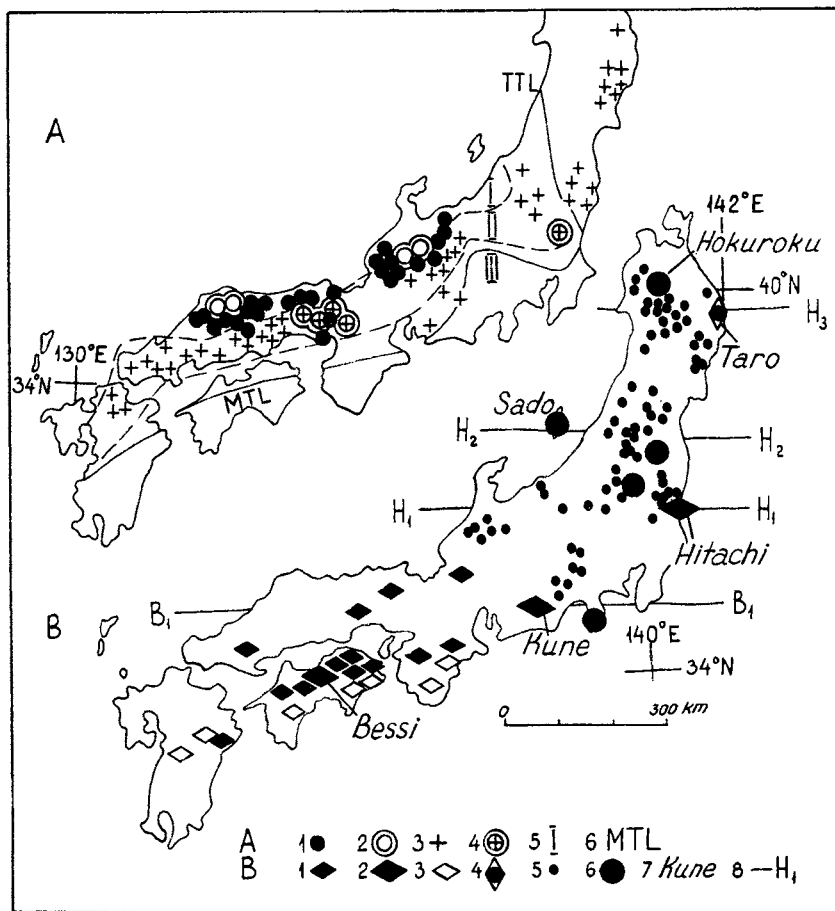
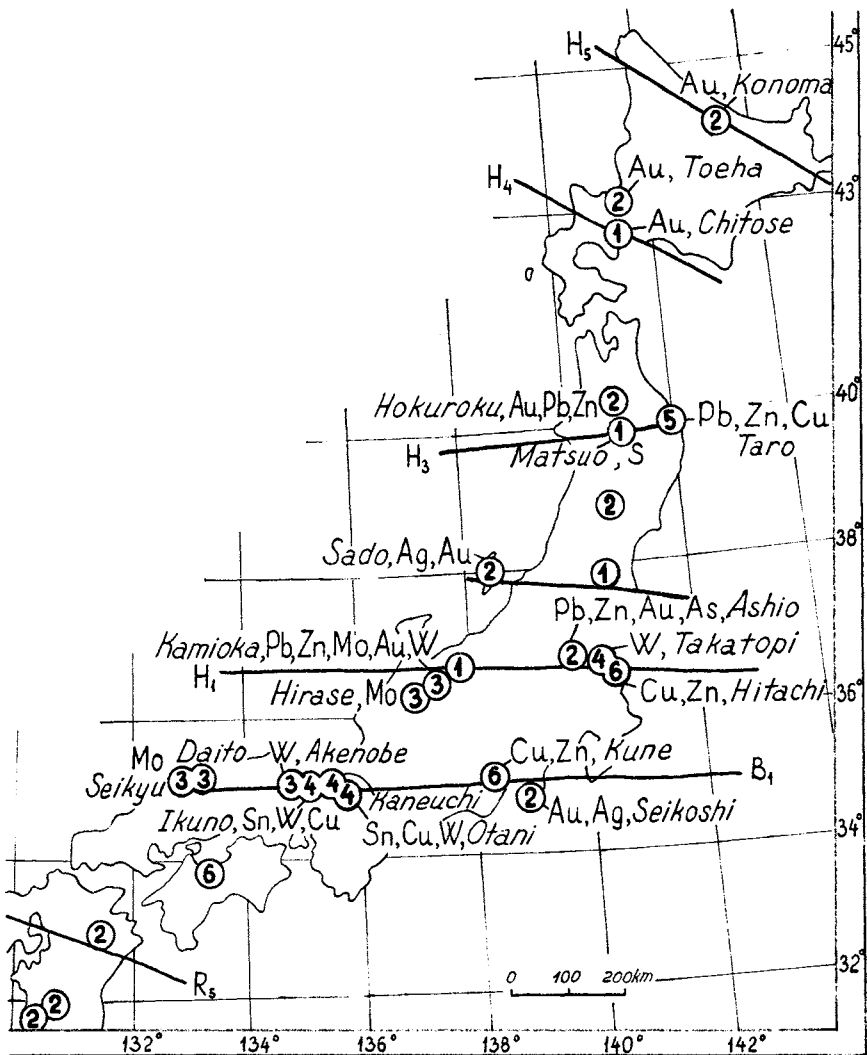


Figure 1. Distribution of some ore deposits in Japan. **A.** Granite related deposits (after Ishihara, 1978, Ishihara et al., 1991). *Legend:* 1, 2 - Paleocene, Pb, Zn, Mo: 1 - small, medium; 2 - large. 3, 4 - Late Cretaceous, Sn, W, Cu: 3 - small, medium; 4 - large. 5 - Belts: 1 - Sanin; 11 - Sanyo; 111 - Outer Zone, Chichibu and Shimanto belts. 6 - MTL-Median Tectonic Line. TTL -Tanakura Tectonic Line. **B.** Volcanogenic deposits (after Tatsumi, 1970; Kamitani and Kanazawa, 1993; Ishihara et al., 1975). *Legend:* 1, 2 - Paleozoic massive sulfide: 1 - small, medium; 2 - large. 3, 4 -Early Mesozoic: 3 - small, medium massive sulfide; 4 - large, kuroko type. 5, 6 - Neogene Au, Ag, Au-bearing kuroko: 5 -small, medium; 6 - large deposits, clusters. 7 - deposit name; 8 - projection of transform fault.



1-N₂-Q 2-N₁₋₂ 3-P₁₋₂ 4-K₂ 5-J-K₁ 6-PZ₃ 7-Kamioka 8-B₁ 9-Cu

Figure 2. Position of the largest ore deposits and clusters in relation to transform faults in Japan. Legend: 1 - 6 - age of deposits: 1 - Recent to Neogene; 2 - Neogene; 3 - Paleocene; 4 - Late Cretaceous; 5 - Jurassic-Early Cretaceous; 6 - Paleozoic. 7 - deposit name; 8 - projection of transform fault; 9 - principal metals.

As it was shown earlier for various regions of the World, some features are generally characteristic for transverse ore-concentrating belts (Favorskaya, 1971; Favorskaya et al. 1974; Kutina, 1980; Baskina, 1982). Among them, there are connection with geophysically manifested steep mantle discontinuities; multiple intermittent ascent of alkali basaltic, ultramafic, potassium rich magmas as well as fluids enriched with mineralizers like F, Li, Cl, P, B, C, and sometimes concentration of those latter as exceptional mineral accumulations. F-Li rich, rare metal bearing granites emplace within the same belts. Besides, multiple activation of ore forming processes is typical, resulted in wide age spectrum of rich deposits along a belt as well as polychronic and polygenic ores in the most part of large deposits, often accompanied by recent thermal activity and mineralization. The transition of continental transverse ore-concentrating zones to ocean transform zones like the "Mendocino line" in North America was also noted in cited papers and elsewhere.

So far we possess no evidence on magmatic anomalies within the B1 belt in south- west Japan, comparable with typical anomalies of case ore concentrating belts, but some facts are noteworthy. Submarine part of the zone in Tokyo Bay is traced by narrow latitudinal chains of Middle-Miocene to Pliocene basalts, andesites, serpentinites (Geol. Map of Tokyo... 1995). Continental areas in the vicinity of 35⁰N, in the Korean Peninsula are a probable continuation of the same belt, as it is found by morphostructural analysis (Ore Concentrating Structures...1983). They are marked by masses of Late Cretaceous monzonites, rare in other parts of peninsula (Geologic Map of Korean... 1990). A chain of small gabbro bodies traces the zone in the Sanin belt (Takagi, 1993), as well as close interconnection of magnetite-series and ilmenite-series granites is typical only for some transverse zones (B1, H1).

As the transverse zones of Japan possess to a great extent most of the typical features of ore concentrating belts described elsewhere, we regard eastward and westward continuation of those zones in Japan as first-rate targets in searching for submarine mineralization. The submarine part between two land blocks could be of special interest: we mean the zone H3, about 40⁰N - 40⁰30'N which controls the Hokuroku cluster and Matsuo deposit in Japan, and is continued in a well known zone of North China with several world famous ore clusters, mostly Precambrian (Zhai, 1996).

In other parts of the Pacific, where unlike Japan much faster change in trends and spatial position of arc tectonic elements is proved, some transfer fractures which control recent ores probably shifted from their earlier position as they are parallel to, but make no direct continuation with continental transverse ore belts. The example of New Guinea and surrounding areas is noteworthy. Most of economic gold deposits of Early Miocene to Pliocene age (from west to east there are Erzberg, Ok-Tedi, Porgera, Yandera, Esis, Panguna) make a narrow latitudinal chain between 5⁰-6⁰S. It is easy to note according to various data that the chain is transverse to the borders of continental plate, collision belt, volcanic arc terrains (Baldwin et al. 1978; Gustafson and Titley, 1978; Lottermother, 1990; Richards and Ledlie, 1993; Rona and Scott, 1993). We believe that "ore concentrating" role of the belt is proved by the recent finding of the Porgera giant deposit (Fleming et al. 1986) under a small placer prospect just between ordinary deposits, within this narrow transverse belt. Transforms and spreading ridges hosting submarine

deposits (Pacmanus, Woodlark) also keep latitudinal trends (Benes et al. 1994; Binns and Scott, 1993), so are parallel to New Guinea- Bougenville "main" belt.

All the above data give additional support to the idea that during geological history an old frame of deep-rooted discontinuities determined inherited trends in a succession of tectonic structures, including those on ocean plate. One of importance is the meridional trend of gold bearing structures in Pacific. The set of repeatedly reactivated longitudinal belts and geofractures hosted the main gold mineralization of Eastern Australia since Proterozoic time and probably influenced the position of the superlarge recent deposit on Lihir island. In Japan the chain of main gold deposits is known along 141°E , within the volcanic belt of Miocene to Recent Japan Arc. To the North the same belt is continued by the rift of Tatar Strait, where Cretaceous - Paleocene gold deposits formed on its borders (like Mnogovershinnoe deposit near the Amur mouth). Further to North dislocations along 141° - 142°E (the border of Proterozoic Okhotsk Central massif) control the large Late Cretaceous gold-silver deposit Khakanzha. Recent sulfide mineralization is found in the vicinity of Nampo islands, in area 26° - 32°N and 139° - 141°E . (Rona and Scott, 1993). That is why we regard this belt as a long-living gold bearing one and believe its continuation to the South from Japan also as the first-rate target in searching for submarine gold mineralization.

CONCLUSIONS

In southwest Japan large and giant ore deposits, various in age, composition, genetic type, compose several latitudinal belts, the latter divided by intervals of 200 -250 km. We believe, that like in other parts of the World, the linear chains of the largest ore deposits and other geochemical anomalies trace systems of persistent deep-rooted dislocations, transverse to boundaries of folded belts and/or continent - ocean plates. According to the ages of deposits, transverse zones in Japan were intermittently active during Phanerozoic time. The case of Southwest Japan is a rare example of a direct transition of transverse zones in continental crust to transforms on ocean plate. The suggestion is made, that submarine continuation of ore-concentrating transverse structures of Japan could be first-rate targets in searching for submarine economic mineralization. Among the zones, two latitudinal (B1, about 35°N and H3, about 40°N , as well as meridional one, 141° - 142°E , are regarded as the most promising.

Acknowledgments

Study was made with the aid of Russian Foundation for Basic Research (Project 95-05-14525).

REFERENCES

- A Bouger Gravity Anomaly Map in Central Japan. 1994. In: Geol. Surv. of Japan. **280**. Tokyo.
- Baskina, V. 1982. Magmatism of ore concentrating structures. Moscow: Nauka. (in Russian).

- Baldwin, I., H. Swain, and G. Clark. 1978. Geology and grade distribution of the Panguna porphyry copper deposit, Bougainville, Papua New Guinea. *Ec. Geol.* **73**:690-703.
- Benes, V., St. Scott, and R. Binns. 1994. Tectonics of rift propagation into a continental margin. *Journ. Geophys. Res.* **99**:4439-4457.
- Billingsley, G., and A. Locke. 1941. Structure of ore deposits in the continental framework. *Trans. Am. Inst. Min. Metal. Eng.* **115**:59-65.
- Binns, R., and S. Scott. 1993. Actively forming polymetal sulfide deposit associated with felsic volcanic rocks in the eastern Manus backarc basin, Papua New Guinea. *Ec. Geol.* **88**:2226-2236.
- Carr, M., R. Stabier, and Ch. Drake. 1973. Discontinuities in the deep seismic zone under the Japanese Arcs. *Geol. Soc. Am. Bull.* **84**:2917-2930.
- Doi, K., S. Hirono, and Yu. Sakamaka. 1975. Uranium mineralization by ground water in sedimentary rocks, Japan. *Ec. Geol.* **70**:628-646.
- Favorskaya, M. 1971. On geochemical indicators of deep rooted tectonics. *Sovetskaya Geologia.* **11**:4-19 (in Russian).
- Favorskaya, M., I. Tomson, V. Baskina, I. Volchanskaya, and O. Pol'akova. Global regularities in distribution of large ore deposits. 1974. Moscow: Nedra. (in Russian)
- Fleming, A., G. Handley, K. Williams, A. Hills and G. Corbett. 1986. The Porgera gold deposit, Papua New Guinea. *Ec. Geol.* **81**:660-681.
- Geological Map of Tokyo Bay and adjacent areas. Scale 1:100000. 1995. Tokyo: Geol. Survey.
- Geological map of Korean Peninsula and adjacent areas. 1990. Russia: Committee on Geol. and Mineral Resources.
- Gustafson, L., and S. Tilley. 1978. Porphyry Copper deposits in the South-Western Pacific islands and Australia. *Ec. Geol.* **73**:597-599.
- Imai, H. 1978. Geological studies of the mineral deposits in Japan and East Asia. Tokyo University Pres.
- Ishihara, S. 1971. Major molybdenum deposits and related granite rocks in Japan. In: *Geol. Survey of Japan.* **239**.
- Ishihara, S. 1978. Metallogenesis in the Japanese island arc system. *Journ. Geol. Soc. London.* **135**:389-406 .

- Ishihara, S., T. Igarashi, and Ch. Nishiwaki. 1975. A re-examination of regional distribution of the Late Cenozoic ore deposits : East Japan arc. *Geol. Soc. Am. Bull.* . **86**:293-297
- Ishihara, S., K. Shibata, and S. Uchiumi. 1988. K-Ar ages of ore deposits related to Cretaceous-Paleocene granitoids. *Bull. Geol. Surv. Japan.* **39**:81-94
- Ishihara, S. and A. Sasaki 1991. Ore deposits related to granitic magmatism in Japan: a magmatic viewpoint. *Episodes.* **3-4**:286-296.
- Kamitani, M., and Y. Kanazawa. 1993. Potential of Au-Ag bearing ore deposits in Japan - particularly on the Kitami area, Hokkaido. *Bull. Geol. Surv. Japan.* **44**:105-126.
- Kutina, J. 1980. Regularities in the distribution of large ore deposits along the "Mendocino Latitude", western United States. *Global Tectonics and Metallogeny.* **1**: 134 -193.
- Laznicka, P. 1985. Empirical Metallogeny. Amsterdam: Elsevier.
- Lottermother, B. 1990. Rare-earth element and heavy metal behavior associated with the epithermal gold deposit on Lihir island, Papua New Guinea. *Journ. of Volcanol. and Geotherm. Res.* **40**:269-291.
- Murakami, N. 1974. Some problems concerning Late Mesozoic to Early Tertiary igneous activity on the inner side of Southwest Japan. *Pacific Geology.* **8**:139-151.
- Ore Concentrating Structures of Asia. 1983. Moscow: Nedra (in Russian).
- Richards, I., and Jan Ledlie. 1993. Alkalic Intrusive Rocks associated with the Mount Kare gold deposit, Papua New Guinea: comparison with the Porgera intrusive complex. *Econ.. Geol.* **88**: 755-782.
- Rona, P., and S. Scott. 1993. Preface to a Special Issue on sea-floor hydrothermal mineralization: new perspectives. *Ec. Geol.* **88**: 1935-1938 .
- Sato, K., 1994. Pyrophyllite deposits in East Asia. *Chishitsu News.* **484.** 40 -50.
- Tatsumi, T. Ed. 1970. Volcanism and ore genesis. Tokyo.
- Takagi, T. 1993. Redox paths of magnetite-series and ilmenite-series granitoid magmas - examples from the central and eastern Chugoku districts, SW Japan. *Journ. Miner. Petrol. Econ. Geol.* **88**:165-178.
- Zhai, Yusheng. 1996. Giant ore deposits related to deep structure in and around North China Block. *Intern. Geol. Review* (in print).

FUNCTION OF BACTERIAL (*HYPHOMONAS SPP.*) CAPSULAR EXOPOLYMERS IN BIOFOULING

Ronald Weiner¹, Stephen Langille¹, Gill Geesey² and Ernesto Quintero³

¹Department of Microbiology, University of Maryland
College Park, MD, USA

²Department of Microbiology, Montana State University
Bozeman, MT, USA

³Oceanix Corporation
Hanover, MD, USA

ABSTRACT

The build-up of biotic communities on surfaces exposed to fresh and marine water can have deleterious effects and is termed biofouling. It results in billions of dollars annual damage and/or degraded performance to pipes, ships and other structures. Bacteria are believed to initiate biofouling and maintain a crucial role in macrobiotic colonization. It is because the pelagic region (mid ocean) is so limited in nutrients that bacteria have developed "ingenious" survival strategies to colonize immersed surfaces which provide enhanced nutrition. They adhere under very adverse conditions. Biofouling bacteria are among the oldest forms of life on this planet. A key to controlling fouling and on obtaining marine coatings and cements is to understand how these bacteria adhere.

It is widely held that bacteria behave like charged colloidal particles when approaching a surface and must pass through a repulsive boundary. They synthesize a variety of adhesive tethers for this purpose (adhesins). This report reviews the complicated and costly biofouling processes and focuses on the complex polysaccharide capsules that function as adhesins of a group of pioneer fouling bacteria (*Hyphomonas spp.*).

INTRODUCTION

Microbial Adhesion and Biofouling

Biofouling and succession of colonizing organisms

Clean surfaces quickly become coated with biotic communities when immersed in seawater. There is an ordered sequence for such colonization. Initially, the substratum becomes coated by organic matter (Lis and Sharon, 1986). Then pioneer bacteria, normally oligotrophic (low nutrient feeders), attach to the surface and begin to grow forming microcolonies within several hours (Corpe, 1973; Marshall et al., 1971). Pioneer bacteria are crucial in initiating the

development of the subsequent complex biotic community and their initial attachment is a key step in the whole process. The survival strategy of these pioneer adherent bacteria is to "bioform" the oligotrophic constraints of the pelagic region (requiring active heterotrophs to adapt a K survival mode), to a richer nutrient niche permitting the r-survival mode. The modified nutrient rich surface now becomes available for colonization by many different species.

Diatoms, fungi, protozoans, micro-algae and other microorganisms attach to the surface, forming what is termed the primary slime layer (Skerman, 1956). However the resulting biofilm (immobilized cells at a substratum in an organic polymer matrix), when formed on man-made structures, may cause corrosion deterioration and promote increased fluid frictional resistance resulting in energy losses and reduced system performance. Furthermore, this primary microbial colonization is often a prerequisite for the final stage of succession in which large organisms, viz., invertebrates, attach and grow on the surface (Crisp and Ryland, 1960; Zobell and Allen, 1935)(biofouling), further deteriorating system performance and often integrity. For example it was reported that corrosion alone has cost the US economy \$167 billion (US Dept of Commerce, 1986) with corrosion prevention over \$100 billion (Wall Street J., 1991) annually.

Physicochemistry of bacterial adhesion

Several related theories govern the probability of bacterial attachment to a substratum in aqueous environments (Marshall, 1988). Each states that the adhesion of microorganisms to surfaces is influenced by long-range, short-range, and hydrodynamic forces. The DLVO (letters after first initials of last names of its proposers) theory assumes that interaction between two objects is comprised of an attractive component, governed by Van der Waals forces, and a potential repulsive component due to overlap of electrical double layers associated with charged groups (Loeb, 1985). These yield two distances at which a particle may be attracted to the substratum. At a primary minimum (ca 1nm), attractive forces are strong; at the secondary minimum (ca 15 nm), forces are weaker. These distances are divided by an intermediate repulsion barrier. Microorganisms may accumulate at the secondary minimum and much of the strategy in surface colonization is concerned with remaining at the secondary minimum and overcoming the repulsive barrier to reach the primary minimum (Okuyawa et al., 1980). Microorganisms synthesize a variety of tethers for this purpose. All have narrow diameter and sufficient length to minimize and "break through" the repulsive layer (Costerton et al., 1985). Such structures have been reported (Costerton et al., 1985) to include long fibular, capsular polysaccharide (CP), pili and flagella, each of which could form an adhesive bridge minimizing electrostatic repulsion (Hammond et al., 1984).

A second, Stern, theory predicts that there will be a net charge distribution at any solid surface and that as a consequence, counter ions are held closely at the surface forming a Stern layer while the rest of the ions are less restricted forming a diffuse ionic zone (Loeb, 1985). This model, probably less applicable in a marine habitat, also predicts a double layer of attractive domains sandwiching a repulsive barrier and would require similar structures to function as tethers as would the DLVO model. The thermodynamic model considers adhesion equilibria in terms of system free energy (Marshall, 1985) with zones of attraction and repulsion approximately those of the other models.

Once the bacteria are attached to the surface, multiple events can transpire to carry it to the primary minimum at which multiple bonds of a more permanent nature may be formed between the organism and substratum. This attachment is generally considered to involve hydrophobic bonds of outer membrane components of Gram negative bacteria or more likely capsular extracellular polymers which form the cement-like biofilm. The roles of bacterial capsules (see below) in this process have been discussed with the conclusion that "much more information is required" (Christensen, 1989; Marshall, 1985).

Adhesins

The term adhesin was originally coined to denote specific bonding molecules to receptors on cell surfaces (Ofek et al., 1985). In this paper, biopolymers that mediate non-specific adhesion on marine surfaces are also referred to as adhesins. As noted above, adhesins include proteinaceous flagella, fimbriae (Swanson et al., 1985) and capsular extracellular polymeric substances (EPS), possibly the capsular polysaccharide (CP) component. EPS is a focus of this report (see below). *Hyphomonas* MHS-3, *Caulobacter crescentus*, *Seliberia stellata* (Hood and Schmidt, 1996) and *Asticcacaulis biprosthecum* are bacteria that make extracellular polymer holdfast (localized "sticky" capsule) and fimbriae at the same pole (Merker and Smit, 1988; Ong et al., 1990). A lectin domain on some fimbriae adheres them to specific cell surface carbohydrates. They may also attach nonspecifically to inanimate surfaces; i.e. since many fimbriae have a low pI and are relatively hydrophobic, they may adhere via salt bridges or hydrophobic bonds.

Capsular Extracellular Polymeric Substances (EPS)

Capsules normally surround bacteria external to the envelope but can also be more localized as in a holdfast. Many are pure polysaccharide (CP; capsular polysaccharide) while a few covalently or otherwise bind a protein (Wrangstadh et al., 1990) and/or fatty acid residues (Sar and Rosenberg, 1988). Consequently, unless the capsule is known to be composed of pure polysaccharide (CP), the term capsular extracellular polymeric substances (EPS) is used.

Bacterial surface polysaccharides have considerable heterogeneity, from the simple α 1-4 linked, unbranched glucose polymers called dextrans, to the highly complex, branched, and substituted heteropolysaccharides made up of oligosaccharide repeating subunits such as xanthan and colanic acid (Christensen et al., 1985). CP can also be substituted with pyruvate, acetate, formate, sulfate, phosphate and other groups (Jann and Westphal, 1975). Two identical sugars can bond to form 11 different disaccharides whereas two identical amino acids can form only one dipeptide. Additionally, CP contain a wide variety of sugars, (Bhattacharjee et al., 1984). Furthermore, the non-carbohydrate side groups that are found in bacterial CP adds to their heterogeneity that, as a consequence of all of these considerations, far exceeds that of proteins (Sutherland, 1982).

Investigations for Model Fouling Bacteria

Fouling films are comprised of complex multispecies communities and a number of species are considered to be primary colonizers. Among these *Hyphomonas* serves as an excellent model to

define the specific roles of the extracellular polymeric substances (EPS) in marine biofouling processes because: 1) it participates in both early colonization of surfaces and subsequent biofilm development; 2) it elaborates proteinaceous fimbriae and capsular polysaccharides at times coincident with cell attachment to surfaces; 3) synthesis of both EPS structures are temporally and polarly regulated; 4) EPS-deficient progeny (rad strain) are "spontaneously" produced (at a rate of 10^{-10} for *Hyphomonas* isolate MHS-3); 5) "footprints" (see below) of *Hyphomonas* spp. left behind on a previously colonized surface can be detected and chemically characterized.

Nearly all underwater marine surfaces are colonized; all support heterogenous populations; no one species appears to be the "linchpin" of the process; and not all species are found in diverse habitats. *Hyphomonas* is important not only as a model, but in nature as well (Baier et al., 1983; Railkin, 1994). It is hypothesized that *Hyphomonas* swarmer cells are chemotactically attracted to both uncolonized conditioning films and biofilm on marine substrata by the concentration of amino acids there. This triggers its differentiation into reproductive cells that synthesize adhesin(s). While adhesion science is still rather empirical (Strausberg and Link, 1990), it may be speculated that EPS or (and?) fimbriae (in the case of strain MHS-3) would tether the cell at the secondary minimum. Given the luxury of time, enough cells would penetrate to the primary minimum where EPS would partition out of the water column and onto the solid substratum, forming hydrogen bonds, not with water but with the surface. This process would continue resulting in a buildup of biofilm which becomes a sink for nutrients and begins to attract a constantly increasing menagerie of other pelagic voyagers.

Life Cycle and Morphogenesis of Hyphomonas

Hyphomonas, like other prosthecate, budding bacteria, has a biphasic life cycle (Wali et al.; Fig. 1) The progeny, swarmer cell, is dispersive (motile) by means of a single flagellum. It can chemotactically sense favorable areas such as nutrient rich surfaces, sometimes nearby; but it also has the capability to form distant colonies, because it is well adapted to survive in the oligotrophic pelagic zone (Emala and Weiner, 1983). It has a low metabolic rate (Emala and Weiner, 1983), polyhydroxybutyrate storage reserves, and is microspherical (0.4 μ m diameter), all properties of deep sea survival cells (Morita, 1985). The prosthecate reproductive stage is morphologically and physiologically equipped to establish, maintain, and survive in marine biofilms. The prosthecate form is larger than the swarmer cell (the main body being a prolate spheroid 1-2 μ m long, with a prosthecum 1-2 μ m long, 0.2 μ m wide).

As the prosthecum emerges from one pole, a "holdfast" has been reported to be synthesized from the other (Moore, 1981). A polar adhesin arrangement would allow the stalk to extend toward regions of richer nutrient and oxygen level. Reproductive budding at the distal tip of the stalk allows the progeny to either escape to the water column to establish a new community, or to settle nearby to extend the existing community. It is interesting that the "holdfast" survival strategy of another genus of procaryotes, *Caulobacter*, may be an example of converging evolution, with the polysaccharide, however, synthesized on the opposite pole (tip of the stalk) so that the reproductive cell body faces upward, with the stalk serving as the anchor (Merker and Smit, 1988).

Physiology of Hyphomonas

By virtue of their specialized physiologies as well as morphologies, motile swarmer cells are well adapted for survival in the oligotrophic water column, while the periphytic, prosthecate, reproductive cell is suited to establish, maintain, and survive in marine biofilms. For heterotrophic growth our laboratory has demonstrated a functional Krebs cycle (Devine and Weiner, 1990) and proteases (Shi et al., 1989), showing that reproductive stages, growing in microbial films, use protein and amino acids for energy (Shi et al., 1988). It was also shown that "autotrophically maintained" *Hyphomonas* assimilates copious quantities of CO₂ (Weiner et al., 1997) growing with repeated transfers in water containing only salts, reduced sulfur, and 10% CO₂. They will not multiply without sulfur and CO₂. Such physiological plasticity confers unusual ability for primary surface colonization. Once a biofilm is established, it would be beneficial to switch to heterotrophic metabolism for rapid multiplication using the accumulating organic material that may be sequestered by the growing biofilm.

RECENT DEVELOPMENTS AND DISCUSSION

Temporal and Spatial Synthesis of EPS Adhesin

The precise timing of EPS synthesis and localization for both strains MHS-3 (Quintero, 1994) and VP-6 (Langille, 1996) has been determined. Using monoclonal antibodies (Busch, 1993) against *Hyphomonas* MHS-3 lipopolysaccharide (LPS) as a negative stain (EPS would sterically hinder the approach of the mAb to its LPS target) in immuno-electron microscopy, we determined that MHS-3 synthesizes EPS only during its adherent (Quintero and Weiner, 1995) reproductive stage and only at the main body of the reproductive cell. No EPS could be detected on the prosthecum. This was also demonstrated probing with gold-labeled *Bauhinia purpurea* lectin and thin sections of polycationic ferritin-stained cells (Quintero and Weiner, 1995) (Fig. 2).

Purification (gel permeation), lectin binding studies (see below) and fine structure micrographs revealed a very different EPS profile for VP-6 than for MHS-3. VP-6 was recently been shown to synthesize two different EPS. One (termed "capsule") surrounds the entire cell, including the prosthecum and the bud (Fig. 3), during all developmental stages; the other is (termed "holdfast") is localized and temporal, being synthesized at one pole of the reproductive cell (Fig. 4) and only during the reproductive stage (Fig. 1, Stages D-F). Structure follows function as MHS-3 does not form rosettes, typical of the hyphomicrobia (i.e. reproductive cells stick to one another with stalks pointing outward in a floral pattern) while VP-6 does form rosettes. The entire capsule of MHS-3 may serve as holdfast, structurally and functionally. Since MHS-3 produces more holdfast adhesin than other species it is an important source of this kind of polymer which is a potentially useful commercial bioadhesive or underwater coating.

MHS-3 produces one cell in 10¹⁰ replications that does not synthesize EPS (rad; Quintero and Weiner, 1995). Among all *Hyphomonas* strains, empirically examined, it also produces the most extensive and adhesive EPS. One may speculate that the rad variant may allow a small number

of reproductive cells to be free of the rare biofilm subject to nutrient depletion, toxin build up or excessive predation.

Purification and Physical Adhesin Properties

The chemical and structural analysis are further along for strain MHS-3 than for VP-6. VP-6 capsular EPS is pyruvylated; MHS-3 EPS is not (Quintero et al., 1990). Crude EPS of MH3 elutes in 5 peaks on an analytical HPLC column (6FC column, 10^4 to 2×10^6 size separation, polystyrene-divinylbenzene packing). Fraction two is the adhesin. The capsular EPS of VP-6 has a much larger molecular weight than that of MHS-3 (500,000 MW to 60,000 MW respectively) and is composed of much larger percentage of uronic acids (Quintero et al., 1990). When the purified EPS of MHS-3 is fractionated by gel permeation chromatography, a single peak is resolved which, remains homogeneous after second dimension anion exchange chromatography. The peak is the putative adhesin. Rad mutants do not yield such polymer. We take this to mean that *Hyphomonas* MHS-3 capsule, "holdfast", and EPS are one and the same (Fig. 2). No protein appears to be tightly associated with this structure. On the other hand, from Commassie blue-stained SDS-PAGE VP-6 capsule putatively contains a tightly associated protein. The holdfast appears to be pure CP which like other holdfasts consists partly of N-acetyl galactosamine (from lectin analysis). This arrangement is similar to that of *S. stellata* (Hood and Schmidt, 1996) which also may be a primary colonizer with a biphasic life cycle.

The Adhesins

Functionally (in adhesion) there are interesting differences and similarities between both strains. MHS-3 synthesizes long, thin fimbriae at the same pole and about the same time as it synthesizes capsule; VP-6 does not (manusc. in prep). Preliminary studies have been carried out to evaluate the importance of the proteinaceous components in adhesion of prosthecate bacteria. Prosthecate MHS-3 attach, even after treatment with protease, at the pole where EPS is deposited. These initial observations suggest that either proteins do not participate in adhesion of *Hyphomonas* MHS-3 to an inanimate surface or that they are protected from or resistant to protease treatment in the presence of the CP. However no protein is detected in the purified adhesin fraction either.

VP-6 on the other hand has reduced ability to adhere after protease treatment, from Coomassie blue stained gels, because of the degradation of the capsular associated proteins (manusc. in prep).

Recent experiments in our laboratory support the necessity for CP in the adhesion of *Hyphomonas* MHS-3 to surfaces. The lectin, *Bauhinia purpurea* (BPA), specific for the CP (Quintero and Weiner, 1995), was found to interfere with cell adhesion (Quintero and Weiner, 1995). Furthermore, the rad strain (CP deficient) synthesizes fimbriae and does not adhere. Thus it appears that CP but not necessarily fimbriae must be present in order for the adhesive process to occur. We have also identified lectins specific for VP-6 holdfast (coral tree) and capsule (sweet pea) and have made monoclonal antibodies (mAb) to the capsular associated protein (Langille, 1996). In preliminary studies these specific reacting agents (not other lectins or mAb) appear to interfere with adhesion (Langille, 1996).

Consistent with the above, a preliminary ATR/FT-IR investigation of the adsorption properties of the crude exopolysaccharide fraction of VP-6 indicated that there was protein present. By contrast, the purified MHS-3 adhesin was shown to form amide bonds in footprint experiments. Therefore, as in the case of other bacteria with adhesive polar CP the adhesive component is possibly an NAG (putatively uronic acid) moiety.

Microbial Footprints

Detection of the adhesive molecules responsible for anchoring bacterial cells to substrata has been achieved through microscopic observations of the "footprints" left on a surface after removal of the surface-associated bacterial cells by one of a variety of techniques. Bacteria, removed by shear force (Marshall et al., 1971), enzymes (Paul and Jeffrey, 1985) or ultrasonication (Neu and Marshall, 1991), leave behind on the substratum the polymers that presumably are responsible for cell adhesion. Surface-sensitive, chemical analytical techniques such as attenuated total reflection infrared spectrometry (ATR/FT-IR) are ideally suited to identify the types of molecules that form the footprints (see Fig. 5). The nature and types of adhesive bonds are revealed. Thus, a chemical analysis of the footprints represents a powerful approach to identifying and characterizing microbial adhesins.

Time-of-flight secondary ion mass spectrometry (ToF-SIMS) is a new surface-sensitive, chemical analytical technique (Niehuis et al., 1989) that developed out of static secondary ion mass spectrometry (S-SIMS)(Fig. 5). ToF-SIMS provides chemical information on chain branching, cross-linking and conformation of polymers in the adsorbed state and has the added advantage of high spatial resolution to investigate the chemistry of a small area containing a footprint. ToF-SIMS provides a spatially-resolved mass spectrum of the molecules located within the top 10-20 angstroms of a surface (Meyer et al., 1992). Spatial resolution ranges from 0.2 mm-12 mm and detection limits are on the order of ppm to ppb. Furthermore, if the primary ion flux is maintained at $\leq 10^{13}$ atoms/cm², organic material such as the adhesive compounds of interest here can be characterized from the fragmentation pattern generated from the mass spectrum. To date, ToF-SIMS has been used to conduct microanalysis of membrane surfaces, molecular microanalysis in soft tissue, microanalysis of peptide diffusion in polymer and patterned arrays (Shamberger et al., 1996). This new instrumentation is, thus, ideally suited to elucidate the chemical identity of the constituents of microbial footprints, and hence, the adhesive molecules excreted by surface fouling microorganisms.

Commercial Promise of the Adhesins

There is a promising beginning to the potential commercialization of MHS-3 adhesin. There is a general purpose growth medium (Marine Broth (MB)), synthetic media (Havenner et al., 1979)(Medium G) and a commercial, low cost medium (Manyak and Weiner, 1994) (LD). We have grown MHS-3 in a fermenter with the finding that there is a higher yield of cells and polymer in the fermentor than in flask culture. The adhesins may have value as underwater surface coatings and as bioadhesives since they are relatively non-immunogenic (MacLeod and Krauss, 1950).

SUMMARY

To control biofouling, it is necessary to understand the primary adhesive interaction between pioneer colonizing bacteria and the substratum. There are apparently several species specific mechanisms involved. One bacterial strategy for adhesion is the synthesis of amino sugar polymeric adhesins. These can be demonstrated by agents that specifically bind these moieties and consequently interfere with the adhesive process. They can be characterized by new spectrometry technology.

ACKNOWLEDGEMENTS

We thank P. Suci and B. Frolund for their contributions to this study. We acknowledge A. Snyder for technical assistance and S. Payne for editing the manuscript. This work was supported by grants from the Office of Naval Research (ONR), the Maryland Industrial Partnerships (MIPS) and Oceanix Corp.

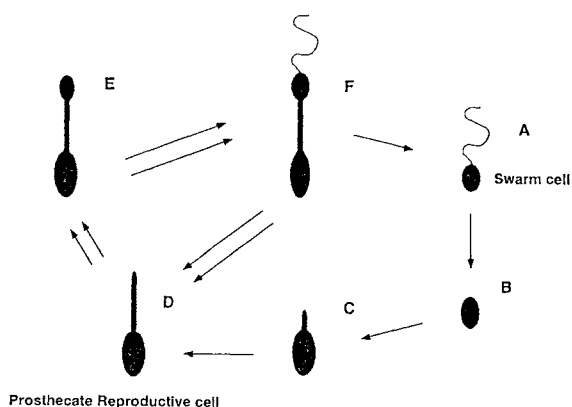


Figure 1. Biphasic life cycle of *Hyphomonas*. Single arrows designate swarm cycle (pelagic form). Double arrows designate reproductive cycle (Adherent, biofilm form).

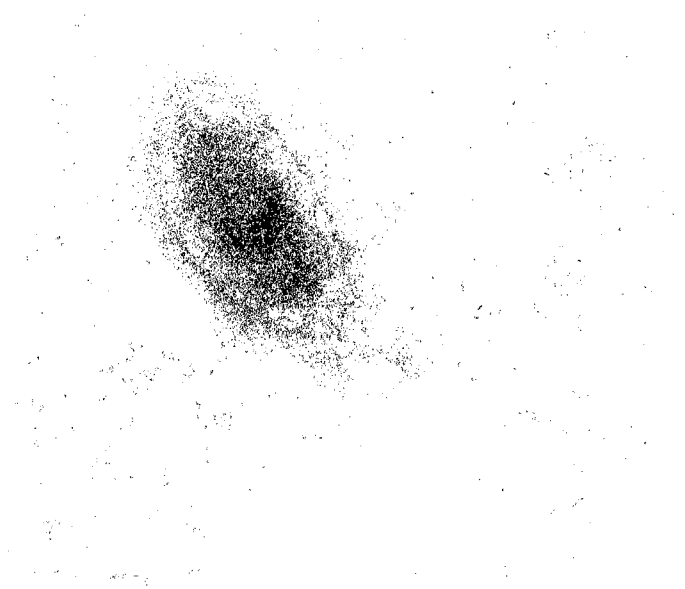


Figure 2. Holdfast capsule of *Hyphomonas*. MHS-3 capsule labelled with *Bauhinia purpurea* lectin. In this electron micrograph, the cell is approx. 2 μ m.



Figure 3. Electron micrograph of *Hyphomonas*. VP-6 showing capsule (surrounding entire cell), stained with cationic cerritin. Bar represents one μ m.

Figure 4. Electron Micrograph of *Hyphomonas* VP-6 showing holdfast. Hostfast (arrow) is clearly visable without staining and other procedures that could induce artifacts.

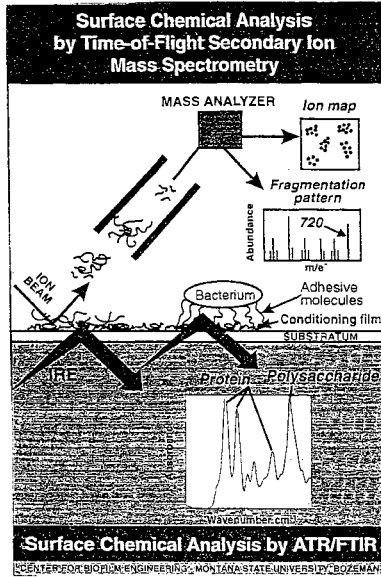


Figure 5. Diagram depicting emerging technologies to determine the nature of bioadhesins and the bonds they form on immersed substrata.

REFERENCES

- Baier, R., A. Meyer, V. DePalma, R. King, M. Fornalik. 1983. Surface microfouling during the induction period. *J. Heat Trans.* **105**:618-624.
- Bhattacharjee, A. K., J. E. Bennett, and C.P.J. Glaudemans. 1984. Capsular polysaccharides of *Cryptococcus neoformans*. *Rev. of Infect. Diseases.* **6**:619-624.
- Busch, K. 1993. Specificity of a monoclonal antibody against *Hyphomonas* MHS-3 polysaccharide. M.S. thesis, 93 pp. MD: University of Maryland.
- Christensen, B., J. Kjosbakken and O. Smidsrod. 1985. Partial chemical and physical characterization of two extracellular polysaccharides produced by marine periphytic *Pseudomonas* sp. strain NCMB 2021. *Appl. and Environ.* **50**:837-845.
- Christensen, B.E. 1989. The role of extracellular polysaccharides in biofilms. *J. Biotechnol.* **10**:181-202.
- Corpe, W.A. 1973. Microfouling: the role of primary film forming bacteria. In: Proceedings of the Third International Congress on Marine Corrosion Fouling. R.F. Ackjer, B.F. Brown, J.R. DePalma and W.P. Iverson, eds. Evanston, IL: Northwestern Univ. pp. 598-609.
- Costerton, J. W., T. Marrie, and K-J. Cheng. 1985. Phenomena of bacterial adhesion. In Bacterial adhesion. D. Savage and M. Fletcher, eds. NY: Plenum Pres. pp. 3-43.
- Crisp, D. J. and J. S. Ryland. 1960. Influence of filming and of surface texture on the settlement of marine organisms. *Nature* **185**:119.
- Devine, R. A. and R. M. Weiner. 1990. *Hyphomonas* species metabolize amino acids using Krebs cycle enzymes. *Microbios.* **62**:137-153.
- Emala, M. A. and R. M. Weiner. 1983. Modulation of adenylate energy charge during the swarmer cycle of *Hyphomicrobium neptunium*. *J. Bacteriol.* **153**:1558-1561.
- Hammond, S. M., P. A. Lambert, and A. N. Rycroft. 1984. The bacterial cell surface. Kent, GB: Croon Helm Ltd.
- Havenner, J., B. McCardell and R. Weiner. 1979. Development of defined, minimal and complete media for the growth of *Hyphomicrobium neptunium*. *Appl. Environ. Microbiol.* **38**:18-23.
- Hood, M. and J. Schmidt. 1996. Examination of *Seliberia stellata* exopolymers using lectin assays. *Microb. Ecol.* **31**:281-290.

- Jann, K., and O. Westphal. 1975. Microbial polysaccharides. In: The antigens. Michael Sela (ed.). Academic Press. New York, San Francisco and London. vol. 3. pp. 1-110.
- Langille, S. 1996. Adhesive capsules of *Hyphomonas* VP-6. Ph.D. Thesis. (In prep.)
- Lis, H. and N. Sharon. 1986. Lectins as molecules and as tools. *Ann. Rev. Biochem.* **55**:35-67.
- Loeb, G. I. 1985. Properties of non-biological surfaces and their characterization. In: Bacterial adhesion. D. Savage and M. Fletcher, eds. NY:Plenum Press. pp. 111-129.
- Macleod, C. M., and M. R. Krauss. 1950. Relation of virulence of pneumococcal strains for mice to the quantity of capsular polysaccharide formed in vitro. *J. Exp. Med.* **92**:1-9.
- Manyak, D. and R. Weiner. 1994. Fermentation of marine bacteria for production of novel biomaterials. In: Abst. Gen. Meet. Amer. Chem. Soc. San Diego.
- Marshall, K. C. 1985. Mechanisms of bacterial adhesion at solid-water interfaces.. In: D. Savage and M. Fletcher (ed.) Bacterial adhesion. NY: Plenum Publishing Corp. pp. 133-160.
- Marshall, K. C. 1988. Adhesion and growth of bacteria at surfaces in oligotrophic habitats. *Can. J. Microbiol.* **34**:503-506.
- Marshall, K. D., R. Stout and R. Mitchell. 1971. Selective sorption of bacteria from seawater. *Can. J. Microbiol.* **17**:1413-1416.
- Merker, R. and J. Smit. 1988. Characterization of the adhesive holdfast of marine and freshwater Caulobacters. *Appl. Environ. Microbiol.* **54**:2078-2085.
- Meyer, K., B. Hagenhoff, M. Deimel, and A. Benninghoven. 1992. Quantification of molecular secondary ion mass spectrometry by internal standards. *Org. Mass Spectr.* **27**:1148-1150.
- Moore, R.L. 1981. The biology of *Hyphomicrobium* and other prosthecate, budding bacteria. *Annu.Rev. Microbiol.* **35**:567-594.
- Morita, R. Y. 1985. Starvation and miniaturization of heterotrophs, with special emphasis on maintenance of the starved viable state. In: Bacteria in their natural environments. M. Fletcher and G. D. Floodgate, eds. Society for General Microbiology Publication #16. Academic Press. pp. 111-130
- Neu, T. R. and K. C. Marshall. 1991. Microbial "footprints"-a new approach to adhesive polymers. *Biofouling* **3**:101-112.
- Niehuis, E., P. N. T. van Velzen, J. Lub, T. Heller and A. Benninghoven. 1989. High mass resolution time-of-flight secondary ion mass spectrometry. *Surface Interface Anal.* **14**:135-142.

- Ofek, I., H. Lis, and N. Sharon. 1985. Animal Cell Surface Membranes. pp. 71-80. In: Bacterial adhesion, D. Savage and M. Fletcher, eds. NY:Plenum Press.
- Okuyawa, K. S. Arnott, R. M. Moorhouse, M.D. Walkinshaw, E.D.T. Atkins, and C. Wolf-Ullish. 1980. *Am. Chem. Soc. Symp. Ser.* **141**:411-419.
- Ong, C., M. Wong and J. Smit. 1990. Attachment of the adhesive holdfast organelle to the cellular stalk of *Caulobacter crescentus*. *J. Bacteriol.* **172**:1448-1456.
- Paul, J. H. and W. H. Jeffrey. 1985. Evidence for separate adhesion mechanisms for hydrophilic and hydrophobic surfaces in *Vibrio proteolytica*. *Appl. Environ. Microbiol.* **50**:431-437.
- Quintero, E. 1994. Characterization of adhesion and biofilm formation by the marine prokaryote MHS-3. Ph.D. Thesis. 200p. MD:University of Maryland.
- Quintero, E., G. Geesey and R. Weiner. 1990. Characterization of adhesive exopolysaccharides of new species of *Hyphomonas*. In: Abst. of Annu. Meeting of Amer. Soc. Microbiol. p. 263.
- Quintero, E. and R. Weiner. 1995. Evidence for the adhesive function of the exopolysaccharide of *Hyphomonas* MHS-3 in its attachment to surfaces. *App. Environ. Microbiol.* **61**:1897-1903..
- Railkin, A. 1994. Self-assembly of marine microfouling communities. *Dokl. Biol. Sci.* **337**:349-357.
- Sar, N., and E. Rosenberg. 1988. Fish skin bacteria: production of friction-reducing polymers. *Microbial Ecol.* **17**:27-38.
- Shamberger, P., F. Caccavo, F. von Ommen Kloche and G. Geesey. 1996. Microbial cell fingerprinting - Development of ToF-SIMS for the study of microbial cell surfaces. Abst. of Surfaces and Biomaterials Conference. Phoenix.
- Shi, J., V. E. Coyne and R. Weiner. 1989. Characterization of the exoproteases of the hydrothermal vent bacterium *Hyphomonas jannaschiana* VP3. 89th Annual Meeting of the American Society for Microbiology, New Orleans, Louisiana. Abst. of Ann. Meeting. p. 253.
- Shi, J., V. E. Coyne and R. M. Weiner. 1988. Characterization of extracellular alkaline protease activity in the budding, hydrothermal vent bacterium *Hyphomonas jannaschiana*. 1st International Symposium on Marine Molecular Biology. Baltimore, Maryland.
- Skerman, T. M. 1956. The nature and development of primary films on submerged surfaces in the sea. N. Zealand, *J. Sci. Technol. B.* **38**:44-57.
- Strausberg, R. and R. Link. 1990. Protein-based medical adhesives. *Tibtech.* **8**:53-57.

Sutherland, I.W. 1982. Biosynthesis of microbial exopolysaccharides. In: *Advances in Microbial Physiology*. vol. 23. A.H. Rose and J.G. Morris (eds). NY: Academic Press.

Swanson, J. S., Bergstrom, K. Robbins, O. Barrera, D. Corwin, J.M. Koomey. 1985. Gene conversion involving the pilin structural gene correlates with pilus⁺--pilus⁻ changes in *Neisseria gonorrhoea*. *Cell* **47**:267-276.

U.S. Department of Commerce, Natl. Bureau of Stds., and Cooperative Research Opportunities at NBS. 1986. Washington, D. C.: U.S. Govt. Print. Off.

Wali, R. M., G. R. Hudson, D. A. Danald and R. M. Weiner. 1980. Timing of swarmer cell cycle morphogenesis and macromolecular synthesis by *Hyphomicrobium neptunium* in synchronous culture. *J. Bacteriol.* **144**:406-412.

Wall Street J. April 19, 1991.

Weiner, R., L. Dagan and J. Tuttle. 1997. Evidence for chemolithotrophic metabolism in *Hyphomonas*. *Appl. and Environ. Microbiol.* (In prep).

Wrangstadh, M., U. Szewzyk, J. Ostling, and S. Kjelleberg. 1990. Starvation-specific formation of a peripheral exopolysaccharide by a marine *Pseudomonas* sp., Strain S9. *Appl. Environ. Microbiol.* **56**:2065-2072.

Zobell, C. E. and E. C. Allen. 1935. The significance of marine bacteria in the fouling of submerged surfaces. *J. Bacteriol.* **29**:230-251.

INTERNAL WAVE INTERACTIONS WITH STEEP SLOPES AND THE RESULTANT INFLUENCE ON OCEAN OUTFALL PERFORMANCE

Patrick K. Sullivan and Dayananda Vithanage

Oceanit Laboratories, Inc.
Honolulu, Hawaii, U.S.A.

ABSTRACT

Standard methods for ocean outfall design and expected performance rely primarily on presumed invariant winter and summer thermocline formation. This information is then used to determine density profiles to calculate the optimum depth for the outfall. Internal waves with tidal and sub-tidal frequencies produce vertical displacement of iso-thermals that are generally enhanced by interaction with steep slopes, such as is found in the Hawaiian Islands. These relatively rapid iso-thermal displacements result in density profile changes, and as a consequence, alter the density gradient and the resultant performance of the ocean outfall. If internal wave induced iso-thermal displacements are considered, environmental and ecological impacts of outfall discharge can be probabilistically described. Applications of this methodology on the Sand Island outfall, with limited available data, indicated that public health risks and environmental impacts of effluent discharge decreased by an order of magnitude over results obtained from conventional methods.

In a continuously stratified ocean, perturbations in the density profile generated at the continental shelf propagate shoreward as free and forced internal waves and undergo amplification from in-shelf topographic effects. Periods of these free waves are the same as the Brunt Vaisala period determined by the density gradient over the depth. Typical free internal wave periods vary from about 5 minutes to tidal periods. These shoreward propagating internal waves are believed to break in many areas, and as a result, cause mass transport of water and entrained sediments in the water layer close to the bottom. The shorter period waves have time scales similar to the buoyancy mixing stage of wastewater plumes and turbulent breaking of these could affect initial mixing and dilution. At a wastewater outfall, this phenomenon could move effluent emanating from the diffuser shoreward along the bottom. Understanding the extent and area of influence of these waves will lead to more realistic environmental and ecological impact evaluations. An experiment has been planned for the spring of 1997 to look into this phenomenon in Mamala Bay, Oahu and Pacific Missile Range Facility (PMRF), Kauai, sponsored by the U.S. Office of Naval Research.

INTRODUCTION

Deep ocean outfall design relies on stratification information to assure that acceptable levels of dilution and wastefield advection occur after effluent is discharged from the outfall diffusers. Usually, stratification measurements are performed seasonally or monthly where summer and winter thermoclines are identified.

During the last decade, continuous temperature measurements were made using recording instruments for Ocean Thermal Energy Conversion (OTEC) research. As part of a current measurement program, temperature data were sampled at 20-minute intervals at several depths for 12 to 18 month periods at Kahe Point and Keahole Point (Edward K. Noda & Associates, 1981). Measurements made in proximity of the Hawaiian Islands showed significant variations in temperature at various depths. These variations occurred at near tidal frequencies indicating significant vertical movement of iso-thermals in response to water level variations from tides.

Spectral analysis of temperature data reveals significant energy concentrations near diurnal and semi-diurnal periods. These peaks are related to internal tides associated with surface tides (Fyre, Leavitt and Noda, 1981). In the literature, these waves are referred to as baroclinic tides. Internal waves could be amplified by topographic effects such as the steep island flanks found in the Hawaiian Islands and, as a result, produce rapid density profile variations. Sand Island data from Mamala Bay showed that temperature variations and associated density stratification varied approximately at tidal periods. This phenomena is considered when calculating the wastefield behavior from deep ocean outfalls.

SAND ISLAND OUTFALL PERFORMANCE

In 1992, Oceanit evaluated mixing characteristics of the Sand Island outfall on Oahu. The outfall discharges about 75 million gallon per day of wastewater from the Sand Island Wastewater Treatment Plant (SIWWTP) through a diffuser at a 70 meters depth. The location of the outfall is shown in Figure 1.

The initial dilution of wastewater emanating from the diffuser is dependent on the density structure and advection currents in the ambient receiving waters. Ocean current data were collected in the vicinity of the outfall at several depths by J.K.K. Look Laboratory of the University of Hawaii. The data collection period was limited from July 1989 to mid September 1989. Current meter data were analyzed to determine effluent dilution and dispersion and to estimate the potential for wastewater effluent to reach the shore and other recreational areas. The currents generally were oriented in an east-west direction parallel to the bottom contours. Frequency distribution of current speed is shown in Figure 2 (Oceanit Laboratories, Inc., 1993).

Temperature data at different depths were also collected by thermistors mounted on the current meters (no salinity information was available and variations of salinity was less than 0.2 ppt). One of the most interesting characteristics of the temperature time series data was the variation of temperature with tidal periods, which varied spatially over various depths. It was observed that a temperature difference of 0.4° C between the surface and bottom affects the initial dilution and the plume surfacing criteria. The frequency distribution of the degree of stratification is shown in Figure 3. Using variations in density profiles calculated from temperature data, the dilution and plume trapping depths were calculated for different combinations of ambient current speeds (Oceanit Laboratories, Inc., 1993).

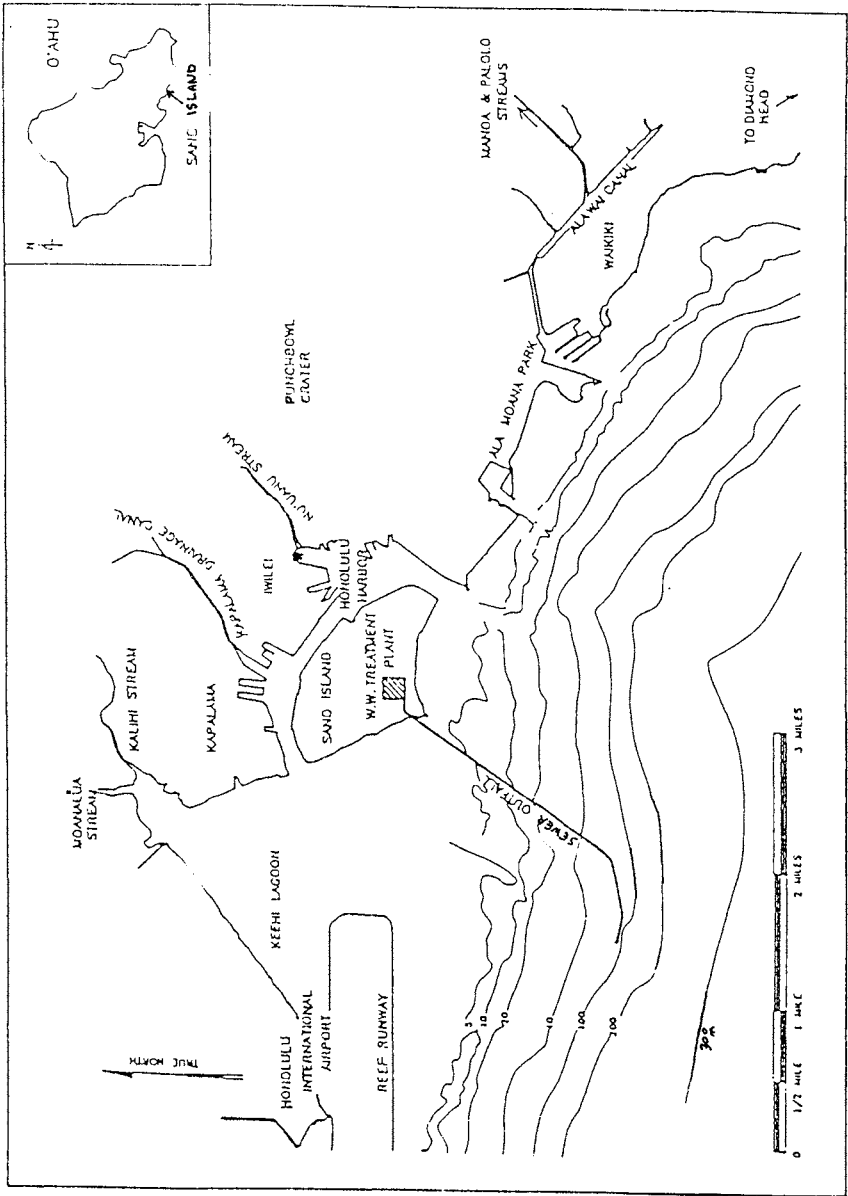


Figure 1. Location of Sand Island Wastewater Treatment Plant (SIWWTP) outfall

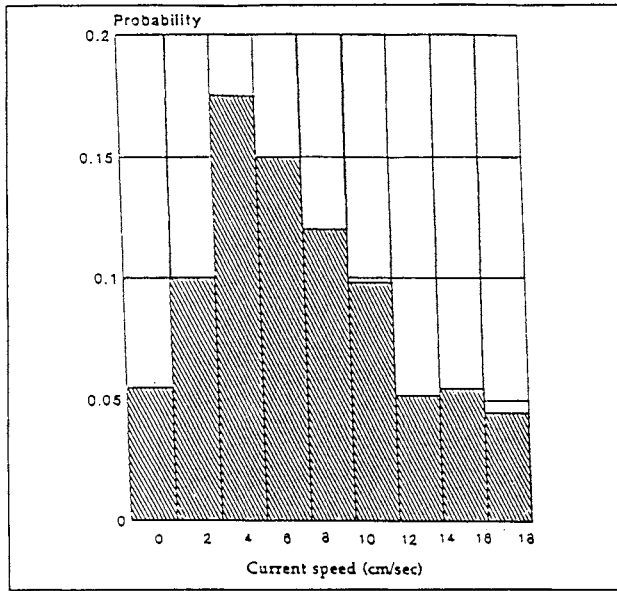


Figure 2. Frequency distribution of current speed at 15-minute average currents taken at mid-depth

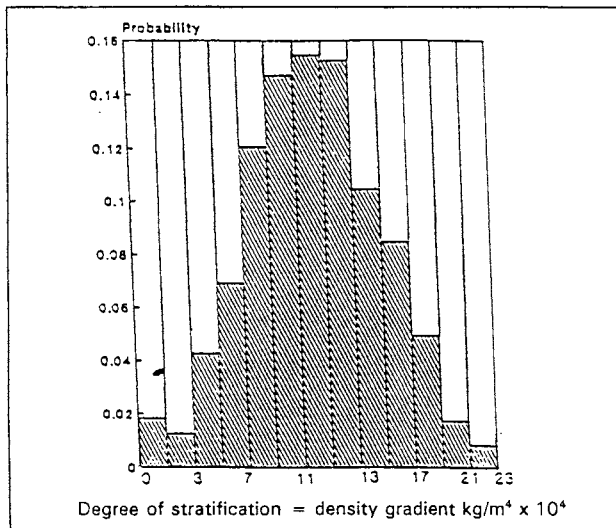


Figure 3. Frequency distribution of degree stratification calculated from 15-minute temperature data at four levels in the water column

Average currents in the study area were generally small due to reversing tidal currents. Tidal currents were roughly one order of magnitude higher than the mean. However, ambient currents were extremely variable; deterministic models could not be used with high confidence. Therefore, a probability approach was used to evaluate mixing and dispersion. A probability distribution of current speeds was calculated using current records. Current and stratification data were combined and used as input in the UPLUME model. The probability of the wastewater plume surfacing was computed from model results (Oceanit Laboratories, Inc., 1993).

Plume Behavior

Results of initial effluent dilution under different conditions were calculated and are shown in Figures 4. Plume trapping depth for similar conditions was calculated, results are graphically displayed in Figures 5 (Oceanit Laboratories, Inc., 1993).

1. The most probable degree of stratification(density gradient) lies between 0.0011 and 0.0013 kg/m^4 , at about 16% probability.
2. The most likely current speed lies between 4 cm/sec and 8 cm/sec.
3. Plume trapping depth is dependent on stratification and current speed, e.g., when stratification is high, dilution is low.

The near-field mixing from buoyancy effects cease after the plume acquires the equilibrium level. Far-field dilution and advection is controlled by eddy diffusion and ambient currents. No information was available for eddy diffusion properties in Mamala Bay. However, probable dilution values were calculated for the plume during advection from the outfall to within 1,000 feet of the shoreline using diffusion coefficients measured at other coastal areas.

In general, currents below a depth of 5 meters are not affected by the local wind. Therefore, plume motion calculated from current meter data are reliable only for submerged plumes. Advection for a surfacing plume is determined to a large extent by the wind climate. Dilution of the surfacing plume shows a minimum of 732 when ambient water current speed is zero. Once at the surface, the plume will undergo further dilution from diffusion as it moves with the ambient currents.

Water current data from current meters moored in shallow water as well as wind data from Honolulu International Airport were analyzed to obtain the percentage of time water moved toward the shoreline. Bacterial contamination of shoreline waters occurs only when the plume reaches the surface. Surface currents are primarily driven by local winds. Data indicate that the wind blows onshore about 55 days in the year, which is 15% of the time (Oceanit Laboratories, Inc., 1993).

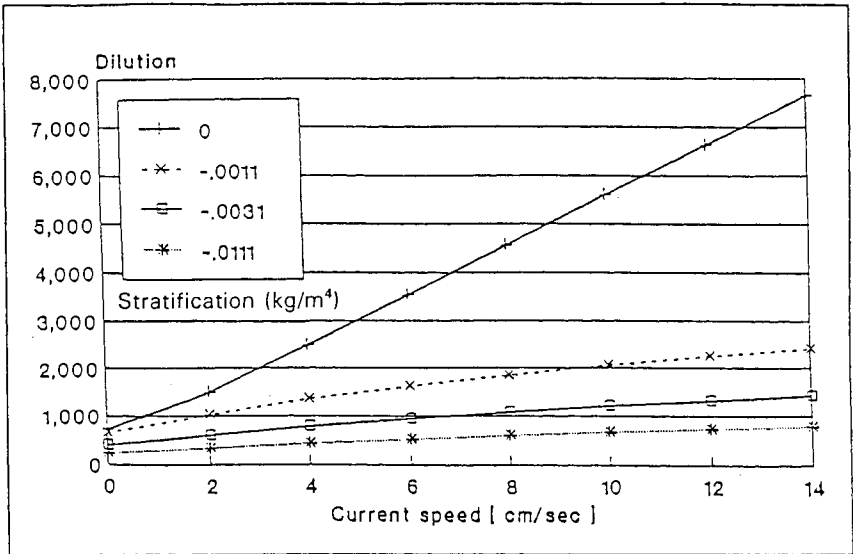


Figure 4. Variation of initial dilution with stratification and current speed at Sand Island outfall diffuser

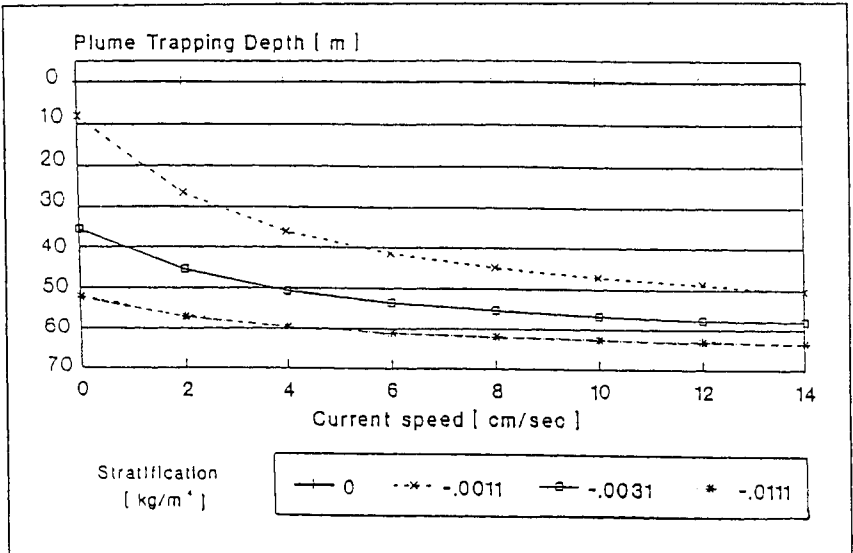


Figure 5. Variation of plume trapping depth with stratification and current speed at Sand Island outfall diffuser

Data indicate that the average onshore wind speed is 6.9 mph and will produce a surface drift of about 6 cm/sec. The average onshore speed of water calculated from current measurements is 6.92 cm/sec. Assuming that the onshore current speed maintains this value as long as it is more than 1000 feet offshore, total onshore average drift can be estimated by adding these two speeds, resulting in a combined speed of 12.92 cm/sec shoreward. At this speed, the surface current will bring the plume within 1,000 feet of the shoreline in approximately 15,220 seconds or about 4.25 hours. During this travel, the plume dilution calculated using Brook's model shows a further dilution of 16. When we combine dilution during initial mixing and eddy diffusion during advection, the resulting total effluent dilution by the time the plume reaches within 1,000 feet of the shoreline is 10,624. With this high degree of dilution and relatively high mortality rate of bacteria in seawater, only viruses will survive when the plume reaches recreational areas.

HEALTH RISKS

Pollutants discharged into the ocean from a wastewater outfall can pose potential risks to human health in two ways including direct exposure to viruses and bacteria as well as the concentration of toxins in the food chain. The risk of contracting disease from exposure to viruses or bacteria in the discharge from the outfall was evaluated using results of indicator bacteria monitoring. Results of receiving water monitoring were used in conjunction with results of earlier studies performed on virus concentration and distribution in Mamala Bay.

Transport of harmful enteroviruses from the effluent to nearshore areas in sufficient concentrations can infect users of these recreational waters. However, most of the bacteria are not present in sufficient concentrations to cause infections because of dilution and the comparatively high mortality rate in seawater. However, enteroviruses have a 90% mortality period on the order of days, which means they can survive the 4 hours needed for shoreward transport with the effluent.

Risks from Beneficial Uses

There have been several studies to determine the health hazard from swimming in sewage contaminated waters. The relationship between numbers of specific disease causing organisms in water and potential for transmission of disease remains elusive since the number of organisms required to cause disease varies depending on the organism, the host, and the manner whereby the organism and the host interact. For example, in some instances a single cell of salmonella or a single plaque forming unit (PFU, a standard means of measuring virus concentrations in tissue culture) may be all that is necessary to cause a disease.

Enterovirus concentrations in the effluent from the Sand Island Wastewater Treatment Plant (SIWWTP) was found to range from 12 to 850 PFU per liter (human enteric viruses in sewage and their discharge into the ocean). Total number of viruses discharged into the ocean daily is estimated at 7.5×10^{10} to 8.5×10^{10} PFU. Using average discharge of 84 mgd, the virus concentration in the effluent is 270 PFU per liter.

Viruses will reach recreational areas by wind induced surface currents. Combinations of a surfacing plume and onshore winds occur about 25 hours in one year. Minimum initial dilution attained by a surfacing plume is 664. A further dilution of 16 will result in a total dilution of 10,624. Concentration of viruses in the effluent after this dilution will be 0.025 PFU per liter; the exposure to risk is therefore 0.025 PFU per liter. This means that a person will ingest an average of one virus for every 40 liters of water swallowed. However, during swimming or bathing it is normal for a person to swallow about 10 ml of water inadvertently. Viruses in water are distributed according to a Poisson distribution. The concentration of viruses in water is 0.00025 PFU per 10 ml. Therefore, the probability of ingesting one PFU under these conditions is about 0.00052 (Oceanit Laboratories, Inc., 1993).

This condition occurs when the plume is surfacing and there is an onshore wind at the same time. This combination of circumstances occurs about 0.3% of time in the year. Therefore, the health risk from viral contamination from Sand Island outfall is estimated to be in the order of 1.56×10^{-6} .

This is a conservative estimate because the travel path of the plume to the shore was assumed to be a straight line. In actual situations this path will be torturous and would take considerably more time to reach the shore than the 4 hours used in the calculations. During this time, dilution by eddy diffusion will be larger; the decrease in the number of viruses from die-off will be considerable. Therefore, the actual risk would be less than this value.

EFFECTS OF INTERNAL WAVE BREAKING

In a continuously stratified ocean, free internal waves generated by topographic and other phenomena do not behave like surface gravity waves or interfacial waves that occur in a layered fluid. The restoring force for these free internal waves is the buoyancy caused by the density gradient. These waves propagate at an angle to the horizontal determined by the ratio of wave frequency to the Brunt Vaisala frequency (buoyancy frequency) (Pond and Pickard, 1983). Forced long period waves such as internal tides propagate horizontally because of their very low frequency and, like barotropic tides, are reflected by topographic boundaries.

However, there is ample evidence that high frequency free internal waves approaching shallow water break rather violently and producing cross shore mass transport in a bottom layer (Jo, 1975). Scaling these parameters to ocean conditions indicate that breaking internal waves could cause mass transport in a layer as thick as 50 feet. This shoreward transport generates additional turbulence and currents that lead to considerable mixing and diffusion by entrainment during the buoyancy phase of the effluent. The additional mixing and dispersion caused by this phenomenon at the early stage of initial dilution may have significant influence on far-field dilution and dispersion characteristics, as well as fate of the wastefield. Currently, there is a scarcity of information on this phenomenon. However, experiments are planned to obtain information on breaking internal waves.

A thermistor string and downward looking Acoustic Doppler Current Profiler (ADCP) can be used to measure internal wave influence as well as the suspended sediment density and cross shore movement of the effluent plume after it emanates from the diffuser. An experiment designed for Mamala Bay will be carried out in proximity to the Sand Island outfall. Results are expected to provide additional effluent dilution and dispersion from the effects of breaking internal waves. The potential public health risks are expected to decrease significantly due to this phenomenon.

CONCLUSIONS

1. Rapid density profile variations have a significant effect on the initial dilution of effluent and plume trapping depth.
2. It is prudent to take into account these rapid variations in the design of ocean outfalls, and the assessment of their environmental and public health impacts.

REFERENCES

- Edward K. Noda & Associates, Inc. 1981. Current Data from Kahe Point, Oahu, and Keahole Point, Hawaii OTEC Benchmark Sites. JKK Look Laboratory of Oceanographic Engineering, Department of Ocean Engineering, University of Hawaii.
- Fyre, D., K. Leavitt, and E. K. Noda. 1981. Current Data from Keahole Point, Hawaii. OTEC Benchmark Sites, June 1980 to April 1981. Prepared for the U.S. Department of Energy.
- Oceanit Laboratories, Inc. 1993. 1990 Sand Island Annual Assessment Reports. Prepared for the Department of Wastewater Management, City and County of Honolulu.
- Pond, S., G. L. Pickard. 1983. Introductory Dynamical Oceanography. Pergamon Press.
- Jo, R. 1975. Internal Gravity Waves. New York: M. Dekker.

PROTECTING THE COASTAL RESOURCES OF PENANG STRAITS OF MALAYSIA: A MODELING PERSPECTIVE

Koh Hock-Lye¹, Lee Hooi-Ling² and Din Zubir¹

¹ Universiti Sains Malaysia
Penang, MALAYSIA

² University of Tennessee
Knoxville, Tennessee, USA

ABSTRACT

The coastal water quality in the Penang Straits of Malaysia has shown indication of progressive deterioration over the years due to the discharge of pollutants particularly domestic sewage, industrial effluent and sediment. Several research and consultancy projects undertaken in the past have indicated the urgent need to preserve and enhance the coastal environment and their resources. All development projects related to the coastal environment must now be subjected to an Environment Impact Assessment (EIA) evaluation to ensure the proper protection of the environment before the project can be approved. In this regard computer modeling and simulation have been effective in helping to assess and evaluate impact and to provide cost effective remedial actions and alternative plans.

More recently a project funded by the UN-ESCAP and another funded by the IRPA Program, Seventh Malaysia Plan have provided an opportunity to refocus the issues involved and to fine tune future research directions. This research will utilize state of the art modeling capability to assess both the fate as well as the effect of pollutants discharged into the coastal seas. This paper will give some description of the models and sample outputs and hope to stimulate exchange of scientific views relevant to the discussion, particularly with respect to cockle and other shellfish culture.

INTRODUCTION

Many research and consultancy studies have been conducted in the past 20 years on the water quality and ecological status of the Southern and Western Channels of the Penang Straits, Malaysia (Fig.1 and 2). A first serious study involving computer modeling of hydrodynamic regimes subject to tidal forcing was initiated by DHI (1972) to support a feasibility study of a bridge connecting the Penang Island and the Peninsular Malaysia. Since then many other studies have been conducted, including float and dye monitoring, water quality sampling and computer modeling of various coastal processes and water quality parameters. Projected development makes it imperative to have available a reliable and robust methodology to assess and predict potential impacts of further discharge of various types of waste into the study area. Such a methodology must

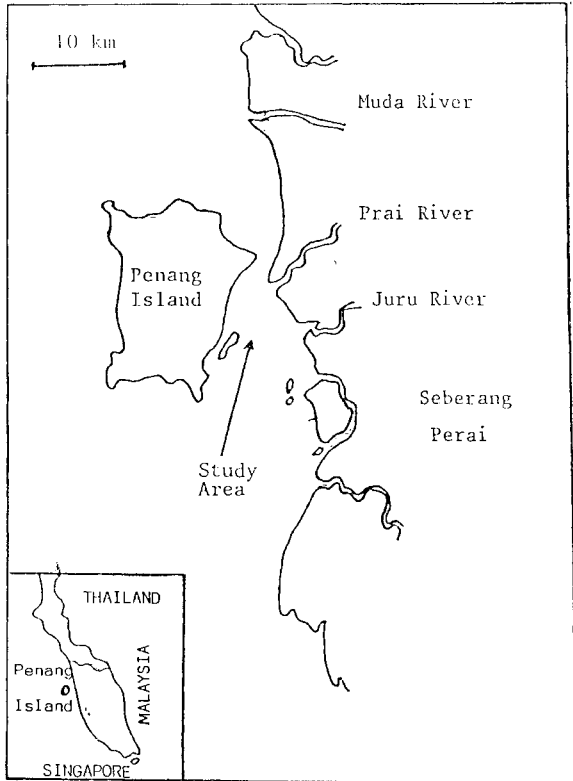


Fig 1. Map showing The Study Area.

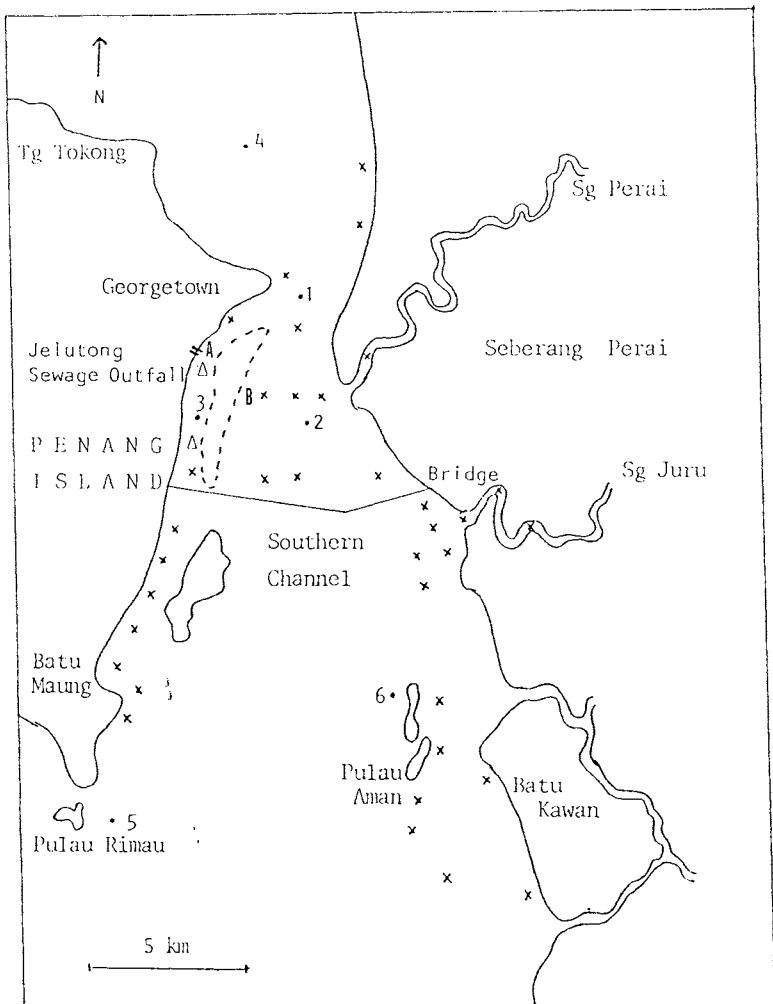


Fig 2. Locations of Current Measurement Stations 1 to 6, and Sampling Stations x. The Channel Δ in which the present Jelutong Sewage Outfall is located is called the Western Channel.

contain an integral component using computer simulations to provide quantitative assessment to augment well acknowledged deficiency and limitation of scientific data observed in a controlled laboratory or limited field study. In view of this, some form of extrapolation, including extrapolation across scales of space, time or ecological organization, is necessary to make impact and risk assessment useful for decision-making (USNRC, 1993). Hence the need to use mathematical models and computer simulation to aid assessment of environmental and ecological risk has been well recognized (USEPA, 1992).

This paper will attempt to describe some of the modeling activities and capability presently available for application to the Penang Straits, as well as other research in progress.

SOME MODELING RESULTS

The major pollutants in the Penang Straits are domestic sewage, suspended sediments (SS) and industrial effluents. The primary concern with regard to sewage is mainly associated with faecal contamination. While the BOD loads from sewage and sullage may be significant, they have not yet created serious problems as the DO levels presently remain above 5 mg/ℓ oxygen. Tidal flow regimes are adequate to dilute BOD to a level of below 2 mg/ℓ at the same time provide sufficient reaeration to maintain DO above 5 mg/ℓ in general. However, the flow regimes are inadequate to provide sufficient dilution and dispersion of faecal coliform bacteria (FC) with the consequence that almost all coastal areas with existing or projected development have FC levels much higher than levels deemed safe for the designated usage, according to the USEPA standards (1986).

A good fundamental understanding of the tidal flows is important, since these provide the basic medium for the transport and fate of all aquatic pollutants including, sewage, SS and industrial wastes, discharged into the area.

Hydrodynamic Regimes

Tidal current measurements were taken at the 6 locations shown in Figure 2 during the study of Koh and Din (1987). The tides are predominantly semi-diurnal with a period of 12.42 hours. A spring tide has an amplitude of about 1 m while a neap tide 0.25 m, with a maximum current speeds of 1.0 m/s and 0.25 m/s respectively. The tidal water elevations between the north (Tg. Tokong) and south entrance (Pulau Rimau) differ by about 50 minutes. Figure 3 shows the vertically averaged current velocity plots at various phases of a spring tide, computed by a finite element technique (Koh, 1988; Koh and Din, 1987), while Figure 4 illustrates current velocity measured at mid-depth at sampling station 1 for 3 consecutive days in 1986. Table 1 provides comparison between measured current velocity and computed velocity (DHI, 1992) as well as velocity computed in this study at 6 locations. The agreement between the 3 sets of values are sufficiently good to justify the use of any one set for further analysis and application.

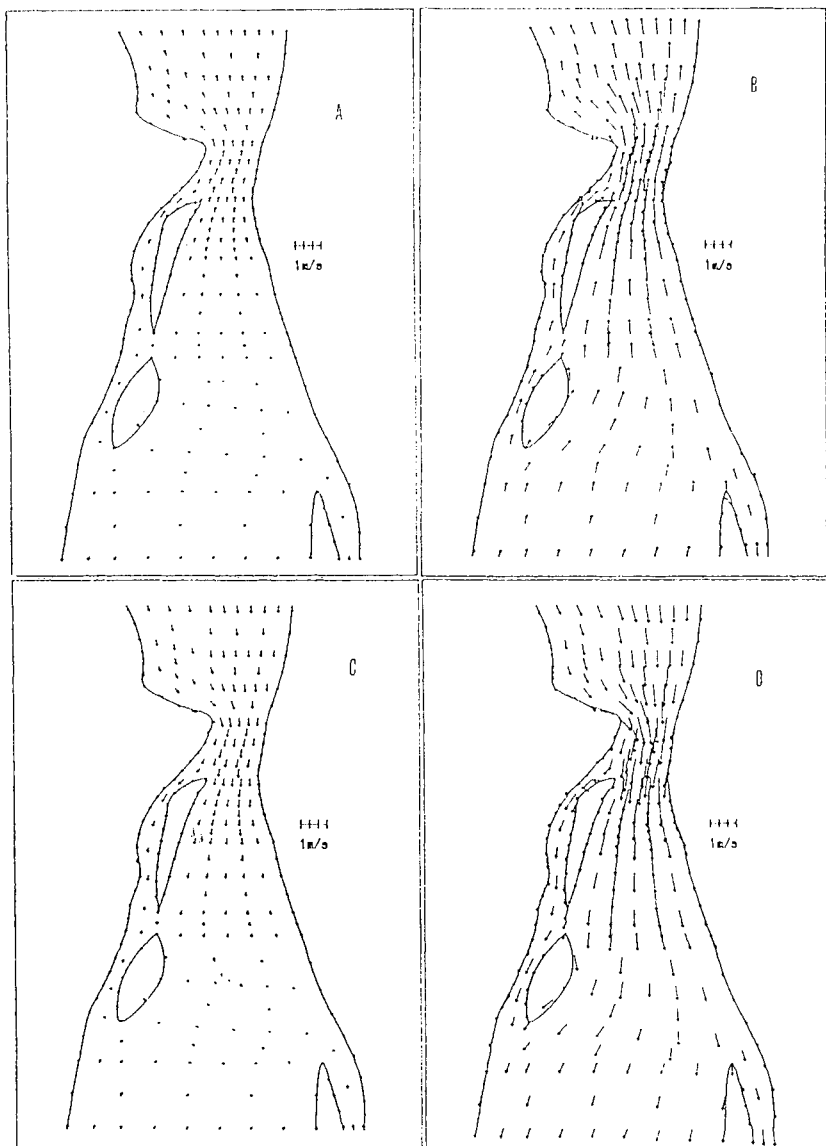


Fig.3. Velocity plots during spring tide in the Straits of Penang:
 (a) slack water, (b) maximum ebb tide, (c) slack water,
 (d) maximum flood tide

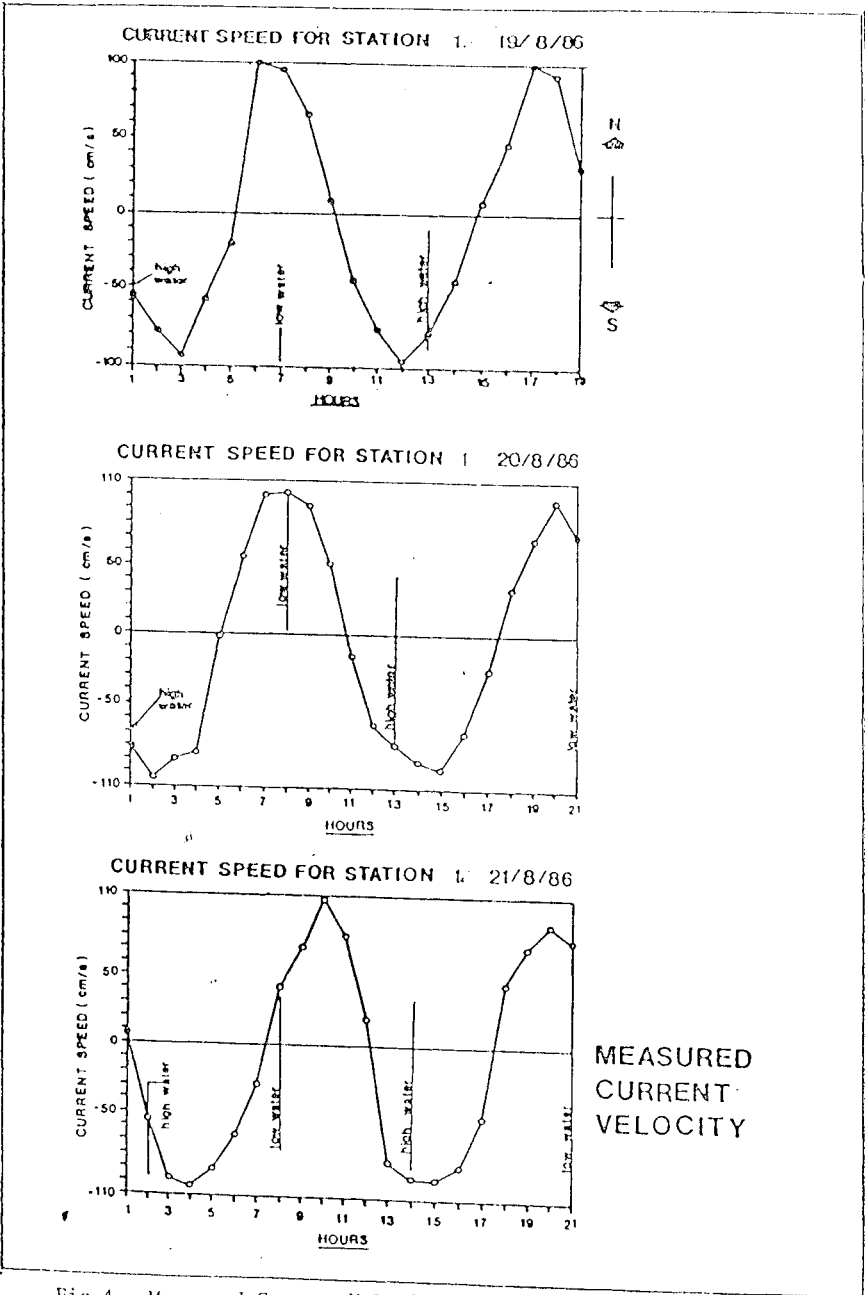


Fig 4. Measured Current Velocity at Sampling Station 1.

Table 1. Comparison Between Measured Velocity and Computed Velocity at 6 Locations (m/s).

Location	Maximum North Flow			Maximum South Flow		
	Measured	Computed (DHI)	Computed (This Study)	Measured	Computed (DHI)	Computed (This Study)
1	1.06	1.01	0.94	1.06	1.05	1.05
2	0.80	0.84	0.77	0.93	0.99	0.88
3	-	0.47	0.45	0.78	0.49	0.50
4	0.78	0.69	0.60	0.85	0.70	0.61
5	0.86	0.71	0.72	0.99	0.72	0.80
6	0.60	0.87	0.50	0.69	0.89	0.60

Sewage Pollution

The Penang Straits is grossly polluted by sewage. The FC concentrations in the Western Channel, for example, consistently vary within the range of 10^3 to 10^6 MPN/100 ml, depending on the distances from the sewage outfall (Owen, 1978; Koh *et al.*, 1996a), which are much higher than the level of 200 MPN/100 ml deemed safe for contact sports and bathing purposes. Yet there are plans to develop tourist recreation resorts in the coastal areas with high FC counts. An EIA is mandatory for this type of development. To achieve the water quality standards commensurate with the designated usage, it is necessary to provide sewage with proper treatment followed by adequate coastal disposal. Simulation models have been developed (Koh and Lee, 1993; Koh *et al.*, 1991) to provide quantitative assessment of the impact of discharge of sewage with given levels of treatment and specified modes of discharge.

Figure 5 provides a prediction of potential FC concentrations in the Western Channel subject to a sewage discharge at site A of 148,000 m³/d with a treated FC concentration of 8×10^5 MPN/100 ml during a mean tide with a maximum tidal current of 0.5 m/s, while Figure 6 depicts the corresponding scenario in Southern Channel for a sewage discharge at site B of 68,000 m³/d with FC concentration of 2×10^7 MPN/100 ml. Various potential scenarios predicted by model simulations subject to different levels of treatment and modes of disposal provide relevant information crucial to informed decision-making for the selection of sewage treatment facilities most suitable for Penang (Koh *et al.*, 1996a).

Suspended Solids

The major sources of SS are mainly land-based activities and coastal zone development projects that produce potentially large quantity of sediments that eventually end up in the sea. Suspended solids can smother corals, reduce light penetration, carry toxicant sorbed

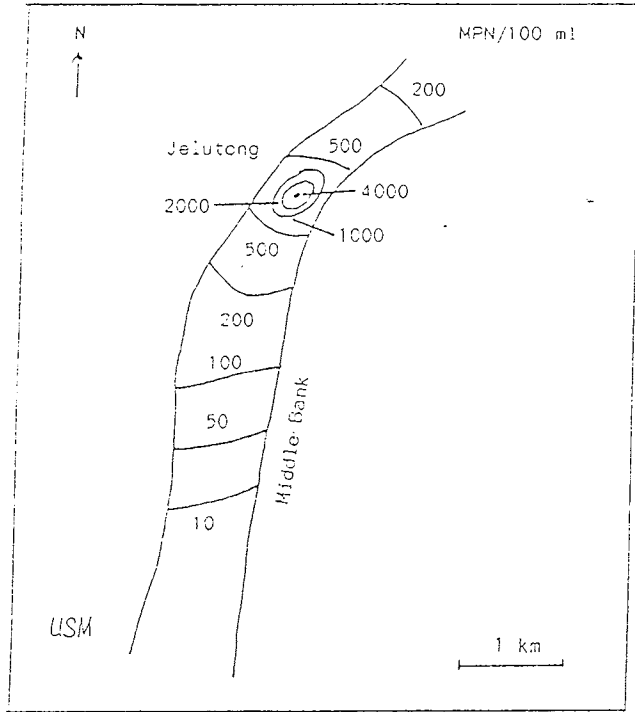


Fig. 5 Tidally averaged FC contours during mean tide for sewage flow of $148,000 \text{ m}^3/\text{d}$, treated to 8×10^5 MPN/100 ml in Western Channel

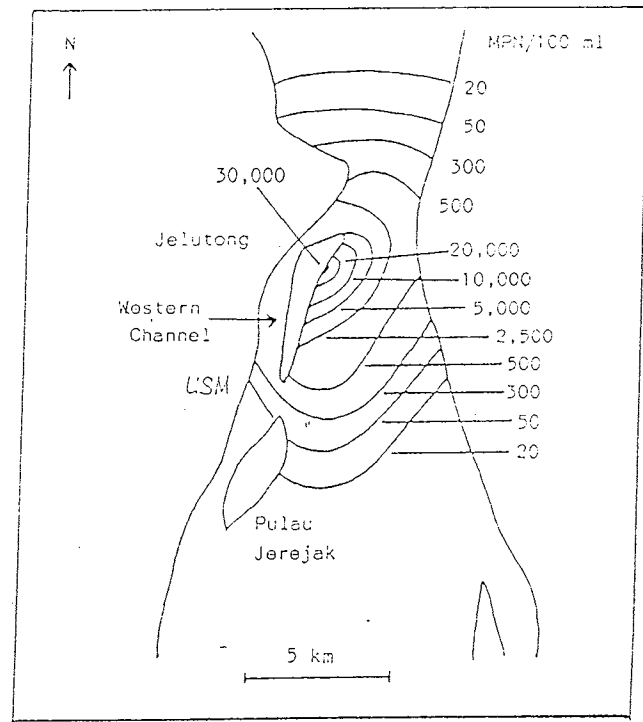


Fig. 6 Tidally averaged FC contours during mean tide for sewage flow of $68,000 \text{ m}^3/\text{d}$, treated to 2×10^7 MPN/100 ml in Southern Channel

onto them and adversely affect marine ecosystems. Various control measures are available to reduce the generation or transport of SS in the water column, the most effective being source control. However, the fast pace of development in the State of Penang has rendered source control an elusive art or simply an “act of nature”. The eventual fate of these SS generated in the coastal environment will depend mainly on the quantity of SS generated at source, and the various physical and chemical processes involved in their transport; knowledge of these processes is sparse. Models of SS transport may be used to quantify the fate of SS in the coastal seas (USEPA, 1991). Figure 7, for example, illustrates the potential SS concentration contours resulting from dredging, predicted by models and averaged over the tidal cycles (Koh and Din, 1995).

We are further enhancing the model capability and robustness through a grant under the UN-ESCAP funding (Postma, 1995; Koh *et al.*, 1995) and an IRPA project funded by the Seventh Malaysia Plan (Koh, *et al.*, 1996b) with the aim to extend the existing models to include uptake and ecosystem modeling.

EFFECT MODELING

Water quality will affect aquatic organisms in many ways. Growth may be slowed down leading to reduced fecundity if the toxicity is sublethal or the organism may bioaccumulate toxicant to a level that rendered them unsuitable for human consumption. Indicative organisms, may be intensively studied so as to provide key indication on the status of the environment. For Penang Straits indicative organisms chosen for this study include the blood cockles (*Anadara granosa* *l.*), the clam (*Donax faba* *c.*), and the oyster (*Crassostrea iredalei* and *Crassostrea belcheri*).

Model for Mussels

While a model of water quality effects on blood cockles is our ultimate goal, we begin with an existing model for mussel, another bivalve species, which will be modified for cockles.

The life cycle of the mussels (Unionids) begins with the fertilization and incubation of eggs that take place in the gill marsupia of the female mussels. Then the glochidia, the parasitic larval stage of the mussels, are released and subsequently attached themselves to suitable fish-hosts before dropping off upon completion of their development into juveniles. A good description of the life cycle of the Unionids is available in Lee and DeAngelis (1996) and the references therein.

The computer model is based upon the Roughgarden *et al.* (1985) concept of a single open marine population with space-limited recruitment and non-overlapping generations. Growth is parameterized by a deterministic function while survival from one age class to the next is probabilistic and is a function of age, species and environment. While the mussels are sessile once they are attached to a substrate, the parasitic stage when they are

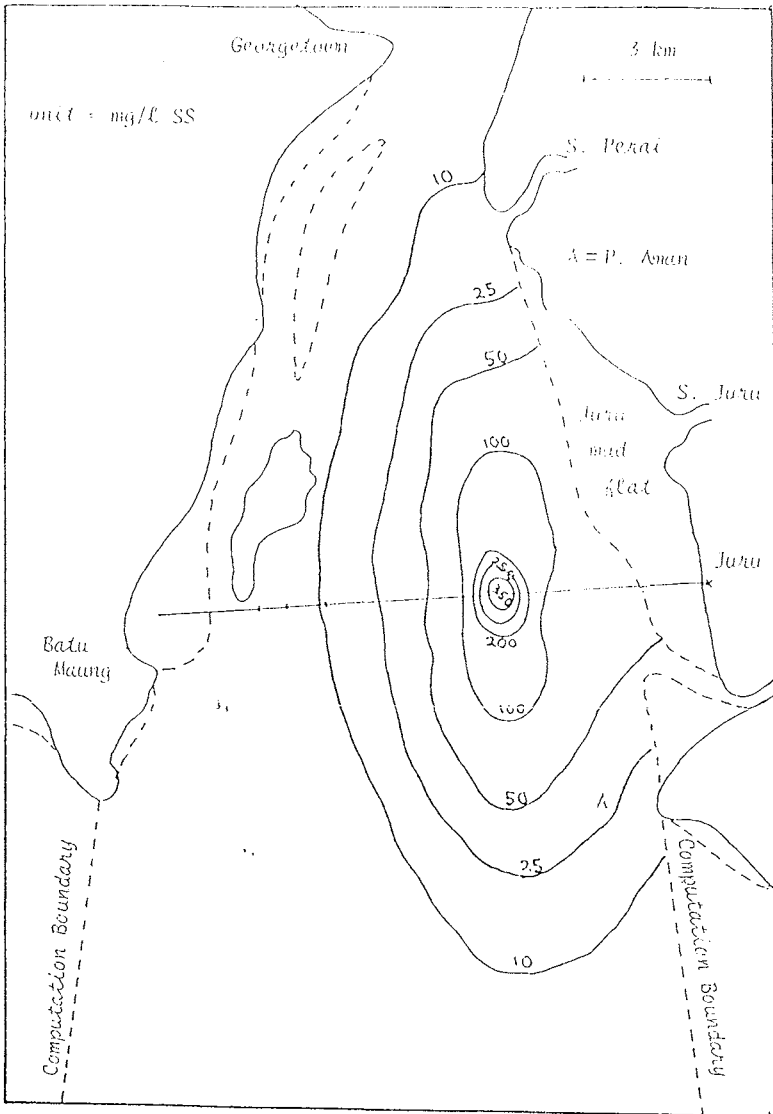


Fig. 7 SS contours for tidally-averaged concentration

attached to a fish-host provides a mechanism to colonize new territory and hence spatial distribution.

A typical distribution of mussel population indicates that the mussels colonize new downstream habitats with the spread of the population taking the appearance of a traveling wave front. More detail regarding the simulations and their ecological implications are available in Lee and DeAngelis (1996). This mussel model is presently under modification to adapt it for the cockles and other molluscs which have different life cycles.

Growth and Update

Dwindling catches from the Penang Straits have raised concerns regarding the adverse impact of pollution on fishery resources, particularly with respect to heavy-metal contamination. In a recent paper, anthropogenic input of heavy metals into the sediments was recorded for the Penang Straits, which was associated with a rise in metal content in molluscs, with the rock oyster *Saccostrea sp* having the highest content and the blood cockle, *Anadara granosa* the least (Din and Jamaliah, 1995). Accumulation of heavy metals by cultured oysters was also noted for the Merbok Estuary, Malaysia (Lim *et al.*, 1995). In addition to bio-accumulation, strong correlation were found between the scope of growth of the blood cockles and seven environmental parameters in the Juru area, which receives domestic and industrial wastes (Din and Ahamad, 1995). Of the metals concerned, copper was found to be most toxic to the clams, *D. faba* and spat of the blood cockles, *A. granosa* followed by cadmium and zinc (Ong and Din, 1996).

Useful as they are, these data are as yet insufficient to provide a general framework to support a modeling endeavour to study the effects of toxicant on the growth and fecundity and hence the dynamics of the organisms involved. However, the modeling efforts done on the mussels mentioned early as well as on the daphnia (Koh *et al.*, 1994) population dynamics subject to environmental stressors would provide strong indications regarding the direction of future research. The aims are to integrate available scientific data with modeling to enhance our understanding of those organisms under environmental stresses to which they are subjected. This forms an integral component of our present research efforts.

ACKNOWLEDGEMENT

A research grant #08-02-05-6007 funded under IRPA, Seventh Malaysia Plan is gratefully acknowledged.

REFERENCES

- DHI. 1972. Full Feasibility Study of a Fixed Linkage Between Penang Island and Province Wellesley. Consultancy Report to Government of Malaysia, Danish Hydraulic Institute.
- DHI. 1992. Penang Borrow Dredging Initial Morphological Impact Assessment. Consultancy Report prepared by Danish Hydraulic Institute to Penta Ocean Construction Ltd.
- Din, Z. and Ahamad, A. 1995. Changes in the Scope of Growth of Blood Cockles (*Anadara granosa*) Exposed to Industrial Discharge. *Marine Pollution Bulletin*. **31**:406-410. Great Britain.
- Din, Z. and Jamaliah, M.R.S.N. 1995. Trace-metal Pollution in the Coastal Areas of Penang Island, Malaysia. *Advances in Marine Environmental Management and Human Health Protection*, edited by D. Watson, K.S. Ong and G. Vigers. Singapore. pp.207-214.
- Koh, H.L. and Din, Z. 1987. Final Report on Coastal Oceanographic Study of the Penang Strait. Consultancy Report submitted to the Penang Development Corporation for an Environmental Impact Assessment related to Coastal Reclamation. March. 120 pp.
- Koh, H.L. 1988 "Finite Element Analysis of Long Period Tidal Propagation in a Channel", Proceedings of the International Conference on Computational Methods in Flow Analysis. Okayama University Press. pp.1262-1269.
- Koh, H.L., Lim, P.E. and Zamali, M. 1991. Management and Control of Pollution in Inner Johore Strait. In: *Journal Environmental Monitoring and Assessment*. The Netherlands:Kluwer Academic Publishers. pp.19: 349-359.
- Koh, H.L. and Lee, H.L. 1993. Lumped Parameter Finite Element Method for Water Quality Analysis. *Jurnal Fizik Malaysia* pp.45-52.
- Koh, H.L., Hallam, T.G. and Lee, H.L. 1994. Combined Effects of Environmental and Chemical Stressors on a Model Daphnia Population. Technical Report M7/94. Universiti Sains Malaysia, Penang.
- Koh, H.L. and Din, Z. 1995. EIA Study of the Proposed Overhead Transmission Line Crossing from Juru to Bayan Lepas: Sediment Transport Study. Final Report submitted to Tenaga Nasional Berhad. May.
- Koh, H.L. and Din, Z., Lee, S.C., Puziah, G. 1995. Environmental Impact of Coastal Development, the Malaysian Case Study in Penang Strait. Report submitted to the Expert Group Meeting on Environmental Impact of Coastal Development, Project UNEP-ESCAP, Bangkok, Thailand. May.

Koh, H.L., Lim, P.E. and Lee, H.L. 1996a Impact Modeling of Sewage Discharge from Georgetown of Penang, Malaysia on Coastal Water Quality. Accepted to Journal Environmental Monitoring & Assessment. The Netherlands:Kluwer Academic Publishers.

Koh, H.L., Din, Z., Lim, P.E. and DeAngelis, D. 1996b. Water Quality and Coastal Ecosystem Modeling for Management. Project 08-02-05-6007, IRPA, Seventh Malaysia Plan.

Lee, H.L. and DeAngelis, D.L. 1996 A Simulation Study of the Spatial-Temporal Dynamics of the Unionid Mussels. Accepted to Ecological Modelling. The Netherlands.

Lim, P.E., Lee, C.K. and Din, Z. 1995 Accumulation of Heavy Metals by Cultured Oysters from Merbok Estuary. Malaysia. *Marine Pollution Bulletin*. **31**:420-423. Great Britain.

Ong, E.S. and Din, Z. 1996 Cadmium, Copper and Zinc Toxicity to Clam, *Donax faba c.* and the Blood Cockles, *Anadara granosa l.* ASEAN-Canada Cooperative Programme on Marine Science II. June. Penang, Malaysia.

Owen, J.D. 1978. Coliform and *E. coli* Bacteria in Seawater Around Penang Island, Malaysia. Water Research, Great Britain. pp.365-370.

Postma, W. 1995. Theory, Practice and Modelling Techniques for Coastal Water Quality Models. Delft Hydraulics and BKH Consulting Engineers. Delft.

Roughgarden, J., Iwasa, Y. and Baxter, C. 1985. Demographic Theory for an Open Marine Population with Space-Limited Recruitment. *Ecology*. **66**(1): 54-67.

USEPA. 1986. Quality Criteria for Water. United States Environmental Protection Agency. Washington, D.C., USA.

USEPA. 1991. WASP4, A Hydrodynamic and Water Quality Model: Theory, User's Manual and Programmer's Guide. USEPA. Athens, Georgia.

USEPA. 1992. Framework for Ecological Risk Assessment", EPA 630/R-92-001, Washington, D.C., USA.

USNRC. 1993. Issues in Risk Assessment. National Research Council, National Academy Press, Washington, D.C., USA.

BASIC STUDY ON THE RENEWAL IN THE COASTAL ZONE OF METROPOLITAN AREAS

Takamasa Miyazaki and Akira Minemura
Nihon University
Chiba, Japan

ABSTRACT

The main purpose of this study is to suggest a new perspective to the present situation of the coastal zone of metropolitan areas which have undergone a rapid environmental alteration according to various industrial interests.

In recent years, the situation of most coasts are that Japan seems to have hit a certain limit without a constructive view. For instance there have appeared waterfront projects, renewal of the port system, developments of recreational resorts at fishing villages, and so forth. These structural alternations, especially, by industrial purposes, indeed have been serving certain interests. However, it has been a long time since various questions in terms of environmental breakdown in these areas were suggested. Inefficiency of industrial concepts as in the past has led the industrial use of many of these areas, substantially, to a collapse, along with the end of high-ratial economical growth in the last decades.

The study therefore consists of analysis and evaluation of the industrial use of the coastal areas. The analysis and evolution are fully developed in order to be prepared for suggesting new values, and simultaneously, activation of the values on the vast industrial areas which have left without constructive importance.

INTRODUCTION

Purpose and Method of Study

This report reviews and reevaluates the environment in the face of the diversified use of the coastline areas brought about by changes in the structure of the location of industry itself, the relocation and the changing character of factories as a result of restructuring and changes in port facilities. It is important that when considering issues that are relevant to the waterfront of large urban areas, the trend of these changes and analyzing the relationship between the cause and effect be kept in mind. This report has been compiled as basic source material for restructuring the coastline as a whole and for planning the formation of a waterfront environment.

This study targets the waterfront of urban centers and extracts the pertinent issues by analyzing the current state of affairs through research on-site and from available materials on the coastlines of Osaka bay and Ise Bay as well as by identifying the current characteristics of these area,

processes of change and the problems that await solutions through investigation of intentions, hearing sessions and on-site research.




THE DETAILS OF THE MAIN BAY AREA IN JAPAN			
	ISE-BAY	TOKYO-BAY	OSAKA-BAY
SHAPE			
POPULATION	5,200,000	25,000,000	15,000,000
SEA SURFACE	210,000ha	120,000ha	140,000ha
COAST LINE	660km	753km	383km
HARBOR AREA	39,000ha	56,000ha	27,000ha
CARGO	201,371,000t	539,820,000t	425,918,000t

Figure 1. The Details of Main Bay Area in Japan

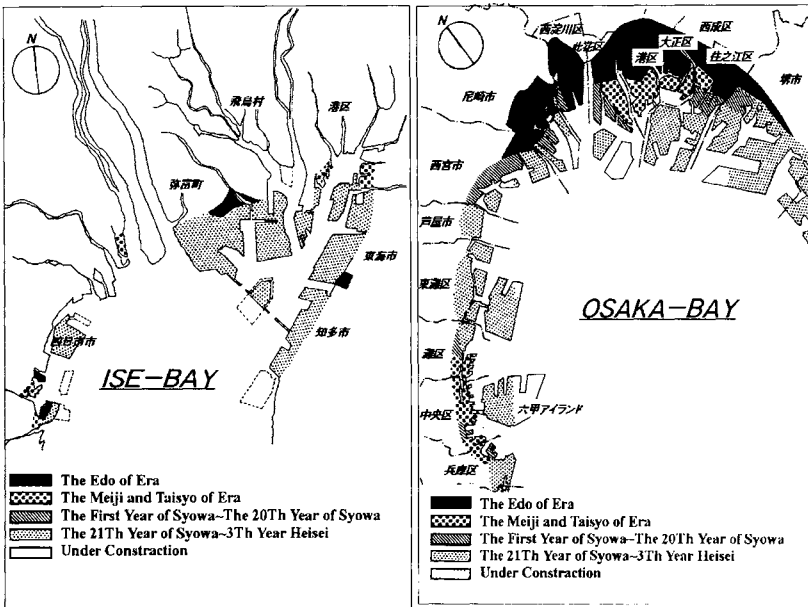


Figure 2. Fill up changes of Ise and Osaka Bay

The production structure and land use by factories in the coastal industrial areas in the years after the end of the high growth years and the collapse of the bubble economy will be investigated and the trends identified. An intent survey was conducted at the factory level on the following issues and the results will be analyzed and reviewed.

Sampling of Target Factories and Method of Survey

Factories located in the Osaka Bay coastal areas of Metropolitan Osaka (Osaka City, Sakai City) and Hyogo Prefecture (Amagasaki City, Nishinomiya City and Kobe City) (as there were no factories in the relevant areas of Ashiya City, this city has been discarded from the target area) and factories located in the Ise Bay coastal areas of Aichi Prefecture (Chita City, Tokai City, Minato Ward of Nagoya City, Tobishima Village, Yatomi Town) and Aichi Prefecture (Kawagoe Town, Yokkaichi City) were selected through random sampling and questionnaires were sent out taking the following into account:

- Companies that have been in existence for 10 years or more
- Factories with total land space of 3,000 square meters or more
- Division by Business Category

Type I (Energy Type): Thermolectric Power Plant, City Gas

Type II (Primary Resource Type): Chemicals, Petroleum, Steel, Non-metals

Type III (Processing and Assembly Type): Metal Products, Machine Products, Electric Products, Automobiles

Type IV (Local Resource Type): Food Products, Fiber Products, Wood Products, Mining Products

Type V (Miscellaneous Type): Clothing Products, Furniture Products, Printing Products, Rubber Products, Leather Products, Others Products

The questionnaires were mailed and collected after a certain number of days.

Content of the Survey (Akimoto and Sasao, 1995)

1. The year in which the coastal area facility began operations
2. Size (size of land)
3. Number of employees
4. Equipment owned (now and when operations first started)
5. Business strategy results and method of implementation

6. Evaluation of the location (overall and by conditions)
7. Desired public sector support structure
8. Future vision for the development of coastal industrial areas

Basic Direction and Vision for Improvements in the Coastal Industrial Areas of the Hanshin and Chukyo Region

The basic direction and vision for improvements in the coastal industrial area of the Hanshin region are seen as 'diversified and composite industrial vision with the physical distribution functions of the harbor organically linked to the industrial functions of the region'.

The basic direction and vision for improvements in the coastal industrial area of the Chukyo Region are seen by the majority as 'diversified and composite industrial zone with the physical distribution functions of the harbor organically linked to the industrial functions of the region', and a diversified and composite zone is envisioned to replace an industry dominated one.

The factor of location in the various industrial zones around Osaka Bay by region shows that in all zones, 40% to 50% show satisfaction so that as a whole, the location can be termed to be satisfactory. However the reason almost 30% are dissatisfied in Sakai City is seen to be linked to the availability of labor, availability of industrial water and the unimproved and underdeveloped urban infrastructure.

Seen by category of industry, 25% in the Energy Type, Primary Resource Type and Processing and Assembly Type expressed dissatisfaction while very little dissatisfaction was expressed by the Local Resource Type and Miscellaneous Type. From these results, it can be said that the evaluation of the area is low among large scale industries and high among medium, small and very small industries.

With regard to land space and buildings, 27.4% expressed the desire that zoning laws be eased thus showing that overall the trend is towards desiring that such laws be eased. The desire to acquire adjacent industrial land or buy out existing facilities was strongest in the Primary Resource Type category (Anon, 1989).

In the Ise Bay area, satisfaction as to location was 40% while dissatisfaction was 15% in the Minato Ward area of Nagoya City. On the other hand, in the neighboring areas of Yatomi Town and Tokai City, dissatisfaction was high on the factors of location (very high), urban infrastructure, industrial water, labor force and information infrastructure and this is seen to be the result of the unimproved state of the infrastructure and the undeveloped industrial location. In Tobishima Village, Kawagoe Town and Yokkaichi City, dissatisfaction was low.

Seen by category of industry, more than 50% in Type II (Primary Resource Type) Chemicals, Petroleum, Steel and Non-metals expressed satisfaction, while this was true of only about 30% of Miscellaneous Type and Local Resource Type industries. Further, among industries in the

Processing and Assembly Type and Energy Type, little dissatisfaction was found. From these results, it can be said that the evaluation of the area is high among large scale industries and low among medium, small and very small industries.

Concerning land space and facilities, on the whole there is a desire to see the easing of zoning restrictions. 'Scrap & Build', a format that may be called a form of self reliance is seen (17.7%) while demands for improvements in such location factors as expansion of available land is also seen (9.2%). When this is observed by category, the need for easing zoning laws is high among the Energy Type and Primary Resource Type industries, motivation to expand land space is present in the Processing and Assembly Type and Miscellaneous Type industries and the Local Resource Type industries are promoting 'Scrap & Build'.

In the Chukyo area, the trend is not towards changing business category or use of land but towards improvements within the status quo and enhancement of conditions so that it is not expected that this would wield sufficient impact to lead to a review of industrial location in coastal regions or to significant redevelopment or changes in the regional structure (Anon, 1995).

Comparison of Location Factors in the Osaka Bay and Ise Bay Areas

In the Osaka Bay area, more than 1/3 of the factories stated that they were 'Satisfied' while those responding with 'Dissatisfied' were few. When the dissatisfaction level is seen by industry category, Energy Type and Primary Resource Type industries make up about 25% of the total.

By region, in Kobe City, 1/2 answered 'Highly Satisfied' while Sakai City registered higher dissatisfaction than other regions.

In the Ise Bay area, 1/3 of the factories stated that they were 'Satisfied' and when combined with the 46.4% who answered 'Average', the total is 85.6% thus indicating that overall, the area is a satisfactory one.

By region, Yatomi Town and Tokai City registered 70% satisfaction and little dissatisfaction. Satisfaction and dissatisfaction were about equal in Tobishima Village, Minato Ward, Kawagoe Town and Yokkaichi City. On the other hand, in contrast to other regions, hardly any factory in Chita City reported satisfaction while 20% answered that they were dissatisfied. Tobishima City and Chita City cannot be seen as being satisfactory locations in relative terms.

By category of industry, dissatisfaction is high in Local Resource Type and Miscellaneous Type industries.

Looking at the two areas by location factors, the merits listed for the Osaka Bay area were transportation factors, proximity factors and production factors while the demerits were the insufficiency of labor and urban infrastructure. A need exists for improving the labor environment by acquiring a larger base of labor force and achieving a balanced urban

infrastructure through building a functional commercial and industrial climate and such amenities as parks.

The evaluation of such factors as industrial water availability, factors related to the region and legal restrictions is low. As these barriers are closely related to the expected move towards high technology, greater sensitiveness and refinement are issues that must be addressed in reviewing location and environment formation in the future.

In the Ise Bay area, the merits were the factors of transportation, proximity and production. The demerits were the availability of labor force and the level of urban infrastructure with the issue of the labor force being considered the greatest demerit.

Characteristics of Location and Future Vision of the Osaka Bay and Ise Bay Coastal Industrial Areas by Region, Zoning and Year of Reclamation

Looking at the situation by zoning in the Osaka Bay area, zoning restrictions and multiple restrictions have made it difficult to expand factory land space in semi-industrial zones and in dedicated industrial zones, despite increases in unused land, redevelopment is difficult and as the waterfront is restricted, being enclosed with a vertical embankment, dissatisfaction over the availability of industrial water, the quality of urban infrastructure, regional factors and legal restrictions is high.

In the Ise Bay area industries function within the confines of restrictions but in industrial and dedicated industrial areas, urban infrastructure, information infrastructure and the labor force are sufficient. The physical distribution function, production function and research function of industry are independent and do not form an integrated whole.

Seen by region, as use objectives and form are diverse in the Osaka Bay area, a need exists for development that takes into account the characteristics of each region with some regions desiring the formation of coastal industry communities or while others desire the formation of urban zones.

In the Ise Bay area, each region is specialized and separated from other reclamation areas by the urban areas connected to them. For this reason most industrial areas are isolated islands with widely different images and characteristics and the development of regional land use that accommodates multiple uses is needed.

Looking at the situation from the zoning point of view, in the Osaka Bay area, in some cases a dedicated industrial zone may be surrounded by industry zones or a semi-industrial zone may exist within the more regulated industrial zone. In other cases, a semi-industrial zone may be surrounded by reclaimed industrial zone and have little access to the waterfront thus impairing harbor functions. In still other cases semi-industrial zones may be far from the interior thus weakening their contact with urban areas. All these make for a less than optimal integration and functionality.

Most of the industrial regions of the Ise Bay area are industrial or dedicated industrial zones. Although the area is unified as an industrial region and is thus efficient, there is no organic link to physical distribution so that a regional development that is multifaceted and integrated in character is required.

Looking at the situation from the year in which reclamation was implemented, the older reclaimed land in the Osaka Bay area is surrounded by the inland sections so that a great many of these industrial regions are landlocked. There is the need for industrial regions that are connected to the inland sections of the region thus providing an urban connection and a high level of integration. Currently there is a scattering of reclaimed regions that are in isolation.

On the other hand, with newer reclamation, use is limited in variety and a more diverse use of land and zoning is awaited in the Osaka Bay area. In the Ise Bay area on the other hand, the newer reclamations are isolated from urban centers so that urban functionality is insufficient.

Characteristics of Waterfront Industrial Regions

1. In Osaka Bay, reclamation of land began relatively early and Suminoe Ward, Nishinari Ward, Taisho Ward, Minato Ward and Konohana Ward which were being used for industrial purposes from the outset, became landlocked and the use of land in this region evolved a multiple dimension that helped develop transport and location conditions. On the other hand, expansion of factory facilities became difficult with the prevailing legal restrictions and redevelopment is seen to be difficult (Inland Multiple Type).
2. Minato Ward in the Ise Bay area has urbanized so that most factories have relocated to reclaimed land (Inland Urban Type).
3. Because of the deterioration of old piers and warehouse facilities and changes in the modes of sea transport, the jetty was reclaimed and harborfunction restored as a container yard. Inanaga Pier in Minato Ward of Nagoya City, Suminoe Ward, Konohana Ward, Taisho Ward, Minato Ward, Amagasaki City, Nishinomiya City, Higashinada Ward, Hyogo Ward and the area around Nagata Ward were reclaimed in the early 1920's and later expanded to become warehouse facilities and industrial container yards but are areas that have significant problems related to safety (Container Yard Type).
4. Yatomi Town and Tobishima Village in the Ise Bay area were originally reclaimed as agricultural land but during the years in which the economy grew at a rapid pace, were diverted to industrial and harbor facilities use. Because the reclamation was on a vast scale, this change of plan was implemented smoothly and many of the areas take an evolved form of the diked communities that were particular to the Ise Bay coastal area (Diverted Use Type).

5. Post war reclamation's were large reclamation's for industrial use for the most part and are petrochemical complexes which are typical of waterfront industrial areas. In Osaka City's Minato Ward in the Osaka Bay area and the area around Yokkaichi City, Minato Ward District 9, Kaneshiro Pier, the areas around Tokai City and Chita City belong to this group (Petrochemical Complex Type).
6. In recent years, reclamation's that were implemented as receiving ground of industrial waste have become artificial islands attracting homes and urban infrastructure to rapidly develop into urban centers. Rokko Island in Kobe City, the area around Nishinomiya, Kaneshiro Pier, and the area around Chita City are examples of this type (Island Type).
7. Garden Pier in Minato Ward in the Ise Bay area, Port Island in Kobe City and Tenhosan Pier in Minato Ward of Osaka City are examples of reclamation's in which amusement centers are being located due to their interrelationship with inland urban centers (Amusement Type).

Thus by year of reclamation and use, industrial land in urban waterfronts can be divided into the above seven types.

- | | | |
|------|-------------------------------|--|
| I. | a. An Inland Multiple Type | b. Inland Urban Type (-1920's) |
| II. | a. Container Yard Type | b. Diverted Use Type (early 1920's - early 1940's) |
| III. | a. Petrochemical Complex Type | b. Island Type (mid 1940's - 1950's) |
| IV. | a. Amusement Type | b. Housing Development Type (late 1980's) |

The various types can be subcategorized into 'I', 'II', 'III' and 'IV' by year of reclamation and into 'a' and 'b' by location characteristics.

It is believed former factory sites in the coastal areas are undergoing change made necessary by the times and by the changes in given conditions influenced by the type categories given above.

For Type I, the issues are the development of such infrastructure as roads and the easing of restrictions while for Type II, as medium and small factories are in close proximity to residential areas, measures for preventing disasters and noise pollution are urgently required. Types III and IV are still developing and the crucial issues here have to do with proximity to housing, industrial waste water, atmospheric pollution and greening of the environment.

Planning Issues and Planning Objectives for Urban Coastal Areas

The Osaka Bay area is the target of legal regulations that are particular to coastal areas and thus the form of land use cannot be changed. This has led to increased incidence of under used and unused land (under used land is found in Sakai City, in the proximity of Amagasaki City and parts of Kobe City and the resulting de-industrialization has detracted from the vigor of the area).

Further, the shoreline is dominated by harbors, physical distribution facilities and industrial functions so that shoreline for the safe recreation of the citizens is insufficient. These facilities are difficult to expand due to restrictions on industrial location. Because of the deteriorated relation with the surrounding area and accessibility, locating amenities and recreational space is also difficult (in the reclaimed areas of Nishinomiya City, the night time population is almost nonexistent).

As can be seen, numerous systems and methods that need to be resolved exist as planning issues for the Osaka Bay area. It is necessary that these be reviewed and resolved in an integrated manner, that legal restrictions be reviewed and restructured and that the introduction of new methodology be reviewed. In place of a single function style of land use, land space that has the functions of residence, workplace, schooling and entertainment in a balanced way must be developed. It is also necessary that the shoreline be opened to construct artificial beaches, ocean recreational space and parks. In coastal areas, achieving proximity of residential areas to the workplace, establishing public services, maintaining commercial functions and providing for green belts and open land space in units of appropriate size thus injecting residential functions into an industry specialized area is indispensable to activating industry (Miwa, 1987).

The Ise Bay area must further enhance its efficient link with industrial and consumption areas while at the same time not limiting itself to ocean transport but developing into an integrated terminal that is capable of responding to all transportation needs including road transport and air transport.

CONCLUSION

The labor force is an issue that has to do with human resources. Given the fact that quality housing space is currently difficult to obtain, it is necessary that such residential space replete with comforts, safety and community amenities be developed addressing not merely the issue of location but ensuring accessibility of the workplace and relationship with the surrounding areas and the accessibility of urban functions.

What is required in the future is the organic positioning of green belts and open space and the development of a residential and industrial base including preserving the integrity of the shoreline and providing for public services. At the same time, given the fact that such industrial zones comprise a part of large urban centers, an integrated environment plan that addresses the issues of functionality and safety from disasters must be implemented.

Further, a restructuring that takes into account the social and location changes caused by the Great Hanshin Earthquake must also be addressed.

The workplace and residential areas must be made more proximate, a regional community formed, facilities needed for living must be maintained, and in particular recreational and commerce creating and leisure functions must be provided for.

This report has taken the intent survey of factories as its fundamental base and in the future, surveys of shop owners in commercial districts and of citizens in the residential districts must be performed in order to study an environment formation plan that answers the needs and intents of citizenry.

REFERENCES

Akimoto, J. and J. Sasao. 1995. Study of Coastal Industry. The report of study in College of Industrial Technology, Nihon University. December.

Anonymous. 1989. Survey of Land Use in the Osaka Bay Coastal Area. Osaka Science & Technology Center. December.

Anonymous. 1995. Conditions in Ise Bay. Harbor 5 Construction Bureau.

Miwa, Kimio. 1987. Vision of the Redevelopment of Coastal Areas. Land of Coastal Zone Question, a Society for the Study of English Poetry, The Minster of International Trade and Industry. March.

REFLECTIONS ON THE DEVELOPMENT OF TROPICAL MARINE STUDIES FOR SOUTH PACIFIC SCHOOLS

Stephen M. Ritchie and David Hopley
James Cook University of North Queensland
Townsville, Australia

ABSTRACT

The *Australian UNESCO Tropical Marine Studies Project for South Pacific Schools* grew out of the need to address the low levels of scientific literacy in the South Pacific Region. A focus on marine studies was perceived to be necessary for the economic future of this region as well as providing an appealing and relevant theme for study in schools. A set of six student texts, three teachers guides and a poster have been published. Each activity-based text has a habitat (e.g., mangroves) or environmental issue (e.g., fisheries) as its focus. The texts were designed to be used separately, within existing curricula, or as the basis of a new additional subject in marine studies. This paper describes the intended and actual development processes of this collaborative project. Our retrospective reflections might help other developers to build on its strengths and to avoid the pitfalls that we experienced.

INTRODUCTION

Fraser and Cohen (1989) expressed concern over the dearth of reports of large-scale curriculum materials development projects. Furthermore, they argued that there was a need for such accounts to emphasise the formative evaluation process so that curriculum developers could benefit from the descriptions of experiences and retrospective reflections of others. Our aim in this paper is to describe the development, including the formative evaluation processes, of the *Australian UNESCO Tropical Marine Studies Project for South Pacific Schools* and share some of the lessons learned by project team members.

BACKGROUND

During the 1988 Australian National Commission's (for UNESCO) sponsored visit to countries of the Pacific Region, the need for marine science school curriculum materials was identified (Wilson-Lo Bianco Report, produced by a joint effort between the Commonwealth Scientific and Industrial Research Organisation - CSIRO - and the Commission). This finding was echoed later by South (1991, p. 2) who reported that, in the Pacific Region, "There is an overwhelming need to develop national and regional programs that focus on the development of appropriate school curriculum materials on marine topics..." South's survey of the school science programs in each of the Pacific nations revealed that, "Very few countries introduce marine-related topics in the curriculum, even though the majority of children in the smaller island nations are surrounded by the ocean and it is an integral part of their daily lives" (p. 41). While education leaders in these nations recognise the importance of relevant curriculum materials for Pacific children, South

found that within-nation curriculum development was constrained by lack of funds, resources, and expertise in marine science curriculum development. Combined with such other constraints as inflexibility and irrelevance of syllabuses (i.e., many Pacific nations have simply adopted syllabuses from such countries as New Zealand, England, France), poor or no laboratory facilities and resources, limited availability of qualified teachers, and the predominance of lecture or expository modes of teaching, a low level of scientific literacy for the population at large has resulted (Broadfoot, 1991; South, 1991). While the extent of these problems varies from school to school and between nations, science education curricula generally are in need of redesign or, at the least, supplementation. In the Kingdom of Tonga, for example, Broadfoot (1991, p.24) observed:

"Due to the examination driven curriculum and the prescriptive syllabuses, most science teachers resort to transmission models of teaching in which lessons are heavily content-based. Students do not have textbooks and spend considerable class time copying notes and diagrams from the blackboard. Very few experiments are done due to the pressure to cover the content."

In recognition of this undesirable position, many Pacific nations are poised to reconceptualise or supplement their school science curricula. Of course, external funding is essential to assist these nations in developing curriculum topics more relevant to the intrinsic interests of the children and the emerging career options in tourism, fisheries, and environmental management.

With funding support from AIDAB (now AusAID), a project team at James Cook University of North Queensland was established in 1991 to develop a series of six marine studies texts that were educationally and culturally relevant to the upper secondary students of South Pacific schools. Although the original project design was planned for a three year period, the project has taken until 1996 to complete. The reasons for the delay are disclosed later along with other relevant reflections.

PROJECT DEVELOPMENT

Several development phases were incorporated in the project design to address the particular goal and contexts for this multi-national project. These general phases included: Awareness of needs and contexts, Pilot study, and Text production. Although there was some overlap in purposes and tasks between these phases, the strategies employed through the three major phases of the project can be summarised linearly for convenience, as shown in Table 1.

Awareness Phase

The Australian National Commission for UNESCO invited Hopley to convene a planning meeting at James Cook University with delegates from member countries (identified by UNESCO) in order to gauge reactions (and preferences for assistance) to the perceived need for school marine studies curriculum materials. This meeting involved school and university education system representatives from the following countries: Cook Islands, Fiji, Kiribati, Papua New Guinea, Solomon Islands, Tonga, and Vanuatu. As well as these delegates, UNESCO representatives from Indonesia, New Zealand and Australia observed proceedings.

Table 1. Summary of the project development phases and strategies

PROJECT PHASE	STRATEGY	PLANNED SCHEDULE	ACTUAL SCHEDULE
1. AWARENESS	a. Australian National Commission report	1988 - 1990	1988 -1990 1988
	b. Planning Workshop with stakeholders at JCU		June 20-21, 1990
2. PILOT STUDY	a. Establishment of a multi-national advisory committee	1991 - 1992 1991	1991 - 1992 1991
	b. Needs Assessment - visit to selected member countries by coordinating team	Apr 1991	Apr 1991
	c. Planning, development and local trial of prototype texts	May 1991 - Nov 1991	May 1991 - Feb 1992
	d. In-country trials	Jan 1992 - Mar 1992	Feb 1992 - Apr 1992
	e. Analysis, revision and further planning	Apr 1992 - Jun 1992	May 1992 - Dec 1992
	3. PRODUCTION	1992 - 1993	1992 - 1996
a. Improvement of prototype texts	Jan 1992 - Apr 1992	1993 - 1995	
b. Development of additional texts	Apr 1992 - Dec 1992	1994 - 1996	
c. Development of Poster	Not scheduled	1995	
d. Production of full set of student texts	Not scheduled - only planned to reach page proof stage: June 1993	1994 - 1996	
c. Development and production of teachers editions	Not scheduled	1995 - 1996	

The planning meeting provided a unique forum for National school system educators, scientists, and educational experts. Delegates were encouraged to disclose particular features of their educational systems and cultures, marine and coastal environments, as well as share their perceptions on what sort of curriculum materials would be most appropriate for the targeted student population. These discussions were helpful in order for the project team, established by Hopley (the project Director), to appreciate the diverse range of cultures, student abilities, languages, resources, and school systems that needed to be considered in the design of any set of pan Pacific curriculum materials.

The scientific delegates from James Cook University outlined possible topics for inclusion in the proposed text. Both university educators (the team led by Ritchie consisted of three science

educators with experience in curriculum development and evaluation, and one education media specialist with expertise in teaching ESOL students, all of whom from JCU) and member country representatives reacted to these proposals in such a way that a clearer image of an appropriate final product emerged. By the end of the meeting, delegates were enthusiastic for the project team to initiate a feasibility study for the development of a set of six ecosystem related marine studies texts and supplementary resources for upper secondary schools in the South Pacific.

Pilot Study Phase

In order to facilitate effective trial and production phases for the project it was essential to establish an appropriate infrastructure within the member countries. As well as providing support for the planned in-country trials it was also essential that the project maximised contributions from the member countries to ensure authenticity of material. Without such involvement and an ongoing commitment to the project from the member countries, the curriculum materials would be less likely to be adopted throughout the region. Therefore, a multi-national advisory committee was established. This committee was made up of representatives from each of the member countries and was consulted regularly throughout the project.

While the planning meeting and the advisory committee provided valuable input to assist project team members conceptualise the particular needs to be addressed, the project team conducted a needs assessment of the particular schools in which the trial would be conducted. The team gathered first hand data about resource requirements and preferred features of the proposed curriculum materials so that guidelines could be drawn to advise scientific authors. These guidelines included the following major points:

1. Language levels should be controlled by: minimising length of sentences (i.e., 12 words per sentence), text density (e.g., wide use of illustrations); careful selection of words so that everyday discourse would be chosen ahead of more descriptive but less familiar expressions, and difficult but essential terms should be included in a glossary.
2. While language needed to be controlled, the intellectual integrity of the texts needed to be maintained. This could be achieved by designing a variety of activities (e.g., excursions and laboratory activities, reading projects, and review questions) with different levels of cognitive demand.
3. The materials needed to take account of differences between the unique cultures and environments of individual Pacific countries (e.g., inclusion of authentic illustrations and photographs, identification of culturally significant applications of concepts and the inclusion of traditional names wherever possible).

Three of the most popular topics (i.e., coral reefs, coral islands, sandy shores) were identified for trial during the needs assessment stage. Writing teams were then established (by Hopley in collaboration with Ritchie) to produce prototype texts for trial with reference to the recommended guidelines. Each team consisted of a principal scientific author, an education consultant from the project team, and two local high school teachers. The intention of including the practicing teachers was so that the author could obtain practical feedback and even try out preliminary activities in classroom and field contexts. In the development of *Tropical Shorelines* (as it became known), for example, the teachers provided helpful feedback on the initial

development of the beach excursion activities. Regrettably, only two of the texts (*Pacific Islands* and *Tropical Shorelines*) were printed in time for the trial.

Teachers who were to trial these prototype texts were called together in each of the three trial countries (i.e., Fiji, PNG, Tonga - these were selected because they offered a variety of cultures and contexts) by the in-country coordinators. Team members addressed each group. During these meetings, the teachers were given the opportunity to familiarise themselves with the content of the texts and were advised on the process of providing helpful evaluative data. In turn, trial teachers asked their students to identify difficult words and annotate their texts with suggestions about how the texts could be improved, during the trial.

The in-country trial phase concluded with a follow-up visit to each country by team members who sought teachers' reactions to the materials. As well as summarising these reactions, team members returned to the scientific authors with detailed suggested changes from both students and teachers who had used them in class. In the case of *Tropical Shorelines*, for example, teachers felt that the opening chapters on the beach excursion provided an abrupt introduction without some form of preliminary overview of what might be found at the beach sites. Accordingly, two introductory chapters were added to the text, along with additional text to prevent possible confusion with the organisation of the excursion. This feedback also was helpful in shaping the accompanying Teacher's Guide. Fortunately, teachers in both Fiji and Tonga were able to suggest names of common organisms in their traditional languages. These alternative names became a feature of the final text. As well, two authentic illustrations, commissioned during the final stage of the trial, were included in the final text.

Prototype texts were distributed to members of the advisory committee and scientists in each of the countries. Feedback from these participants was considered by each author during the revision process.

Production Phase

The first step in the production phase was the revision of the prototype texts. Most student comments related to the need to improve the quality of illustrations while the trial teachers were more concerned about the layout. The prototype texts were printed in draft form and the final production was planned to provide better illustrations by virtue of the higher resolution selected and better quality paper. Many of the illustrations were enlarged and those which did not appeal to students were deleted or replaced. Nevertheless, it was decided that a relevant colour photograph, to capture the essence of the topic, should be featured on the cover of each text to enhance the appeal of the texts. Such a photograph might also provide a possible referent for class discussion. As well, a colour interactive poster was designed to further enhance the quality of illustrations. The poster featured vivid colour photographs relating to the first three planned texts (*Pacific Islands*, *Tropical Shorelines*, *Corals*). The poster focused on the evolution of oceanic islands, from volcanoes to atolls. Challenging questions were designed for each set of photographs to initiate class discussion on the topic as well as to supplement text material. The layout of the texts was improved considerably by uniformly adopting two columns for text, boxes for activities and projects, and different levels of shading to distinguish between boxed text.

Confusing words, as identified by trial participants, were either replaced or highlighted and added to the glossary. For example, in *Tropical Shorelines*, the word "staff" was replaced by "measuring rod" in the beach profile activities. The authors made every attempt to modify the texts in accordance with the suggestions made by the trial participants. From a scientific perspective, *Tropical Shorelines* was clearly about shorelines in the tropics rather than the sandy shores (the original title) that could be found in temperate regions. For this reason the text was renamed. Similarly, because the *Coral Islands* text described continental islands as well as coral cays and motus found in the Pacific, it was renamed *Pacific Islands*. The in-country coordinators also suggested that the prototype texts would fit the current syllabuses better if there was a focus on ecological interactions. In *Tropical Shorelines*, Chapters 7 and 8 (Interactions and associations, and ecology of shorelines, respectively) were included to address this concern.

Generally, all trial participants were pleased with the size of the texts and the relevance of the subject material. They were particularly appreciative of the excursion activities in *Tropical Shorelines*, but indicated the need for teaching suggestions (e.g., recommended time allocations for activities and planning advice). Similarly, while the teachers valued the detailed information within the texts, they felt somewhat insecure about their own limitations in knowledge about marine environments. These concerns suggested the need for the release of teachers' editions of the texts, where such concerns could be addressed, simultaneously with the student editions. So, immediately on completion of the revised texts, a teacher's edition for *Pacific Islands* and *Tropical Shorelines* was prepared. This edition provided advice to teachers about structuring their sequence of lessons in different ways, included additional information, and suggested possible answers to questions. However, even though they were printed, mass circulation of the students' and teachers' editions was delayed until September 1996, so that not only were the teachers fully briefed, but that the impact of a comprehensive set of materials could be maximised.

During the revision of the prototype texts, authors for the remaining texts were identified. In light of the experiences gained from the trial of the prototype texts, these authors were briefed by team members. Initial drafts were prepared and revised several times after editorial comments were made by team members. This phase of the project was the most time consuming and there were several unexpected delays which set the project behind schedule by about three years. Some of these problems are discussed below.

As each new text was produced team members started preparing the teacher's editions. Each teacher's edition includes the text of two student books plus interleaved notes for teachers. The combinations of texts were selected on the basis of perceived scientific relatedness. *Pacific Islands* and *Tropical Shorelines* was the first set. Other combinations were: *Corals and Coral Reefs*, and *Mangroves; Oceanography & Plankton*, and *Fisheries*.

REFLECTIONS

It was difficult for team members and scientific authors to appreciate fully the diversity of cultures and the differential access to school learning resources across the South Pacific nations. Writing the texts in a vacuum, without conducting the needs assessment and trial, would have hastened the project's progress, but delivered a set of irrelevant and unusable texts. The

significant modifications made to the prototype texts were made possible only by the fruitful infrastructure and evaluation processes established for the purposes of the in-country trials. In-country teacher and student feedback provided compelling evidence for the authors to modify their texts; to write to a lay audience with different cultural orientations. Authentic illustrations, stories, and traditional names of flora and fauna are now striking features of this series.

Writing the texts for upper secondary Pacific students was a real challenge for the scientific authors. Describing the complexities of the scientific concepts without indulging in the overuse of technical genres was a time consuming enterprise. At times, the authors were forced to compromise their usually precise specialist discourse so that non-specialists could make sense of the text. Some authors did not appreciate the time needed for the necessary intellectual reorientation (to write for such a different audience) and the several redrafts required.

The original plan was for senior marine scientists to be the chief authors. However, with a couple of exceptions, these were the people who were least able to make the deadlines. In some cases, authorships had to be reallocated to more junior scientists. While this partially addressed the worrying problem of operating well after the planned project closure, it created other problems. In particular, changing authors during the preparation of the texts (there were three different sets of authors in *Corals*) meant more work for the educational team members (i.e., each author had to be briefed), stylistic anomalies, and some discussion was needed between authors as to the scientific integrity of some sections (i.e., some authors were more prepared to compromise scientific precision than others). In hindsight, a single scientific author (or team) who was able to relinquish all other teaching and research for the duration of the project, might have solved many of these problems. However, this plan would have added substantially to the project's budget. It also would have moved the project away from what we believe is one of its greatest assets: that the scientific input however modified for the target audience, is from marine scientists who are at the leading edge of their respective disciplines. An alternative approach worthy of consideration is that all of the initial authors could have been asked to write just a chapter or two for trial. In this way, authors would have committed themselves earlier in the project and any reallocations could have been made then. However, such a plan still does not take into consideration unforeseen career moves, or personal changes in priorities. As well, the reason why the team was reluctant to adopt such an approach in the planning stage was that a multi-topic text would present a different and perhaps even more complex set of problems for teachers and students involved in the trial. At the time, any plan which might have risked the implementation of the trial and the quality of feedback returned was not given serious consideration.

CONCLUSIONS

The set of texts, teacher's guides and poster provide a range of resources for Pacific teachers to integrate into existing upper secondary curricula. Teachers are now able to use these resources to select an appropriate habitat for detailed study or simply to use the materials to illustrate scientific phenomena in a range of habitats. These resources not only provide relevant learning experiences related to several typical Pacific habitats (i.e, coral reefs, islands, shorelines, mangroves) featured by the series, but also engage learners in important environmental debates likely to impact on their future lives (i.e., fisheries exploitation, global climate change).

Apart from supplementing existing curricula, these resources have the potential to form the basis of the development of an exciting new upper secondary subject for study (i.e., marine studies). Such a program would not only be personally meaningful for many Pacific students, but also lead to a wide range of career options, for example, in resource management and fisheries. Given that each text has listed the main learning objectives and included a range of review questions, it is realistic to expect in-country curriculum developers to prepare new syllabuses without excessive additional support. Upon release of this series to Pacific nations, the demand for additional teacher support in the form of inservice training in marine studies can be expected.

During the needs assessment and trial stages of the project, team members became aware of the demand for similar materials at the lower secondary and even primary level of schooling. From our experience, it would be unwise for university-based scientists to be invited to prepare materials for such an audience. Instead, we would recommend that Pacific educators be supported to rewrite and modify these texts by external consultants, but that the actual writing be conducted within the countries by local experts.

Most Pacific Island nations have declared their 200 nautical mile EEZ, giving them responsibilities for an area of ocean, at least an order of magnitude, greater than their land. However, these enormous marine and coastal resources have always been part of their heritage and tradition. Ultimately it is the hope of the project team that the series we have produced will help the school students of the region to appreciate and understand their oceans and that this in turn in the future will result in their resources being utilised in a sustainable way.

REFERENCES

- Broadfoot, J. (1991). Science teaching in Tonga. *The Queensland Science Teacher*, **17(3)**, 23-26.
- Fraser, B.J., and Cohen, D. (1989). A retrospective account of the development and evaluation process of a science curriculum project. *Science Education*, **73(1)**, 25-44.
- South, G.R. (1991). *Education in the Pacific islands, including a review of opportunities and constraints for education and training in marine studies*. Technical Report No. 4, Marine Studies Programme. Suva: The University of the South Pacific.

POST 1995 CHALLENGES TO MARITIME EDUCATION AND TRAINING ESTABLISHMENTS

Rod Haigh
Australian Maritime College
Launceston, Australia

ABSTRACT

Forthcoming changes to the regulatory environment i.e. the 1995 amendments to the International Convention on the Standards for Training and Certification of Watchkeepers (STCW) 1978, with reference to the training of seafarers will mean that training establishments and governments will have to be more rigorous with the establishment, delivery and assessment of training programmes leading to the award of Certificates of Competency for the personnel intending to pursue a career at sea. The challenge to training establishments is to deliver training courses which are recognised by government and the international maritime community, which are relevant to ship owners and students, and which are delivered in a way which reflects the strengths of the various learning environments which are currently available. This paper details those changes and what they will mean for establishments engaged in the training of mariners.

INTRODUCTION

Changes in standards in the maritime industry are generally driven by disaster. In the mid 19th century catastrophic losses of British ships and seafarers caused the introduction of Government-controlled testing and certification of seafarers. A derivative of this system is still used today, and Governments issue a "Certificate of Competency" to seafarers who are deemed to be competent to act in some capacity on board ship.

The loss of the *Titanic* in 1912, where the 'unsinkable' vessel had insufficient lifeboats to accommodate all her passengers, caused the introduction, in 1914, of the first version of the internationally accepted Safety of Life at Sea (SOLAS) Convention.

A whole spate of radar assisted collisions in the early 1950's when radar became a common navigational instrument in ships, notably the *Andrea Doria-Stockholm* collision off Nantucket lightship in 1956, on the approach to New York (Hoffer, W. 1979), was the catalyst for the introduction of the first internationally accepted training requirement for seafarers. Proficiency in the use and interpretation of radar information was made mandatory for keepers of a navigational watch in the late 1950's.

The grounding and subsequent loss of the 120,000 tonne *Torrey Canyon* (Republic of Liberia, 1967), spilling all her crude-oil cargo, in the English channel in 1967, which caused massive oil

pollution on both the French and English coastlines and damaged fisheries, alerted public opinion world wide to the environmental dangers which the new supertankers posed. This accident and others, which had lower public profile, led to the introduction of the International Convention on Marine Pollution (MARPOL) in 1973 and the international requirement that seafarers employed on oil tankers be specially trained for the work required of them.

It was around this period that the problems associated with the continuing trends to use Flags of Convenience (FOC's) and to reduce crew sizes were coming to light. Ship owners, looking to reduce the running costs of their ships, were employing low cost crews from emerging nations, and at the same time reducing the size of these crews. There were still no international standards for the training of mariners, and the nations from which seafarers were now being drawn and where the majority of the world's fleet was registered, had no maritime background and had little or no infrastructure to support their maritime activities.

Traditional and progressive maritime nations had accepted the responsibility for ensuring the competence of their own seafarers, through their respective Governments and national Maritime Administrations. However many of the emerging maritime countries did not have the expertise to do this and relied on "overseas" standards.

The international maritime community was represented by the International Maritime Consultative Organisation (IMCO), later to become the International Maritime Organisation (IMO). IMO was charged by the United Nations with the responsibility to formulate internationally acceptable Conventions and recommendations which will provide guide-lines to Governments for the purpose of promoting safety of life at sea, safety of property at sea and protection of the marine environment.

In 1978, IMO, through an IMO conference, adopted the *International Convention on Standards of Training, Certification and Watchkeeping for Seafarers 1978 (STCW 1978)*.

BACKGROUND

The STCW Convention of 1978

This was a first attempt to proclaim an overall training standard. It gave the minimum knowledge requirements for persons who sailed as Master, mate, engineer or rating in a navigational or watchkeeping capacity, on ships over a certain tonnage.

It was promulgated by IMO in 1978 and in 1993, 101 countries, controlling 92.93% of the worlds tonnage (IMO, 1993) have acceded to it and written it into their respective national legislation.

The objectives of this Convention were:-

- 1/ To establish minimum global standards of competence for the various levels of officer and ratings,
- 2/ to achieve a global standard for training and examination of seagoing personnel,
- 3/ to facilitate global recognition and acceptance of the certificates granted under STCW 1978, and
- 4/ to ensure global safe manning of ships.

The Convention listed the minimum standards required in terms of the knowledge required by certificate holders, and also minimum requirements such as age, minimum sea-service for the granting of certificates of competency, and any special training required.

It must be recognised that the standards laid out in STCW '78 were minimum standards only and were the result of compromise during the formative stages. Nonetheless they were an important first step to internationalise training in what is an international industry.

On accession to the Convention it is the responsibility of the member state to implement the regulations by :-

- 1/ ensuring safe manning of ships under its flag.
- 2/ ensuring proper and adequate education and training of seafarers, and
- 3/ arranging for examination and certification of seafarers.

It is in this area that the limitations of STCW '78 lie, as, while it lays down the minimum knowledge base for certification at the various levels, it does not specify how to ensure that the minimum knowledge has been assimilated by an individual seafarer, nor does it specify the mechanism by which each member state will discharge its responsibilities as outlined above. The Convention simply requires that each will be implemented "*to the satisfaction of the flag state administration*".

It is therefore open to interpretation by each member state how it will achieve this, and so over the 18 years during which STCW '78 has been in operation, many differing standards and systems for maintaining such standards have evolved.

Further Developments

During those 18 years there have been continuing maritime disasters which have been publicised world wide, amongst them being :-

Vessel	Place	Date	Casualty	Reference
<i>Amoco Cadiz</i>	Europe	1978	220,000 tonnes crude oil spilled	Chelminski, 1987
<i>Herald of Free Enterprise</i>	Europe	1987	188 lives lost	Dept of Transport, UK. 1987
<i>Exxon Valdez</i>	USA	1989	36,000 tonnes crude oil spilled	National Transportation Safety Board, USA. 1990
<i>Mega Borg</i>	USA	1990	13,000 tonnes oil spilled	IMO, 1995
<i>Braer</i>	Europe	1993	84,700 tonnes crude oil spilled	Dept of Transport, UK. 1993
<i>Estonia</i>	Europe	1994	900+ lives lost	Lloyds, 1994

All of the above have contributed to change in the maritime regulatory environment, these changes are still being implemented, such as special training for employment on board a Ro-Ro passenger vessel and more stringent anti-pollution regulations.

In addition to the above there have been an increasing number of maritime accidents which have gone unnoticed to the general public

In the USA alone during the period 1983-1993 there have been about 2600 fatalities in maritime operations, about half of which were related to vessel casualties (e.g. sinkings or collisions) and half due to operational hazards (mainly falls, either overboard or on-board). During the same time there were approximately 160,000 tonnes of oil spilled from maritime sources (IMO, 1995).

It has been estimated that 80% of all accidents are caused by human error, some experts say that the percentage is even higher and so the training which seafarers receive has come under criticism again.

There have been three developments over the past few years which impinge upon the competence of ships' personnel :-

- 1/ The Paris Memorandum of Understanding on Port State Control (1982), leading to IMO Resolutions on Ship Safety and Pollution Prevention and Ship Management and Port State Control (1991),
- 2/ the IMO International Safety Management (ISM) Code (1993) and,
- 3/ the 1995 revision of STCW 1978

Port State Control

The ship's flag state is legally responsible for the ship's compliance with international standards, however it is possible that a ship may never visit her country of registry, and if a vessel is in a dangerous condition, it is the ports, coastlines and populations of the country visited which are at risk. Port State Control is a mechanism whereby the administration in the Port State can inspect a visiting ship for compliance with certain required standards related to safety, and may detain such ships which do not comply until all deficiencies have been rectified.

ISM Code

This is an integrated code of quality management practices which outlines the responsibilities of both shipboard and shore personnel in ensuring that the ship operates efficiently and safely. It attempts to provide all ship operators with guide-lines for efficient hazard management on board and ashore. The requirements of this convention must be implemented on all vessels before 2001.

The 1995 Amendment to STCW 1978

The new amendment, which comes into force on 1st February 1997, has been developed because the provisions of the existing Convention have been open to interpretation and have failed to establish a minimum level of competence to an acceptable international standard.

In addition, due to a multitude of accidents and incidents, there has been a world wide loss of confidence in the reliability of the STCW certificates of competency as an indicator of seafarers' abilities. (International Shipping Federation, 1995) Critics of the 1978 Convention have also argued that there was little emphasis on ensuring that mariners were competent to actually perform the tasks/functions in which they were certificated as 'competent'.

The 1995 amendment attempts to remove these weaknesses in the original Convention by incorporating measures to :-

- 1/ ensure implementation by Governments,
- 2/ ensure implementation by ship operators, and
- 3/ ensure a true international standard of competence.

Responsibilities of Governments

The principal responsibilities of each acceding government is to ensure that all training, assessment of competence and certification carried out by non Government agencies under its authority are continuously monitored through a quality standards system to ensure the achievement of defined objectives. This monitoring is to include the qualifications and experience of instructors/assessors and:-

- 1/ where Government agencies perform such activities there shall be a quality standard system in place, and
- 2/ provide to the Secretary-General all information as is required to confirm that the Convention has been given full and complete effect.

Responsibilities of Ship Operators

Operators are required to:-

- 1/ ensure that the seafarers they employ meet minimum standards for the function in which they are employed,
- 2/ crew their ships in accordance with flag state requirements,
- 3/ maintain detailed records of all personnel employed, and
- 4/ ensure that seafarers assigned to their ships undergo familiarisation training

Uniform Standards of Competence

The revision of the Convention contains specific criteria detailing the standards of knowledge and proficiency to be achieved by candidates for certification and the criteria for evaluating them. The Convention now states not only the competencies which each function requires but also how those competencies may be attained and assessed.

Responsibilities of IMO

IMO is under obligation to:-

- 1/ convene a panel of experts, the Maritime Safety Committee, who will assess each member state's submission as outlined above and report on its suitability, and
- 2/ maintain and publish a list (the 'White List') of member states whose training systems comply with the requirements.

The revised Convention also contains many other provisions including the use of simulators in training, measures to prevent fatigued personnel from being at work and continued in-service training. Together the above inter-related measures are designed to overcome the inadequacies of the current Convention and ensure that the factors determining competence will be regulated internationally.

IMPACTS ON MARITIME EDUCATION AND TRAINING INSTITUTIONS

The major impacts on training establishments will be felt in 4 areas, namely:

- 1/ the curriculum
- 2/ the delivery of the training
- 3/ the assessment of trainees, and
- 4/ the implementation of a quality system.

The Curriculum

When the Convention comes into force, for a nation to have its certificates of competency recognised internationally, that nation must have the systems outlined in the Convention in place, vetted and approved by IMO and its name on the White List. This means that the three parties to be involved with training i.e. Governments, through their Maritime Safety Administrations, the nation's shipping industry and education establishments must co-operate to implement a workable national system which complies with the Convention. A further consideration is that the qualifications obtained by a successful trainee are such that they will enhance career prospects and fit in with the aspirations of the trainee. This curriculum must therefore contain a common core curriculum which would embrace all the competency requirements of the Convention.

The Convention, however, is purely concerned with the safe and efficient operation of the ship and such a core would not include other competencies which are highly desirable for the successful commercial operation of the ship. Subject areas such as budgeting, computing, industrial relations etc. are required of a ship's officer in the day to day running of the ship and, in addition, it is almost certain that, there would be some requirements which could be labelled as being strictly national in tenor. These additional subject areas would, with the core, embrace a national curriculum which would be suitable for officers who are to sail under that state's flag, but which may be quite unsuitable for a person who is studying and wishes to sail under a foreign flag. Such a person would certainly require the core and may need the desirable subjects but the subjects with a national flavour would be quite unsuitable.

The curriculum therefore should be separated into the following areas:-

- 1/ core (STCW requirements),
- 2/ desirable (non-safety oriented subject matter), and
- 3/ national requirements.

There is also a fourth category which may be added. A specific ship operator (or group of operators) may require special training to reflect their company's special operational requirements or indeed their commercial ethos. Such requirements may be labelled:-

- 4/ industry requirements

Such a division of study areas for candidates gives great flexibility and would allow them to study the minimum which is required for certification and choose any other career enhancing subjects as extras.

The Delivery

The delivery of the appropriate training to attain the objectives is one of the greater challenges which all parties involved have to meet. A candidate for a certificate of competency under the

new Convention will have undergone a training package, part of which will have taken place on board ship, part in the classroom ashore and part in a simulated environment using ship operations simulator(s). This is the challenge to the maritime educators, to design a cost effective and efficient training scheme.

There is no doubt that, for some needs, on board training is much more meaningful than any other type of training and this is recognised in the Convention.

Industrial experience, commonly known as sea time, is one of the basic requirements of certification, for example someone wishing to obtain a basic watchkeeper's certificate will need to obtain 3 years of sea time unless the candidate has undergone an approved training programme which **includes on-board training**, in which case the sea time requirement may be reduced.

This is a fast track for training which most shipping companies would like to take advantage of. However the new Convention also states that :-

Any person on board or ashore conducting in-service training intended to be used in qualifying for certification under the Convention shall:

- .1 have an appreciation of the training programme and an understanding of the specific training objectives for the particular type of training being conducted, and*
- .2 be qualified for the task for which the training is being conducted (STCW, 1995b)*

Any person on board or ashore conducting in-service assessment intended to be used in qualifying for certification under the Convention shall:

- .1 have an appropriate level of knowledge and understanding of the competence to be assessed and,*
- .2 be qualified for the task for which the training is being conducted*

This begs the questions:

- 1/ under reduced manning regimes where manpower is at a minimum who has the time to be involved in training? and
- 2/ should the time be found, does the trainer have the necessary skills in training or assessment to be competent?

This is a new challenge for ship operators and solutions must be found in order to develop an acceptable, comprehensive, and cost effective package of training.

One solution is to have a dedicated training ship in which all trainees undergo their in-service training. Many nations have such a vessel or vessels. The disadvantage of the training vessel (other than its cost and who bears it) is that, while being excellent for initial training in order to

gain initial qualifications, any further training for higher certificates is, in general, not possible. A variant of this is to use a commercial vessel as a 'training ship' and rotate new entrant trainees through it, using trained educators to deliver the training. This approach has been (and still is) used in many instances, however it has most of the same disadvantages as the dedicated training vessel.

For the training of personnel requiring higher certificates a possible solution for the training is to train ship's personnel as trainers and assessors. This approach is being used currently in Europe where the Maersk Line of the Isle of Man selected 6 Masters and 6 Chief Engineers for training as assessors and used the newly developed Merchant Navy Training Board (MNTB) Development of Certificated Officer Scheme (DOCS) as a pilot training scheme.

This scheme contains the study material and procedures for competency-based qualifications, with the objective of improving on board performance, job satisfaction and career potential.(Cowley, 1996)

A more innovative solution which makes use of modern communication techniques is for training establishments to develop distance education packages for seafarers and use satellite communications to exchange information between the ship and the college. The disadvantage of this is the high cost of exchanging lengthy messages which more traditional distance education methods may require. However a new generation of interactive, PC based situation simulators almost certainly will overcome these disadvantages and be part of the answer to in-service training problems. Such simulators can offer meaningful training scenarios and in addition can record and assess both the scenario and the trainee's responses. An assessor therefore need not be *in situ* when a trainee is undergoing either training or assessment, but may review the trainees' efforts at a more convenient time. It is conceivable that the data files from such a training session may be compressed and transmitted to a shore based training establishment for appraisal. Communication media such as the INTERNET may also be used to give almost real-time interaction between a sea-going trainee and a shore based trainer.

The Convention recognises the value of such simulations for training and advocates their use where possible under prescribed performance standards (STCW, 1995a).

On board training is also mandatory in as far as familiarisation for new crew members which is a new development. It is not yet clear how this will be done however the constraints on the trainers, as outlined above, still apply.

It is a possibility that videos, interactive CD's etc. can be developed for the general requirements of ship familiarisation. However there will be in every case, ship-specific items which need the personal touch.

Whichever regime is adopted there is no doubt that a range of on-board training, properly conducted and assessed, will benefit the industry as a whole, by producing better trained

personnel more quickly. A competency trained and assessed crew member will be ready for the function or rank being assessed for immediately on passing, which is certainly not the case today.

In conclusion, delivery systems are not yet clear and require development, however it is clear that some degree of innovation must be displayed to achieve the required aims.

Assessment

Each candidate for certification must provide evidence of having achieved the required standards of competence, demonstrating an ability to perform tasks and duties and to assume responsibilities.

The Convention lays down levels of knowledge, understanding and proficiency along with methods for demonstrating competence and the criteria for evaluating it.

As an example, the STCW 1978 states:-

Knowledge of automatic pilot systems and procedures

The 1995 amendment states:-

Competence

Plan and conduct a passage...

Knowledge, Understanding and proficiency

Steering control systems

Knowledge of steering control systems, operational procedures and change over from manual to automatic and vice-versa. Adjustment of controls for optimum performance

Methods for demonstrating competence

Examination and assessment of evidence obtained from one or more of the following:

- 1. Approved in-service experience.*
- 2. Approved training ship experience.*
- 3. Approved simulator training where appropriate.*
- 4. Approved laboratory equipment training.*

Criteria for demonstrating competence

The selection of the mode of steering is the most suitable for the prevailing weather, sea and traffic conditions and intended manoeuvres.

This is one of the major revisions in the Convention. The candidate must actually demonstrate the ability to perform the task/function safely and efficiently and meet the performance criteria relevant to each function required to be performed. Such assessment is extremely time consuming, as trainees have different learning abilities. It also demands that the assessor rigorously pursues the task, as there must be a quality assurance system in place in which the assessor is as much under the microscope as the assessed. This makes it vital that any assessment is performed by qualified persons. The assessment of trainees is one of the major variables in the

debate on the optimum mode of delivery of the training, as the resources, both human and hardware, for assessment must be found.

Quality Assurance

As stated above the 1995 amendment states an acceding Government must put “...*quality standards system in place to ensure achievement of defined objectives...*”

This quality standards system will cover:-

- 1/ The administration of the certification system, i.e. the Government agency which issues certificates
- 2/ The training course itself which requires that the provider of the training has a quality standards system in place

Such systems would assess the standards of:-

- 1/ delivery of courses,
- 2/ examinations,
- 3/ assessments, and
- 4/ qualifications and experience of instructors and assessors.

This system is to be independently audited at periods not exceeding 5 years, and the findings communicated to IMO.

The independent audit is required to verify that:-

- 1/ all internal management control and monitoring measures and follow-up actions comply with planned arrangements and documented procedures and are effective in ensuring achievement of defined objectives,*
- 2/ the results of each independent evaluation are documented and brought to the attention of those responsible for the area evaluated, and*
- 3/ timely action is taken to correct deficiencies.*

The report of the independent evaluation required.....shall include the terms of reference for the evaluation and the qualifications and experience of the evaluators.

It is thought that the maintenance and publication of a list of countries by IMO which is conducting their training and issuing their certificates according to the requirements of the new amendments to the Convention will provide assurance to other administrations of the quality of another's standards and maybe provide an encouragement to nations who are lax in their implementation of the Convention.

CONCLUSION

The 1995 amendment to STCW 1978 is one of a number of current international initiatives designed to improve the safety and operational standards of maritime activities and remove marginal operators as far as possible from the market place. If it is implemented in the full spirit of its intent then it will mean an enormous change in the format of training, the delivery of courses and the assessment of competence. Ship owners and managers will no longer be able to look upon training as someone else's responsibility. National maritime administrations which wish to issue certificates of competency will have to do more than simply print them. Educational and training institutions will have to change their methods of delivery and administration of training courses in order to give their customers the training which is required. Innovation in course design will be necessary to sell their educational product. It is also desirable that the training package is seen by the trainee, to be a career enhancing programme and not just designed to optimally interface the watchkeeper with the ship system. Educators will also have to work hand in glove with Government, Industry, and other providers to maintain common standards. Regional co-operation groups may be required to assist the smaller nations to conform. Such a group for the Asia-Pacific region was formed in Auckland (New Zealand) in December 1995, the Association of Maritime Education and Training in the Asia Pacific with (currently) 15 members from 10 nations around the Pacific basin. The revised Convention promises to provide a challenge for all concerned, a challenge which must be addressed. To meet this challenge, and succeed, will along with parallel initiatives, give rise to safer and cleaner seas.

REFERENCES

- Chelminski, R. 1987. Superwreck. Amoco Cadiz: The Shipwreck that had to Happen. New York: W Morrow & Co. N. Y.
- Cowley, J. 1996. Vocational Qualifications and On-Board Assessment. Seaways. April.
- Department of Transport (UK). 1987. Marine Accident Report No. 8074. UK:H.M.S.O.
- Department of Transport (UK). 1993. The *Braer* Incident. Marine Pollution Control Unit. UK:H.M.S.O.
- Hoffer, W. 1979. Saved! London:MacMillan London Limited.
- IMO Document. 1993. FSI 2/3/2 9/11/93.
- IMO Document. 1995. MSC 65.Inf.5.
- International Shipping Federation. 1995. The Revised STCW Convention: A Guide for the Shipping Industry. International Shipping Federation.
- Lloyds List International. 1994. June 10.

National Transportation Safety Board (USA). 1990. Marine Accident Report NTSB/Mar-90/04.

Republic of Liberia. 1967. Report of the Board of Investigation in the matter of the stranding of the s.s. *Torrey Canyon* on 18.3.67. Republic of Liberia Marine Accident Investigation.

STCW 1995 Amendment. 1995. Section A-I/12. International Maritime Organisation.

STCW 1995 Amendment. 1995. Section A-I6. International Maritime Organisation.

BASIC RESEARCH ON BARRIER-FREE COASTAL RECREATIONAL FACILITIES IN JAPAN

Tsuyoshi Kobayashi, Takeo Kondo and Eiichi Matsuura
Nihon University
Chiba, Japan

ABSTRACT

The aging of the population is an issue that is common to all industrialized nations. In recent years, the Japanese population has aged rapidly and by the year 2020, it is reported that Japan will become an ultra-aged society in which one fourth of the population will be aged 65 or above. As a response to this trend of an aging society, various measures in city planning and in the life environment are progressing, but to date, measures for access and the creation of facilities convenient for disabled people have not been adopted relevant to the waterfront.

In this study, questionnaire surveys were conducted to elicit information concerning the interface of the aged and disabled people with waterfronts, current status of achievement of barrier-free coastal recreational facilities by local authorities and on measures towards the creation of such barrier-free facilities and field surveys of beaches and marinas which constitute coastal recreational facilities were conducted. As a result, a comprehensive understanding of the interface between waterfronts and the aged and the disabled as well as the status and future of barrier-free facilities was attained.

INTRODUCTION

The aging of Japanese society is an issue of extreme importance (Welfare Policy Study, 1995; U.S. Architectural and Transportation, 1990). In 1970, the ratio of aged citizens in Japan exceeded 7% and by 1994, had exceeded 14%. In the period of only 24 years, a rapid increase never before seen in any country had occurred. Reportedly, Japan will face an aged society in which 1/4 of all citizens will be aged 65 or older by the year 2020 (Prime Minister's Office, 1994). The issue of the aging of society is being addressed as one of urgency in the fields of welfare and construction, and in 1994, a law concerning the promotion of specialized buildings that afford convenience of use to the aged and disabled people was promulgated (Nishijima and Shimada, 1994).

In the industrialized nations of Europe and America, the aging of society is already a reality and city planning and life environment measures that respond to the circumstances are in progress. In some coastal cities, the ease with which the disabled are able to access waterfronts is positioned as an important factor, and progress is being made in constructing coastal recreational facilities that incorporate the barrier-free concept.

In recent years, greater demand for recreation brought on by the increased availability of leisure time, changing life styles and diversifying values have raised the potential demand for active leisure. The potential demand for waterfront recreation as a means of spending free time is increasing also among the aged and disabled (Recreational Development Center, Inc., 1994). However, the current status is one in which the infrastructure that aged or disabled persons can avail themselves of waterfront recreation has yet to be put in place.

AIM OF STUDY

Barrier-free is a concept that is used in employment, insurance, welfare, education, sports, cultural facilities and in all aspects of the life environment. However there has yet been no case in which the concept was applied to riverbanks and beaches. On the other hand, as with parks, the waterfront is an important venue for relaxation and human exchange for the aged and disabled, while at the same time, is highly important for the mental and spiritual benefits that are involved.

Through questionnaire surveys targeting local authorities and associations of aged people and through field surveys of coastal recreational facilities, this study attempted to achieve an understanding of the current status of the application of the barrier-free concept at beaches and marinas that offer numerous and diverse opportunities for recreation.

METHOD OF STUDY

Questionnaire Survey of Local Authorities

In order to understand the current status of barrier-free access and the intent of local authorities, a mailed questionnaire survey was conducted targeting the Public Works Divisions (Department of Rivers, Department of Harbors) of 47 prefectures and districts and 12 cities incorporated under law (cities with a population of 1 million or more). The term of the survey was 2 months, from August to September, 1995. Of the 61 questionnaire mailed, 57 (93.4%) were returned completed.

Questionnaire Survey of Associations of Aged and Disabled Persons

In order to understand the views, evaluation and trends of the aged and disabled people relative to the waterfront, a questionnaire survey was conducted among disabled people and aged living in areas proximate to waterfronts and in inland areas of Kanagawa Prefecture using a combination of the mailing and drop-off method. The term of the survey was 2 months, from August to September 1995. The response rate for aged people was 190 mailed or dropped off with 190 responding (100%) while for the disabled people, 450 were mailed or dropped off with 197 (43.8%) responding. The areas targeted for the survey are as shown in Figure 1.

Field Study of Coastal Recreational Facilities

A total of 51 frequently visited beaches and 29 Marinas in the Kanto Area were targeted for the study and the barrier-free level of these facilities was ascertained. The areas targeted for this study are as shown in Figure 1.

In this study, access to the seaside or waterfront and the convenience of facilities were viewed from the perspective of disabled people (with locomotion difficulties) and the existence of steps and slopes, the height and depth of steps, the height of handrails and the grading of slopes were studied to ascertain the level to which the forms of access and the facilities give consideration to the aged or the disabled people through comparison of the actual data with average values (hereinafter "Standard Values") established by local authority ordinance or guidance.

RESULTS AND CONSIDERATION

Questionnaire Survey Targeting Local Authorities

On the existence or otherwise of a barrier-free manual

The existence or otherwise of a barrier-free manual (such as guidelines for city planning based on welfare consideration, guidelines for improvement, etc.) is shown in Figure 2. Of the responding local authorities, 38 (66%) responded that a barrier-free manual did exist and if those local authorities currently reviewing and in the process of producing such a manual are included, this figure increases to 70% of the total. More local authorities are beginning to produce barrier-free manuals yearly and reviews of standards applicable to facilities have begun.

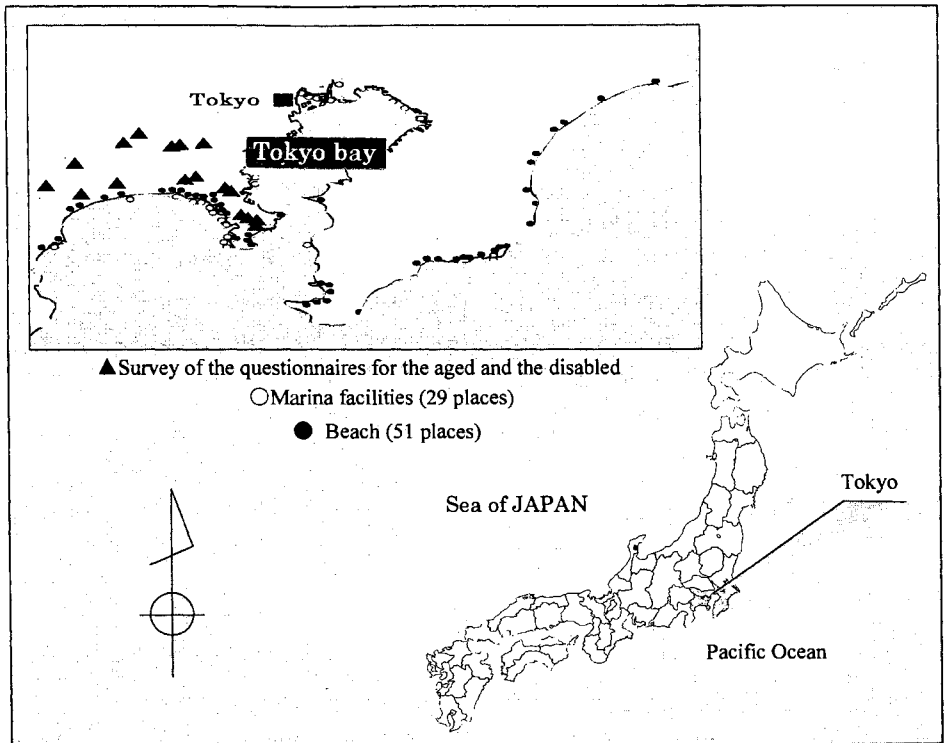


Figure 1. The sites of a field survey

Status of waterfront public facilities and future actions

Responses to the question "Are current waterfront public facilities appropriate for use by aged and disabled people?" are as shown in Figure 3. The number of local authorities responding "The facilities are sufficiently appropriate" was 0 (0%) while 2 (4%) responded that "The facilities are appropriate" and the fact of the insufficiency of the current status is clear. However, a significant

number or 38 (70.2%) of local authorities responded that "Though insufficient, some facilities are appropriate".

To the question "In the face of the coming aging of society, what steps are contemplated relevant to waterfront public facilities appropriate for use by aged and disabled people?", the responses of local authorities as evaluated (Figure 3) show that 44 (80.7%) intend to take action, and when those "Intend to take action in certain areas" are included, 90% of local authorities have the intention of improving waterfront public facilities giving consideration to use by aged and disabled people.

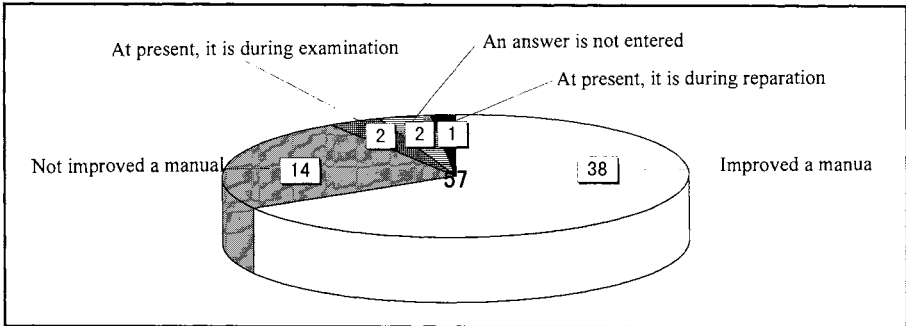


Figure 2. As for who or has not barrier-free manuals

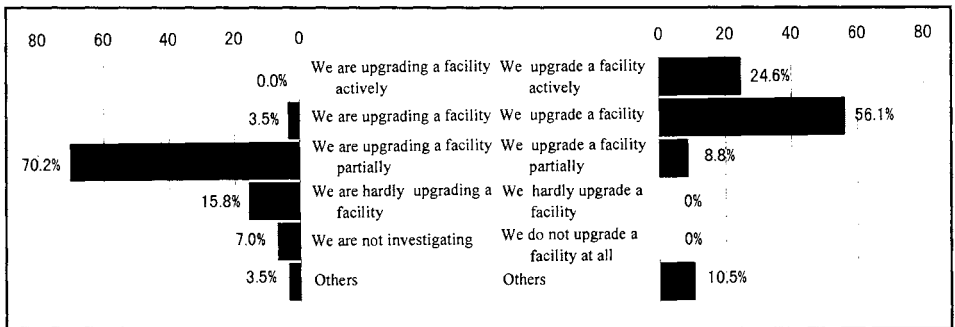


Figure 3. Trend for waterfront facilities

Questionnaire survey of associations of aged and disabled persons

On frequency of visits to the waterfront

The frequency of visits to the waterfront by aged and disabled people is shown in Figure 4. In the case of both the aged and disabled, those responding "Once a week" accounted for 25% or 1/4 of the total. Those answering "Never" comprised 15% of the aged and 8% of the disabled people. The fact that visits to the waterfront by the aged are less frequent than by disabled people points to the fact that disabled people are more motivated towards an active life.

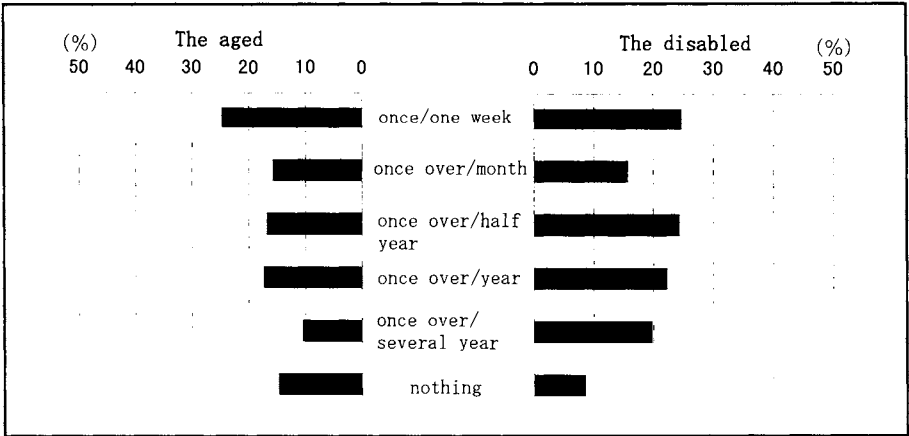


Figure 4. Frequency of visits to the seaside

Comparison of visits by those living proximate to the waterfront and those living inland

The comparison of visits by those who live proximate to the waterfront and those living inland is as shown in Figure 5. Among those aged people living proximate to the waterfront, 47% responded "Once or more a week" while among those living inland, only 2% responded in this way. Only 7% of those living proximate to the waterfront responded "Never", while 24% of those living inland responded in this way, thus testifying to the fact that the propensity to visit the waterfront is higher among those living near the waterfront. Among those disabled people living

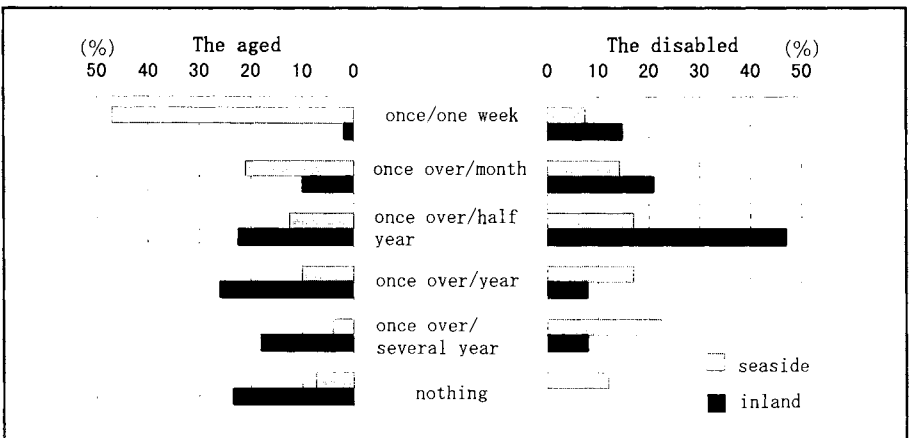


Figure 5. Comparison of visits by those living proximate to the waterfront and those living inland

inland, 15% answered "Once or more a week", a level that is about double the number of those living proximate to the waterfront who responded in this manner. Similarly, those responding "Once or more a month" and "Once or more every 6 months" were greater in number among the inland group and it was seen that overall, those disabled people living inland are more apt to visit than those living proximate to the waterfront. Among aged people, those living near the waterfront are more apt to visit due to distance and accessibility considerations while among disabled people, those living inland visit the waterfront more frequently than those living close.

Field Study of Coastal Recreational Facilities

Study of slopes and steps at beaches

The existence of slopes is as shown in Figure 6. In Kanagawa Prefecture and Chiba Prefecture, about 60% of beaches have slopes. However, slopes that have grades that are within the Standard Value for convenient use by the aged and disabled people account for only 20% of beaches in Kanagawa Prefecture and 10% in Chiba Prefecture. On the other hand, though both prefectures meet the Standard Value for width (135 centimeters or more), this is thought to be because entry of vehicles for supplying ships and stores on the beach was taken into consideration.

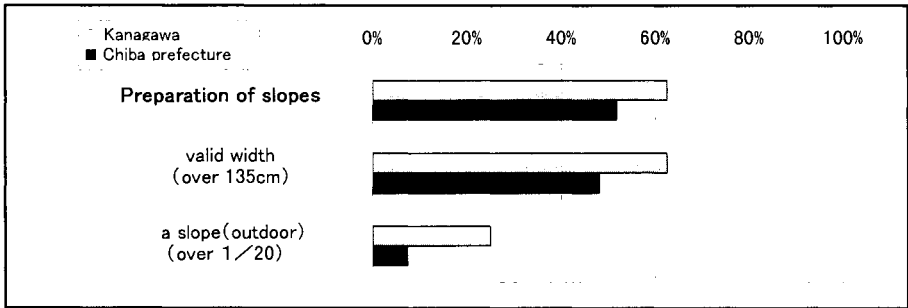


Figure 6. The present condition of slopes

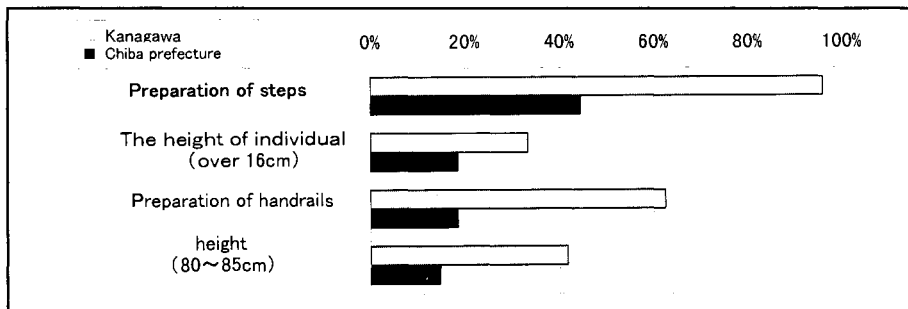


Figure 7. The present condition of steps

The existence of steps is as shown in Figure 7. In Kanagawa Prefecture, the incidence of steps is high at 90% while in Chiba Prefecture, the level is lower at 40%. As for whether or not steps are equipped with handrails, in Kanagawa Prefecture 65% have handrails while in Chiba Prefecture, the number is 43%. In regards to the height of the handrails are appropriate, 67% of handrails in Kanagawa Prefecture are appropriate while in Chiba Prefecture 79% are appropriate. Only about one third of the steps found in both prefectures were found to be appropriate for use by the aged or disabled people.

Study of piers at marinas

The condition of piers at marinas is as shown in Figure 8. Whereas 93.1 % of piers can be accessed by ordinary people, only 10.3% are accessible in a wheelchair. Also, only 13.8% of piers have slopes to eliminate sudden changes of grade and in only 1 case (3.5%) was such a slope the result of having consciously given consideration to access by disabled people. Such facilities as stoppers to prevent wheelchairs from falling off piers, lighting, fencing or poles were only found in very few cases.

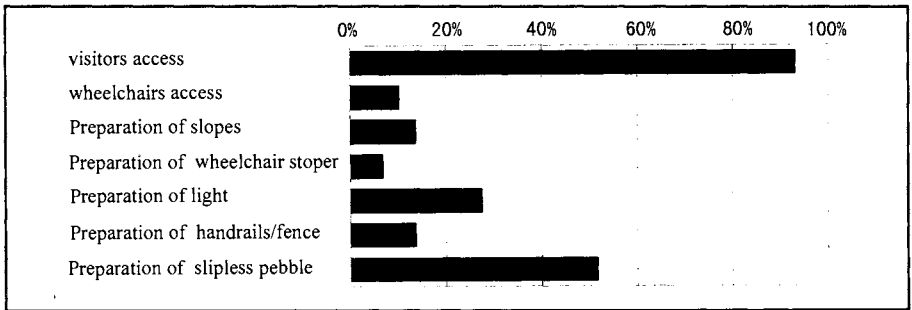


Figure 8. Possibility of accessibility to piers

CONCLUSION

Through this study, a comprehensive understanding of the status of the application of the barrier-free concept to waterfront public facilities which have various possibilities as the venue for coastal recreational activities was obtained through questionnaire surveys of associations for the aged and disabled people and local authorities, as well as through field study of coastal recreational facilities.

As a result, it was found that local government recognizes the importance of achieving a barrier-free waterfront environment and that there is a move to see the waterfront not only from the point of view of protection of the coastline but as part of the life environment and to take active measures towards making the waterfront more accessible as a response to the aging of society. The frequency of visits to the waterfront by the aged and disabled people clearly points to the need for greater accessibility and convenience of the facilities at waterfronts. The high incidence of visits by disabled people living inland shows the need to improve transportation facilities from inland areas to the waterfront. The steps and slopes found at beaches do not take into consideration human engineering as relates to the aged and disabled people relevant to their dimensions and the number of convenience facilities is insufficient. Consideration is not sufficiently given to the aged and disabled people in marinas and future improvement is a matter of urgency.

As seen, it has been determined that such coastal recreational facilities as beaches and marinas do not give sufficient consideration to use by the aged and disabled people. However, to such insufficiently improved facilities, 1/4 of all aged and disabled people make visits "Once or more a week" and this fact emphasizes the need for improvement.

Since facilities dedicated for use by disabled people are costly and internalize problems of maintenance, the first step is not the construction of such dedicated facilities but of facilities for use by all people. Further, rather than attempting to improve all marinas and beaches, one facility per given area should be chosen for such improvement so that a balance is achieved and facilities for use become widespread. In making improvements to coastal recreational facilities, each facility should be interconnected and have continuity with clear signs and easy accessibility assured and amenities that can be used by disabled people should be built within reasonable intervals and after the upper shores have been significantly developed, the shore line should be developed so that such disabled people are able to come to the water line safely and comfortably.

Physical safety and security are especially important at beaches and clear traffic signs and visitor guide signs as well as audio signs that can guide those visitors with seeing difficulties should be positioned. Since the intensity of ultra violet rays is strong at beaches, huts, pergolas and trees should be positioned in order to protect people from sunburns that can be caused by strong sunlight. Further, nighttime lighting for aesthetic purposes as well as for ensuring security is called for. In addition to improvements in the infrastructure to afford comfortable use by the aged and the disabled, the formation of a universal society together with the intangible improvements required must be implemented taking in the views of numerous people.

REFERENCES

- Nishijima, E. and S. Shimada. 1994. Survey Research on Barrier-Free Design Manual (2), Kumamoto University of Engineering.
- Prime Minister's Office. 1994. White Paper of Handicaps. Ministry of Finance Printing Bureau.
- Recreation Development Center Incorporated. 1995. White Paper on Leisure '95. Recreation Development Center Incorporated, Buneisha.
- U.S. Architectural and Transportation Barriers Compliance Board. 1990. Americans With Disabilities Act, Accessibility Guidelines for Buildings and Facilities. U.S. Architectural and Transportation Barriers Compliance Board.
- Welfare Policy Study Group, Ministry of Construction. 1995. Building a Welfare Life Environment. Gyosei.

PARTICIPATION OF SEaweEDS IN WATER PURIFICATION AND MARINE BIOTA PROTECTION

O.N. Selivanova

Russian Academy of Sciences
Petropavlovsk-Kamchatsky, RUSSIA

ABSTRACT

Ecological situation in one of the regions of Russian Pacific coasts, the Avacha Bay (Eastern Kamchatka), has been studied by the author for 10 years. The waters of the Bay belong to the class "dirty". A constant tendency of the loss of the species diversity is marked (up to 60% in Rhodophyta, 50% in Phaeophyta and 25 % in Chlorophyta). Sterilizing effect of pollution on reproductive structures of Rhodophyta appears to be the principal cause of their loss. More primitive reproductive processes in green and brown algae probably makes them more resistant to pollution. The pollution influence on vegetative structures of macrophytes (e.g. teratogenous effects, cellular anomalies etc.) is not obvious probably due to their high ability to repara damage.

Some algae (e.g. Laminariales) withstand high concentrations of pollutants playing an active role in the processes of water self-cleaning. But in the process of kelp death toxic substances return to the water again producing a secondary source of pollution. Experimental removal of old decaying fronds helped to improve ecological conditions in a small enclosed inlet within the Bay and prevented marine organisms from suffocation. So this method may serve as one of immediate protective measures against biota's decrease in the Bay.

INTRODUCTION

Anthropogenic pressure on the waters of the Pacific Ocean including northern parts of the Far Eastern seas of Russia has dramatically increased in the latest decades of this century. Ecological conditions in one of these regions, the Avacha Bay (Eastern Kamchatka), have been studied for more than 10 years.

The Avacha Bay is considered to be the largest (S = 215 square kilometers, coast line 110 kilometers long) and one of the most beautiful harbours of the Pacific coasts of Russia (Fig. 1). It was formed in the Pleistocene and its geologic history is connected with volcanic and tectonic processes of

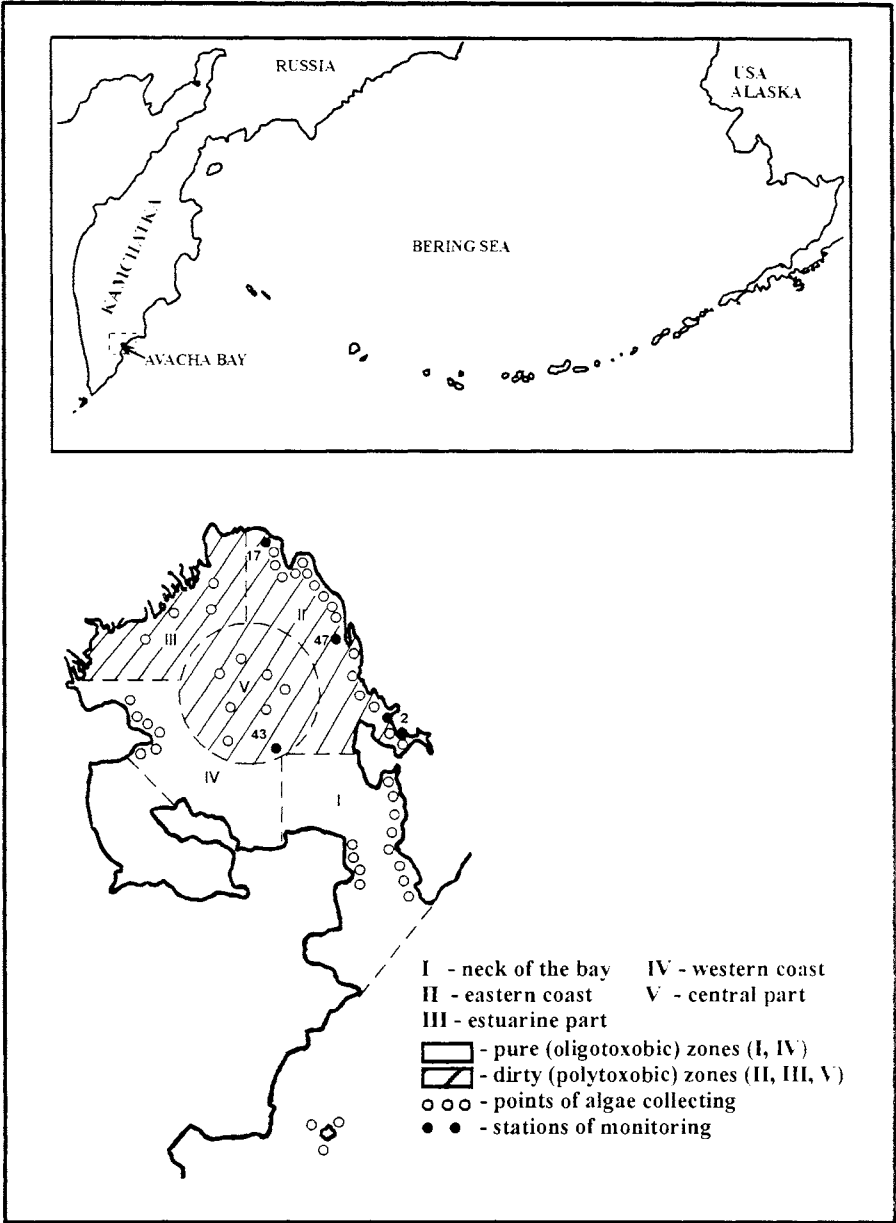


Figure 1. Ecological map of the Avacha Bay. Inset shows the position of the studied area on the Pacific coast of Kamchatka

development of the Eastern Kamchatka relief. Submarine extrusive dome is located in the northern part of the Avacha Bay. Underwater terraces of ring shapes are supposed to be formed as a result of tectonic sinking of the bottom caused by formation of tectonic depression in the paleovolcanic center (Dmitriev and Yezhov, 1977).

The coast line of the Bay is very winding, forming many small inlets. It is very convenient for navigation. This basin has a unique combination of the peculiarities of a fiord and a lagoon with a great variety of substrata, salinity, temperature and oxygen regimes in its different parts, providing diversity of ecotops and thus favourable conditions for development of rich marine biota, including benthic algae.

Macrophytes play the leading role in marine coastal biosystem. Owing to stenotopic character and high sensitivity of some algae species to the environmental conditions they can be used for ecological control, as test-objects in the studies of pollution processes in soil and water, especially caused by oil-products and heavy metals (Shtina, 1985; Khristoforova, 1989).

At the same time algae are active agents in the processes of water self-cleaning. Some species can withstand high degree of pollution not losing photosynthetic ability. They saturate water with oxygen necessary for aerobic organisms and processes of bacterial decay of polluting substances. Such toxicants as oil products, benzene, ethanol, phenol etc. can be taken up by marine algae. Radioactive elements and heavy metals can be accumulated in the fronds of macrophytes and thus inactivated. The role of algae in the processes of purification of the waters of the Black Sea was studied by Kovardakov and co-authors (Kovardakov et al., 1987). They showed that carbon from carbonates can be recycled completely in *Cystoseira's* thallus during 7-16 hours in spring and 5-11 hours in summer. Similar works in the Far Eastern seas of Russia, particularly Pacific coasts of Kamchatka, are rather scanty (Gusarova and Khristoforova, 1979; Selivanova and Shebyakina, 1994; 1995). But it is obvious that the processes of decomposition of organic substances are less intensive in cold waters as compared with warm ones. Even in the Black Sea which is the warmest one in Russia, algae are already unable to fulfil processes of natural water purification and artificial protective measures are necessary. So in our region the problem of water purification seems to become more urgent.

Our long-term observations on marine benthic communities of the Avacha Bay confirm that the ecosystem, having been in the extreme conditions for a long time, cannot tolerate further unfavourable factors, and the process of loss of biodiversity in this basin is reflected in this response. In order to cease inevitable extinction of marine biota, immediate protective measures

should be taken. We proposed sanitary kelp removal in a small inlet within the Bay as one of those measures and it proved to be helpful.

MATERIALS AND METHODS

This work is based on long-term field observations and studies of phycological material collected in the Avacha Bay since 1982 till 1992. Algae were collected in the intertidal zone during low water, from the boat with the help of a long hook (kanza) from the depths of 1-3 meters, using SCUBA technique from the depths of 3-30 meters. Algae cast ashore were also picked up. Collections were made all year round. Algae examination was made using light microscopes of the type 'Ergaval' and 'Olympus'. Material was sectioned freehand with razor blades. Some of the slides were stained with Lugol solution. We have examined above 2000 algae samples.

Water quality in the Avacha Bay was estimated on the basis of chemical analyses carried out by the staff of the Hydrochemical Laboratory (Petropavlovsk-Kamchatsky). Estimation of the ecologic conditions was based on personal field observations on marine benthic vegetation. The state of the biota's components permits to reveal unfavourable ecologic conditions more precisely than pollution itself. Having analysed and compared these data we determined general character, dynamics and peculiarities of main pollutants inflow and distribution in the Avacha Bay and their effect on macrophytes. From numerous analysed water samples we used only those which corresponded to the places of growth of the algae examined.

RESULTS

Main sources of the Avacha Bay's pollution are produced by fishery and ship-repairing enterprises and by sewage waters of Petropavlovsk-Kamchatsky. Being accumulated here for many years they have considerably changed the hydrochemical regime of the Bay.

During our investigations seasonal and annual dynamics of the Avacha Bay's ecologic conditions were observed. We analysed maximum and mean concentrations of main pollutants: oil-products, phenols and detergents and also annual and seasonal dynamics of oxygen contents which is considered to be directly dependent on the pollution level. It can be stated for sure that there is a constant oxygen deficiency in the Bay especially in early autumn.

The Avacha Bay waters according to the sea water pollution index belong to the class "dirty". Main polluting agents (oil- products, phenols and

detergents) in the waters of the Bay exceed 400-3900, 15-80, 200-900 mkg per liter accordingly. These toxicants are particularly dangerous in the period of the most active growth and reproduction of the organisms of benthic communities, including macrophytes.

Relative stabilization of the water quality in the Avacha Bay doesn't adequately characterize the real ecological conditions. The processes of decomposition of chemical substances are low and most toxicants are retained at the bottom. The data of drilling show that sediment layers in some parts of the Bay reach 7 m. These layers are unexposed to wave current and sedimented toxicants produce secondary pollution source and reduce dissolved oxygen contents. Zones with oxygen deficiency are obviously increasing and spreading in most shallow water regions which are natural ecotops for marine vegetation.

But despite such unfavourable ecological situation in the basin as a whole, there are some relatively undamaged ecotops here (which we called oligotoxobic zones in contrast to the most dirty ones which were called polytoxobic) due to the unique geomorphological and hydrological conditions in the Bay. Marine benthic flora of the Avacha Bay is still relatively rich and diverse. We have found more than 100 species, three of them being new for the Bay: *Percursaria percursa* (Ag.) Bory, *Beringia castanea* Perest., *Scagelia pylaisaei* (Mont.) Wynne and six new for the Pacific coasts of Kamchatka.): *Porphyra gardneri* (Smith et Hollenb.) Hawkes, *P. kurogii* Lindstrom, *P. torta* Krishn., *Neoabbottiella araneosa* (Perest.) Lindstrom, *Palmaria callophyloides* Hawkes et Scagel, *Membranoptera multiramosa* Gardn. Even in the polytoxobic zones of the Bay we found about 50 species of algae (Tabl. 1).

We used the term "toxobic" also to characterize algal resistance to pollution by organic and inorganic substances. It is more correct as compared to the term "saprobic" which is currently accepted in Russian ecologic literature as the latter corresponds only to organic pollutants. Algae resistant to high, middle and low degrees of pollution are called accordingly poly-, meso- and oligotoxobic. As it becomes clear from our data, the majority of Chlorophyta belong to polytoxobic group, Phaeophyta are mainly mesotoxobic and most Rhodophyta represent oligotoxobic group of species. Of course, these ecologic groups are conventional, and representatives of each of them may be met in all divisions of macroalgae.

Table 1. Macrophytes of polytoxobic zones of the Avacha Bay

Algae species names and systematic position	Collection places	Depths, substrata	Frequency of find	Ecologic group
CHLOROPHYTA				
Cladophoraceae				
1. <i>Rhizoclonium implexum</i> (Dillw.) Kuetz.	II	cast ashore	very rare	mesotoxobic
Chlorochytriaceae				
2. <i>Chlorochytrium inclusum</i> Kjellm.	II	5-10m, endophytic	frequent	polytoxobic
Ulotrichaceae				
3. <i>Ulothrix flacca</i> (Dillw.) Thur.	II	0-1m, stones	rare	mesotoxobic
Acrosiphoniaceae				
4. <i>Acrosiphonia arcta</i> (Dillw.) J. Ag	II	0-4 m, sand, stones, silt	very rare	mesotoxobic
5. <i>Spongomorpha duriuscula</i> (Rupr.) Collins	II	3-4 m, sand, stones	rare	mesotoxobic
6. <i>Urospora penicilliformis</i> (Roth) Aresch.	II	0-0.5 m, stones	frequent	polytoxobic
Monostromataceae				
7. <i>Monostroma grevillei</i> (Thur.) Wittr.	II	1-4 m, sand, stones	frequent	polytoxobic
8. <i>Blidingia minima</i> (Naeg. ex Kuetz.) Kylin	II,V	0-27 m, rocks, stones	rare	mesotoxobic
Kornmanniaceae				
9. <i>Kornmannia leptoderma</i> (Tild.) Blid.	II	0-4m, stones	rare	mesotoxobic

Algae species names and systematic position	Collection places	Depths, substrata	Frequency of find	Ecologic group
Ulvaceae				
10. * <i>Percursaria percursa</i> (Ag.) Bory	II	cast ashore	very rare	mesotoxobic
11. <i>Ulva fenestrata</i> P. et R.	II	0-3m, stones	frequent	polytoxobic
12. <i>Ulvaria splendens</i> Rupr.	II	1.5-4 m, stones	frequent	polytoxobic
13. <i>Enteromorpha flexuosa</i> (Wulf. ex Roth) J.Ag.	II	0-1 m, stones	frequent	polytoxobic
14. <i>E. linza</i> (L.) J. Ag.	II	0-4m, stones epiphytic	frequent	polytoxobic
15. <i>E. procera</i> Ahlner	II	0-1 m, stones	frequent	polytoxobic
16. <i>E. prolifera</i> (Muell.) J.Ag.	II	0-1m, stones	frequent	polytoxobic
PHAEOPHYTA				
Ectocarpaceae				
17. <i>Pilayella littoralis</i> (L.) Kjellm.	II	0-4 m, silt, sand, stones, epiphytic	rare	mesotoxobic
18. <i>Ectocarpus arctus</i> Kuetz.	II	cast ashore	rare	mesotoxobic
Chordariaceae				
19. <i>Chordaria flagelliformis</i> (Muell.) Ag.	II, III, V	cast ashore	frequent	polytoxobic
Dictyosiphonaceae				
20. <i>Dictyosiphon foeniculaceus</i> (Huds.) Grev.	II	0-1m, stones pebbles	rare	mesotoxobic

Algae species names and systematic position	Collection places	Depths, substrata	Frequency of find	Ecologic group
Laminariaceae				
21. <i>Laminaria bongardiana</i> P. et R.	II, III, V	2-4m, stones	frequent	polytoxobic
22. <i>L. gurjanovae</i> A. Zin.	II	1-4 m, sand	rare	mesotoxobic
23. <i>Laminaria</i> sp.	II	3-4 m, silt, sand, stones	vary rare	mesotoxobic
24. <i>Agarum clathratum</i> Dumortier	II	3-8m, stones	rare	mesotoxobic
Alariaceae				
25. <i>Alaria angusta</i> Kjellm. emend. Petrov	II	4 m, sand	rare	mesotoxobic
26. <i>A. marginata</i> P. et R.	II, III, V	2-3m, stones	frequent	polytoxobic
Ficaceae				
27. <i>Fucus evanescens</i> C. Ag.	II	0-1 m, stones	rare	mesotoxobic
RHODOPHYTA				
Bangiaceae				
28. ** <i>Porphyra kurogii</i> Lindstrom	II	0-3 m, stones	rare	mesotoxobic
29. <i>P. miniata</i> (Ag.) Ag,	II	3-4 m, stones	rare	mesotoxobic
30. ** <i>P. torta</i> Krishn.	II	cast ashore	rare	mesotoxobic
Corallinaceae				
31. <i>Corallina pilulifera</i> P. et R.	II	3-5 m, rocks	frequent	polytoxobic

Algae species names and systematic position	Collection places	Depths, substrata	Frequency of find	Ecologic group
32. <i>Clathromorphum circumscriptum</i> (Stroemf.) Foslie	II	3-8 m, rocks, stones	frequent	polytoxobic
33. <i>C. compactum</i> (Kjellm.) Foslie	II	3-8 m, rocks, stones	rare	mesotoxobic
34. <i>Lithothamnion pacificum</i> (Foslie) Foslie	II	3-5 m, stones	rare	mesotoxobic
Kallymeniaceae				
35. <i>Callophyllis rhynchocarpa</i> Rupr.	II	0-4 m, rocks	rare	mesotoxobic
Palmariaceae				
36. <i>Devaleraea compressa</i> (Rupr.) Selivanova et Kloczcova	II	0-1 m, stones pebbles	rare	mesotoxobic
37. <i>D. microspora</i> (Rupr.) Selivanova et Kloczcova	II	cast ashore	rare	mesotoxobic
38. ** <i>Palmaria callophyloides</i> Hawkes et Scagel	II	cast ashore	rare	mesotoxobic
39. <i>P. stenogona</i> (Perest.) Perest.	II, III, V	1.5 -3 m, stones	frequent	polytoxobic
Ceramiaceae				
40. * <i>Scagelia pilaysaei</i> (Mont.) Wynne	II	4 m, sand, epiphytic	rare	mesotoxobic

Algae species names and systematic position	Collection places	Depths, substrata	Frequency of find	Ecologic group
41. <i>Neoptilota asplenioides</i> (Turn.) Kylin	II, III, V	0.5-4 m, rocks, stones	frequent	polytoxobic
Rhodomelaceae				
42. <i>Pterosiphonia bipinnata</i> (P. et R.) Falkenb.	II	2-3m, stones	frequent	polytoxobic
43. <i>P. hamata</i> Sinova	II	3-4, stones	rare	mesotoxobic
44. <i>Odonthalia corymbifera</i> (Gmel.) J. Ag.	II	cast ashore	rare	mesotoxobic
45. <i>O. kamtschatica</i> (Rupr.) J. Ag.	II	4-5 m, rocks	rare	mesotoxobic
46. <i>O. setacea</i> (Rupr.) Perest.	II	cast ashore	very rare	mesotoxobic

DISCUSSION

It seems impossible now to estimate damage caused by each pollutant separately without special laboratory experiments. So in the field we observed accumulative effects of anthropogenic pressure on benthic flora and communities as a whole. This total pollution leads to obvious loss of the species diversity.

Comparing algae species composition of very dirty ecotops (polytoxobic) and relatively pure (oligotoxobic) ones we found that pollution causes reduction of the species number up to 60% in Rhodophyta, 50% in Phaeophyta and 25% in Chlorophyta.

Having analysed data from the literature since the beginning of the century up to 1970's (Savich, 1914; Voronikhin, 1914; Sinova, 1933; 1954;

Spasskii, 1961; Blinova and Gusarova, 1970; 1971; Klochkova, 1977) and personal long-term field observations in the Bay (Selivanova, 1988 a; b; 1989) we mark a constant tendency of marine flora of the region to decrease in species number. A series of algae, mainly representatives of Rhodophyta can be considered as very rare and vanishing species in the Bay : *Membranoptera beringiana* (Rupr.) A.Zin., *M. multiramosa* Gardn., *Hymenena ruthenica* (P. et R.) A. Zin., *Pantoneura juergensii* (J.Ag.) Kyl.

Thus it is clear that red algae are most sensitive to unfavourable environmental factors. We suppose sterilizing effect of pollution to be the main cause of their disappearance. As it was shown by Gusarova and Khristoforova (1987) pollution leads to a fortnight delay in spore release of macrophytes growing in waters with high concentrations of heavy metals. We observed total absence of reproductive structures in red algae growing in polytoxic zones during the period of intensive reproduction of these species in normal conditions. More primitive reproductive processes in green and brown algae probably make them more resistant to pollution.

Loss of species diversity is accompanied by serious changes in phytocenoses: in the character of dominance; in the number and correlation of the co-dominant species and abrupt growth of epiphytism (in 1.5-2 times as compared to pure zones).

The influence of pollution on vegetative structures of benthic algae including morphologic, histologic, cellular anomalies is not so obvious. We observed rare morphological anomalies only in some representatives of Laminariales (e.g. *Agarum clathratum*, *Alaria marginata*). But these cases can not be for sure considered as teratological caused by pollution because anomalous specimens were also sometimes found in pure zones. And we failed to find any evident pathologic changes while studying vegetative cells and tissues of macrophytes. This is probably due to ability of marine benthic algae to repair damage which assists their survival even in the extremely unfavourable ecologic conditions.

Most numerous and massive algae of the order Laminariales are able to withstand harmful environmental factors without any evident morphologic changes and not losing physiologic and reproductive activity. Moreover they are active agents in the processes of sea water self-cleaning, absorbing toxicants and making complexes with alginates in their fronds and thus inactivating poisons. But on the other hand, algae themselves become toxic and unfit for use. In the process of kelp elimination pollutants return to the water. Destroyed fronds sedimenting at the bottom and decaying produce the secondary source of pollution and make oxygen regime worse. So processes of natural water purification are obviously insufficient in the unfavourable conditions presently observed in the

Avacha Bay. Urgent artificial measures are necessary to improve its ecologic situation in order to prevent further process of marine biota extinction. Of course, introduction of modern technical devices of water purification will be of much help in this case. But biological methods also may play important role in this process.

One of those methods turned out to be successful. After experimental removal of old decaying fronds (analogous with sanitary felling in the woods) in a small enclosed inlet within the Bay we managed to improve its ecologic conditions and prevent other marine organisms from suffocation. Due to photosynthetic activity of the rest of the algae, oxygen contents considerably increased.

This method of sanitary kelp removal may be successfully combined with other biological methods of water cleaning, for instance, marine culture with application of filtrating organisms (mussels etc. also with their further withdrawal) and serve as one of the immediate measures of water purification and marine biota protection in the Bay.

ACKNOWLEDGEMENTS

We are thankful to the staff of Kamchatka Hydrochemical Laboratory and personally to senior engineer L.I. Kodnyanskaya for chemical analyses of the Bay's waters.

REFERENCES

- Blinova, E.I. and I.S. Gusarova. 1970. Marine algae, new for the coasts of the Eastern Kamchatka. *Novosti Sistematiki Nizshikh Rastenii*. Leningrad. 7 : 68-71. (In Russian).
- Blinova, E.I. and I.S. Gusarova. 1971. Algae of the sublittoral zone of the south-eastern coast of Kamchatka. *Izvestia TINRO* 76 : 139-145. (In Russian).
- Dmitriev, V.D. and B.V. Yezhov. 1977. To the question of the origin of the Avacha Bay. *Voprosy geografii Kamchatki* 7 : 45-48. (In Russian).
- Gusarova, I.S. and N.K. Khristoforova. 1979. Micro-elemental composition of *Cystoseira crassipes* (Turn.) Ag. from one of the bays of the north-western coast of the Sea of Japan. *Kiev, Naukova Dumka*, pp. 38-40. (In Russian).
- Gusarova, I.S. and N.K. Khristoforova. 1987. Floro-coenotic changes in the macrobenthos produced by heavy metals. *Kiev, Naukova Dumka*, pp. 94-95. (In Russian).

- Klochkova, N.G. 1977. Additions to the flora of the Kronotsky and Avachinsky Bays of the south-eastern Kamchatka. *Biologiya Morya* 5 : 24-32. (In Russian).
- Khrstoforova, N.K. 1989. How to characterize the environments judging by the algal chemical composition. *Morskaya Niva, Vladivostok*. pp. 124-134. (In Russian).
- Kovardakov, S.A., Yu.K. Firsov and S.E. Zavalko. 1987. *Cystoseira* and its epiphytes in the marine recreation area. Dynamics and biomass of absorbing surface. Possible participation in self-cleaning. I All-Union Conference 'Actual problems of modern phycology'. Kiev, Naukova Dumka, pp. 112-113. (In Russian).
- Savich, V.P. 1914. Algological observations in the Avacha Bay in May, 1909. *Trudy Kamchatskoi ekspeditsii F.P. Ryabushinskogo*. 2 : 451-472. (In Russian).
- Selivanova, O.N. 1988a. Additions to marine algal flora of the south-eastern Kamchatka. *Novosti Sistematiki Nizshikh Rastenii*. (Leningrad) St. Petersburg 25:57-63. (In Russian).
- Selivanova, O.N. 1988 b. Species composition of the benthic flora of the Avachinskaya Inlet (South-Eastern Kamchatka). In : (A.I. Kafanov, ed.) *Biota and Communities of the Far Eastern Seas. Lagoons and Bays of Kamchatka and Sakhalin*. Academia Nauk Press, Vladivostok: 84-92. (In Russian).
- Selivanova, O.N. 1989. The list of macrophytes of the Avacha Bay. In: (O.G. Kussakin, ed.) *Hydrobiological Investigations in the Avacha Bay*. Academia Nauk Press, Vladivostok : 93-98. (In Russian).
- Selivanova, O.N. and G.V. Shebyakina. 1994. Effect of pollution on benthic algae of the Avacha Bay (south-eastern Kamchatka). All-Russian Conference 'Ecosystems of Russian Seas in the Conditions of Anthropogenic Press': 521-523. (In Russian).
- Selivanova, O.N. and G.V. Shebyakina. 1995. The pollution influence on seaweeds of the Avacha Bay (Kamchatka). Long-term changes in marine ecosystems. Arcachon, France : 72.
- Shtina, E.A. 1985. Principles and methods of the application of soil algae for bioindication of the soil pollution. *Trudy VNIISKH Mikrobiologii* 52 : 26-32. (In Russian).
- Sinova, E.S., 1933. Algae of Kamchatka. *Issledovaniya morei SSSR*. Issue 17 : 7-42. (In Russian).
- Sinova, E.S. 1954. Marine algae of the south-eastern Kamchatka. *Trudy Botanicheskogo Instituta AN SSSR*. Seria II, issue 9 : 365-400. (In Russian).

Spasskii, N.N. 1961. Littoral zone of the south-eastern coasts of Kamchatka. Issledovaniya dalnevostochnykh morei SSSR, 7 : 261-311. (In Russian).

Voronikhin, N.N. 1914. Marine algae of Kamchatka. Trudy Kamchatskoi ekspeditsii F.P.Ryabushinskogo. 2 : 475-524. (In Russian).

THE SEISMIC SEQUENCE, GEOTECTONICS AND PETROLEUM GEOLOGY IN NANSHA REGION

Shaoren Jiang and Xiaozhong Zhou
South China Sea Institute of Oceanology, Academia Sinica
Guangzhou, China

ABSTRACT

The Nansha Islands regions is located in the southern part of the South China Sea. From 1987 to 1991, four geophysical cruises have been carried out in this region. Based on seismic data, three seismic sequences, corresponding to three structural layers respectively, can be separated by two regional unconformities. They have different seismic facies and different features of tectonic deformations, representing a different tectonic evolutionary history. The crust under the Nansha Islands region, including Nansha Trough, is considered to be thinned and block-faulted micro-continental crust. It is a split paleo-platform in geotectonics. The Nansha Trough was formed by the gravitational isostatic response of the nappe zone. Six sedimentary basins are identified in the Nansha region. They are mostly of polycyclic marine facies sedimentary basins with three sets of source-reservoir-caprock associations. The Nansha Island region seems to be full of promise for oil and gas.

INTRODUCTION

The Nansha Islands region is located to the east of the Natuna Islands, west of the Kalimantan Islands and south of Latitude 12° N, with an area of about 1,000,000 km² in total. From 1987 to 1991, the Nansha Investigation Team of Academia Sinica has completed four geophysical survey cruises, including 19 seismic lines with a total length of 6,883 km and 14 stations of refraction sonabuoy (Fig. 1), covering most of the waters in this region and crossing different geotectonic units. Some important information has been obtained through this investigation for evaluating the petroleum resources and understanding the tectonics of the Nansha area.

The marine seismic data were acquired by the SHIYAN 2 Geophysical Investigation vessel with 24 seismic channels, 50 m interval. The source was an airgun with volume of 25 ltr., pressure of 125 kg/cm² and shooting space of 50 m. The seismograms were made by a DFS-V digital recording system and the positioning was conducted by MX-200B Comprehensive Geophysical Satellite Positioning System.

Most of the data were processed by the Geophysical Exploration Institute of the National Petroleum and Gas General Corp., on IBM3033 and IBM 3083 computers. The seismic profiles show clear features, high signal/noise ratio and good quality, and also show that a number of Mesozoic and Cenozoic basins developed over this marine region.

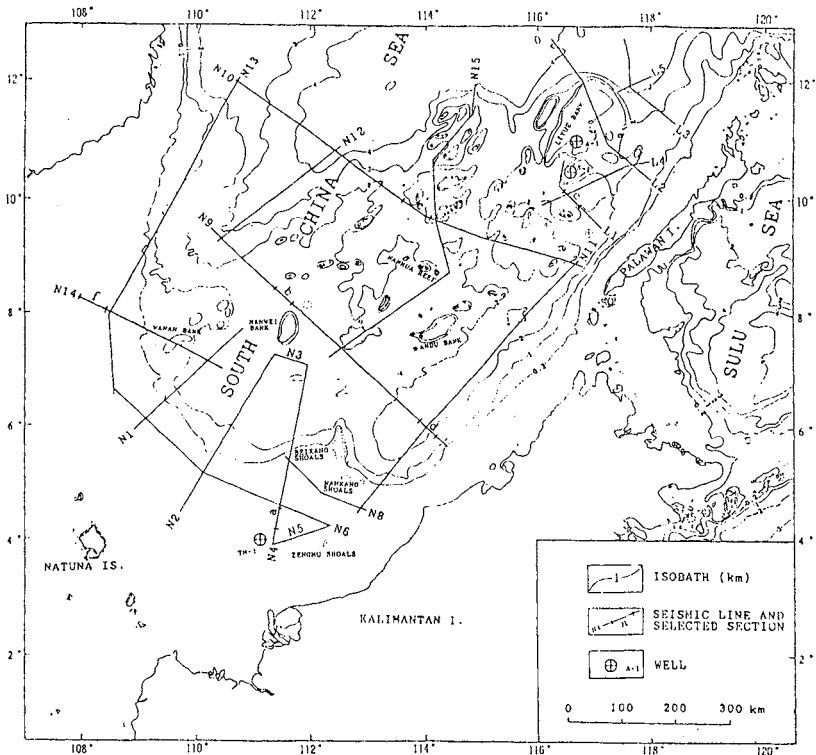


Fig. 1 Layout of the survey lines

THE SEISMIC SEQUENCES

Based on the synthetic analysis of reflection seismic data, three seismic sequences could be separated by two regional unconformities: T_8 and T_h . They correspond to three structural layers characterized by different seismic facies, different tectonic deformation and representing a different geotectonic evolutionary history (Fig. 2, Fig. 3, Fig. 4).

1. The upper seismic sequence is the reflection series between seabed and reflector T_8 , where the seismic facies is of strong amplitude, high apparent frequency, consistent continuity, clear stratification, subdued relief and sheeted draping. It can be traced and compared over a great range. Its thickness varies greatly over a large area. The maximum thickness of this layer is over 9 km in the center of Zengmu Basin. But around the margins and the uplifted zone of the basins, the sediments become thinner and locally pinched out. According to drilling data from wells off Salaoyue - Natuna

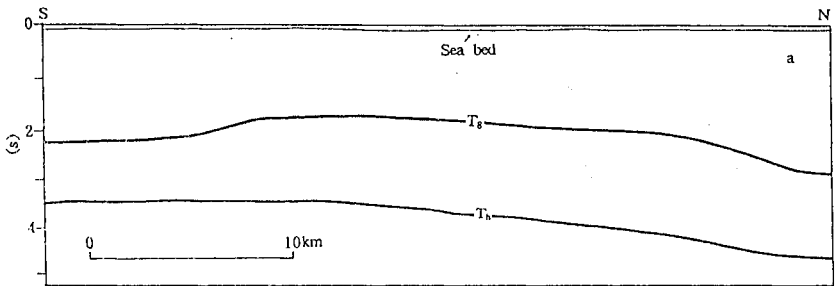
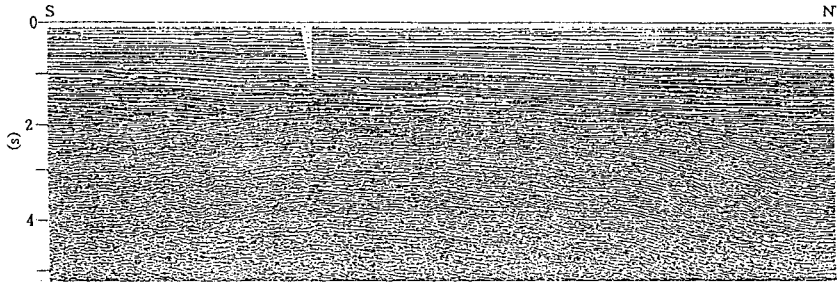


Fig. 2 Selected section of seismic profiles over Zengmu Basin (N4-a in Fig. 1)

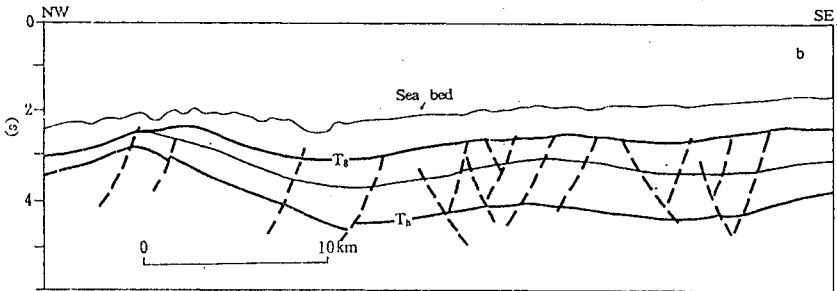
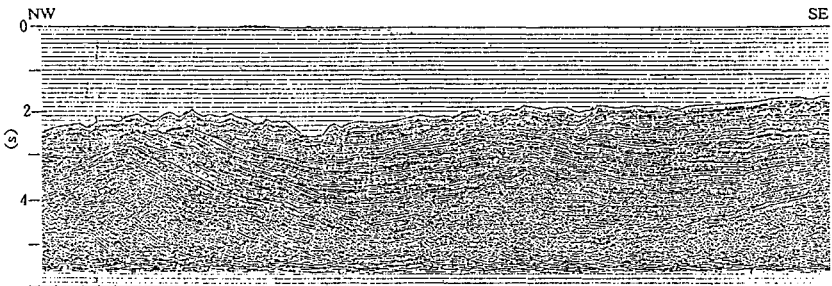


Fig. 3 Selected section of seismic profiles over Nanwei Bank (N9-b in Fig. 1)

Islands (Ernst, 1981), the sediment was mainly clastic rock interlaced with organic reef or carbonate rock. The age of this layer may be Oligocene to Recent, locally including late Eocene. Drilling data from the Sampagita-1 (S-1) in the eastern Liyue Beach illustrates that the series is of organic reef limestone and sandy shale of littoral facies of upper Eocene-Quaternary (Taylor, 1980).

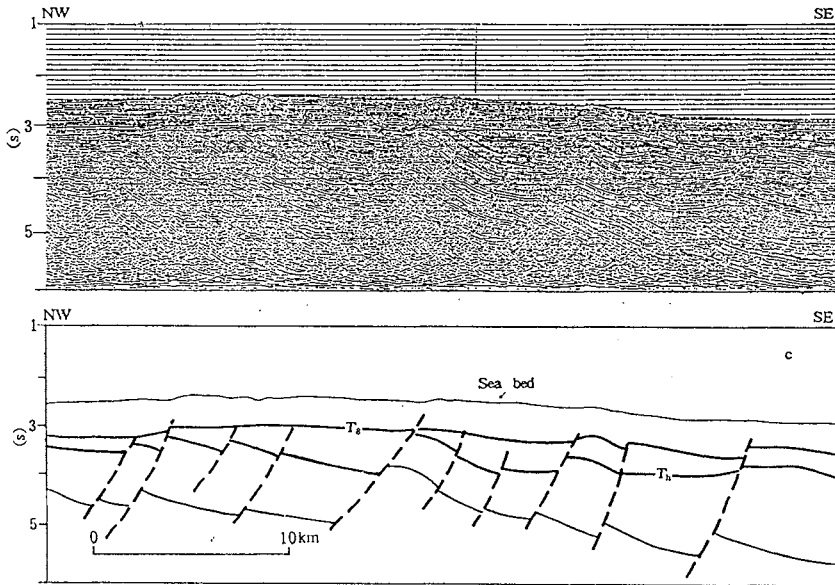


Fig. 4 Selected section of seismic profiles over Liyue Bank (L1-c in Fig. 1)

2. The middle seismic sequence lies between reflectors T_8 and T_{11} . Its seismic facies is of middle amplitude, middle frequency, good continuity, clear stratification and subparallel-divergent textures. It is a gently folded Paleocene to Eocene sequence, angularly unconformable with overlain sequence. After deposition, this layer had suffered fault-cutting and tilting to form a series of half graben structures. The thickness of this layer is generally about 1-3 km, thinned or absented over uplift areas. It could be another important target layer for oil-gas exploration in the Nansha region. Tenggiri Marine-1 (TM-1) near the N_4 survey line in southern Zengmu Basin (Fig. 1) met Eocene clastic rocks at 2854 m (Soeparjadi, 1986). Based on the drilling data of well Sampagita-1 in Reed Bank (Taylor, 1980), the layer consists of Paleocene-Eocene detrital sediments of deltaic facies and outer neritic-bathyal facies.

3. The lower seismic sequence lies beneath reflector T_{11} . Its base is not well defined. This sequence is characterized by weak amplitude, low frequency,

poor continuity and is separated from the middle sequence by an angular unconformity. This layer is assumed to consist of pre-Tertiary sedimentary, metamorphic and igneous rocks, among which sedimentary rocks are mainly distributed in the southeast part of this region. Early Cretaceous littoral-neritic sediments were drilled through in well Sampagita-1 and A-1 in Reed Bank (Fontaine, 1983). Triassic and Jurassic marine sedimentary rocks were found by dredge near Renai and Meiji Reefs (Kudras, 1985).

TECTONIC MOVEMENTS

Two large-scale tectonic movements occurred in late Cretaceous and late Eocene time, respectively resulting in two obvious regional unconformities, which divided the sediments into three structural layers. The tectonic movement in late Cretaceous caused a large-scale uplifting and subsequent high erosion, which formed the regional unconformity T_h and a series of basement faults in this region.

The tectonic movement in late Eocene was intensive and widespread. From Kalimantan-Palawan Island to the Nansha Islands, a strong regional compression fold-deformed and uplifted the middle seismic sequence, and caused epimetamorphism in the south (CCOP-IOC, 1980). In the middle Oligocene, the tectonic movement transformed from a regional compression to a regional extension in most of the region except the southern margin. Large scale block-faulting and tilting occurred, forming a series of fault sags. Then regional uplifting transformed into differential subsidence. Because of this tectonic movement, lower and middle Oligocene formations were mostly absent and the upper Oligocene or younger formations unconformably overlie the folded Eocene and older formations.

CRUSTAL TYPE

According to the initial investigation, the crust under the Nansha Islands region, including the Nansha Trough, is considered to be thinned and faulted microcontinental blocks and split paleoplatforms in the tectonics. Mesozoic unmetamorphosed sedimentary rocks were found under the pre-Tertiary unconformity. Pre-Mesozoic metamorphic rocks are exposed in the northern uplifted area. During late Oligocene time, most of the Nansha Trough region has uplifted to form land and the middle structural layer was removed by erosion. Afterwards the overthrust and nappe kept shifting from the southern margin of the Trough to the north. It caused a strong subsidence north of the nappe zone and formed Nansha Trough (Fig. 5) as a result of the gravity isostatic response (Hinz, 1985; 1989).

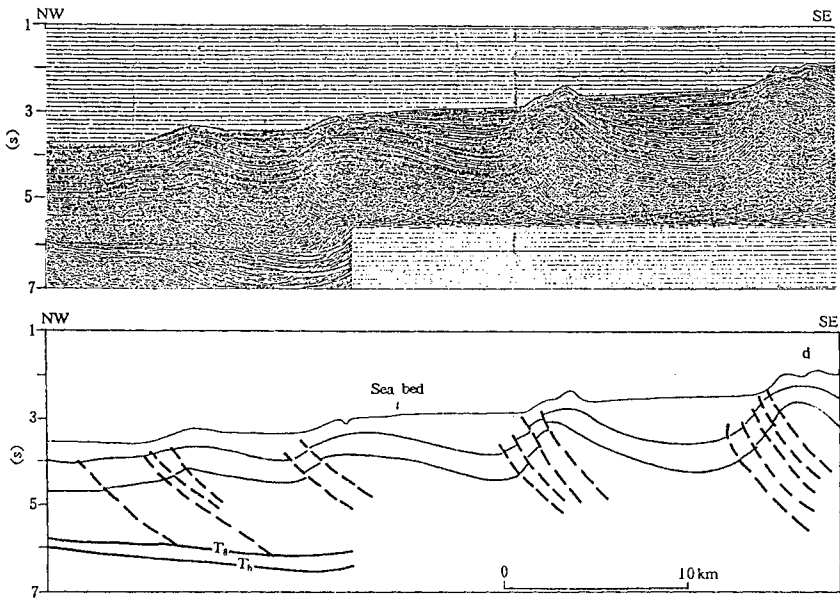


Fig. 5 Overthrust-nappe structure at the southern margin of Nansha Trough (N9-d in Fig. 1)

TECTONIC EVOLUTION AND OUTLINE OF THE PALEOGEOGRAPHY

In the Nansha region, the sedimentary cover consists of three series of marine facies i.e., Mesozoic, Paleocene-Eocene and Oligocene-Quaternary strata. They represent three tectonic-sediment cycles, but their paleogeography and sediment environment have undergone significant changes. According to the explanation of magnetic lineation by Taylor and Hayes (1980), the South China Sea central basin was formed in the middle of Oligocene-early Miocene time (32-17 Ma). Therefore, the South central basin did not exist before the Oligocene, and at that time, the Nansha region was connected directly with the South China continent. Ophiolite and abyssal sediment outcropped at Kalimantan-south Palawan suggests that a pre-Oligocene ancient South China Sea existed to the south of the Nansha region.

According to tectonostratigraphic studies, we concluded that since Cretaceous time, the South China continental margin had rifted twice to form the ancient and current South China Sea basins respectively.

During the middle to the late Cretaceous time, the South China continental margin uplifted and extended regionally to form a series of half grabens and tilted fault blocks. To the south of this area, rifting and sea-floor spreading created the ancient South China

Sea basin, which separated the original Kalimantan microcontinental block from the South China continental margin (including Nansha microcontinental block). From the Paleocene to the Eocene, the Nansha region gradually subsided as a continental margin sea with a topography higher in the north and lower in the south. The marine transgression expanded from south to north submerged most of the basement high and formed overlap draping sediment. South China continent became mainly a sedimentary terrigenous province.

In the late Eocene, the original South China continent creep-dispersed further to the southeast and strongly extended and uplifted again, leading to collision and the joining of the Nansha microcontinental block with the previous Kalimantan microcontinental block. The ancient ocean crust between these two blocks subducted southward and consumed (Sarawak), or partly faulted and obducted northward onto the Nansha microcontinental block (east Sabah-south Palawan). This collision resulted in widespread up-folding in the Nansha region with much area turning into land. On the south margin, the nappe-thrust created an orogenic belt and foredeep (foreland basin). During the early-middle Oligocene, the continued regional extension and rifting of the South China continent caused strong block-faulting in the central and northern parts of this area.

From late Oligocene to early Miocene, with the spreading and forming of the South China Sea basin, the Nansha microcontinental block separated from the South China continent and drifted southward, becoming a reef island region far from the continent and depositing platform facies and biohermal carbonates. The south margin of this region was in compressive tectonic surroundings, which led to the napping extending to the north and forming the Nansha (Palawan) trough with abyssal turbidity current deposits at the front of the huge nappe. Meanwhile, Kalimantan Island gradually uplifted and enlarged to become a mainly sedimentary terrigenous province.

Since middle Miocene, sea-floor spreading in the South China Sea has stopped. The cooling of the oceanic crust has led to regional subsidence and most of the Nansha region gradually became a bythal-abyssal sedimentary environment. As the Australian microcontinental block was rotated counterclockwise, obducted northward and compressed further, leading the nappe zone at the south margin of Nansha microcontinental block to keep advancing to the north and complicating. Meanwhile, the Nansha trough retreated northward and deepened gradually.

BASIN DIVISION AND GENETIC TYPE

Based on the thickness variation of three sedimentary sequences and the tectonically deformed features, six basins are identified in Nansha region. They are West Wanan basin, Zengmu basin, Nanwei basin, Nanhua basin, Liyue basin (Reed bank) and Nansha Trough basin (Fig. 6).

West Wanan basin developed on the intersection of the Nansha block with the Sunda block. The middle structural layer was lacking in most of the basin. The upper one without deformation has a great thickness (two-way traveltime of the seismic wave is over 4s), in which the middle and lower sections are deltaic facies sediments filling a half graben and characteristic of clear divergent structure (Fig. 7). The upper section is marine ingression onlap of parallel-subparallel texture. Consequently, West Wanan basin was formed mainly since Oligocene and obviously controlled by the Natuna Fault Belt, which strikes north-southward. Its origin was hypothetically related to the dextral strike slip of the fault and belonged to the pull-apart basin.

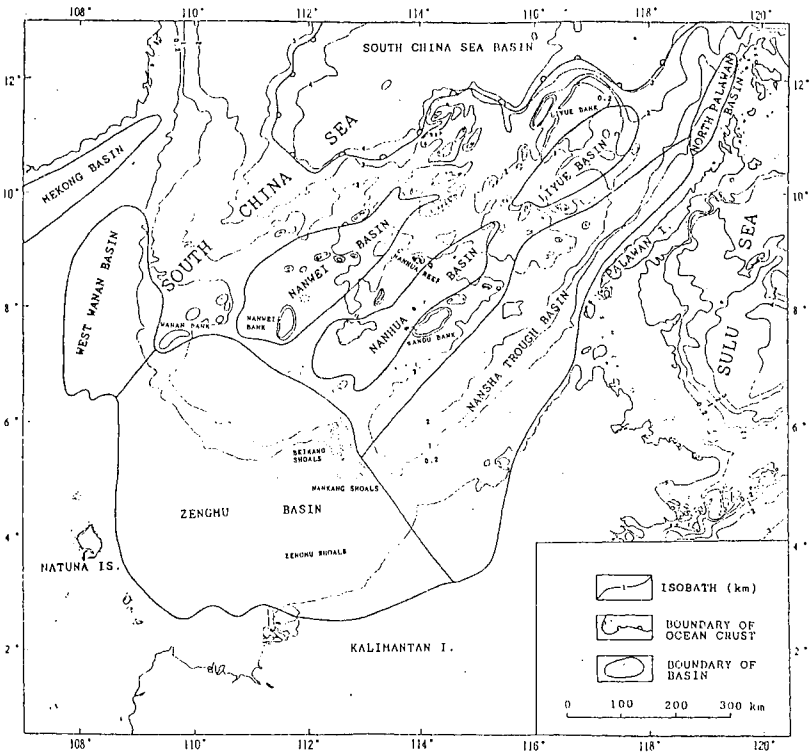


Fig. 6 Sketch map of sedimentary basins in Nansha region

In addition to West Wanan basin, three sedimentary layers (e.g. Mesozoic group, Paleocene-Eocene series and Oligocene-Quaternary system), were developed in the other five basins in Nansha region to various extents. Therefore, these basins are Mesozoic and Cenozoic basins with multiple depositional cycles. Particularly, the Paleocene-Eocene series distributed widely over this region, with thickness of 1-3 km or zero in uplift areas. The features of sedimentary development show that during Paleocene to Eocene time,

Zengmu, Nanwei, Nanhua, Liyue and Nansha Trough basins were joined with each other, to have formed a huge Nansha continental margin depression area.

Since the late Eocene, as the two microcontinental blocks, Nansha and primitive Kalimantan collided with each other, Zengmu and Nansha Trough basins have transformed into foreland basins. Characteristics of compression in the south and extension in the north are shown very clearly in these two basins. On their south margins they developed a folding and thrust nappe zone, while in the middle and the north areas, tensile block-faulting and strong subsidence mainly developed. Their sedimentary features in the upper structural layer are of rapid cumulation with successively prograded deltaic sedimentation in their southern parts, and mainly of neritic terrace facies-organic reef or abyssal turbidity current deposits in the central and northern parts. After Miocene time, there appears non-compensative sedimentary environments, and pelagically suspended pelitic deposition in some local parts. Because of the expanding and developing of the Central South China Sea Basin, the Nansha microcontinental block block-faulted further and drifted south gradually (Taylor, 1980). Therefore these three basins developed in the northern part of Nansha microcontinental block. Liyue (Reed bank) basin, Nanhua basin and Nanwei basin, transformed into tensional detached land-block basins after the Eocene period.

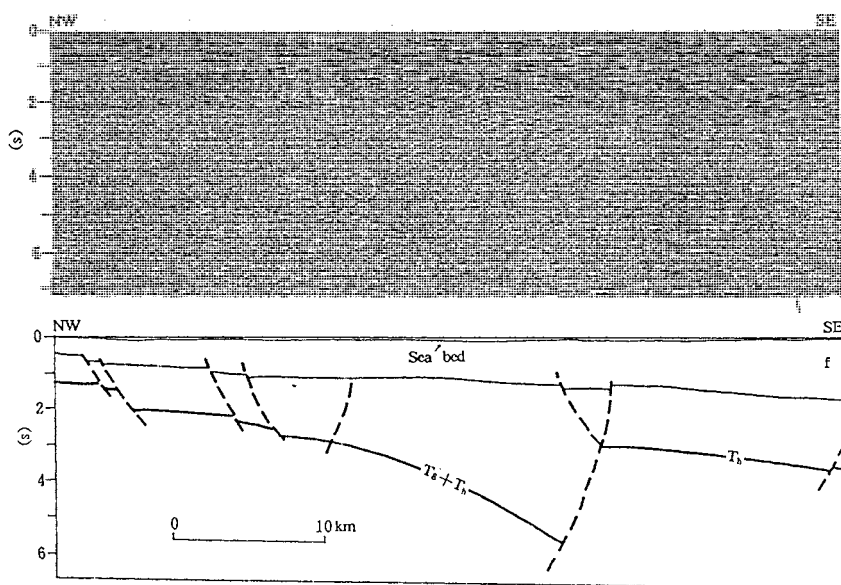


Fig. 7 Selected section of seismic profile in s Wanan Bank (N14-f in Fig. 1)

GEOLOGICAL CONDITIONS OF PETROLEUM

Many oil companies have drilled wells in the West Wanan basin, Zengmu basin and shelves of Nansha Trough basin and have found a number of large to medium sized oil-gas fields, all producing formations of which are of sandstone or of carbonate rock of the upper structural layer. Oil-gas from the Paleocene sandstone has been found in the Sampagita-1 well in Liyue basin, which reveals that the middle structural layer distributed pervasively over the Nansha region may be another target series for an oil-gas prospect. In terms of the basin type, both Zengmu basin and Nansha Trough basin are of foreland which bear the richest oil and gas. The other basins, of strike-slip pull-apart and tensional detached land-block, also have wonderful oil-gas prospects. As a result, the Nansha region might be the focus of world attention for its great potential prospects.

Based on the seismic facies and drilling data, oil and gas might be formed in unmetamorphic deltaic to bathyal sediments in the three tectonic layers. Deltaic, neritic-littoral or abyssal turbidite sandstone masses developed during the later Cretaceous, Paleocene-Eocene and Miocene periods and stratified carbonate rocks and biological reefs developed during the Paleocene-Eocene period. These might be favorable source rocks. Pliocene-Miocene and Eocene overlap deposits could be muddy caprocks in a regional scale while the lower Cretaceous muddy rocks could be locally caprocks.

In Liyue basin, the block-faulting (Fig. 4) in the middle and lower tectonic layers created traps of faulted blocks type. In the Nanwei basin, the large-scale compressive anticlines in the middle structural layers might be the favorable traps (fig. 3). The Zengmu basin and the southern margin of the Nansha Trough have many compressive anticlines and mud diapir structures in the upper tectonic layer. In the outer shelf from East Natuna to Nankang, a vast buried organic reef doming was developed. These three types of trap might contain oil-gas fields in medium to large sizes.

REFERENCES

- CCOP-IOC. 1980. Studies in East Asia tectonics and resources. Russia: CCOP Project Office. RAS/80/003 (RAS/77/037). pp. 141-151.
- Du Bois, E. P. 1981. Review of principal hydrocarbon-bearing basins of the South China Sea area. *Energy*. **6**:1113-1140.
- Fontaine, H. et al. 1983. The Jurassic in Southeast Asia. *CCOP Tech. Bull.* **16**:1-75.
- Hinz, K. and H. U. Schul Ter. 1985. Geology of the dangerous grounds, South China Sea and continental margin off Southwest Palawan: Results of SONNE Cruises SO-23 and SO-27. *Energy*. **10**:297-315.

Hinz, K. et al. 1989. Thrust Tectonics along the North-Western Continental margin of Sabah/Borneo. *Geologische Rundschau*. **78/3**:705-730.

Kudrass, H. R. et al. 1985. Mesozoic and Cenozoic rocks dredged from the South China Sea (Reed Bank Area) and Sulu Sea and their significance for plate-tectonic reconstructions. *Marine and Petroleum Geology* 3. pp. 19-30.

Soeparjade, R. A., L. Z. Valachi and S. Sosromihardjo. 1986. Oil and gas developments in Far East in 1985. *AAPG Bull.* **70(10)**:1497-1565.

Taylor, B. and D. E. Hayes. 1980. The tectonic evolution of South China Sea Basin in the tectonic and geologic evolution of Southwest Asian Seas and Islands. *Geophys. Monograph Series*. Vol. 23. D. E. Hayes (ed.). Washington, D.C.: American Geophysical Union. pp. 89-104.

WILD DOLPHIN BASED TOURISM: MINIMIZING THE RISKS AND MAXIMIZING THE BENEFITS

Mark B. Orams

Massey University Albany
Auckland, NEW ZEALAND

ABSTRACT

Tourism that is based upon interacting with dolphins in the wild has become popular in the past decade. Twelve such operations currently exist in New Zealand and at least eight in Australia. Previous records of dolphins which have become habituated to human contact have shown that dolphins can become aggressive and sometimes endanger humans. In addition, a number of sociable dolphins have been injured by humans. There are, therefore, risks for both the dolphins and for the tourists in this new industry. Proponents of the industry state that there are significant educational and conservation benefits which result from these kinds of interactions. Potential benefits also include stimulation and entertainment for the dolphins, and economic and psychological benefits for humans. Widespread debate exists over how these interactions should be managed.

Management strategies which have the potential to minimize and risks and maximize the potential benefits from these interactions include: ensuring operators and participants are knowledgeable about dolphins, independent and long term monitoring of dolphin behavior, prohibiting interaction when dolphins are resting, feeding, or in nursery pods, restricting the number of boats, human participants and the frequency and duration of interactions, including education programs as part of the experience, encouraging interactions to be stimulating and “fun” and prompting people to become more environmentally responsible as a result of their experience with dolphins. When combined with sensible management the dolphin based tourism industry has the potential to be sustainable and ethically acceptable. Without it, it is neither.

INTRODUCTION

Dolphins have been popular images for humans for centuries (Cousteau and Dirole 1975). Early accounts of dolphins befriending humans are available from the first century (Pline L’Ancien 1955) and many examples exist for more recent times (Lockyer 1990). Unfortunately many of these “friendships” have ended in tragedy for the dolphin and in a number of cases humans have been endangered as well. Despite their passive and gentle image, and despite the majority of people wishing to interact with dolphins having good intentions, a number of cases have shown that there are considerable risks involved in these kinds of interactions, both for dolphins and for humans (Orams in press^a).

In the past five years, particularly in New Zealand and Australia, a tourism industry based upon interacting with dolphins in the wild has developed (Orams 1995). Large numbers of people are now being taken out into coastal waters and are swimming with dolphins. Several others use food for the dolphins as a mechanism by which close interaction is facilitated in a shallow water environment. The rapid increase in the number of these types of operations has caused concern regarding the impact of such regular interaction on the dolphins. Concern is seldom expressed regarding the safety of humans, however, history suggests that this risk must also be addressed in the management of this industry (Orams 1996^a).

This paper provides a brief overview of the social relations between humans and dolphins throughout history. It emphasises that these historical accounts reveal that there are some very real risks involved in these interactions and specifies these potential negative impacts. The potential positive impacts are also acknowledged and a management regime which can be used to maximize these, whilst minimizing the risks is offered.

HISTORICAL ACCOUNTS OF HUMAN - DOLPHIN INTERACTION

Stories and legends about “friendly” dolphins have been around for centuries and are found in many cultures (Lockley 1979). It is apparent that, for many peoples, these animals have held a special place in their culture, as represented in writings, art and folklore (Burr-Stebins 1929). Of particular interest have been those dolphins which have become “sociable” with humans. These situations have become major attractions which were often recorded. One notable account, which is of direct relevance to the issues discussed in this paper, is that of the relationship between a boy and a dolphin in North Africa during the first century (Alpers 1963). The story claims that the boy and the dolphin, which was named “Simo”, swam, played and frolicked together in the shallows with the boy often being taken for rides on the dolphin’s back. The games and antics of the dolphin and boy became a major attraction which eventually resulted in many visitors (dolphin tourists?) crowding the town to watch. Morris (1988) states that the crowding of the town caused major divisions in the community and that the town leaders eventually killed the dolphin in order to restore peace and quiet to the area!

In more recent times a similar scenario was played out in the small town of Opononi in northern New Zealand. “Opo” was a large female bottlenose dolphin which began to interact regularly with people during the summer of 1955. The dolphin quickly became a major tourist attraction resulting in an influx of thousands of people into the small coastal community. As the infrastructure of the town struggled to cope with the large numbers controversy arose over the benefit of having such a dolphin resident in the area. Some locals felt the need to offer some formal protection for Opo and an Act of Parliament was passed in order to protect the dolphin from harm. Unfortunately, however, Opo was found dead towards the end of the summer and it is suspected that she was deliberately killed by the detonation of an underwater explosive (Doak 1984).

There have been many cases of sociable dolphins being deliberately harmed by humans. Examples include, a friendly dolphin named “Chira” which was shot and killed off the coast of

Costa Rica (Lockyer 1990). A sociable bottlenose dolphin at Bunbury in Western Australia which was reported to have been killed by a "star - picket" thrown by a local fisherman (Wilson 1994). A dolphin named "Old Charlie" was reportedly shot at Monkey Mia in Western Australia as was "Donald" off the Isle of Man in the United Kingdom (Lockyer 1990). A number of fishermen are reported to have deliberately attempted to hook and land dolphins which were accepting fish handouts from humans in Florida (National Marine Fisheries Service 1994). There are, therefore, a number of accounts which show that dolphins which have become "friendly" with humans have been deliberately harmed by humans.

Similarly, there are a number of accounts of wild sociable dolphins which have deliberately harmed humans. Despite a common perception that dolphins are gentle and passive creatures by nature, dolphins do have aggression as part of their behavioral makeup (Leatherwood and Reeves 1990). Dolphins which become used to frequent human contact often become increasingly forceful in their physical relationships with people (Orams et al 1996). There are reported examples of sociable dolphins holding people under the water (Webb 1978), carrying people out to sea (Dobbs 1977), attempting to copulate with people (Morris and Lockyer 1988), aggressively attacking people (Lockyer and Morris 1985) and biting people (Orams 1996^a). An extreme case, recently reported, relates a situation where an extremely popular dolphin in Brazil deliberately injured a number of swimmers and caused the death of one swimmer (Santos 1995).

It is clear from the numerous accounts reported throughout history that there are significant risks associated with close relationships between dolphins and humans. Despite these accounts, the popular image of dolphins as being friendly playful and safe wild animals persists. In addition, the assumption that dolphins wish to have human "friends" and human contact is also widespread. These views, a reaction against the keeping of dolphins in captivity, and a recognition of an opportunity has resulted in operators setting up boat trips which promote people swimming and otherwise interacting with dolphins. The next section will detail some of these more recent developments in Australasia.

RECENT DEVELOPMENTS IN AUSTRALASIA

In the past five years 12 commercial operators have established "swim with wild dolphin" programs off the coast in New Zealand (Doak 1994). Similarly, in Australia, at least eight operators are now offering paying tourists the opportunity to enter the water and interact with wild dolphins (Orams in press^a). The Department of Conservation in New Zealand has many more proposals for additional "dolphin swimming" programs (Doak pers comm) and Queensland's (Australia) Department of Environment has found a similar high level of interest in its area of jurisdiction (Queensland Department of Environment 1994). It is apparent, therefore, that demand exists for these kinds of dolphin - human interaction operations and that government agencies are having to respond to these demands (at least in Australasia). Research into the impacts of such interactions is still in its infancy (Constantine 1995).

The dolphin encounters offered by commercial operators follow a variety of patterns. Most involve locating a group of dolphins (most typically bottlenose species - *Tursiops truncatus*),

manoeuvring a boat close to the dolphins and then allowing tourists to enter the water with snorkel, masks and fins. The tourists then swim over to initiate visual and occasionally physical contact with the dolphins (although sometimes the dolphins initiate the interaction) (Constantine 1995). A number of operators tow snorkellers on a line dragged behind the boat through the area where the dolphins are swimming. One operator (in Western Australia) uses underwater motorised “scooters” to manoeuvre amongst the animals (Orams 1995). At two Australian locations (Monkey Mia, Western Australia and Tangalooma, Queensland) hand feeding of fish in shallows adjacent to a beach is used to facilitate close interaction between dolphins and tourists (Conner and Smolker 1985; Orams 1994^a).

There have been few investigations into the effect of these interactions (the notable exceptions being Constantine 1995; Amante-Helweg 1995, Weir et al 1996 and Orams 1996^a) and concern over the potential for harm to dolphins and controversy over management of these interactions has arisen. In New Zealand, the first prosecution against an unlicensed operator under the Marine Mammal Protection Act has been undertaken (Department of Conservation versus Crapper, Kaikohe District Court). This case and other problems with controlling private boaters attempting to swim with wild dolphins, programs for feeding wild dolphins and other forms of interaction have received much attention in the mass media in Australasia during the past year.

There is no doubt that huge demand exists for opportunities to interact with dolphins in the wild. This is not surprising given the extremely positive image that dolphins have for many people. Commercial operators and private individuals are now realising, in ever increasing numbers, that regular interaction with wild dolphins is possible. Furthermore, they are also realising that these interactions can form the basis of commercially viable tourism businesses. Consequently, more people are establishing close contact with dolphins than ever before. Unfortunately, however, very few commercial operators and virtually no members of the “general public” are aware of the potential risks involved in such interactions. Given the problems associated with sociable dolphins reported in the literature it is important that such risks are detailed and that management strategies developed to minimize them. The following sections provide a brief overview of the potential impacts of these human - dolphin interactions. To a certain degree they represent the author’s personal assessment with regard to the potential impacts, both negative and positive. Where possible, literature to support these points is referred to, however, the reader is advised that there is currently little evidence regarding the impacts of this new industry.

POTENTIAL NEGATIVE IMPACTS

Risks for Dolphins

Habituation to the close proximity of humans

As dolphins become more accustomed to people they begin to lose their natural wariness of them. Some dolphins, after a period of adapting to human contact, actually begin to seek out humans and initiate contact themselves (Doak 1984). Whilst this situation is commonly viewed as an extremely positive outcome from a human perspective - ie. a friendly dolphin - it places the

dolphin at risk. Unfortunately, not all humans who approach dolphins have good intentions toward them, the dolphin has no way of telling if a human intends to harm them or not. Because the dolphin has grown accustomed to human contact, those people who wish to harm them have a greater opportunity to do so. A number of cases in the past (see above) have shown that “friendly dolphins” have been harassed, injured and killed by humans. Dolphins which become accustomed to regular human contact are at a greater risk of harm than those dolphins which retain their natural wariness.

Disruption of natural behavior patterns

Wild dolphins that become sociable with humans have been known to abandon “normal” behavioral routines. Examples include remaining in particular locations for long periods, interacting with humans more frequently than with other dolphins (Lockyer 1990), adopting unusual and dangerous behavior such as closely following moving propeller blades (Lockyer and Morris 1985), entering extremely shallow tidal waters and playing with objects such as plastic or chemical containers (Doak 1984).

Disturbance during critical phases

Like all animals, dolphins have aspects of their lives which are particularly important to their survival. These include, giving birth and the caring of the very young, resting and hunting (Shane et al 1986). During these times the approach of boats or the presence of humans can be disturbing and stressful for the dolphins (Conner and Micklewaith-Peterson 1994). This is particularly so because in each of these situations the dolphins are less able to move to avoid human approaches. Unfortunately, unless one is trained to do so, it is difficult to recognise these critical phases. Consequently, dolphins are often approached by boats irrespective of their activity at the time (for example, if resting or hunting) or the make up of their group (for example, if in a “nursery pod” with very young calves) and disturbance results (Orams pers obs).

Increased exposure to health risks

One of the major threats to dolphins is the health of marine ecosystems (Dobbs 1981). In many areas where urban development or other human activities have resulted in marine pollution all marine based life, including dolphins, is threatened. Dolphins which become sociable with humans often do so in coastal areas close to major human activity (Lockyer 1990). If due to this regular contact dolphins remain closer to centres of human activity than they otherwise would, they increase their exposure to pollution based risks to their health. In addition to these indirect risks, dolphins health has been directly harmed through humans feeding wild dolphins inappropriate or contaminated food such as old bait fish, candy bars, bread, pretzels and even golf balls! (National Marine Fisheries Service 1994).

Risks for Humans

Subject to possible aggressive behavior

Dolphins are predators, they have aggression as part of their behavioural makeup and they can become aggressive towards humans. This is far more likely to occur when a dolphin has become accustomed to frequent close contact from humans (Orams et al 1996). The wild dolphin based tourism industry has only become established recently, consequently long term frequent contact has not yet become a feature of the wild dolphin - tourist relationship. However, previous experience has shown that as contact continues aggressive acts become a greater possibility (Lockyer and Morris 1985). These aggressive attacks can be relatively minor, such as pushing and biting (Orams 1996^a) or severe resulting in the hospitalisation of victims and rarely, even fatal injuries (Santos 1995).

Risk of harmful accidents

Any recreational activity which involves placing people into the open sea carries the risk of accident. Most commercial operators are aware of these risks and carefully monitor dolphin swimmers (Constantine 1995). However, many private boaters, who get caught up in the excitement of swimming with dolphins, pay little attention to the risks involved with entering the water in the open ocean. In an indirect sense, interacting with wild dolphins is likely to result in a drowning sometime in the future. Furthermore, the excitement of seeing dolphins and the possibility of swimming with them has resulted in vessel operators paying insufficient attention to the handling of their craft and a number of narrow misses with other boats have been observed (Orams pers obs).

POTENTIAL POSITIVE IMPACTS

Potential Positive Impacts for Dolphins

Entertainment/stimulation

Play is an important part of dolphins' behavioral routine. In particular it is an important way that young dolphins practice and learn skills that are essential for their survival. Consequently many dolphins find unusual objects and activities stimulating and an opportunity for play (Orams and Pulice 1995). It is not uncommon for dolphins to actively participate in interaction with humans - it is even possible to interpret their involvement in swim programs as "fun" and to conclude that it is enjoyable for the dolphins (Doak 1994).

Improved adaptability to human influences

Increased access to and interest in the marine environment, for example, through SCUBA diving, personal water craft, para-sailing and the myriad of other marine recreational activities, has resulted in increasing contact between marine creatures and humans. A number of animals have suffered as a result of the increase in human marine recreational activities (for example, the West Indian Manatee). The increasing influence of humans in the marine environment means that those animals that are better able to adapt to these influences are those that are more likely to survive. It is possible (but not proven) that dolphins which are exposed to regular interaction with

humans may learn to avoid risks, such as fast moving vessels, engine propellers and fishing hooks.

Environmentally responsible human behavior - marine conservation

If, as a result of their experience with dolphins, humans adopt more environmentally responsible attitudes and practices there may be indirect long term conservation benefits for dolphins. There is a widespread notion that people will protect those things that they know and love. There is some truth to this as evidenced by the large number of organizations which are dedicated to the protection of dolphins and whales.

Stranding assistance, injury treatment and rehabilitation

A number of stranding networks gain additional support and members as a result of people's interests being aroused as a result of their participation in an interaction with dolphins. Similarly, groups which establish facilities and programs for treating and rehabilitating injured and sick animals can gain support through increased interest in cetaceans prompted by close encounters with dolphins.

Potential Benefits for Humans

Psychological

There is no doubt that interacting with dolphins results in extremely positive feelings of enjoyment and connection with nature for humans (Amante-Helweg 1995) and that these kinds of "peak experiences" are beneficial for humans (Haddock 1993).

Educational

When an educational program is associated with these kinds of interactions significant learning can result. For example, a study of tourists who interacted with dolphins at Tangalooma, Queensland, Australia revealed that tourists who received educational material as part of their experience with the dolphins improved their knowledge about dolphins and marine environmental issues (Orams 1996^a).

Economic

Hoyt (1996) reports that "whale watching" (which also includes dolphin watching and other wild dolphin based tourism) occurs in over 65 countries and that in 1994 around 5.4 million tourists participated in this industry spending over US\$500 million. The industry continues to grow rapidly and has transformed many coastal communities. A good example is the New Zealand South Island town of Kaikoura. This small coastal community has seen an over twenty-fold increase in visitors and the establishment of 44 new businesses since whale watching and dolphin swimming began in 1987 (Hoyt 1995). The economic impact of cetacean (dolphin and whale) based tourism has been transformational for some 295 communities worldwide (Hoyt 1996).

Environmental awareness and action

If, as a result of their interacting with dolphins, people become more environmentally aware and responsible, it is possible that local communities may benefit. This can occur as more environmentally aware citizens work to improve the quality of their local area (for example, through involvement in beach clean-ups, recycling programs or re-vegetation projects).

SUGGESTIONS FOR MANAGEMENT

Management of wild dolphin based tourism is currently conducted in a variety of ways by a diverse range of agencies. Because the industry has developed recently and rapidly, management approaches have tended to be reactive and regulatory (for example, by restricting numbers of commercial permits or by imposing minimum approach distances). Research is also in its infancy and, as a consequence, agencies (most typically governmental bodies responsible for the conservation of marine mammals) are attempting to manage the industry in the absence of information on the impacts of human - dolphin interactions. Thus, at present, the way the industry is managed is largely a result of personal opinion, legal responsibilities and agency resources. The following brief suggestions are offered as a starting point for further research and debate, most represent the author's opinions on strategies, and some are already part of the management regime in place in Australia and New Zealand. However, issues regarding education as a management approach has been empirically tested and the reader should refer to Orams (1994^b, 1996^a, 1996^b, in press^b and also Orams and Hill 1996) for a more complete discussion of this.

Minimizing the Risks

Operators must be knowledgeable

In order to minimize the risk of disturbance and harm, operators must understand the biology and behavior of dolphins, in particular they must be aware of the risks outlined in this paper and learn to recognize the behavioral cues which may be a preliminary to unsafe situations.

Education of operators and participants is essential

Of particular importance is the extension of knowledge to private boat owners. A series of guidelines (code of behavior) which advises both commercial operators and private boaters of the behavior appropriate around dolphins is useful. This code can reinforce and extend regulations governing interactions.

Independent monitoring of dolphins' behavior is needed

Because commercial operators have commercial priorities and because private boaters are seldom aware of their impacts, an independent agency/agencies must monitor the impact of the

interactions. This monitoring must be long term, scientifically credible and practical in terms of developing management strategies for reducing problems.

Limit the frequency and duration of interaction

By limiting the amount of interaction to a brief number of encounters per day (less than three) and limiting the interaction to a short time period (half an hour or less) the habituation of dolphins to human contact is reduced. Of particular value is a period of the year where no interaction at all occurs.

Limit the number boats and the number of people in close proximity to dolphins

An example of a reasonable restriction could be; no more than three boats within 300 metres of a group of dolphins for the purposes of swimming with them. No more than 15 people permitted to swim with a group of dolphins at one time.

No interaction during sensitive phases/with sensitive groups

Regulations should restrict interaction when dolphins are resting, hunting/feeding or when there are nursery pods.

Expectations must be controlled

One of the difficulties with regard to dolphin - human interaction is that people's expectations of the encounter have often been shaped by media portrayals of dolphins or marketing promotions of commercial operators. The images often projected are of "mind blowing" encounters where participants get to "cuddle" dolphins and "make a friend for life". This of course is seldom the case, however, if participants expectations are unrealistic they often try to create that experience and subsequently place the dolphins under pressure of close contact.

Maximizing the Benefits

Education must be used

In order to prompt more environmentally responsible behavior in participants, well planned, high quality education programs must be incorporated as part of the experience. Research has shown that this can be effective (Orams in press^b).

A proportion of fees should be used to support monitoring and conservation efforts

If commercial operators are deriving a profit from dolphins it can be argued that there is an ethical obligation that operators contribute to the maintenance and health of that "attraction" (ie. the dolphins). One way of doing this is to impose a small conservation fee on all commercial "dolphin tourists" and use this money to support research, regulation enforcement and conservation initiatives.

Build in other marine attractions

In order to extend participants' knowledge and appreciation for the marine environment, other aspects of that environment should be incorporated into the trip. This can also assist in reducing the entire focus of the trip on the dolphins, thereby reducing the pressure on operators to find dolphins and facilitate interaction.

Encourage stimulating interaction

Both dolphins and humans benefit more from interesting, playful and stimulating interaction. Games, unusual sounds, mimicking, appreciation and respect enhance interactions (Doak 1995).

Use follow-up networks

In order to prompt longer term benefits for dolphins, participants should be encouraged to continue with their interest in dolphins through joining an environmental group or a stranding assistance network. The interaction with the dolphins is an opportunity to turn people into dolphin conservation advocates and workers.

CONCLUSION

Dolphin based tourism will become increasingly popular. History has shown that there are significant risks involved in these interactions, there are also however, benefits from these relationships. The challenge is to develop management approaches that successfully minimize the negative and maximize the positive. We must do this, for if we cannot, we will look back on dolphin based tourism as yet another example of humans exploiting and destroying wildlife for our own entertainment and profit.

ACKNOWLEDGEMENTS

I wish to thank two anonymous reviewers for their comments.

REFERENCES

- Alpers, A. 1963. Dolphins. London: John Murray.
- Amante-Helweg, V.L.U. 1995. Cultural perspectives of ecotourists participating in a swim with wild dolphins programme in the Bay of Islands, New Zealand. Unpublished Master of Arts Thesis, The University of Auckland.
- Burr-Stebbins, E. 1929. The Dolphin in the Literature and Art of Greece and Rome.

- Connor, R.C. and Micklethwaite-Petersen, D. 1994. *The Lives of Whales and Dolphins*. Chatswood, NSW: Reed Books.
- Connor, R.C. and Smolker, R.S. 1985. Habituated dolphins (*Tursiops* sp.) in Western Australia. *Journal of Mammalogy* 66(2): 398-400.
- Constantine, R. L. 1995. Monitoring the commercial swim-with-dolphin operations with the bottlenose (*Tursiops truncatus*) and common dolphins (*Delphinus delphis*) in the Bay of Islands, New Zealand. Unpublished Master of Science Thesis. The University of Auckland.
- Cousteau, J.Y. and Dirole, P. 1975. *Dolphins*. London: Cassell.
- Doak, W. 1984. *Encounters With Whales and Dolphins*. Auckland: Hodder and Stoughton.
- Doak, W. 1994 *Swimming With Dolphins in New Zealand*. Auckland: Hodder and Stoughton.
- Dobbs, H.E. 1977. *Follow a Wild Dolphin*. London: Souvenir Press.
- Dobbs, H.E. 1981. *Save the Dolphins*. London: Souvenir Press.
- Haddock, C. 1993. *Managing Risks in Outdoor Activities*. Wellington: New Zealand Mountain Safety Council Inc.
- Hoyt, E. 1995. The worldwide extent and value of whale watching: 1995, 1-34. In report IWC/47/WW2 to the Whale Watching Working Group, International Whaling Commission (IWC) annual meeting Dublin, Ireland May 1995.
- Hoyt, E. 1996. Whale watching: A global overview of the industry's rapid growth and some implications and suggestions for Australia, 31-36. In Colgan, K, Prasser, S. And Jeffery, A. (eds). *Encounters With Whales*. Canberra: Australian Nature Conservation Agency.
- Leatherwood, J.S. and Reeves, R.R. (eds) 1990. *The Bottlenose Dolphin*. San Diego: Academic Press.
- Lockley, R.M. 1979. *Whales, Dolphins and Porpoises*. Sydney: Methuen.
- Lockyer, C. 1990. Review of incidents involving wild, sociable dolphins, worldwide, 337-353. In Leatherwood, J.S. and Reeves, R.R. (eds). *The Bottlenose Dolphin*. San Diego: Academic Press.
- Lockyer, C. and Morris, R.J. 1985. A wild but sociable dolphin off Portreath, North Cornwall. *Journal of Zoological Society of London* 207: 605-607.
- Morris, R.J. 1988. Human contact, 204-207. In Harrison, R. and Bryden, M. (eds). *Whales, Dolphins and Porpoises*. New York: Facts on File Publishing.

Morris, R.J. and Lockyer, C. 1988. Twenty-two months in the life of a juvenile wild bottlenose dolphin. *Aquatic Mammals* 14(2): 49-62.

National Marine Fisheries Service. 1994. NMFS Report to Congress on Results of Feeding Wild Dolphins: 1989 - 1994. Washington DC: National Marine Fisheries Service, Office of Protected Natural Resources.

Orams, M.B. 1994^a. Tourism and marine wildlife: The wild dolphins of Tangalooma, Australia. *Anthrozoos* 7(20): 195-201.

Orams, M.B. 1994^b. Creating effective interpretation for managing interaction between tourists and wildlife. *Australian Journal of Environmental Education* 10, 21-34.

Orams, M.B. 1995. Development and management of a wild dolphin feeding program at Tangalooma, Australia. *Aquatic Mammals* 21(2), 39-51.

Orams, M.B. 1996^a. Managing interaction between wild dolphins and tourists at a dolphin feeding program, Tangalooma, Australia. Unpublished PhD thesis. The University of Queensland.

Orams, M.B. 1996^b. An interpretation model for managing marine wildlife - tourist interaction. *Journal of Sustainable Tourism* 4(2), 81-95.

Orams, M.B. in press ^a. Historical accounts of human-dolphin interaction and recent developments in wild dolphin based tourism in Australasia. *Aquatic Mammals*.

Orams, M.B. in press^b The effectiveness of environmental education: Can we turn tourists into "greenies"? *Progress in Tourism and Hospitality Management*.

Orams, M.B., Hill, G.J.E. and Baglioni, A.J. 1996. "Pushy" behaviour in a wild dolphin feeding program at Tangalooma, Australia. *Marine Mammal Science* 12(1): 107-117.

Orams, M.B. and Pulice, D.L. 1995. *Learning About Whales and Dolphins*. Brisbane: Tangalooma Island Resort.

Pline L'Ancien. 1955. *Histoire Naturelle, Livre IX*, French translation by E. De Saint-denis. Societe d'Edition les Belles Letters. Paris: Universites de France.

Queensland Department of Environment. 1994. Draft Management Plan for the Conservation and Management of Whales and Dolphins (Order Cetacea) in Queensland. Brisbane: Queensland Department of Environment.

Santos, M.C. de O. 1995. Behavior of a lone, wild, sociable bottlenose dolphin, *Tursiops truncatus*, and a case of human fatality in Brazil. Eleventh Biennial Conference on the Biology of Marine Mammals, Abstracts, p101. The Society for Marine Mammalogy.

Shane, S.H., Wells, R.S. and Wursig, B. 1986. Ecology, behavior and social organization of the bottlenose dolphin: A review. *Marine Mammal Science* 2(1): 34-63.

Webb, N.G. 1978. Women and children abducted by a wild, but sociable adult male bottlenosed dolphin. *Carnivore* 1(1): 89-94.

Weir, J., Dunn, W., Bell, A. And Chatfield, B. 1996. An investigation into the impact of "dolphin-swim ecotours" in southern Port Phillip Bay. Unpublished report. The Dolphin Research Project Inc, Victoria, Australia.

Wilson, B. 1994. Review of dolphin management Monkey Mia. Unpublished report to the Executive Director, Department of Conservation and Land Management, Western Australia.

INFRASTRUCTURE DEVELOPMENT IN CORAL REEF ENVIRONMENTS: THE NEED FOR ENGINEERING GUIDELINES

Stanislaw R. Massel¹ and I. R. Kapitzke²

¹Australian Institute of Marine Science
Townsville, Australia

²James Cook University
Townsville, Australia

ABSTRACT

The opportunity for ecologically sustainable use of coral reef regions is dependent on providing sound engineering and environmental bases for infrastructure developments in reefal and adjoining coastal waters. This involves an integrated approach to the design, construction and operation of facilities to ensure that, whilst safety and protection of projects are provided for, minimum detrimental impact is caused to sensitive marine ecosystems. This paper describes a research project which is developing guidelines for infrastructure developments in coral reef and coastal environments.

INTRODUCTION

The imperative for ecologically sustainable development applies to coral reef environments world-wide. Australia's Great Barrier Reef, for example, whilst still in a relatively pristine condition, is subject to increasing pressures from tourism, mariculture, agriculture, and coastal development. Although the Great Barrier Reef is carefully managed, marine park managers, scientists and engineers must maintain the balance between its protection and wise use to provide for a sustainable future. In the Pacific Islands, tourism developers often construct substantial buildings close to the shore, threatening the fragile coastal environment. Furthermore, global warming poses a threat to Pacific Island communities living on coral atolls which barely rise above sea level. Without protection, these atolls could be partly or wholly reclaimed by the sea.

Sound engineering and environmental bases for infrastructure developments are required for the ecologically sustainable development of these and other coral reef regions. This involves an integrated approach to the design, construction and operation of facilities to ensure that minimum negative impact is caused to sensitive marine ecosystems.

Many standardised marine engineering approaches to hydrodynamics, geotechnics, design and construction techniques (for example SPM, 1984) do not apply to coral reefs. Researchers working on the Great Barrier Reef, as part of the Australian government's Cooperative Research Centre program, are developing new engineering guidelines for infrastructure developments in coral reef and coastal environments. The guidelines apply innovative engineering techniques to

reef moorings, coral cay structures, waste discharges, and other coral reef installations for which established marine engineering procedures are not always appropriate. Whereas management issues are dependent on local legislative provisions, technical matters addressed in the guidelines are common to most reef and coastal environments. The researchers intend that the guidelines will be adaptable to sustainable infrastructure development in coral reef regions around the world, particularly in the Pacific region.

IMPACTS ON CORAL REEF ENVIRONMENTS

Structural and Process Type Impacts

The marine environment, particularly coastal areas, has great significance to the people, cultures and economies of the Pacific region (Kenchington and Bleakley, 1994). Coral reefs are the major feature of shallow marine environments in this region. They have substantial ecological and economic importance as their productivity and biological diversity provide the natural resource base for fisheries and tourism. The majority of human habitation is located on the coastal areas, which are targeted by most forms of economic development. The coral reefs and other marine habitats are increasingly threatened by over-exploitation and land-based development. Whilst tourism is the fastest growing activity in much of the Pacific region, urbanisation and industrialisation, rural agriculture, and fishing each have impacts on the marine environment.

These impacts can be of a structural or process nature. Structural impacts occur mainly in shallow reefal and coastal environments from infrastructure development at specific sites, and from disturbance of bottom communities through trawling. This may be due to island and mainland resorts and townships; land reclamation; excavations, dredging and breakwater construction for ports and marinas; construction of fixed structures such as jetties and underwater observatories; construction, operation and removal of moored facilities and structures; floating structures such as pontoons; vessel operation; and mariculture facilities.

The process impacts result from widespread phenomena such as pollution and overfishing, and are more threatening to marine areas and to the overall health of the marine ecosystems than the structural impacts. Polluted marine waters may impact public health and amenity, but may also affect the ecology of the reef. As the effects of chronic pollution on coral reefs is becoming widely known, reef managers are recognising the importance of maintaining water quality for the conservation of the natural resources of the reefs (Woodley, 1989). Hence concern about the effects of pollution on reefs is growing relative to sewage discharge, nutrients, toxic contaminants, oil, litter and marine debris, reclamation and dredging, sedimentation and anti-fouling.

The greatest source of marine pollution is commonly land-based human activity (Kelleher, 1994). The degree of pollution at different locations is often closely related to the size of the adjacent human population, with the exception being the major river systems that discharge pollutants from inland to the sea. Agriculture, industrial processes and urbanisation (outfall sewers and stormwater drains) contribute nutrients, herbicides, pesticides, toxic chemicals and heavy metals

which may cause local eutrophication, loss of seagrass beds, build up of toxic metal levels in sediments and organisms, and loss of public amenity.

These adverse land-use practices commonly result in sedimentation and enhanced nutrient levels which present major long-term threats to reefs. Sediments have the dual effect of increasing turbidity in reefal waters, and transporting nutrients which contribute to eutrophication of the system. Increased turbidity reduces light levels reaching photosynthetic organisms, and sediment deposition may cause periodic blanketing of reef organisms, and sometimes burial (Kinsey, 1990). This substrate modification leads to poor recolonisation of corals, metabolic stress and frequently death. Enhanced nutrients such as nitrogen and phosphorus adversely affect coral reef ecosystems, reducing the strength of calcium carbonate skeletons and smothering corals by algae, which in turn may stunt coral growth and release toxins that poison organisms such as fish.

Whereas pollution and fishing produce the most significant impacts on the regional health and status of reefs, site specific impacts from island and coastal development and from tourism activities are also significant for ecologically sustainable use. The tourism industry's reliance on a sustained reef environment provides an impetus for management of these impacts.

Tourism Activity

Tourism activity on the Great Barrier Reef and other Pacific regions is expanding substantially. GBR tourism, as well as experiencing a rapid growth in recent years, has undergone a dramatic change in style from an unsophisticated, relatively inexpensive, family style of activity to one which emphasises high technology and corporately financed activities (Craik, 1994). Large stable high speed catamarans provide ready access to the outer barrier reefs and the industry is now well supported by increased domestic and international air travel. For some Pacific counties, tourism is a major source of employment and foreign currency income, and the industry represents the sole opportunity for significant economic development. The reefs are also important in indigenous customary culture in many countries.

Coastal and island development associated with tourism may impact on the reef environment through habitat destruction in mangroves, estuaries and tidal marshes, and from pollution, particularly if dredging is involved. This affects the biological diversity of coastal and marine ecosystems in general, and threatens the survival of coral reefs and seagrass beds. Offshore tourism activities within the reef areas are less likely to be a serious threat to conservation of the reef environment as a whole. The important issues are to ensure that the particular sites are conserved and to ensure that the concentrations of people and tourist facilities in particular areas do not detract from the experience of other users (Massel et al., 1995).

Impacts from offshore tourism activities tend to be focused on a number of relatively heavily used areas that are attractive and easily accessible, and which provide good anchorages. Tourist pontoon installations on the Great Barrier Reef provide a good example of a high demand and high intensity activity that has the potential for adverse impact at individual sites if inappropriately managed. These pontoons are semi-permanently moored floating structures which support tourist activities operated by shore based tour companies. The pontoons are

serviced on day trips by fast catamaran vessels, and provide for a range of activities, including reef viewing, snorkelling, scuba diving, underwater viewing, and fish feeding. They act as bases for semi-submersible craft, glass bottomed boats and dive tenders, and provide a berthing facility for the transit vessels.

Protection of pontoon sites is vital to the continued viable operation of the installed facilities, since very few sites are available in any particular area which meet the strict criteria for suitability. A pontoon may impact on the biophysical environment of a site as a result of coral damage from mooring system components such as anchor blocks and chains; shading of coral; fish aggregation; waste disposal; and fin damage by snorkellers and divers. Furthermore, the structural integrity of the installation is crucial to visitor safety and to ensuring that the pontoon does not break free under severe weather conditions and therefore endanger shipping.

Present Limitations in Technical Provisions for Development

Proposals for project developments in the Great Barrier Reef Marine Park and in many other coral reef regions are presently affected by a lack of uniformity in approach and standards across responsible agencies, and by limitations in the technical provisions for development. This indicates the need for sound engineering and environmental bases for the development of structures and other major facilities to ensure functional, environmental and safety requirements are met.

Such guidelines should clarify requirements for proponents and marine parks authorities at all stages of the project assessment process. Technical provisions for design, construction and monitoring of infrastructure developments are required in order to rationalise environmental conditions and loadings and to incorporate a risk assessment philosophy for the installations.

DESIGN PHILOSOPHY FOR REEF AND COASTAL ENVIRONMENTS

Deterministic versus Probabilistic Approach

Those involved in the design, construction and operation of infrastructure developments in coral reef regions should recognise and understand the philosophy that applies for installations in such an environment. Some standardised coastal engineering techniques and assumptions may not apply to coral reefs, because they exhibit unusual growth and geomorphological patterns. Coral reefs behave as living substrates that can respond to changes in wave action, currents, storms, cyclones and other climatic variables. Designers should employ 'environmentally friendly' alternatives to traditional engineering approaches to account for the sensitivity of these marine ecosystems.

The two main approaches to dealing with loading and strength of a structure are the deterministic approach and the probabilistic approach. In the deterministic approach, a safety factor margin is adopted between the "characteristic strength" and the "design load". The safety factor does not

exclude failure, but is a measure of the probability of failure, based only on loading statistics (e.g. significant wave height H_s).

Probabilistic techniques give the designer a more objective means of building an appropriate degree of safety into a design. The random character of the marine environment causes great uncertainty in loadings. Waves induced by random fluctuation of wind over the sea surface generate surface waves which are also random, and the full description of a random wave field is only possible in terms of probability and spectral methods. To properly design marine structures and to plan marine operations, designers should estimate the probability of extreme events (such as tropical cyclones) and the associated parameters for winds, waves (significant wave height, wave period etc.) and currents. In the regional (global) sense, this will involve the statistics of occurrence and intensity of severe weather systems (typically tropical cyclones), whilst site-by-site investigations will also be required to account for significant localised influences imposed by the reef systems themselves. The return period of extreme events combined with the design life of marine structures or installations yields the probability of exposure to such an event. This probability represents the level of risk for the structure, and hence indicates the likelihood of damage or survival in the reef and coastal environment.

Environmental and Engineering Risk Analysis

Risk analysis provides a method of dealing with uncertainty. Conventional engineering analyses on structure integrity and safety are typically conducted for extreme events such as tropical cyclones, but these analyses should be supplemented by an environmental risk analysis in coral reef environments. The aim of ecological risk assessment at a coral reef site is to provide for sustainable bioconstruction and biodiversity (Done, 1996). This involves an evaluation of the area at risk, quantification of the risk, and assessment of recoverability and consequences in terms of ecological succession and bioconstruction. The analysis should be based on a clear understanding of the ecological and geomorphological implications of the final decision. The likelihood of various scenarios is assigned by taking account of the level of acceptable change, which may range from zero to complete, depending on the ecological value of the site. For example, the decision should be 'preserve' when considering development at a reef of high value when the risk of total loss is high. Conversely, if the risk of total loss is low, the decision still depends on the capacity of the affected area to quickly recover to its pre-loss condition.

System Approach

Infrastructure developments in reef and coastal locations are closely linked with ambient environmental conditions, forming a complex system with many feed-back relationships. This is demonstrated in the structure - environment interaction diagram (Fig. 1), where the central position relates to the structure or installation under consideration. The structure is affected by hydrodynamic, geotechnical and ecological factors, which in themselves are strongly interrelated.

The design approach for reef and coastal environments incorporated in engineering guidelines should reflect the relationships between these factors. Attention should be given to the determination of hydrodynamic impact on the coastline and the structure, assessment of geotechnical conditions for structure foundations on reefs and in the coastal zone, optimal

structural design to minimise negative impact on the environment, and application of appropriate construction techniques.

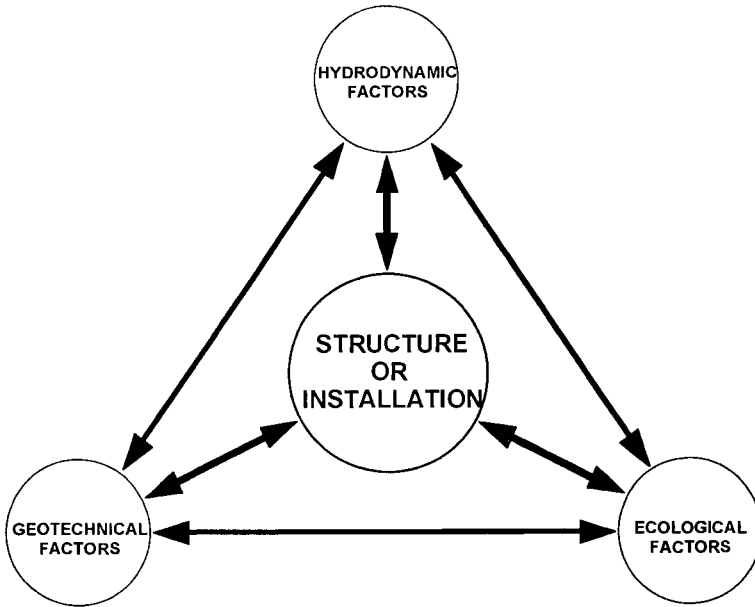


Figure 1. Structure - environment interaction diagram

CONTROLLING PROCESSES AND METHODS OF THEIR DETERMINATION

Hydrodynamic Factors

The assessment of hydrodynamic impacts for installations should consider atmospheric conditions (wind speed and direction, probability of occurrence) and hydrodynamic conditions (sea level, storm surge, currents and waves) during operational and cyclonic events. Hydrodynamic design inputs for cyclones are difficult to determine accurately.

The existing guidelines for pontoons in the Great Barrier Reef Marine Park have some shortcomings in that they require that the pontoons should withstand loadings associated with a Category 4 cyclone. Such a criterion is not well defined and structures in some areas of the GBR are overdesigned, whereas others are exposed to greater risk due to underestimation of the

environmental loadings. Furthermore, hydrodynamic loadings depend on the location of the structure within the GBR reef matrix and on the degree of sheltering provided by the adjacent reefs. It is not possible to design such structures with 100 percent safety, and there will always be some level of risk which should be accepted by engineers, scientists and managers. It is therefore appropriate to use a risk assessment approach instead of the adoption of a particular cyclone category.

Geotechnical Factors

The geotechnical properties of coral reef areas are complex and very little is known of the mechanics of coral and coral sand. The reefs provide very poor foundations for many engineering structures due to their extremely heterogeneous structural characteristics. Engineering structures such as drilling platforms, navigation aids, harbour and port structures founded on modern coral reefs are generally supported on piled foundations. For shallow foundations, the foundation elements are placed on the sea floor and any burial of foundations that occurs is through self weight loading. Cavities and loosely packed sands and gravels frequently occur within the reef structure, providing conditions for rapid flow of water through the high permeability zones (Hopley, 1991).

The shortage of suitable engineering aggregates in coral reef areas commonly requires that expensive aggregates are imported for use in foundations, concrete and pavements. Coral detritus has been successfully used as an alternative aggregate in engineering works, although mining of live reefs or beach deposits may not be an appropriate alternative to importing aggregates. Use of surplus excavation material for construction reduces importation requirements.

Coral cays are delicate morphological structures that are sometimes developed for tourist resorts, remote weather stations and navigational aids; commonly with adverse consequences. The cays are formed from the sediments produced by the reef on which they occur. This process depends on the shape and size of the reef, the pattern of wave refraction over the reef top, and diffraction around the reef. Coral cays readily migrate as a result of shifts in weather patterns, although vegetation and beachrock may give some protection against cay movement.

It is therefore important in designing and constructing structures on coral reefs, reef flats and coral cays, to take account of the special morphological and geotechnical conditions that apply for anchoring, foundations, fill materials etc.

Environmental Factors

The interaction of environmental factors with structures or installations should be considered at a range of spatial and temporal scales. Whereas long-term, broad-scale impacts are unlikely from individual structures, they may cause short-term and long-term local impacts which are unacceptable for sustainable use of the reef.

For pontoon installations on the Great Barrier Reef, the Great Barrier Reef Marine Park Authority requires that the pontoon mooring system be designed and installed to minimise the

risk of the anchors, chains and associated components damaging the coral in the vicinity of the pontoon. The design criteria used for this condition are commonly less conservative than the criteria for integrity and overall safety of the structure.

Structural and Construction Conditions

Designs must provide for the function, safety and comfort of visitors and resist severe cyclone conditions. For example, the tourist pontoon installations should provide for a period of serviceability when operations can be maintained up to some limiting wind speed. In tropical weather conditions, characterised by predominantly calm weather interrupted by cyclonic episodes, the safety requirements can be considered for three different stages: operational, cyclone stand-by, and cyclone. Construction techniques for marina excavation, de-watering, dredging and disposal of dredge spoils, for example, must consider the proximity of coral reefs and seagrass beds.

GUIDELINES FOR INFRASTRUCTURE DEVELOPMENTS

In order to implement the design philosophy described here, a research program is being undertaken by the Cooperative Research Centre for the Ecologically Sustainable Development of the Great Barrier Reef, based in Townsville, Australia. The Reef Infrastructure Guidelines developed here, although primarily related to the Great Barrier Reef region, will be adaptable to other coral reef regions. These guidelines are to help industry and environmental managers increase the opportunity for ecologically sustainable use of the reef and coastal zone, and to achieve a balance between protection of, and access to the reefs. They will assist project proponents and marine park authorities in the permit assessment process, and will facilitate developments having minimum detrimental impact on the physical, biological, cultural and social values of the reefs.

The guideline documents are divided into three parts (Fig. 2): Part 1-Project Assessment, Part 2-Structures and Installations, and Part 3-Design Procedures, Environmental Conditions and Loadings. Part 1 provides general information on the reef region and on the project application and assessment process. It identifies the general information required to assess a project application, defines the steps in the approval process, and is tailored to the management agency's approval procedures and documentation. Part 2 describes specific approaches and techniques for particular structures and installations, and is used by the proponent for the planning and design of these installations. Part 3 provides detailed information applicable across the range of reef and coastal conditions and types of installations and deals with the basic controlling processes and their methods of determination.

The guidelines will cover pontoons; single point moorings; marinas; mariculture; waste discharge; dredging and dumping; coral cays and coastal structures; and ship operations.

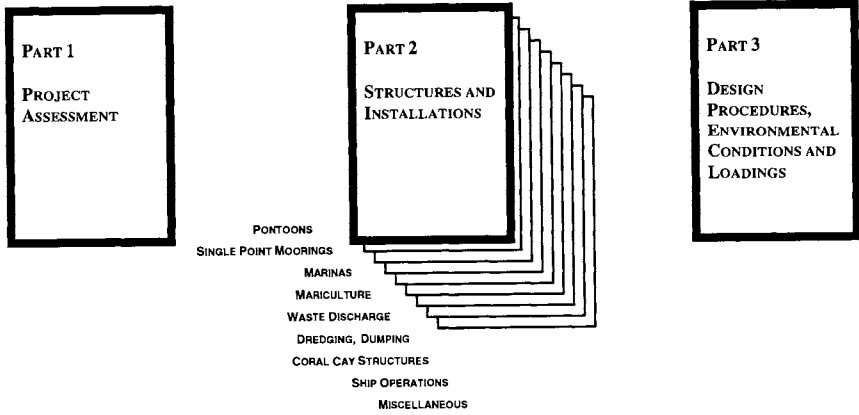


Figure 2: Engineering Guideline structure

CONCLUSIONS

Development pressures in coral reef regions provide an imperative for careful management of coral reef ecosystems and the provision of sound engineering and environmental bases for infrastructure developments in reefal and adjoining coastal areas. Whereas water pollution, fishing and coastal and island development produce major impacts on the regional health and status of coral reefs, other site specific impacts relating to tourism activities, for example, are significant for the ecologically sustainable use of the reefs.

Moreover, many standardised marine engineering approaches to hydrodynamics, geotechnical properties, structural designs and construction techniques do not apply to coral reef environments. Hydrodynamic and structural designs must allow for prevailing weather and severe cyclonic conditions, and designers should pay careful attention to risk assessment and the use of design criteria for structures that are reasonable and practicable. The Reef Infrastructure Guidelines will form a comprehensive, standardised set of criteria to assist in the planning and assessment process. They will provide project proponents with a basis for understanding and applying sound engineering practice for coral reef regions, and allow marine management agencies to apply these same principles in assessing the environmental impacts and safety of the project.

ACKNOWLEDGMENTS

This research was supported by the Australian Cooperative Research Centres Program through the Cooperative Research Centre for the Ecologically Sustainable Development of the Great Barrier Reef.

REFERENCES

- Craik, W. 1994. Tourism developments in offshore and coastal environments. In: Proceedings of Tourism Ecodollars Conference. Mackay, Australia.
- Done, T. 1996. Ecological criteria for evaluating coral reefs and their implications for managers and researchers. *Coral Reefs*. **14** : 183-192.
- Hopley, D. 1991. The geology and geomorphology of the Great Barrier Reef in relation to engineering problems. In: Proceedings of Engineering in Coral Reef Regions Conference. James Cook University, Townsville, Australia. pp. 61-74.
- Kelleher, G. 1994. The Pacific Basin: Humans in a complex system. In: Bellwood, O., Choat, H., and N. Saxena (eds). Proceedings of PACON 1994 Conference. James Cook University, Townsville, Australia. pp. 1-6.
- Kenchington, R., and C. Bleakley. 1994. Identifying priorities for Marine Protected Areas in the insular Pacific. *Marine Pollution Bulletin*. **29**:3-9.
- Kinsey, D. W. 1990. Water quality and its effects on reef ecology. In: Proceedings of Engineering in Coral Reef Regions Conference. James Cook University, Townsville, Australia. pp. 105-109.
- Massel, S. R., Kapitcke, I. R., and C. Cook. 1995. Providing a sound basis for infrastructure developments in coral reef environments. In: Proceedings of National Environmental Engineering Conference 1995. Melbourne, Australia.
- Shore Protection Manual (SPM). 1984. U.S. Army, Coastal Engineering Research Center, Washington, D.C. Vol. I-III.
- Woodley, S. 1989. Management of water quality in the Great Barrier Reef Marine Park. *Water Sci. Tec.*, **21**:31-38.

COMPETITION AMONG NORTH AMERICAN CONTAINERPORTS: CURRENT CHARACTERISTICS INVOLVED

Henry S. Marcus¹ and William A. Cowart²

¹Massachusetts Institute of Technology
Cambridge, Massachusetts, U.S.A.

²World Bank
Washington, D.C. U.S.A.

ABSTRACT

If you ask someone employed by a North American port authority to describe the competition among containerports, the person will undoubtedly reply, "Fierce". While the answer may be accurate, it doesn't really tell us much. We may be more interested in knowing whether competition is going on "as expected" or in some "surprising" manner. Typically, we have in mind a paradigm of how we expect competition to take place.

This paper will consider some dominant paradigms of containerport competition and explain why they are lacking. Data on competition among North American containerports will be presented and a new conceptual approach for analyzing port competition will be considered. This discussion will show how the current characteristics of ports and their competitive strategies are an inherent part of the overall conceptual approach.

INDUSTRY BACKGROUND

The first fully cellular containership service in international trade started in 1966. The transition from break-bulk cargo operations to higher fixed-cost containership activities had obvious implications for port competition. Consultants, such as McKinsey and Co., Inc., saw an obvious reduction in port calls that would accompany the introduction of high cost containerships (1967). The logic was that while inexpensive break-bulk cargo vessels could make a huge number of port calls on a single voyage, expensive containerships could not afford to spend their time sitting in port. Consequently, they would reduce the number of ports on their itineraries and serve other areas by truck, rail or feeder vessels.

THE DOMINANT PARADIGM: LOAD CENTERING

Over the past 30 years, the obvious paradigm of more port concentration has continued with every new generation of larger and more expensive containerships resulting in similar predictions that these vessels would have to have fewer port calls each voyage to better utilize their capital-intensive investment. Therefore, today we still hear that 6,000 plus TEU containerships will

result in fewer major containerports, the ports that are not served by these giants being left to fade away from the lack of cargo.

The two highest volume containerports in the world, Hong Kong and Singapore, are major transshipment centers. These load centers have grown with the use of feeder systems to move the cargo to or from its origin/destination.

ANOTHER PARADIGM: PUBLIC INVESTMENT

One might argue that since containerports are managed by quasi-public port authorities, taxpayers' money will be used to build containerports as well as maintain them even if they operate at a loss. In North America (specifically, Canada, U.S. and Mexico), there are 64 containerports. While the transition from break-bulk cargo vessels to small containerships to giant containerships may have resulted in the demise of ports, we still have plenty left. We might conclude that all 64 ports will remain alive and continue to grow at the same rate over time.

Examples of public investment include taxpayers' funding of new facilities in Charleston, Savannah and Jacksonville, in what is a zero sum game. Further north Boston and Philadelphia have committed tens of millions of dollars to develop double-stack container trains.

RECENT RESEARCH AND SHORTCOMINGS OF CURRENT PARADIGMS

While the dominant port competition paradigm of greater port concentration over time seems to make sense, it is not fully accurate. Professor Jon Helmick of the U.S. Merchant Marine Academy has shown that on the U.S. East Coast the degree of port concentration is actually decreasing over time (Helmick, 1996). On a worldwide basis the percent of container cargo carried by the top 20 ports has declined from 1992 to 1993. The percent of container cargo carried has gone from 51.8% in 1992, to 51.6% for 1993 (NMCL, 1995). However, it did increase in 1994 to 51.9%. The key conclusion here appears to be that port concentration won't change much over the short run.

The public investment paradigm is too simplistic and inaccurate. The difference in volume between the largest and smallest is enormous, a factor of more than 2,000. Similarly, growth rates also vary as shown by the difference in world ranking of various ports between 1993 and 1994.

Before presenting a different conceptual approach for analyzing containerport competition, let's consider some recent research performed at MIT (based on work originally done as a Master's thesis by William Cowart.) In order to focus on major levels of competition among North American containerports, the researcher only included containerports that are "rail-capable", that is, rail service exists at or near the port. This constraint brings the total from 64 to 33 ports that moved a total of 16.7 million TEU in 1993. Of this total 6.0 million TEU moved by rail and 10.7 million by truck.

To differentiate among the 33 rail-capable ports, those with more than 150,000 TEU of rail movements in 1993 were selected. These 14 ports handled 5.7 million TEU by rail, or 95% of all railed containers, and 8.6 million TEU by truck, or 80% of the truck traffic. Six of these ports are on the West Coast, 8 on the East Coast.

The remaining 19 ports moved only 2.4 million TEU or 14% of the containers, handling 0.3 million TEU by rail and 2.1 million TEU by truck. From a competitive standpoint these 19 ports without major rail movements are in a different category than the 14 major ports.

One part of what we are seeing is a reflection of the geographic range of truck and rail movements. In North America containers are typically carried by rail when the distance to be moved is more than 500 miles, while they are normally trucked when the distance is less than 500 miles. Consequently, the 19 smaller ports are geographically restricted in the impact they can have and will normally compete only with ports within 400 or 500 miles of them. In contrast, the major ports can use rail service to move containers from coast to coast. In some instances they can compete with almost all the rest of the major 13 ports since ocean carriers have a choice between all-water routes and mini-landbridge service.

Another part of this picture is that economies of scale exist in some port operations, particularly as they relate to double-stack unit train activities. A huge volume of container movements needs to exist before a frequent double-stack unit train service is viable.

PROPOSED CONCEPTUAL APPROACH

The authors feel that it is useful to think of containerports in three tiers or categories. (This assumes that ports neatly fit into one of these categories, which is not always the case.) The first tier is for the containerports with the largest volume. These ports are the industry leaders or load centers. The third tier ports are the smallest; they exist because they serve a market niche. The second tier represents medium-sized ports. This tier is the most vulnerable because they lack the long-lasting competitive advantage exhibited by many first and third tier ports.

Ports in each category possess characteristics that are within their control as well as some totally outside their control. Probably the most important factor in the latter category is population size in the immediate vicinity. It is not a coincidence that the four containerports with the highest volume on the North American mainland (Long Beach, Los Angeles, New York/New Jersey, and Oakland) are located in major population centers. Access to the open sea and natural water depth are also important. Dredging can, of course, alter water depth. However, as New York/New Jersey and Oakland have found out, environmental issues can make it difficult to increase, or even maintain, water depth.

First tier ports must also possess a number of man-made accomplishments on the landside. Good rail access (unless the port is on an island) and good road access are critical to being a first tier port. As the MIT research shows, if the port is not "rail-capable", its market is fundamentally restricted to a radius of a few hundred miles, thereby severely restricting potential growth. Of

course, even if a port is "rail-capable", it may not have the rail service needed to attract regional or transcontinental cargo. Examples would be Boston, prior to its investment to introduce double-stack trains, as well as San Francisco.

Modern large terminals and on-dock or near-dock double-stack container train facilities characterize first tier ports. While port efficiency may be very important in growing to be a first tier port, it may not be as important once this tier level has been achieved. A first tier that is blessed with a major population center has a certain characteristic that might be described as critical mass, entrenched infrastructure, or simply inertia. Consider the Port of New York/New Jersey. While it has steadily lost market share to other East Coast ports over the last several years, it still handles more than twice the number of TEU's of its closest East Coast rival.

Reconcilable environmental concerns and political support are also important for first tier ports. We don't think that any first tier ports can totally avoid environmental problems, but the successful ports find a way to resolve their problems. Political support may be even more important than public funding in this process. Some first tier ports, particularly in California, worry more about municipal governments taking money from the port coffers rather than the reverse.

At the other end of the size spectrum is the third tier ports. Their geographic reach is limited because they do not use major rail services. However, the successful third tier ports possess some type of competitive advantage or market niche within the geographic boundaries of their hinterlands. A variety of factors may contribute to their competitive advantage such as: remote location, specialized cargo handling facilities, unique labor contract or unique relationship with customers. The Port of Richmond, Virginia, ranking number 40 out of 64 displays some of these characteristics. Richmond possesses the only US Department of Agriculture inspected and approved livestock facility on the East Coast. In addition, it uses Teamsters rather than the International Longshoremen's Association (ILA) and has good relationships with its customers. As small specialized ports, third tier players often rely on government financial support, particularly to build new specialized facilities.

The second tier category of medium sized ports is made up of all the ports that do not fit into either the first or third tier classifications. These ports are the most vulnerable because they do not have the competitive advantage of the first or third tier ports. The second tier ports, such as Boston or Portland, Oregon, lack either the built-in population base or the level of terminal capacity or intermodal service possessed by the industry leaders. At the same time they are too big to rely on market niches like the third tier ports. Consequently, they struggle to match all the facilities and services provided by the first tier ports, but are not perceived to be doing so by ocean carriers. In some ways the second tier ports need financial government support the most since they do not have the entrenched customer base of the first or third tier ports.

A MORE BASIC PARADIGM

In trying to apply the conceptual approach described above, the authors realized that they had to articulate a more basic paradigm as to how the maritime industry operated. Fundamental assumptions as to the marine industry included:

- There is -- and will continue to be -- an overcapacity of shipbuilding facilities in the world. While there may be a period of time near the end of this decade when supply and demand for shipbuilding may be in balance, for the last few decades, and for the foreseeable future, this seems to be a safe assumption.
- Shipbuilding overcapacity will always result in vessel over-capacity as long as governments around the world keep directly or indirectly subsidizing their underutilized shipyards to build new ships that wouldn't otherwise be constructed. OECD is on the verge of implementing a financing agreement among its members and others that would basically end the traditional subsidies to shipyards. If this agreement is actually implemented, it might eventually have a major impact on vessel overcapacity in the world. Otherwise, we assume it's business as usual.
- As long as the conference system exists in U.S. inter-national trades, non-conference or independent carriers will operate in U.S. trades at reduced tariffs.
- Taxpayers in the U.S. (and elsewhere) will continue to subsidize the construction of new container handling facilities at their local ports in order to reap the perceived local benefits from such investments. Therefore, we will continue to have an overcapacity of container facilities in the U.S. (although such excess container terminal capacity may not be in the ideal terminal size and design).
- The international liner market will continue to be a dynamic industry. The constantly changing nature of this market is shown by looking at how the numbers of competitors has varied in the major two U.S. international trades over the time period 1980-1995 (NMCL, 1981; 1996). On the North American West Coast-Far East trade the number of liner operators decreased from 37 to 24 in this 15 year period, while on the Europe-North American East Coast trade the number increased from 14 to 36 over the same period.

When you put together all these assumptions, you have an overcapacity of containerports chasing after an overcapacity of containerships. The first and third tier containerports have the best chance of filling their capacity because of the competitive advantages they possess. The underutilized second tier ports chase after the remaining carriers, cutting price when necessary to get someone in their terminals.

In theory, a major operator may try to serve a few first tier ports with direct calls and then serve the rest of the first tier ports, as well as the second and third tier calls, by feeder system. From the viewpoint of an ocean carrier that is not an industry leader, rather than compete head-on with a major containership operator by having the same itinerary, the weaker carrier can improve his

competitive position by providing direct service to ports served only by the major competitors feeder systems. Such a strategy may force the major carrier to provide direct service to more ports than he would otherwise. (Note that in the case of the new 6,000 TEU containerships, the carrier's number of port calls has not yet decreased.)

USING THE CONCEPTUAL APPROACH

The authors don't pretend that the conceptual approach described above will explain all the interactions among ports; the liner industry is simply too complex for that. However, we hope this concept may be useful to those following containerport activities. (We also think that the dominant existing paradigms can be useful supplements as well.) We can see from the conceptual approach that many different activities are going on at the same time in a dynamic environment. Some will cause a greater concentration of traffic in containerports, while others will have the opposite effect.

Third tier ports should rarely be expected to grow beyond the size of their niche market. Second tier ports without great rail service should not expect to significantly increase their volume with cargo much beyond a few hundred miles away. A first tier may lose cargo in a given year, but will not lose its first tier status without a basic change in the competitive structure of the market (described below).

The authors would argue that a major change in technology (e.g., giant containerships too big to fit into many ports, giant container terminals required by global alliances where the facility can only exist in a small number of ports, or a new type of double-stack rail service that is only available to a limited number of ports) or regulation (e.g., restricting the number of ports that can be dredged) is needed to allow ports to move between tiers. As long as ports can copy the industry leaders in new facilities, new double stack rail service and new information systems, don't expect to see major shifts of ports between categories.

In the future we hope to do further research in the application of the conceptual approach presented here. While one might hypothesize that all continents contain ports that can be placed in the three tiers or categories that we have described, we have not done the research to prove it. In addition, more research could be performed matching port characteristics to the types of trade routes they serve.

Modifications may also be appropriate to the paradigm presented by the authors. Paul Chilcote of the Port of Tacoma has suggested that when two ports seem to function as one in the same geographic area, they should be considered as one "gateway" (Chilcote, 1996). In our terminology, we might consider two ports in the same general location (e.g., Long Beach and Los Angeles) as one port for purposes of calculating port concentration.

While we know we do not have all the answers, we hope that the conceptual approach presented here will help people understand the ever-changing containerport industry.

REFERENCES

- Chilcote, P. 1996. Gateway to Heaven. *Containerization International*. **29(8)**:13.
- Cowart, W. A. 1996. Operationalizing a Model of Landside Access and Seaport Container Activity. M.C.P. and M.S. thesis, Massachusetts Institute of Technology.
- Helmick, J. S. 1996. Network Evolution in the North Atlantic Liner Route System: A Longitudinal Investigation. In: Proc. Intermodal Distribution Education Academy (IDEA). March. p. 82.
- Lauriat, G. 1996. Port of Richmond: Classic Niche Port. *Atlantic Journal of Transportation*. Iss. 31. p. 5a.
- McKinsey and Company, Inc. 1967. Containerization: The Key to Low-Cost Transport. A report for the British Transport Docks Board. London: McKinsey and Company, Inc.
- National Magazine Co., Ltd. (NMCL). 1981 *Containerization International Yearbooks*. London:National Magazine Co., Ltd.
- National Magazine Co., Ltd. (NMCL). 1995 *Containerization International Yearbooks*. London:National Magazine Co., Ltd.
- National Magazine Co., Ltd. (NMCL). 1996 *Containerization International Yearbooks*. London:National Magazine Co., Ltd.

INDEX OF AUTHORS

- Aoki, Taro..... 89
 Ayukai, Tenshi..... 227

 Balasuriya, B. A. A. P..... 119
 Baskina, Valentina A..... 45, 363
 Blain, Cheryl Ann..... 177
 Burke, R. J..... 191

 Cai, Deling..... 205
 Chang, Man..... 269
 Clark, T..... 259
 Collins, R. L..... 191
 Cowart, William A..... 501

 Dacey, John W. H..... 277
 Davies, Peter J..... 297
 Din, Zubir..... 397

 Everson, James F..... 277

 Garrood, Dennis..... 19
 Geesey, Gill..... 373
 Geng, Xueyi..... 33
 Graham, T. L..... 305

 Haigh, R..... 429
 Hall, T..... 259
 Helsley, C. E..... 191
 Henry, R. F..... 167
 Holland, Paul M..... 277
 Hopley, David..... 249, 305, 421
 Huang, Weigen..... 11

 Itoh, Sadahiko..... 55

 Jiang, Shaoren..... 465

 Kapitzke, I.R..... 491
 Kawana, Ikuo..... 89
 Kim, Woong-Seo..... 269
 Kobayashi, Tsuyoshi..... 443
 Koh, Hock-Lye..... 397
 Kolotyrkina, Irina Y..... 217

 Kondo, Takeo..... 443
 Korchagin, Nickolay..... 317
 Kozuki, Yasunori..... 55
 Kumar, Muneendra..... 131

 Langille, Stephen..... 373
 Lay, G. F. Terry..... 347
 Leach, Joseph H. J..... 1
 Lee, Jong Soo..... 269
 Lee, Soo Hyung..... 269
 Lee, Hooi-Ling..... 397
 Lehtomaki, Norman..... 19
 Liu, Qinyu..... 239
 Ludbrook, G..... 259
 Luick, J. L. 167
 Luk, Tony..... 19

 Malahoff, Alexander..... 217
 Mao, Zhihua..... 11
 Marchuk, Andrei..... 77
 Marcus, Henry S..... 501
 Massel, Stanislaw..... 141, 491
 Matsuura, Eiichi..... 443
 Minemura, Akira..... 411
 Miyazaki, Takamasa..... 411
 Murakami, Hitoshi..... 55
 Murphy, Doug..... 97
 Murray, Steve..... 97
 Murty, T.S..... 167
 Mustacich, Robert V..... 277

 Nakamura, Shigehisa..... 65
 Neudorfer, Mark..... 19

 Orams, Mark B..... 477

 Pan, Yuqiu..... 11
 Pan, Delu..... 11
 Patel, C. K. N..... 191
 Paul, Linda M.B..... 329
 Petrenko, Victor..... 77

 Quintero, Ernesto..... 373

Rasmussen, C. E.....	305
Ritchie, Stephen M.....	421
Rognstad, Mark.....	19
Sato, Hiroaki.....	55
Selivanova, O. N.....	451
Sharma, S. K.....	191, 227
Shpigun, Lilly K.....	217
Sullivan, Patrick K.....	387
Sun, Jilin.....	239
Takagawa, Shinichi.....	89
Takai, Motoyuki.....	107
Tratt, D. M.....	191
Troedson, Alexa.....	297
Ura, Tamaki.....	107, 119
Vithanage, Dayananda....	387
Wang, Lu.....	287
Watson, Gary.....	153
Weiner, Ronald.....	373
Wiltshire, John C.....	337, 347
Yamamoto, Naoaki.....	55
Yamashita, Takao.....	153
Zhou, Xiaozhong.....	465
Zhu, Baozhen.....	239
Zielinski, Adam.....	33

